INTERNATIONAL DOCTORAL
SCHOOL OF THE USC

Marcos
Vilela Picos

PhD Thesis

STIMULI-RESPONSIVE CONTROL OF CYCLIC PEPTIDE NANOTUBES TOWARDS BIOLOGICAL APPLICATIONS

Santiago de Compostela, 2025

Doctoral Programme in Chemical Science and Technology

ESCOLA DE DOUTORAMENTO
INTERNACIONAL DA USC

DOCTORAL THESIS

STIMULI-RESPONSIVE CONTROL OF CYCLIC PEPTIDE NANOTUBES TOWARDS BIOLOGICAL APPLICATIONS

Marcos Vilela Picos

Supervisors: Juan Ramón Granja Guillán and Manuel Amorín López

Tutor: Juan Ramón Granja Guillán

PHD PROGRAMME IN CHEMICAL SCIENCE AND TECHNOLOGY

SANTIAGO DE COMPOSTELA

A mis padres, hermana y abuelos

USC
UNIVERSIDADE
DE SANTIAGO
DE COMPOSTELA

Agradecimientos

"Recuerda que lo que hoy tienes alguna vez fue aquello que deseaste" - Epicuro

Las siguientes personas son las que alguna vez deseé para acompañarme en este largo camino y estoy seguro que la gran experiencia de la tesis habría sido mucho peor sin todas ellas. Como siempre digo, la gente es lo mejor que me llevo de esta etapa. Después de tanto tiempo es probable que me olvide de mencionar a alguien, pero os estoy eternamente agradecido a todos los que me acompañasteis en este camino.

En primer lugar, me gustaría agradecer a mis directores de tesis, Juan R. Granja y Manuel Amorín. A **Juan**, muchas gracias por transmitirme todo tu entusiasmo por la investigación y guiarme en todo momento. Me alegro de haber llegado a tener una relación más coloquial contigo y poder conocer a esa gran persona que se esconde detrás de ese magnífico profesor e investigador. A **Manuel**, eres la persona que me recibió el primer día en el laboratorio y desde el principio me acogiste con los brazos abiertos. Gracias por tu predisposición para ayudarme siempre.

A **Federica**, no me llegan las palabras para agradecerte todo lo que hiciste por mí, en mi corazón eres una directora más de mi tesis. Sin ti esta tesis no sería posible. Gracias por todo lo que me enseñaste, por inculcarme esa pasión por el trabajo y por estar disponible siempre que lo necesité, incluso cuando ya no estabas en el grupo y no tenías ninguna obligación de hacerlo. Eres un ejemplo a seguir para tu Marcolino. ¡Muchísimas gracias Fede!

A **Alejandro Lamas**, mi primer maestro. Aunque en su momento no fuera el mejor alumno del mundo para ti, supiste mantener la paciencia y enseñarme muchas de las cosas que sé hoy en día. Creo que parte de las buenas manías que tengo vienen de aquellos meses siendo tu pupilo. Me integraste en el grupo y fuera del laboratorio te convertiste en un gran amigo. ¡Muchísimas gracias Lamiñas!

A **Rebeca G. Fandiño**, muchas gracias por todas las sugerencias en los seminarios que me ayudaron a mejorar esta tesis. A **Javier Montenegro**, **Julián**, **Nacho** y **Adrián**, gracias por estar dispuestos a ayudarme siempre que lo necesité. A **Alejandro Méndez**, muchas gracias por tu infinita ayuda y enseñarme todo cuanto sé de microfluídica. A **Alessandro Moretto** y **Pepo Brea**, por las colaboraciones y ayuda científica durante estos años.

A **Samuel I. Stupp**, por abrirme las puertas de tu grupo y acogerme como un miembro más desde el primer día. Gracias a ti pude vivir una experiencia que nunca olvidaré. A **Liam Palmer**, por la ayuda científica e introducirme en el grupo. A **Todd Linton**, por la ayuda burocrática para hacer posible mi estancia. A **Hiro**, por ser una enciclopedia humana y la persona a la que siempre pude recurrir con cualquier consulta científica durante mi estancia. A **Cara**, sin duda la persona más importante de mi estancia en el grupo. Siempre dispuesta a ayudarme o enseñarme. A pesar de ser un momento complicado para ti por estar en la recta final de tu tesis, siempre me

USC UNIVERSIDADE DE SANTIAGO

transmitías una gran pasión por todo lo que hacías. Nunca olvidaré aquellos días sacrificando ratones para los experimentos, todavía sigo traumado. A **Suvendu**, por tu entusiasmo y todo el tiempo compartido en el laboratorio. A **Rade** y **Yang Yang**, por todos los momentos en el despacho y convertir Northwestern en mi casa de acogida. Al resto de miembros del grupo, gracias por acogerme en vuestra gran familia. A **Joaquín**, por todas las grandes vivencias que pasamos por Evanston y Chicago adelante. A **Ila**, **Alessandra**, **Miranda** y **Gwen**, por acogerme en vuestro hogar cuando ya me veía durmiendo en la calle. Once a wildcat, always a wildcat!

Al **Ministerio de Universidades**, por el contrato de Formación de Profesorado Universitario (FPU19/01011) y la Ayuda complementaria de movilidad (EST22/00065). A la **Xunta de Galicia** (ED431C 2017125, ED431C 2021/21), al **Ministerio de Ciencia e Innovación** y la **Agencia Estatal de Investigación** (PID2019-111126RB-I00, PID2022-142440NB-I00) por todos los proyectos del grupo que financiaron la investigación de esta tesis doctoral. A la **Real Academia de Farmacia de Galicia**, por el accésit de excelencia del X Premio Julián Francisco Suárez Freire para jóvenes investigadores. A **Lilly** y la **Real Sociedad Española de Química**, por el XXII Premio Lilly de Investigación para Alumnos de Doctorado.

A todo el **personal del CiQUS** que hizo que mi día a día fuera mucho más llevadero: Mencha, Arcadio, Laura, Carmen, Ángel, Noela, Mariano, Adrián y Almudena. Especialmente a **Andrea**, con quien comparto la sonrisa con la que ella nos alegra los días. ¡Soltad a los perros porque me he escapado! A **Rebeca Menaya**, por tu interminable paciencia cuidando de nuestras células y estar disponible siempre que lo necesité. A **Patri Lago**, por ser siempre mi salvadora con cualquier tema burocrático.

A la **RIAID** de la Universidad de Santiago de Compostela por las facilidades para usar su equipamiento. Especialmente, a **Raquel** y **María José** del servicio de microscopía por la cantidad de muestras analizadas y pelearse constantemente con el equipo de plasma para que pudiera usarlo.

A todos mis compañeros de laboratorio durante estos años, gracias por las experiencias vividas y por convertiros en mis grandes amigos.

A **Alfonso**, espero que estas palabras no se te suban a la cabeza, pero esta experiencia habría sido mucho peor sin ti. Eres una pieza clave e insustituible. Capaz de desesperarme como nadie, pero me siento un auténtico afortunado de tenerte como amigo. Tienes un corazón enorme, por eso Javi Fernández y yo te queremos un montón. Ya sea en Francia, Islandia o la otra punta del mundo, eres un amigo para siempre y mi gran compañero de patinaje. Gracias por todo tu apoyo. ¡No cambies nunca!

A **Victoria**, gracias por estar siempre dispuesta a ayudarme en lo que sea o a darme unas clases del refranero. La chica opuesta a mi manía por el orden y la que me avisó desde el principio que acabaría mal de la cabeza. Ahora puedo confirmar que tenías toda la razón. Eres una alegría en el laboratorio con tus risas interminables o esas arrancadas de moto. Gracias por toda tu locura y amistad durante estos años. ¡Siempre saldrán tres por dos calles!

USC UNIVERSIDADE DE SANTIAGO DE COMPOSTELA

A **Ezequiel (Zeko)**, o quizás debería decir: I'm not talking to you! Eres la única persona presente en todas mis etapas en Santiago. No podría haber tenido un mejor amigo para recorrer todo este camino. Gracias por estar presente desde el primer día que pisé la facultad hasta hoy, tanto en los buenos como en los malos momentos. Eres un compañero incondicional de experiencias. También eres la persona con más paciencia conmigo y a la que más caña metí durante todos estos años, todavía no sé cómo no me pegaste. ¡Eres un amigo muy grande Zekolino!

A **Sergio Serantes**, mi primer alumno. Aunque tuviste que sufrir mi inexperiencia como maestro, espero que aprendieras algo científicamente productivo. En todo este tiempo yo aprendí muchas cosas de una gran persona y amigo como eres tú. Ahora te toca ser mi sucesor, pero no se me ocurre nadie mejor para ello. Nunca pierdas esa personalidad y alegría que te caracterizan porque eres un tesoro de amigo. A ver si te vienes un día por Ferrol que estoy cansado de invitarte y de que rechaces mis planes. Además, me queda la espinita clavada de ir a Zaragoza contigo. Si no coincide con el día de la madre, ¡me tienes para lo que sea!

A **Amaia**, mi segunda alumna, la reina del brownie de chocolate y de las presentaciones en los seminarios. Espero que guardes un muy buen recuerdo de nuestro tiempo como maestro y pupila. Siempre intenté hacerlo lo mejor que pude para que fuera una experiencia productiva para ti. No pierdas nunca esa pasión que te caracteriza y sigue poniéndole tantas ganas a todo lo que haces.

A **Kaddy**, mi última alumna, espero que aprendieras mucho y que siempre recuerdes con una sonrisa nuestros días juntos en el laboratorio. Llegaste en una etapa más complicada para mí como es la recta final de la tesis, pero aun así nunca perdiste la paciencia y siempre estuviste dispuesta a ayudarme cuando lo necesité. Aunque ya no vaya a estar en el laboratorio, me seguirás teniendo y te seguiré ayudando cuando lo necesites. Te deseo lo mejor en la tesis que estás empezando y nunca pierdas la ilusión.

A **Alba**, te tengo un cariño especial por ser mi pupila durante solo una semana y por ser capaz de cuidar aquel vial como si fuera tu vida. Aunque nunca conseguiste que me apuntara a CrossFit, tu llegada trajo un soplo de aire fresco y alegría al laboratorio. Eres una gran compañera y una magnífica amiga.

A **Román**, como siempre digo un auténtico crack. Aunque tienes todo lo que Juan odia de nosotros, no tengo dudas de que te espera una tesis brillante por delante.

A **Alicia Moreno**, mi gran compañera de comidas en la última época de la tesis. Gracias por encajar perfectamente en nuestra locura desde el primer día.

A **Yeray**, gracias por la interminable paciencia, por soportar todos los experimentos y por convertirte en mi biólogo de confianza. Seguro que no fue fácil aguantar las preguntas de un químico pretendiendo ser biólogo, pero yo no podría haber tenido un mejor maestro. Cuando quieras te enseño a hacer un MTT. A **Sandra**, mi rival en el laboratorio por la comida. Aunque digas que me gusta quedar bien con la gente, siempre estuviste presente desde el principio hasta el final de la tesis. Nunca desvelaré

USC DE SANTIAGO

lo que vi en aquella playa. A **Patri Fulias** (¿o era Fulías?), gracias a ti empecé a deconstruirme y ahora soy una mejor persona. Gracias por todos los momentos Party. Eres un lujo de amiga. A **Lucía** (la auténtica Motomami), gracias por tu compañía todos aquellos días de soledad en el P1L5. Sigue siendo la máxima liante que conozco. A **Jose María**, por ser sin ningún tipo de duda la persona más graciosa del grupo. A **Rebeca**, por ser una gran compañera y una alegría en el laboratorio. A **Mayra**, una chambeadora profesional, creo que eres la única persona que hice llorar el día que la conocí. Me enseñaste que en esta vida no todo es pajita de coco. A **Manu Pérez**, por defender siempre los intereses de Ferrolterra. A todos los que estáis empezando este largo camino de la tesis, os deseo lo mejor: **Fernando**, **Diego**, **Irene**, **Álex Fiel** o **Miguel**.

A **Alberto**, por ser el máximo fan de pantera o león. A **Eva**, por sufrir juntos el proyecto de la doxorrubicina. A **Ángel**, por ser la persona más buena que pasó por el laboratorio. A **Marta**, por ser la madre del laboratorio que siempre cuidaba de sus polluelos. A **Giulia**, por ser la organizadora de los eventos sociales, confieso que hasta echo de menos los gritos que nos dabas por los olores. A **Marisa**, mi otra química/bióloga a la que recurrir, muchas gracias por toda la ayuda y consejos. A **Manuel** de León (no me acuerdo si te llamabas Manuel o Miguel), por todos los grandes momentos de cruceta o por los golpes que me pegabas. A **Mini Patri**, por ser la pupila de la que aprendí yo más de ella que ella de mí. A **Martín Calvelo**, por ser el chico de computacional que al que siempre recurrir. A **Antía**, por tus consejos de como convivir con la terremoto italiana. Al resto de compañeros con los que tuve la oportunidad de compartir laboratorio y de los que guardo un recuerdo enorme: **Charlene**, **Alicia Rioboo**, **Iván**, **Héctor**, **Jose Juan**, **Irene Lostalé**, **Richard**, **Guibom**, **Geert**, **Sahnawaz** y **Augustina**. A los alumnos que pasaron en algún momento por el laboratorio y que supieron adaptarse a convivir con nosotros: **María**, **Borja** y **Sara Seoane**.

A todos los chicos de computacional: **Alfonso Cabezón**, **Álex Seco**, **Dani Conde**, **Xandre**, **Fabián** y **Paula Antelo**. Gracias por todo el tiempo juntos y sufrir el calendario de seminarios sin quejaros demasiado.

A mis compañeros de piso durante todos estos años, sois mi gran familia santiaguesa. A **Isa**, se podría decir que eres como mi madre en Santiago. Gracias por cuidarme y preocuparte siempre por mí. Se que no fue fácil aguantar todos mis vaciles, pero aun así siempre estuviste para levantarme cuando así lo necesité ¡Eres un amor! A **Álex (Mogo)**, eres la persona más agradecida que conozco en todo Santiago. Siempre dispuesto a entregar tu vida por los demás. Gracias a ti aprendí a no comer queso en exceso o la parrilla completa de Fórmula Uno. Tenemos citas pendientes con nuestro amigo Manolo en las Betanceiras o el Viña Rock. A **Sergio Otero**, por ser mi compañero de carrera, mi compañero de piso, pero por encima de todo mi amigo. Cuando quieras te doy unas clases de cocina porque veo que las tartas aún no las tienes controladas. A **Jesús**, para mi eres como un compañero más del piso y un gran amigo. Un sufridor de mi humor porque ya sabes que busco elegancia en el diccionario y sale tu nombre. No cambies nunca porque tienes un corazón enorme. A **Laura**, gracias por tu alegría y por enseñarle a Mogo a cocinar fajitas.

USC DE SANTIAGO

A **Martín**, eres la persona que me tenía calado desde el principio y que nunca fui capaz de engañar. Gracias por perdonarme por no limpiarte el chorizo atrapado en la barba o por ser un cutre con la cinta para pegar las fotos. ¡Patético! ¡No lo supero! Siempre apoyándome en los buenos momentos y animándome en los malos. Vales oro Martino porque eres un amigo de diez. Lo que unió ese tortillazo que no lo separe nadie.

A **Lara**, probablemente te sorprenda aparecer aquí, pero como tú siempre dices hay cosas que no hay quien las entienda y me ayudaste mucho más de lo que te imaginas en la recta final de la tesis. Eres una auténtica suerte. Gracias por todos tus ánimos, tu felicidad y conseguir que no perdiera la sonrisa. ¡Pero mira que sonrisa! Sigue así de cañera y con esa potencia que te caracteriza porque eres única, Escairón mola. ¡Un poco!

Gracias al resto de compañeros y amigos del CiQUS que alegraron mi día a día y consiguieron que este tiempo fuera mucho más especial: **Celia**, **Paula**, **Fer Salgado**, **Ricardo**, **Roi** y **Axel**, entre muchos otros. Especialmente, gracias a **Noa** y **Andrés**, no solo presentes en Santiago, sino por acompañarme durante el tiempo de la estancia. Tenemos juntos experiencias y momentos únicos que siempre voy a recordar. Ya nos tomaremos un Bloody Mary para celebrar nuestras tesis. Let's go Brewers!

Al resto de mis amigos de la carrera no mencionados previamente, muchas gracias por todos estos años juntos, sois amigos para siempre: **Gonzalo**, **Laura**, **Dani Nieto**, **Santi**, **Loli** y **Gemma**. A mis amigos de Ferrol, por todos los grandes momentos vividos y los que aún nos quedan por vivir: **Sergio**, **Dani**, **Álvaro**, **Jessica**, **Paula** y **Andrea**.

A **Sara**, gracias por haber formado parte del gran equipo verde que me ayudó a llevar mejor todos los malos momentos, siempre dispuesta a alegrarme y a sacar lo mejor de mí. Sin duda eres la persona que mejor sabe por todas las etapas que pasé durante este tiempo. Eres un pilar fundamental de esta tesis y no me llegan las palabras para expresar lo super agradecido que te estoy por todo ello. Gracias por todo lo que hiciste por mí. Sabes que puedes contar conmigo para lo que necesites.

El párrafo más importante y emocionante va dedicado a toda mi **familia**. A mi madrina, primos y tíos, pero especialmente a mis abuelos, hermana y padres. Esta tesis lleva vuestro nombre. A **mis abuelos** Amelia, Antonio, Dolores y Agustín, gracias por cuidar de nosotros y construir esta gran familia. Sois el ejemplo perfecto de esfuerzo, una fuente de inspiración y un modelo a seguir para mí. Siempre os llevo en mi corazón y vuestro cariño me quedará marcado para siempre. A **mi hermana** Sandra, una racinguista obligada, a veces me cuesta saber si te quiero o te odio, pero sin duda eres una hermana maravillosa. Gracias por tu interminable felicidad y por estar presente siempre que lo necesito. A **mi madre** Rosa y **mi padre** Abel, sin vuestro esfuerzo a lo largo de los años yo hoy no sería nadie y no estaría escribiendo estas páginas. Siempre estáis dispuestos a apoyarnos y a renunciar a lo que sea por nuestro bien para que no nos falten oportunidades. Imposible estar más agradecido por todo vuestro esfuerzo y cariño. Los mejores padres que se puede tener y por suerte sois los míos. Esta tesis va dedicada a todos vosotros. ¡Os quiero muchísimo!

¡Muchísimas gracias a todos!

USC
DE SANTIAGO
DE COMPOSTELA

INDEX

1. ABBREVIATIONS 10

2. RESUMO 14

3. SUMMARY 21

4. INTRODUCTION 27

4.1. SUPRAMOLECULAR CHEMISTRY 28

4.2. PHOTO-RESPONSIVE SYSTEMS 32

4.2.1. Molecular photoswitches based on isomerizations 35

4.2.2. Molecular photoswitches based on photocyclization reactions 39

4.2.3. Molecular photoswitches based on the combination of mechanisms 40

4.3. STIMULI-RESPONSIVE SYSTEMS FOR ANTICANCER DRUG DELIVERY 42

4.3.1. pH-responsive drug delivery systems 45

4.3.2. Redox-responsive drug delivery systems 48

4.3.3. Enzyme-responsive drug delivery systems 50

4.3.4. Magnetic field-responsive drug delivery systems 51

4.3.5. Light-responsive drug delivery systems 52

4.3.6. Ultrasound-responsive drug delivery systems 54

4.4. SELF-ASSEMBLING CYCLIC PEPTIDES 56

4.4.1. SCPNs as artificial channels 61

4.4.2. SCPNs as antimicrobial agents 63

4.4.3. SCPNs as drug delivery systems 64

4.4.4. Control of the assembly properties of SCPNs 66

5. OBJECTIVES 70

6. RESULTS AND DISCUSSION 73

6.1. ANTHRACENE PHOTODIMERIZATION TO BEND SELF-ASSEMBLING CYCLIC PEPTIDE NANOTUBES 74

6.1.1. Precedents 76

6.1.2. Objective 78

6.1.3. Results and discussion 79

6.1.4. Conclusions 101

6.2. PHOTO-ASSEMBLING CYCLIC PEPTIDES FOR DYNAMIC LIGHT-DRIVEN PEPTIDE NANOTUBES 102

6.2.1. Precedents 104

USC UNIVERSIDADE DE SANTIAGO DE COMPOSTELA

6.2.2. Objective 110
6.2.3. Results and discussion 111
6.2.4. Conclusions 137
6.3. SELF-ASSEMBLING CYCLIC PEPTIDE NANOTUBES FOR THE TRANSPORT OF DOXORUBICIN INTO CANCER CELLS 138
6.3.1. Precedents 139
6.3.2. Objective 141
6.3.3. Results and discussion 143
6.3.4. Conclusions 162
7. CONCLUSIONS 163
8. METHODOLOGY AND EXPERIMENTAL SECTION 165
8.1. General remarks 166
8.2. Particular remarks 169
8.2.1. ANTHRACENE PHOTODIMERIZATION TO BEND SELF-ASSEMBLING CYCLIC PEPTIDE NANOTUBES 169
8.2.2. PHOTO-ASSEMBLING CYCLIC PEPTIDES FOR DYNAMIC LIGHT-DRIVEN PEPTIDE NANOTUBES 211
8.2.3. SELF-ASSEMBLING CYCLIC PEPTIDE NANOTUBES FOR THE TRANSPORT OF DOXORUBICIN INTO CANCER CELLS 234
9. REFERENCES 273
10. ANNEXES 285
10.1. Annex I: List of publications 286
10.2. Annex II: Conflict of interest 289
10.3. Annex III: Rights and permissions of the images 289
10.4. Annex IV: Declaration of all other images 313

USC UNIVERSIDADE DE SANTIAGO DE COMPOSTELA

1. ABBREVIATIONS

ABA	4-Aminobenzoic acid
ADA	1-Adamantylamine
AFM	Atomic Force Microscopy
Ala	Alanine
AMF	Alternating magnetic field
Ant	Anthracene
aS	α-Synuclein
Asp	Aspartic acid
Bcl-xL	B-cell lymphoma-extra large
br	Broad
BTA	Benzenetricarboxamide
bZIP	Basic leucine zipper
cac	Critical aggregation concentration
CB	Cucurbituril
CD	Circular Dichroism
CG-MD	Coarse-grained molecular dynamic
COSY	Homonuclear Correlation Spectroscopy
CP	Cyclic peptide
CPT	Camptothecin
CuAAC	Cu(I)-catalyzed alkyne-azide cycloaddition
d	Doublet
DAE	Diarylethene
DCM	Dichloromethane
DEPT	Distortionless Enhancement by Polarization Transfer
dsGUVs	Droplet-stabilized giant unilamellar vesicles
DMF	*N*,*N*-Dimethylformamide
DMSO	Dimethyl sulfoxide
DNA	Deoxyribonucleic acid

USC UNIVERSIDADE DE SANTIAGO DE COMPOSTELA

DOX	Doxorubicin
DSF	Disulfiram
EDT	1,2-Ethanedithiol
EGFR	Epidermal growth factor receptor
ESI-MS	Electrospray Ionisation Mass Spectrometry
et al.	And others
FBS	Fetal Bovine Serum
FITC	Fluorescein isothiocyanate
Fmoc	Fluorenylmethoxycarbonyl
FR	Folate receptor
FRET	Fluorescence resonance energy transfer
FT-IR	Fourier transform infrared spectroscopy
5-FU	5-Fluorouracil
Gln	Glutamine
Glu	Glutamic acid
GOx	Glucose oxidase
GSH	Glutathione
Glu	Glutamic acid
HATU	1-[bis(dimethylamino)methylene]-1H-1,2,3-triazolo[4,5-b]pyridinium 3-oxide hexafluorophosphate
HBC	Hexabenzocoronene
HBTU	3-[bis(dimethylamino)methyliumyl]-3H-benzotriazol-1-oxide hexafluorophosphate
HEPES	4-(2-hydroxyethyl)piperazine-1-ethanesulfonic acid
HFIF	Hexafluoroisopropanol
HI	Hemiindigo
His	Histidine
HMBC	Heteronuclear multiple bond correlation
HPLC	High performance liquid chromatography
HR-MS	High resolution mass spectrometry

USC UNIVERSIDADE DE SANTIAGO DE COMPOSTELA

HSQC	Heteronuclear single quantum coherence spectroscopy
HTI	Hemithioindigo
IR	Infrared
LC-MS	Liquid chromatography-mass spectrometry
LND	Lonidamine
LUVs	Large unilamellar vesicles
Lys	Lysine
m	Multiplet
MC	Merocyanine
MMP	Metalloproteinase
MNPs	Magnetic nanoparticles
MPS	Methyl phenyl sulfide
MS	Mass spectrometry
Mtt	4-Methyltrityl
MTT	3-[4,5-Dimethylthiazol-2-yl]-2,5-diphenyltretrazolium bromide
MV	Methyl viologen
NBD	Nitrobenzoxadiazole
NIR	Near-infrared
NMM	*N*-methylmorpholine
NMR	Nuclear magnetic resonance
Np	Naphthol-modified copolymer
NR	Nile red
nNOS	Neural NO synthase
o-NB	*o*-Nitrobenzyl
PBS	Phosphate buffered saline
PCB	Phycocyanobilin
PDI	Perylene diimide
P-gp	P-glycoprotein
ppm	Part per million

USC UNIVERSIDADE DE SANTIAGO DE COMPOSTELA

PTA	Phosphotungstic acid
PyAOP	(7-Azabenzotriazol-1-yloxy)trispyrrolidinophosphonium hexafluorophosphate
RGD	Arginine-glycine-aspartic acid
ROESY	Rotating Frame Overhauser Enhancement Spectroscopy
RPMI	Roswell Park Memorial Institute
R_t	Retention time
SCPN	Self-assembling cyclic peptide nanotube
SCPPN	Supramolecular cyclic peptide-polymer nanotube
s	Singlet
Ser	Serine
SP	Spiropyran
STEM	Scanning transmission electron microscopy
t	Triplet
TFA	Trifluoroacetic acid
TFE	Trifluoroethanol
ThT	Thioflavin T
TIS	Triisopropylsilane
TOCSY	Total correlation spectroscopy
UPy	Ureido-pyrimidinone
UV	Ultraviolet
Vis	Visible
ZFs	Zinc fingers

USC UNIVERSIDADE DE SANTIAGO DE COMPOSTELA

2. RESUMO

A aparición da química supramolecular fixo posible aumentar o nivel de complexidade das estruturas químicas. En concreto, este campo da química é definido como "a química máis aló das moléculas" xa que fai uso de interaccións non covalentes entre moléculas sinxelas para obter estruturas máis complexas e organizadas. Por exemplo, a química supramolecular contribuíu a dilucidar estruturas biolóxicas como a dobre hélice do ADN. Exemplos de sistemas supramoleculares sintéticos son os macrociclos capaces de acomodar ións metálicos na súa cavidade desenvoltos por C. J. Pedersen, J. M. Lehn e D. J. Cram ou as máquinas moleculares desenvoltas por J. P. Sauvage, J. F. Stoddart e B. L. Feringa. Outro tipo destas estruturas son os polímeros supramoleculares, nos cales interaccións non covalentes entre os bloques construtores dan lugar a estruturas con forma de fibras. Estes polímeros supramoleculares caracterízanse por un carácter dinámico que fixo posible a obtención de estruturas para unha ampla variedade de aplicacións.

Esta natureza dinámica dos sistemas supramoleculares, baseada no uso de interaccións non covalentes, levou a explorar a adición de resposta a estímulos para ampliar as súas propiedades e aplicacións. Un caso relevante é o desenvolvemento de sistemas que responden á luz e que poden mudar as súas propiedades en resposta a un estímulo luminoso. A maioría destes materiais están baseados na conversión dun fotoconmutador molecular entre diferentes formas como resultado da irradiación luminosa. Unha ampla variedade de fotoconmutadores moleculares foron desenvoltos, aínda que a maioría deles están baseados na isomerización dun dobre enlace, en reaccións de fotociclación ou na combinación de diferente mecanismos de fotoconmutación. En particular, grupos azobenzeno son os fotoconmutadores moleculares máis empregados, nos que o seu dobre enlace pode isomerizarse entre o *trans*-azobenzeno e o *cis*-azobenceno mediante irradiación luminosa apropiada. Un exemplo de fotoconmutadores moleculares baseados en reaccións de fotociclación son os derivados de diariletenos, nos cales unha 6π-electrociclación converte a forma aberta na forma pechada. A combinación de mecanismos pode ser ilustrada cos espiropiranos, nos que a fotoconmutación está baseada na ruptura dun enlace C-O e unha isomerización.

Sistemas supramoleculares sensibles a estímulos foron tamén propostos como vehículos de entrega de fármacos contra o cancro. Esta enfermidade representa un dos maiores problemas de saúde no mundo, xa que é unha das principais causas de morte. A selectividade e eficacia dos tratamentos actuais están limitados por unha serie de factores, como a baixa internalización celular e a aparición de resistencias aos fármacos. Por isto, a procura de novos nanotransportadores de fármacos dentro das células cancerígenas é de gran relevancia para superar estas limitacións. Un sistema ideal de transporte de fármacos debe facilitar a liberar controlada do axente terapéutico no sitio de acción desexado para realzar a súa eficacia. Ademais, resulta esencial minimizar as interaccións con células sans para reducir os efectos secundarios. O mecanismo de acción destes sistemas de entrega está normalmente baseado na liberación do fármaco

USC

no interior da célula en resposta a un estímulo intrínseco ou externo, como cambios en pH, condicións redox, enzimas, campos magnéticos, luz ou ultrasóns. Por exemplo, as células de cancro caracterízanse por un pH lixeiramente máis baixo que as células sans. Lisosomas e endosomas tardíos tamén presentan un pH máis baixo comparado con outros compartimentos celulares. Estas diferenzas poden ser aproveitadas para deseñar sistemas que poidan liberar o fármaco atrapado mediante ruptura dun enlace ácido-lábil ou un cambio conformacional da estrutura co pH.

Neste contexto, os nanotubos de péptidos cíclicos autoensamblantes xorden como unha alternativa prometedora para a construción de novos sistemas sensibles a estímulos. Estes polímeros supramoleculares con forma de tubo están formados polo amoreamento ordenado de macrociclos planos de péptidos cíclicos. En xeral, os péptidos cíclicos formados por un número par de aminoácidos con alternancia de quiralidade *D*- e *L*- poden adoptar unha conformación de lámina β, a cal permite o amoreamento sucesivo dunha unidade sobre outra mediante a formación de enlaces de hidróxeno. Ademais, a capacidade destes nanotubos para ensamblase en nanoláminas 2D ou incorporar cadeas de polímeros na estrutura do péptido cíclico foi demostrada. A fácil modificación das súas propiedades internas e externas fixo posible obter nanotubos con diferentes aplicacións. O diámetro interno do nanotubo pode ser modificado en función do número e tipo de aminoácidos que compoñen o péptido cíclico, mentres as propiedades externas poden controlarse porque as cadeas laterais dos α-aminoácidos quedan proxectadas cara o exterior do nanotubo. O uso doutros aminoácidos pode empregarase para modificar as propiedades internas, como a incorporación de γ-aminoácidos cíclicos. Neste sentido, nanotubos hidrofóbicos teñen a habilidade de inserirse en membranas lipídicas e actuar como canles artificiais. Por exemplo, o transporte de ións, glucosa ou ácido glutámico con nanotubos de péptidos cíclicos transmembrana foi xa descrito. Ademais, péptidos cíclicos anfipáticos poden ser empregados como axentes antimicrobianos debido á interacción paralela do nanotubo con membranas, desencadeando a morte bacteriana. Exemplos de nanotubos de péptidos cíclicos como sistemas de entrega de fármacos tamén foron desenvoltos, pero estes deseños están principalmente limitados ao emprego de nanotubos transmembrana ou conxugados péptido cíclico-polímero.

A pesar dos diferentes exemplos de nanotubos de péptidos cíclicos desenvoltos, un dos grandes desafíos destes polímeros supramoleculares é a dificultade de controlar de forma precisa a dinámica do nanotubo. A súa formación é un proceso cooperativo no cal é difícil controlar o proceso de autoensamblaxe ou a lonxitude e empaquetamento do nanotubo final. Neste sentido, diferentes deseños con conxugados de péptidos cíclico-polímero foron desenvoltos para gañar control nestes aspectos. En xeral, estas estratexias están baseadas en interaccións anfitrión-hóspede ou no uso de polímeros que son protonados co pH ou rotos cun redutor. A menor natureza dinámica deste tipo de conxugados péptidos cíclico-polímero fai necesario a busca doutras alternativas para estender este control do proceso de autoensamblaxe para todos os tipos de nanotubos de péptidos cíclicos. O uso dun fotoácido externo foi proposto como unha alternativa para inducir con luz a polimerización e despolimerización supramolecular. Con todo,

esta estratexia require o uso dun fotoácido externo e o proceso de desensamblaxe ocorre rapidamente cando a irradiación luminosa é retirada.

Polas razóns previamente mencionadas, o obxectivo principal desta tese doutoral é desenvolver novas estratexias para controlar o proceso de autoensamblaxe dos nanotubos de péptidos cíclicos e atopar novas aplicacións biolóxicas para este tipo de estruturas supramoleculares. Con este fin, a adición de resposta a estímulos foi proposto como método para modificar a forma da ensamblaxe do nanotubo, controlar a súa polimerización e despolimerización supramolecular ou explorar o seu uso como axentes de entrega de fármacos.

En primeiro lugar, deseñouse unha nova clase de péptidos cíclicos híbridos compostos por α- e β-aminoácidos e modificados cun grupo antraceno. O péptido cíclico preparouse por síntese en fase sólida e a incorporación do grupo antraceno levouse a cabo mediante a formación dun enlace oxima. Para este propósito, a cadea lateral dunha lisina modificouse cun grupo hidroxilamina acetilado que se fixo reaccionar con 9-antracenocarboxaldehído. No modelo de nanotubo proposto, os β-aminoácidos deberían inducir o amoreamento do péptido cíclico formando estruturas de lámina paralela xa que estes dispoñen os seus grupos amino e carbonilo orientados en direccións opostas. Ademais, cambios co pH no estado de ionización dos residuos de histidina deberían permitir controlar o proceso de autoensamblaxe. A formación de nanotubos confirmouse por unha ampla variedade de técnicas como espectroscopía de fluorescencia, dicroísmo circular ou microscopia. A formación destes nanotubos só ten lugar a pH neutro ou básico debido a protonación/desprotonación dos residuos básicos do péptido. Ademais, detectáronse agrupacións de nanotubos, as cales deben formarse por interaccións intermoleculares antraceno-antraceno mediante unha autoensamblaxe xerárquica. A continuación, avaliouse a cicloadición [4+4] do grupo antraceno mediante irradiación a 350 nm e seguindo a redución na súa banda de absorción cando a reacción ten lugar. Descubriuse que a reacción é máis rápida nas condicións de pH nas cales o nanotubo está formado, suxerindo que a organización dos grupos antraceno na estrutura tubular debe acelerar a cicloadición. Curiosamente, observouse un movemento de dobramento da estrutura macromolecular mediante esta irradiación luminosa. O proceso está baseado na formación dos correspondentes fotodímeros mediante a cicloadición [4+4] dos grupos antraceno. Esta reacción de fotodimerización provoca cambios na ensamblaxe do nanotubo inducindo a súa curvatura. Microscopia de epifluorescencia mostrou un cambio na emisión do conxunto de nanotubos dende verde a azul mediante a irradiación luminosa, seguido do movemento de dobramento inducido por luz. Ademais, a deposición de mostras irradiadas mostrou por microscopia electrónica de transmisión de barrido a presenza de estruturas tubulares con forma de zigzag que confirman o movemento de dobramento proposto. O cambio do antraceno por un grupo non sensible á luz, como naftaleno ou pireno, proporciona péptidos cíclicos que experimentan unha ruptura do enlace N-O da oxima mediante irradiación con luz. Sorprendentemente, a análise por microscopia de epifluorescencia do derivado con pireno antes da irradiación mostrou a inesperada formación de fibras con forma de hélices. As consecuencias da irradiación na

ensamblaxe e a perda do grupo pireno foron avaliadas con experimentos de fluorescencia e microscopia. Ademais, explorouse a substitución de antraceno por un grupo azobenceno isomerizable. Desafortunadamente, a pesar de que a isomerización entre os isómeros *Z* e *E* foi avaliada, ningún dos dous isómeros mostrou a capacidade de ensamblarse en nanotubos.

En segundo lugar, en vez de modificar unha cadea lateral do péptido cíclico cun grupo sensible á luz, decidiuse incorporar na secuencia peptídica un aminoácido insaturado que pode ser fotoisomerado. O péptido cíclico tamén incorpora un grupo pireno na cadea lateral dunha lisina para axudar na formación de nanotubos mediante π,π-interaccións. As propiedades espectroscópicas do pireno tamén permiten estudar o proceso de autoensamblaxe por técnicas como fluorescencia. O deseño proposto foi preparado de novo mediante síntese en fase sólida. Inicialmente, a olefina do aminoácido fotoconmutador foi protexida como un cicloaducto de furano. O quentamento dunha disolución acuosa proporcionou selectivamente a formación do isómero *Z* mediante unha reacción de retro-Diels-Alder. A continuación, a isomerización inducida por luz entre o isómero *Z* e o *E* foi avaliada. A irradiación a 290-320 nm dunha disolución acuosa do isómero *Z* proporcionou unha mestura 7:3 de ambos os dous isómeros, mentres a conversión dende o isómero *E* ao isómero *Z* pode ser conseguida en case unha relación 1:1 mediante irradiación a 254 nm. En ambos os dous casos, o estado fotoestacionario logrouse tras só uns minutos de irradiación e o proceso ocorre independentemente do pH. A aplicación de varios ciclos ou longos tempos de irradiación non causa a descomposición do péptido cíclico ou a aparición de novos produtos, suxerindo unha boa fotoestabilidade destes deseños. As diferentes propiedades de ensamblaxe de ambos os dous isómeros foron demostradas cunha ampla variedade de técnicas. O isómero *Z* presenta un conformación pregada e permanece como monómero debido a súa incapacidade de autoensamblarse. Pola contra, o isómero *E* adopta a necesaria conformación plana para formar nanotubos. Como resultado, este proceso de isomerización pode empregarse para controlar a conformación e a ensamblaxe deste tipo de nanotubos de péptidos cíclicos. En concreto, a ensamblaxe ou desensamblaxe inducida por luz pode provocarse pola isomerización de unicamente un aminoácido insaturado. Ademais, a autoensamblaxe só ocorre a pH neutro ou básico debido a desprotonación dos residuos de histidina do péptido cíclico. Isto permite un control dual por medio do pH e a luz sobre a formación dos nanotubos. Curiosamente, estudouse a substitución no deseño orixinal dunha glutamina por unha lisina para aumentar a solubilidade en auga. Porén, esta substitución proporciona isómeros de péptidos cíclicos con propiedades de ensamblaxe diferentes, xa que o isómero *Z* forma estruturas con forma de lámina e o isómero *E* forma nanotubos.

A polimerización supramolecular espacialmente controlada de ambos os dous isómeros foi avaliada no espazo confinado de gotas acuosas de microfluídica suspendidas en aceite. A tecnoloxía microfluídica baseada en gotas xurdiu como un método atractivo para analizar o comportamento de estruturas fibrilares nun espazo confinado e controlado. Por exemplo, estas gotas poden empregarse para construír células sintéticas artificiais ou avaliar a potencial aplicación de estruturas fibrilares

sintéticas como miméticos do citoesqueleto celular. Neste sentido, empregouse un dispositivo de microfluídica para fabricar gotas co isómero apropiado a ser estudado no seu interior. Ademais, explorouse o uso de diferentes condicións dentro das gotas. En particular, a ensamblaxe do péptido cíclico é inducida nun primeiro cruzamento do dispositivo de microfluídica ao mesturar unha corrente que contén unha disolución acuosa do péptido cíclico lixeiramente ácida con dúas correntes cunha disolución capaz de inducir a ensamblaxe. Empregáronse cambios de pH ou unha alta forza iónica para inducir a ensamblaxe. A continuación, a formación das gotas ten lugar ao converxer esta nova corrente acuosa cunha corrente de aceite. As gotas foron recollidas á saída do dispositivo de microfluídica e analizadas por técnicas de microscopia. A análise por microscopia de epifluorescencia de gotas a pH neutro que conteñen o isómero *Z* mostrou unha apagada fluorescencia azul, suxerindo que non hai agregación deste isómero. Un resultado similar foi obtido para gotas contendo o isómero *E* en condicións ácidas. Pola contra, gotas co isómero *E* a pH neutro mostraron estruturas fibrilares azul fluorescente principalmente localizadas en contacto cos bordes das gotas. Esta distribución na periferia das gotas foi confirmada por microscopia confocal. Curiosamente, esta acumulación en contacto cos bordes é capaz de inducir a fusión entre dúas gotas veciñas contendo o isómero *E*. A substitución do pireno por unha cadea alquílica de seis carbonos proporciona gotas sen propiedades de fusión, suxerindo que as π,π-interaccións dos grupos pireno son necesarias para a ensamblaxe xerárquica e a indución da fusión entre gotas. Polo tanto, a fusión é probablemente debido á formación dunha superficie hidrófoba que ao interactuar cos bordes das gotas causa a súa fusión. Ademais, non se observou fusión entre gotas co isómero *Z* e gotas co isómero *E*. Estruturas fibrilares foron tamén observadas principalmente localizada no centro das gotas e con propiedades de fusión reducidas cando o proceso de ensamblaxe do isómero *E* foi provocado cunha alta forza iónica. A indución da ensamblaxe con luz avaliouse tamén no interior das gotas. Para este propósito, gotas contendo o isómero *Z* a pH neutro foron irradiadas a 290-320 nm. Microscopia de epifluorescencia mostrou a formación de estruturas fibrilares no interior das gotas despois da irradiación. Ademais, a análise por HPLC do interior das gotas proporcionou outra vez un estado fotoestacionario composto dunha mestura en proporción 7:3 de ambos os dous isómeros, o cal confirma a isomerización do péptido cíclico neste espazo confinado.

En terceiro lugar, diferentes conxugados de péptido cíclico-doxorrubicina cun enlace hidrazona ácido-lábil foron preparados para o transporte de doxorrubicina ao interior de células de cancro. En particular, os péptidos cíclicos foron preparados por síntese en fase sólida e, cando foi necesario, unha cola de carbono foi incorporada na rexión non polar do péptido cíclico mediante unha estratexia de *química click* en resina. A incorporación do fármaco ao esqueleto do péptido levouse a cabo mediante reaccións en disolución. Experimentos de fluorescencia, dicroísmo circular ou técnicas de microscopia revelaron a habilidade destes conxugados para ensamblarse en fibras ou estruturas 2D con forma de lámina. A actividade anticancerosa *in vitro* foi avaliada en tres liñas celulares de cancro diferentes: unha liña de células de cancro de peito (MCF-7), unha liña de células de cancro de pulmón (NCI-H460) e unha liña de células de

cancro de ovario resistentes a doxorrubicina (NCI/ADR-RES). Todos os conxugados péptido cíclico-doxorrubicina propostos amosaron unha boa actividade contra as dúas liñas de células non resistentes (MCF-7 e NCI-H460). Porén, só os péptidos cíclicos que incorporan unha cadea de 10 carbonos, 14 carbonos ou unha cola con un grupo NBD presentaron unha boa actividade contra a liña de células resistentes (NCI/ADR-RES). Ademais, a súa actividade foi avaliada nunha liña de células embrionarias de pulmón non cancerosas (MRC-5), mostrando que a unión de doxorrubicina ao péptido cíclico aumentaba a biocompatibilidade do fármaco. O mecanismo de acción destes conxugados foi investigado na liña de células resistentes ao fármaco. A resistencia das células de cancro é normalmente o resultado da sobreexpresión de proteínas de membrana que expulsan o fármaco dende o interior ao exterior da célula obxectivo, evitando que o fármaco exerza o seu efecto terapéutico. En particular, a liña de células de cancro NCI/ADR-RES sobreexpresa a glicoproteína-P, a cal é capaz de expulsar doxorrubicina ao exterior das células. Imaxes de microscopia confocal e experimentos de citometría de fluxo con inhibidores de endocitose foron empregados para avaliar o mecanismo de internalización. Especificamente, o patrón punteado no interior da célula, a colocalización con Lysotracker e a redución na internalización na presenza de inhibidores de endocitose suxire que o camiño endocítico é un dos principais mecanismos de internalización destes derivados. Ademais, os experimentos de microscopia confocal revelaron que só os péptidos cíclicos cunha cola de carbono apropiada son capaces de transportar doxorrubicina ao núcleo para inducir a morte destas células resistentes. Como resultado, especulamos que a incorporación dunha cola hidrocarbonada no deseño do péptido cíclico é necesaria para o escape endosomal, o transporte do fármaco ao núcleo e superar a resistencia das células.

En conclusión, nesta tese doutoral propúxose a adición de resposta a estímulos aos nanotubos de péptidos cíclicos. En particular, desenvolvéronse diferentes estratexias para controlar o proceso de ensamblaxe ou para estender o seu uso como vehículos de transporte de fármacos. Inicialmente, un movemento de dobramento dos nanotubos foi inducido por irradiación luminosa baseándose na cicloadición [4+4] de grupos antraceno. Agardamos que esta primeira aproximación permita o deseño doutras novas estratexias para controlar a forma dos nanotubos de péptidos cíclicos e desenvolver novas funcións. A continuación, a incorporación na secuencia peptídica dun aminoácido insaturado fotoconmutador e o estudo da súa isomerización permitiu controlar con irradiación luminosa o proceso de ensamblaxe e desensamblaxe dos nanotubos de péptidos cíclicos. Ademais, avaliouse o control espacial da polimerización supramolecular inducida pola luz e o medio no espazo confinado de gotas acuosas de microfluídica suspendidas en aceite. Curiosamente, a acumulación do isómero autoensamblante en contacto cos bordes das gotas induce a fusión entre dúas gotas veciñas. Este traballo representa un novo paso no estudo da polimerización supramolecular de fibras de péptidos cíclicos en modelos miméticos artificiais, xa que estas propiedades de fusión poderían atopar novas aplicacións. Finalmente, prepararonse diferentes conxugados de péptidos cíclico-doxorrubicina para o transporte deste fármaco dentro de células de cancro. Todos os conxugados estudados

amosaron boa actividade contra liñas celulares non resistente, mentres só os deseños que incorporan unha cola de carbono amosaron a capacidade de exercer a súa acción terapéutica nunha liña de células de cancro resistentes ao fármaco. Os resultados desta tese doutoral representan unha primeira aproximación cara a un mellor control do proceso de autoensamblaxe e as propiedades dos nanotubos de péptidos cíclicos. Ademais, estes resultados poderían habilitar no futuro novas funcións para os nanotubos de péptidos cíclicos, especialmente aplicacións biolóxicas.

USC
UNIVERSIDADE DE SANTIAGO DE COMPOSTELA

3. SUMMARY

The emergence of supramolecular chemistry has made possible to increase the level of complexity of chemical structures. In particular, this field of chemistry is defined as the "chemistry beyond the molecule" because it uses non-covalent interactions between simple molecules to obtain more complex and organized structures. For example, supramolecular chemistry has contributed to the elucidation of biological structures such as the DNA double helix. Examples of synthetic supramolecular systems are the macrocycles able to bind metal ions in their cavity reported by C. J. Pedersen, J. M. Lehn and D. J. Cram or the molecular machines developed by J. P. Sauvage, J. F. Stoddart and B. L. Feringa. Another type of structures are the supramolecular polymers, in which non-covalent interactions between the building blocks give rise to filamentous structures. These supramolecular polymers are characterized by a dynamic character that has made possible to obtain structures for a wide range of applications.

This dynamic nature of supramolecular systems, which rely on the use of non-covalent interactions, has led to explore the addition of stimuli-responsiveness to extend their properties and applications. A relevant case is the development of photo-responsive systems that are capable of altering their properties in response to a light stimulus. Most of these materials are based on the interconversion of a molecular photoswitch between different forms as a result of light irradiation. A wide variety of molecular photoswitches have been reported, but most of them are based on isomerization around a double bond, photocyclization reactions or the combination of different photoswitching mechanisms. In particular, azobenzene moieties are the most commonly used molecular photoswitches, whose double bond can undergo isomerization from *trans*-azobenzene to *cis*-azobenzene in response to appropriate light irradiation. An example of molecular photoswitches that rely on photocyclization reactions is that of diarylethene derivatives, in which a 6π-electrocyclization process converts the open form into the closed one. The combination of mechanisms can be illustrated with spiropyran, whose photoswitching is based on the cleavage of a C-O bond and an isomerization.

Also, stimuli-responsive supramolecular systems have been proposed as anticancer drug delivery vehicles. Cancer represents a significant global health problem, as it is one of the leading causes of mortality. The efficacy and selectivity of current treatments are limited by a number of factors, including a low rate of cellular internalisation and the emergence of drug resistance. Therefore, the search for new drug nanocarriers inside cancer cells is of great relevance to overcome these limitations. An ideal drug delivery system should facilitate the controlled release of the therapeutic agent at the targeted site of action to enhance its efficacy. Moreover, it is essential to minimize interactions with healthy cells to reduce side effects. The mechanism of action of these delivery systems is usually based on the release of the trapped drug inside the cell in response to intrinsic or external stimuli, such as changes in pH, redox conditions, enzymes, magnetic fields, light or ultrasounds. For example, cancer cells are characterized by a slightly lower pH than healthy cells. Lysosomes and late endosomes

USC Universidade de Santiago de Compostela

also exhibit a lower pH than other cellular compartments. These differences can be exploited to design systems capable of releasing the trapped drug through the cleavage of acid-labile bonds or a conformational change in the structure with the pH.

In this context, self-assembling cyclic peptide nanotubes emerge as a promising alternative for the construction of new stimuli-responsive systems. These tubular supramolecular polymers are formed by the orderly stacking of planar cyclic peptide macrocycles. In general, cyclic peptides composed of an even number of amino acids with alternating *D*- and *L*- chirality can adopt a planar β-sheet conformation, which allows the successive stacking of one unit on top of another through the formation of hydrogen bonding interactions. Moreover, the ability of these nanotubes to assemble into 2D nanosheet structures or the attachment of polymer chains to the cyclic peptide scaffold has been reported. The easy modification of their internal and external properties has made possible to obtain nanotubes with different applications. The inner diameter of the nanotube can be modified according to the number and type of amino acids that compose the cyclic peptide backbone, while the external properties can be controlled because the side chains of the α-amino acids face outwards from the nanotube. Additionally, other amino acids can be employed to modify the internal properties, such as the incorporation of cyclic γ-amino acids. In this regard, hydrophobic nanotubes have the ability to insert into lipid membranes and act as artificial channels. For example, the transport of ions, glucose or glutamic acid with transmembrane cyclic peptide nanotubes has already been described. Moreover, amphipathic cyclic peptides can be used as antimicrobial agents due to the parallel interaction of the nanotube with membranes, leading to bacterial death. Examples of cyclic peptide nanotubes as drug delivery systems have also been reported, but these designs are particularly limited to the use of transmembrane nanotubes or cyclic peptide-polymer conjugates.

Despite the different examples of cyclic peptide nanotubes that have been developed, one of the great challenges of these supramolecular polymers is the difficulty to precisely control the nanotube dynamics. Their formation is a cooperative process in which it is difficult to control the self-assembly process or the length and packing of the final nanotube. Several designs with cyclic peptide-polymer conjugates have been reported to achieve some control in this regard. In general, these strategies are based on host-guest interactions or the use of polymers that can be protonated with pH or cleaved with a reductant. However, the less dynamic nature of this type of cyclic peptide-polymer conjugates makes necessary to look for other alternatives to extend the control of the assembly process to all types of cyclic peptide nanotubes. The use of an external photoacid has already been proposed as an alternative to photo-induce their supramolecular polymerization and depolymerization. However, this strategy requires the use of an external photoacid and the disassembly process occurs very quickly as soon as the light irradiation is removed.

USC DE SANTIAGO

For the reasons mentioned above, the main objective of this doctoral thesis is to develop new strategies to control the assembly process of cyclic peptide nanotubes and find new biological applications for this type of supramolecular structures. For this

purpose, the addition of stimuli-responsiveness was proposed as a method to modify the shape of the nanotube packing, control their supramolecular polymerization and depolymerization or explore their use as drug delivery agents.

Firstly, a new class of cyclic peptide hybrid was designed made of α- and β-amino acids and functionalized with an anthracene moiety. The cyclic peptide was prepared by solid-phase peptide synthesis and the incorporation of the anthracene group was achieved through the formation of an oxime bond. For this purpose, a lysine side chain modified with a hydroxylamine acetyl moiety was reacted with 9-anthracenecarboxaldehyde. In the proposed nanotube model, the β-residues should induce the stacking of the cyclic peptide by forming parallel β-sheet structures because they predispose their amino and carbonyl groups pointing in opposite directions. Also, changes with pH in the ionization state of histidine residues should allow control of the self-assembly process. The nanotube formation was confirmed by a wide range of techniques such as fluorescence spectroscopy, circular dichroism or microscopy. Nanotube formation only takes place at neutral or basic pH due to the protonation/deprotonation of the peptide basic residues. Moreover, nanotube bundles were detected, which should be formed by anthracene-anthracene intermolecular interactions through a hierarchical self-assembling process. Then, the [4+4] cycloaddition of the anthracene moiety was assessed by irradiation at 350 nm and following the reduction of the absorption band when the reaction takes place. The reaction was found to be faster at the pH conditions at which the nanotubes are formed, suggesting that the organization of anthracene in the tubular structure accelerates the cycloaddition. Interestingly, a bending motion of the macromolecular structure was observed under this light irradiation. The process is based on the formation of the corresponding photo-dimers through the [4+4] cycloaddition of the anthracene moiety. This photodimerization reaction causes changes in the packing of the nanotube inducing its curvature. Epifluorescence microscopy revealed an emission switching of the bundles from green to blue under light irradiation, followed by the light-induced bending motion. Also, the deposition of irradiated samples showed by scanning transmission electron microscopy the presence of zigzag tubular structures that confirm the proposed bending motion. Replacement of this anthracene moiety for a non-photosensitive group, such as a naphthalene or a pyrene pendant, resulted in cyclic peptides that under irradiation undergo a photo-cleavage of the oxime N-O bond. Surprisingly, epifluorescence microscopy analysis of the pyrene derivative before the irradiation showed the formation of unexpected helical fibres. The consequences on the assembly of the irradiation and loss of the pyrene group were evaluated with fluorescence and microscopy experiments. In addition, the replacement of anthracene by an isomerizable azobenzene moiety was explored. Unfortunately, although the isomerization between the *Z*- and *E*-isomers was studied, neither of the two isomers showed the ability to assemble into nanotubes.

Secondly, instead of functionalizing a side chain of the cyclic peptide with a photo-responsive moiety, it was decided to introduce into the peptide sequence an unsaturated amino acid that could be photo-isomerized. The cyclic peptide also

incorporates a pyrene moiety in a lysine side chain to help nanotube formation through π,π-interactions. The spectroscopic properties of pyrene also allow to study the self-assembly process by techniques such as fluorescence. Again, this proposed design was prepared by solid-phase peptide synthesis. Initially, the olefin moiety of the photoswitchable amino acid was protected as a furan cycloadduct. Then, heating of an aqueous solution enabled the selective formation of the *Z*-isomer by a retro-Diels-Alder reaction. The light-induced isomerization between the *Z*- and the *E*-isomer was evaluated. Irradiation at 290-320 nm of an aqueous solution of the *Z*-isomer resulted in the formation of a 7:3 mixture of both isomers, while the conversion from the *E*- to the *Z*-isomer can be achieved in almost a 1:1 ratio by irradiation at 254 nm. In both cases, the photostationary state is reached within a few minutes of irradiation and the process occurs independently of pH. The application of several irradiation cycles or the use of long irradiation times does not cause cyclic peptide decomposition or the appearance of new products, suggesting a good photostability of these designs. The different assembly properties of both isomers were demonstrated using a wide range of techniques. The *Z*-isomer exhibits a folded conformation and remains as a monomer due to its inability to self-assemble. In contrast, the *E*-isomer adopts the planar conformation required to assemble into nanotubes. Consequently, this switching process can be employed to control the conformation and the assembly of this type of cyclic peptide nanotubes. The light-induced assembly and disassembly can be triggered by the isomerization of this single unsaturated amino acid. Also, the self-assembly process only occurs at neutral or basic pH, as a consequence of the deprotonation of the histidine residues in the cyclic peptide scaffold. This allows a dual control by pH and light over the nanotube formation process. Interestingly, the substitution in the original design of the glutamine for a lysine amino acid was studied to increase the water solubility. However, this substitution resulted in cyclic peptide isomers with different assembly properties, as the *Z*-isomer assembles into sheet-like structures and the *E*-isomer forms nanotubes.

The spatially controlled supramolecular polymerization of both isomers in the confined space of microfluidic water-in-oil droplets was evaluated. Droplet-based microfluidic technology has emerged as an attractive method for analysing the behaviour of fibrillar structures in a confined and controlled space. For example, these droplets can be used to construct artificial synthetic cells or evaluate the potential application of synthetic fibrillar structures as mimetics of cell cytoskeleton. In this sense, a microfluidic device was used to create droplets containing the appropriate isomer to be studied in their interior. In addition, the use of different conditions inside of the droplets was explored. In particular, the cyclic peptide assembly is induced in a first junction of the microfluidic device by mixing a stream containing a slightly acidic aqueous solution of the cyclic peptide with two streams containing a trigger solution responsible for inducing the assembly. Changes in pH or the use of a high ionic strength were employed to induce the assembly. Then, droplet formation occurs by merging this new aqueous stream with an oil stream. Droplets were collected at the outlet of the microfluidic device and analysed by microscopy techniques. Epifluorescence microscopy analysis of droplets at neutral pH containing the *Z*-isomer showed quenched blue

USC DE SANTIAGO

fluorescence, suggesting no aggregation of this isomer. A similar result was obtained for droplets containing the *E*-isomer under acidic conditions. In contract, droplets containing the *E*-isomer at neutral pH showed blue fluorescent fibrillar structures mainly located in contact with the edges of the droplets. This distribution at the periphery of the droplets was confirmed by confocal microscopy. Interestingly, this accumulation in contact with the edges is able to induce the fusion between two neighbouring droplets containing the *E*-isomer. The substitution of the pyrene by an alkyl chain of six carbons provided droplets with no fusogenic properties, suggesting that the π,π-stacking of pyrene moieties is necessary for the hierarchical assembly and the induction of droplet fusion. Therefore, the fusion is probably due to the formation of a hydrophobic surface that interacts with the droplets interface causing their merging. Moreover, no fusion was observed between droplets with the *Z*-isomer and droplets with the *E*-isomer. In addition, fibre-like structures mainly located in the core of the droplets and with reduced fusogenic properties were observed when the assembly process of the *E*-isomer was triggered with a high ionic strength. Light-induced assembly was also evaluated inside of the droplets. For this purpose, droplets containing the *Z*-isomer at neutral pH were irradiated at 290-320 nm. Fluorescence microscopy revealed the formation of fibrillar structures inside the droplets after irradiation. HPLC analysis of the droplet interior also revealed again a photostationary state consisting of a 7:3 ratio mixture of the two isomers, confirming the isomerization of the cyclic peptide in this confined space.

Thirdly, different cyclic peptide-doxorubicin conjugates with an acid-labelled hydrazone linkage were prepared for the transport of doxorubicin inside cancer cells. In particular, the cyclic peptide scaffold was prepared by solid-phase peptide synthesis and, when necessary, a carbon tail was incorporated in the non-polar region of the cyclic peptide using an on-resin *click chemistry* strategy. The incorporation of the drug into the peptide backbone was carried out by reactions in solution. Fluorescence experiments, circular dichroism or microscopy techniques revealed the ability of these conjugates to assemble into fibres and 2D sheet-like structures. The *in vitro* anticancer activity was tested in three different cancer cell lines: a breast cancer cell line (MCF-7), a lung cancer cell line (NCI-H460) and a doxorubicin-resistant ovarian cancer cell line (NCI/ADR-RES). All the proposed cyclic peptide-doxorubicin conjugates showed good activity against the two non-resistant cell lines (MCF-7 and NCI-H460). However, only the peptides incorporating a 10-carbon, 14-carbon or NBD tail showed good activity against the resistant cell line (NCI/ADR-RES). Their activity was also evaluated in a non-cancerous human embryonic lung cell line (MRC-5), showing that the binding of doxorubicin to the cyclic peptides increased the biocompatibility of the drug. The mechanism of action of these conjugates was investigated in the drug-resistant cell line. Cancer cell resistance is usually the result of the overexpression of membrane proteins that expel the drug from the inside to the outside of the target cell, preventing the drug from exerting its therapeutic effect. In particular, the NCI/ADR-RES cancer cell line overexpresses the P-glycoprotein, which is capable of expelling doxorubicin from the cells. Confocal microscopy images and flow cytometry experiments with endocytosis inhibitors were

USC DE SANTIAGO

employed to evaluate the internalization mechanism. Specifically, the observed dotted pattern inside of the cell, the colocalization with Lysotracker and the reduction of the internalization in the presence of endocytosis inhibitors suggest that the endocytosis pathway is one of the main internalization mechanisms of these derivatives. Furthermore, confocal microscopy experiments revealed that only the peptides with an appropriate carbon tail are able to transport doxorubicin to the nucleus to induce the death of these resistant cells. Therefore, we speculate that the incorporation of a hydrocarbon tail into the peptide design is necessary to undergo endosomal escape, transport the drug to the nucleus and overcome cell resistance.

In conclusion, the addition of stimuli-responsiveness to cyclic peptide nanotubes was proposed in this doctoral thesis. In particular, different strategies have been developed to control the assembly process or to extend their use as drug delivery vehicles. First, a bending motion of the nanotubes was induced by light irradiation based on a [4+4] cycloaddition of an anthracene moiety. We expect that this first approach will allow the design of other new strategies to control the shape of cyclic peptide nanotubes and develop new functions. Then, the incorporation of a photoswitchable unsaturated amino acid into the peptide sequence and the study of its isomerization allowed to control the assembly and disassembly process of cyclic peptide nanotubes by light irradiation. The spatially controlled supramolecular polymerization triggered by light and media was also studied in the confined space of microfluidic water-in-oil droplets. Interestingly, the accumulation of the self-assembling isomer in contact with the droplet interface induces the fusion between two neighbouring droplets. This work represents a new step forward in the study of the supramolecular polymerization of cyclic peptide fibres in artificial minimal models, as these fusogenic properties might find new applications. Finally, different cyclic peptide-doxorubicin conjugates were prepared for the transport of this drug inside cancer cells. All the conjugates studied showed good activity against non-resistant cell lines, but only the designs incorporating a carbon tail showed the ability to exert their therapeutic effect in a drug-resistant cell line. The results of this doctoral thesis represent a first approach towards a better control of the self-assembly process and the properties of cyclic peptide nanotubes. Moreover, they could enable new functions for cyclic peptide nanotubes in the future, especially in biological applications.

USC
UNIVERSIDADE DE SANTIAGO DE COMPOSTELA

4. INTRODUCTION

USC
UNIVERSIDADE
DE SANTIAGO
DE COMPOSTELA

4.1. SUPRAMOLECULAR CHEMISTRY

The ambition of chemists to obtain more complex chemical entities beyond those accessible by covalent methods led to the development of the supramolecular systems. Their formation is based on dynamic and reversible non-covalent interactions between single molecules to form more complex structures (Figure 1A).[1] The origin of this branch of chemistry can be traced back to the discovery of the first intermolecular force in 1873 by Johannes Diderik van der Waals.[2] This finding was followed by other significant developments, including the description by Fischer in 1894 of the "Lock and Key" model (Figure 1B) to elucidate the interaction between a substrate and an enzyme or the first indication of the hydrogen bonds by M. L. Huggins, W. L. Latimer and W. H. Rodebush in the 1920s.[3,4] Later, K. L. Wolf introduced the concept of "Supramolecule (german: Übermoleküle)" in 1937. However, it was not until 1993 that J. M. Lehn provided the first definition of supramolecular chemistry as the "chemistry beyond the molecule".[5]

The great expansion of supramolecular chemistry has contributed to the discovery of both natural systems, including the DNA double helix in 1953 (Figure 1C),[6,7] and the development of more complex synthetic systems. In particular, supramolecular materials are characterized by an enhanced structural complexity beyond the molecular level, forming organized systems based on intermolecular interactions. Moreover, the reversibility of these non-covalent interactions enables the design of more dynamic systems with modulable properties or that can respond to the environmental conditions.[8] Relevant examples are the macrocycles reported by the laureate chemists C. J. Pedersen, J. M. Lehn and D. J. Cram in the 1960s, such as the crown ethers and cryptands (Figures 1D and 1E).[9] These ring-shaped molecules can bind specific metallic ions within their cavity through non-covalent interactions. A more recent example is the development by the laureates J. P. Sauvage, J. F. Stoddart and B. L. Feringa of molecular machines that are capable of producing mechanical motions, such as catenanes and rotaxanes (Figure 1F).[10,11]

---

[1] J. W. Steed, J. L. Atwood. *Supramolecular Chemistry*, 3rd Edition. John Wiley & Sons Ltd, Chichester, UK, **2022**.
[2] J. D. van der Waals, *On the Continuity of the Gaseous and Liquid States*, University of Leiden, Leiden, **1873**.
[3] E. Fischer, *Ber. Dtsch. Chem. Ges.* **1894**, *27*, 2985-2993.
[4] W. M. Latimer, W. H. Rodebush, *J. Am. Chem. Soc.* **1920**, *42*, 1419-1433.
[5] J. M. Lehn, *Science* **1993**, *260*, 1762-1763.
[6] a) J. D. Watson, F. H. C. Crick, *Nature* **1953**, *171*, 737-738; b) M. H. F. Wilkins, A. R. Strokes, H. R. Wilson, *Nature* **1953**, *171*, 738-740; c) R. E. Franklin, R. G. Gosling, *Nature* **1953**, *172*, 156-157.
[7] S. Neidle, *J. Biol. Chem.* **2021**, *296*, 100553.
[8] a) D. B. Amabilino, D. K. Smith, J. W. Steed, *Chem. Soc. Rev.* **2017**, *46*, 2404-2420; b) M. J. Webber, E. A. Appel, E. W. Meijer, R. Langer, *Nat. Mater.* **2016**, *15*, 13-26.
[9] a) C. J. Pedersen, *Science* **1988**, *241*, 536-540; b) J. M. Lehn, *Acc. Chem. Res.* **1978**, *11*, 49-57; c) J. M. Lehn, *Angew. Chem. Int. Ed. Engl.* **1988**, *27*, 89-112; d) D. J. Cram, *Angew. Chem. Int. Ed. Engl.* **1988**, *27*, 1009-1020; e) C. J. Pedersen, *Angew. Chem. Int. Ed. Engl.* **1988**, *27*, 1021-1027.
[10] a) J.-P. Sauvage, *Angew. Chem. Int. Ed.* **2017**, *56*, 11080-11093; b) J. F. Stoddart, *Angew. Chem. Int. Ed.* **2017**, *56*, 11094-11125; c) B. L. Feringa, *Angew. Chem. Int. Ed.* **2017**, *56*, 11060-11078; d) D. A. Leigh, *Angew. Chem. Int. Ed.* **2016**, *55*, 14506-14508; e) V. Balzani, A. Credi, F. M. Raymo, J. F. Stoddart, *Angew. Chem. Int. Ed.* **2000**, *39*, 3348-3391; f) S. Erbas-Cakmak, D. A. Leigh, C. T. McTernan, A. L. Nussbaumer, *Chem. Rev.* **2015**, *115*, 10081-10206.
[11] S. Kassem, T. van Leeuwen, A. S. Lubbe, M. R. Wilson, B. L. Feringa, D. A. Leigh, *Chem. Soc. Rev.* **2017**, *46*, 2592-2621.

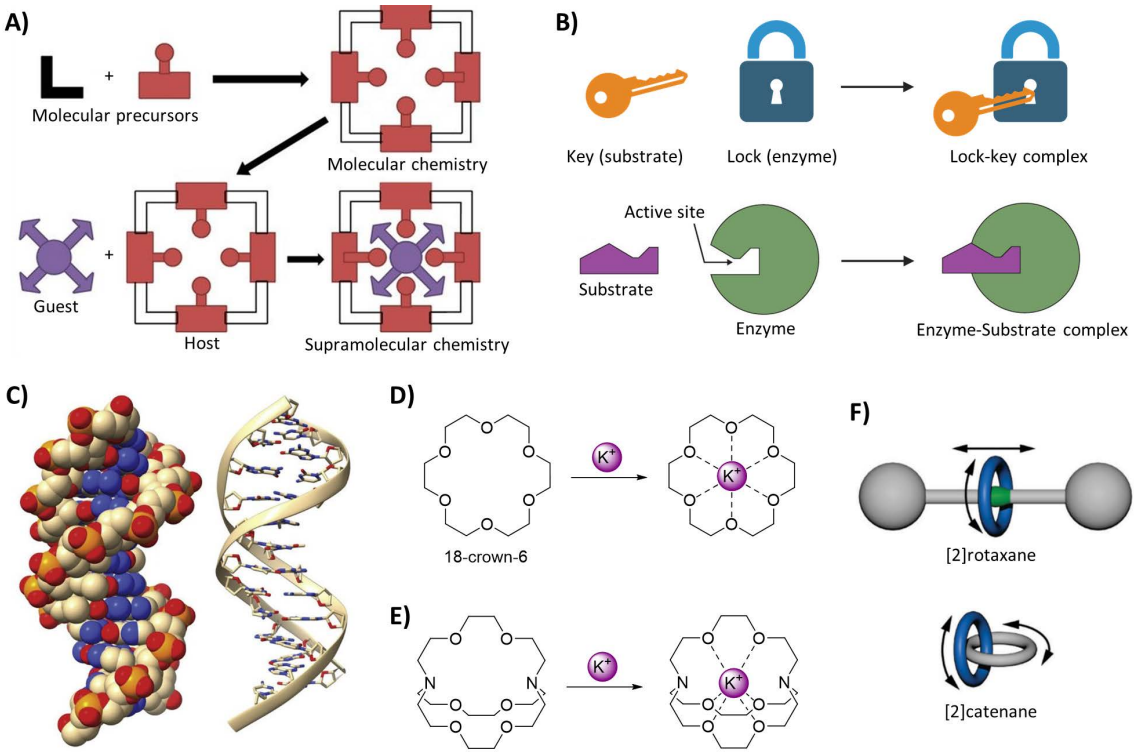

Figure 1. (A) Different scope of molecular and supramolecular chemistry. Reprinted with permission from Ref. 12. Copyright © 2012 Wiley-VCH Verlag GmbH & Co. (B) "Lock and Key model" to explain the interaction between and enzyme and a substrate. (C) Structure of the DNA double helix. Reprinted with permission from Ref. 7. Copyright © 2021 Elsevier. (D) Structure of a crown ether for potassium recognition. (E) Structure of a cryptand for potassium recognition. (F) Schematic representation of the mechanical motion of a rotaxane and a catenane. Adapted with permission from Ref. 11. Copyright © 2017 Royal Society of Chemistry.

Another type of structures based on non-covalent interactions are the supramolecular polymers. In contrast to the synthetic polymers in which small molecules are covalently and repeatedly bonded, in supramolecular polymers the building blocks interact in a non-covalent manner to form filamentous structures.[13] As this type of materials are based on non-covalent interactions, the supramolecular polymers are characterized by a strong dynamic and adaptive character compared to the covalent ones. Moreover, the rational design of the building blocks that constitute them allows for their easy preparation.

Natural examples of supramolecular polymers are the actin filaments and the microtubules that compose the cell cytoskeleton. These are formed by the self-assembly of protein monomers into long ordered filaments (Figure 2A).[14,15] Examples of synthetic

[7] S. Neidle, *J. Biol. Chem.* **2021**, *296*, 100553.
[11] S. Kassem, T. van Leeuwen, A. S. Lubbe, M. R. Wilson, B. L. Feringa, D. A. Leigh, *Chem. Soc. Rev.* **2017**, *46*, 2592-2621.
[12] D. Kumar, D. Sharma, G. Singh, M. Singh, M. S. Rathore, *ISRN Pharm* **2012**, *2012*, 474830.
[13] a) L. Brunsveld, B. J. B. Folmer, E. W. Meijer, R. P. Sijbesma, *Chem. Rev.* **2001**, *101*, 4071-4097; b) T. Aida, E. W. Meijer, S. I. Stupp, *Science* **2012**, 335, 813-817; c) E. Krieg, M. M. C. Bastings, P. Besenius, B. Rybtchinski, *Chem. Rev.* **2016**, *116*, 2414-2477.
[14] a) T. D. Pollard, G. G. Borisy, *Cell* **2003**, *112*, 453-465; b) A. Akhmanova, M. O. Steinmetz, *Nat. Rev. Mol. Cell Biol.* **2015**, *16*, 711-726.
[15] C. Conde, A. Cáceres, *Nat. Rev. Neurosci.* **2009**, *10*, 319-332.

supramolecular polymers are those described by the group of E. W. Meijer, who reported the use of the benzenetricarboxamide (BTA) motif, which stacks through the formation of three hydrogen bonds between amides (Figure 2B).[16,17] Furthermore, the same group exploited the use of the ureido-pyrimidinone (UPy) motif as a four-hydrogen bond forming unit (Figure 2C).[18,19]

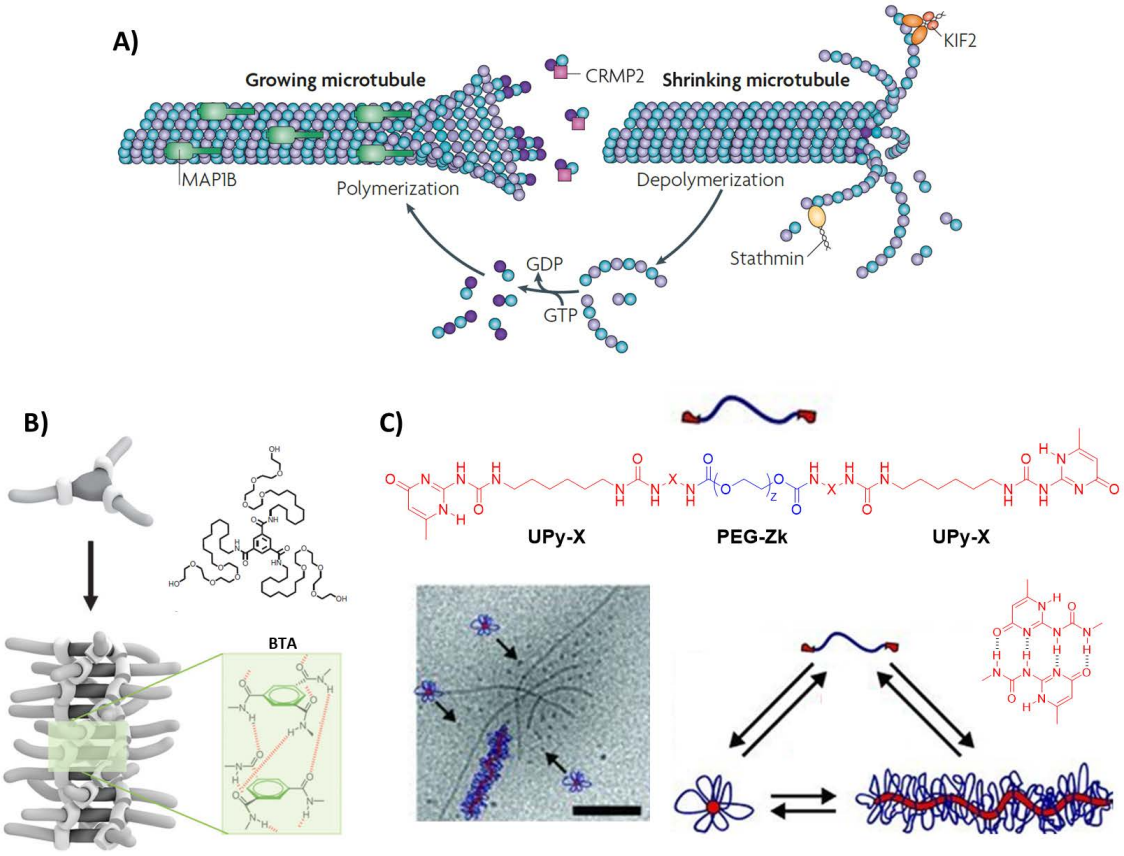

Figure 2. (A) Tubulin assembly and disassembly to form microtubules. Reprinted with permission from Ref. 15. Copyright © 2009 Springer Nature. (B) Supramolecular polymers made by the self-assembly of BTA by three intermolecular hydrogen bonds. Adapted with permission from Ref. 17. Copyright © 2012 Royal Society of Chemistry. (C) Representation of an UPy dimer and the corresponding supramolecular polymerization. Adapted with permission from Ref. 19 Copyright © 2012 Wiley-VCH Verlag GmbH & Co.

Another strategy to obtain a supramolecular polymer is the assembly of long conjugated π-molecules into columnar structures through π,π-interactions. For example, the group of F. Würthner has made great contributions to the use of perylene

[15] C. Conde, A. Cáceres, *Nat. Rev. Neurosci.* **2009**, *10*, 319-332.
[16] a) L. Albertazzi, F. J. Martinez-Veracoechea, C. M. A. Leenders, I. K. Voets, D. Frenkel, E. W. Meijer, *Proc. Natl. Acad. Sci. U.S.A.* **2013**, *110*, 12203-12208; b) L. Albertazzi, D. van der Zwaag, C. M. A. Leenders, R. Fitzner, R. W. van der Hofstad, E. W. Meijer, *Science* **2014**, *344*, 491-495.
[17] S. Cantekin, T. F. A. de Greef, A. R. A. Palmans, *Chem. Soc. Rev.* **2012**, *41*, 6125-6137.
[18] R. P. Sijbesma, F. H. Beijer, L. Brunsveld, B. J. B. Folmer, J. H. K. K. Hirschberg, R. F. M. Lange, J. K. L. Lowe, E. W. Meijer, *Science* **1997**, *278*, 1601-1604.
[19] P. Y. W. Dankers, T. M. Hermans, T. W. Baughman, Y. Kamikawa, R. E. Kieltyka, M. M. C. Bastings, H. M. Janssen, N. A. J. M. Sommerdijk, A. Larsen, M. J. A. van Luyn, A. W. Bosman, E. R. Popa, G. Fytas, E. W. Meijer, *Adv. Mater.* **2012**, *24*, 2703-2709.

diimide (PDI) for the construction of supramolecular polymers (Figure 3A).[20,21] Similarly, the group of T. Aida proposed the use of hexabenzocoronene (HBC) as a motif to obtain supramolecular nanotubes (Figure 3B).[22,23] Peptide amphiphiles represent another of the most explored building blocks. The research group of Samuel I. Stupp mainly investigated the use of amphiphilic peptides consisting of a hydrocarbon tail and a β-sheet forming sequence, to which a bioactive moiety can be attached (Figure 3C).[24,25] The resulting peptides showed the ability to undergo supramolecular polymerization in aqueous solutions giving rise to nanofibers.

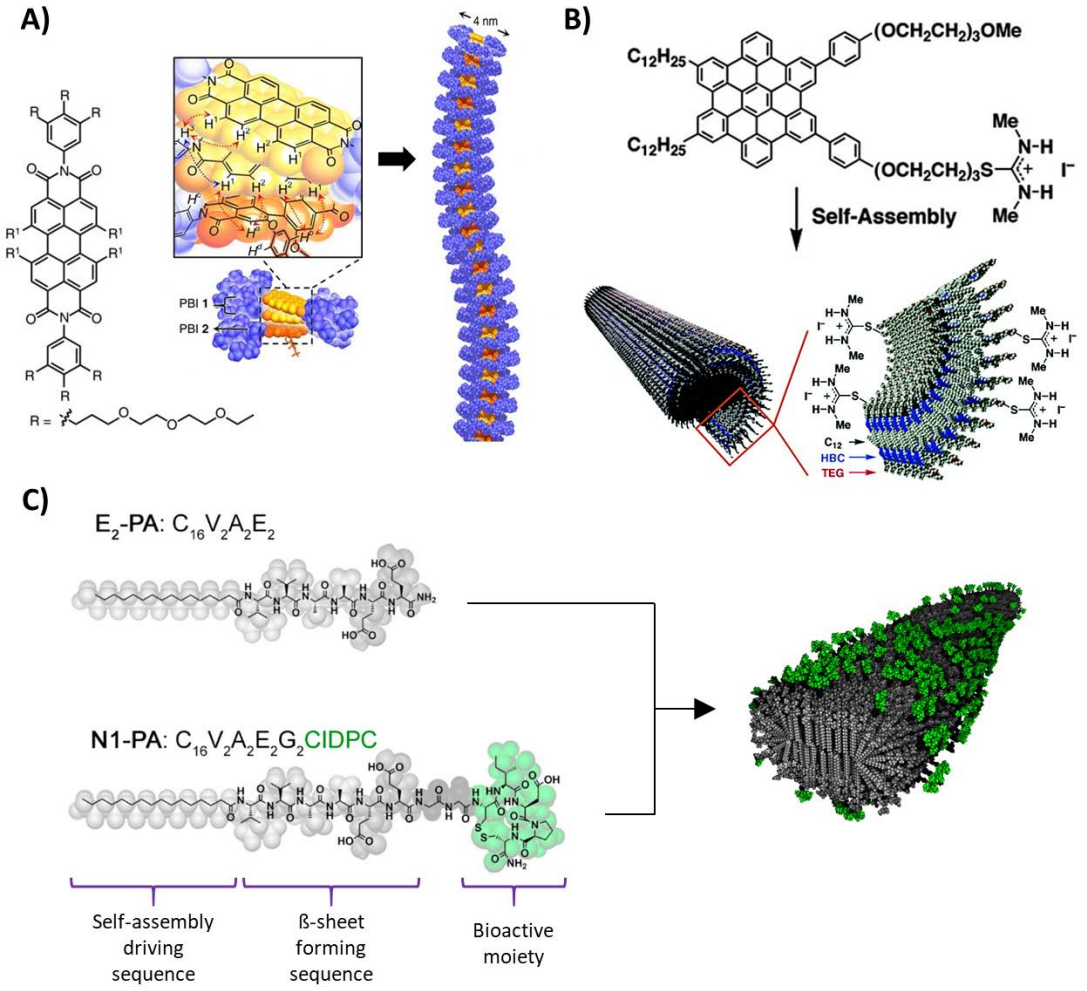

Figure 3. (A) Assembly of a PDI moiety though π,π-interactions. Adapted with permission from Ref. 21. Copyright © 2015 Springer Nature. (B) Nanotube composed of a bilayer wall resulting from the assembly of HBC units. Adapted with permission from Ref. 23. Copyright © 2007 American Chemical Society. (C) Coassembly of two peptide amphiphiles to form a supramolecular nanofiber. Adapted with permission from Ref. 25. Copyright © 2023 American Chemical Society.

[20] X. Zhang, D. Görl, V. Stepanenko, F. Würthner, *Angew. Chem. Int. Ed.* **2014**, *53*, 1270-1274.
[21] D. Görl, X. Zhang, V. Stepanenko, F. Würthner, *Nat. Commun.* **2015**, *6*, 7009.
[22] J. P. Hill, W. Jin, A. Kosaka, T. Fukushima, H. Ichihara, T. Shimomura, K. Ito, T. Hashizume, N. Ishii, T. Aida, *Science* **2004**, *304*, 1481-1483.
[23] G. Zhang, W. Jin, T. Fukushima, A. Kosaka, N. Ishii, T. Aida, *J. Am. Chem. Soc.* **2007**, *129*, 719-722.
[24] a) J. D. Hartgerink, E. Beniash, S. I. Stupp, *Science* **2001**, *294*, 1684-1688; b) Z. Álvarez, A. Kolberg-Edelbrock, I. Sasselli, J. Ortega, R. Qiu, Z. Syrgiannis, P. Mirau, F. Chen, S. Chin, S. Weigand, E. Kiskinis, S. I. Stupp, *Science* **2021**, *374*, 848-856.
[25] C. S. Smith, Z. Álvarez, R. Qiu, I. R. Sasselli, T. Clemons, J. A. Ortega, M. Vilela-Picos, H. Wellman, E. Kiskinis, S. I. Stupp, *ACS Nano* **2023**, *17*, 19887-19902.

The dynamic behaviour of supramolecular systems has led to the addition of stimuli-responsiveness to these materials, thus broadening their range of potential applications.[26] The general approach is to modify their physicochemical properties in response to a stimulus, such as light,[27] redox conditions,[28] enzymatic activity[29] or pH[30], among others. Taking into account the objective of this PhD thesis, the next sections will be focused on light-sensitive systems and stimuli-responsive drug delivery systems.

4.2. PHOTO-RESPONSIVE SYSTEMS

Light is able to regulate different biological functions in living organisms. For example, phytochromes are photoreceptor proteins able to isomerize between a molecular structure that absorbs red light (Pr state) and one that absorbs far-red light (Pfr state) (Figure 4A). This photoswitching process is able to control the growth, reproduction and movement of plants, fungi and bacteria based on the different biological response of each state.[31,32] Another example found in nature is the photo-isomerization between 11-*cis*- and all-*trans*-retinal in the protein Rhodopsin to regulate the vision in humans.[33] Also, the isomerization from all-*trans*- to 13-*cis*-retinal controls the transport of ions in bacterial membranes (Figure 4B). In this last case, the process occurs only at a specific double bond in the binding pocket of the microbial Rhodopsin to activate the transport of protons from the cytoplasm to the extracellular environment.[34,35]

[26] a) X. Yan, F. Wang, B. Zheng, F. Huang, *Chem. Soc. Rev.* **2012**, *41*, 6042-6065; b) X. Ma, H. Tian, *Acc. Chem. Res.* **2014**, *47*, 1971-1981.
[27] a) X. Yao, T. Li, J. Wang, X. Ma, H. Tian, *Adv. Optical Mater.* **2016**, *4*, 1322-1349; b) M. Baroncini, J. Groppi, S. Corra, S. Silvi, A. Credi, *Adv. Optical Mater.* **2019**, *7*, 1900392; c) F. Xu, B. L. Feringa, *Adv. Mater.* **2023**, *35*, 2204413.
[28] a) A. K. Miller, Z. Li, K. A. Streletzky, A. M. Jamieson, S. J. Rowan, *Polym. Chem.* **2012**, *3*, 3132-3138; b) Q. Yan, A. Feng, H. Zhang, Y. Yin, J. Yuan, *Polym. Chem.* **2013**, *4*, 1216-1220.
[29] a) J. Hu, G. Zhang, S. Liu, *Chem. Soc. Rev.* **2012**, *41*, 5933-5949; b) Y. Ding, Y. Kang, X. Zhang, *Chem. Commun.* **2015**, *51*, 996-1003; c) X. Xiao, J. Huang, *Langmuir* **2024**, *40*, 15407-15420.
[30] a) K. C. Leung, C. Chak, C. Lo, W. Wong, S. Xuan, C. H. K. Cheng, *Chem. Asian J.* **2009**, *4*, 364-381; b) H. Frisch, P. Besenius, *Macromol. Rapid Commun.* **2015**, *36*, 346-363.
[31] H. Takala, P. Edlund, J. A. Ihalainen, S. Westenhoff, *Photochem. Photobiol. Sci.* **2020**, *19*, 1488-1510.
[32] a) P. W. Kim, N. C. Rockwell, L. H. Freer, C. Chang, S. S. Martin, J. C. Lagarias, D. S. Larsen, *J. Phys. Chem. Lett.* **2013**, *4*, 2605-2609; b) D. Morozov, V. Modi, V. Mironov, G. Groenhof, *J. Phys. Chem. Lett.* **2022**, *13*, 4538-4542.
[33] a) R. Hubbard, A. Kropf, *Proc. Natl. Acad. Sci. U S A*. **1958**, *44*, 130-139; b) K. Palczewski, *J. Biol. Chem.* **2012**, *287*, 1612-1619.
[34] P. Nogly, T. Weinert, D. James, S. Carbajo, D. Ozerov, A. Furrer, D. Gashi, V. Borin, P. Skopintsev, K. Jaeger, K. Nass, P. Båtch, R. Bosman, J. Koglin, M. Seaberg, T. Lane, D. Kekilli, S. Brünle, T. Tanaya, W. Wu, C. Milne, T. White, A. Barty, U. Weierstall, V. Panneels, E. Nango, S. Iwata, M. Hunter, I. Schapiro, G. Schertler, R. Neutze, J. Standfuss, *Science* **2018**, *361*, eaat0094.
[35] O. P. Ernst, D. T. Lodowski, M. Elstner, P. Hegemann, L. S. Brown, H. Kandori, *Chem. Rev.* **2014**, *114*, 126-163.

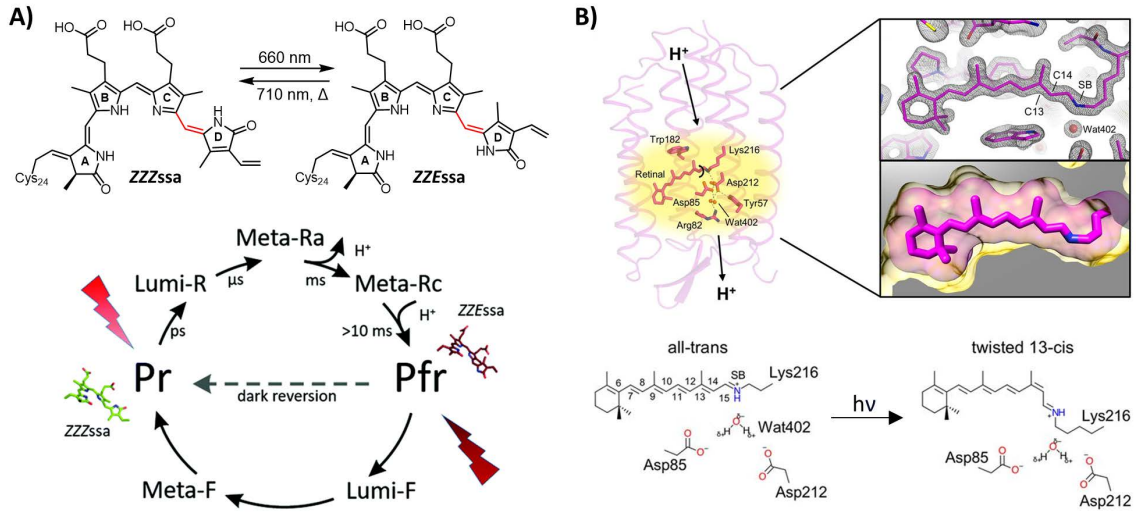

Figure 4. (A) Representation of the biliverdin chromophore in *Deinococcus radiodurans* phytochrome (DrBphP) and photocycle of isomerization between two states (Pr and Pfr states). Adapted with permission from Ref. 31. Copyright © 2020 Royal Society of Chemistry. (B) All-*trans*- to 13-*cis*-retinal isomerization in the binding pocket of Bacteriorhodopsin to control the transport of protons in a bacterial membrane. Adapted with permission from Ref. 34. Copyright © 2018 AAAS.

Based on this type of examples in nature, the research for new light-sensitive materials is of great interest with the aim of obtaining innovative properties and functions. In fact, the 21st century has even been named as the "Age of Enlightenment" in molecular sciences.[36] In this sense, the concept of "molecular photoswitches" has emerged to describe any chromophore that can be converted between two or more different isomers by appropriate light irradiation.[36,37,38] The initially thermodynamic isomer can be usually brought through light irradiation to an excited state, followed by a relaxion process to a new metastable isomer (Figure 5A). This new metastable isomer is higher in energy than the initial one, so it can be usually isomerized again in a reversible manner to the initial thermodynamic form. An ideal photoswitch should present a fast conversion process and high thermal stability, extinction coefficients and quantum yields. In addition, each isomer must be characterised by different properties. Multiple examples of molecular photoswitches have been described, but most of them are based on isomerization around a double bond, photocyclization reactions or combination of mechanisms (Figure 5B).[36,37,38]

[31] H. Takala, P. Edlund, J. A. Ihalainen, S. Westenhoff, *Photochem. Photobiol. Sci.* **2020**, *19*, 1488-1510.
[34] P. Nogly, T. Weinert, D. James, S. Carbajo, D. Ozerov, A. Furrer, D. Gashi, V. Borin, P. Skopintsev, K. Jaeger, K. Nass, P. Båtch, R. Bosman, J. Koglin, M. Seaberg, T. Lane, D. Kekilli, S. Brünle, T. Tanaya, W. Wu, C. Milne, T. White, A. Barty, U. Weierstall, V. Panneels, E. Nango, S. Iwata, M. Hunter, I. Schapiro, G. Schertler, R. Neutze, J. Standfuss, *Science* **2018**, *361*, eaat0094.
[36] Z. L. Pianowski, *Chem. Eur. J.* **2019**, *25*, 5128-5144.
[37] J. Volarić, W. Szymanski, N. A. Simeth, B. L. Feringa, *Chem. Soc. Rev.* **2021**, *50*, 12377-12449.
[38] a) M. Russew, S. Hecht, *Adv. Mater.* **2010**, *22*, 3348-3360; b) J. Boelke, S. Hech, *Adv. Optical Mater.* **2019**, *7*, 1900404; c) B. L. Feringa. *Molecular Photoswitches: Chemistry, Properties, and* Applications, *2 Volume Set.* John Wiley & Sons Ltd, Chichester, UK, **2022**.

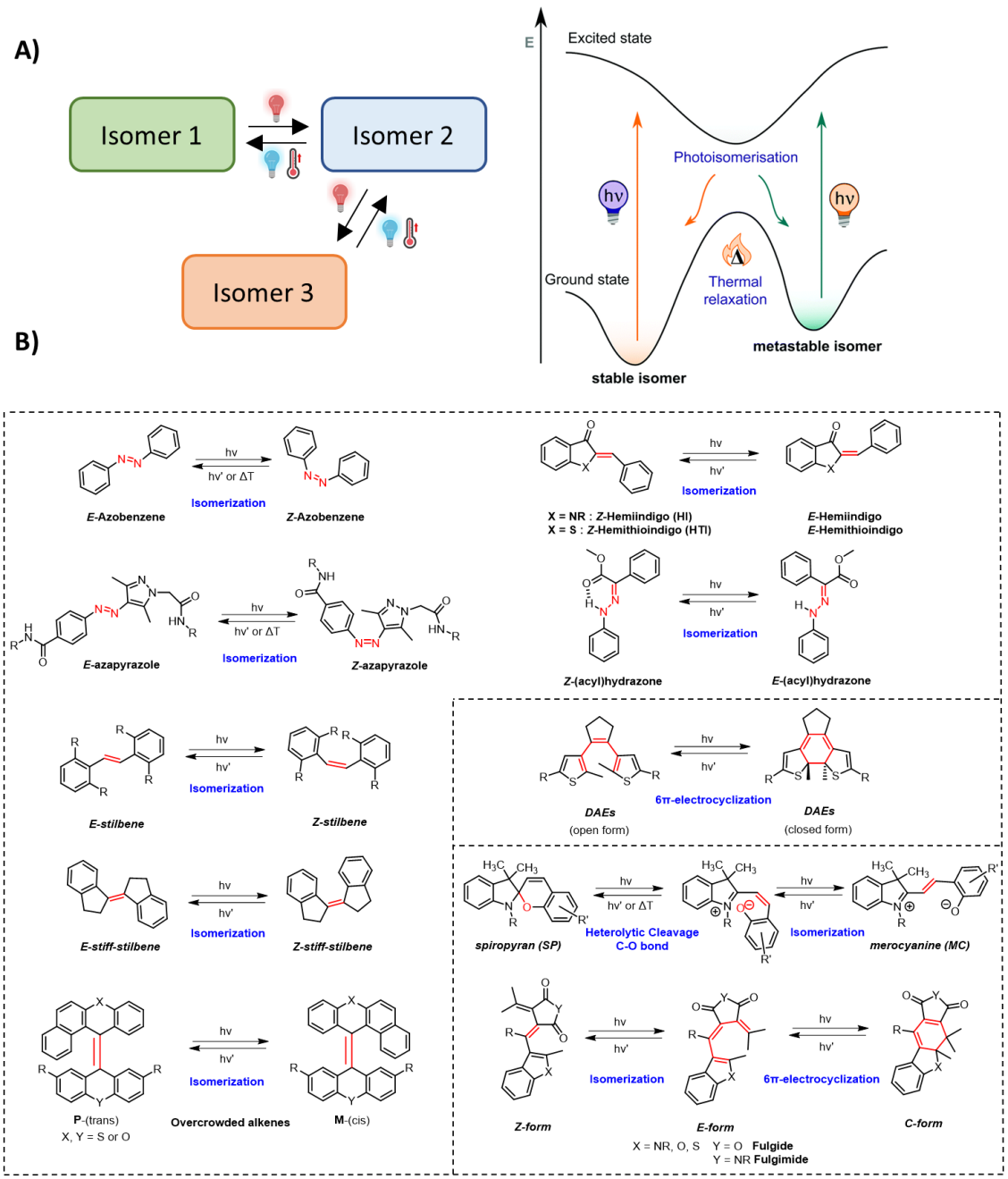

Figure 5. (A) Potential energy surfaces during photoisomerization of a molecular photoswitch. Adapted with permission from Ref. 37. Copyright © 2021 Royal Society of Chemistry. (B) Examples of molecular photoswitches based on double bond isomerization, photocyclization reactions or the combination of mechanisms.

4.2.1. Molecular photoswitches based on isomerizations

The main mechanism of photo-switching is the isomerization of a double bond between the *E* and *Z* form or *vice versa* to induce structural changes in the molecular system. This is the case of azobenzene derivatives, which are the most widely used molecular photoswitches for biomolecules.[39] Unsubstituted *trans*-azobenzene can be converted in around an 80% into the *cis*-azobenzene by irradiation with UV light (∼360 nm), while the reverse process can be thermally achieved in around a 100% or by irradiation with visible light in around a 95% (∼430 nm). As unmodified azobenzene isomerizes in the UV region, other substituted azobenzenes were reported for red-shifting the absorption wavelength, especially when a biological application is desired.[40] For example, electron-donating amino groups can be introduced in the *ortho* or *para* position to considerably red-shift the absorption.[41] Also, a similar effect is obtained by substitution of the four *ortho* positions with methoxy groups.[42] Another strategy for the red-shifting is the "push-pull azobenzenes", which contain an electron donating group in the *para* position of one of the phenyl rings and an electron acceptor group also in the *para* position of the other phenyl group.[43] However, these strategies usually afford azobenzene derivatives characterised by a faster thermal relaxation time which can limit their applications when a long-term effect is desired. In contrast, the tetra-substitution with halogens has been shown to increase the half-life, like the 2,2',6,6'-tetrafluoroazobenzene which has a half-life of 700 days at 25°C.[44]

An example of a supramolecular assembly controlled by azobenzene isomerization is its combination with the host-guest chemistry of α-cyclodextrin. The *trans*-azobenzene is recognized by α-cyclodextrin, while the *cis*-azobenzene is unable to interact. Based on this feature, the group of X. Zhang developed a method for photo-controlling the assembly and disassembly of vesicle-like structures (Figure 6A).[45] Another example of an azobenzene-based assembly system is the supramolecular tubules reported by the group of T. Kudernac (Figure 6B).[46] In particular, they designed an aromatic core with two azobenzene moieties and with hydrophilic oligoether chains to increase the water solubility. The structural changes resulting from the *trans* to *cis* isomerization are capable of triggering the disassembly of these tubules by simple light irradiation.

---

[39] a) A. A. Beharry, G. A. Woolley, *Chem. Soc. Rev.* **2011**, *40*, 4422-4437; b) H. M. D. Bandarab, S. C. Burdette, *Chem. Soc. Rev.* **2012**, *41*, 1809-1825; c) F. A. Jerca, V. V. Jerca, R. Hoogenboom, *Nat. Rev. Chem.* **2022**, *6*, 51-69.
[40] M. Dong, A. Babalhavaeji, S. Samanta, A. A. Beharry, G. A. Woolley, *Acc. Chem. Res.* **2015**, *48*, 2662-2670.
[41] O. Sadovski, A. A. Beharry, F. Zhang, G. A. Woolley, *Angew. Chem. Int. Ed.* **2009**, *48*, 1484-1486.
[42] a) A. A. Beharry, O. Sadovski, G. A. Woolley, *J. Am. Chem. Soc.* **2011**, *133*, 19684-19687; b) S. Samanta, A. A. Beharry, O. Sadovski, T. M. McCormick, A. Babalhavaeji, V. Tropepe, G. A. Woolley, *J. Am. Chem. Soc.* **2013**, *135*, 9777-9784.
[43] a) S. Kobayashi, H. Yokoyama, H. Kamei, *Chem. Phys. Lett.* **1987**, *138*, 333-338; b) F. Aleotti, A. Nenov, L. Salvigni, M. Bonfanti, M. M. El-Tahawy, A. Giunchi, M. Gentile, C. Spallacci, A. Ventimiglia, G. Cirillo, L. Montali, S. Scurti, M. Garavelli, I. Conti, *J. Phys. Chem. A* **2020**, *124*, 9513-9523.
[44] a) D. Bléger, J. Schwarz, A. M. Brouwer, S. Hecht, *J. Am. Chem. Soc.* **2012**, *134*, 20597-20600; b) C. Knie, M. Utecht, F. Zhao, H. Kulla, S. Kovalenko, A. M. Brouwer, P, Saalfrank, S. Hecht, D. Bléger, *Chem. Eur. J.* **2014**, *20*, 16492-16501; c) S. Axelrod, E. Shakhnovich, R. Gómez-Bombarelli, *ACS Cent. Sci.* **2023**, *9*, 166-176.
[45] Y. Wang, N. Ma, Z. Wang, X. Zhang, *Angew. Chem. Int. Ed.* **2007**, *46*, 2823-2826.
[46] J. W. Fredya, A. Méndez-Ardoy, S. Kwangmettatama, D. Bochicchio, B. Matt, M. C. A. Stuart, J. Huskens, N. Katsonis, G. M. Pavan, T. Kudernac, *Proc. Natl. Acad. Sci. USA* **2017**, *114*, 11850-11855.

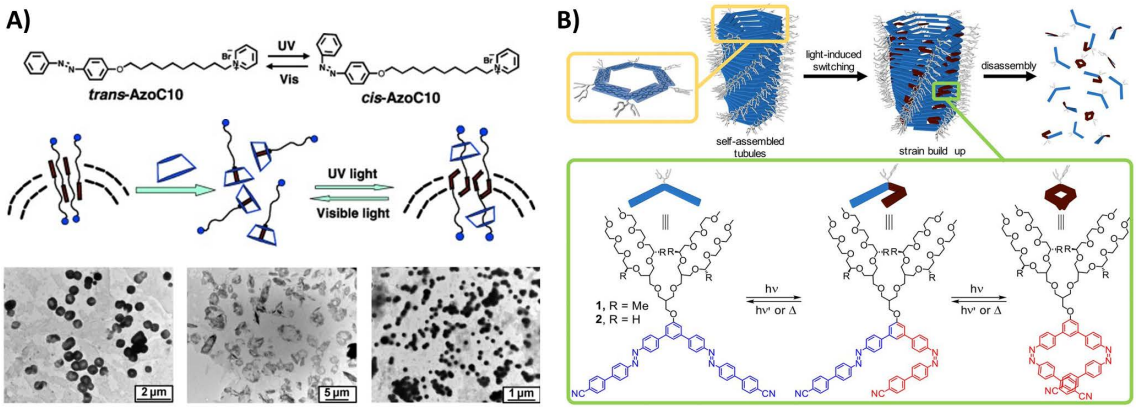

Figure 6. (A) Reversible light-induced assembly and disassembly of vesicle-like structures. Adapted with permission from Ref. 45. Copyright © 2007 Wiley-VCH Verlag GmbH & Co. (B) Disassembly by light irradiation of water-soluble supramolecular tubules. Adapted with permission from Ref. 46. Copyright © 2017 National Academy of Sciences.

In this regard, azobenzene has also been widely incorporated into peptides to regulate various biological functions, such as their interaction with nucleic acids and proteins.[47,48] For example, the group of J. L. Mascareñas reported for the first time in the year 2000, an azobenzene-based basic leucine zipper (bZIP) in which its binding to DNA can be induced by light (Figure 7A).[49] However, the strong binding of the *cis*-isomer to DNA prevented this process from being reversible. For this reason, a few years later different strategies were developed by the group of G. A. Woolley to make this binding of bZIPs to DNA reversible.[50] More recently, the group of B. L. Feringa extended the use of azobenzene to control the binding of zinc fingers (ZFs) to DNA.[51] In another sense, the group of R. K. Alleman developed different peptides with a crosslinker of azobenzene for photo-switching the peptide conformation between an α-helix and a random coil conformation to control the interaction with the B-cell leukaemia protein Bcl-x_L (Figure 7B).[52,53] In another example, the group of M. Beyermann developed a cyclic peptide with an azobenzene amino acid, in which the *cis*-isomer was able to bind to the protein α-1-syntrophin (Figure 7C).[54,55] This peptide binding avoids the protein-protein

[45] Y. Wang, N. Ma, Z. Wang, X. Zhang, *Angew. Chem. Int. Ed.* **2007**, *46*, 2823-2826.
[46] J. W. Fredya, A. Méndez-Ardoy, S. Kwangmettatama, D. Bochicchio, B. Matt, M. C. A. Stuart, J. Huskens, N. Katsonis, G. M. Pavan, T. Kudernac, *Proc. Natl. Acad. Sci. USA* **2017**, *114*, 11850-11855.
[47] a) L. Albert, O. Vázquez, *Chem. Commun.* **2019**, *55*, 10192-10213; b) C. Renner, L. Moroder, *ChemBioChem* **2006**, *7*, 868-878; c) R. J. Mart, R. K. Allemann, *Chem. Commun.* **2016**, *52*, 12262-12277.
[48] J. Rodríguez, J. Mosquera, S. Learte-Aymamí, M. Eugenio Vázquez, J. L. Mascareñas, *Acc. Chem. Res.* **2020**, *53*, 2286-2298.
[49] A. M. Caamaño, M. E. Vázquez, J. Martínez-Costas, L. Castedo, J. L. Mascareñas, *Angew. Chem. Int. Ed.* **2000**, 39, 3104-3107.
[50] a) G. A. Woolley, A. S. I. Jaikaran, M. Berezovski, J. P. Calarco, S. N. Krylov, *Biochemistry* **2006**, *45*, 6075-6084; b) F. Zhang, K. A. Timm, K. M. Arndt, G. A. Woolley, *Angew. Chem. Int. Ed*. **2010**, *49*, 3943-3946.
[51] G. M. Murawska, C. Poloni, N. A. Simeth, W. Skymanski, B. L. Feringa, *Chem. Eur. J.* **2019**, *25*, 4965-4973.
[52] S. Kneissl, E. J. Loveridge, C. Williams, M. P. Crump, R. K. Allemann, *ChemBioChem.* ***2008****, 9, 3046-3054.*
[53] R. J. Mart, R. J. Errington, C. L. Watkins, S. C. Chappell, M. Wiltshire, A. T. Jones, P. J. Smith, R. K. Allemann, *Mol. BioSyst.* **2013**, *9*, 2597-2603.
[54] C. Hoppmann, S. Seedorff, A. Richter, H. Fabian, P. Schmieder, K. Rück-Braun, M. Beyermann, *Angew. Chem. Int. Ed.* **2009**, *48*, 6636-6639.
[55] C. Hoppmann, P. Schmieder, P. Domaing, G. Vogelreiter, J. Eichhorst, B. Wiesner, I. Morano, K. Rück-Braun, M. Beyermann, *Angew. Chem. Int. Ed.* **2011**, *50*, 7699-7702.

interaction of α-1-syntrophin with the neural NO synthase (nNOS) in the skeletal muscle, providing a photo-control of the muscle contraction. Also, the introduction of azobenzene into peptides has been exploited as a method to regulate their interaction with membrane receptors (Figure 7D).[56,57] Another biologically relevant azobenzene-based peptides are those use to control by light irradiation their cell uptake or their use as antibiotics.[58]

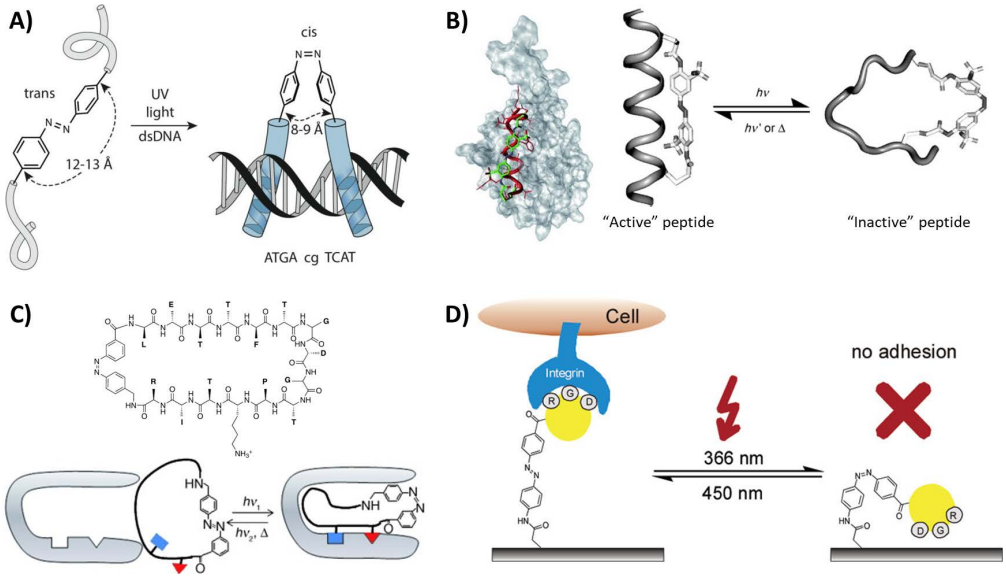

Figure 7. (A) Photo-induction of DNA binding of an azobenzene bZIP. Reprinted with permission from Ref. 48. Copyright © 2020 American Chemical Society. (B) Control of peptide helicity by isomerization of an azobenzene crosslinker to regulate the interaction with the Bcl-xL protein. Adapted with permission from Ref. 52. Copyright © 2007 Wiley-VCH Verlag GmbH & Co. (C) Cyclic peptide with an azobenzene amino acid for the photo-conversion between the non-binding and the protein-binding conformation. Adapted with permission from Ref. 54. Copyright © 2009 Wiley-VCH Verlag GmbH & Co. (D) Light-controlled adhesion to an integrin receptor of an azobenzene-modified RGD peptide. Reprinted with permission from Ref. 56. Copyright © 2005 American Chemical Society.

Other examples of molecular photoswitches that rely on double bond isomerization are azapyrazol,[59] stilbene,[60] stiff-stilbene,[61] hemi(thio)indigo,[62]

[48] J. Rodríguez, J. Mosquera, S. Learte-Aymamí, M. Eugenio Vázquez, J. L. Mascareñas, *Acc. Chem. Res.* **2020**, *53*, 2286-2298.
[52] S. Kneissl, E. J. Loveridge, C. Williams, M. P. Crump, R. K. Allemann, *ChemBioChem.* ***2008****, 9, 3046-3054.*
[54] C. Hoppmann, S. Seedorff, A. Richter, H. Fabian, P. Schmieder, K. Rück-Braun, M. Beyermann, *Angew. Chem. Int. Ed.* **2009**, *48*, 6636-6639.
[56] J. Auernheimer, C. Dahmen, U. Hersel, A. Bausch, H. Kessler, *J. Am. Chem. Soc.* **2005**, *127*, 16107-16110.
[57] T. Podewin, J. Broichhagen, C. Frost, D. Groneberg, J. Ast, H. Meyer-Berg, N. H. F. Fine, A. Friebe, M. Zacharias, D. J. Hodson, D. Trauner, A. Hoffmann-Roder, *Chem. Sci.* **2017**, *8*, 4644-4653.
[58] a) A. Prestela, H. M. Mölle, *Chem. Commun.* **2016**, *52*, 701-704; b) Y. Q. Yeoh, J. Yu, S. W. Polyak, J. R. Horsley, A. D. Abell, *ChemBioChem* **2018**, *19*, 2591-2597; c) X. Just-Baringo, A. Yeste-Vázquez, J. Moreno-Morales, C. Ballesté-Delpierre, P. J. Vila, E. Giralt, *Chem. Eur. J.* **2021**, *27*, 12987-12991.
[59] a) S. Crespi, N. A. Simeth, B. König, *Nat. Rev. Chem.* **2019**, *3*, 133-146; b) C. E. Weston, R. D. Richardson, P. R. Haycock, A. J. P. White, M. J. Fuchter, *J. Am. Chem. Soc.* **2014**, *136*, 11878-11881; c) L. Stricker, E. Fritz, M. Peterlechner, N. L. Doltsinis, B. J. Ravoo, *J. Am. Chem. Soc.* **2016**, *138*, 4547-4554.
[60] a) D. H. Waldeck, *Chem. Rev.* **1991**, *91*, 415-436; b) W. Fuß, C. Kosmidis, W. E. Schmid, S. A. Trushin, *Angew. Chem. Int. Ed.* **2004**, *43*, 4178-4182.
[61] a) D. Villarón, S. J. Wezenberg, *Angew. Chem. Int. Ed.* **2020**, *59*, 13192-13202; b) F. Xu, J. Sheng, C. N. Stindt, S. Crespi, W. Danowski, M. F. Hilbers, W. J. Buma, B. L. Feringa, *Chem. Sci.* **2024**, *15*, 6763-6769.
[62] a) C. Petermayer, H. Dube, *Acc. Chem. Res.* **2018**, *51*, 1153-1163; b) C. Petermayer, S. Thumser, F. Kink, P. Mayer, H. Dube, *J. Am. Chem. Soc.* **2017**, *139*, 15060-15067; c) S. Wiedbrauk, H. Dube, *Tetrahedron Lett.* **2015**, *56*, 4266-4274.

overcrowded alkenes[63] or hydrazones,[64] among others. For example, the group of A. Harada developed a dimer of cyclodextrins linked by a stilbene moiety (Figure 8A).[65] Specifically, in the presence of a ditopic adamantly guess molecule, the *trans*-isomer encapsulates both adamantane moieties and remains in a dimeric state. In contrast, the *cis*-isomer is unable to fit both adamantanes with the two cyclodextrins of the same molecule, leading to the formation of linear assemblies. In a different attempt to construct photo-responsive supramolecular polymers, the group of B. L. Feringa designed stiff-stilbene-based bis-urea monomers (Figure 8B) for the reversible control of their assembly/disassembly process, switching from liquid solution to organogels upon light irradiation.[66]

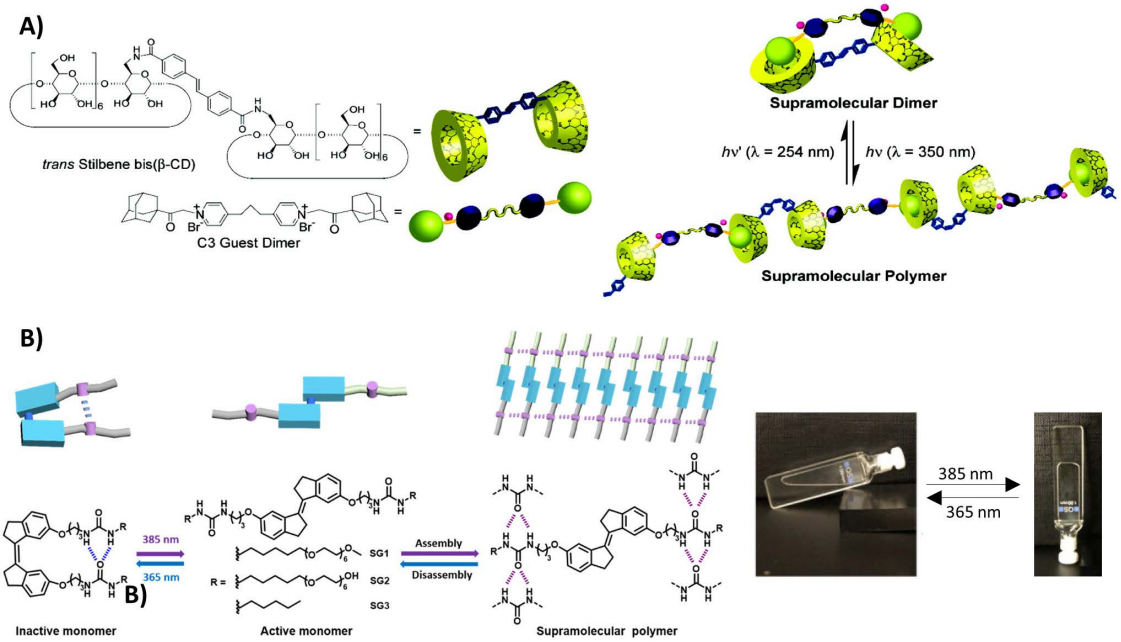

Figure 8. (A) Dimer formation or supramolecular polymerization based on the *trans*/*cis*-isomerization of stilbene-based cyclodextrins. Adapted with permission from Ref. 65. Copyright © 2007 American Chemical Society. (B) Light control of the assembly/disassembly process of bis-urea monomers modified with stiff-stilbene and the reversible organogels formation. Adapted with permission from Ref. 66. Copyright © 2021 American Chemical Society.

The research group of B. L. Feringa also exploited the isomerization around an overcrowded alkene to obtain a molecular motor with muscle-like behaviour (Figure 9A).[67] Depending on the olefin geometry, the supramolecular polymer can go

[63] a) N. Koumura, R. W. J. Zijlstra, R. A. van Delden, N. Harada, B. L. Feringa, *Nature* **1999**, *401*, 152-155; b) N. Koumura, E. M. Geertsema, M. B. van Gelder, A. Meetsma, B. L. Feringa, *J. Am. Chem. Soc.* **2002**, *124*, 5037-5051; c) J. C. M. Kistemaker, P. Štacko, D. Roke, A. T. Wolters, G. H. Heideman, M. Chang, P. van der Meulen, J. Visser, E. Otten, B. L. Feringa, *J. Am. Chem. Soc.* **2017**, *139*, 9650-9661; d) D. R. S. Pooler, A. S. Lubbe, S. Crespi, B. L. Feringa, *Chem. Sci.* **2021**, *12*, 14964-14986.

[64] a) H. Qian, S. Pramanik, I. Aprahamian, *J. Am. Chem. Soc.* **2017**, *139*, 9140-9143; b) M. Jeong, J. Park, Y. Seo, K. Lee, S. Pramanik, S. Ahn, S. Kwon, *Chem. Eur. J.* **2022**, *28*, e202103972; c) A. Ryabchun, Q. Li, F. Lancia, I. Aprahamian, N. Katsonis, *J. Am. Chem. Soc.* **2019**, *141*, 1196-1200.

[65] P. Kuad, A. Miyawaki, Y. Takashima, H. Yamaguchi, A. Harada, *J. Am. Chem. Soc.* **2007**, *129*, 12630-12631.

[66] F. Xu, L. Pfeifer, S. Crespi, F. King-Chi Leung, M. C. A. Stuart, S. J. Wezenberg, B. L. Feringa, *J. Am. Chem. Soc.* **2021**, *143*, 5990-5997.

[67] J. Chen, F. K.-C. Leung, M. C. A. Stuart, T. Kajitani, T. Fukushima, E. van der Giessen, B. L. Feringa, *Nat. Chem.* **2018**, *10*, 132-138.

from the extended to the contracted form. Moreover, the group of E. W. Meijer synthetized hydrazone monomers that isomerize between the *E*- and *Z*-isomer when irradiated with the appropriate light wavelength (Figure 9B).[68] The geometry of the *Z*-isomer monomer provides shorter supramolecular polymers due to the capping properties of this isomer.

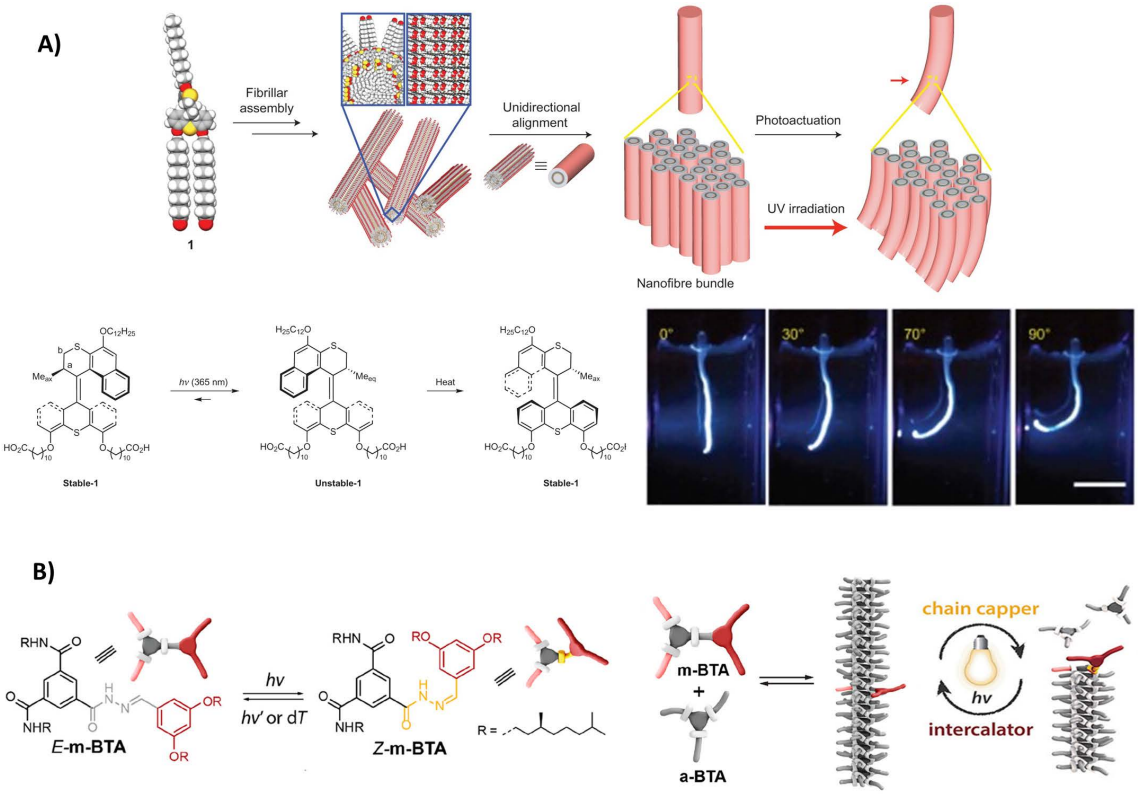

Figure 9. (A) Photoactuation of a molecular motor and bending of its macroscopic strings. Scale bar, 0.5 cm. Adapted with permission from Ref. 67. Copyright © 2018 Springer Nature. (B) Control of the chain length in a supramolecular polymer by the *E* to *Z* photo-isomerization of a hydrazone chain capper. Adapted with permission from Ref. 68. Copyright © 2020 American Chemical Society.

4.2.2. Molecular photoswitches based on photocyclization reactions

Another type of photo-switching mechanism is the photocyclization reactions.[37] One of the most relevant examples are diarylethenes (DAEs), which can be converted from the open to the closed form by a 6π-electrocyclization reaction when irradiated with UV light. The process can be reverted by a ring-opening reaction promoted with visible light. Moreover, this molecular photoswitch is characterized by a good thermal stability and fatigue resistance.[69]

[37] J. Volarić, W. Szymanski, N. A. Simeth, B. L. Feringa, *Chem. Soc. Rev.* **2021**, *50*, 12377-12449.
[67] J. Chen, F. K.-C. Leung, M. C. A. Stuart, T. Kajitani, T. Fukushima, E. van der Giessen, B. L. Feringa, *Nat. Chem.* **2018**, *10*, 132-138.
[68] E. Weyandt, G. M. ter Huurne, G. Vantomme, A. J. Markvoort, A. R. A. Palmans, E. W. Meijer, *J. Am. Chem. Soc.* **2020**, *142*, 6295-6303.
[69] a) H. Tian, S. Yang, *Chem. Soc. Rev.* **2004**, *33*, 85-97; b) J. Zhang, H. Tian, *Adv. Optical Mater.* **2018**, 1701278; c) H. Cheng, S. Zhang, E. Bai, X. Cao, J. Wang, J. Qi, J. Liu, J. Zhao, L. Zhang, J. Yoon, *Adv. Mater.* **2022**, *34*, 2108289.

In this context, the group of W. Zhu modified a DAE with two S- or R-phenylalanines and two naphthalimide chromophores to obtain a supramolecular helical material (Figure 10A).[70] The open form of the DAE self-assembles into a helix stabilized by intermolecular hydrogen bonds between carboxylic acids. The left- or right-handed twist of the helix is determined by the chirality of the amino acid, while the DAE provides light control of the assembly and disassembly process. Alternatively, the group of H. Tian reported a benzene-1,3,5-tricarboxamide (BTA) molecule modified with three DAEs, whose photocyclization can be used to regulate its disassembly and reassembly into microrods in a reversible way (Figure 10B).[71]

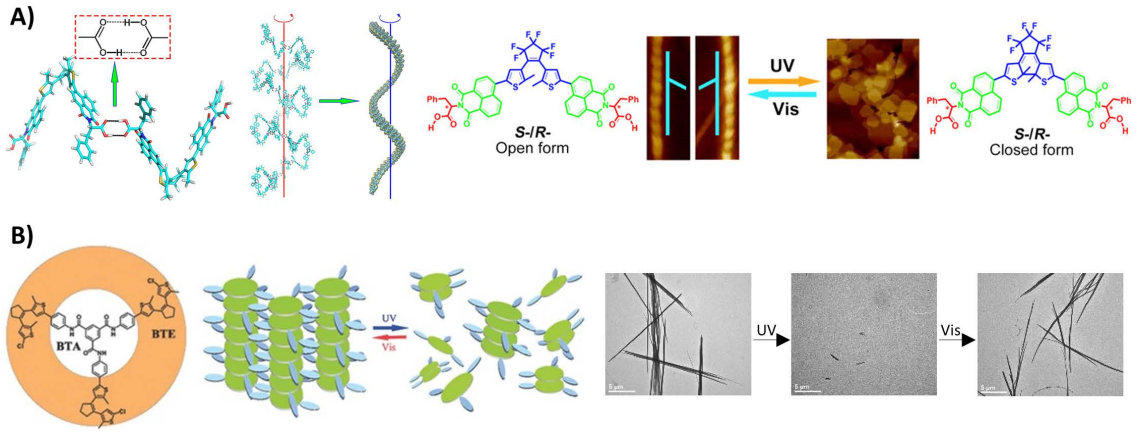

Figure 10. (A) Light-induced assembly/disassembly of a modified DAE into a helical structure. Adapted with permission from Ref. 70. Copyright © 2016 American Chemical Society. (B) Photo-assembling BTA molecule modified with DAEs for obtaining microrods. Adapted with permission from Ref. 71. Copyright © 2016 Wiley-VCH Verlag GmbH & Co.

4.2.3. Molecular photoswitches based on the combination of mechanisms

A mechanism of photo-responsiveness is also the combination of different switching processes.[37] One example is spiropyran (SP), which is based on the heterolytic cleavage of a C-O bond upon UV light irradiation to provide the open-ring merocyanine (MC), followed by *Z-E* isomerization of the central double bond.[72] The process can be reverted spontaneously or by irradiation with visible light. In addition, this photoswitching is associated with a proton release or capture. For example, the group of Samuel I. Stupp reported the contraction or expansion of spiropyran hydrogels by means of light irradiation (Figure 11A).[73] In particular, polymeric hydrogels with a sulfonated spiropyran expand in the opposite direction to the light source, while a design without the sulfonic group contracts towards the light. More recently, they have

[37] J. Volarić, W. Szymanski, N. A. Simeth, B. L. Feringa, *Chem. Soc. Rev.* **2021**, *50*, 12377-12449.
[70] Y. Cai, Z. Guo, J. Chen, W. Li, L. Zhong, Y. Gao, L. Jiang, L. Chi, H. Tian, W. Zhu, *J. Am. Chem. Soc.* **2016**, *138*, 2219-2224.
[71] T. Li, X. Li, J. Wang, H. Ågren, X. Ma, H. Tian, *Adv. Optical Mater.* **2016**, *4*, 840-847.
[72] a) R. Klajn, *Chem. Soc. Rev.* **2014**, *43*, 148-184; b) L. Kortekaas, W. R. Browne, *Chem. Soc. Rev.* **2019**, *48*, 3406-3424; c) J. K. Rad, Z. Balzade, A. R. Mahdavian, *J. Photochem. Photobiol. C.* **2022**, *51*, 100487.
[73] C. Li, A. Iscen, L. C. Palmer, G. C. Scharz, S. I. Stupp, *J. Am. Chem. Soc.* **2020**, *142*, 8447-8453.

also developed a hybrid material which contains amphiphilic peptide assemblies to reinforce the bending motion.[74] Also, the group of T. Aida discovered the light-controlled supramolecular polymerization to form nanotubes of a barrel-shaped chaperonin protein that was modified with a spiropyran moiety (Figure 11B).[75] The ionic merocyanine unit is generated by irradiation with UV light, allowing the generation of nanotubes due to the formation of Mg^{2+} bridges between different units. Moreover, these nanotubes can be dissociated into the non-ionic spiropyran monomers when irradiated with visible light. In another example, the group of D. L. Officer published the 3D movement of photoactive spiropyran organic droplets through water, which can be moved in any direction just by using the appropriate light irradiation (Figure 11C).[76]

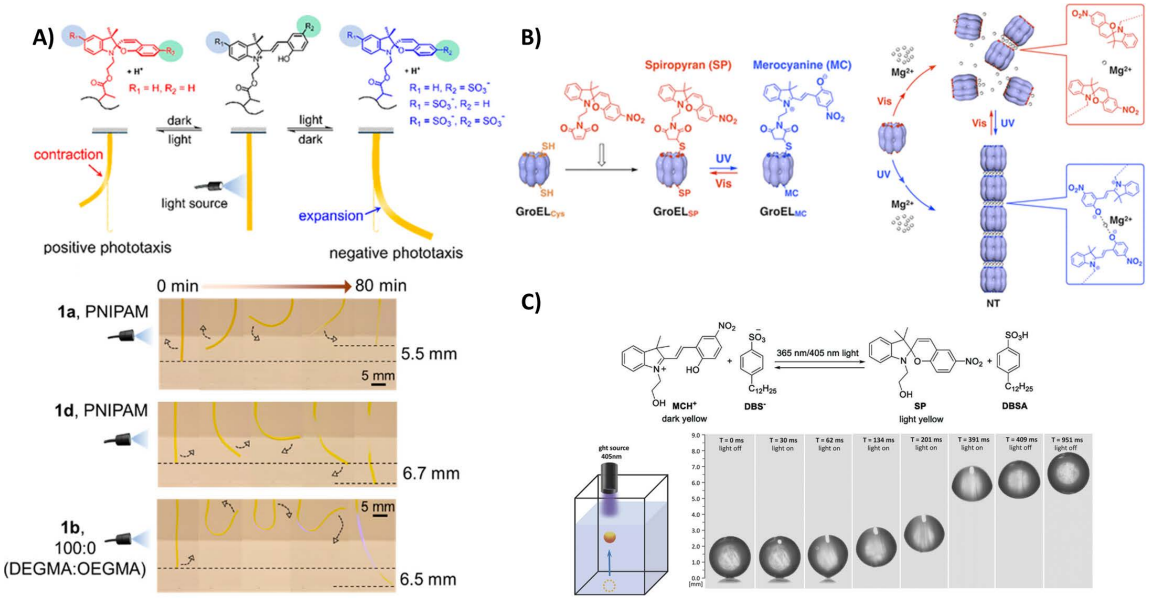

Figure 11. (A) Photo-contraction or photo-expansion of spiropyran hydrogels. Adapted with permission from Ref. 73. Copyright © 2020 American Chemical Society. (B) Light-controlled formation and dissociation of chaperonin nanotubes. Adapted with permission from Ref. 75 Copyright © 2013 American Chemical Society. (C) Photo-induced movement in water of a spiropyran-based organic droplet. Adapted with permission from Ref. 76. Copyright © 2018 Wiley-VCH Verlag GmbH & Co.

In a similar manner, fulgides and fulgimides contain a 6π-electron core which can undergo a *Z-E* isomerization of the central double bond, followed by a ring-opening/closing reaction under appropriate light irradiation.[77] However, fewer applications have been developed for these photoswitches so far. The most notably ones are their use in surface processes or for optical memory applications.[78]

[73] C. Li, A. Iscen, L. C. Palmer, G. C. Scharz, S. I. Stupp, *J. Am. Chem. Soc.* **2020**, *142*, 8447-8453.
[74] C. Li, Q. Xiong, T. D. Clemons, H. Sai, Y. Yang, M. H. Sangji, A. Iscen, L. C. Palmer, G. C. Schatz, S. I. Stupp, *Chem. Sci.* **2023**, *14*, 6095-6104.
[75] T. Sendai, S. Biswas, T. Aida, *J. Am. Chem. Soc.* **2013**, *135*, 11509-11512.
[76] Y. Xiao, S. Zarghami, K. Wagner, P. Wagner, K. C. Gordon, L. Florea, D. Diamond, D. L. Officer, *Adv. Mater.* **2018**, *30*, 1801821.
[77] R. Matsushima, H. Sakaguchi, *J. Photochem. Photobiol.* A, **1997**, *108*, 239-245.
[78] a) M. Vlajić, W. Unger, J. Bruns, K. Rueck-Braun, *Appl. Surf. Sci.* **2019**, *465*, 686-692; b) S. Klaes, C. Henry-de-Villeneuve, F. Ozanam, C. Barta, K. Rück-Braun, R. Métivier, P. Allongue, *J. Phys. Chem. C* **2019**, *123*, 12223-12233; c) Y. Jiao, R. Yang, Y. Luo, L. Liu, B. Xu, W. Tian, *CCS Chem.* **2022**, *4*, 132-140.

4.3. STIMULI-RESPONSIVE SYSTEMS FOR ANTICANCER DRUG DELIVERY

Cancer is one of the main diseases affecting the world population, with an expected increase in the number of people affected in the next few years.[79] The clinical application of conventional anticancer drugs is limited by their reduced cellular internalization, their lack of selectivity and the appearance of drug resistance phenomena after prolonged treatments.[80] This resistance usually arises from the overexpression of efflux pumps in the cancer cell membrane, which are able to expel the drug from the target cell.[81] Moreover, many of the current pharmaceutical agents interact with the healthy cells before reaching the cancer cells, requiring high doses and causing serious side effects. Consequently, there has been a significant interest in the development of novel chemical systems that can selectively transport and release the already existing antitumour drugs inside cancer cells.[82]

A "drug delivery system" is defined as a formulation that releases a therapeutic agent in a controlled manner at the targeted site of action to enhance its efficacy (Figure 12).[83] In an optimal situation, the drug delivery system would facilitate the targeted release of the therapeutic agent, avoiding interactions with healthy cells. In this way, this type of systems would have the potential to reduce the adverse effects associated with current treatments.[82,83]

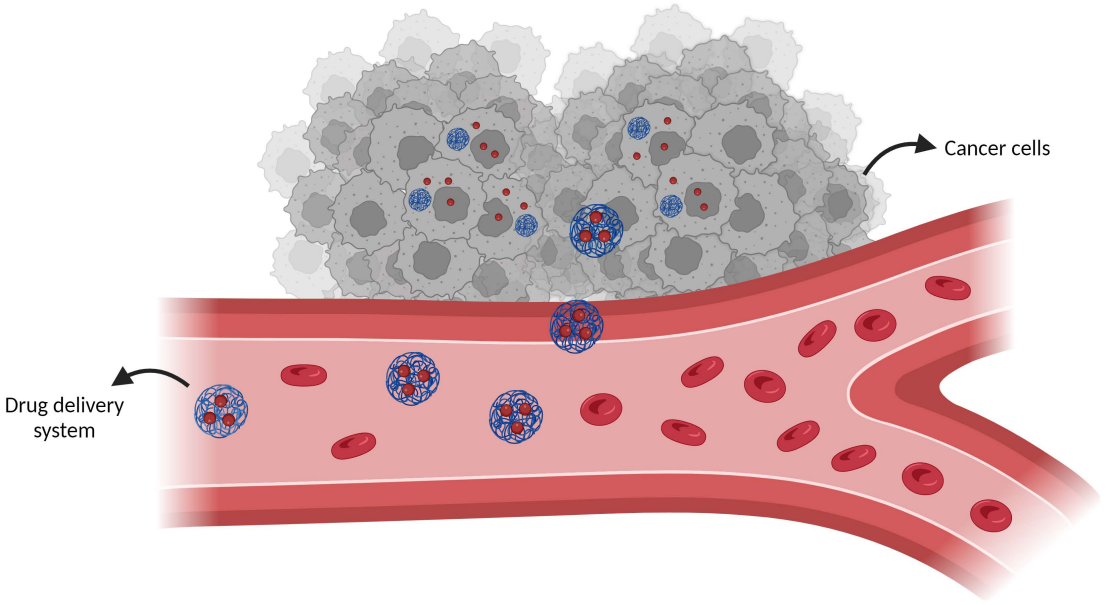

Figure 12. Schematic representation of the circulation of a drug delivery system in the bloodstream and the selective release of the drug at the site of action. Figure created with Biorender.com.

[79] E. Weiderpass, B. W. Stewart, World Cancer Report, **2020** (IARC Press, Lyon, 2020).
[80] N. Vasan, J. Baselga, D. M. Hyman, *Nature* **2019**, *575*, 299-309.
[81] M. M. Gottesman, T. Fojo, S. E. Bates, *Nat. Rev. Cancer* **2002**, *2*, 48-58.
[82] a) D. Peer, J. Karp, S. Hong, O. Farokhzard, R. Margalit, R. Langer, *Nat. Nanotechnol.* **2007**, *2*, 751-760; b) S. Senapati, A. K. Mahanta, S. Kumar, P. Maiti, *Sig. Transduct. Target. Ther.* **2018**, *3*, 7; c) A. M. Vargason, A. C. Anselmo, S. Mitragotri, *Nat. Biomed. Eng.* **2021**, *5*, 951-967; d) W. Li, J. Tang, D. Lee, T. R. Tice, S. P. Schwendeman, M. R. Prausnitz, *Nat. Rev. Mater.* **2022**, *7*, 406-420; e) J. Gao, J. M. Karp, R. Langer, N. Joshi, *Chem. Mater.* **2023**, *35*, 359-363.
[83] K. K. Jain, *Drug Delivery Systems-An Overview* in *Drug Delivery Systems*. Eds. K. K. Jain. Humana Press: Totowa, **2008**, pp. 1-50.

The concept of drug delivery appeared in 1952 with the development of a formulation for the time-controlled release of Dextroamphetamine (Dexedrine).[84] In particular, this first design incorporated a coating barrier to protect the drug and provide a controlled release mechanism. Since then, this technology has evolved until achieving the nanoscale manipulation of transport systems. Currently, there are many examples of drug delivery systems based on structures such as liposomes, micelles, nanoparticles or hydrogels, among others (Figure 13).[82,83] In fact, some of them have already been approved for their clinical use in humans.

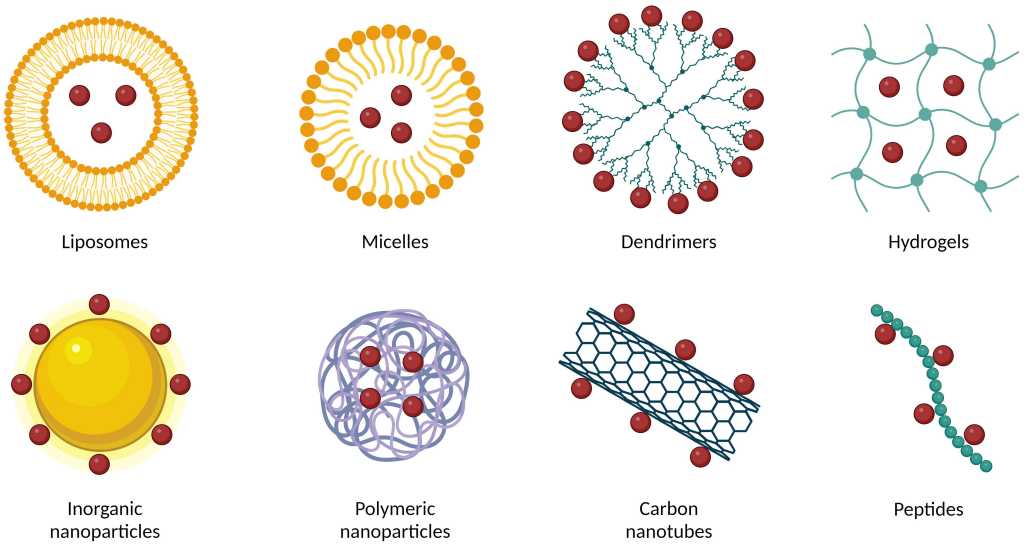

Figure 13. Schematic representation of different formulations of drug delivery systems. Figure created with Biorender.com.

Liposomes are ideal nanocarriers for the encapsulation of hydrophilic or lipophilic drugs due to their phospholipid bilayer that provides a hydrophilic core.[85] These liposomes are characterized by their excellence biocompatibility, while the encapsulation of the drug protects it from degradation and enhances its half-life. For example, Doxil® was the first liposome-based delivery system.[86] It consists of a formulation to encapsule the anticancer drug doxorubicin (DOX), which is commonly used for the treatment of ovarian cancer, metastatic breast cancer, Kaposi´s sarcoma or myeloid melanoma. **Micelles** have also been proposed as a potential solution for the transport of hydrophobic drugs.[87] In this regard, some amphiphilic polymers are able to

[82] a) D. Peer, J. Karp, S. Hong, O. Farokhzard, R. Margalit, R. Langer, *Nat. Nanotechnol.* **2007**, *2*, 751-760; b) S. Senapati, A. K. Mahanta, S. Kumar, P. Maiti, *Sig. Transduct. Target. Ther.* **2018**, *3*, 7; c) A. M. Vargason, A. C. Anselmo, S. Mitragotri, *Nat. Biomed. Eng.* **2021**, *5*, 951-967; d) W. Li, J. Tang, D. Lee, T. R. Tice, S. P. Schwendeman, M. R. Prausnitz, *Nat. Rev. Mater.* **2022**, *7*, 406-420; e) J. Gao, J. M. Karp, R. Langer, N. Joshi, *Chem. Mater.* **2023**, *35*, 359-363.

[83] K. K. Jain, *Drug Delivery Systems-An Overview* in *Drug Delivery Systems*. Eds. K. K. Jain. Humana Press: Totowa, **2008**, pp. 1-50.

[84] a) R.H. Blythe (**1956**). *Sympathomimetic Preparation* (U.S. Patent No. US2738303A). United States Patent Office; b) K. Park, *J. Control. Release* **2014**, *190*, 3-8; c) H. Park, A. Otte, K. Park, *J. Control Release* **2022**, *342*, 53-65.

[85] a) T. M. Allen, P. R. Cullis, *Adv. Drug Deliv. Rev.* **2013**, *65*, 36-48; b) S. Saraf, A. Jain, A. Tiwari, A. Verma, P. K. Panda, S. K. Jain, *Drug Deliv. Sci. Technol.* **2020**, *56*, 101549; c) D. Guimarães, A. Cavaco-Paulo, E. Nogueira, *Int. J. Pharm.* **2021**, *601*, 120571.

[86] Y. Barenholz, *J. Control Release* **2012**, *160*, 117-134.

[87] a) Z. Ahmad, A. Shah, M. Siddiq, H. Kraatz, *RSC Adv.* **2014**, *4*, 17028-17038; b) D. Hwang, J. D. Ramsey, A. V. Kabanov, *Adv. Drug Deliv. Rev.* **2020**, *156*, 80-118.

assemble into micelles in aqueous environments providing a suitable pocket for the encapsulation of non-polar drugs, proteins or DNA. **Dendrimers** represent another interesting strategy for the development of drug delivery nanostructures due to their low polydispersity and their excellent biocompatibility.[88] **Hydrogels** are a biocompatible tool for the transport of hydrophilic drugs due to their high water content.[89] **Inorganic or polymeric nanoparticles** have also been exploited due to the possibility of modifying their size, shape and properties to enhance the stability of the cargo, the transport across biological barriers or increase the circulation time.[90] **Carbon nanotubes** have been functionalized to make them soluble in water and to load them with drugs.[91] **Peptides** have also been proposed as drug delivery systems based on their structural versatility, their high biocompatibility, their ability to reduce drug toxicity and their high delivery efficiency.[92]

Some of these delivery systems have the limitations of a low solubility, instability in the body, difficulties in crossing natural barriers or reduced biocompatibility and specificity.[93] As a result, a wide range of drug delivery vehicles have been chemically modified with "targeting agents" to increase their efficacy.[94] It consists mainly of using molecules that are specifically recognized by receptors overexpressed on the surface of tumour cells (Figure 14). The ligand-receptor interactions facilitate the internalisation of the vector into the cell, thus enhancing the release of the drug.

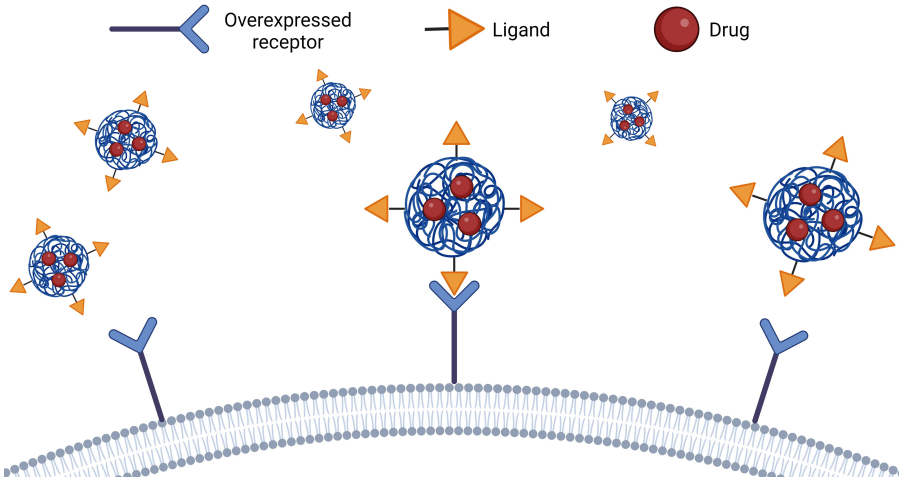

Figure 14. Ligand-receptor interaction for the targeting of a drug delivery system to a cancer cell. Figure created with Biorender.com.

[88] a) P. Kesharwani, K. Jain, N. K. Jain, *Prog. Polym. Sci.* **2014**, *39*, 268-307; b) A. Caminade, C. Turrin, *J. Mater. Chem. B* **2014**, *2*, 4055-4066; c) H. Wang, Q. Huang, H. Chang, J. Xiao, Y. Cheng, *Biomater. Sci.* **2016**, *4*, 375-390.
[89] a) J. Li, D. J. Mooney, *Nat. Rev. Mater.* **2016**, 16071; b) Z. Sun, C. Song, C. Wang, Y. Hu, J. Wu, *Mol. Pharmaceutics* **2020**, *17*, 373-391.
[90] a) D. Bobo, K. J. Robinson, J. Islam, K. J. Thurecht, S. R. Corrie, *Pharm. Res.* **2016**, *33*, 2373-2387; b) M. J. Mitchell, M. M. Billingsley, R. M. Haley, M. E. Wechsler, N. A. Peppas, R. Langer, *Nat. Rev. Drug Discov.* **2021**, *20*, 101-124; c) M. A. Beach, U. Nayanathara, Y. Gao, C. Zhang, Y. Xiong, Y. Wang, G. K. Such, *Chem. Rev.* **2024**, *124*, 5505-5616.
[91] W. Zhang, Z. Zhang, Y. Zhang, *Nanoscale Res. Lett.* **2011**, *6*, 555.
[92] a) Z. Song, X. Chen, X. You, K. Huang, A. Dhinakar, Z. Gu, J. Wu, *Biomater. Sci.* **2017**, *5*, 2369-2380; b) Z. Lian, T. Ji, *J. Mater. Chem. B* **2020**, *8*, 6517-6529; c) J. Yang, H. An, H. Wang, *ACS Appl. Bio Mater.* **2021**, *4*, 24-46; d) Y. Zhu, K. Tang, J. Lv, *Trends Pharmacol. Sci.* **2021**, *42*, 857-869.
[93] T. Christian Ezike, U. S. Okpala, U. L. Onoja, C. P. Nwike, E. C. Ezeako, O. J. Okpara, C. C. Okoroafor, S. C. Eze, O. L. Kalu, E. C. Odoh, U. G. Nwadike, J. O. Ogbodo, B. U. Umeh, E. C. Ossai, B. C. Nwangumaa, *Heliyon* **2023**, *9*, e17488.
[94] M. T. Manzari, Y. Shamay, H. Kiguchi, N. Rosen, M. Scaltriti, D. A. Heller, *Nat. Rev. Mater.* **2021,** *6*, 351-370.

One targeting option is to modify the systems with antibodies that are capable of specifically binding to overexpressed antigens on the surface of cancer cells.[95] While the drug exerts anti-tumour activity, the antibody confers specificity. For example, the epidermal growth factor receptor (EGFR) is overexpressed on pancreatic tumour cells and can be recognised by the C225 antibody. In one study, polymeric micelles containing the anticancer drug Gemcitabine were modified on their outer surface with this antibody to increase their efficacy.[96]

Another targeting strategy is to exploit the overexpression of specific receptors on the membrane of tumour cells. For example, the folate receptor (FR) is overexpressed in several types of cancer and, as a consequence, many transport systems have been modified with folic acid or monoclonal antibodies against FR to increase their activity.[97] Another commonly overexpressed receptor is the $\alpha_v\beta_3$ integrins, which can be recognised by the RGD (arginine-glycine-aspartic acid) tripeptide, especially in its cyclic form. The incorporation of this cyclic peptide into drug delivery systems has been widely used to improve their efficacy and tumour penetration.[98]

In this context, single- or multi-stimulus responsive designs have emerged as one of the most promising alternatives in this field. These systems are usually designed to release the entrapped drug in response to intrinsic stimuli, such as variations in pH, redox conditions and enzymes, or externally applied stimuli, such as magnetic fields, light or ultrasounds.[99,100]

4.3.1. pH-responsive drug delivery systems

A wide variety of delivery systems take advantage of the slight pH difference between healthy cells (extracellular pH ≈ 7.4 and intracellular pH ≈ 7.2) and tumour cells (extracellular pH ≈ 6.7-7.1 and intracellular pH ≥ 7.2) to trigger the controlled release of the cargo.[101] Also, lysosomes and late endosomes are characterized by a lower pH (4.5-5.5) compared to other subcellular compartments, which is of special relevance as many delivery systems are internalised via an endocytosis pathway.[102] Based on these differences, two main strategies have been developed: structures that

[95] J. Di, F. Xie, Y. Xu, *Adv. Drug Deliv. Rev*. **2020**, *154-155*, 151-162.
[96] G. Mondal, S. Almawash, A. K. Chaudhary, R. I. Mahoto, *Mol. Pharmaceutics* **2017**, *14*, 3121-3133.
[97] a) J. Sudimack, R. J. Lee, *Adv Drug Deliv Rev.* **2000**, *41*, 147-162; b) M. Ahmadi, C. A. Ritter, T. von Woedtke, S. Bekeschus, K. Wende, *Chem. Sci.* **2024**, *15*, 1966-2006.
[98] a) Y. Sun, C. Kang, F. Liu, Y. Zhou, L. Luo, H. Qiao, *Drug Dev. Res.* **2017**, *78*, 283-291; b) Y. Cheng, Y. Ji, *Eur. J. Pharm. Sci.* **2019**, *128*, 8-17.
[99] S. Mura, J. Nicolas, P. Couvreur, *Nat. Mater.* **2013**, *12*, 991-1003.
[100] a) C. Álvarez-Lorenzo, A. Concheiro, *Chem. Commun.* **2014**, *50*, 7743-7765; b) V. P. Torchilin, *Fundamentals of Stimuli-responsive Drug and Gene Delivery Systems* in *Stimuli-responsive Drug Delivery Systems*. Eds. A. Singh, M. M. Amiji. Royal Society of Chemistry, **2018**, 1-32.
[101] a) B. A. Webb, M. Chimenti, M. P. Jacobson, D. L. Barber, *Nat. Rev. Cancer* **2011**, *11*, 671-677; b) J. Liu, Y. Huang, A. Kumar, A. Tan, S. Jin, A. Mozhi, X. Liang, *Biotechnol. Adv.* **2014**, *32*, 693-710.
[102] a) I. Mellman, R. Fuchs, A. Helenius, *Ann. Rev. Biochem.* **1986**, *55*, 663-670; b) X. He, J. Li, S. An, C. Jiang, *Ther. Deliv.* **2013**, *4*, 1499-1510; c) Z. Kaźmierczak, K. Szostak-Paluch, M. Przybyło, M. Langner, W. Witkiewicz, N. Jędruchniewicz, K. Dąbrowska, *Bioorg. Med. Chem.* **2020**, *28*, 115556.

undergo a pH-dependent conformational change or the use of components containing acid-labile bonds that are broken to release the attached drugs.[99]

Probably the most remarkable systems of the first alternative are the amphiphilic polymers capable of self-assembling into micelles.[103] This property allows the encapsulation of drugs in the hydrophobic cavity at physiological pH. However, at the slightly acidic pH of tumour cells, ionization of some of the functional groups of the polymer takes place, usually imidazole moieties, leading to destabilisation of the micelle and release of the drug into the cell medium. For example, the group of V. P. Torchilin used this strategy to develop a micelle based on three grafted copolymers for the encapsulation and pH-controlled release of the anticancer drug paclitaxel (Figure 15).[104]

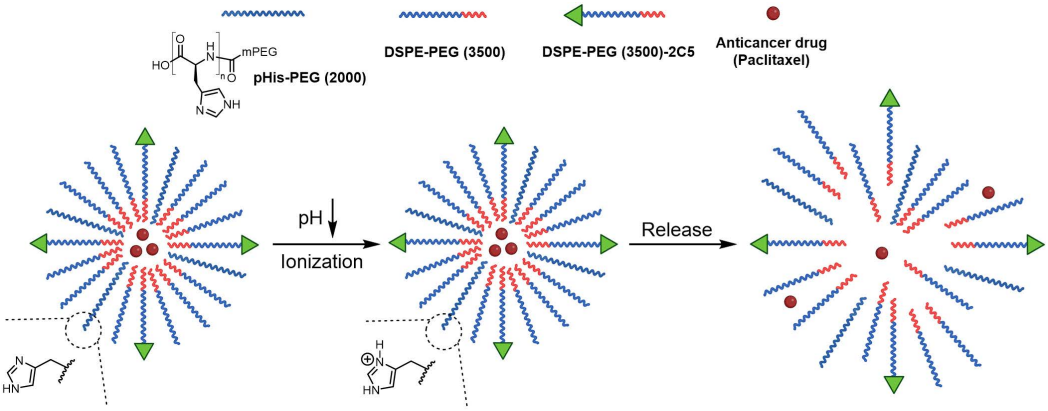

Figure 15. pH-sensitive polymeric micelle based on ionization of histidine residues. Adapted with permission from Ref. 104. Copyright © 2013 Elsevier.

On the other hand, acid-labile bonds can be used to attach the drugs to the nanocarriers. As a result, these bonds are selectively cleavage in the tumour environment releasing the active form. Suitable bonds for this purpose are vinyl ethers,[105] imines,[106] oximes,[107] hydrazones[108] or ortho esters[109], among others.[110] Each

[99] S. Mura, J. Nicolas, P. Couvreur, *Nat. Mater.* **2013**, *12*, 991-1003.

[103] a) D. Kim, E. S. Lee, K. T. Oh, Z. G. Gao, Y. H. Bae, *Small* **2008**, *4*, 2043-2050; b) B. Zhao, Y. Zhao, Y. Huang, L. Luo, P. Song, X. Wang, S. Chen, K. Yu, X. Zhang, Q. Zhang, *Biomaterials* **2012**, *33*, 2508-2520; c) W. Hao, D. Liu, Y. Shang, J. Zhang, S. Xu, H. Liu, *RSC Adv.* **2016, *6*,** 29149-29158.

[104] H. Wu, L. Zhu, V. P. Torchilin, *Biomaterials* **2013**, 34, 1213-1222.

[105] a) J. Shin, P. Shum, D. H. Thompson, *J. Control Release* **2003**, *91*, 187-200; b) J. A. Boomer, M. M. Qualls, H. D. Inerowicz, R. H. Haynes, V. S. Patri, J. Kim, D. H. Thompson, *Bioconjugate Chem.* **2009**, *20*, 47-59; c) H. Kim, J. Van den Bossche, S. Hyun, D. H. Thompson, *Bioconjugate Chem.* **2012**, *23*, 2071-2077; d) J. Shin, P. Shum, J. Grey, S. Fujiwara, G. S. Malhotra, A. González-Bonet, S. Hyun, E. Moase, T. M. Allen, D. H. Thompson, *Mol. Pharmaceutics* **2012**, *9*, 3266-3276.

[106] a) C. Ding, J. Gu, X. Qu, Z. Yang, *Bioconjugate Chem.* **2009**, *20*, 1163-1170; b) X. Qu, Z. Yang, *Chem. Asian J.* **2016**, *11*, 2633-2641; c) X. Zeng, G. Liu, W. Tao, Y. Ma, X. Zhang, F. He, J. Pan, L. Mei, G. Pan, *Adv. Funct. Mater.* **2017**, *27*, 1605985.

[107] Y. Jin, L. Song, Y. Su, L. Zhu, Y. Pang, F. Qiu, G. Tong, D. Yan, B. Zhu, X. Zhu, *Biomacromolecules* **2011**, *12*, 3460-3468.

[108] a) J. B. Matson, S. I. Stupp, *Chem. Commun.* **2011**, *47*, 7962-7964; b) S. J. Sonawane, R. S. Kalhapure, T. Govender, *Eur. J. Pharm. Sci.* **2017**, *99*, 45-65; c) J. Wahbeh, S. Milkowski, *SLAS Technol.* **2019**, *24*, 161-168.

[109] a) L. Li, K. Knickelbein, L. Zhang, J. Wang, M. Obrinske, G. Z. Ma, L. Zhang, L. Bitterman, W. Du, *Chem. Commun.* **2015**, *51*, 13078-13081; c) G. Yan, J. Wang, P. Zhang, L. Hu, X. Wang, G. Yang, S. Fu, X. Cheng, R. Tang, *Polym. Chem.* **2017**, *8*, 2063-2073; c) M. Sun, D. Li, X. Wang, L. He, X. Lv, Y. Xu, R. Tang, *J. Mater. Chem. B* **2019**, *7*, 3692-3703.

[110] a) Z. Shi, Q. Li, L. Mei, *Chin. Chem. Lett.* **2020**, *31*, 1345-1356; b) H. Ding, P. Tan, S. Fu, X. Tian, H. Zhang, X. Ma, Z. Gu, K. Luo, *J. Control Release* **2022**, *348*, 206-238.

of them is characterised by a pH-dependent release rate, allowing a greater variety of options when creating new designs. In particular, the use of hydrazones to conjugate the drug doxorubicin should be highlighted, since multiple formulations have been developed with this drug conjugated through a hydrazone to structures of different nature.[111] In this regard, the group of J. Wang reported polymeric nanoparticles in which doxorubicin is conjugated with a hydrazone bond (Figure 16A).[112] These structures can respond to the extracellular pH to enhance cellular uptake by changing their surface charge and to trigger the intracellular drug release at the lower pH inside endosomes and lysosomes. This acid-triggered drug release was able to cause the death of drug-resistant cancer stem cells. Also, the same group proposed the hydrazone-bonded incorporation of doxorubicin to gold nanoparticles for overcoming drug resistance (Figure 16B).[113] In another example, the group of R. Zhao published the hydrazone conjugation of doxorubicin to a tumour-targeting peptide which increases drug specificity (Figure 16C).[114] This conjugate presented a good stability at neutral pH and a fast drug release under slightly acidic conditions.

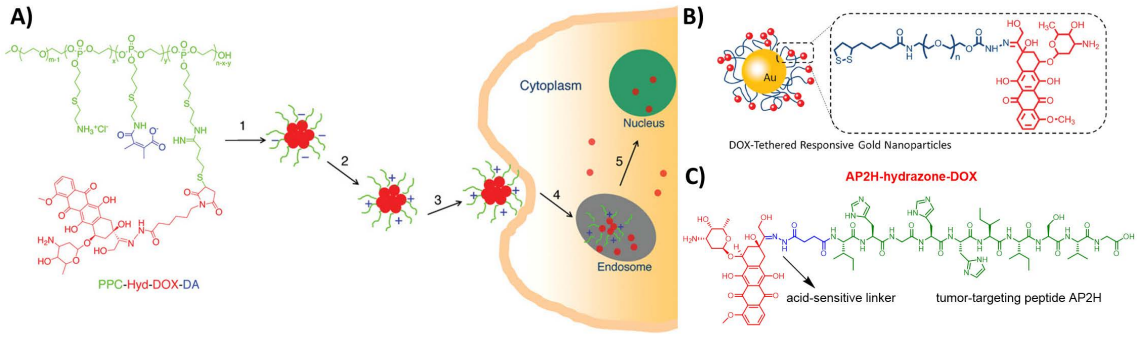

Figure 16. (A) Release of doxorubicin conjugated to a polymeric nanoparticle by cleavage of a hydrazone bond under acidic endosome conditions. Reprinted with permission from Ref. 112. Copyright © 2011 American Chemical Society. (B) Doxorubicin conjugation to gold nanoparticles through a hydrazone bond. Reprinted with permission from Ref. 113. Copyright © 2011 American Chemical Society. (C) Chemical structure of a tumour-targeting peptide modified with a hydrazone-bonded doxorubicin. Adapted with permission from Ref. 114. Copyright © 2015 Royal Society of Chemistry.

There are also some examples of pH-sensitive systems that transport simultaneously more than one compound. That is the case of the polymeric micelles reported by the group of Y. Li capable of encapsulating disulfiram (DSF), which is a cell resistance modulator, while transporting doxorubicin via hydrazone bonding (Figure 17).[115] The resulting micelle allows the rapid release of disulfiram causing the inhibition

[111] a) C. Lee, S. Cheng, I. Huang, J. S. Souris, C. Yang, C. Mou, L. Lo, *Angew. Chem. Int. Ed.* **2010**, *49*, 8214-8219; b) D. Ren, F. Kratz, S. Wang, *Small* **2011**, *7*, 1051-1560; c) V. Rao N, S. R. Mane, A. Kishore, J. D. Sarma, R. Shunmugam, *Biomacromolecules* **2012**, *13*, 221-230; d) J. D. Wallat, J. K. Harrison, J. K. Pokorski, *Mol. Pharmaceutics* **2018**, *15*, 2954-2962; e) H. Cai, P. Tan, X. Chen, M. Kopytynski, D. Pan, X. Zheng, L. Gu, Q. Gong, X. Tian, Z. Gu, H. Zhang, R. Chen, K. Luo, *Adv. Mater.* **2022**, *34*, 2108049.
[112] J. Du, X. Du, X. Mao, J. Wang, *J. Am. Chem. Soc.* **2011**, *133*, 17560-17563.
[113] F. Wang, Y. Wang, S. Dou, M. Xiong, T. Sun, J. Wang, *ACS Nano* **2011**, *5*, 3679-3692.
[114] Y. Jin, Y. Huang, H. Yang, G. Liu, R. Zhao, *Chem. Commun.* **2015**, *51*, 14454-14457.
[115] X. Duan, J. Xiao, Q. Yin, Z. Zhang, H. Yu, S. Mao, Y. Li, *ACS Nano* **2013**, *7*, 5858-5869.

of the activity of the P-gp glycoprotein responsible of the resistance. On the other hand, doxorubicin is released gradually over time, increasing its accumulation in the cell and its therapeutic efficacy. This system resulted to be an excellent inhibitor of the growth of doxorubicin-resistant breast cancer cells through the combined action of the two drugs.

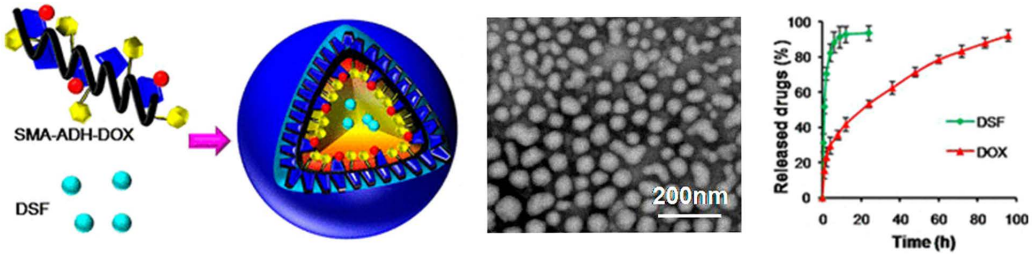

Figure 17. DSF and DOX transport with polymeric micelles for a combinatorial treatment of cancer cells. Adapted with permission from Ref. 115. Copyright © 2013 American Chemical Society.

4.3.2. Redox-responsive drug delivery systems

Disulphide bonds have been widely used to obtain redox-sensitive structures due to their rapid reduction and cleavage in the presence of the tripeptide glutathione (GSH). Intracellular compartments such as the cytosol, mitochondria or nucleus contain a higher concentration of GSH (≈ 2-10 mM) than extracellular fluids (≈ 2-20 μM).[116] For this reason, while pH-sensitive vehicles are mainly designed to release the drug into the acidic environment of endosomes and lysosomes, redox-sensitive delivery systems usually release the drug into the cytosol of the tumour cell.

Based on the characteristics of the disulphide bond, it has been mostly used in peptides, micelles and nanoparticles.[117] One example is a supramolecular strategy developed by the group of H. Cui for the transport of the anticancer drug camptothecin (CPT) with amphiphilic peptide structures (Figure 18A).[118] Depending on the number of drug molecules attached to the peptide, it self-assembles into nanotubes or nanofibers. These nanostructures showed a good activity against cancer cells due to the effective release of the drug in the presence of GSH. In another example, the group of J. Yang prepared polymeric nanoparticles in which again camptothecin is conjugated with a disulphide bond (Figure 18B).[119] Interestingly, these nanoparticles also allowed the drug doxorubicin to be encapsulated. The cleavage of the disulphide bond with GSH releases the drug camptothecin into the cytoplasm and triggers the disassembly of the nanoparticle for DOX release. Consequently, a higher activity is achieved as a result of the combined release and effect of both drugs.

[115] X. Duan, J. Xiao, Q. Yin, Z. Zhang, H. Yu, S. Mao, Y. Li, *ACS Nano* **2013**, *7*, 5858-5869.
[116] R. Cheng, F. Feng, F. Meng, C. Deng, J. Feijen, Z. Zhong, *J. Control. Release* **2011**, *152*, 2-12.
[117] a) J. Wu, L. Zhao, X. Xu, N. Bertrand, W. Choi, B. Yammen, J. Shi, V. Shah, M. Mulvale, J. L. MacLean, O. C. Farokhzad, *Angew. Chem. Int. Ed.* **2015**, *54*, 9218-9223; b) N. Liu, Y. Tan, Y. Hu, T. Meng, L. Wen, J. Liu, B. Cheng, H. Yuan, X. Huang, F. Hu, *ACS Appl. Mater. Interfaces* **2016**, *8*, 33148-33156; c) X. He, K. Cai, Y. Zhang, Y. Lu, Q. Guo, Y. Zhang, L. Liu, C. Ruan, Q. Chen, X. Chen, C. Li, T. Sun, J. Cheng, C. Jiang, *ACS Appl. Mater. Interfaces* **2018**, *10*, 39455-39467.
[118] A. G. Cheetham, P. Zhang, Y. Lin, L. L. Lock, H. Cui, *J. Am. Chem. Soc.* **2013**, *135*, 2907-2910.
[119] J. Shen, Q. Wang, J. Fang, W. Shen, D. Wu, G. Tang, J. Yang, *RSC Adv.* **2019**, *9*, 37232-37240.

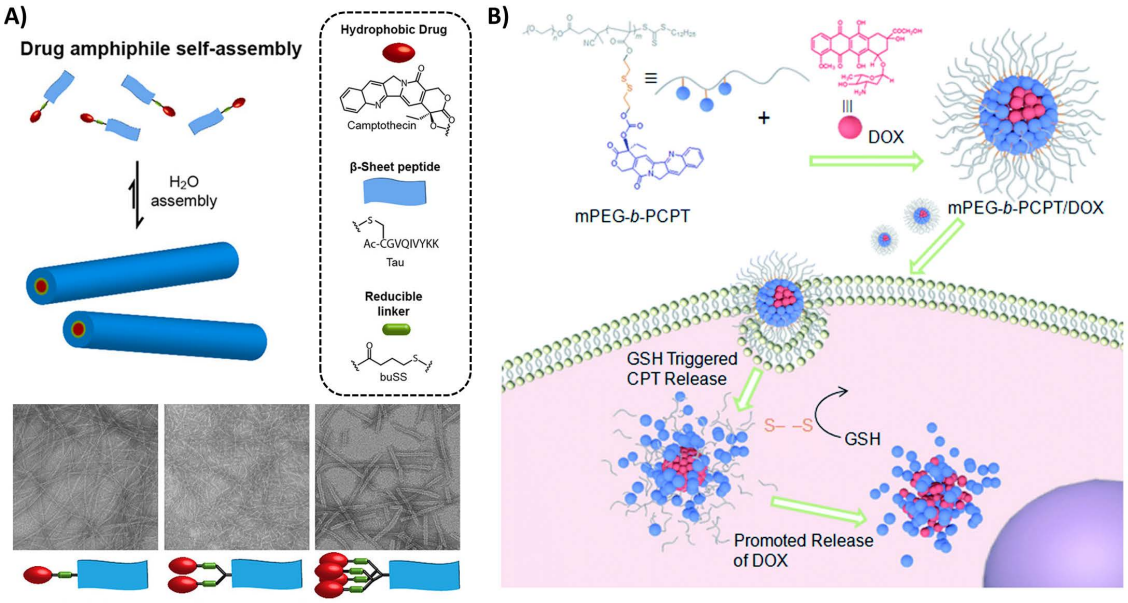

Figure 18. (A) Amphiphilic peptides for the release of camptothecin by reduction of a disulphide bond. Adapted with permission from Ref. 118. Copyright © 2013 American Chemical Society. (B) Polymeric nanoparticles for the combined release of camptothecin and doxorubicin in the presence of GSH. Reprinted with permission from Ref. 119. Copyright © 2019 Royal Society of Chemistry.

The objective of incorporating several stimuli-sensitive groups in the same nanocarrier enhances the importance of a dual sensitive release through both pH and redox conditions. For example, the group of J. Chang developed polymeric vesicles loaded with doxorubicin and coated with both an acid-sensitive and a GSH-sensitive layer for preventing the premature release of the encapsulated drug (Figure 19A).[120] Another prominent example of polymeric entities are the micelles reported by the group of S. Zhou, which incorporate the drug via a pH-sensitive hydrazone bond, but they do not release it into the cytosol until the micellar structure is lost in response to the reducing conditions of GSH (Figure 19B).[121]

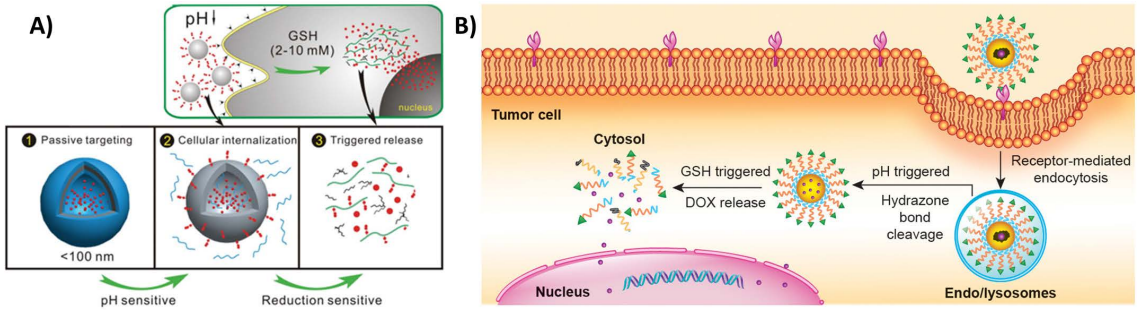

Figure 19. (A) pH and redox-sensitive polymeric vesicles for DOX encapsulation. Adapted with permission from Ref. 120. Copyright © 2014 Royal Society of Chemistry. (B) Polymer micelles for DOX release triggered by acidic pH and GSH. Reprinted with permission from Ref. 121. Copyright © 2016 American Chemical Society.

[118] A. G. Cheetham, P. Zhang, Y. Lin, L. L. Lock, H. Cui, *J. Am. Chem. Soc.* **2013**, *135*, 2907-2910.
[119] J. Shen, Q. Wang, J. Fang, W. Shen, D. Wu, G. Tang, J. Yang, *RSC Adv.* **2019**, *9*, 37232-37240.
[120] S. Wang, H. Wang, Z. Liu, L. Wang, X. Wang, L. Su, J. Chang, *Nanoscale*, **2014**, *6*, 7635-7642.
[121] Y. Wang, L. Zhang, X. Zhang, X. Wei, Z. Tang, S. Zhou, *ACS Appl. Mater. Interfaces* **2016**, *8*, 5833-5846.

4.3.3. Enzyme-responsive drug delivery systems

Tumour cells overexpress certain enzymes that allow to differentiate them from healthy cells, such as proteases, phospholipases and oxidoreductases.[122] In particular, matrix metalloproteinases (MMPs) are the most exploited tumour cell enzymes for drug delivery applications. The main strategy is to incorporate synthetic linear peptides into the nanocarrier that can act as substrates of MMPs.[123]

As an example, the group of J. R. Lu found peptides with the appropriate sequence Gly-Pro-Leu-Gly-Leu-Ala (GPLGLA) required for MMP-7 enzyme action (Figure 20A).[124] These peptides are capable of self-assembling into fibres with a hydrophobic interior ideal for the encapsulation of doxorubicin molecules. The fibres are selectively degraded in the tumour environment by amide hydrolysis between Gly and Leu, resulting in the selective release of the drug in the tumour cells. Similar approaches have been used to obtain liposomes or nanoparticles sensitive to MMPs.[125]

This release mechanism is not limited to MMPs. The tetrapeptide Gly-Phe-Leu-Gly (GFLG) is considered to be a suitable substrate for cathepsin B, a protease overexpressed in many tumour cells.[126] Other enzymes exploited by drug delivery systems include kinase A for phosphorylating serine residues,[127] lipases or esterases for cleaving ester bonds[128] and glycosidases for the hydrolysis of glycosidic bonds.[129]

In order to improve drug release, enzyme-responsive systems often incorporate other stimuli-responsive bonds into their structure. An example illustrating this feature is a multi-responsive dendritic assembly that is MMP-, GSH- and pH-sensitive (Figure 20B).[130] The initial enzymatic activation by MMP removes the outer layer of the dendrimer, enhancing its cellular internalisation. Next, disulphide bond cleavage occurs, releasing Lonidamine (LND), which is an inhibitor capable of combating cellular drug resistance. Finally, the drug release is triggered by the acidic conditions of the lysosomes.

---

[122] a) Q. Hu, P. S. Katti, Z. Gu, *Nanoscale*, **2014**, *6*, 12273-12286; b) M. Shahriari, M. Zahiri, K. Abnous, S. M. Taghdisi, M. Ramezani, M. Aliboland, *J. Control. Release* **2019**, *308,* 172-189.

[123] Q. Yao, L. Kou, Y. Tu, L. Zhu, *Trends Pharmacol. Sci.* **2018**, *39*,766-781.

[124] M. Cao, S. Lu, N. Wang, H. Xu, H. Cox, R. Li, T. Waigh, Y. Han, Y. Wang, J. R. Lu, *ACS Appl. Mater. Interfaces* **2019**, *11*, 16357-16366.

[125] a) L. Zhu, P. Kate, V. P. Torchilin, *ACS Nano* **2012**, *6*, 3491-3498; b) X. Gao, J. Zhang, Z. Huang, T. Zuo, Q. Lu, G. Wu, Q. Shen, *ACS Appl. Mater. Interfaces* **2017**, *9*, 29457-29468.

[126] V. S. Egorova, E. P. Kolesova, M. Lopus, N. Yan, A. Parodi, A. A. Zamyatnin, *Pharmaceutics* **2023**, *15*, 1848-1868.

[127] M. J. Webber, C. J. Newcomb, R. Bitton, S. I. Stupp, *Soft Matter* **2011**, *7*, 9665-9672.

[128] Y. Li, Y. Chen, H. Dong, C. Dong, *Med. Chem. Commun.* **2015**, *6*, 1874-1881.

[129] R. Barat, T. Legigan, I. Tranoy-Opalinski, B. Renoux, E. Péraudeau, J. Clarhaut, P. Poinot, A. E. Fernandes, V. Aucagne, D. A. Leigh, S. Papot, *Chem. Sci.* **2015**, *6*, 2608-2613.

[130] Y. Li, X. Xu, X. Zhang, Y. Li, Z. Zhang, Z. Gu, *ACS Nano* **2017**, *11*, 416-429.

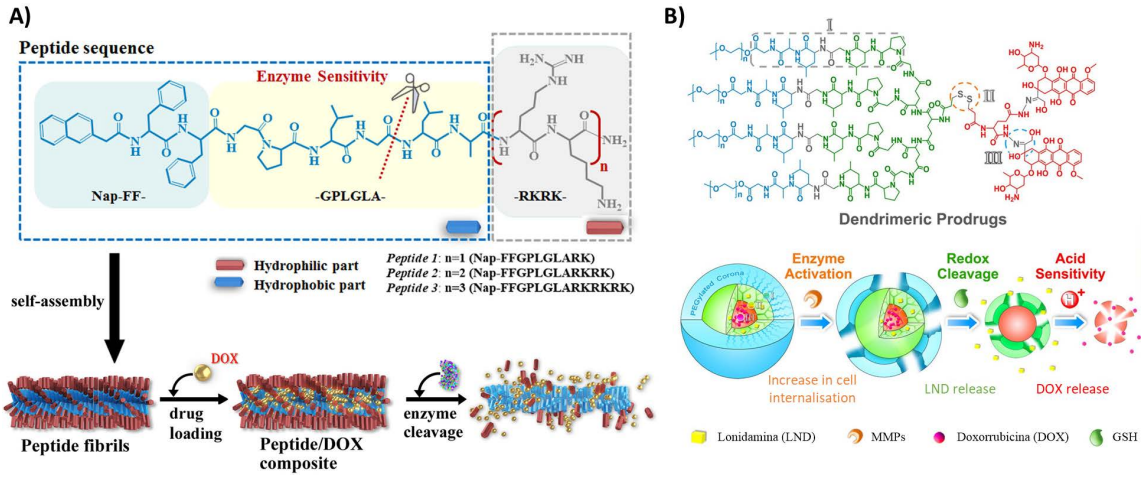

Figure 20. (A) Peptide fibre for DOX release by enzymatic cleavage with MMP-7 of the Gly-Leu amide bond. Adapted with permission from Ref. 124. Copyright © 2019 American Chemical Society. (B) Dendritic nano-assembly sensitive to MMPs, GSH and pH. Adapted with permission from Ref. 130. Copyright © 2017 American Chemical Society.

4.3.4. Magnetic field-responsive drug delivery systems

Magnetic nanoparticles (MNPs) are the main magnetic field-sensitive drug delivery systems.[131] Among the wide variety of available MNPs, superparamagnetic nanoparticles of iron oxides, such as magnetite (Fe_3O_4) and maghemite (γ-Fe_2O_3), have shown the greatest potential for biomedical application.[132] Although for decades they have been used exclusively as contrast agents in magnetic resonance imaging, in recent years they have also been used as drug carriers. One of the advantages of applying a magnetic field is to guide magnetically sensitive vehicles to the target. In the presence of a magnetic field, they rapidly reach saturation by magnetisation. However, as soon as the field is removed, they demagnetise without retaining residual magnetism. In addition, the external surface of the magnetic nanoparticles can be modified with organic or inorganic compounds to improve their efficacy.[131,132] For example, in a work developed by the group of T. Pellegrino in collaboration with our research group, four Pt complexes derived from the anti-tumour drug cisplatin were covalently attached to magnetic nanoparticles by a pH-sensitive dicarboxylic group (Figure 21A).[133] As a result, cell internalisation and cytotoxicity were enhanced when an external magnetic field was applied, while the acidic hydrolysis of the complex allowed drug release.

Another effective method in cancer therapy is to increase the temperature of the tumour tissues (hyperthermia). However, the main problem lies in reaching the

[124] M. Cao, S. Lu, N. Wang, H. Xu, H. Cox, R. Li, T. Waigh, Y. Han, Y. Wang, J. R. Lu, *ACS Appl. Mater. Interfaces* **2019**, *11*, 16357-16366.
[130] Y. Li, X. Xu, X. Zhang, Y. Li, Z. Zhang, Z. Gu, *ACS Nano* **2017**, *11*, 416-429.
[131] a) J. Dobson, *Drug. Dev. Res.* **2006**, *67*, 55-60; b) A. Grillone, G. Ciofani, *Chem. Eur. J.* **2017**, *23*, 16109-16114; c) Y. Liu, M. Li, F. Yang, N. Gu, *Sci. China Mater.* **2017**, *60*, 471-486; d) G. M. Ziarani, M. Malmir, N. Lashgari, A. Badiei, *RSC Adv.* **2019**, *9*, 25094-25106.
[132] H. Arami, A. Khandhar, D. Liggitt, K. M. Krishnan, *Chem. Soc. Rev.* **2015**, *44*, 8576-8607.
[133] A. Quarta, M. Amorín, M. J. Aldegunde, L. Blasi, A. Ragusa. S. Nitti, G. Pugliese, G. Gigli, J. R. Granja, T. Pellegrino, *Nanoscale* **2019**, *11*, 23482-23497.

necessary temperatures without affecting normal cells.[131] To solve this, the concept of "intracellular hyperthermia" has emerged based on the ability of magnetic nanoparticles to induce an increase in temperature when an alternating magnetic field (AMF) is applied.[134] One example was reported by the group of J. I. Zink, who developed mesoporous silica nanoparticles containing in the interior Fe_3O_4 and doxorubicin (Figure 21B).[135] The structure was also modified on the outer surface with pseudorotaxane derivatives. The implementation of an alternating magnetic field generates internal heat that causes disassembly of the structure, leading to the release of the encapsulated drug.

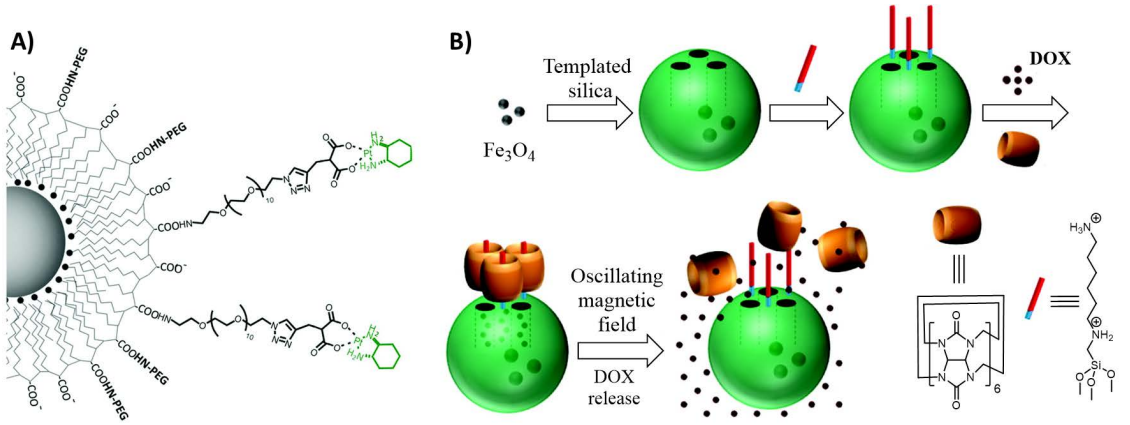

Figure 21. (A) Binding of a cisplatin derivative to magnetic nanoparticles. Reprinted with permission from Ref. 133. Copyright © 2019 Royal Society of Chemistry. (B) Schematic representation of the application of an alternating magnetic field for doxorubicin release from mesoporous silica nanoparticles containing Fe_3O_4. Adapted with permission from Ref. 135. Copyright © 2010 American Chemical Society.

4.3.5. Light-responsive drug delivery systems

Photoactivatable nanomaterials have gained special attention as drug delivery vehicles due to the non-invasive nature of light. In general, these systems make use of ultraviolet (UV, 200-400 nm) or visible (Vis, 400-700 nm) irradiation.[136] However, these wavelengths present low tissue penetration due to dispersion phenomena and the presence of biocomponents capable of absorbing them.[137] As a solution, other alternatives using light of lower energy have started to be applied, especially wavelengths in the near infrared region (NIR, 700-1000 nm).[136,137] In particular, the strategies for designing this type of systems can be classified into three categories: photochemical, photoisomerization or photothermal release.[138]

---

[131] a) J. Dobson, *Drug. Dev. Res.* **2006**, *67*, 55-60; b) A. Grillone, G. Ciofani, *Chem. Eur. J.* **2017**, *23*, 16109-16114; c) Y. Liu, M. Li, F. Yang, N. Gu, *Sci. China Mater.* **2017**, *60*, 471-486; d) G. M. Ziarani, M. Malmir, N. Lashgari, A. Badiei, *RSC Adv.* **2019**, *9*, 25094-25106.

[133] A. Quarta, M. Amorín, M. J. Aldegunde, L. Blasi, A. Ragusa. S. Nitti, G. Pugliese, G. Gigli, J. R. Granja, T. Pellegrino, *Nanoscale* **2019**, *11*, 23482-23497.

[134] A. Ito, M. Shinkai, H. Honda, T. Kobayashi, *J. Biosci. Bioeng.* **2005**, *100*, 1-11.

[135] C. R. Thomas, D. P. Ferris, J. Lee, E. Choi, M. H. Cho, E. S. Kim, J. F. Stoddart, J. Shin, J. Cheon, J. I. Zink, *J. Am. Chem. Soc.* **2010**, *132*, 10623-10625.

[136] W. Zhao, Y. Zhao, Q. Wang, T. Liu, J. Sun, R. Zhang, *Small* **2019**, *15*, 1903060.

[137] C. Álvarez-Lorenzo, L. Bromberg, A. Concheiro, *Photochem. Photobiol.* **2009**, *85*, 848-860.

[138] C. S. Linsley, B. M. Wu, *Ther. Deliv.* **2017**, *8*, 89-107.

The photochemical release involves the cleavage of a covalent bond under light irradiation. Therefore, these systems require wavelengths with sufficient energy per photon to break bonds, such as UV and high-energy Vis.[138] The most commonly used photolabile groups are *o*-nitrobenzyl (*o*-NB) derivatives, whose irradiation with UV light produces its irreversible cleavage, generating *o*-nitrobenzaldehyde.[139,140] For example, the group of K. Zhang developed nucleic acid nanostructures with a photolabile 2-nitrobenzyl ether moiety that acts as a link between DNA and camptothecin (Figure 22A).[141] When this conjugate is activated by UV irradiation, it degrades and releases camptothecin from the nanostructure. Other examples of photolabile groups are coumarin and pyrene modified with ester groups that are susceptible to cleavage upon irradiation.[138,139]

Drug release can also be achieved by conformational changes due to light-induced isomerization. Photoisomerization of azobenzene is the most commonly used for this purpose.[138,142] When irradiated with UV light, an isomerization between the thermodynamically stable *trans* to the metastable *cis* isomer occurs. In contrast to other methods, this change can be reversed by Vis light, thermally or spontaneously in the dark due to the higher thermodynamic stability of the *trans* isomer. In order to avoid the use of UV light, lower energy light has started to be used. In this sense, the group of S. Wu exploited the higher affinity of cyclodextrins for the *trans*-isomer than for the *cis*-one (Figure 22B).[143] This system is based on mesoporous silica nanoparticles in which the *trans*-isomer binds to cyclodextrins to close the nanopores. However, the red-light irradiation photoisomerize the azobenzene, expelling the cyclodextrins and releasing the encapsulated drug. Spiropyran (SP) is another photoconvertible group used in drug delivery systems,[144] while others such as diarylethenes (DAEs) or hemithioindigos (HTIs) have not yet been widely explored for this purpose.[145]

Finally, the photothermal release refers to the use of materials that generate heat under photoexcitation to thermally affect the transport system and release the drug.[138] This requires the efficient conversion of light energy into thermal energy and the use of materials that quickly respond to the temperature increase, modifying the system properties and releasing the drug. Some of the structures most commonly used are Au components such as nanoparticles,[146] nanocapsules,[147] nanorods[148] and

[138] C. S. Linsley, B. M. Wu, *Ther. Deliv.* **2017**, *8*, 89-107.
[139] A. P. Pelliccioli, J. Wirz, *Photochem. Photobiol. Sci.* **2002**, *1*, 441-458.
[140] H. Zhao, E. S. Sterner, E. B. Coughlin, P. Theato, *Macromolecules* **2012**, *45*, 1723-1736.
[141] X. Tan, B. B. Li, X. Lu, F. Jia, C. Santori, P. Menon, H. Lui, B. Zhang, J. J. Zhao, K. Zhang, *J. Am. Chem. Soc.* **2015**, *137*, 6112-6115.
[142] J. Zhu, T. Guo, Z. Wang, Y. Zhao, *J. Control. Release* **2022**, *345*, 475-493.
[143] D. Wang, S. Wu, *Langmuir* **2016**, *32*, 632-636.
[144] A. Fagan, M. Bartkowski, S. Giordani, *Front. Chem.* **2021**, *9*, 720087.
[145] S. Jia, W. Fong, B. Graham, B. J. Boyd, *Chem. Mater.* **2018**, *30*, 2873-2887.
[146] a) N. S. Abadeer, C. J. Murphy, *J. Phys. Chem. C* **2016**, *120*, 4691-4716; b) K. Sztandera, M. Gorzkiewicz, B. Klajnert-Maculewicz, *Mol. Pharmaceutics* **2019**, *16*, 1-23.
[147] H. Ke, X. Yue, J. Wang, S. Xing, Q. Zhang, Z. Dai, J. Tian, Sh. Wang, Y. Jin, *Small* **2014**, *10*, 1220-1227.
[148] a) X. Huang, I. H. El-Sayed, W. Qian, M. A. El-Sayed, *J. Am. Chem. Soc.* **2006**, *128*, 2115-2120; b) W. I. Choi, A. Sahu, Y. H. Kim, G. Tae, *Ann. Biomed. Eng.* **2012**, *40*, 534-546.

nanostars,[149] due to their strong absorption of NIR light and their ability to transform it into heat. For example, the group of B. Liu reported doxorubicin-loaded liposomes which present a core based on Au nanostars and a heat-sensitive lipid bilayer (Figure 22C).[150] The irradiation with NIR light produces an efficient drug release due to the photothermal effect of the Au nanostars in the lipid bilayer.

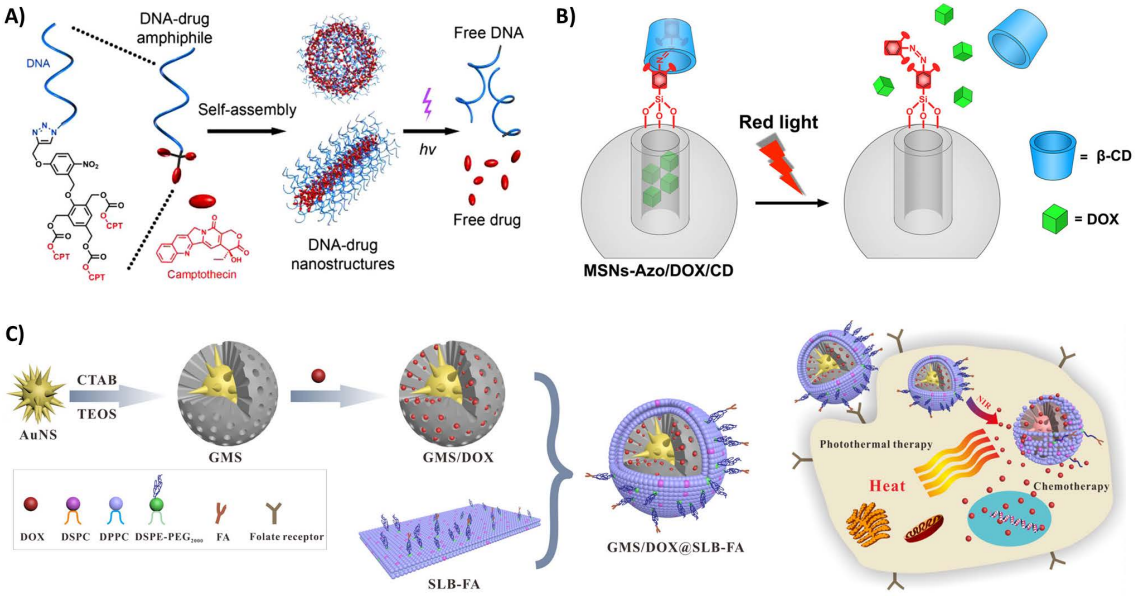

Figure 22. (A) Photochemical release of camptothecin from nucleic acid nanostructures by irreversible cleavage of a *o*-nitrobenzyl moiety. Reprinted with permission from Ref. 141. Copyright © 2015 American Chemical Society. (B) Release of doxorubicin from the nanopores of silica nanoparticles by photoisomerization of an azobenzene group. Adapted with permission from Ref. 143. Copyright © 2016 American Chemical Society. (C) Schematic illustration of the photothermal release of doxorubicin from liposomes with an Au nanostar core. Adapted with permission from Ref. 150. Copyright © 2017 American Chemical Society.

4.3.6. Ultrasound-responsive drug delivery systems

The application of ultrasounds represents a promising approach due to their non-invasive nature and deep tissue penetration. In addition, they provide a high drug release specificity at the desired site of action. This drug release mechanism usually consists of a temperature increase in the irradiated tissue or a cavitation process due to the ultrasound irradiation.[151]

[141] X. Tan, B. B. Li, X. Lu, F. Jia, C. Santori, P. Menon, H. Lui, B. Zhang, J. J. Zhao, K. Zhang, *J. Am. Chem. Soc.* **2015**, *137*, 6112-6115.
[143] D. Wang, S. Wu, *Langmuir* **2016**, *32*, 632-636.
[149] a) H. Yuan, A. M. Fales, T. Vo-Dinh, *J. Am. Chem. Soc.* **2012**, *134*, 11358-11361; b) Y. Liu, H. Yuan, A. M. Fales, J. K. Register, T. Vo-Dinh, *Front. Chem.* **2015**, *3*, 51.
[150] J. An, X. Yang, K. Cheng, X. Song, L. Zhang, C. Li, X. Zhang, Y. Xuan, Y. Song, B. Fang, X. Hou, Y. Zhao, B. Liu, *ACS Appl. Mater. Interfaces* **2017**, *9*, 41748-41759.
[151] a) S. R. Sirsi, M. A. Borden, *Adv. Drug Deliv. Rev.* **2014**, *72*, 3-14; b) X. Cai, Y. Jiang, M. Lin, J. Zhang, H. Guo, F. Yang, W. Leung, C. Xu, *Front. Pharmacol*. **2020**, *10*, 1650; c) P. Wei, E. J. Cornel, J. Du, *Drug Deliv. Transl. Res.* **2021**, *11*, 1323-1339.

The most used nanocarriers for an ultrasound-responsive drug delivery are microbubbles,[152] nanobubbles,[153] nanodroplets,[154] nanoemulsions,[155] polymeric vesicles[156] or hydrogels.[157] For example, the group of K. Nam reported paclitaxel-loaded nanodroplets that convert into microbubbles under ultrasound irradiation (Figure 23A).[158] This conversion triggers the paclitaxel release at the site of action. In a similar manner, the group of J. Du developed a pH- and ultrasound-responsive polymersome for doxorubicin encapsulation based on the self-assembly of a block copolymer (Figure 23B).[159] The pH sensitivity facilitates endosomal escape, while ultrasound allows drug release.

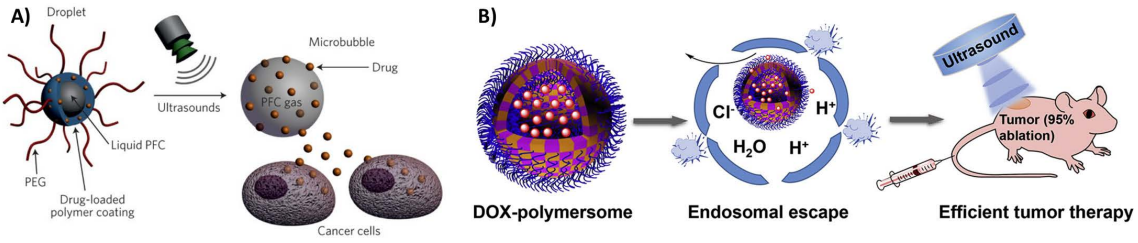

Figure 23. (A) Ultrasound-induced droplet-to-bubble transition for drug release. Reprinted with permission from Ref. 99. Copyright © 2013 Springer Nature and Ref. 158. Copyright © 2009 Elsevier. (B) pH- and ultrasound-responsive polymersome for controlled DOX delivery. Reprinted with permission from Ref. 159. Copyright © 2020 Elsevier.

As a conclusion of this section, research into chemical systems that transport existing drugs has increased in recent years. In particular, the use of targeting agents and the sensitivity to intrinsic or external stimuli represent a solution to the problems of conventional treatments. Despite the large number of examples in this field to date, there is still a long way to go until obtaining fully efficient drug delivery systems. In addition, structural complexity and difficulties to scale-up the synthesis are the main barriers that prevent many alternatives to enter into the market. However, the good health of this area of research suggests that new and better chemical methods will be described in the future.

---

[99] S. Mura, J. Nicolas, P. Couvreur, *Nat. Mater.* **2013**, *12*, 991-1003.

[152] a) M. C. Cochran, J. Eisenbrey, R. O. Ouma, M. Soulen, M. A. Wheatley, *Int. J. Pharm.* **2011**, *414*, 161-170; b) C. Niu, Z. Wang, G. Lu, T. M. Krupka, Y. Sun, Y. You, W. Song, H. Ran, P. Li, Y. Zheng, *Biomaterials* **2013**, *34*, 2307-2317; c) C. McEwan, C. Fowley, N. Nomikou, B. McCaughan, A. P. McHale, J. F. Callan, *Langmuir* **2014**, *30*, 14926-14930.

[153] a) T. Yin, P. Wang, J. Li, Y. Wang, B. Zheng, R. Zheng, D. Cheng, X. Shuai, *Biomaterials* **2014**, *35*, 5932-5943; b) C. Hernandez, S. Gulati, G. Fioravanti, P. L. Stewart, A. A. Exner, *Sci. Rep.* **2017**, *7*, 13517.

[154] a) W. Tang, Z. Yang, S. Wang, Z. Wang, J. Song, G. Yu, W. Fan, Y. Dai, J. Wang, L. Shan, G. Niu, Q. Fan, X. Chen, *ACS Nano* **2018**, *12*, 2610-2622; b) L. Zhang, T. Yin, B. Li, R. Zheng, C. Qiu, K. S. Lam, Q. Zhang, X. Shuai, *ACS Nano* **2018**, *12*, 3449-3460.

[155] a) N. Rapoport, K. Nam, R. Gupta, Z. Gao, P. Mohan, A. Payne, N. Todd, X. Liu, T. Kim, J. Shea, C. Scaife, D. L. Parker, E. Jeong, A. M Kennedy, *J. Control Release* **2011**, *153*, 4-15; b) M. Javadi, W. G. Pitt, D. M. Belnap, N. H. Tsosie, J. M. Hartley, *Langmuir* **2012**, *28*, 14720-14729.

[156] a) Z. Gao, H. D. Fain, N. Rapoport, *Mol. Pharm.* **2004**, *1*, 317-330; b) P. Wu, Y. Jia, F. Qu, Y. Sun, P. Wang, K. Zhang, C. Xu, Q. Liu, X. Wang, *ACS Appl. Mater. Interfaces* **2017**, *9*, 25706-25716.

[157] a) N. Huebsch, C. J. Kearney, X. Zhao, J. Kim, C. A. Cezar, Z. Suo, D. J. Mooney, *Proc. Natl. Acad. Sci. U. S. A.* **2014**, *111*, 9762-9767; b) Y. Zhou, G. Liu, S. Guo, *J. Mater. Chem. B* **2022**, *10*, 3947-3958.

[158] N. Y. Rapoport, A. M. Kennedy, J. E. Shea, C. L. Scaife, K. Nam, *J. Control. Release* **2009**, *138*, 268-276.

[159] P. Wei, M. Sun, B. Yang, J. Xiao, J. Du, *J. Control. Release* **2020**, 322, 81-94.

4.4. SELF-ASSEMBLING CYCLIC PEPTIDES

In 1974, De Santis *et al.* proposed theoretical studies of cyclic peptides (CPs) composed of an even number of α-amino acids of alternating *D*- and *L*- chirality. In particular, they suggested that these cyclic peptides could adopt a planar β-sheet conformation with the CO and NH groups pointing in opposite directions of the ring plane (Figure 24A).[160] As a result of this conformation, the cyclic peptides could stack one on top of each other in a parallel or antiparallel fashion to form tubular structures through the formation of hydrogen bonds between neighbouring units. In 1987, the group of G. P. Lorenzi, in an attempt to demonstrate the previous theoretical studies, described the synthesis of different cyclic oligopeptides formed by the same number of alternating *D*- and *L*-amino acids.[161] Although they turned out to be insoluble in most organic solvents, the authors were able to shown by IR the presence of a strong network of hydrogen bonds. Later, in 1993, the group of M. R. Ghadiri reported the first self-assembling cyclic peptide nanotube (SCPN).[162] This first design consisted of an α-(*D*,*L*)-cyclic octapeptide with two glutamic acids in the sequence (Figure 24B). The protonation of these residues in aqueous solution induces the crystallization into hollow tubular structures with several nanometres in length. In addition to α-CPs, multiple nanotube designs have also been proposed including β-CPs,[163] α,γ-CPs,[164] α,δ-CPs[165] or α,ε-CPs,[166] among others (Figure 24C).[167,168]

One of the advantages of this type of hollow supramolecular polymers is that their internal and external properties can be easily modified. In this sense, the internal diameter of the nanotube can be changed by adjusting the number and type of amino acids in the cyclic peptide. In particular, the diameter of an α-CP of 8 residues is around 7.5 Å,[162] while the 10 residues α-CP is around 10 Å and the 12 residues α-CP is around 13 Å.[169] Moreover, the side chains of the α-amino acids face outwards from the nanotube, allowing the possibility of modifying the properties of the outer surface. Also, the internal cavity can be tuned by incorporating other amino acids, such as

[160] P. De Santis, S. Morosetti, R. Rizzo, *Macromolecules* **1974**, *7*, 52-58.
[161] L. Tomasic, G. P. Lorenzi, *Helv. Chim. Acta* **1987**, *70*, 1012-1016.
[162] M. R. Ghadiri, J. R. Granja, R. A. Milligan, D. E. McRee, N. Khazanovich, *Nature*, **1993**, *366*, 324-327.
[163] a) D. Seebach, J. L. Matthews, A. Meden, T. Wessels, C. Baerlocher, L. B. McCusker, *Helv. Chim. Acta* **1997**, *80*, 173-182; b) T. D. Clark, L. K. Buehler, M. R. Ghadiri, *J. Am. Chem. Soc.* **1998**, *120*, 651-656; c) F. Fujimura, T. Hirata, T. Morita, S. Kimura, *Biomacromolecules* **2006**, *7*, 2394-2400; d) F. Fujimura, Y. Horikawa, T. Morita, J. Sugiyama, S. Kimura, *Biomacromolecules* **2007**, *8*, 611-616; e) Y. Ishihara, S. Kimura, *J. Pept. Sci.* **2010**, *16*, 110-114.
[164] a) M. Amorín, L. Castedo, J. R. Granja, *J. Am. Chem. Soc.* **2003**, *125*, 2844-2845; b) C. Reiriz, R. J. Brea, R. Arranz, J. L. Carrascosa, A. Garibotti, B. Manning, J. M. Valpuesta, R. Eritja, L. Castedo, J. R. Granja, *J. Am. Chem. Soc.* **2009**, *131*, 11335-11337; c) R. Hourani, C. Zhang, R. van der Weegen, L. Ruiz, C. Li, S. Keten, B. A. Helms, T. Xu, *J. Am. Chem. Soc.* **2011**, *133*, 15296-15299.
[165] a) M. Calvelo, A. Lamas, A. Guerra, M. Amorín, R. Garcia-Fandino, J. R. Granja, *Chem. Eur. J.* **2020**, *26*, 5846-5858; b) A. Blanco-González, M. Calvelo, P. F. Garrido, M. Amorín, J. R. Granja, Á. Piñeiro, R. Garcia-Fandino, *Front. Chem.* **2021**, *9*, 704160.
[166] a) W. S. Horne, C. D. Stout, M. R. Ghadiri, *J. Am. Chem. Soc.* **2003**, *125*, 9372-9376; b) S. M. Darnall, C. Li, M. Dunbar, M. Alsina, S. Keten, B. A. Helms, T. Xu, *J. Am. Chem. Soc.* **2019**, *141*, 10953-10957.
[167] a) R. J. Brea, C. Reiriz, J. R. Granja, *Chem. Soc. Rev.* **2010**, *39*, 1448-1456; b) R. Chapman, M. Danial, M. L. Koh, K. A. Jolliffe, S. Perrier, *Chem. Soc. Rev.* **2012**, *41*, 6023-6041.
[168] Q. Song, Z. Cheng, M. Kariuki, S. C. L. Hall, S. K. Hill, J. Y. Rho, S. Perrier, *Chem. Rev.* **2021**, *121*, 13936-13995.
[169] N. Khazanovich, J. R. Granja, D. E. McRee, R. A. Milligan, M. R. Ghadiri, *J. Am. Chem. Soc.* **1994**, *116*, 6011-6012.

cyclic γ-amino acids because their β position is placed facing the interior of the cavity (Figure 24C).[164,170]

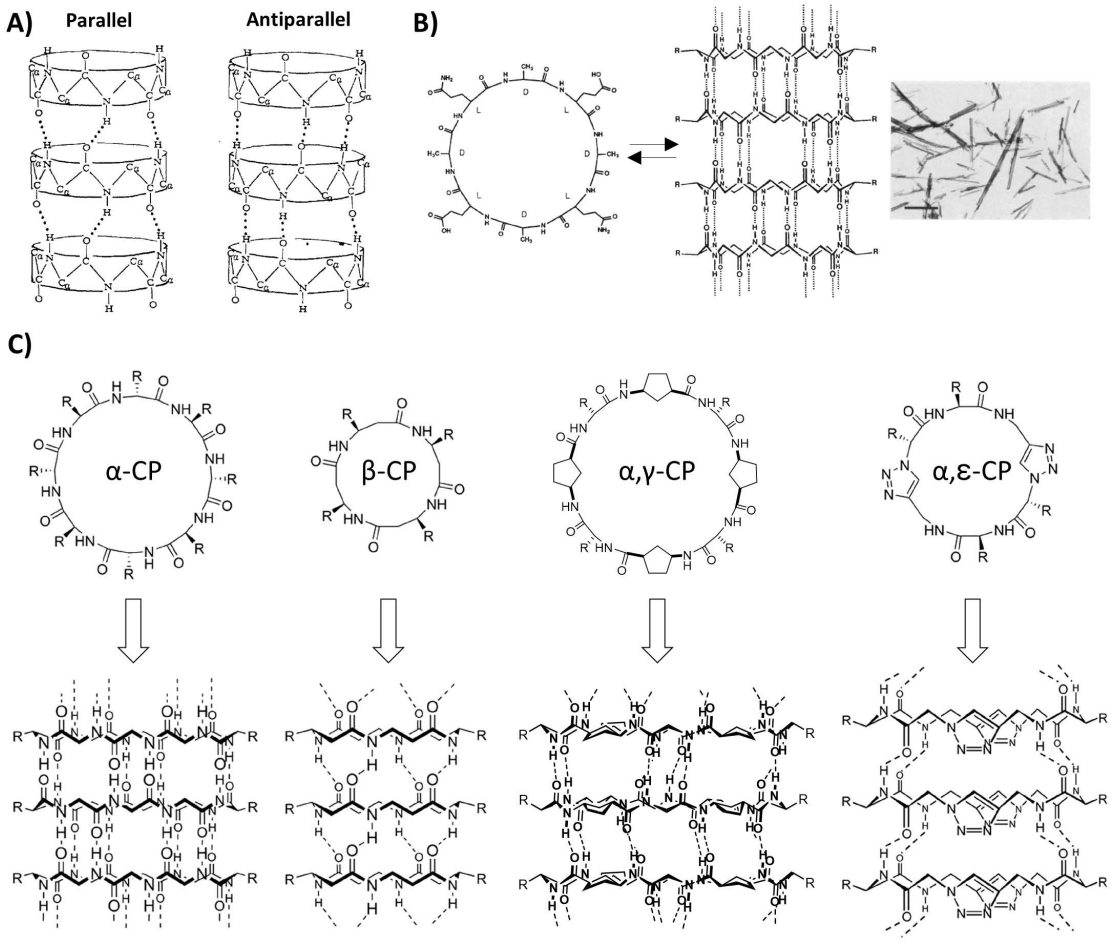

Figure 24. (A) Interaction schemes of parallel and antiparallel tubular structures composed of β-sheet cyclic peptides proposed by De Santis *et al.* in 1974. Reprinted with permission from Ref. 160. Copyright © 1974 American Chemical Society. (B) First example of a self-assembling cyclic peptide nanotube described by the group of M. R. Ghadiri in 1993 showing the antiparallel stacking and the network of hydrogen bonds. Reprinted with permission from Ref. 162. Copyright © 1993 Springer Nature. (C) Examples of nanotubes composed of α-CPs, β-CPs, α,γ-CPs or α,ε-CPs. Adapted with permission from Ref. 168. Copyright © 2021 American Chemical Society.

To get a better understanding of the conformation and thermodynamic aspects of these SCPNs, simple models formed by only two CPs were reported (Figure 25A).[171,172] Their formation is based on blocking one of ring faces by *N*-alkylation of the amino acids

[160] P. De Santis, S. Morosetti, R. Rizzo, *Macromolecules* **1974**, *7*, 52-58.

[162] M. R. Ghadiri, J. R. Granja, R. A. Milligan, D. E. McRee, N. Khazanovich, *Nature*, **1993**, *366*, 324-327.

[164] a) M. Amorín, L. Castedo, J. R. Granja, *J. Am. Chem. Soc.* **2003**, *125*, 2844-2845; b) C. Reiriz, R. J. Brea, R. Arranz, J. L. Carrascosa, A. Garibotti, B. Manning, J. M. Valpuesta, R. Eritja, L. Castedo, J. R. Granja, *J. Am. Chem. Soc.* **2009**, *131*, 11335-11337; c) R. Hourani, C. Zhang, R. van der Weegen, L. Ruiz, C. Li, S. Keten, B. A. Helms, T. Xu, *J. Am. Chem. Soc.* **2011**, *133*, 15296-15299.

[168] Q. Song, Z. Cheng, M. Kariuki, S. C. L. Hall, S. K. Hill, J. Y. Rho, S. Perrier, *Chem. Rev.* **2021**, *121*, 13936-13995.

[170] N. Rodríguez-Vázquez, M. Amorín, J. R. Granja, *Org. Biomol. Chem.* **2017**, *15*, 4490-4505.

[171] a) M. R. Ghadiri, K. Kobayashi, J. R. Granja, R. K. Chadha, D. E. McRee, *Angew. Chem. Int. Ed. Engl.* **1995**, *34*, 93-95; b) T. D. Clark, J. M. Buriak, K. Kobayashi, M. P. Isler, D. E. McRee, M. R. Ghadiri, *J. Am. Chem. Soc.* **1998**, *120*, 8949-8962.

[172] K. Kobayashi, J. R. Granja, M. R. Ghadiri, *Angew. Chem. Int. Ed. Engl.* **1995**, *34*, 95-98.

with the same chirality. As a result, the formation of hydrogen bonds and the corresponding assembly process can just take place through the non-blocked face, restricting the assembly process to the dimers formation. This strategy was used to evaluate the differences between the parallel and the antiparallel β-sheet structures.[171,172] Although initially the blocking group was mainly restricted to a methyl group, later other alkyl chains were also used for the preparation of structures such as transmembrane transporters (Figure 25B),[173,174] Venturi-like nanotubes (Figure 25C)[175] or capsules (Figure 25D).[176,177]

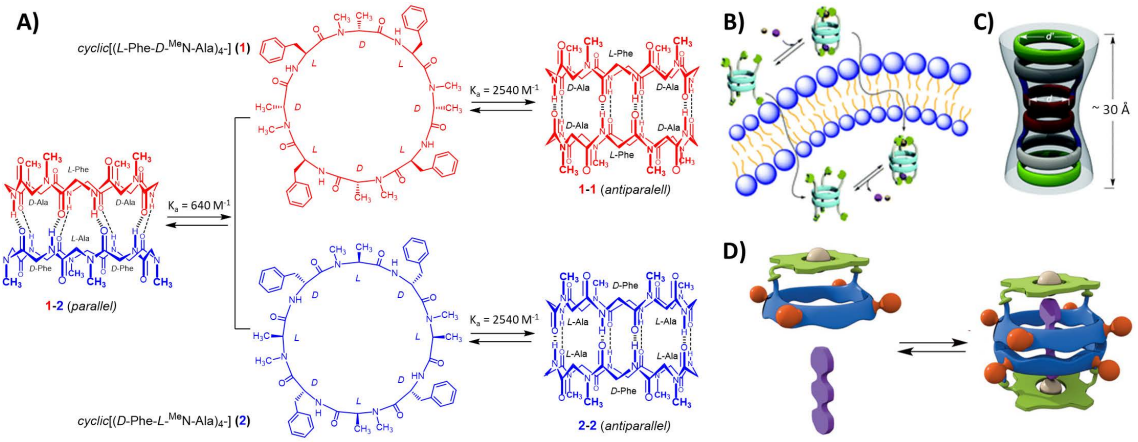

Figure 25. (A) Schematic representation of two *N*-methylated cyclic peptides and the corresponding assembly into parallel or antiparallel dimers. Adapted with permission from Ref. 172. Copyright © 1995 Wiley-VCH Verlag GmbH & Co. (B) Transmembrane transport of cations and anions with cyclic peptide dimers. Reprinted with permission from Ref. 173. Copyright © 2020 Royal Society of Chemistry. (C) Self-assembling Venturi-like peptide nanotube. Reprinted with permission from Ref. 175. Copyright © 2017 Royal Society of Chemistry. (D) Ligand recognition with a self-assembling cyclic peptide capsule. Adapted with permission from Ref. 176. Copyright © 2017 American Chemical Society.

In this regard, the group of M. R. Ghadiri reported the photoswitching between inter- and intramolecular dimer formation (Figure 26).[178,179] The process is based on the linkage via an azobenzene moiety of two *N*-methylated cyclic octapeptides. The *E*-isomer is able to form oligomers through intermolecular hydrogen bonds, while the *Z*-isomer assembles into single intramolecular hydrogen-bonded dimers. As a result, the *Z*/*E*-isomerization under light irradiation allows to control the type of dimer obtained both in solution and in thin films.

[171] a) M. R. Ghadiri, K. Kobayashi, J. R. Granja, R. K. Chadha, D. E. McRee, *Angew. Chem. Int. Ed. Engl.* **1995**, *34*, 93-95; b) T. D. Clark, J. M. Buriak, K. Kobayashi, M. P. Isler, D. E. McRee, M. R. Ghadiri, *J. Am. Chem. Soc.* **1998**, *120*, 8949-8962.
[172] K. Kobayashi, J. R. Granja, M. R. Ghadiri, *Angew. Chem. Int. Ed. Engl.* **1995**, *34*, 95-98.
[173] A. Fuertes, M. Amorín, J. R. Granja, *Chem. Commun.* **2020**, *56*, 46-49.
[174] a) A. Fuertes, M. Amorín, J. R. Granja, *Supramol. Chem.* **2020**, *32*, 239-246; b) V. López-Corbalán, A. Fuertes, A. L. Llamas-Saiz, M. Amorín, J. R. Granja, *Nat. Commun.* **2024**, *15*, 6055.
[175] A. Fuertes, H. L. Ozores, M. Amorín, J. R. Granja, *Nanoscale*, **2017**, *9*, 748-753.
[176] H. L. Ozores, M. Amorín, J. R. Granja, *J. Am. Chem. Soc.* **2017**, *139*, 776-784.
[177] a) N. Rodríguez-Vázquez, R. García-Fandiño, M. J. Aldegunde, J. Brea, M. Isabel Loza, M. Amorín, J. R. Granja, *Org. Lett.* **2017**, *19*, 2560-2563; b) A. Pizzi, H. L. Ozores, M. Calvelo, R. García-Fandiño, M. Amorín, N. Demitri, G. Terraneo, S. Bracco, A. Comotti, P. Sozzani, C. X, Bezuidenhout, P. Metrangolo, J. R. Granja, *Angew. Chem. Int. Ed.* **2019**, *58*, 14472-14476.
[178] M. S. Vollmer, T. D. Clark, C. Steinem, M. R. Ghadiri, *Angew. Chem. Int. Ed.* **1999**, *38*, 1598-1601.
[179] C. Steinem, A. Janshoff, M. S. Vollmer, M. R. Ghadiri, *Langmuir* **1999**, *15*, 3956-3964.

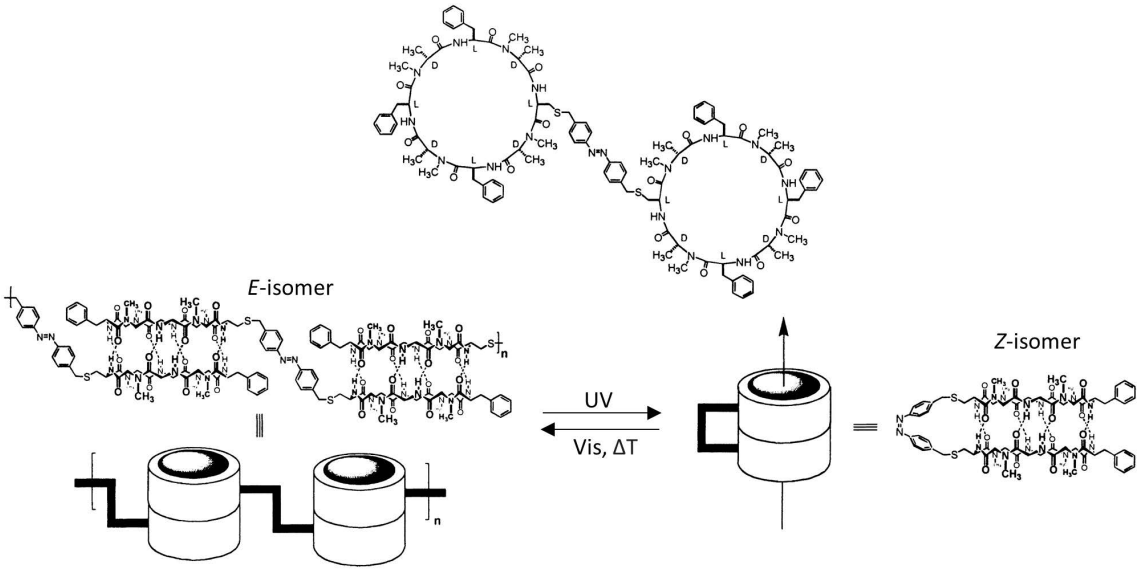

Figure 26. Schematic representation of the photoswitching between inter- and intramolecular hydrogen-bonded cyclic peptide dimers based on azobenzene isomerization. Adapted with permission from Ref. 178. Copyright © 1999 Wiley-VCH Verlag GmbH & Co.

More recently, the ability of SCPNs to form 2D nanosheet structures has been reported. The first example consisted of an amphiphilic cyclic peptide of 8 residues that self-assembled into nanotubes in aqueous solution, followed by a lateral growth to form bilayer structures (Figure 27).[180] This 2D growth was promoted by the interaction of the hydrophobic regions of different nanotubes with the aim of avoiding the contact with the external water. Specifically, this hydrophobic core was composed of a kind of Leu zippers and Trp stacks, but later it was shown that changes in this region by other hydrophobic amino acids do not prevent the formation of nanosheets.[181] However, the ionizable glutamic acid and histidine must always be placed together in the sequence to maintain these 2D materials. Also, designs with low or no electrostatic repulsions did not show the formation of nanosheets. Moreover, the incorporation of two confronted hydrophobic faces in the peptide sequence can promote the elongation in a 180° angle to prepare cyclic peptide monolayers.[182] This type of 2D materials were also found with other amphipathic cyclic peptides, such as those with antimicrobial properties.[183]

[178] M. S. Vollmer, T. D. Clark, C. Steinem, M. R. Ghadiri, *Angew. Chem. Int. Ed.* **1999**, *38*, 1598-1601.
[180] I. Insua, J. Montenegro, *J. Am. Chem. Soc.* **2020**, *142*, 300-307.
[181] S. Díaz, I. Insua, G. Bhak, J. Montenegro, *Chem. Eur. J.* **2020**, 26, 14765-14770.
[182] I. Insua, A. Cardellini, S. Díaz, J. Bergueiro, R. Capelli, G. M. Pavan and J. Montenegro, *Chem. Sci.* **2023**, *14*, 14074–14081.
[183] E. González-Freire, F. Novelli, A. Pérez-Estévez, R. Seoane, M. Amorín, J. R. Granja, *Chem. Eur. J.* **2021**, *27*, 3029-3038.

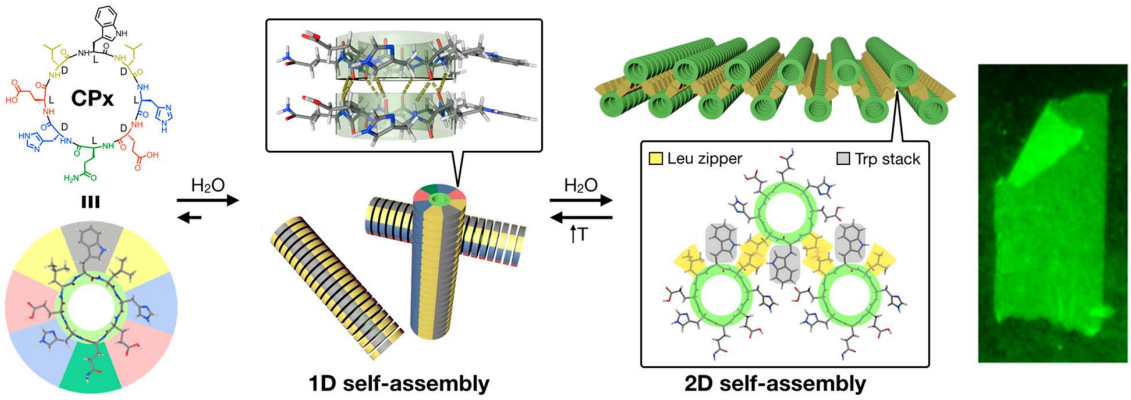

Figure 27. Schematic illustration of the self-assembly of cyclic peptides from 1D nanotubes to 2D nanosheets. Adapted with permission from Ref. 180. Copyright © 2020 American Chemical Society.

The introduction of polymeric chains into the core of the cyclic peptide was explored by S. Perrier and other authors (Figure 28A).[168,184] The main objectives were to increase the peptide solubility, as well as to avoid the lateral aggregation to prevent the formation of bundles. As a result, these cyclic peptide-polymer conjugates can self-assemble into supramolecular cyclic peptide−polymer nanotubes (SCPPN) with a variety of functions due to the versatility of the polymers. At a higher level of the hierarchical assembly, modification of the cyclic peptide with hydrophobic and hydrophilic polymers on opposite faces of the ring allows the construction of tubisomes (Figure 28B).[185]

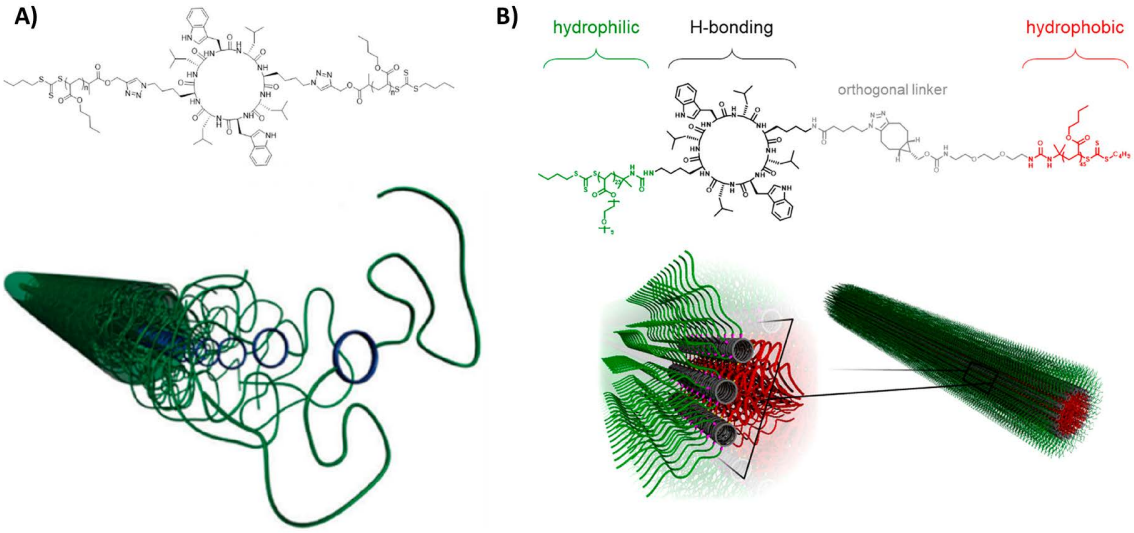

Figure 28. (A) Example of a cyclic peptide-polymer conjugate and the corresponding assembly into SCPPNs. Adapted with permission from Ref. 184. Copyright © 2011 Royal Society of Chemistry. (B) Asymmetric cyclic peptide-polymer conjugate for the formation of tubisomes. Adapted with permission from Ref. 185. Copyright © 2018 Wiley-VCH Verlag GmbH & Co.

[168] Q. Song, Z. Cheng, M. Kariuki, S. C. L. Hall, S. K. Hill, J. Y. Rho, S. Perrier, *Chem. Rev.* **2021**, *121*, 13936-13995.
[180] I. Insua, J. Montenegro, *J. Am. Chem. Soc.* **2020**, *142*, 300-307.
[184] R. Chapman, K. A. Jolliffe, S. Perrier, *Polym. Chem.* **2011**, *2*, 1956-1963.
[185] J. C. Brendel, J. Sanchis, S. Catrouillet, E. Czuba, M. Z. Chen, B. M. Long, C. Nowell, A. Johnston, K. A. Jolliffe, S. Perrier, *Angew. Chem. Int. Ed.* **2018**, *57*, 16678-16682.

The appropriate nanotube design allows for a wide variety of applications, ranging from the construction of hydrogels to the encapsulation of molecules in the internal cavity.[168,170,186,187] Specifically, membrane-interacting SCPNs are of special interest, as they can be used for different biologically relevant applications.[188] In particular, hydrophobic CPs can form ion channels in phospholipid bilayers,[189] while amphipathic CPs can be used as antimicrobial agents since they lye parallel to the membrane (Figure 29).[183]

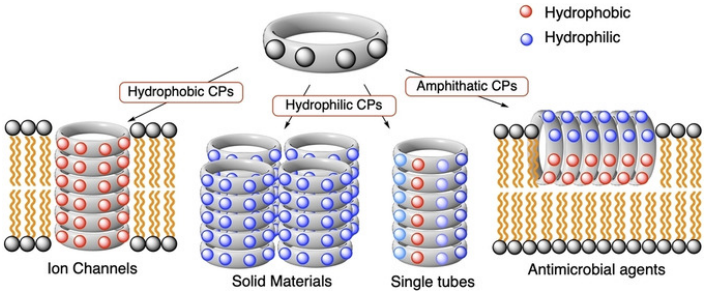

Figure 29. Applications of self-assembling cyclic peptide nanotubes depending on their amino acid sequence. Reprinted with permission from Ref. 183. Copyright © 2021 Wiley-VCH Verlag GmbH & Co.

4.4.1. SCPNs as artificial channels

Lipid bilayers are responsible for maintaining the cellular machinery in the interior of the cell, as well as defining its shape, size and isolate cellular components from the environment. Although this bilayer allows some diffusion of apolar molecules across it, they are impermeable to polar molecules such as ions, sugars or amino acids. Natural membrane proteins, such as channels, offer an optimal solution due to their high degree of selectivity and efficiency. In this sense, supramolecular chemists have tried to develop artificial channels that mimic the natural properties and functions.[190]

In this context, cyclic peptide nanotubes have emerged as a promising alternative. The easy modification of the amino acid sequence to modulate the properties facilitates the development of hydrophobic nanotubes with the ability to insert into lipid membranes (Figure 30A).[189] The first example was reported in 1994 by the group of M. R. Ghadiri, who used *cyclo*-[*D*-Leu-*L*-Gln-(*D*-Leu-*L*-Trp-)$_3$] as a transmembrane channel for the efficient transport of small alkaline ions.[191] This system represented one of the first examples of a supramolecular ion channel. Absorption and

[168] Q. Song, Z. Cheng, M. Kariuki, S. C. L. Hall, S. K. Hill, J. Y. Rho, S. Perrier, *Chem. Rev.* **2021**, *121*, 13936-13995.
[170] N. Rodríguez-Vázquez, M. Amorín, J. R. Granja, *Org. Biomol. Chem.* **2017**, *15*, 4490-4505.
[183] E. González-Freire, F. Novelli, A. Pérez-Estévez, R. Seoane, M. Amorín, J. R. Granja, *Chem. Eur. J.* **2021**, *27*, 3029-3038.
[186] A. Bayón-Fernández, A. Méndez-Ardoy, C. Alvarez-Lorenzo, J. R. Granja, J. Montenegro, *J. Mater. Chem. B* **2023**, *11*, 606-617.
[187] A. Lamas, A. Guerra, M. Amorín, J. R. Granja, *Chem. Sci.* **2018**, *9*, 8228-8233.
[188] N. Rodríguez-Vázquez, H. L. Ozores, A. Guerra, E. González-Freire, A. Fuertes, M. Panciera, J. M. Priegue, J. Outeiral, J. Montenegro, R. García-Fandino, M. Amorín, J. R. Granja, *Curr. Top. Med. Chem.* **2014**, *14*, 2647-2661.
[189] J. Montenegro, M. R. Ghadiri, J. R. Granja, *Acc. Chem. Res.* **2013**, *46*, 2955-2965.
[190] T. M. Fyles, *Chem. Soc. Rev.* **2007**, *36*, 335-347.
[191] M. R. Ghadiri, J. R. Granja, L. K. Buehler, *Nature* **1994**, *369*, 301-304.

fluorescence spectroscopy revealed the incorporation of the peptide in large unilamellar vesicles (LUVs) and the ion transport ability of the channel was confirmed. Biophysical studies using polarized FT-IR showed that this channel have a central axis tilted 7° with respect to the phospholipid bilayer.[192]

These transmembrane nanotubes can also be used as transporters of small polar molecules such as glucose (Figure 30B).[193] Molecular modelling revealed that a pore size larger than 9 Å is necessary to accommodate and transport glucose. Therefore, the group of M. R. Ghadiri used the 10-residues *cyclo*-[*D*-Leu-*L*-Gln-(*D*-Leu-*L*-Trp-)$_4$] for this purpose. This represents one of the first examples of an artificial transmembrane channel able to transport neutral hydrophilic substrates across lipid bilayers. The same cyclic decapeptide was later exploited for the transport of glutamic acid.[194] Other examples of systems developed are heteromeric nanotubes with modified transport capabilities or diffusion-limited size-selective ion sensors.[195] Also, transmembrane nanotubes made of α,γ-CPs[196] or CP-polymer conjugates[197] were reported.

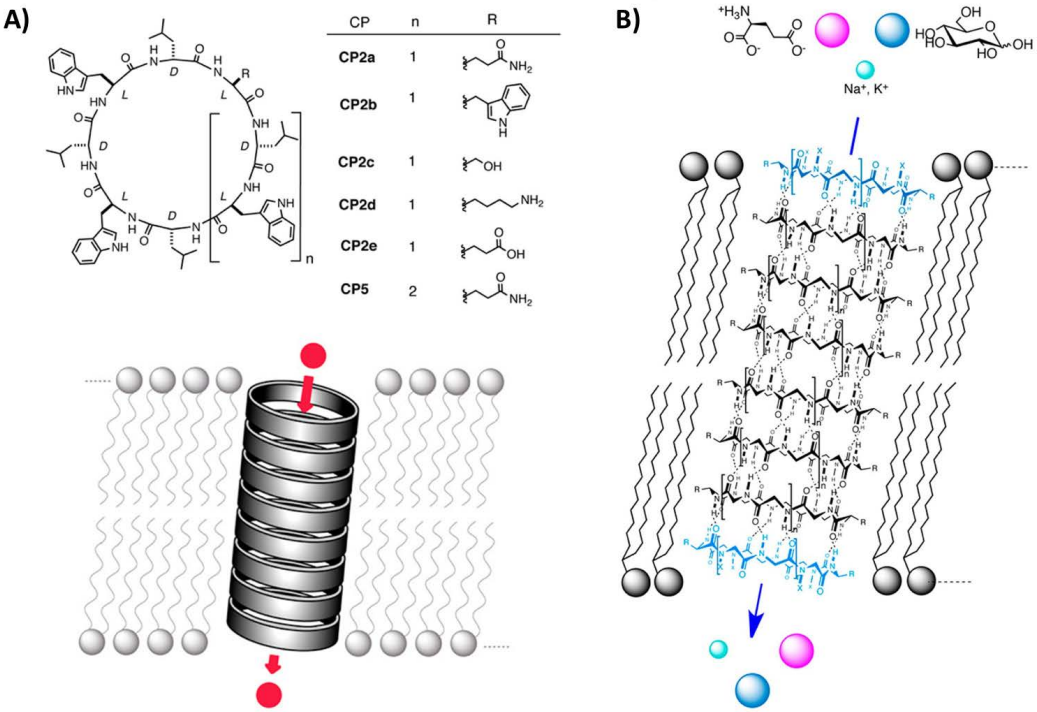

Figure 30. (A) Examples of hydrophobic CPs that can form transmembrane channels in lipid bilayers. Adapted with permission from Ref. 189. Copyright © 2013 American Chemical Society. (B) Transmembrane cyclic peptide nanotube for the transport of ions (green), glucose (blue) or glutamic acid (pink). Reprinted with permission from Ref. 189. Copyright © 2013 American Chemical Society.

[189] J. Montenegro, M. R. Ghadiri, J. R. Granja, *Acc. Chem. Res.* **2013**, *46*, 2955-2965.
[192] H. S. Kim, J. D. Hartgerink, M. R. Ghadiri, *J. Am. Chem. Soc.* **1998**, *120*, 4417-4424.
[193] J. R. Granja, M. R. Ghadiri, *J. Am. Chem. Soc.* **1994**, *116*, 10785-10786.
[194] J. Sánchez-Quesada, H. S. Kim, M. R. Ghadiri, *Angew. Chem. Int. Ed.* **2001**, *40*, 2503-2506.
[195] a) J. Sánchez-Quesada, M. P. Isler, M. R. Ghadiri, *J. Am. Chem. Soc.* **2002**, *124*, 10004-10005; b) K. Motesharei, M. R. Ghadiri, *J. Am. Chem. Soc.* **1997**, *119*, 11306-11312.
[196] a) R. García-Fandiño, J. R. Granja, M. D'Abramo, M. Orozco, *J. Am. Chem. Soc.* **2009**, *131*, 15678-15686; b) R. García-Fandiño, M. Amorín, L. Castedo, J. R. Granja, *Chem. Sci.* **2012**, *3*, 3280-3285; c) L. Ruiz, A. Benjamin, M. Sullivan, S. Keten, *J. Phys. Chem. Lett.* **2015**, *6*, 1514-1520; d) M. Calvelo, C. I. Lynch, J. R. Granja, M. S. P. Sansom, R. Garcia-Fandiño, *ACS Nano* **2021**, *15*, 7053-7064.
[197] M. Danial, C. M.-N. Tran, K. A. Jolliffe, S. Perrier, *J. Am. Chem. Soc.* **2014**, *136*, 8018-8026.

4.4.2. SCPNs as antimicrobial agents

Antibiotic resistance represents one of the major health problems worldwide, with the number of deaths expected to increase in the coming years. Therefore, it is necessary to find new strategies that can overcome the problems related with the appearance of drug resistance.[198] In this regard, cyclic peptide nanotubes emerge as an interesting alternative for the treatment of bacterial infections.[188]

The first examples of cyclic peptide nanotubes with antimicrobial activity were developed by the group of M. R. Ghadiri in 2001.[199] In particular, they reported a screening of 6- and 8-residues amphipathic cyclic peptides composed of a hydrophilic segment of 3 amino acids and a hydrophobic segment that alternates *L*-Trp and *D*-Leu. The best candidates showed high antimicrobial activity against Gram-positive and Gram-negative bacteria. A "carpet-like" mechanism was proposed based on the insertion of the nanotube in the bacterial membrane, the collapse of transmembrane potentials and the consequent cell death. Later, the same research group confirmed the prolonged systemic antimicrobial activity of this type of cyclic peptide nanotubes.[200] More recently, our group in collaboration with M. Bastos explored their mechanism of action by combining experimental techniques with Coarse-grained molecular dynamic (CG-MD) simulations (Figure 31A).[201] The cyclic peptide nanotubes showed a strong interaction with anionic membranes, while a reduce affinity for zwitterionic ones. The results also showed that, in most of the cases, the peptide nanotubes interact with a parallel orientation to the membrane to cause its collapse.

Other strategies were proposed to decorate the outer surface of the cyclic peptides and improve their activity. For example, again the group of M. R. Ghadiri developed *D*,*L*-α-glycopeptides with side chains modified with *D*-glucosamine, *D*-galactose or *D*-mannose (Figure 31B).[202] The incorporation of these sugars reduces the toxicity in mammalian cells without compromising the antimicrobial activity in Gram-positive strains. Also, our group described two orthogonal clickable reactions to modified antimicrobial cyclic peptide side chains with hydrophobic or hydrophilic moieties (Figure 31C).[183] In particular, a Cu-catalysed azide-alkyne [3+2] cycloaddition (CuAAC) was used to incorporate different hydrophobic tails to a propargylglycine residue, while an *O*-alkoxyamine moiety allowed the attachment of polar aldehydes

[183] E. González-Freire, F. Novelli, A. Pérez-Estévez, R. Seoane, M. Amorín, J. R. Granja, *Chem. Eur. J.* **2021**, *27*, 3029-3038.
[188] N. Rodríguez-Vázquez, H. L. Ozores, A. Guerra, E. González-Freire, A. Fuertes, M. Panciera, J. M. Priegue, J. Outeiral, J. Montenegro, R. García-Fandino, M. Amorín, J. R. Granja, *Curr. Top. Med. Chem.* **2014**, *14*, 2647-2661.
[198] a) A. H. Holmes, L. S. P. Moore, A. Sundsfjord, M. Steinbakk, S. Regmi, A. Karkey, P. J Guerin, L. J. V. Piddock, *Lancet.* **2016**, *387*, 176-187; b) T. Pulingam, T. Parumasivam, A. M. Gazzali, A. M. Sulaiman, J. Y. Chee, M. Lakshmanan, C. F. Chin, K. Sudesh, *Eur. J. Pharm. Sci.* **2022**, 170, 106103.
[199] S. Fernandez-Lopez, H.-S. Kim, E. C. Choi, M. Delgado, J. R. Granja, A. Khasanov, K. Kraehenbuehl, G. Long, D. A. Weinberger, K. M. Wilcoxen, M. R. Ghadiri, *Nature* **2001**, *412*, 452-455.
[200] V. Dartois, J. Sanchez-Quesada, E. Cabezas, E. Chi, C. Dubbelde, C. Dunn, J. Granja, C. Gritzen, D. Weinberger, M. R. Ghadiri, T. R. Parr, *Antimicrob. Agents Chemother*. **2005**, *49*, 3302-3310.
[201] B. Claro, E. González-Freire, M. Calvelo, L. J. Bessa, E. Goormaghtigh, M. Amorín, J. R. Granja, R. Garcia-Fandiño, M. Bastos, *Colloids Surf. B Biointerfaces*. **2020**, *196*, 111349.
[202] L. Motiei, S. Rahimipour, D. A. Thayer, C. Wong, M. R. Ghadiri, *Chem. Commun.* **2009**, *25*, 3693-3695.

such as sugars. The hydrocarbon tails enhance antimicrobial activity, while the sugars reduce the toxicity in hemolytic experiments.

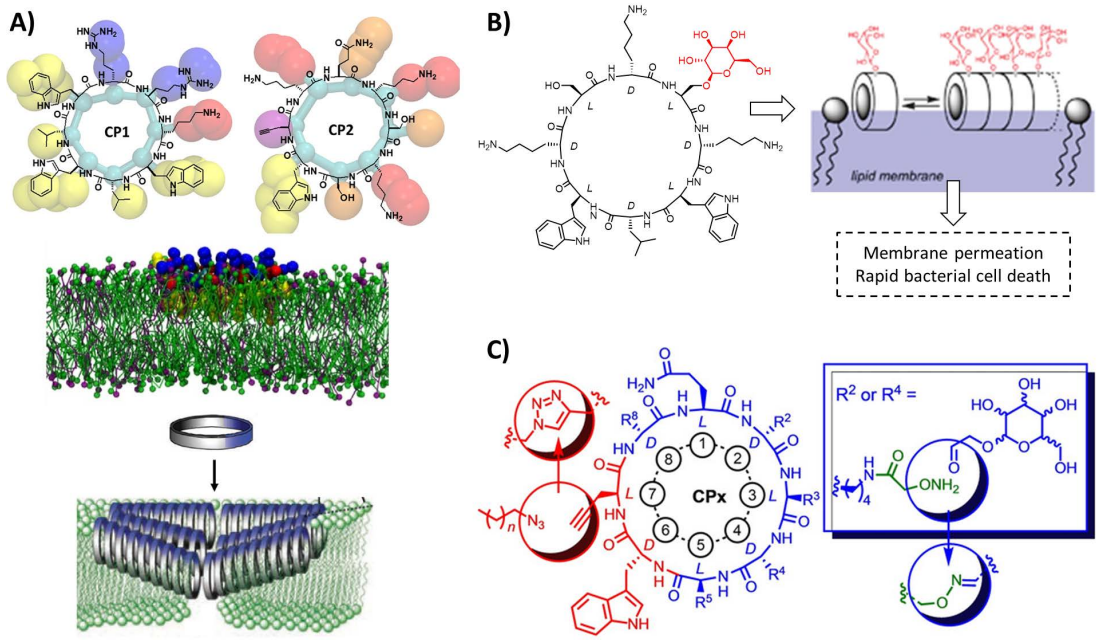

Figure 31. (A) Proposed model of interaction of antimicrobial cyclic peptide nanotubes with lipid bilayers through a "carpet-like" mechanism. Adapted with permission from Ref. 201. Copyright © 2020 Elsevier. (B) Example of an antimicrobial cyclic *D*,*L*-α-glycopeptide. Adapted with permission from Ref. 202. Copyright © 2009 Royal Society of Chemistry. (C) Antimicrobial cyclic peptides based on side chain modifications with two orthogonal clickable reactions. Reprinted with permission from Ref. 183. Copyright © 2021 Wiley-VCH Verlag GmbH & Co.

4.4.3. SCPNs as drug delivery systems

The versatility and biocompatibility of cyclic peptide nanotubes also made possible to study their application for cancer treatment. Initial computational studies raised the possibility of using the previously mentioned transmembrane nanotubes for the transport of the anti-tumour drug 5-fluorouracil (5-FU) across lipid membranes (Figure 32A).[203,204] Later, the group of W. Wu experimentally demonstrated the transport of 5-FU by transmembrane nanotubes composed of the hydrophobic cyclic peptide previously used for glucose transport.[193,205] In the presence of these artificial channels, the drug was able to internalize into the cancer cell faster than by passive diffusion. Moreover, 5-FU and CPs showed a synergistic anticancer effect on different tumour cells.

[183] E. González-Freire, F. Novelli, A. Pérez-Estévez, R. Seoane, M. Amorín, J. R. Granja, *Chem. Eur. J.* **2021**, *27*, 3029-3038.
[193] J. R. Granja, M. R. Ghadiri, *J. Am. Chem. Soc.* **1994**, *116*, 10785-10786.
[201] B. Claro, E. González-Freire, M. Calvelo, L. J. Bessa, E. Goormaghtigh, M. Amorín, J. R. Granja, R. Garcia-Fandiño, M. Bastos, *Colloids Surf. B Biointerfaces*. **2020**, *196*, 111349.
[202] L. Motiei, S. Rahimipour, D. A. Thayer, C. Wong, M. R. Ghadiri, *Chem. Commun.* **2009**, *25*, 3693-3695.
[203] H. Liu, J. Chen, Q. Shen, W. Fu, W. Wu, *Mol. Pharmaceutics* **2010**, *7*, 1985-1994.
[204] R. Vijayaraj, S. V. Damme, P. Bultinck, V. Subramanian, *Phys. Chem. Chem. Phys.* **2013**, *15*, 1260-1270.
[205] J. Chen, B. Zhang, F. Xia, Y. Xie, S. Jiang, R. Su, Y. Lua, W. Wu, *Nanoscale*, **2016**, *8*, 7127-7136.

PEG-modified nanotube bundles were also described by the group of M. Zhang for the encapsulation and transport of doxorubicin (Figure 32B).[206] The CP contained a glutamic acid whose protonation triggered the assembly process into bundles. However, this residue can be also used to load doxorubicin via the formation of an ion-pair, while a cysteine was incorporated to attach a maleimide-mPEG chain. This PEGylation process led to the formation of smaller bundles that showed the ability to increase doxorubicin cellular accumulation and overcome resistance in a human breast cancer cell line.

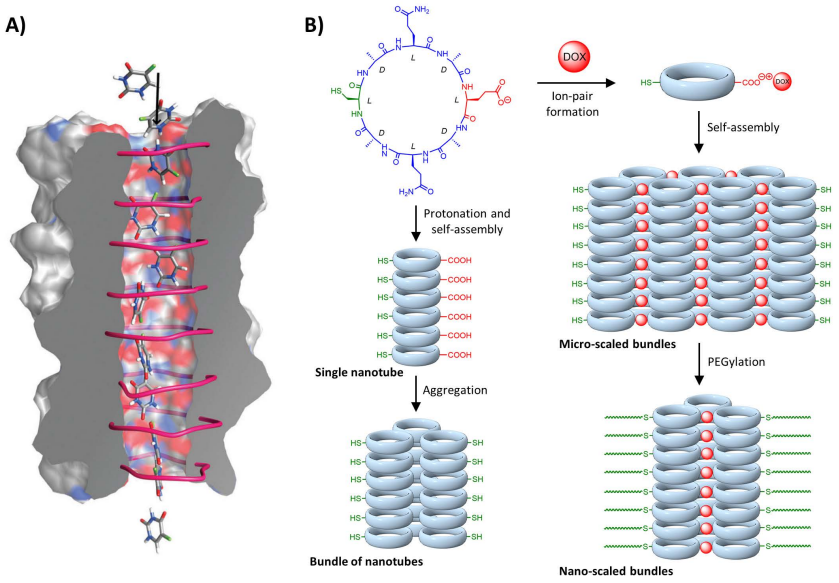

Figure 32. (A) Transport of 5-fluorouracil across lipid membranes with cyclic peptide transmembrane nanotubes. Reprinted with permission from Ref. 204. Copyright © 2013 Royal Society of Chemistry. (B) PEG-modified cyclic peptide nanotube bundles loaded with doxorubicin.

Other conjugates of cyclic peptides with polymers have been widely used as drug delivery systems due to the advantage of polymers to increase aqueous solubility. In this sense, the group of S. Perrier developed several cyclic peptide-polymer conjugates for the transport of antitumour drugs based on ruthenium or iridium complexes.[207] More recently, the same group attached camptothecin through a linker that was susceptible to esterase cleavage (Figure 33A).[208] The nanotube was also modified with a hydrophilic or amphiphilic RAFT polymer to protect the drug in the final structure. Specifically, the hydrophilic polymer increased the water solubility, while with the amphiphilic polymer they obtained nanotubes with a higher stability and size. These nanotubes showed a good cargo release, leading to cell death in 2D and 3D cellular models. Also, they reported photo-responsive tubisomes for the transport of doxorubicin (Figure 33B).[209] In particular, the cyclic peptide scaffold was modified with one hydrophilic and one hydrophobic polymer containing a photo-sensitive *o*-nitrobenzyl ester moiety. The

[204] R. Vijayaraj, S. V. Damme, P. Bultinck, V. Subramanian, *Phys. Chem. Chem. Phys.* **2013**, *15*, 1260-1270.
[206] Y. Wang, S. Yi, L. Sun, Y. Huang, S. C. Lenaghan, M. Zhang, *J. Biomed. Nanotechnol.* **2014**, *10*, 445-454.
[207] a) B. M. Blunden, R. Chapman, M. Danial, H. Lu, K. A. Jolliffe, S. Perrier, M. H. Stenzel, *Chem. Eur. J.* **2014**, *20*, 12745-12749; b) S. C. Larnaudie, J. C. Brendel, I. Romero-Canelón, C. Sanchez-Cano, S. Catrouillet, J. Sanchis, J. P. C. Coverdale, J. Song, A. Habtemariam, P. J. Sadler, K. A. Jolliffe, S. Perrier, *Biomacromolecules* **2018**, *19*, 239-247.
[208] S. K. Hill, R. M. England, S. Perrier, *J. Control Release* **2024**, *367*, 687-696.
[209] J. Yang, J. Song, Q. Song, J. Y. Rho, E. D. H. Mansfield, S. C. L. Hall, M. Sambrook, F. Huang, S. Perrier, *Angew. Chem. Int. Ed.* **2020**, *59*, 8860-8863.

resulting design was able to self-assemble into tubisomes in aqueous solution, allowing the encapsulation of doxorubicin in the interior. Upon light irradiation, cleavage of the *o*-nitrobenzyl ester takes place, changing the nature of the polymer from hydrophobic to hydrophilic and causing the disassembly of the tubisome for drug release.

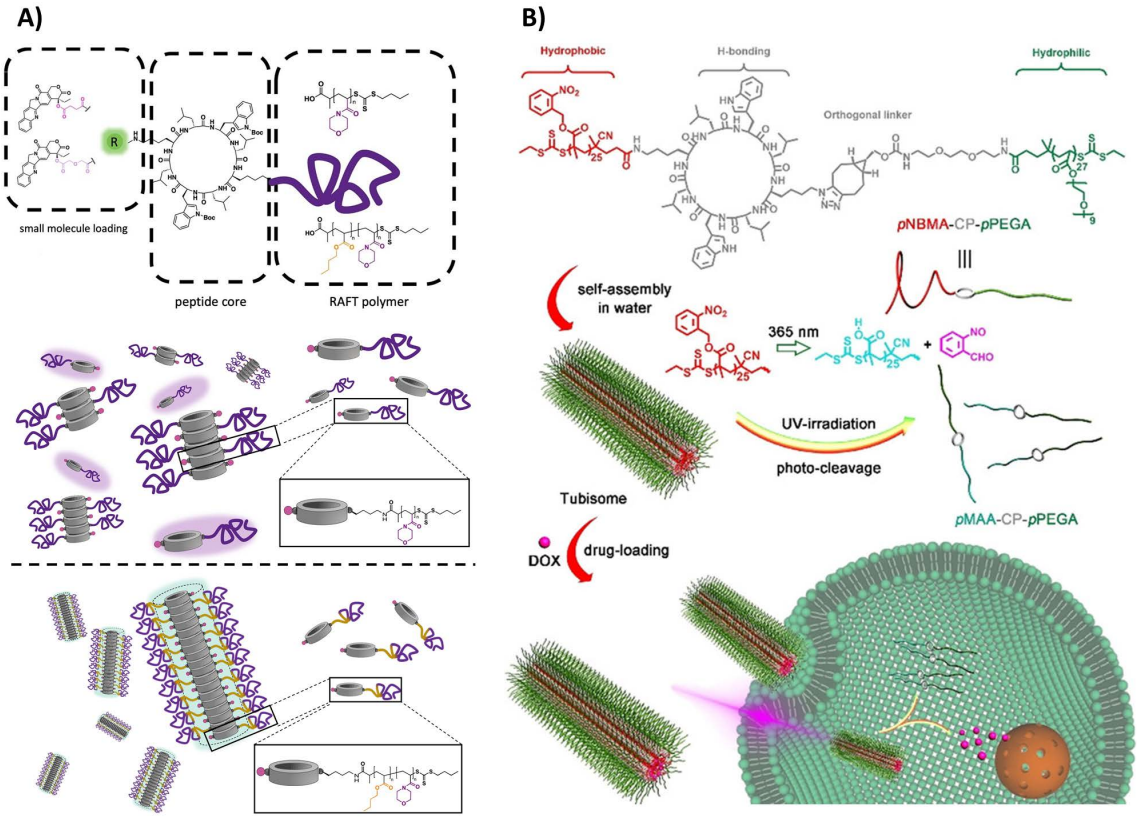

Figure 33. (A) Self-assembled nanotubes made by cyclic peptides modified with the drug camptothecin and a hydrophilic or amphiphilic polymer. Adapted with permission from Ref. 208. Copyright © 2024 Elsevier. (B) Tubisomes loaded with doxorubicin for photo-sensitive intracellular drug release. Reprinted with permission from Ref. 209. Copyright © 2020 Wiley-VCH Verlag GmbH & Co.

4.4.4. Control of the assembly properties of SCPNs

More recently, great efforts have been made to control the assembly process of cyclic peptide nanotubes. In general, once the nanotube formation is triggered, the process continues in a cooperative manner making difficult to control the final nanotube length or packing. Specifically, the group of S. Perrier has made major contributions with CP-polymer conjugates. For example, CPs functionalized with a polymer that can be protonated allow reversible control of the assembly process with pH changes (Figure 34A).[210] The conjugate is able to form nanotubes at physiological pH, while the disassembly can be achieved by protonation of the polymer at low pH. Later, they also developed redox-responsive cyclic peptide-polymer conjugates (Figure 34B).[211] The

[208] S. K. Hill, R. M. England, S. Perrier, *J. Control Release* **2024**, *367*, 687-696.
[209] J. Yang, J. Song, Q. Song, J. Y. Rho, E. D. H. Mansfield, S. C. L. Hall, M. Sambrook, F. Huang, S. Perrier, *Angew. Chem. Int. Ed.* **2020**, *59*, 8860-8863.
[210] S. C. Larnaudie, J. C. Brendel, K. A. Jolliffe, S. Perrier, *ACS Macro Lett.* **2017**, *6*, 1347-1351.
[211] Q. Song, J. Yang, S. C. L. Hall, P. Gurnani, S. Perrier, *ACS Macro Lett.* **2019**, *8*, 1347-1352.

cleavage with a reductant of the disulphide bond between a CP and a polymer induces the transition from a non-assembling monomeric form to self-assembled polymeric nanotubes. A similar strategy was used to prepare conjugates with membrane activity (Figure 34C).[212] Initially, the polymer acts as a shell that prevents interaction of the nanotube with membranes or other undesired components. The cleavage of disulphide linkers detaches the shielding polymer to generate membrane active nanotubes. In addition, larger nanotubes are obtained after the cleavage due to changes in the lateral aggregation and an enhanced tendency to stack. In another example, they reported the reversible switching of the self-assembly of cyclic peptide-polymer conjugates using host-guest interactions (Figure 34D).[213] This strategy consists of introducing phenylalanine moieties in the cyclic peptide scaffold as binding sites for CB[7] to generate nanotubes. Also, their dissociation can be achieved by the addition of a competitive 1-adamantanamine molecule.

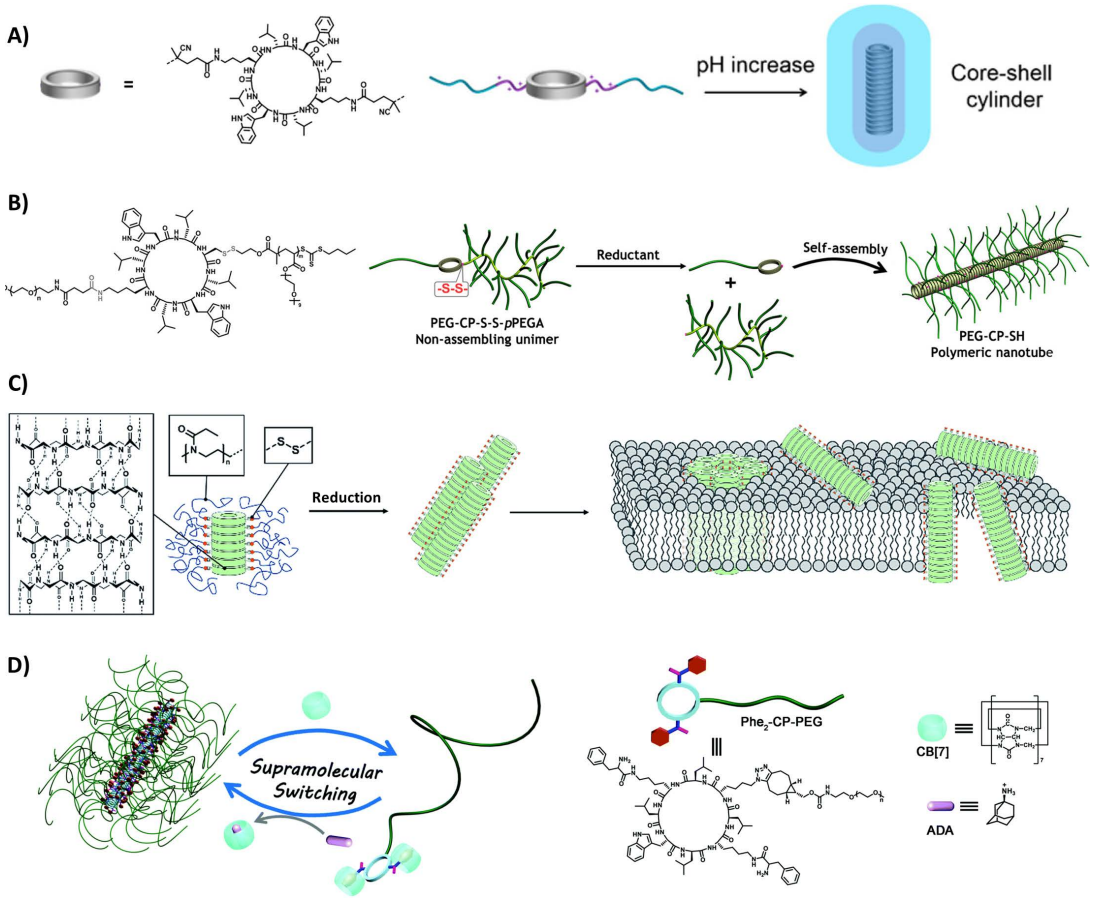

Figure 34. (A) pH-controlled assembly of CP-polymer conjugates. Adapted with permission from Ref. 210. Copyright © 2017 American Chemical Society. (B) Transition from non-assembling monomers to nanotubes based on redox-responsive CP-polymer conjugates. Adapted with permission from Ref. 211. Copyright © 2019 American Chemical Society. (C) Reduction of a disulphide linker to induce the interaction of nanotubes with membranes. Reprinted with permission from Ref. 212. Copyright © 2019 Royal Society of Chemistry. (D) Switching of cyclic peptide-polymer conjugates assembly via host-guest chemistry. Adapted with permission from Ref. 213. Copyright © 2019 Royal Society of Chemistry.

[210] S. C. Larnaudie, J. C. Brendel, K. A. Jolliffe, S. Perrier, *ACS Macro Lett.* **2017**, *6*, 1347-1351.
[211] Q. Song, J. Yang, S. C. L. Hall, P. Gurnani, S. Perrier, *ACS Macro Lett.* **2019**, *8*, 1347-1352.
[212] M. Hartlieb, S. Catrouillet, A. Kuroki, C. Sanchez-Cano, R. Peltier, S. Perrier, *Chem. Sci.* **2019**, *10*, 5476-5483.
[213] Q. Song, J. Yang, J. Y. Rho, S. Perrier, *Chem. Commun.* **2019**, *55*, 5291-5294.

However, the use of polymeric chains attached to CPs reduces the dynamism of the final supramolecular structure. For this reason, other strategies are needed to control the assembly process of all types of SCPNs. In this context, the group of T. Kudernac reported cyclic peptide nanotubes in which cycles of fast supramolecular polymerization and depolymerization can be photoinduced through protonation by a photoacid (Figure 35).[214] In particular, they designed a cyclic peptide with three glutamic acid residues, susceptible of being protonated, and a pyrene moiety to study the nanotube formation. A spiropyran derivative was used as an external photoacid because when the merocyanine form switches to the closed spiropyran form, a proton is released that induce a decrease in the pH value. At pH higher than 6.0, the carboxylic acid residues are negatively charged and the different CPs repel each other avoiding the assembly. In contrast, at values of pH lower than 5, these residues protonate inducing the assembly into nanotubes. In the presence of the photoacid, the pH oscillates between 6.1 and 4.9 under light irradiation triggering the supramolecular polymerization. The process can be quickly reverted in the dark. This example represents one of the first cases of control of cyclic peptide nanotubes assembly with light. However, the use of an external photoacid is required and the disassembly process occurs very quickly in the dark when irradiation is removed. Therefore, it is still necessary to find new strategies to control the assembly process in a less invasive and more durable way.

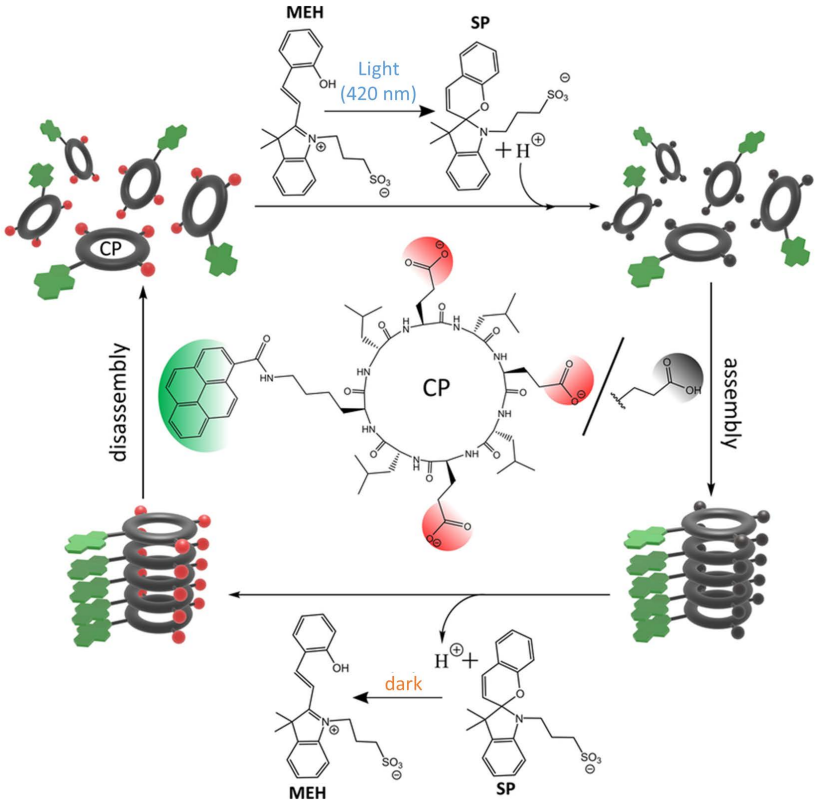

Figure 35. Assembly/disassembly cycle of cyclic peptides into nanotubes induced by a spiropyran photoacid that cause protonation/deprotonation of the glutamic acid residues. Reprinted with permission from Ref. 214. Copyright © 2020 Wiley-VCH Verlag GmbH & Co.

UNIVERSIDADE DE SANTIAGO DE COMPOSTELA

[214] N. Cissé, T. Kudernac, *ChemSystemsChem*, **2020**, *2*, e2000012.

Our research group also studied a pH-responsive CP that polymerize into nanotubes and fibres through a hierarchical assembly process after the external addition of base (Figure 36A).[215] The process is based on the deprotection of the imidazole moiety of two histidine residues. The assembly process could also be induced inside the confined space of water-in-oil droplets prepared by emulsification methods. Moreover, this basification can give rise to viscoelastic hydrogels.[186,215] Later, the spatially controlled supramolecular polymerization of the same peptide scaffold was evaluated in water-in-oil droplets fabricated with a microfluidic device, which allows to control the signal that triggers the self-assembly process (Figure 36B).[216] The fibrillation process occurred at the interface of the water-in-oil droplets when a base was used as a triggering agent, while the use of a high ionic strength triggered the assembly at the core of the droplets. These works represent the first examples of the supramolecular polymerization of cyclic peptide nanotubes in artificial minimal models.

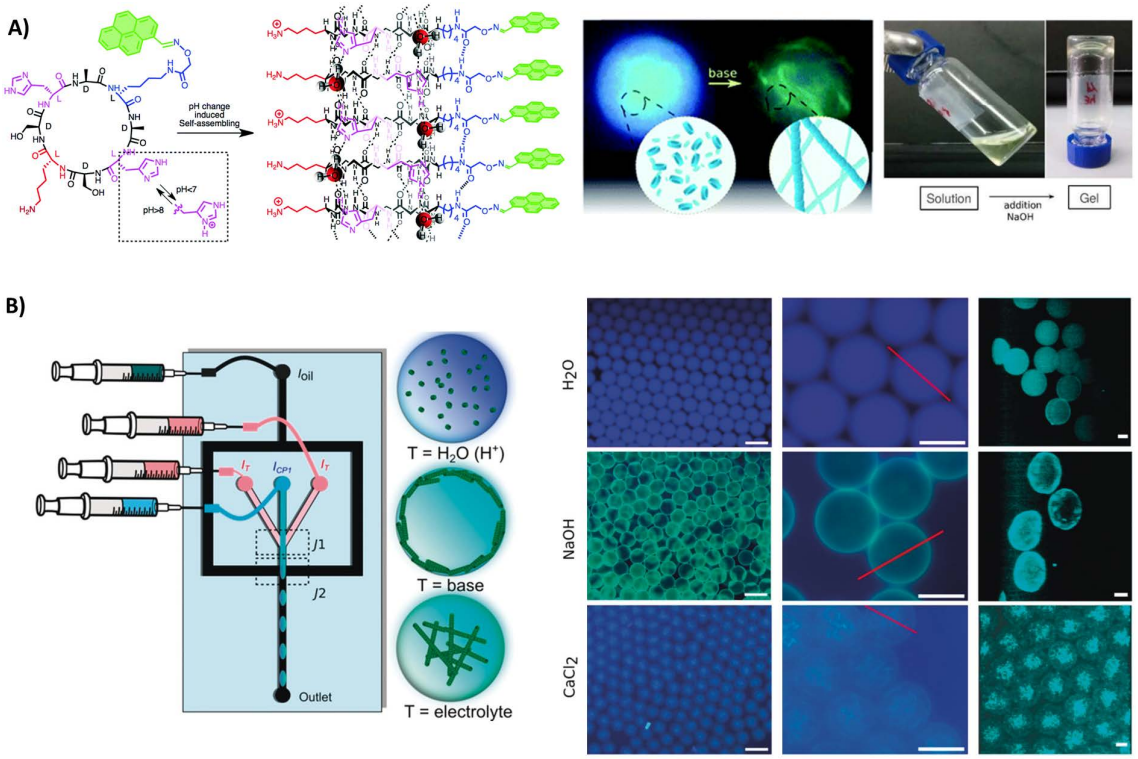

Figure 36. (A) Supramolecular polymerization of a pH-responsive cyclic peptide by addition of an external base. Adapted with permission from Ref. 215. Copyright © 2018 Royal Society of Chemistry. (B) Spatially controlled supramolecular fibrillation of a cyclic peptide at the interface or the core of microfluidic droplets. Adapted with permission from Ref. 216. Copyright © 2020 Wiley-VCH Verlag GmbH & Co.

[186] A. Bayón-Fernández, A. Méndez-Ardoy, C. Alvarez-Lorenzo, J. R. Granja, J. Montenegro, *J. Mater. Chem. B* **2023**, *11*, 606-617.
[215] A. Méndez-Ardoy, J. R. Granja, J. Montenegro, *Nanoscale Horiz.* **2018**, *3*, 391-396.
[216] A. Méndez-Ardoy, A. Bayón-Fernández, Z. Yu, C. Abell, J. R. Granja, J. Montenegro, *Angew. Chem. Int. Ed.* **2020**, *59*, 6902-6908.

5. OBJECTIVES

USC
UNIVERSIDADE
DE SANTIAGO
DE COMPOSTELA

The examples presented in the introduction illustrate that self-assembling cyclic peptide nanotubes represent a highly versatile class of supramolecular structures. However, as previously stated, one of the most significant challenges in this field is to achieve the on-demand control of the nanotube self-assembly process and the packaging of the final supramolecular entity. For these reasons, the main objective of this doctoral thesis is to add stimuli-responsiveness to cyclic peptide nanotubes in order to gain some control over their assembly process and obtain supramolecular structures with new properties and applications.

In particular, the first partial objective (Figure 37) is the orthogonal functionalization of the side chain of one of the amino acids that compose a cyclic peptide by condensation with a photo-responsive anthracene group. The resulting design should be capable of assembling into nanotubes through a hierarchical assembly process. In addition, the structural modifications induced by light irradiation would facilitate the control of the final nanotubes shape.

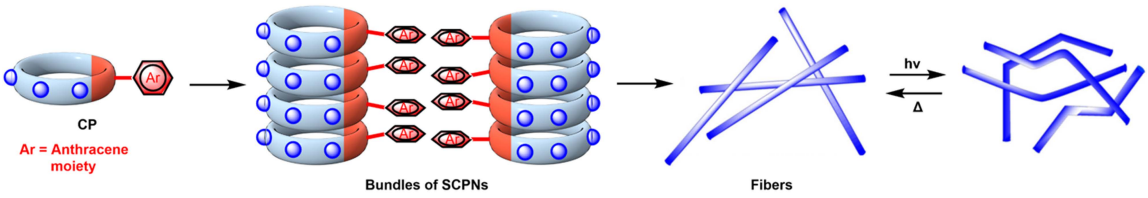

Figure 37. Objective 1: Anthracene photodimerization to bend self-assembling cyclic peptide nanotubes.

The second partial objective (Figure 38) is to introduce a photo-sensitive amino acid into a cyclic peptide sequence with the aim of gaining light control of the assembly/disassembly process. The appropriate light irradiation should induce a transition between a monomeric folded conformation and a flat conformation, which represents an essential step towards nanotube formation. The objective is also to evaluate their spatially controlled polymerization and the feasibility of triggering this process with light within confined aqueous droplets created by microfluidic techniques.

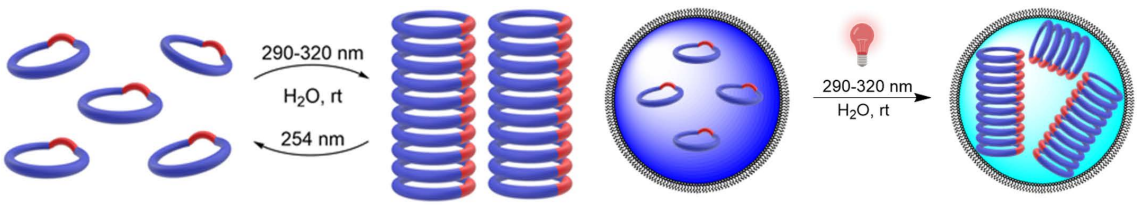

Figure 38. Objective 2: Photo-assembling cyclic peptides for dynamic light-driven peptide nanotubes.

USC UNIVERSIDADE DE SANTIAGO DE COMPOSTELA

The third and final partial objective (Figure 39) is to develop a library of cyclic peptides for the treatment of cancer cells. This will be achieved by condensation of the antitumour drug doxorubicin via an acid-labile bond, which should selectively release the drug in the more acidic environment of tumour cells. This stimulus-responsive strategy should facilitate the intracellular delivery of the antitumour drug.

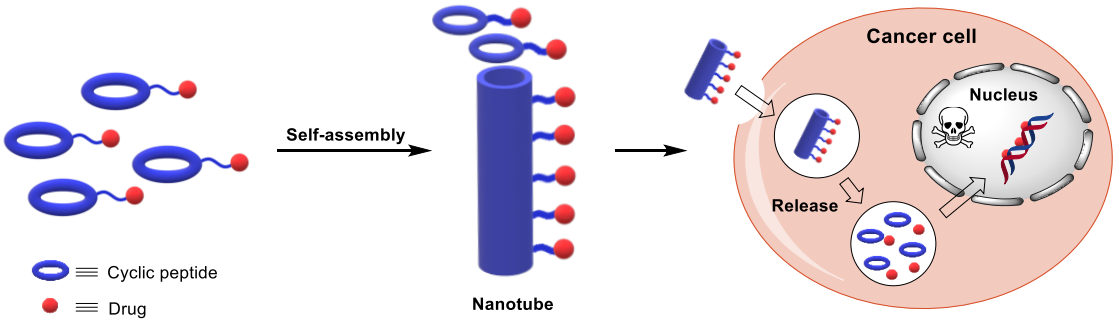

Figure 39. Objective 3: Self-assembling cyclic peptide nanotubes for the transport of doxorubicin into cancer cells.

USC UNIVERSIDADE DE SANTIAGO DE COMPOSTELA

6. RESULTS AND DISCUSSION

USC
UNIVERSIDADE
DE SANTIAGO
DE COMPOSTELA

6.1. ANTHRACENE PHOTODIMERIZATION TO BEND SELF-ASSEMBLING CYCLIC PEPTIDE NANOTUBES

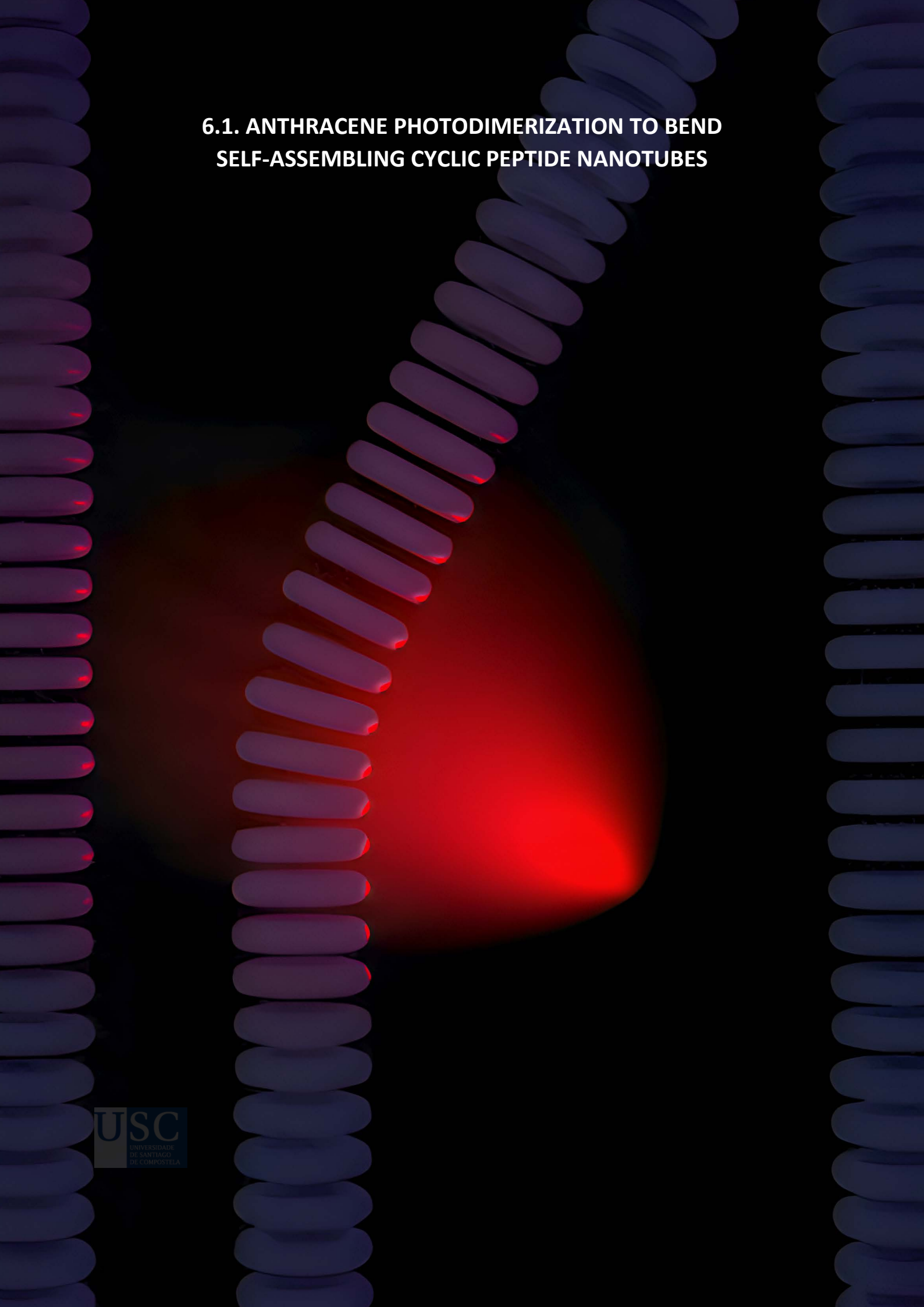

The results of this chapter have been published in *Angewandte Chemie International Edition* as:

F. Novelli, M. Vilela, A. Pazó, M. Amorín, J. R. Granja. Molecular Plumbing to Bend Self-Assembling Peptide Nanotubes. *Angew. Chem. Int. Ed.* **2021**, *60*, 18838-18844. DOI: 10.1002/anie.202107034

Affiliations

Centro Singular de Investigación en Química Biolóxica e Materiais Moleculares (CiQUS), Departamento de Química Orgánica, Universidade de Santiago de Compostela, 15782 Santiago de Compostela, Spain.

Information in this chapter is reproduced from Ref. 217 with permission from Wiley-VCH Verlag GmbH & Co.

USC UNIVERSIDADE DE SANTIAGO DE COMPOSTELA

[217] F. Novelli, M. Vilela, A. Pazó, M. Amorín, J. R. Granja. *Angew. Chem. Int. Ed.* **2021**, *60*, 18838-18844.

6.1.1. Precedents

Anthracene is a photo-responsive moiety that under UV light irradiation (~350 nm) undergoes a dimerization process through a [4+4] cycloaddition reaction.[218] The resulting dimer can be reverted again to the monomers when irradiated with light of higher energy (~250 nm) or by heating at high temperature.

This moiety has been specially used as a photo-cross-linking component.[219] For example, the group of M. Watanabe reported the photohealing of ion gels based on anthracene photodimerization (Figure 40A).[220] In particular, a tetra-arm poly(ethylene glycol) modified with anthracene moieties was combined with an ion liquid to form an ion gel through light irradiation. The group of L. A. Connal developed a light-driven hydrogel actuator by modifying a hydrophilic copolymer with anthracene (Figure 40B).[221] A benzylimine functionalized group was used to red-shift the absorption and the visible-light photo-dimerization induces a change in the hydrogel network causing a macroscopic bending of the hydrogel.

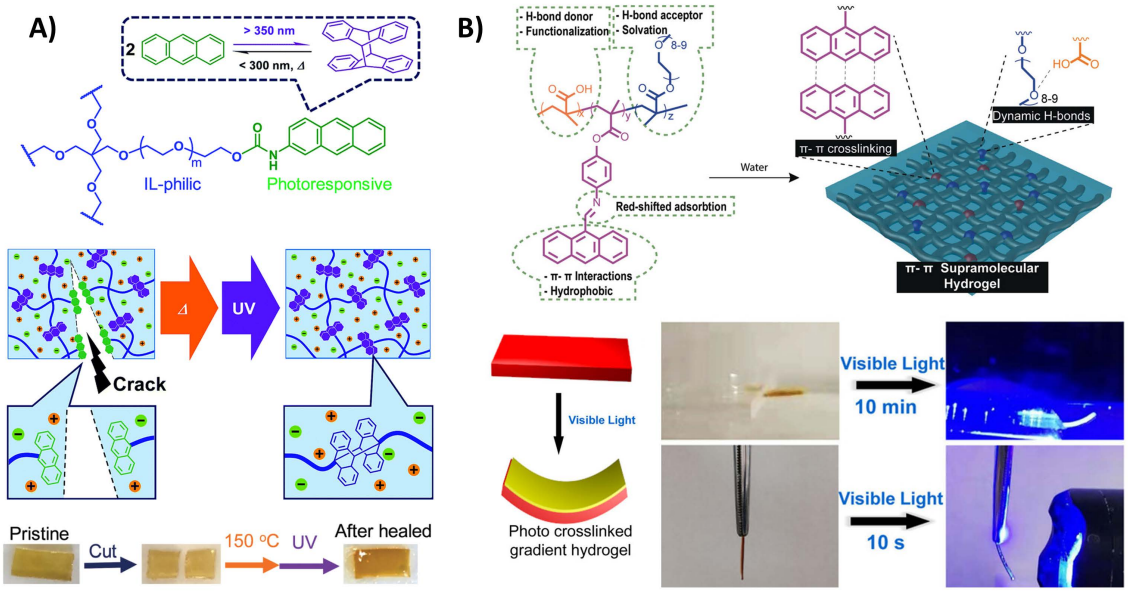

Figure 40. (A) Photohealing of an ion gel based on the photo-dimerization of anthracene. Reprinted with permission from Ref. 220. Copyright © 2018 Royal Society of Chemistry. (B) Supramolecular photo-responsive hydrogel and light-induced bending motion. Reprinted with permission from Ref. 221. Copyright © 2020 Wiley-VCH Verlag GmbH & Co.

[218] a) D. Greene, S. L. Misrock, J. R. Wolfe, *J. Am. Chem. Soc.* **1955**, *77*, 3852-3855; b) D. E. Applequist, R. L. Litle, E. C. Friedrich, R. E. Wall, *J. Am. Chem. Soc.* **1959**, *81*, 452-456; c) H. Becker, *Chem. Rev.* **1993**, *93*, 145-172; d) H. Bouas-Laurent, A. Castellan, J.-P. Desvergnea, R. Lapouyadec, *Chem. Soc. Rev.* **2000**, *29*, 43-55; e) H. Bouas-Laurent, A. Castellan, J.-P. Desvergnea, R. Lapouyadec, *Chem. Soc. Rev.* **2001**, *30*, 248-263; f) M. Yoshizawa, J. K. Klosterman, *Chem. Soc. Rev.* **2014**, *43*, 1885-1898.

[219] a) Z. Hou, W. M. Nau, R. Hoogenboom, *Polym. Chem.* **2021**, *12*, 307-315; b) J. Bai, Z. Shi, J. Yin, M. Tian, R. Qu, *Adv. Funct. Mater.* **2018**, *28*, 1800939; c) Z. Wang, L. Guo, H. Xiao, H. Cong, S. Wang, *Mater. Horiz.* **2020**, *7*, 282-288; d) M. C. Paderes, M. J. Diaz, C. Angelo Pagtalunan, D. A. Bruzon, G. A Tapang, *Chem Asian J.* **2022**, *17*, e202200193.

[220] A. Saruwatari, R. Tamate, H. Kokubo, M. Watanabe, *Chem. Commun.* **2018**, *54*, 13371-13374.

[221] Z. Jiang, M. L. Tan, M. Taheri, Q. Yan, T. Tsuzuki, M. G. Gardiner, B. Diggle, L. A. Connal, *Angew. Chem. Int. Ed.* **2020**, *59*, 7049-7056.

Also, the group of Q. Yang reported double-dynamic supramolecular polymers based on the combination of anthracene photodimerization and the host-guest interaction between pillar[5]arene and imidazole groups (Figure 41A).[222] The polymerization/depolymerization process can be controlled by changes in temperature and irradiation that induce a macroscopic gel/sol transition. In a similar manner, the group of S. J. Webb published the photo-disassembly and dissociation of amino acid hydrogels modified in the amino group with an anthracene that undergoes photo-induced gel-phase dimerization (Figure 41B).[223] A photo-change in the morphology was also observed by the group of C. J. Bardeen with crystals of 9-methylanthracene (Figure 41C).[224] In particular, this molecule can crystalize into microneedles or microribbons depending on the conditions. Upon light irradiation and subsequent anthracene photodimerization, the authors found that the microneedles bent, while the microribbonds twisted.

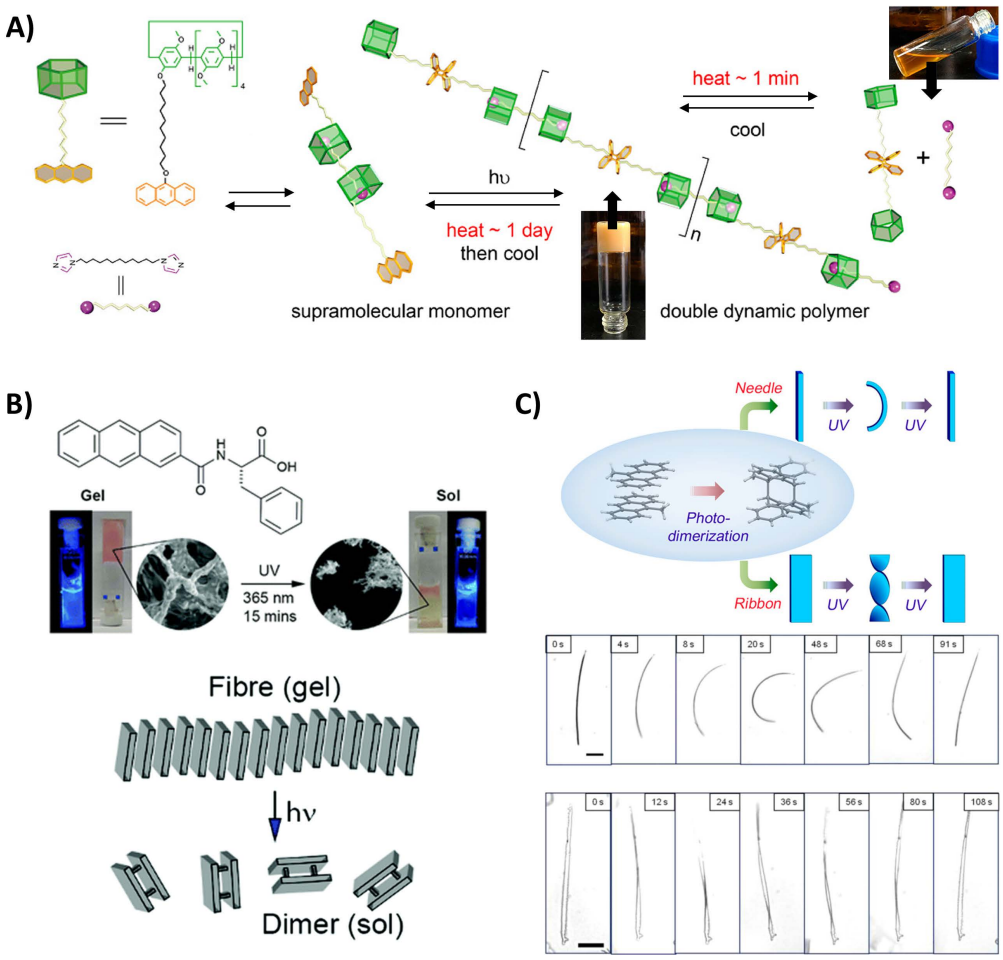

Figure 41. (A) Double-dynamic supramolecular polymer based on anthracene photodimerization and host-guest chemistry. Adapted with permission from Ref. 222. Copyright © 2013 American Chemical Society. (B) Photodimerization of self-assembled anthracene-amino acids and subsequent hydrogel dissociation. Reprinted with permission from Ref. 223. Copyright © 2020 Royal Society of Chemistry. (C) Photo-bending of a microneedle and photo-twisting of a microribbon made of 9-methylanthracene. Reprinted with permission from Ref. 224. Copyright © 2014 American Chemical Society.

[222] J. Xu, Y. Chen, L. Wu, C. Tung, Q. Yang, *Org. Lett.* **2013**, *15*, 6148-6151.
[223] P. R. A. Chivers, R. S. Dookie, J. E. Gough, S. J. Webb, *Chem. Commun.* **2020**, *56*, 13792-13795.
[224] T. Kim, L. Zhu, L. J. Mueller, C. J. Bardeen, *J. Am. Chem. Soc.* **2014**, *136*, 6617-6625.

6.1.2. Objective

As mentioned before, one of the main difficulties of self-assembling cyclic peptide nanotubes is to control their final packing. In fact, some progress has been achieved in the last years by using CPs/polymers hybrids, but further control in these nanotube structural parameters is still required.[225]

Moreover, our group previously described the side chain functionalization of CPs by the orthogonal incorporation of aryl groups.[215,216] In particular, it consists of a condensation between aryl aldehydes with CPs bearing an alkoxyamine moiety. In these peptides, the interdigitation of the aromatic moieties not only helps the stacking of CPs into nanotubes, but also promotes the formation of small bundles through a hierarchical self-assembling process.

In this chapter, we propose to use this orthogonal transformation to attach an anthracene moiety to a cyclic peptide (Figure 42). We envisage that the light-induced anthracene dimerization process could be used to induce changes in the SCPN packing and properties.

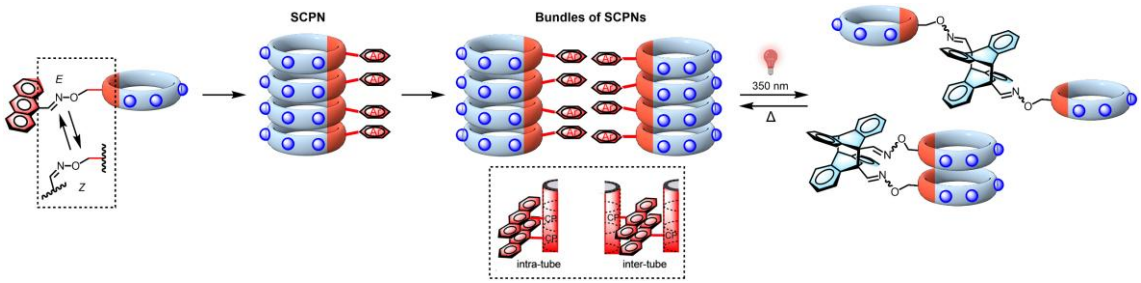

Figure 42. Objective of this chapter: supramolecular hierarchical process and anthracene [4+4] photodimerization to induce changes in the SCPN packing.

[215] A. Méndez-Ardoy, J. R. Granja, J. Montenegro, *Nanoscale Horiz.* **2018**, *3*, 391-396.
[216] A. Méndez-Ardoy, A. Bayón-Fernández, Z. Yu, C. Abell, J. R. Granja, J. Montenegro, *Angew. Chem. Int. Ed.* **2020**, *59*, 6902-6908.
[225] a) J. Y. Rho, S. Perrier, *ACS Macro Lett.* **2021**, *10*, 258-271; b) S. Catrouillet, J. C. Brendel, S. Larnaudie, T. Barlow, K. A. Jolliffe, S. Perrier, *ACS Macro Lett.* **2016**, *5*, 1119-1123; c) R. Chapman, M. L. Koh, G. G. Warr, K. A. Jolliffe, S. Perrier, *Chem. Sci.* **2013**, *4*, 2581-2589; d) J. Y. Rho, J. C. Brendel, L. R. MacFarlane, E. D. H. Mansfield, R. Peltier, S. Rogers, M. Hartlieb, S. Perrier, *Adv. Funct. Mater.* **2017**, *27*, 201704569.

6.1.3. Results and discussion

6.1.3.1. Design

To carry out this work, we decided to create a new class of cyclic peptide hybrids made of α- and β-amino acids, which should allow to precisely control the interpeptide register and the β-sheet type structure (Figure 43).[226] For this purpose, we used a *D*,*L*-α-alternating sequence combined with two β-amino acids. In the required flat conformation, this type of β-residues with an even number of carbons between the carbonyl and NH moieties predispose the amide groups (NH and C=O) pointing in opposite directions.[227] Therefore, the insertion of these β-residues should induce the CPs to stack by forming parallel β-sheet structures.[228] The incorporation of the His residues was aimed to provide aqueous solubility to the peptide and control of the self-assembling capability due to its ionization state changes at almost neutral pH. Moreover, a Lys modified with a hydroxylamine acetyl moiety was place at the opposite side of the β-residues to allow the incorporation of anthracene-9-carbaldehyde through the formation of an oxime bond. Consequently, in the proposed parallel model, the arene stacking and the β-residues would provide nanotubes in which each residue would be aligned with itself along the tubular structure (Figure 43). In this organization, His, Ser or Gln side chains could also participate in stabilizing the tubular structure by forming additional hydrogen bonds assisted, in some cases, by water molecules.

[226] M. R. Silk, J. Newman, J. C. Ratcliffe, J. F. White, T. Caradoc-Davies, J. R. Price, S. Perrier, P. E. Thompson, D. K. Chalmers, *Chem. Commun.* **2017**, *53*, 6613-6616.
[227] R. P. Cheng, S. H. Gellman, W. F. DeGrado, *Chem. Rev.* **2001**, *101*, 3219-3232.
[228] a) M. R. Silk, J. Newman, J. C. Ratcliffe, J. F. White, T. Caradoc-Davies, J. R. Price, S. Perrier, P. E. Thompson, D. K. Chalmers, *Chem. Commun.* **2017**, *53*, 6613-6616; b) T. D. Clark, L. K. Buehler, M. R. Ghadiri, *J. Am. Chem. Soc.* **1998**, *120*, 651-656; c) D. Seebach, J. L. Matthew, T. W. A. Meden, C. Baerlocher, L. B. McCusker, *Helv. Chim. Acta* **1997**, *80*, 173-182; d) T. Marmin, Y. L. Dory, *Chem. Eur. J.* **2019**, *25*, 6707-6711; e) S. Leclair, P. Baillargeon, R. Skouta, D. Gauthier, Y. Zhao, Y. L. Dory, *Angew. Chem. Int. Ed.* **2004**, *43*, 349-353; f) Y. Tabata, Y. Kamano, H. Uji, T. Imai, S. Kimura, *Chem. Lett.* **2019**, *48*, 322-324.

USC

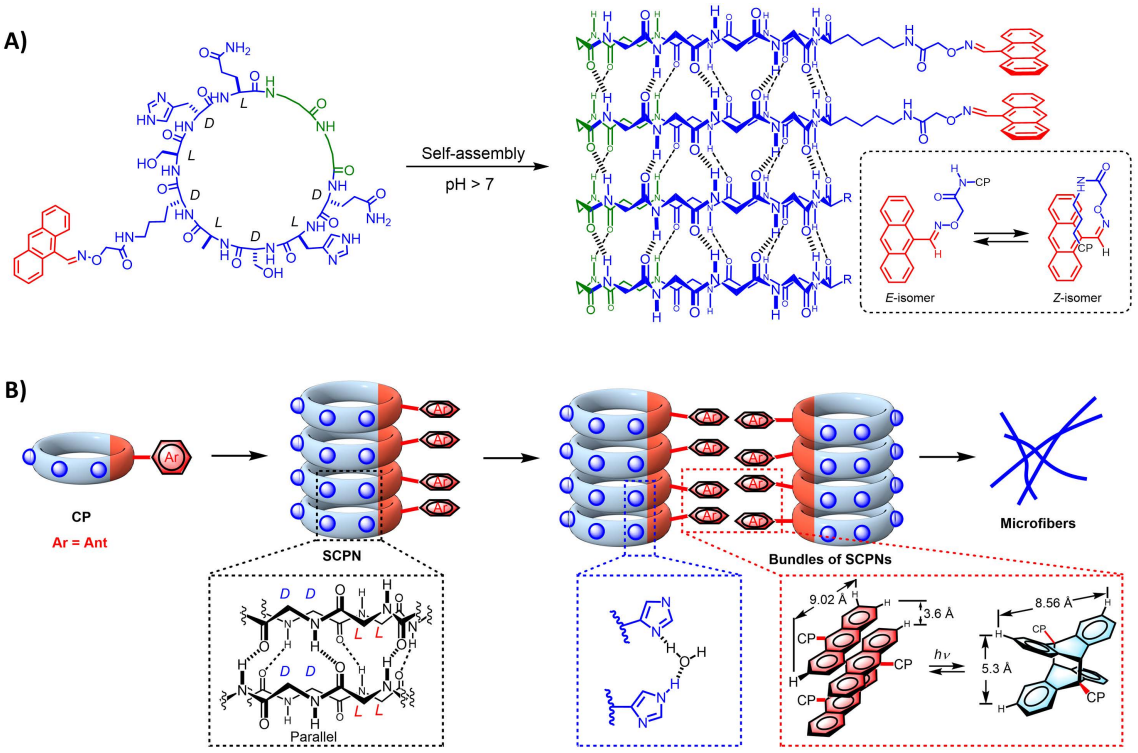

Figure 43. (A) Structure of the cyclic peptide used in this chapter and model for nanotube formation guided by the stacking of anthracene moieties and the β-residues. Right inset: proposed structures for the *E*- and *Z*- isomers of the *o*-alkyloxime linker. (B) Supramolecular hierarchical process responsible for SCPN bundles formation. Right inset: proposed changes in dimensions of anthracene moieties upon photodimerization.

6.1.3.2. Solid-phase peptide synthesis

CP1 was prepared by solid-phase methods and following an strategy previously reported by our group (Figure 44).[215,216,229] First, an α-allyl-protected glutamic acid was attached through its side chain to a Rink amide resin. Next, cycles of deprotection of the Fmoc group with 25% piperidine/DMF and coupling of the next Fmoc-protected amino acid with *N*-HBTU were performed. Once the full linear peptide was synthetized, the *C*-terminal allyl-protecting group was removed with π-allyl palladium chemistry. Then, the *N*-terminal protecting group was removed with 25% piperidine/DMF and the cyclization reaction was performed using PyAOP as a coupling agent. The Lys side chain functionalization was carried out by deprotection of the Mtt group with mild acidic conditions (hexafluoroisopropanol [HFIP]/trifluoroethanol [TFE]/triisopropylsilane [TIS]/dichloromethane [DCM] [20:10:5:65]), followed by coupling with *N*-HATU of (Boc-aminooxy)acetic acid. Cleavage of the peptide from the resin and the side chain

[215] A. Méndez-Ardoy, J. R. Granja, J. Montenegro, *Nanoscale Horiz.* **2018**, *3*, 391-396.
[216] A. Méndez-Ardoy, A. Bayón-Fernández, Z. Yu, C. Abell, J. R. Granja, J. Montenegro, *Angew. Chem. Int. Ed.* **2020**, *59*, 6902-6908.
[229] a) J. M. Palomo, *RSC Adv.* **2014**, *4*, 32658-32672; b) P. Rovero, L. Quartara, G. Fabbri, *Tetrahedron Lett.* **1991**, *32*, 2639-2642; c) A. El-Faham, F. Albericio, *Chem. Rev.* **2011**, *111*, 6557-6602; d) F. Albericio, *Biopolymers* **2000**, *55*, 123-139.

deprotection was performed by treatment with a solution of TFA, H_2O and TIS (95:2.5:2.5). After HPLC purification, the resulting pure peptide (**CP1**) was condensed with 9-anthracenecarboxaldehyde by mixing both components in DMSO at 60°C to provide **CP2**. The HPLC analysis of this peptide showed one single peak, confirming its purity, which did not require further purification.

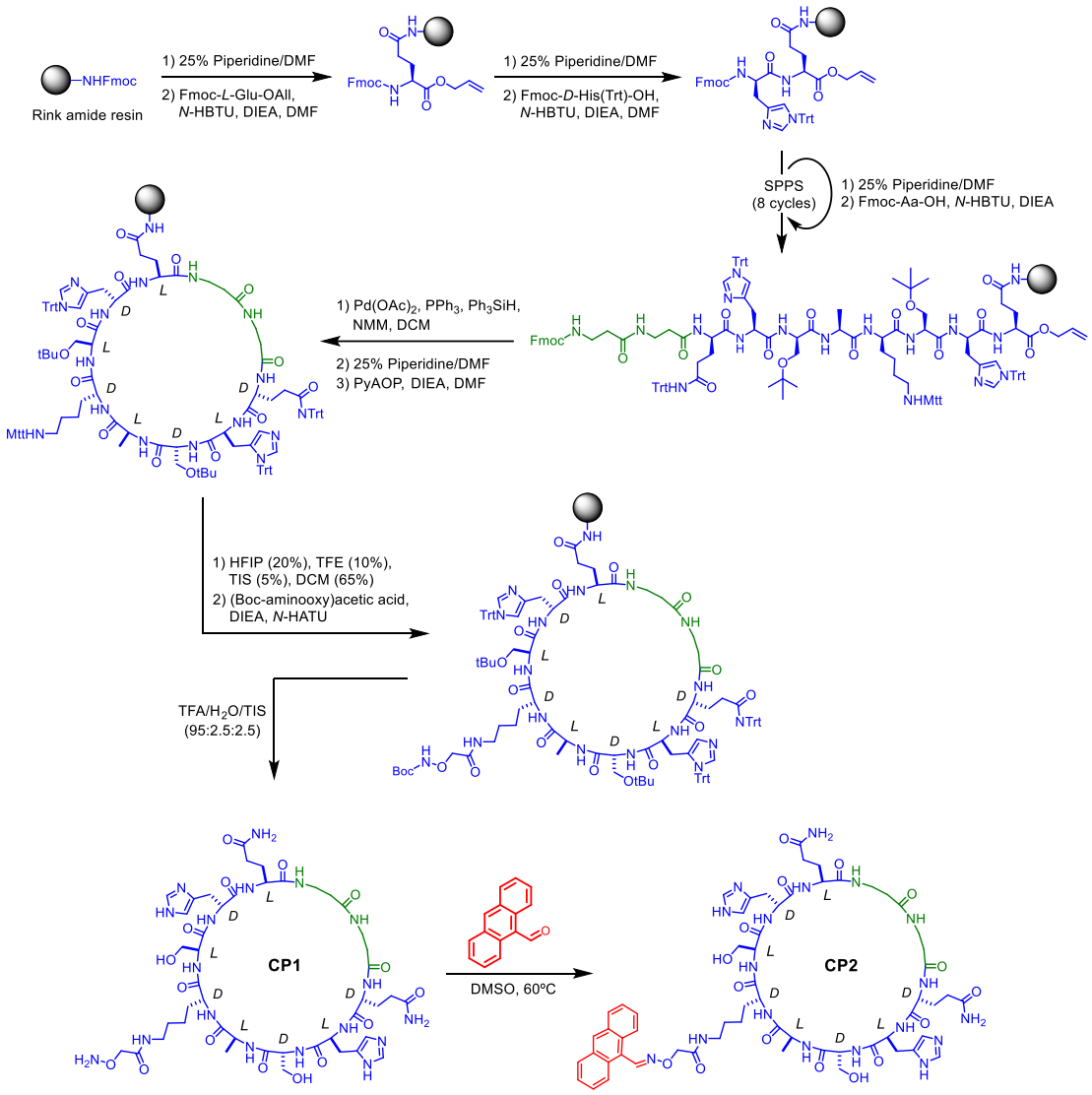

Figure 44. Synthetic strategy for the preparation of **CP1** and **CP2**.

6.1.3.3. Self-assembly properties

Our initial studies were directed to demonstrate the ability of this new *D,L*-α,β-CP hybrid to assemble into nanotubes both in solution and solid-state. **CP2** was soluble in double distilled water, whose resulting pH (3-5) depended on CP concentration as a consequence of its protonation state after the HPLC purification. At neutral pH (HEPES buffer), the solubility is reduced, starting to precipitate at concentrations above 400 µM. The fluorescence spectra at native pH showed a band

centred around 475 nm whose intensity slightly decreases as pH is raised until a critical point (pH 7.3), after which emission starts to increase upon further base addition (Figure 45A). Such behaviour might be explained by the imidazolium ring deprotonation as the pH increases that might trigger the CP self-assembly. This assembly of CPs must cause the stacking of the aromatic fluorophore and, consequently, lead to a higher fluorescent output. Experiments using Nile red (NR) were also carried out to determine the critical aggregation concentration (*cac*), which represents the lowest concentration in which CP assembly starts to take place. NR is a hydrophobic dye that exhibits a significant increase together with a blue shift of the maximum emission wavelength when incorporated in hydrophobic environments.[230] The fluorescence experiments of **CP2** at different concentrations (6-500 µM) in HEPES buffer (10 mM, pH 7.0) and in the presence of NR (1 µM) allowed to estimate a *cac* around 50 µM (Figure 45B). A similar value (45 µM) was obtained in the same conditions but using the Thioflavin T (ThT) probe (Figure 45C), which is a dye that only emits fluorescence upon binding to β-sheet structures.[231] These results suggest that the β-sheet formation takes place together with a hydrophobic packing when the aggregation occurs.

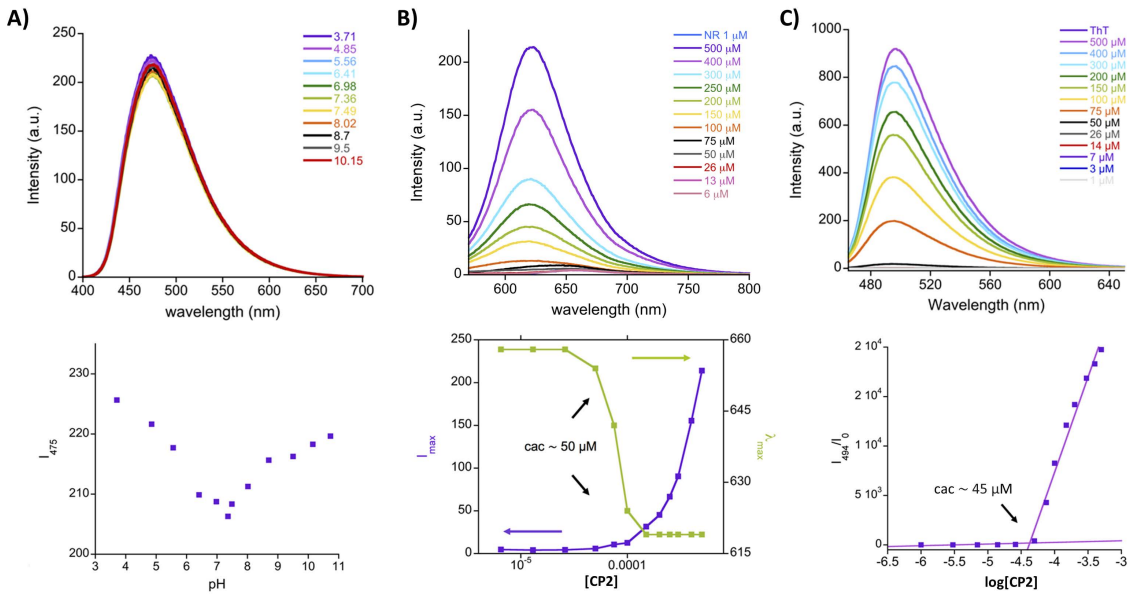

Figure 45. (A) **CP2** fluorescence spectra at different pH obtained upon addition of NaOH (0.1 M) to an aqueous solution of **CP2** at 350 µM (λ_{exc} = 385 nm, T = 20°C) and trend of fluorescence emission at 475 nm versus pH. (B) NR (1 µM) fluorescence spectra at different concentrations of **CP2** in HEPES buffer (10 mM, pH 7.0) and maximum intensity (data in purple) with the corresponding wavelength at maximum intensity (data in green) for calculating a *cac* of 50 µM (λ_{exc} = 550 nm, T = 20°C). (C) Overlaid ThT (20 µM) fluorescence spectra of solutions of **CP2** at different concentrations in HEPES buffer (10 mM, pH 7.0) and intensity ratio I_{494}/I_0 versus the logarithm of the concentration of **CP2** (λ_{exc} = 440 nm, T = 20°C). I_0 is the fluorescence intensity at 494 nm of ThT alone. The break point indicates a *cac* of 45 µM.

[230] a) R. M. P. Da Silva, D. Van Der Zwaag, L. Albertazzi, S. S. Lee, E. W. Meijer, S. I. Stupp, *Nat. Commun.* **2016**, *7*, 11561; b) R. Mishra, D. Sjölander, P. Hammarström, *Mol. BioSyst.* **2011**, *7*, 1232-1240; c) M. C. A. Stuart, J. C. van de Pas, J. B. F. N. Engberts, *J. Phys. Org. Chem.* **2005**, *18*, 929-934.

[231] a) H. Naiki, K. Higuchi, M. Hosokawa, T. Takeda, *Anal. Biochem.* **1989**, *177*, 244-249; b) M. Girych, G. Gorbenko, I. Maliyov, V. Trusova, C. Mizuguchi, H. Saito, P. Kinnunen, *Methods Appl. Fluoresc.* **2016**, *4*, 034010; c) M. J. Groenning, *J. Chem. Biol.* **2010**, *3*, 1-18.

FT-IR measurement was carried out to investigate the CP structure (Figure 46A). The FT-IR spectrum on a freeze-dried powder after basification supports the formation of a parallel β-sheet structure with a strong peak at 1633.3 cm^{-1} and a shoulder at 1664.6 cm^{-1}.[192,232] The amide A band at 3292.5 cm^{-1} is highly indicative of a well-established network of backbone-backbone hydrogen bonds.[233] Circular dichroism (CD) studies were also performed to evaluate the pH-induced supramolecular self-assembly (Figure 46B). No CD signals were detected at native pH (~3.6). On the contrary, a strong signal was observed at 240-290 nm and, to a lesser extent, for the anthracene band at 340-420 nm with increasing pH. Such an outcome suggests the formation of long-range-ordered supramolecular assemblies as the pH increases, with the transfer of chirality from the peptide to the anthracene unit. Plotting the CD signal at 275 nm as a function of the pH provided mean values of pKa = 7.3 and a Hill coefficient of n = 1.6 ± 0.3, suggesting a cooperative self-assembly process.

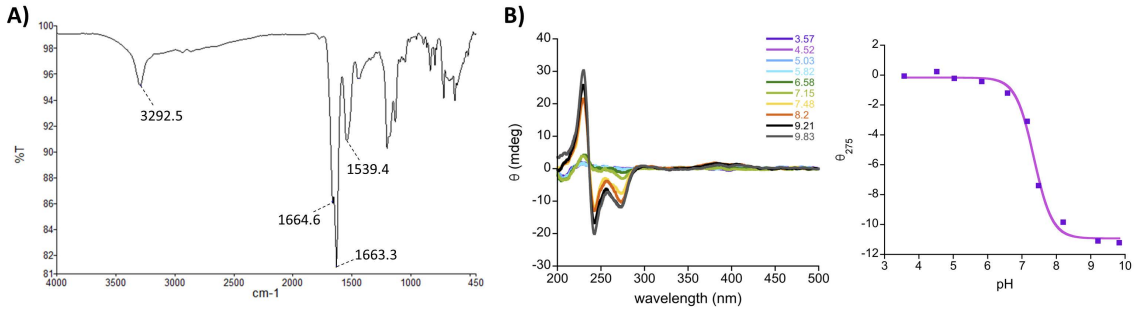

Figure 46. (A) FT-IR spectrum of **CP2** (solid, 298 K). (B) Overlaid CD spectra of a **CP2** aqueous solution (350 µM) at different pH and trend of the ellipticity changes measured at 275 nm as a function of the pH. The data were fitted with the adapted Henderson-Hasselbalch equation (pH - pKa) = log[(θ_{max} – θ)/(θ – θ_{min}), providing a mean values of pKa = 7.3 and Hill coefficient of n = 1.6 ± 0.3.

Scanning Transmission Electron Microscopy (STEM) microscopy was employed to evaluate the self-assembled structure of **CP2** at different pH. The deposition of a **CP2** solution (350 µM) at native pH (3.5) on Cu grids provided mainly amorphous aggregates or, to a lesser extent, small tubes with diameters of about 2-3 nm and lengths ranging between 150-200 nm (Figure 47A). This behaviour was expected since the protonation of the His side chains and the corresponding repulsive intermolecular interactions of charged imidazolium rings would avoid the build-up of nanotubes. On the other hand, at neutral pH (350 µM), individual SCPNs with a diameter of approximately 2-3 nm and lengths of a few microns together with bundles of them with an average diameter of ~5-6 nm were observed (Figure 47B). Atomic force microscopy (AFM) analysis also corroborated these dimensions (Figure 47C). Nanotube bundles must arise from

[192] H. S. Kim, J. D. Hartgerink, M. R. Ghadiri, *J. Am. Chem. Soc.* **1998**, *120*, 4417-4424.
[232] a) J. Kubelka, T. A. Keiderling, *J. Am. Chem. Soc.* **2001**, *123*, 12048-12058; b) Y. Zou, Y. Li, W. Hao, X. Hu, G. Ma, *J. Phys. Chem. B* **2013**, *117*, 4003-4013.
[233] S. Krimm, J. Bandekar in Advances in Protein Chemistry, *Vol. 38* (Eds.: C. B. Anfinsen, J. T. Edsall, F. M. Richards), Elsevier, Amsterdam, **1986**, pp. 181-364.

intermolecular anthracene-anthracene interactions and the coexistence of both types of structure corroborate the existence of the mentioned hierarchical assembling process illustrated in Figure 43B. Therefore, the neutralization of aqueous media favours the formation of a unique synergistic interplay between hydrogen bonding, hydrophobic, and π,π-interactions with subsequent organization in hierarchical tubular architectures.

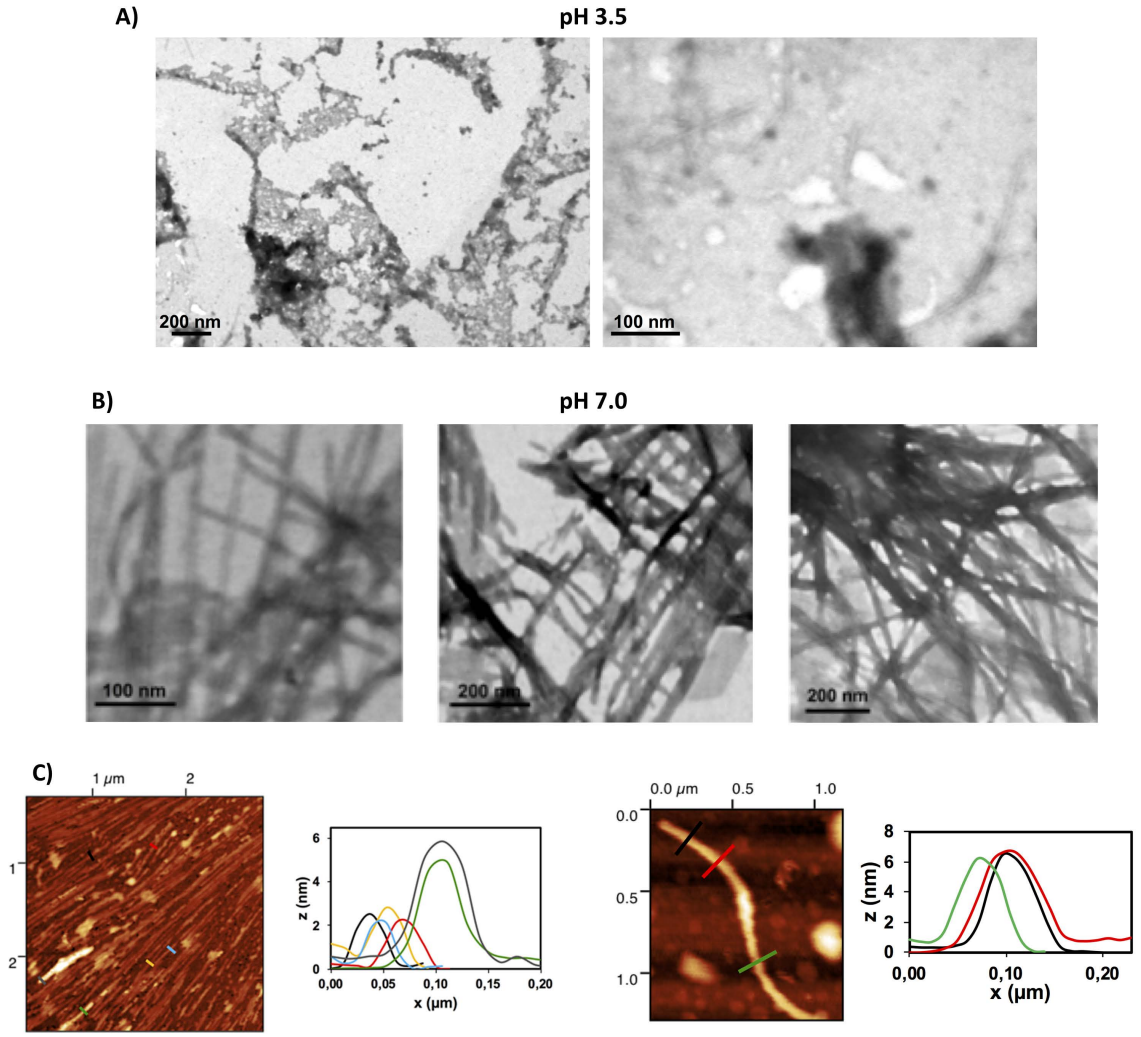

Figure 47. (A) STEM micrographs of a deposited solution of **CP2** (400 µM) at native pH (3.5) on Cu grids. Staining was obtained with 2% w/v phosphotungstic acid (PTA). (B) STEM micrographs achieved by deposition of a solution of **CP2** (350 µM) at neutral pH (7.0) on Cu grids. Staining was obtained with 2% w/v phosphotungstic acid (PTA). (C) AFM micrographs of an aqueous solution of **CP2** (350 µM, pH 7.0). The height profiles were achieved along the colour lines shown in the image.

6.1.3.4. Anthracene photodimerization

Once confirmed the nanotube formation, we started to evaluate the anthracene photodimerization.[218] Therefore, we decided to investigate it upon UV irradiation at 350 nm at different pH (Figure 48): acidic (pH 1.85), native (pH 4.95) and neutral (10 mM HEPES, pH 7.0). The degassed solutions of **CP2** (250 µM) were irradiated at 350 nm, and the process was followed by the reduction in the absorption of the band at 386 nm due to the loss of aromaticity of the anthracene moiety upon

the [4+4] cycloaddition reaction.[234] The reaction proceeds smoothly at pH 7.0 after 90 min. At native (pH 4.95) and acidic conditions (pH 1.85), the conversion was smaller, 80% and 60%, respectively. The kinetic studies allowed to estimate a velocity constant k_1 of 0.14 min^{-1} at neutral pH, five times faster than for acidic conditions (0.03 min^{-1} at pH 1.85). These results suggest that the anthracene preorganization, favoured at the conditions in which nanotubes are already forms, speeds up the [4+4] cycloaddition.

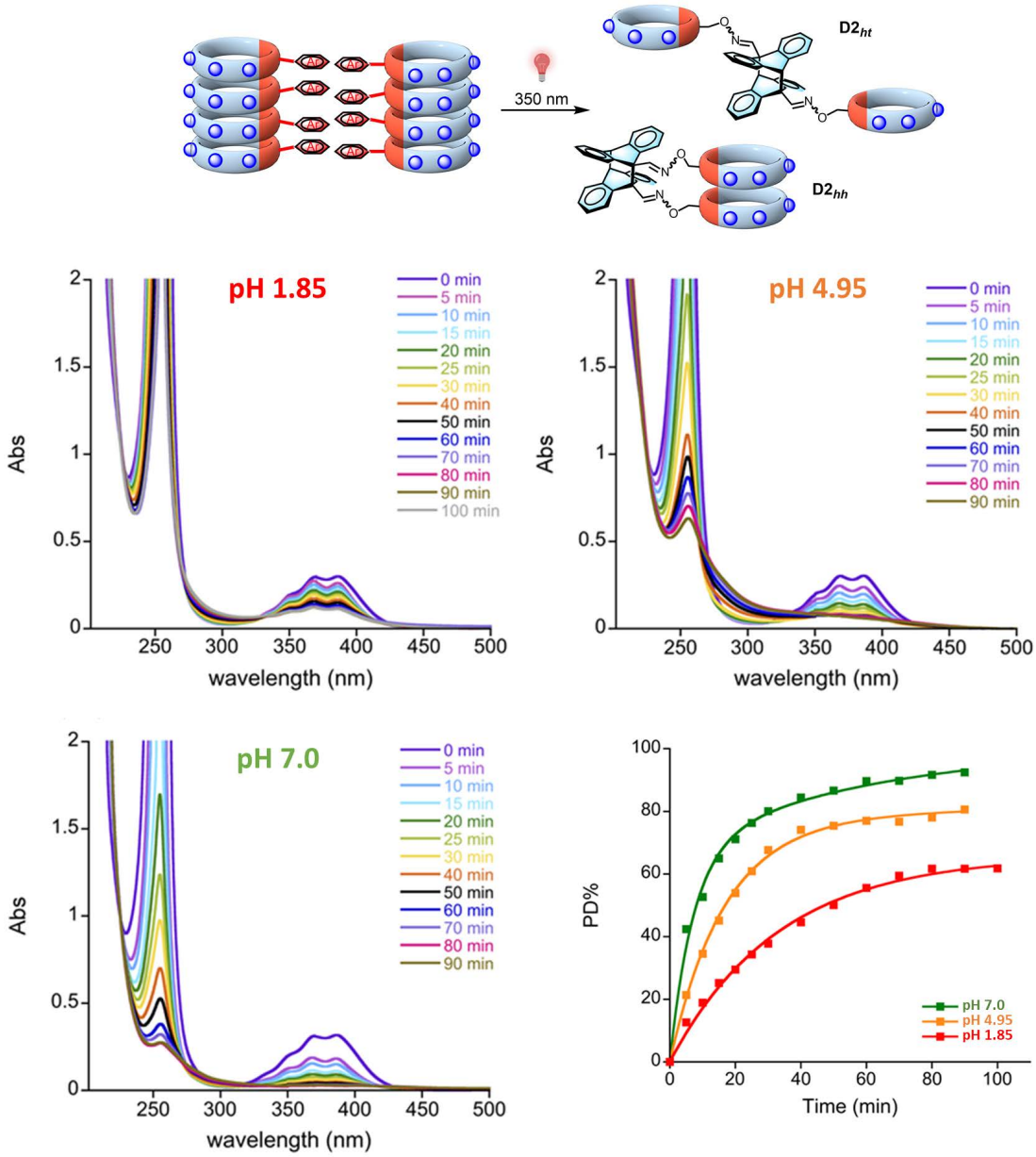

Figure 48. Time-course UV-Vis spectra and photodimerization degree followed at 386 nm versus time of solutions of **CP2** (250 µM) at acidic (pH 1.85), native (pH 4.95) and neutral conditions (10 mM HEPES, pH 7.0) upon irradiation at 350 nm. The photodimerization degree was evaluated through the equation PD = ((A_0 − A)/A_0)*100, where A_0 is the initial intensity at 386 nm. The solid curve derived from the biexponential fit $PD\ (t) = X_1(1 - e^{-k_1 t}) + X_2(1 - e^{-k_2 t})$, where $PD(t)$ corresponds to the time-dependent photodimerization degree, k_1 and k_2 are rate constants, X_1 and X_2 are the relative weighting fractions. Fitting the curves with this equation allowed to estimate a k_1 of 0.14 min^{-1} at pH 7.0, of 0.06 min^{-1} at pH 4.95, and 0.03 min^{-1} at pH 1.85.

UNIVERSIDADE DE SANTIAGO DE COMPOSTELA

[234] C.-H. Tung, J.-Q. Guan, *J. Org. Chem.* **1998**, *63*, 5857-5862.

To confirm that these differences in rates are related with nanotube structure and not with media conditions, model anthracene derivative (**Ant1**) was prepared as described in Figure 49A. Then, irradiations at 350 nm and at acidic (pH 3.93) or neutral (10 mM HEPES, pH 7.0) conditions were carried out (Figure 49B). The photodimerization reaction of model **Ant1** at both pH is slower than for **CP2**. Additionally, and contrary to what was observed for **CP2**, the reaction is slower at neutral pH than at acidic media. This confirms the importance of the nanotube induced preorganization of anthracene moieties to speed up the photodimerization.

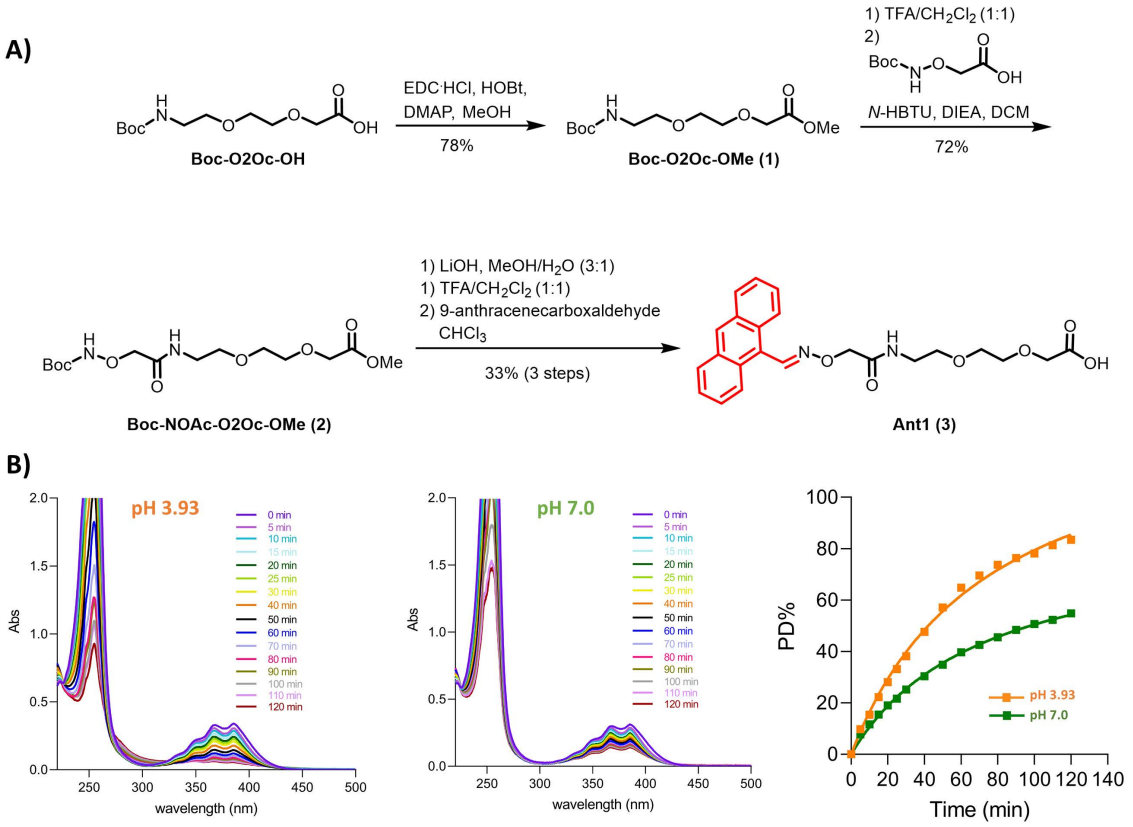

Figure 49. (A) Synthetic strategy for the preparation of **Ant1**. (B) Time-course UV-Vis spectra and photodimerization degree followed at 386 nm versus time of solutions of model **Ant1** (250 µM, 1:3 MeOH/H_2O) at native (pH 3.93) and neutral conditions (10 mM HEPES, pH 7.0) upon irradiation at 350 nm.

HPLC analysis of the irradiated mixture of **CP2** at pH 7.0, provided information regarding products formation (Figure 50A). In addition to the starting material, four new peaks were observed during the irradiation process. One of them raised very fast at the initial stage of irradiation to decrease later as the other three products start rising. MS analysis (Figure 50C) shows that this product has the molecular weight of the monomer, whose absorption spectra coincide with anthracene derivatives (Figure 50D). This suggests that this product must be an isomer (**^{Z}CP2**) of the starting material. However, the molecular weight of the other three products (Figure 50C) coincides with dimeric structures (**D2**) and whose UV spectra also confirm the [4+4] cycloadduct structures (Figure 50D). The formation of the same type of products was observed with the **Ant1** model, although the reaction proceeds slower (Figure 50B).

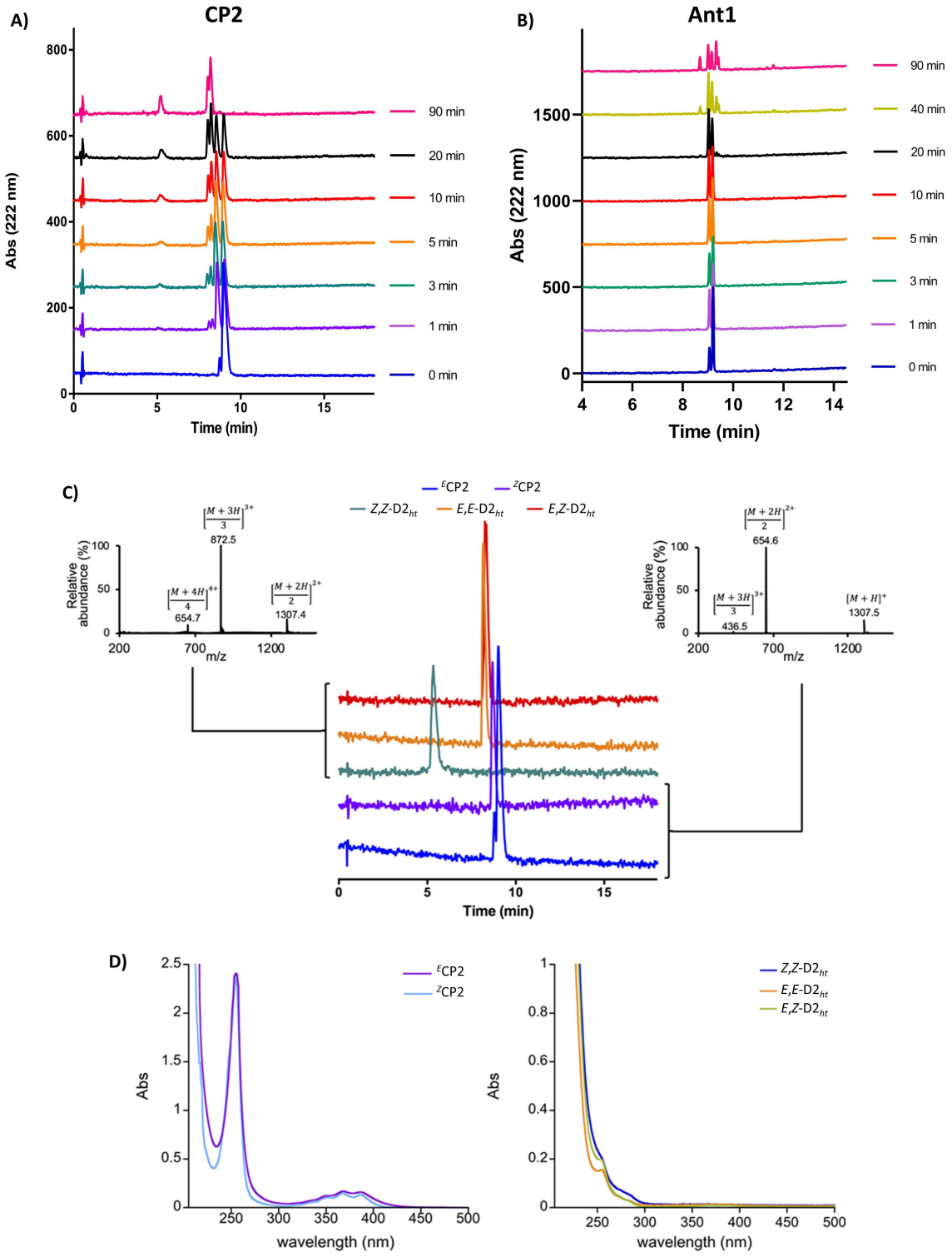

Figure 50. (A) HPLC analysis (HPLC conditions: H_20 (0.1% TFA)/MeCN (0.1% TFA), 80:20 → 80:20 (2 min) and 80:20 → 50:50 (19 min)) of the mixture of **CP2** (250 µM) irradiated at pH 7.0 at different time intervals. After 1 minute of irradiation (purple line), the formation of a new product (**^{Z}CP2**) with retention time 8.59 min is distinctly observable. After 90 min of irradiation, only the three dimeric structures can be observed. (B) HPLC analysis (HPLC conditions: H_20 (0.1% TFA)/MeCN (0.1% TFA), 80:20 → 80:20 (2 min) and 80:20 → 5:95 (19 min)) of the mixture of **Ant1** (250 µM, 1:3 MeOH/H_2O) irradiated at pH 7.0 at different time intervals. (C) HPLC traces and corresponding MS analysis of the different purified products obtained after irradiation of an aqueous solution of **CP2** at pH 7.0, showing the formation of **^{Z}CP2** (R_t = 8.59 min) and three dimeric species with retention time of 5.37 min (***Z,Z*-D2$_{ht}$**), 8.19 min (***E,E*-D2$_{ht}$**) and 8.26 min (***E,Z*-D2$_{ht}$**), respectively. (D) UV-Vis spectra of **^{E}CP2**, **^{Z}CP2**, ***Z,Z*-D2$_{ht}$**, ***E,E*-D2$_{ht}$** and ***E,Z*-D2$_{ht}$** (200 µM).

Additionally, to rule out the formation of photo-oxygenated products,[235] the reaction was also carried out with an air-equilibrated solution at pH 7.0 (Figure 51). Under these conditions a variety of new products, some of them assigned to endoperoxides and/or anthraquinones, were formed. Any of these products were detected under the previous oxygen-free irradiation conditions (Figure 50A).

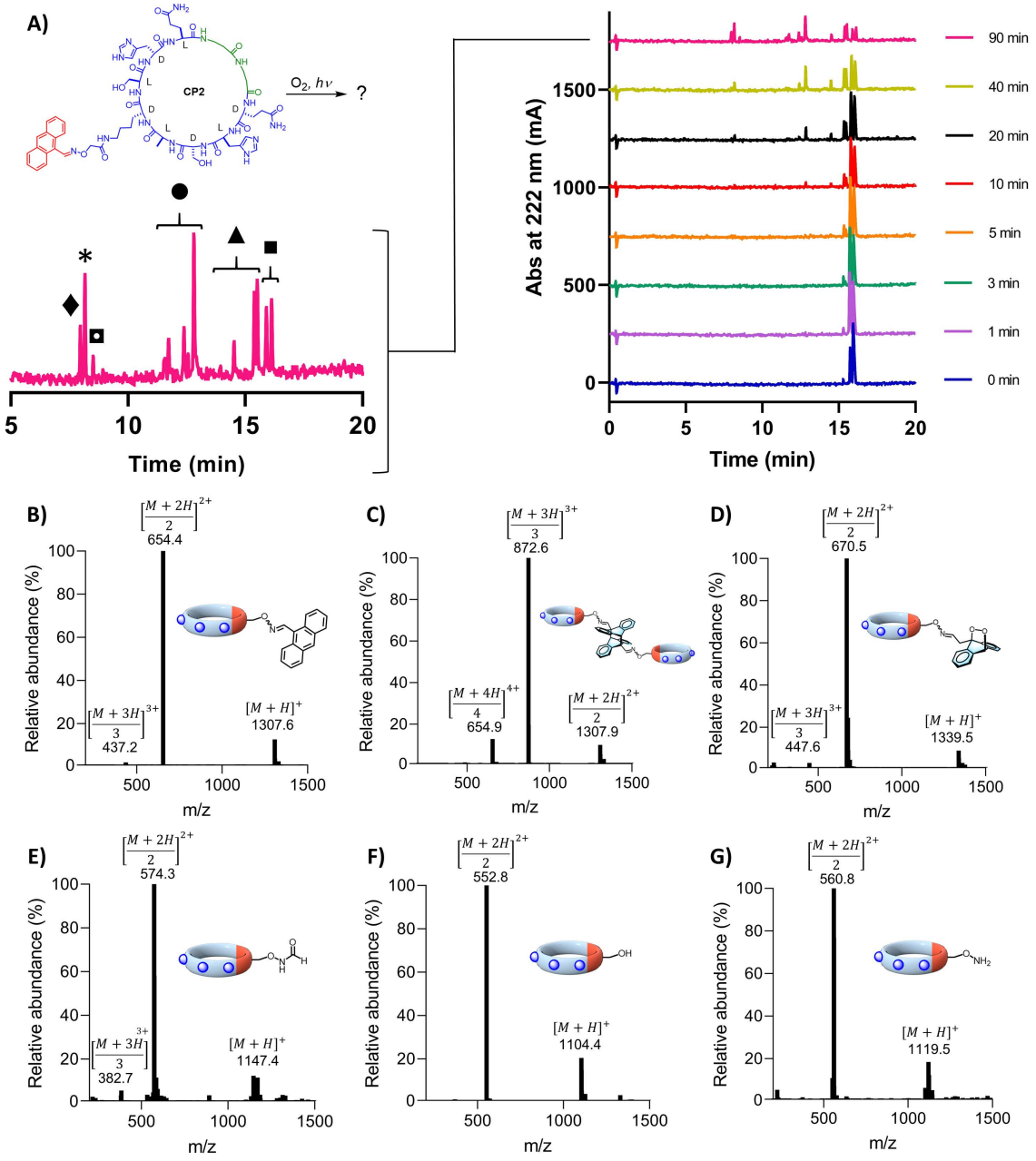

*Figure 51. (*A) HPLC analysis [HPLC conditions: $H_2$0 (0.1% TFA)/MeCN (0.1% TFA), 100:0 → 100:0 (2 min) and 100:0 → 50:50 (19 min)] of the mixture of **CP2** (250 μM) irradiated at pH 7.0 (HEPES, 10 mM) under oxygen atmosphere at different time intervals. (B) ESI-MS of ^{Z}**CP2** and ^{E}**CP2** (■, 15.7 min and 15.9 min). (C) ESI-MS of ***Z,Z*-D2$_{ht}$**, ***E,E*-D2$_{ht}$** and ***E,Z*-D2$_{ht}$** (▲, 14.5 min, 15.4 min and 15.6 min). (D) ESI-MS of endoperoxides (●, 12.8 min, 12.4 min and 11.7 min). (E) ESI-MS of product at 8.6 min (◘). (F) ESI-MS of the N-O photolytic product (*, 8.2 min). (G) ESI-MS of the oxime hydrolysis product (♦, **CP1**, 8.0 min).

[235] a) W. Fudickar, T. Linker, *Chem. Eur. J.* **2011**, *17*, 13661-13664; b) W. Fudickar, T. Linker, *J. Am. Chem. Soc.* **2012**, *134*, 15071-15082; c) Y. Han, M. Liu, R. Zhong, Z. Gao, Z. Chen, M. Zhang, F. Wang, *Inorg. Chem.* **2019**, *58*, 12407-12414.

The NMR analysis (Figure 52) of the newly formed monomer (**^{Z}CP2**) suggested that the thermodynamic oxime *E*-isomer is photo-transformed into the *Z*-form[236] that is kinetically stable remaining in this geometry even when its aqueous solution is allowed to equilibrate on the bench for a few days. The observed shielding effect on the Lys side chain protons, the NH at 6.92 ppm or the methylene groups at 1.00 ($^{\gamma}CH_2$) and 1.17 ($^{\delta}CH_2$) ppm, derived from the ring current of the anthracene moiety, suggest that the hydrophobic contacts must stabilize this form (Figure 52B and inset in Figure 43A).

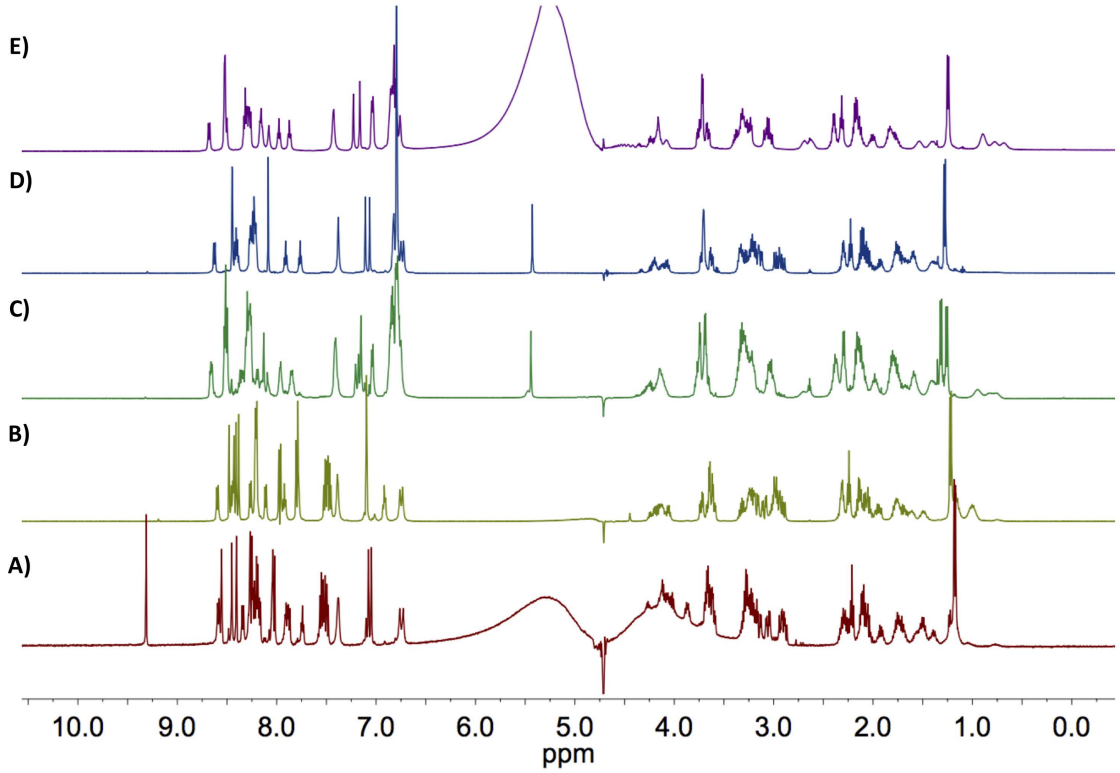

Figure 52. ^{1}H-NMR (500 MHz, D_2O/H_2O, 298K) of: (A) **^{E}CP2**, (B) **^{Z}CP2**, (C) ***E,Z*-D2$_{ht}$**, (D) ***E,E*-D2$_{ht}$**, (E) ***Z,Z*-D2$_{ht}$**.

In our initial evaluation, we considered the formation of two types of dimers, the head-to-head (**D2$_{hh}$**) and the head-to-tail (**D2$_{ht}$**) (Figure 48), based on whether the reaction occurs through inter-tubular or intra-tubular processes.[218,237] However, NMR analysis of the resulting dimers (Figure 52C-E), obtained in a 1:2:4 (***Z,Z*-D2$_{ht}$**: ***E,E*-D2$_{ht}$**: ***E,Z*-D2$_{ht}$**) ratio, rules out the formation or isolation of **D2$_{hh}$**. The complexity of the spectrum of the major isomer (Figure 52C) compared with the other two suggests that this corresponds to the ***E,Z*-D2$_{ht}$**. The ***Z,Z*-D2$_{ht}$** was assigned to the minor product

[218] a) D. Greene, S. L. Misrock, J. R. Wolfe, *J. Am. Chem. Soc.* **1955**, *77*, 3852-3855; b) D. E. Applequist, R. L. Litle, E. C. Friedrich, R. E. Wall, *J. Am. Chem. Soc.* **1959**, *81*, 452-456; c) H. Becker, *Chem. Rev.* **1993**, *93*, 145-172; d) H. Bouas-Laurent, A. Castellan, J.-P. Desvergnea, R. Lapouyadec, *Chem. Soc. Rev.* **2000**, *29*, 43-55; e) H. Bouas-Laurent, A. Castellan, J.-P. Desvergnea, R. Lapouyadec, *Chem. Soc. Rev.* **2001**, *30*, 248-263; f) M. Yoshizawa, J. K. Klosterman, *Chem. Soc. Rev.* **2014**, *43*, 1885-1898.

[236] a) H. D. Roth, *Light-Induced Chemistry of Oximes and Derivatives*, John Wiley & Sons Ltd, Chichester, UK, **2010**; b) S. Mondal, P. Chakraborty, P. Bairi, D. P. Chatterjee, A. K. Nandi, *Chem. Commun.* **2015**, *51*, 10680-10683; c) B. Bai, M. Zhang, N. Ji, J. Wei, H. Wang, M. Li, *Chem. Commun.* **2017**, *53*, 2693-2696.

[237] A. Castellan, R. Lapouyade, H. Boutas-Laurent, J. Y. Lallemand, *Tetrahedron Lett.* **1975**, *29*, 2467-2470.

according, again, to the shielding effect of the Lys side chain protons (Figure 52E). The ^{1}H-NMR spectra of ***E,Z*-D2$_{ht}$** and ***E,E*-D2$_{ht}$** (Figure 52C-D and Figure 53) display a singlet at around 5.45 ppm that can be assigned to the bridge hydrogen H10 according to the integral value and the chemical shift. For the ***Z,Z*-D2$_{ht}$** photodimer, this signal is covered by the water peak (Figure 52E). HMBC spectra show a cross-signal between this singlet at 5.45 ppm and the ^{13}C-NMR signal at around 57.9-57.7 ppm that was assigned to the C9 carbon (Figure 53). This observed cross-signal in the HMBC spectra between H10 and the bridgehead carbon C9 discards the isolation of head-to-head (**D2$_{hh}$**) photodimers and suggests the formation of only head-to-tail derivatives (**D2$_{ht}$**).

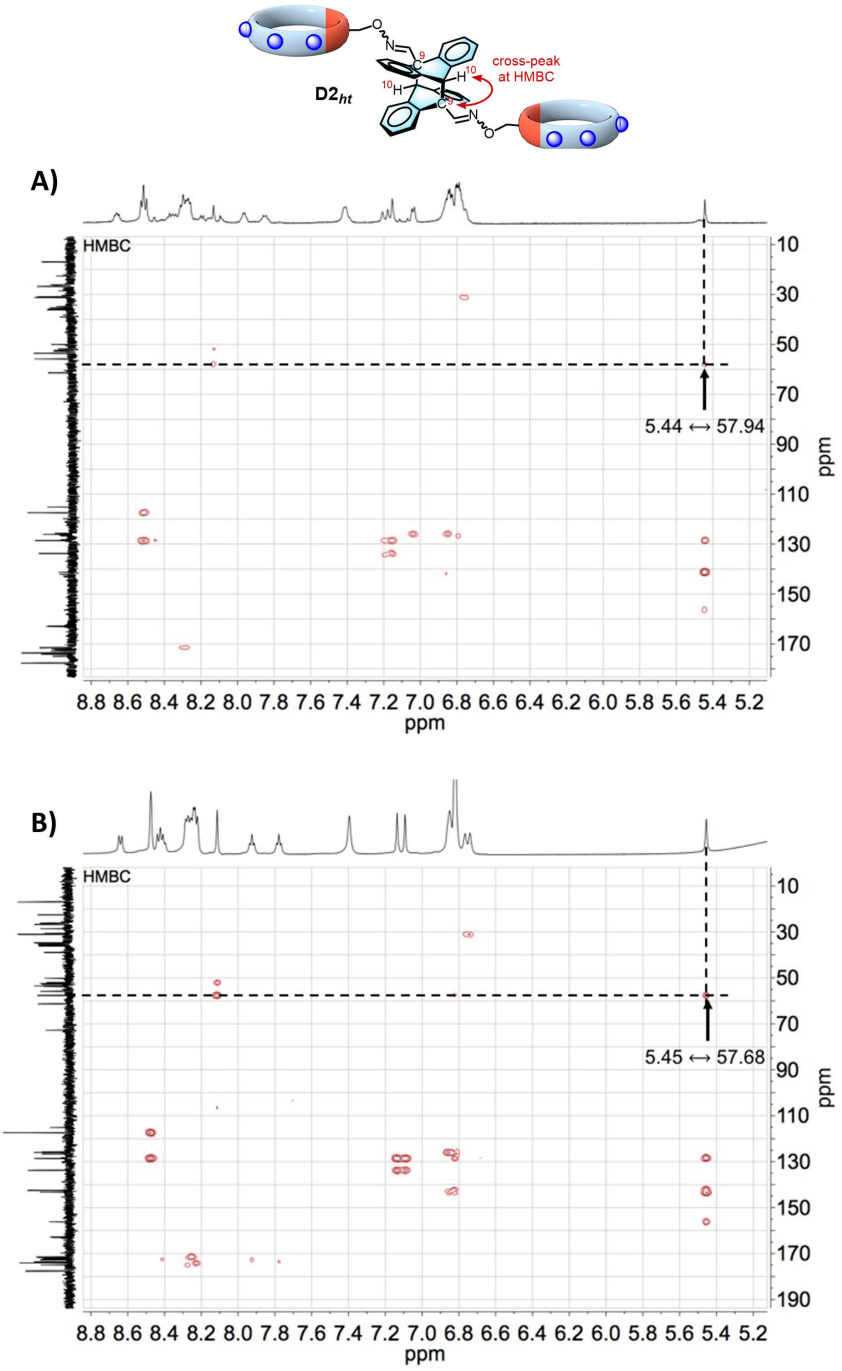

Figure 53. (A) HMBC magnification of ***E,Z*-D2$_{ht}$** at 3.4 mM (500 MHz, D_2O/H_2O, 298K). (B) HMBC magnification of ***E,E*-D2$_{ht}$** at 3.7 mM (500 MHz, D_2O/H_2O, 298K).

In order to discard the formation of unstable head-to-head dimers (**D2$_{hh}$**), which could revert under the analysis conditions, a new experiment using irradiation-dark cycles was carried out (Figure 54A).[238] The formation of photodimers **D2$_{hh}$** was dismissed by following the changes in the anthracene absorption band (386 nm) upon sequential cycles of irradiation at 350 nm for a short time (5-10 min) followed by an equilibration time in the dark (40 min) at 298 K. During the time in the dark, the absorption band of anthracene was not recovered, confirming that head-to-head dimers were not formed under these conditions. Consequently, all three isomers are head-to-tail derivatives differentiated by the geometry of the *o*-alkyloxime: the *E*,*E*-, *Z*,*Z*- and *E*,*Z*-derivatives. Therefore, in the inter-tubular cycloaddition process, it seems that the more favourable packing is the one in which one *Z*-isomer is close to the *E*-derivative. Also, no recovery of the anthracene absorption band during the equilibration time in the dark was observed for the **Ant1** model (Figure 54B).

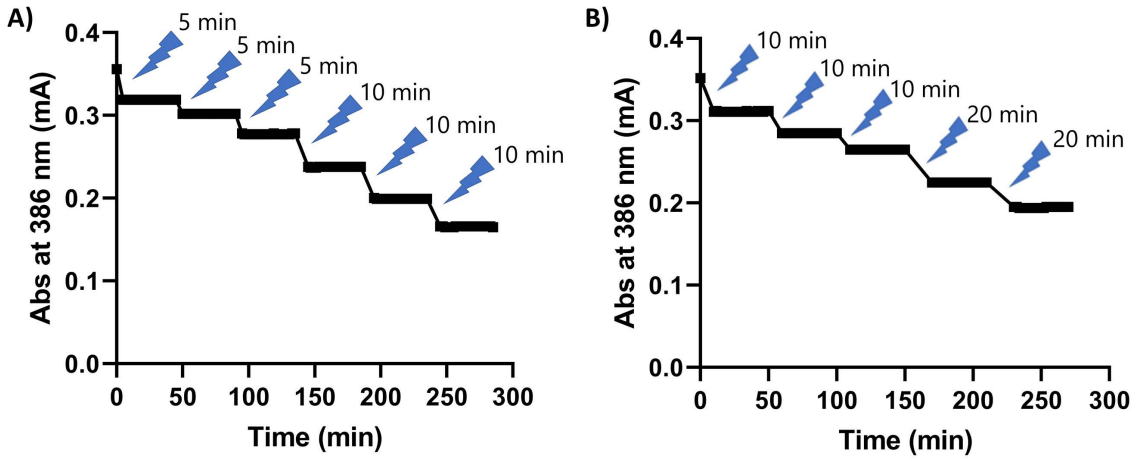

*Figure 54. (*A) Evolution of the absorption at 386 nm of **CP2** (250 µM) at neutral conditions (10 mM HEPES, pH 7.0), after cycles of irradiation (5 or 10 min) and darkness (40 min). (B) Evolution of the absorption at 386 nm of **Ant1** (250 µM) in a 3:1 mixture of MeOH and an aqueous solution (10 mM HEPES, pH 7.0), after cycles of irradiation (10 or 20 min) and darkness (40 min).

These dimers can be reverted to the monomeric structure by heating the aqueous solutions containing each of the dimers (250 µM) for 800 min at 80°C. The process was followed by UV-Vis (Figure 55A-D) and HPLC (Figure 55E) analysis. Interestingly, each of the dimers reverted into the corresponding monomers maintaining their oxime geometry without isomerization to the more stable form. The stability of the corresponding dimers (Figure 55D) is quite different, while ***Z*,*Z*-D2$_{ht}$** only provided a 12% of the **^{Z}CP2** after 800 min of heating, the ***E*,*E*-D2$_{ht}$** provided a 25% of **^{E}CP2** and the heterodimeric form (***E*,*Z*-D2$_{ht}$**) provided a 47% of monomeric anthracene derivatives (**^{E}CP2** and **^{Z}CP2**).

USC UNIVERSIDADE DE SANTIAGO DE COMPOSTELA

[238] A. Tron, P. J. Thornton, C. Lincheneau, J.-P. Desvergne, N. Spencer, J. H. R. Tucker, N. D. McClenaghan, *J. Org. Chem.* **2015**, *80*, 988-996.

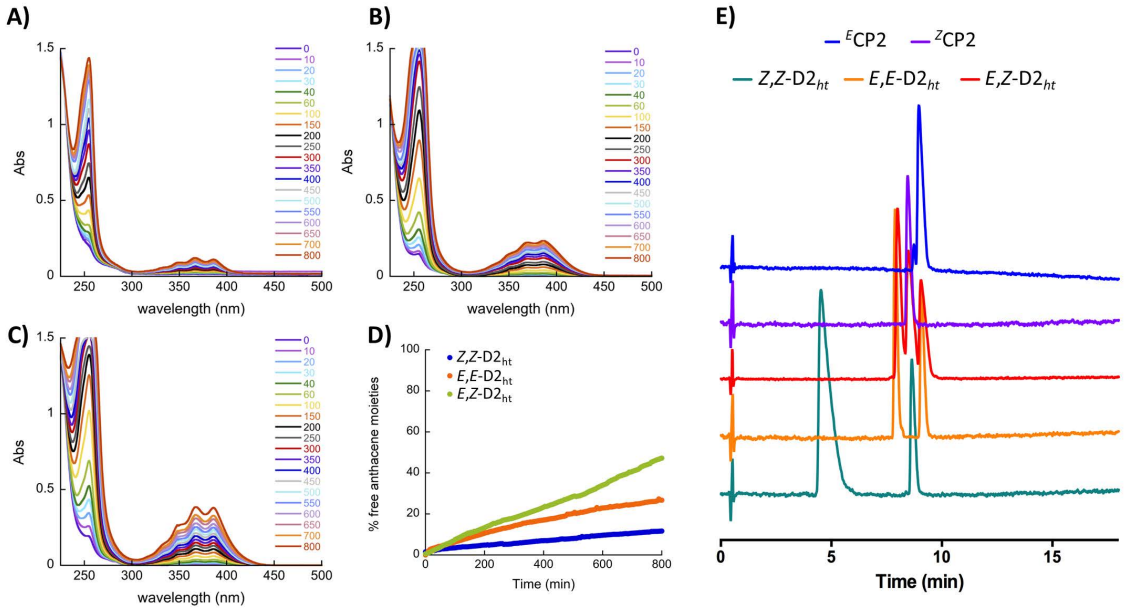

Figure 55. (A-C) Time-course UV-Vis spectra of the thermal dissociation of dimers upon heating at 80°C of the corresponding aqueous solutions of (A) ***Z,Z*-D2*ht***, (B) ***E,E*-D2*ht***, and (C) ***E,Z*-D2*ht*** at a concentration of 250 µM. (D) Percentage of formed monomeric anthracene moieties (%) as a function of the heating time at 80°C. The percentage of monomeric anthracene (%) was calculated through the equation % = [100-(A_0 − A)/A_0]*100, where A_0 is the maximum absorption at 386 nm before irradiation. Concentration of monomeric anthracene moieties calculated using an extinction coefficient at 386 nm of ε = 6300 $M^{-1}.cm^{-1}$: ***Z,Z*-D2*ht***: 12% (blue), ***E,E*-D2*ht***: 25% (orange), and ***E,Z*-D2*ht***: 47% (green). (E) HPLC traces (HPLC conditions: H_20 (0.1% TFA)/MeCN (0.1% TFA), 80:20 → 80:20 (2 min) and 80:20 → 50:50 (19 min)) obtained after the thermal dissociation experiments for ***Z,Z*-D2*ht*** (green), ***E,E*-D2*ht*** (orange) and ***E,Z*-D2*ht*** (red) derivatives. The HPLC traces of **^{Z}CP2** (purple) and **^{E}CP2** (blue) were included for comparison.

6.1.3.5. Light-induced bending motion of cyclic peptide nanotubes

After confirming the dimerization process, we decided to study the consequences of this transformation at the macroscopic level. Therefore, solutions of **CP2** (350 µM) before the irradiation were analysed by epifluorescence microscopy (Figure 56A). Under these conditions, bright and green needle-shaped structures (ø 1.5-2 µm) were observed denoting that the pH-triggered hierarchical assembly process was maintained from the nanotubes to the micro-scale tubular architectures. Notably, by increasing the irradiation time, the fluorescence emission of the bundles switched irreversibly from green to blue (Figure 56B). Moreover, the change in fluorescence emission was accompanied with a light-induced bending motion of the bigger fibres (Figure 56C). The differences in reaction time observed between the bulk solution (90 min, Figure 48) with the single fibre (30 s) must be related with the differences between the intra-bundle photochemical reaction and the combination of intra-bundle and inter-tubular dimerization that must take place in solution.

USC UNIVERSIDADE DE SANTIAGO DE COMPOSTELA

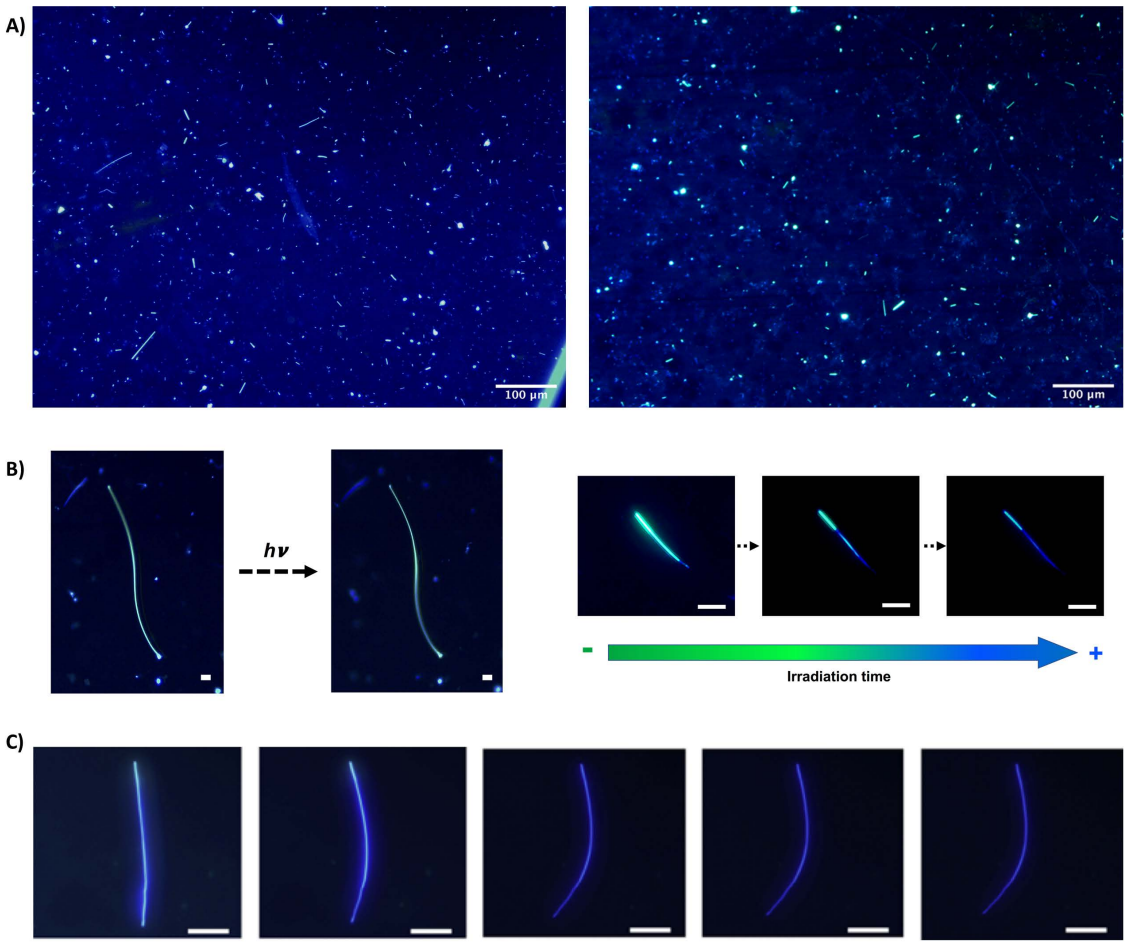

Figure 56. (A) Epifluorescence images of an aqueous solution of **CP2** (350 µM, pH 8.0). Scale bars: 100 µm. (B) Epifluorescence images of **CP2** (350 µM, pH 8.0) fibres exposed to different irradiation time in which the emission switching off suggests structural changes in the anthracene moiety. Scale bars: 10 µm. (C) Bending motion of the nanorods of **CP2** (350 µM, pH 8.0) resulting from the increase in irradiation time. Scale bars: 25 µm.

The resulting irradiated solutions were also evaluated by STEM (Figure 57). To our delight, zigzag-shaped tubular structures were observed, suggesting that the light-induced process provided structures that retained the tubular structure but a variety of elbows in these hollow fibres were observed. Therefore, the light-induced anthracene dimerization is able to change the inter-nanotube packing, forcing a bending motion to satisfy the structural restrictions induced by the cycloadduct formation.

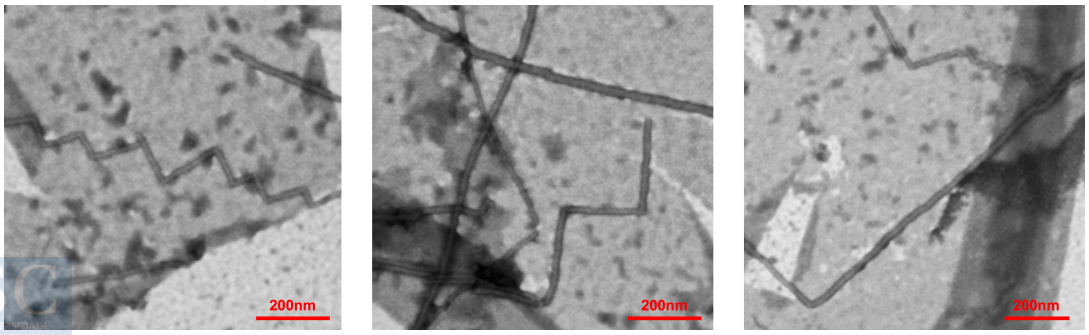

Figure 57. STEM micrographs of grids resulting of the deposition of a solution of **CP2** (250 µM, pH 7.0) that was irradiated for 90 min. Scale bars: 200 nm.

6.1.3.6. Cyclic peptide modifications with other aromatic groups

To study if the main driving force of the bending motion is the photodimerization reaction or the *E-Z* isomerization of the oxime bond, cyclic peptide derivatives were prepared in which the anthracene moiety was replaced by aromatic groups unable to photodimerize, such as naphthalene (**CP2N**) or pyrene (**CP2P**). As a result, these compounds could only undergo *E-Z* isomerization when irradiated. Both derivatives were synthesized by condensation of **CP1** with the corresponding aromatic aldehyde in DMSO at 60°C, as previously described for **CP2**. The resulting derivatives were submitted to irradiation conditions similar to those previously mentioned for **CP2**. After 1 min of irradiation the *E-Z* isomerization starts to take place but in a lesser extension than with the anthracene derivative (Figure 58). Surprisingly, with these new aromatic derivatives, longer irradiation times provoke the formation of new products that correspond by MS analysis to the cleavage of the N-O bond of the oxime.[239] This cleavage did not take place with the previous anthracene derivative **CP2** even after long irradiation times, suggesting that anthracene excitation and dimerization is preferred to *o*-alkyloxime excitation.

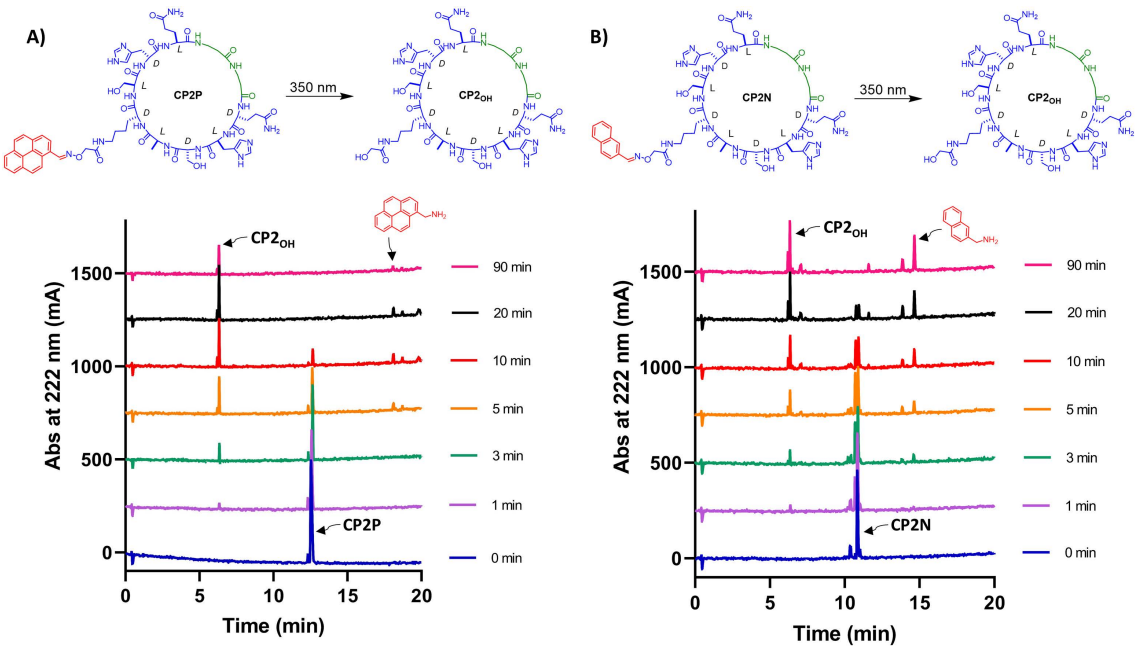

Figure 58. HPLC analysis (HPLC conditions: H_2O (0.1% TFA)/MeCN (0.1% TFA), 100:0 → 100:0 (2 min) and 100:0 → 25:75 (19 min)) of the mixture of (A) **CP2P** (250 µM) or (B) **CP2N** (250 µM) irradiated at pH 7.0 at different time intervals (1, 3, 5, 10, 20 and 90 min).

[239] a) M. Fréneau, P. de Sainte Claire, N. Hoffmann, J. Vors, J. Geist, M. Euvrardd, C. Richard, *RSC Adv.* **2016**, *6*, 5512-5522. b) B. Sevilla-Morán, P. Sandín-España, M. J. Vicente-Arana, J. L. Alonso-Prados, J. M. García-Baudín, *J. Photochem. Photobiol. A Chem.* **2008**, *198*, 162-168.

The self-assembly properties of **CP2P** were also evaluated. Studies carried out with **CP2P** using the ThT assay[231] showed an increase in ThT emission with increasing peptide concentration, confirming that this peptide is also able to adopt the β-sheet structure necessary to assemble into nanotubes (Figure 59A). The resulting critical aggregation concentration (*cac* 20 µM) was smaller than the one previously obtained for the anthracene derivative (**CP2**, *cac* 45 µM), as expected considering the higher hydrophobic character of the pyrene moiety. A similar *cac* value (10 µM) was determined with the NR assay (Figure 59B).[230] In contrast, the appearance of a CD signal at 340-400 nm with increasing peptide concentration provided a *cac* of 100 µM (Figure 59C). This value differs in almost one order of magnitude (10 µM and 100 µM), suggesting that the different techniques may be measuring different aggregation states of the hierarchical assembly process. The nanotube formation was confirmed with STEM images of a **CP2P** solution at neutral pH that revealed the formation of long fibres (Figure 59D). Also, the analysis by epifluorescence microscopy at the micro-scale revealed the formation of linear fibres, together with some unexpected helical ones, confirming the **CP2P** hierarchical assembly (Figure 59E).

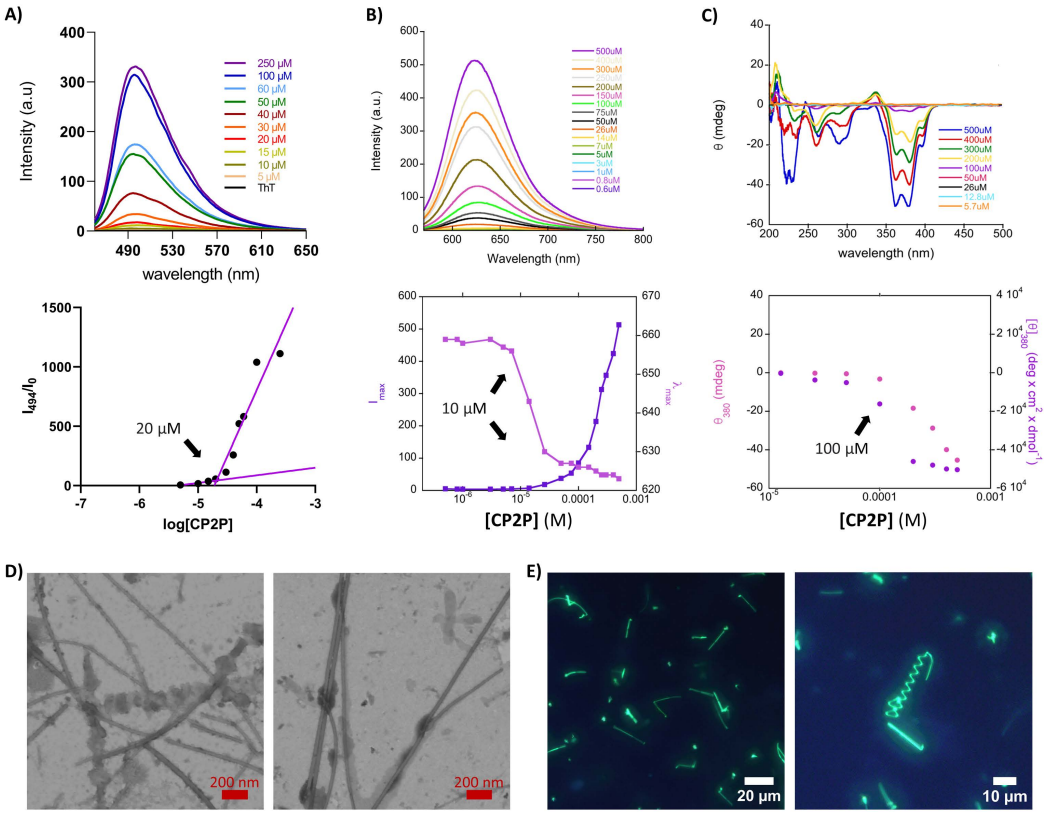

Figure 59. (A) Overlaid ThT (20 µM) fluorescence spectra of solutions of **CP2P** at different concentrations (10 mM HEPES, pH 7.0) and intensity ratio I_{494}/I_0 versus the logarithm of the concentration of **CP2P** (λ_{exc} = 440 nm, T = 20°C). I_0 is the fluorescence intensity at 494 nm of ThT alone. The break point indicates a *cac* of 20 µM. (B) Overlaid NR (1 µM) fluorescence spectra of solutions of **CP2P** at different concentrations (10 mM HEPES, pH 7.0) and maximum intensity (data in purple) and corresponding wavelength at maximum intensity (data in magenta) plotted as a function of the peptide concentration to estimate a *cac* around 10 µM (λ_{exc} = 550 nm, T = 20°C). (C) Overlaid CD spectra (T = 20°C) of aqueous solutions of **CP2P** (10 mM HEPES, pH 7.0) at different concentrations and minimum intensity (data in purple) plotted as a function of the peptide concentration to estimate the concentration at which the CD signal band at 380 nm was observed (~100 µM). (D) STEM micrographs of grids resulting of the deposition of an aqueous solution of **CP2P** (250 µM, pH 7.0). (E) Epifluorescence images of **CP2P** (350 µM, pH 8.0).

The evolution of the assembly properties of **CP2P** after the irradiation and consequent N-O bond cleavage was studied. Clearly, the ThT emission is reduced in the samples of **CP2P** that were irradiated (Figure 60A). Almost no emission of the ThT was observed after 10 min of irradiation, time at which all the pyrene group was already detached from the peptide as determined by previous HPLC analysis (Figure 58A). This result suggests the nanotube disassembly after the loss of the aromatic moiety, but unfortunately no information was obtained about the importance of the *E-Z* isomerization. However, STEM micrographs achieved by direct deposition on Cu grids of a solution of **CP2P** (250 µM, pH 7.0) irradiated for 30 minutes still showed the formation of long nanotubes (Figure 60B). Contrary, amorphous aggregates were observed after HPLC isolation of **CP2$_{OH}$** from the irradiated solution and subsequent deposition on Cu grids of an aqueous solution (250 µM, pH 7.0) (Figure 60C).

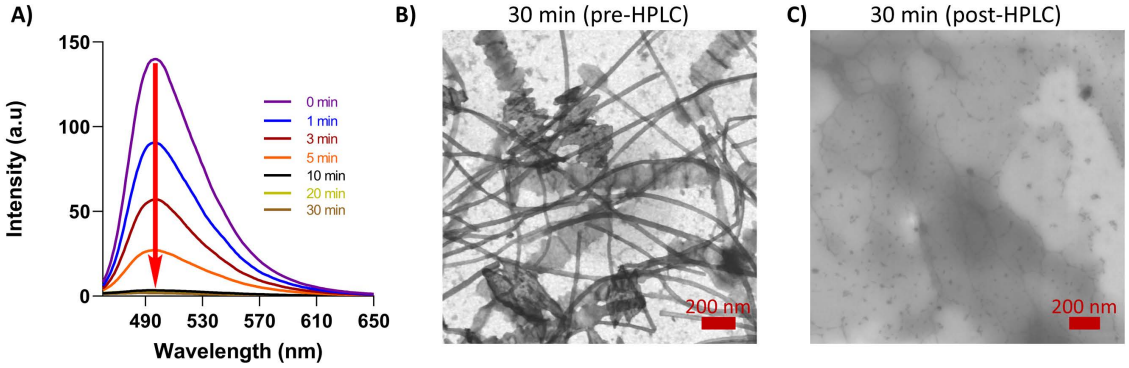

Figure 60. (A) Evolution of the ThT (20 µM) fluorescence of **CP2P** solutions (50 µM) at neutral pH (10 mM HEPES, pH 7.0) upon irradiation at 350 nm, showing the disappearance of the emission band characteristic of the dye that suggests the disassembly of the nanotube (λ_{exc} = 440 nm, T = 20°C). (B) STEM micrographs of grids resulting of the direct deposition of an aqueous solution of **CP2P** (250 µM, pH 7.0) irradiated at 350 nm for 30 minutes. (C) STEM micrographs of grids resulting of the deposition of a purified aqueous solution of **CP2$_{OH}$** (250 µM, pH 7.0).

Substitution of anthracene by another photo-sensitive group was also explored. In particular, it was decided to choose azobenzene due to the many examples in the literature that make use of this moiety, in which double bond isomerization could give rise to different aggregation states.[39] Based on the N-O bond cleavage observed with the previous derivatives, two versions were proposed in which the azobenzene was incorporated as an oxime (**^{E}CP2azo-ox**) or as an amide bond (**^{E}CP2azo-am**). The **^{E}CP2azo-ox** was again synthesized by condensation to **CP1** of the azobenzene aldehyde (**5**) in DMSO at 60°C. This aldehyde was prepared in two synthetic steps starting from the corresponding carboxylic acid (Figure 61A). The **^{E}CP2azo-am** was obtained by the previously described on-resin deprotection of the Mtt-protected lysine and subsequent coupling of 4-(phenylazo)benzoic acid. Ideally, in both designs the *E*-isomer could be converted into the *Z*-isomer by irradiation with UV light (350 nm), while the reverse process could be achieved by irradiation with visible light (450 nm) or by heating (Figure

61B). Depending on the geometry of the azobenzene, changes in the planarity of the aryl group could be expected and, as a result, differences in the assembly properties for each isomer.

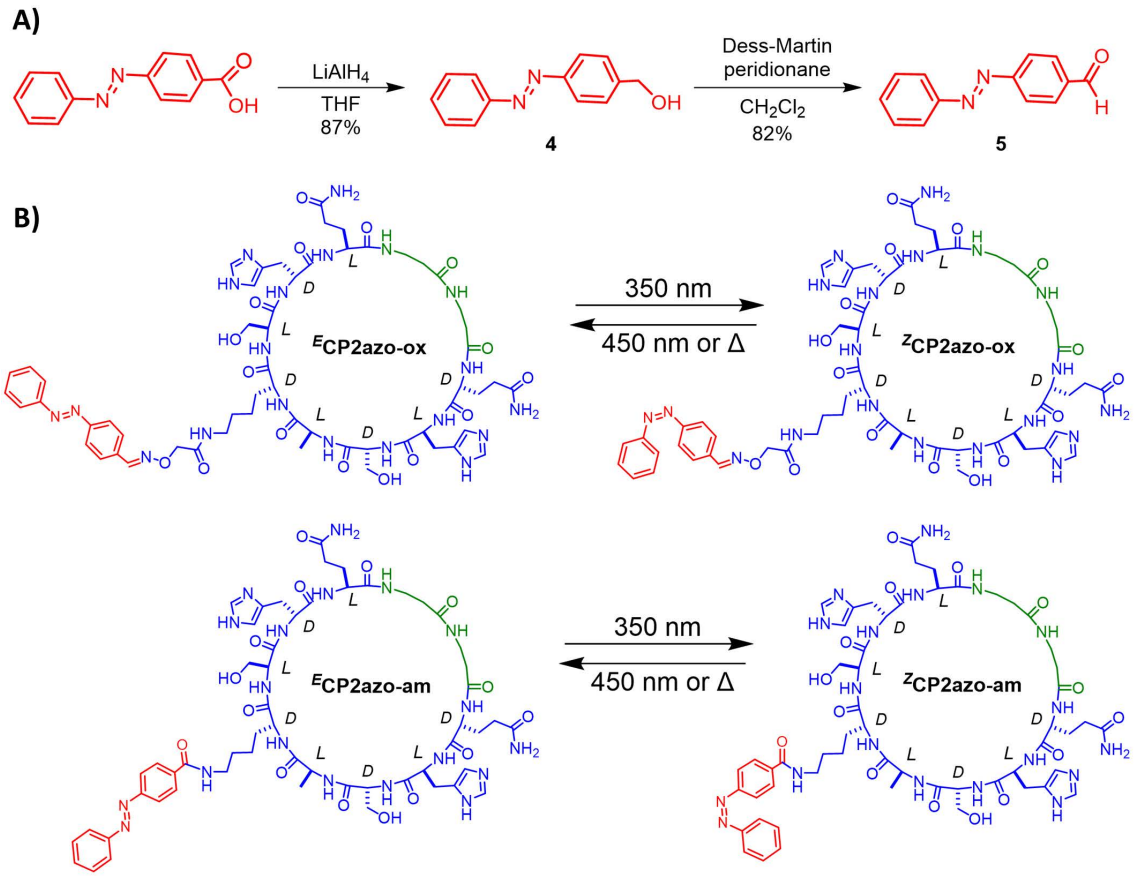

Figure 61. (A) Synthetic scheme to obtain 4-(phenylazo)benzaldehyde (**5**). (B) Isomerization between the two isomers of **CP2azo-ox** and **CP2azo-am** under irradiation with the appropriate wavelength.

The self-assembly properties of ^{E}**CP2azo-ox** and ^{E}**CP2azo-am** were studied. However, the ThT assay did not show emission at neutral (10 mM HEPES, pH 7.0) or basic pH (10 mM Boric acid, pH 9.0) for either design (Figure 62A-D). This suggests the inability of these two derivatives to adopt the β-sheet conformation to assemble into nanotubes even at high concentration (300 µM). In fact, STEM micrographs revealed the formation of amorphous aggregates for both designs (Figure 62E-F).

USC
UNIVERSIDADE DE SANTIAGO DE COMPOSTELA

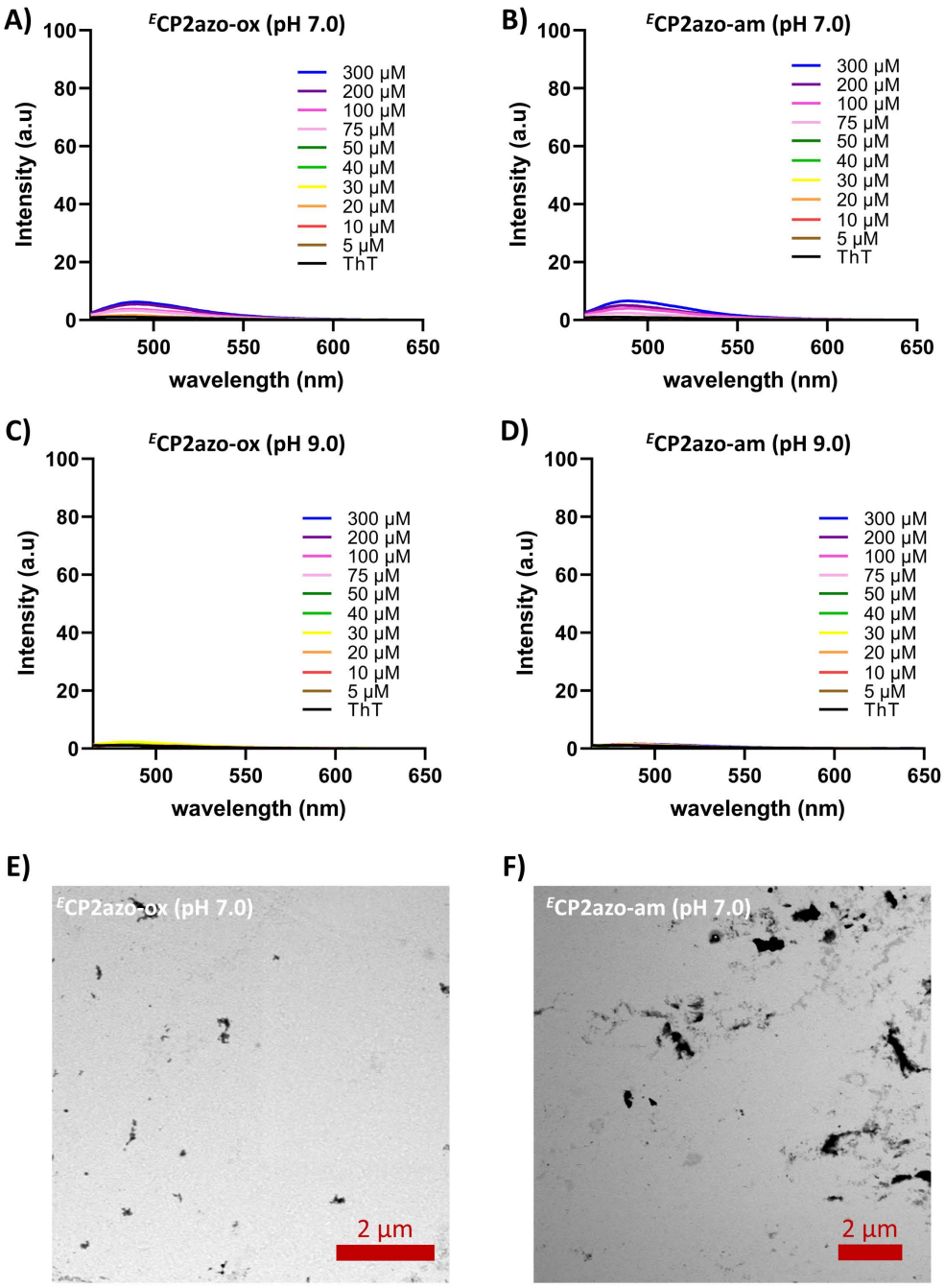

Figure 62. (A-B) Overlaid ThT (20 µM) fluorescence spectra of solutions of (A) **^{E}CP2azo-ox** or (B) **^{E}CP2azo-am** in HEPES buffer (10 mM, pH 7.0) at different concentrations (λ_{exc} = 440 nm, T = 20°C). (C-D) Overlaid ThT (20 µM) fluorescence spectra of solutions of (C) **^{E}CP2azo-ox** or (D) **^{E}CP2azo-am** in Boric acid buffer (10 mM, pH 9.0) at different concentrations (λ_{exc} = 440 nm, T = 20°C). (E-F) STEM micrographs of grids resulting of the deposition of a 250 µM solution of (E) **^{E}CP2azo-ox** or (F) **^{E}CP2azo-am** at neutral pH (10 mM HEPES, pH 7.0).

The isomerization of **^{E}CP2azo-ox** or **^{E}CP2azo-am** (250 µM) into the *Z*-isomer was investigated at neutral pH (10 mM HEPES, pH 7.0) upon irradiation at 350 nm (Figure 63A-B). In both cases, the photostationary state was achieved after 6-8 minutes of irradiation and it was composed of a 7:3 mixture of both isomers. Also, the UV spectrum after the irradiation confirms the isomerization, as denoted by the decrease

of the characteristic absorption band of the *E*-isomer around 325 nm and the increase of the absorption band of the *Z*-isomer around 425 nm.[39] Interestingly, no cleavage of the N-O bond in **CP2azo-ox** was observed. Also, the process can be reverted to recover around an 80% of the *E*-isomer by irradiation with visible light (450 nm) at neutral pH (10 mM HEPES, pH 7.0) (Figure 63C-D).

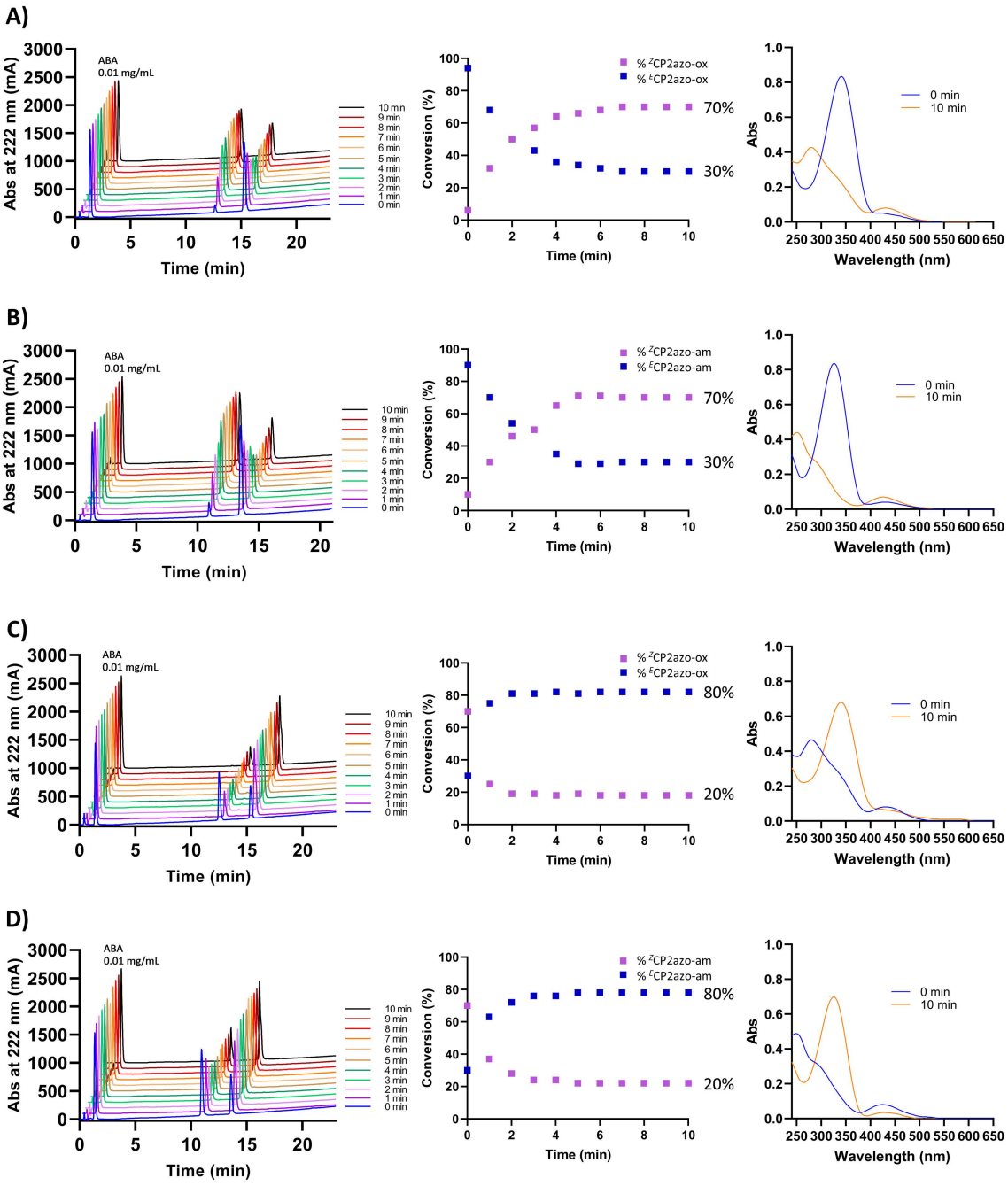

Figure 63. Pilled HPLC chromatograms, time-dependent conversion and UV-Vis spectrum evolution at neutral pH (10 mM HEPES, pH 7.0) corresponding to the isomerization of 250 µM solutions of (A) **^{E}CP2azo-ox** by irradiation at 350 nm, (B) **^{E}CP2azo-am** by irradiation at 350 nm, (C) the re-isomerization of **CP2azo-ox** by irradiation at 450 nm or (D) the re-isomerization of **CP2azo-am** by irradiation at 450 nm. An aqueous solution of 4-aminobenzoic acid (ABA, 0.01 mg/mL) was added as an internal standard in the HPLC analysis to quantify the peptide concentration. HPLC conditions: H_2O (0.1% TFA)/MeCN (0.1% TFA), 100:0 → 90:10 (2 min) and 90:10 → 40:60 (19 min).

The spontaneous reversibility of the isomerization was also evaluated (Figure 64). For that, a solution of **^{E}CP2azo-ox** or **^{E}CP2azo-am** (250 µM) at neutral pH (10 mM HEPES, pH 7.0) was again isomerized by irradiation at 350 nm during 10 minutes to obtain a 70% of the *Z*-isomer. Then, these samples were allowed to equilibrate in the dark and after only 12 hours an 80% of the *E*-isomer was recovered in both cases. This result suggests a fast thermal relaxation time for both designs.

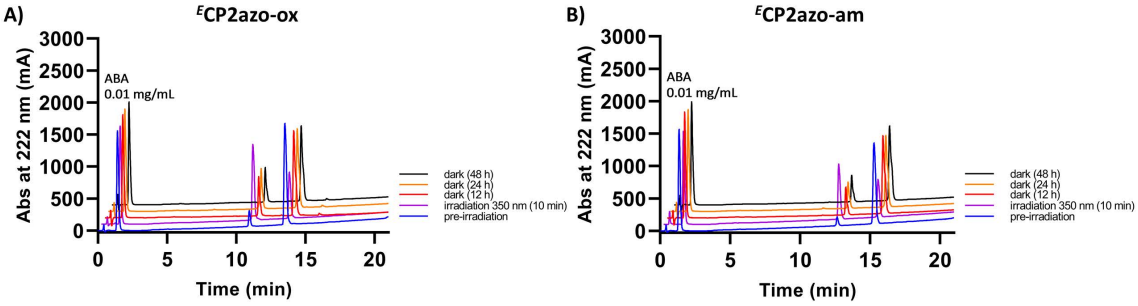

Figure 64. Spontaneous reversibility of a solution of (A) **^{E}CP2azo-ox** or (B) **^{E}CP2azo-am** (250 µM, 10 mM HEPES, pH 7.0) irradiated at 350 nm for 10 minutes, followed by equilibration in the dark. HPLC conditions: H_2O (0.1% TFA)/MeCN (0.1% TFA), 100:0 → 90:10 (2 min) and 90:10 → 40:60 (19 min).

Finally, it was evaluated if this isomerization has any implication on the self-assembly properties of the cyclic peptides. The process was monitored by following the ThT emission, but no increase in emission was observed after the irradiation (Figure 65A-B). Also, STEM images did not reveal the presence of nanotubes after irradiation for 10 minutes (Figure 65C-F). These results confirm that neither of the two isomers of these azobenzene derivatives are able to assemble into nanotubes.

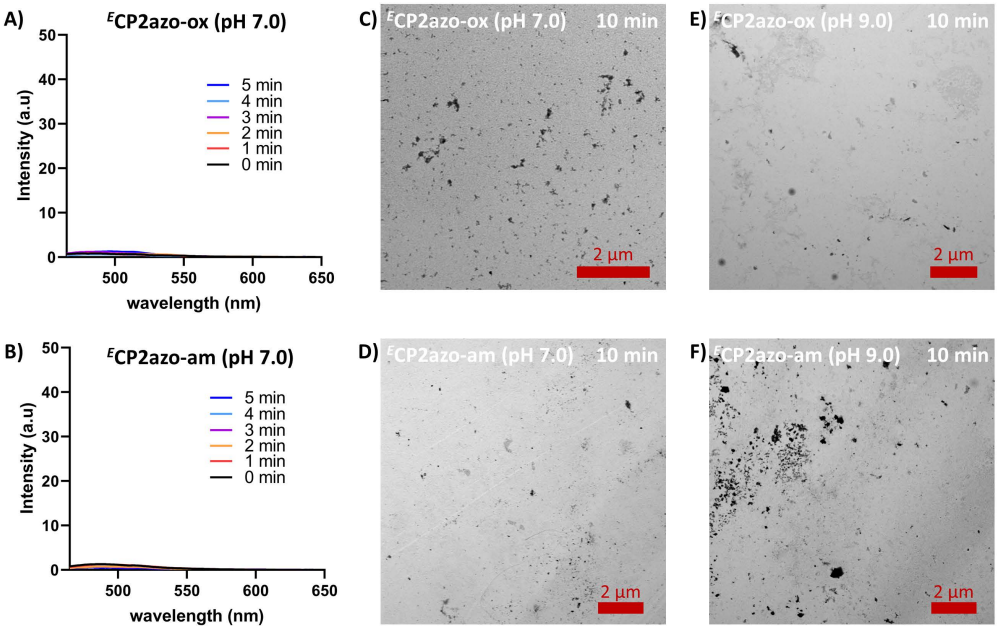

Figure 65. (A-B) Evolution of ThT (20 µM) fluorescence of solutions at neutral pH (10 mM HEPES, pH 7.0) of (A) **^{E}CP2azo-ox** (100 µM) or (B) **^{E}CP2azo-am** (100 µM) upon irradiation at 350 nm (λ_{exc} = 440 nm, T = 20°C). (C-D) STEM micrographs of grids resulting of the deposition of a 500 µM solution at pH 7.0 of (C) **^{E}CP2azo-ox** or (D) **^{E}CP2azo-am** irradiated at 350 nm for 10 min. (E-F) STEM micrographs of grids resulting of the deposition of a 500 µM solution at pH 9.0 of (E) **^{E}CP2azo-ox** or (F) **^{E}CP2azo-am** irradiated at 350 nm for 10 min.

6.1.4. Conclusions

In this chapter, we have shown a new class of cyclic peptide hybrid modified with an anthracene moiety. This cyclic peptide was designed to stack in a parallel fashion and form nanotubes at neutral or basic pH. Under these conditions, the resulting nanotube can bend as a result of a light stimulus. The anthracene pendant that bears each cyclic component forms a hydrophobic pocket in the nanotube bundle and dimerizes under appropriate light irradiation. The resulting changes in dimensions that accompanies this cycloaddition, perhaps together with *E*,*Z*-oxime isomerization, induce structural changes in the nanotube packing that force the nanotube to curve. Interestingly, the irradiation of the same peptide scaffold modified with naphthalene or pyrene provoke the cleavage of the N-O bond of the oxime. Finally, analogue cyclic peptides bearing an azobenzene moiety instead of anthracene were not able to assemble into nanotubes even after light irradiation. We envisage that these light-induced dynamic changes in shape can enable new functions for this type of nanotubes, particularly in a biological context.

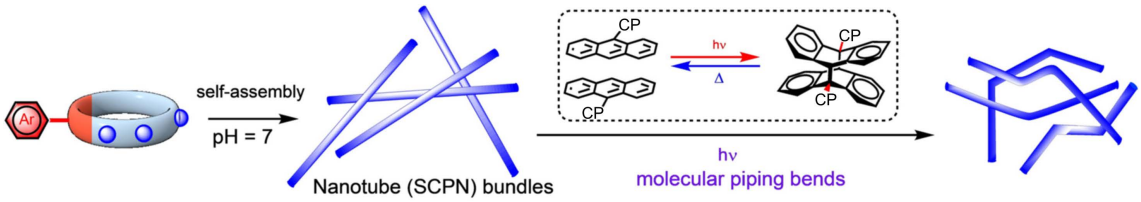

Figure 66. Nanotube bending developed in this chapter based on anthracene [4+4] photodimerization.

USC UNIVERSIDADE DE SANTIAGO DE COMPOSTELA

6.2. PHOTO-ASSEMBLING CYCLIC PEPTIDES FOR DYNAMIC LIGHT-DRIVEN PEPTIDE NANOTUBES

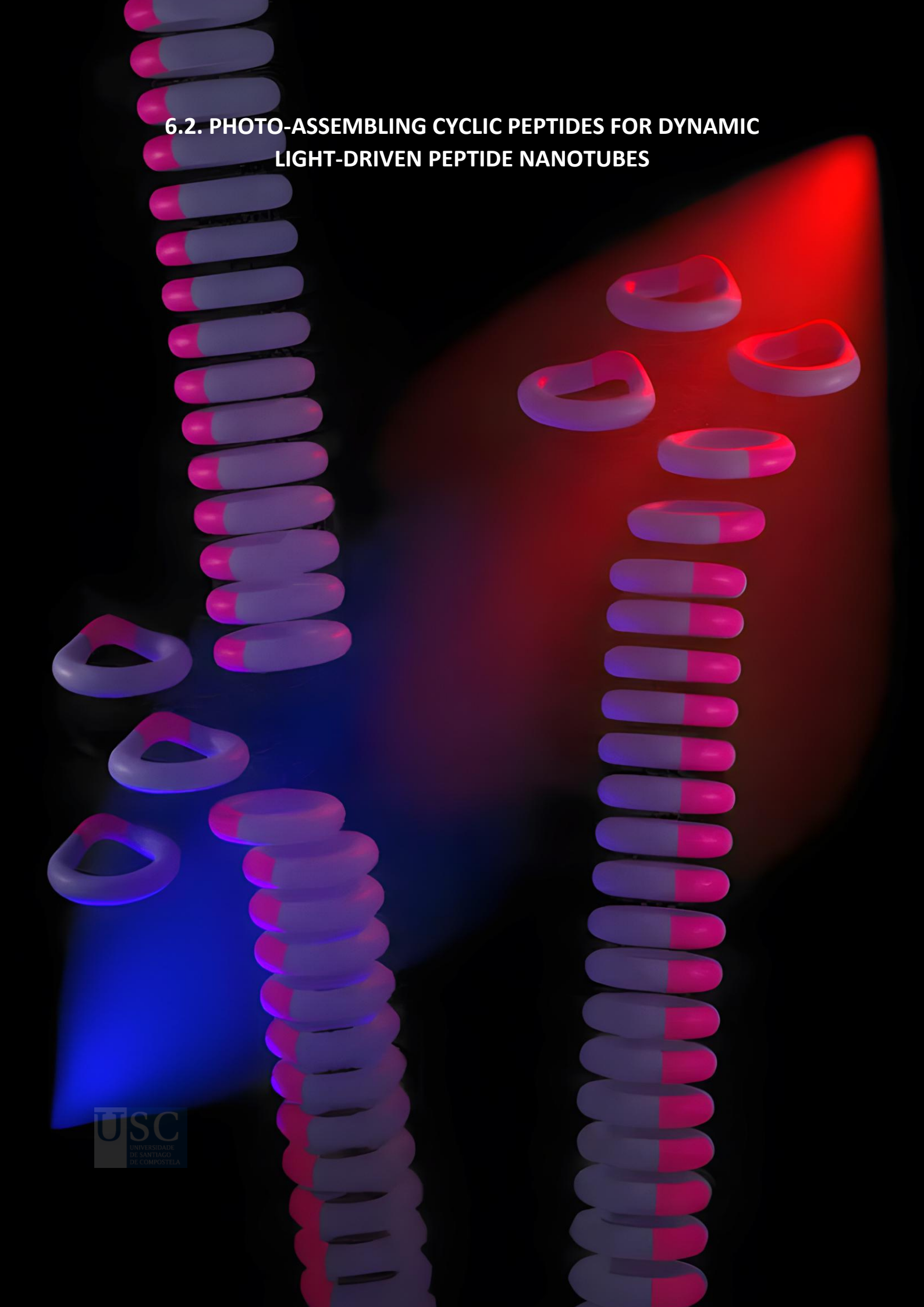

The results of this chapter have been published in *Chem* and *STAR Protocols* as:

M. Vilela-Picos,[a] F. Novelli,[a] A. Pazó,[a] A. Méndez-Ardoy,[a] G. Marafon,[b] M. Amorín,[a] A. Moretto,[b] J. R. Granja.[a] Photo-assembling Cyclic Peptides for Dynamic Light-driven Peptide Nanotubes. *Chem* **2023**, *9*, 3365-3378. DOI: 10.1016/j.chempr.2023.10.005

M. Vilela-Picos,[a] F. Novelli,[a] A. Méndez-Ardoy,[a] A. Moretto,[b] J. R. Granja.[a] Protocol for Photo-controlling the Assembly of Cyclic Peptide Nanotubes in Solution and Inside Microfluidic Droplets. *STAR Protocols* **2024**, *5*, 103031. DOI: 10.1016/j.xpro.2024.103031

Affiliations

[a] Centro Singular de Investigación en Química Biolóxica e Materiais Moleculares (CiQUS), Departamento de Química Orgánica, Universidade de Santiago de Compostela, 15782 Santiago de Compostela, Spain.

[b] Department of Chemical Sciences, University of Padova, via Marzolo, 1, Padova, Italy.

Information in this chapter is reproduced from Ref. 240 and 241 with permission from Elsevier and Cell Press.

[240] M. Vilela-Picos, F. Novelli, A. Pazó, A. Méndez-Ardoy, G. Marafon, M. Amorín, A. Moretto, J. R. Granja. *Chem* **2023**, *9*, 3365-3378.
[241] M. Vilela-Picos, F. Novelli, A. Méndez-Ardoy, A. Moretto, J. R. Granja. *STAR Protocols* **2024**, *5*, 103031.

6.2.1. Precedents

6.2.1.1. Light-induced assembly/disassembly of supramolecular polymers

Photo-assemblers are molecular units whose assembly/disassembly properties are modulated by light-induced conformational changes.[67,242] Most of these materials are related to changes in their secondary structure derived from the light-induced isomerization of a photo-switchable component. This allows the on-demand generation and disaggregation of supramolecular materials under mild conditions.

In this sense, the group of A. Moretto described the use of an unsaturated β-alanine derivative (3-aminoprop-2-enoic acid) to prepare peptide conformational switchers through its *Z* to *E* isomerization (Figure 67A).[243] The *Z*-isomer adopts a loop-like structure, while the *E*-isomer presents an extended conformation that allows the generation of ribbons through the formation of β-sheet type structures. This reversible isomerization induces the activation and deactivation of the peptide self-assembly process. The initial synthetic strategy based on a Pd/Cu catalysed olefin oxidative amidation only allowed the incorporation of one photoswitchable amino acid per peptide. Therefore, the same research group developed a new synthetic strategy to introduce multiple units of this residue into a single peptide.[244] To this end, the authors protected the double bond as a furan cycloadduct, which by a retro-Diels-Alder reaction provided multiple units of the *Z*-isomer, even in a consecutive manner in the peptide sequence (Figure 67B).

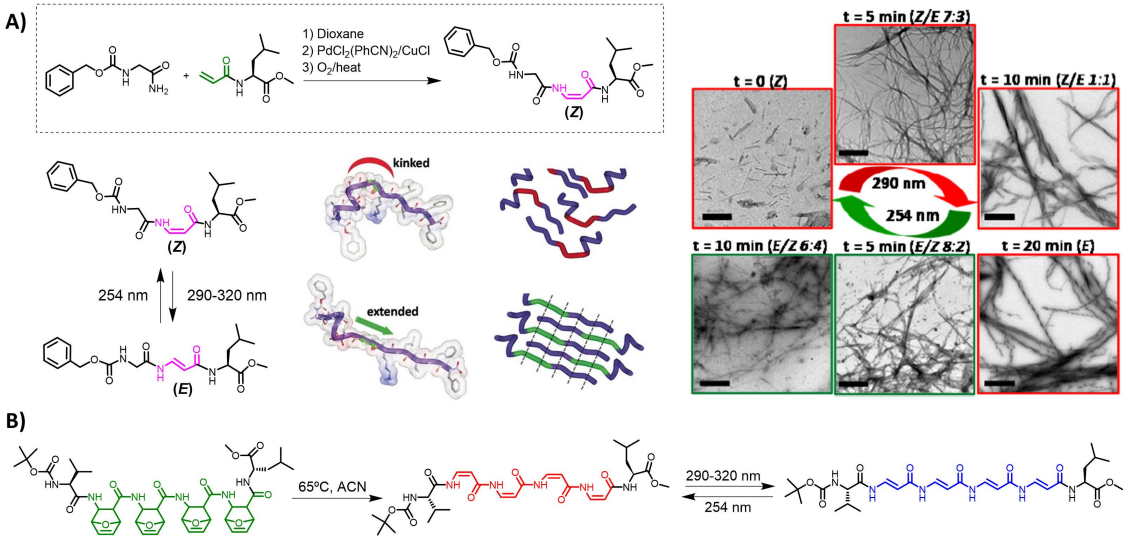

Figure 67. (A) Light-induced assembly/disassembly of a linear peptide that incorporates an unsaturated β-alanine derivative that isomerize between the *Z* and *E*-isomers. Adapted with permission from Ref. 243. Copyright © 2018 Wiley-VCH Verlag GmbH & Co. (B) Strategy to incorporate multiple unsaturated amino acids in a single peptide sequence. Adapted with permission from Ref. 244. Copyright © 2019 American Chemical Society.

[67] J. Chen, F. K.-C. Leung, M. C. A. Stuart, T. Kajitani, T. Fukushima, E. van der Giessen, B. L. Feringa, *Nat. Chem.* **2018**, *10*, 132-138.
[242] Q. Zhang, D. Qu, H. Tian, *Adv. Opt. Mater.* **2019**, *7*, 1900033.
[243] G. Marafon, M. Crisma, A. Moretto, *Angew. Chem. Int. Ed.* **2018**, *57*, 10217-10220.
[244] G. Marafon, M. Crisma, A. Moretto, *Org. Lett.* **2019**, *21*, 4182-4186.

The group of A. Moretto also developed a photo-responsive foldamer, which incorporates two units of this unsaturated amino acid, to control and trigger with light irradiation the aggregation of the protein α-synuclein (aS), whose aggregation has been associated to Parkinson disease etiopathogenesis (Figure 68A).[245] In another example, they introduced this amino acid into a catalytic foldamer in which isomerization brings together the residues Ser, His and Asp (nucleophile, base and acid moieties) to trigger esterase activity (Figure 68B).[246]

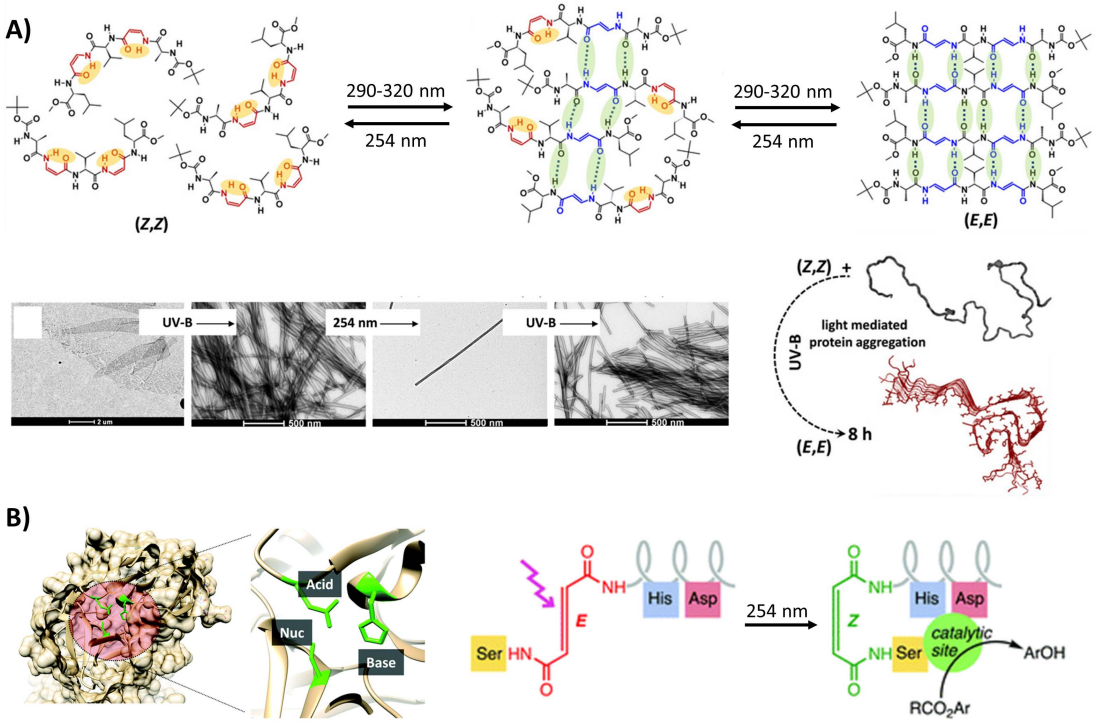

Figure 68. (A) Light activation of a peptide foldamer for inducing the conformational transition and aggregation of α-synuclein. Adapted with permission from Ref. 245. Copyright © 2021 Wiley-VCH Verlag GmbH & Co. (B) Photo-responsive peptide foldamer with esterase activity after light isomerization. Adapted with permission from Ref. 246. Copyright © 2021 Royal Society of Chemistry.

The control of the assembly process of cyclic peptide nanotubes also represents one of the great challenges in the field of these supramolecular materials. Although the strong cooperativity in nanotube formation allows triggering the assembly under specific mild conditions, unfortunately, the reverse process (nanotube dissociation) is not so simple, usually requiring slightly more severe conditions. As mentioned in the introduction, the attachment of polymeric chains to CPs[210,211,212,213] or the use of an external photoacid[214] allowed the implementation of milder conditions, but further studies are still needed to make this reversibility available for all types of SCPNs.

[210] S. C. Larnaudie, J. C. Brendel, K. A. Jolliffe, S. Perrier, *ACS Macro Lett.* **2017**, *6*, 1347-1351.
[211] Q. Song, J. Yang, S. C. L. Hall, P. Gurnani, S. Perrier, *ACS Macro Lett.* **2019**, *8*, 1347-1352.
[212] M. Hartlieb, S. Catrouillet, A. Kuroki, C. Sanchez-Cano, R. Peltier, S. Perrier, *Chem. Sci.* **2019**, *10*, 5476-5483.
[213] Q. Song, J. Yang, J. Y. Rho, S. Perrier, *Chem. Commun.* **2019**, *55*, 5291-5294.
[214] N. Cissé, T. Kudernac, *ChemSystemsChem*, **2020**, *2*, e2000012.
[245] G. Marafon, M. Crisma, A. Masato, N. Plotegher, L. Bubacco, A. Moretto, *Angew. Chem. Int. Ed.* **2021**, *60*, 5173-5178.
[246] M. Pollastrini, G. Marafon, J. Clayden, A. Moretto, *Chem. Commun.* **2021**, *57*, 2269-2272.

6.2.1.2. Confinement inside microfluidic droplets

In the last years, droplet-based microfluidic technology has become an effective method for analysing molecular behaviour, among other applications.[247] This technique allows the fabrication of droplets with a control size, volume, composition and concentration. In general, microfluidic droplets give a more controlled and monodisperse environment than bulk, especially when aggregate visualization is required. Also, microfluidic experiments are characterized by a low reagent consumption and a fast droplet generation that provides an ideal tool for screening applications. In this sense, the behaviour of multiple structures in these confined spaces has been evaluated, such as proteins,[248] drugs,[249] cells,[250] or supramolecular structures,[251] among others.

The works reported by the research groups of C. Abell and O. A. Scherman are especially relevant in this field. In particular, they widely exploited the combination of host-guest chemistry with microfluidic droplets to generate monodisperse and reproducible microcapsules.[252] In one of their first examples they published supramolecular microcapsules based on the formation of a 1:1:1 complex between cucurbit[8]uril (CB[8]), gold nanoparticles functionalized with methyl viologen moieties (MV^{2+}) and a naphthol-modified copolymer (Np) (Figure 69A).[253] The droplets were generated in a microfluidic device with a T-junction geometry in which an oil phase flowed perpendicular to the aqueous phase containing the three assembling components. This setup allowed the encapsulation of cargos in the interior of these droplets, such as fluorescein isothiocyanate-labelled dextran (FITC-dextran) or *Escherichia coli* cells. Interestingly, the release of the cargo could be achieved in a stimuli-responsive manner by a one-electron reduction of the MV^{2+} moiety to cause the degradation of the capsule. The supramolecular nature of these systems allowed the design of other microcapsules with different cargo release mechanisms based on breaking the host-guest interaction and cause the microcapsule degradation (Figure 69B). For example, the modification with a photoswitchable azobenzene leads to a light-triggered release, while a competitive guest-triggered release mechanism can

[247] a) G. M. Whitesides, *Nature*, **2006**, *442*, 368-373; b) L. Shang, Y. Cheng, Y. Zhao, *Chem. Rev.* **2017**, *117*, 7964-8040; c) D. Khoeini, T. F. Scott, A. Neild, *Lab Chip*, **2021**, *21*, 1661-1675; d) P. Zhu, L. Wang, *Lab Chip* **2016**, *17*, 34-75.

[248] a) B. Zheng, L. S. Roach, R. F. Ismagilov, *J. Am. Chem. Soc.* **2003**, *125*, 11170-11171; b) Y. Zhu, L. Zhu, R. Guo, H. Cui, S. Ye, Q. Fang, *Sci. Rep.* **2014**, *4*, 5046.

[249] a) M. N. Hsu, R. Luo, K. Z. Kwek, Y. C. Por, Y. Zhang, C. Chen, *Biomicrofluidics* **2015**, *9*, 052601; b) M. Windbergs, Y. Zhao, J. Heyman, D. A. Weitz, *J. Am. Chem. Soc.* **2013**, *135*, 7933-7937.

[250] a) S. Köster, F. E. Angilè, H. Duan, J. J. Agresti, A. Wintner, C. Schmitz, A. C. Rowat, C. A. Merten, D. Pisignano, A. D. Griffiths, D. A. Weitz, *Lab Chip*, **2008**, *8*, 1110-1115; b) J. Clausell-Tormos, D. Lieber, J. C. Baret, A. El-Harrak, O. J. Miller, L. Frenz, J. Blouwolff, K. J. Humphry, S. Köster, H. Duan, C. Holtze, D. A. Weitz, A. D. Griffiths, C. A. Merten, *ACS Chem. Biol.* **2008**, *15*, 427-437; c) E. Brouzes, M. Medkova, N. Savenelli, D. Marran, M. Twardowski, J. B. Hutchison, J. M. Rothberg, D. R. Link, N. Perrimon, M. L. Samuels, *Proc. Natl. Acad. Sci. U. S. A.* **2009**, *106* , 14195-14200; d) S. Sart, G. Ronteix, S. Jain, G. Amselem, C. N. Baroud, *Chem. Rev.* **2022**, *122*, 7061-7096.

[251] a) H. Lin, L. Zhou, F. Mei, W. Dou, L. Hu, H. Yang, L. Xu, *Angew. Chem. Int. Ed.* **2023**, *62*, e202301900; b) S. Bai, S. Debnath, K. Gibson, B. Schlicht, L. Bayne, M. Zagnoni, R. V. Ulijn, *Small* **2014**, *10*, 285-293; c) A. Levin, T. C. T. Michaels, T. O. Mason, T. Müller, L. Adler-Abramovich, L. Mahadevan, M. E. Cates, E. Gazit, T. P. J. Knowles, *ACS Appl. Mater. Interfaces* **2018**, *10*, 27578-27583.

[252] J. Liu, Y. Lan, Z. Yu, C. S.Y. Tan, R. M. Parker, C. Abell, O. A. Scherman, *Acc. Chem. Res.* **2017**, *50*, 208-217.

[253] J. Zhang, R. J. Coulston, S. T. Jones, J. Geng, O. A. Scherman, C. Abell, *Science* **2012**, *335*, 690-694.

be achieved by the addition of a molecule with a higher affinity for CB[8], such as 1-adamantylamine (ADA).[254]

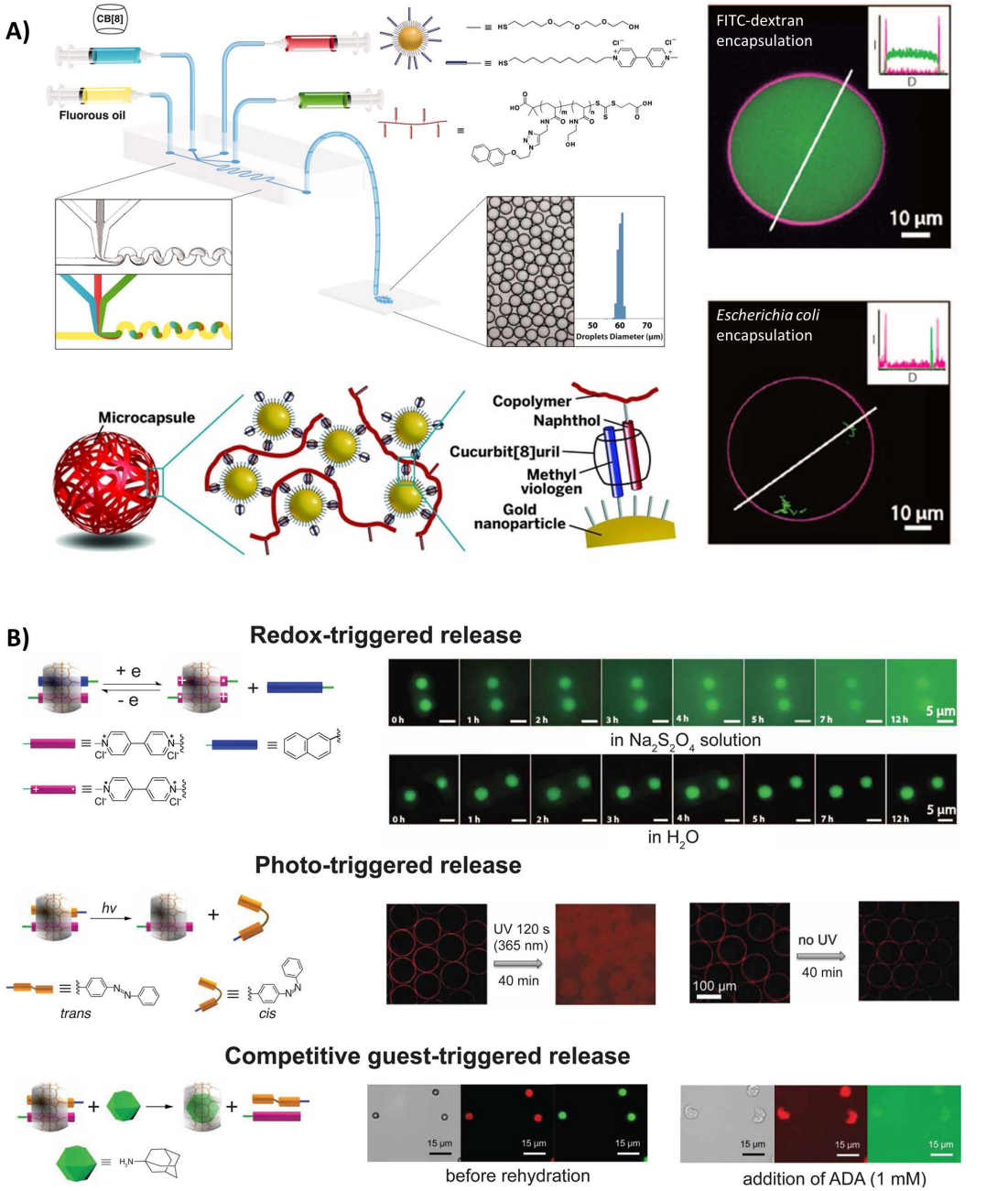

Figure 69. (A) Droplet generation for creating microcapsules made from the host-guest interaction of CB[8], gold nanoparticles functionalized with MV^{2+} and a naphthol-modified copolymer. The microcapsules allowed the encapsulation in the interior of cargos such as FITC-dextran or *Escherichia coli* cells. Adapted with permission from Ref. 253. Copyright © 2012 AAAS. (B) Representation of three different release mechanisms of a cargo from a microfluidic microcapsule. Reprinted with permission from Ref. 252. Copyright © 2017 American Chemical Society.

[252] J. Liu, Y. Lan, Z. Yu, C. S.Y. Tan, R. M. Parker, C. Abell, O. A. Scherman, *Acc. Chem. Res.* **2017**, *50*, 208-217.
[253] J. Zhang, R. J. Coulston, S. T. Jones, J. Geng, O. A. Scherman, C. Abell, *Science* **2012**, *335*, 690-694.
[254] a) Y. Zheng, Z. Yu, R. M. Parker, Y. Wu, C. Abell, O. A. Scherman, *Nat. Commun.* **2014**, 5, 5772; b) X. Xu, E. A. Appel, X. Liu, R. M. Parker, O. A. Scherman, C. Abell, *Biomacromolecules* **2015**, *16*, 2743-2749; c) Z. Yu, J. Zhang, R. J. Coulston, R. M. Parker, F. Biedermann, X. Liu, O. A. Scherman, C. Abell, *Chem. Sci.* **2015**, *6*, 4929-4933; d) Z. Yu, Y. Zheng, R. M. Parker, Y. Lan, Y. Wu, R. J. Coulston, J. Zhang, O. A. Scherman, C. Abell, *ACS Appl. Mater. Interfaces* **2016**, *8*, 8811-8820.

Microfluidic techniques have also been applied to construct artificial synthetic cells.[255] The research group of W. T. S. Huck reported the encapsulation of liposomal droplets into another liposomal droplets to obtain multicompartmental liposomal structures called vesosomes (Figure 70A).[256] These structures showed the ability to generate RNA in their interior or create nanopores in their membrane to transport small molecules between the different compartments, converting this technique in an interesting approach to prepare artificial cells. As an alternative, the group of J. P. Spatz reported droplet-stabilized giant unilamellar vesicles (dsGUVs) created by microfluidics (Figure 70B).[257] These water-in-oil structures are composed of a membrane that combined lipid vesicles with copolymer-stabilized droplets. By means of pico-injections inside the microfluidic device, they were able to introduce transmembrane proteins (integrin and ATP synthase) or cytoskeletal proteins (G-actin and tubulin) into the interior. In addition, this approach allows to eliminate the oil phase and stabilize the droplets in the water phase without disrupting the lipids or affecting the biological functions of the synthetic cell.

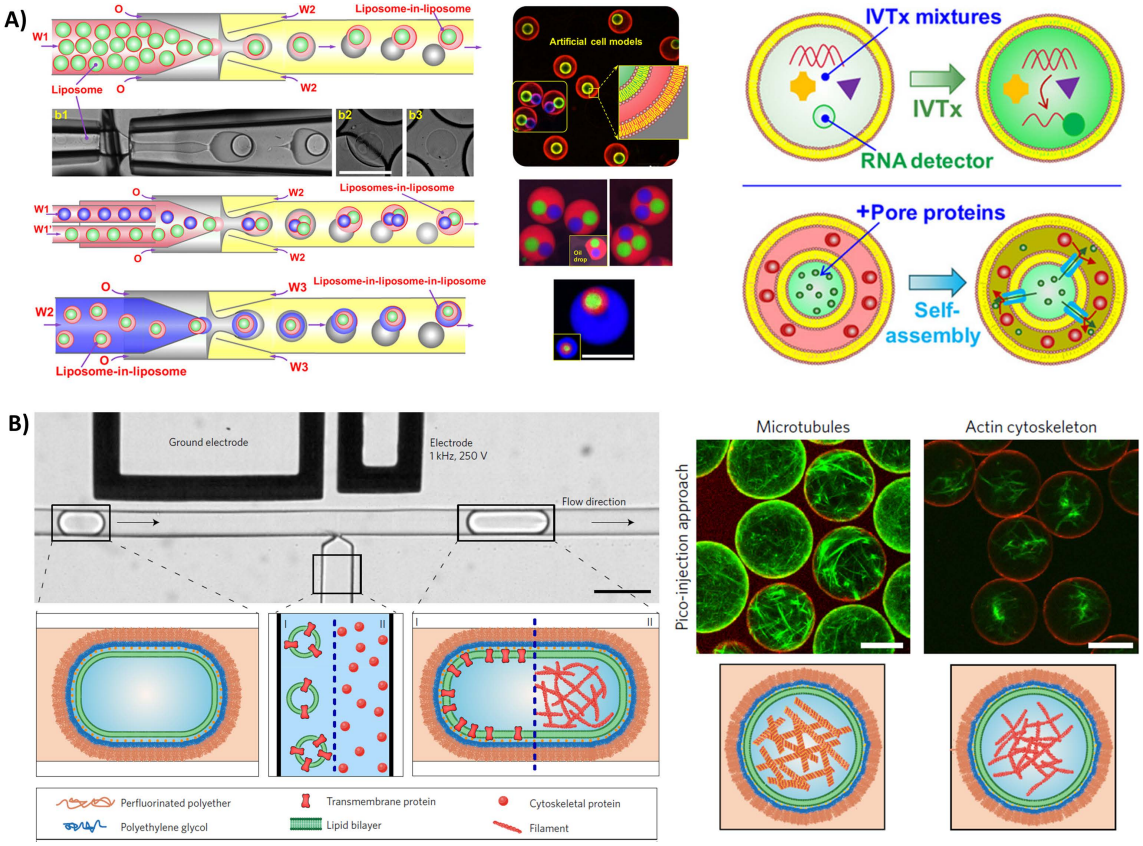

Figure 70. (A) Vesosomes created by a microfluidic technique to allow RNA generation or nanopore formation in their interior. Adapted with permission from Ref. 256. Copyright © 2017 American Chemical Society. (B) Microfluidic pico-injections for incorporating transmembrane and cytoskeletal proteins inside dsGUVs. Adapted with permission from Ref. 257. Copyright © 2018 Springer Nature.

[255] a) C. Martino, A. J. deMello, *Interface Focus* **2016**, *6*, 20160011; b) S. Tan, Y. Ai, X. Yin, Z. Xue, X. Fang, Q. Liang, X. Gong, X. Dai, *Adv. Funct. Mater.* **2023**, *33*, 2305071; c) S. Fasciano, S. Wang, *SLAS Technol.* **2024**, *29*, 100090.
[256] N. Deng, M. Yelleswarapu, L. Zheng, W. T. S. Huck, *J. Am. Chem. Soc.* **2017**, *139*, 587-590.
[257] M. Weiss, J. P. Frohnmayer, L. T. Benk, B. Haller, J. Janiesch, T. Heitkamp, M. Börsch, R. B. Lira, R. Dimova, R. Lipowsky, E. Bodenschatz, J.Baret, T. Vidakovic-Koch, K. Sundmacher, I. Platzman, J. P. Spatz, *Nat. Mater.* **2018**, *17*, 89-96.

These microfluidic droplets also allow to evaluate the behaviour of fibrillar and hydrogel-like supramolecular systems in confined spaces, especially for assessing their potential application as synthetic mimetics of cell cytoskeleton.[258] The group of Y. Wang published supramolecular microcapsules created by a microfluidic technique composed of hydrazone hydrogelators that self-assemble at water-water interfaces (Figure 71A).[259] In particular, the use of a catalyst transforms the water soluble hydrazide and aldehyde precursors into a supramolecular hydrogel that accumulates at the water-water interface creating a microcapsule. The encapsulation of the enzyme glucose oxidase (GOx) in their interior converts a redox-responsive molecule (CSH) into a self-assembling monomer (CSSC) causing the enzymatic growth of supramolecular fibres that mimic the self-assembly of microtubules in living cells (Figure 71B).

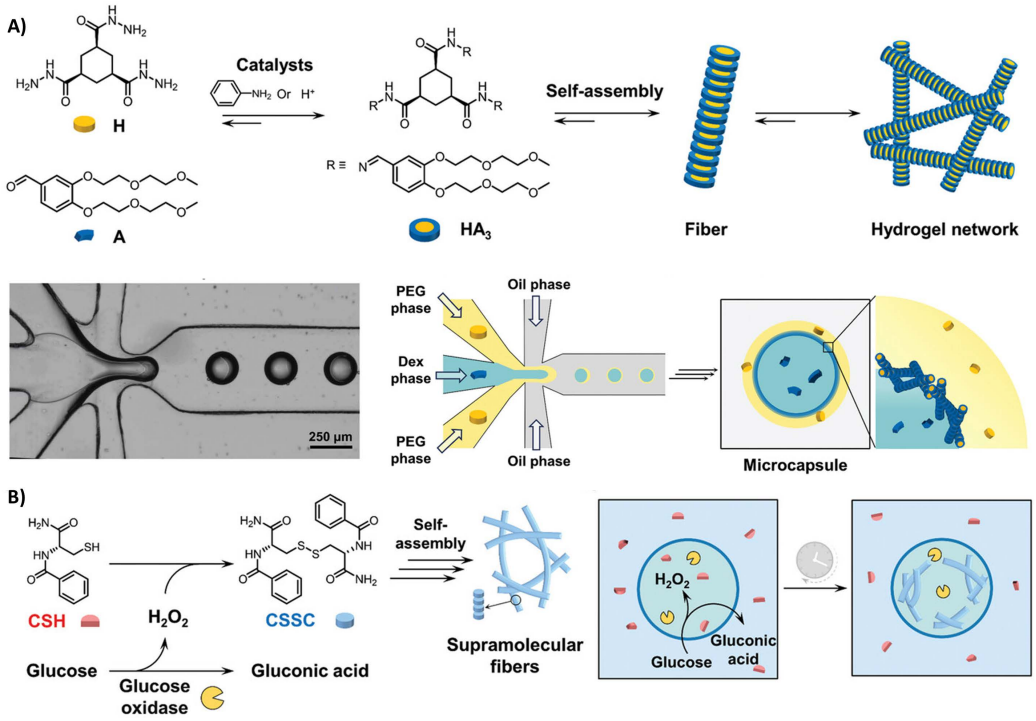

Figure 71. (A) Fabrication of supramolecular microcapsules with a microfluidic technique by self-assembly of hydrazone hydrogelators at water-water interfaces. Reprinted with permission from Ref. 259. Copyright © 2024 Wiley-VCH Verlag GmbH & Co. (B) Enzymatic growth in the interior of microfluidic microcapsules of supramolecular fibres that mimic the self-assembly of microtubules in cells. Adapted with permission from Ref. 259. Copyright © 2024 Wiley-VCH Verlag GmbH & Co.

In this context, our research group has recently focused on the study of the spatiotemporally controlled supramolecular polymerization of CPs within aqueous droplets. As explained in the introduction, in a first work, it was designed a pH-responsive CP that polymerize into nanotubes, after the external addition of base, inside water-in-oil droplets prepared by emulsification methods.[215] In a second work, the spatially controlled supramolecular polymerization of the same cyclic peptide scaffold was achieved in the interior of microfluidic water-in-oil droplets.[216]

[215] A. Méndez-Ardoy, J. R. Granja, J. Montenegro, *Nanoscale Horiz.* **2018**, *3*, 391-396.
[216] A. Méndez-Ardoy, A. Bayón-Fernández, Z. Yu, C. Abell, J. R. Granja, J. Montenegro, *Angew. Chem. Int. Ed.* **2020**, *59*, 6902-6908.
[258] P. Zhan, K. Jahnke, N. Liu, K. Göpfrich, *Nat. Chem.* **2022**, *14*, 958-963.
[259] Z. Li, H. Wang, Y. Gao, J. Chen, G. Gu, J. Liu, Y. Chen, X. Guo, Y. Wang, *Small* **2024**, 2403085.

6.2.2. Objective

In this chapter, we propose to introduce the 3-aminoprop-2-enoic acid (ΔβAla) reported by the group of A. Moretto[243,244,245,246] in a cyclic peptide that can assemble into nanotubes. In particular, this residue can exist as either the *Z*- or *E*-isomer (Δ^{Z}βAla or Δ^{E}βAla) and both forms can be interconverted by appropriate UV light irradiation. The shorter wavelength (254 nm) is used to transform the *E*- into the *Z*-isomer, while irradiation with a longer wavelength light (290-320 nm) provides the thermodynamically more stable *E*-isomer. We intend to use this process to change the conformational shape of the cyclic peptide from a folded conformation (monomeric component) to a flat ring-shaped conformation that is programmed to self-assemble and *vice versa*. In addition, we plan to study this process inside microfluidic aqueous droplets to evaluate the spatiotemporally controlled supramolecular polymerization. Based on the work of the previous chapter in which the incorporation of two β-alanine to *D*,*L*-α-CPs provided a new kind of SCPN constituted by parallel oriented stacks,[217] now we decided to replace one of the β-Ala by the corresponding unsaturated residue (**^{Z}CP3** and **^{E}CP3**) (Figure 72) . The designed cyclic peptide also incorporates a pyrene moiety that should help in the nanotube formation by establishing π,π-interactions and, in addition, its spectroscopic properties should allow to study the self-assembly process.

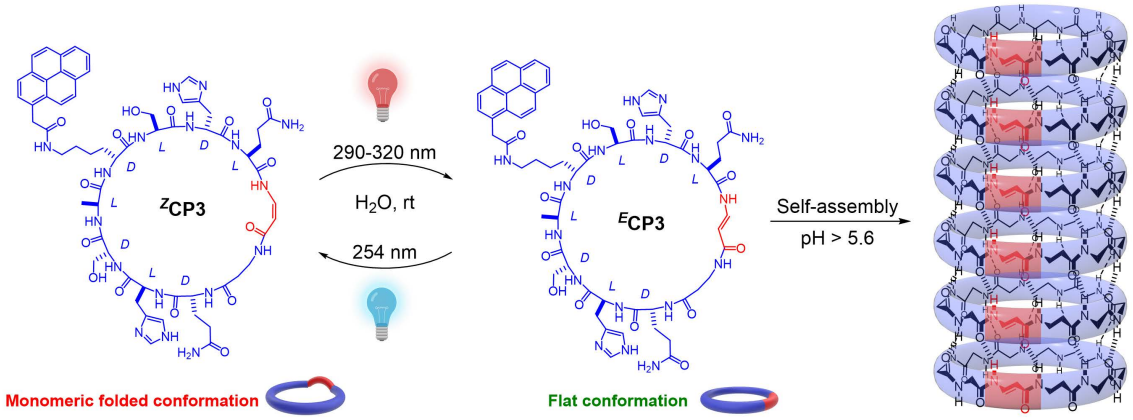

Figure 72. Illustration of the photo-modulated assembly/disassembly process of peptide nanotubes proposed in this chapter. The amino acid side chains in the nanotube model are omitted for clarity.

6.2.3. Results and discussion

6.2.3.1. Synthesis of CPs

The proposed peptide was prepared by Fmoc-methodologies on solid phase synthesis using a Rink amide resin (Figure 73).[215,216,229] For this purpose, the Glu residue was attached through its side chain using an α-allyl-protected glutamic acid derivative (Fmoc-*L*-Glu-OAll). Then, the linear peptide was prepared by repetitive cycles of deprotection of the Fmoc group with 25% piperidine/DMF and coupling with *N*-HBTU of the next Fmoc-protected amino acid. The olefinic moiety of the unsaturated residue was masked as a furan cycloadduct (Fmoc-Δ^{P}βAla-OH) and it was attached, as a racemic mixture, at the end of the linear peptide sequence. After this, the cyclization was carried out on solid support. To this end, the *C*-terminal allyl-protecting group was removed using typical π-allyl palladium chemistry, and then, the *N*-terminal Fmoc group was eliminated using standard conditions (25% piperidine/DMF). The cyclization was carried out using PyAOP as a coupling reagent. Full cyclization was achieved after 2 h of reaction, and then, the pyrene moiety was incorporated on the Lys side chain by treatment with mild acidic conditions (HFIP/ TFE/ TIS/ DCM [20:10:5:65]) to deprotect the Mtt group followed by coupling of 1-pyreneacetic acid using *N*-HATU as coupling agent. Peptide cleavage was initially carried out using standard conditions (TFA/DCM/H_2O/TIS [90:5:2.5:2.5]). Unfortunately, the resulting major product under these conditions had a molecular weight two units higher than expected. This compound was assigned to the CP with the double bond of the cycloadduct moiety reduced. We attributed this problem to the strong reducing properties of the silane scavenger. Therefore, substitution of this reagent by thioanisole (methyl phenyl sulfide; MPS) (TFA/DCM/H_2O/MPS [90:5:2.5:2.5]) provided, after HPLC purification, **^{P}CP3** in an overall 18% yield.

USC UNIVERSIDADE DE SANTIAGO DE COMPOSTELA

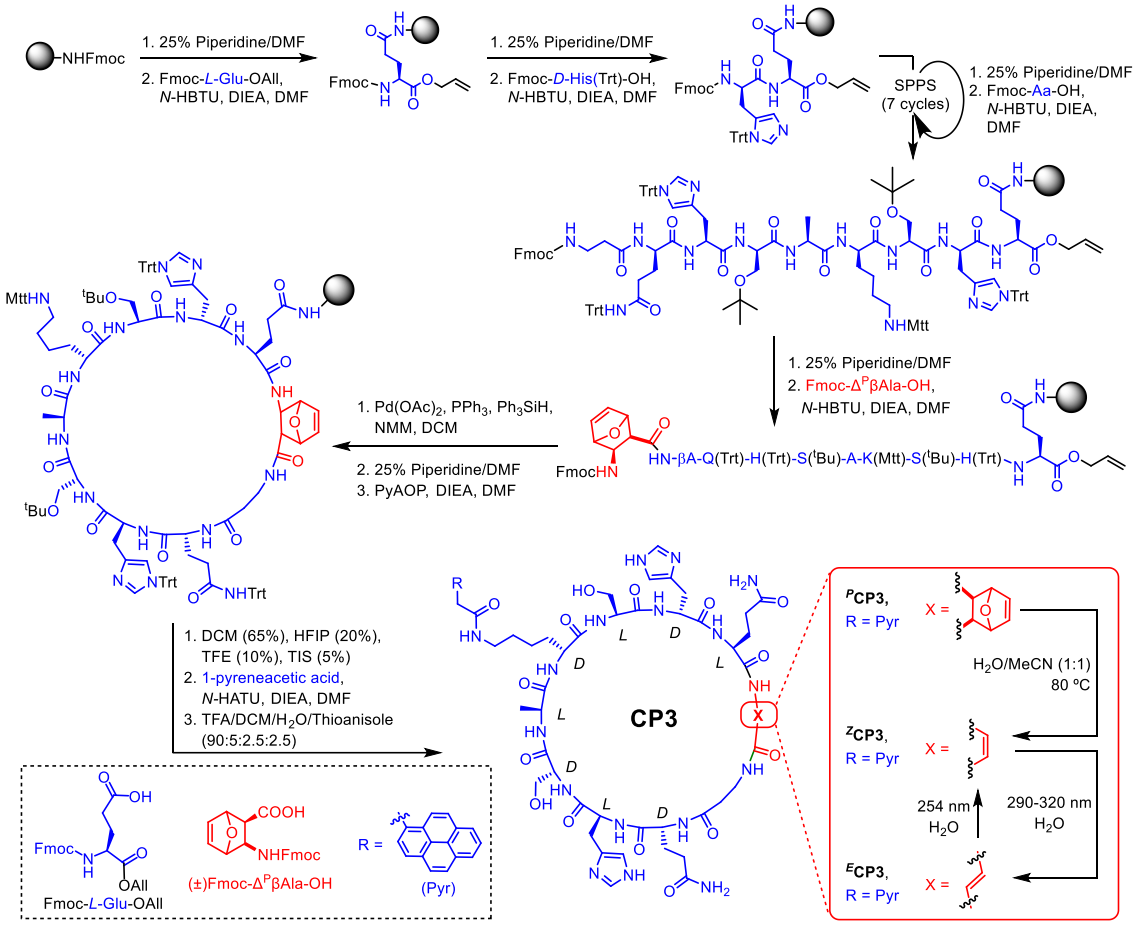

Figure 73. Synthetic scheme used for the preparation of **^{P}CP3**, **^{Z}CP3** and **^{E}CP3**.

Heating an aqueous solution (H_2O/MeCN, 1:1) of **^{P}CP3** for 24 h at 80°C yielded the expected **^{Z}CP3**. The chemical shift of amide proton of Δ^{Z}βAla at 11.28 ppm supports the proposed folded conformation of **^{Z}CP3** (Figure 74), consistent with the previously reported behaviour of peptides containing this residue due to the formation of a strong hydrogen bond with its carbonyl moiety.[243] The sharp and fine resolution of most of the proton signals of this CP confirms that it is unaggregated.

USC UNIVERSIDADE DE SANTIAGO DE COMPOSTELA

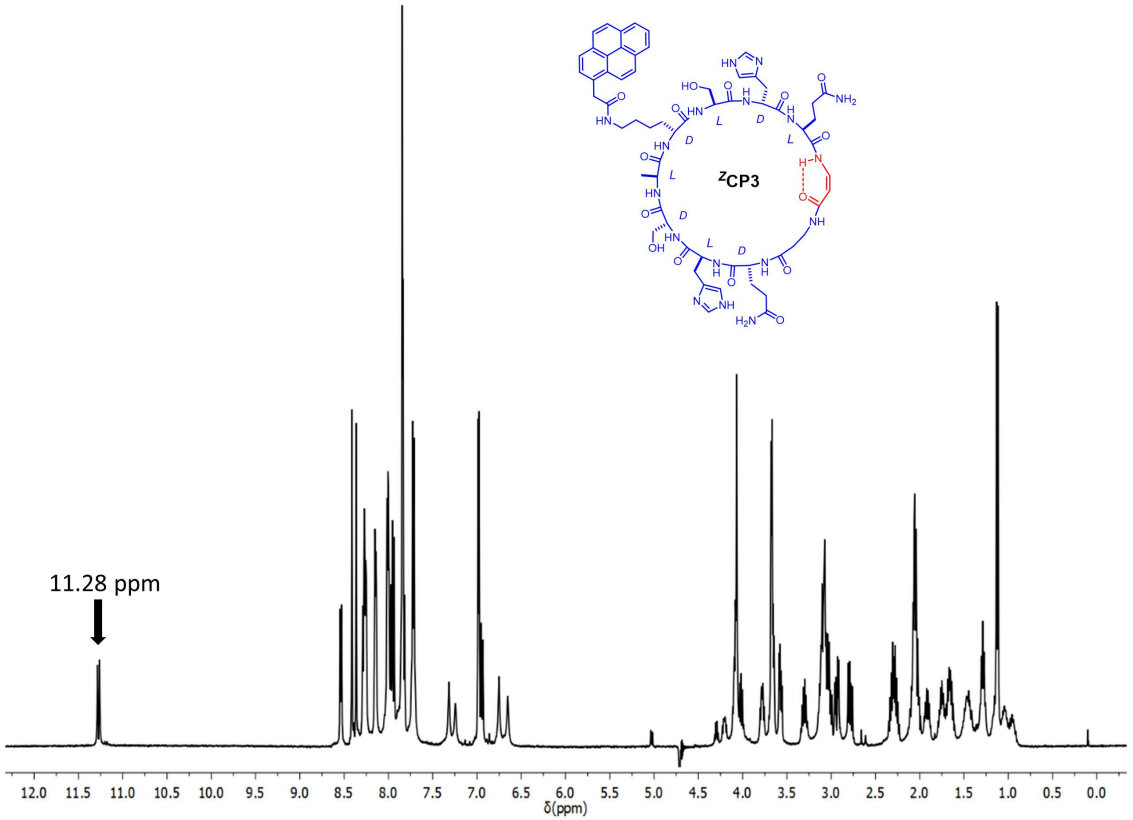

Figure 74. ^{1}H-NMR of **^{Z}CP3** at 4.4 mM (500 MHz, D_2O/H_2O, 298K) showing the amide proton signal of Δ^{Z}βAla at 11.28 ppm that is forming a hydrogen bond with its carbonyl moiety.

6.2.3.2. Studies of CP isomerization

The *E*-isomer was obtained by irradiation (290-320 nm) of an aqueous solution of **^{Z}CP3** (400 µM) for 10 min (Figure 73). Under these conditions, **^{E}CP3** was obtained as a major product, in a 7:3 mixture with the starting peptide. Both isomers were separated by HPLC, and the new compound was characterized. The NMR signals under acidic conditions (Figure 75A) confirm the up-field shift (9.79 ppm) of the amide proton of Δ^{E}βAla, suggesting that it is not anymore participating in the above-mentioned strong intramolecular hydrogen bond. The FT-IR spectrum (Figure 75B) of a lyophilized sample after neutralization supports the formation of a parallel-like β-sheet structure with a strong band at 1633.3 cm^{-1} and a shoulder at 1659.0 cm^{-1}.[217] In addition, the band at 3293.9 cm^{-1} (amide A) is highly indicative of a well-established network of hydrogen bonds.[233]

USC UNIVERSIDADE DE SANTIAGO DE COMPOSTELA

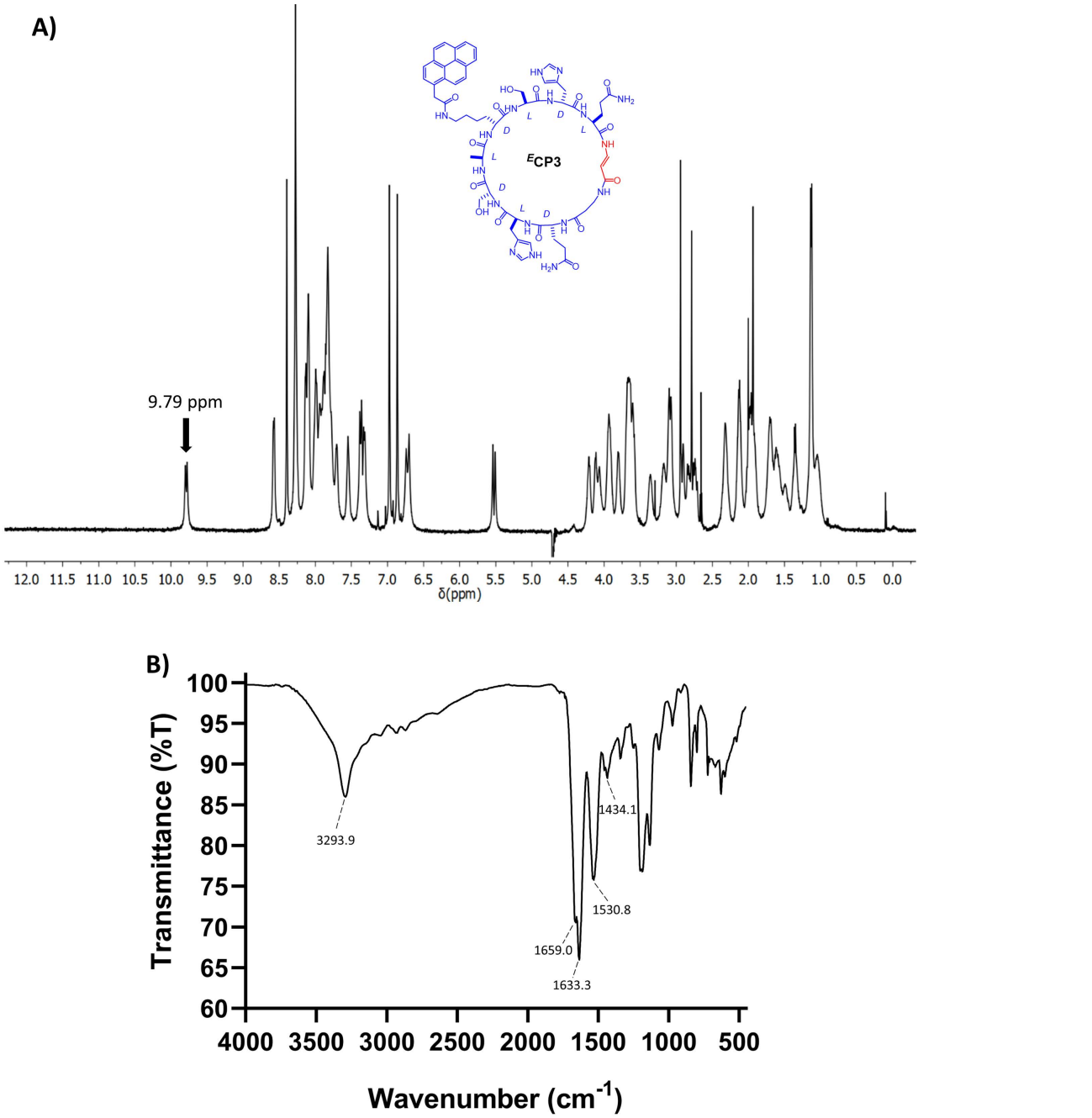

Figure 75. (A) ^{1}H-NMR of **^{E}CP3** at 3.5 mM (500 MHz, D_2O/H_2O, 298K) showing the amide proton signal of Δ^{E}βAla at 9.79 ppm. (B) FT-IR spectrum of **^{E}CP3** (solid, 298 K).

The kinetic of this *Z* to *E* isomerization was followed by HPLC (200 µM) (Figure 76). After 10 min of irradiation, the mixture already reaches the steady state as a 7:3 mixture of both isomers. This ratio is slightly smaller than the previously reported by A. Moretto with linear peptides,[243,244,245,246] suggesting that the internal hydrogen bond in the CP must stabilize the *Z*-isomer. The isomerization is independent of the pH of the media, as confirmed by the similar ratios and yields obtained at either acidic (pH 1.8), native (pH 5.1), neutral (pH 7.0) or basic conditions (pH 9.0). Under neutral and basic conditions, the peptide starts to precipitate during irradiation, most likely due to pH-induced self-assembly, as denoted by the reduction of the sample signals with time.

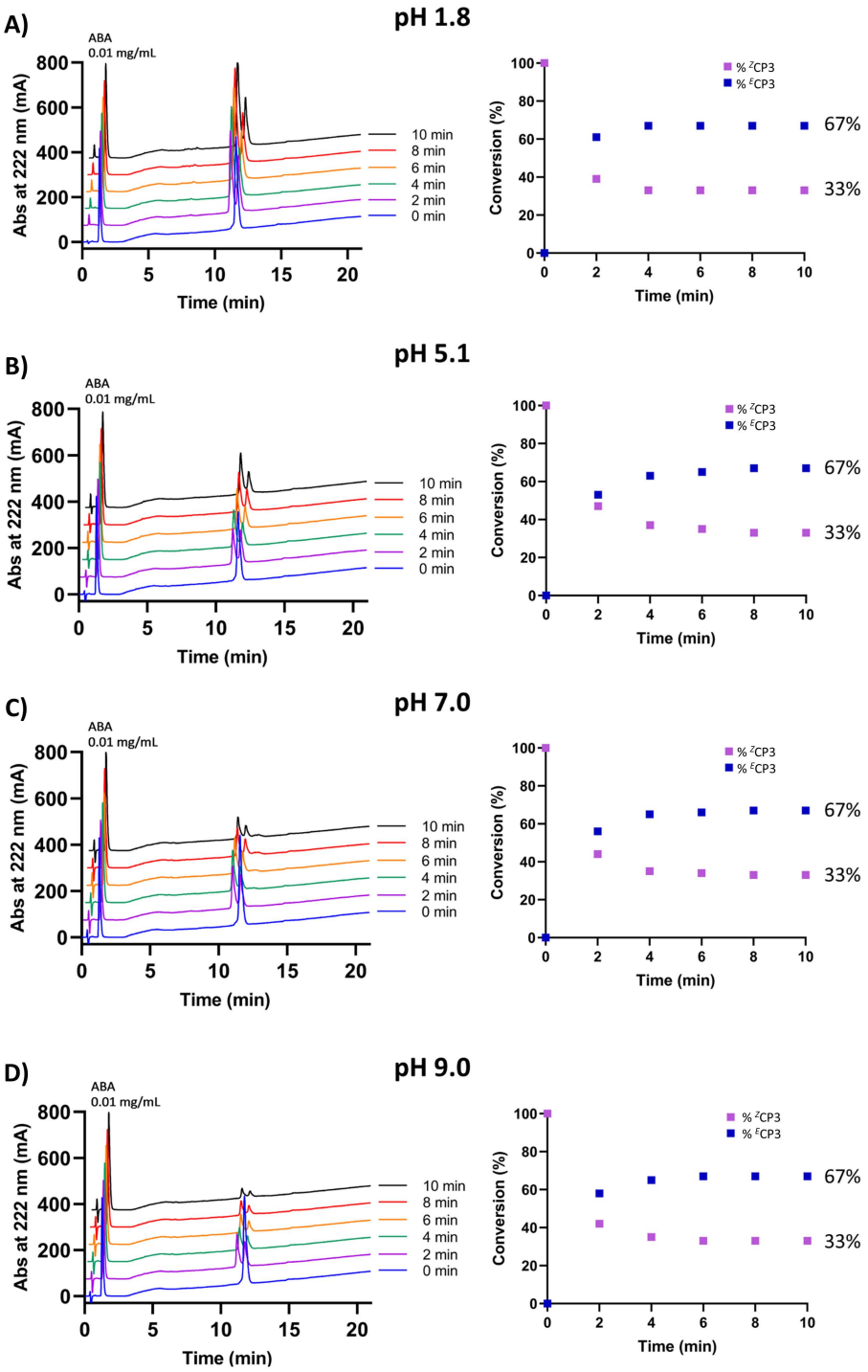

Figure 76. Photoisomerization of **^{Z}CP3**. HPLC analysis (HPLC conditions: H_2O (0.1% TFA)/MeCN (0.1% TFA), 100:0 → 80:20 (2 min) and 80:20 → 50:50 (19 min)) and photoisomerization conversion of a solution of **^{Z}CP3** (200 µM) irradiated at 290-320 nm at acidic (A, pH 1.8), native (B, pH 5.1), neutral (C, pH 7.0, 10 mM HEPES) or basic pH (D, pH 9.0, 10 mM Boric acid). An aqueous solution of 4-aminobenzoic acid (ABA, 0.01 mg/mL) was added as an internal standard.

The isomerization of **^{E}CP3** (200 µM) (Figure 77) into **^{Z}CP3** was also investigated but using a shorter wavelength (254 nm). The reaction was also studied at a different pH, and the isomerization rate was followed by HPLC analysis. In all cases, after 2 min, the reactions have already reached the photostationary state consisting of an almost 1:1

mixture of both isomers. Once again, the isomerization occurs independently of the pH media. However, as observed previously, peptide signals on the HPLC traces decrease due to their precipitation at neutral or basic conditions.

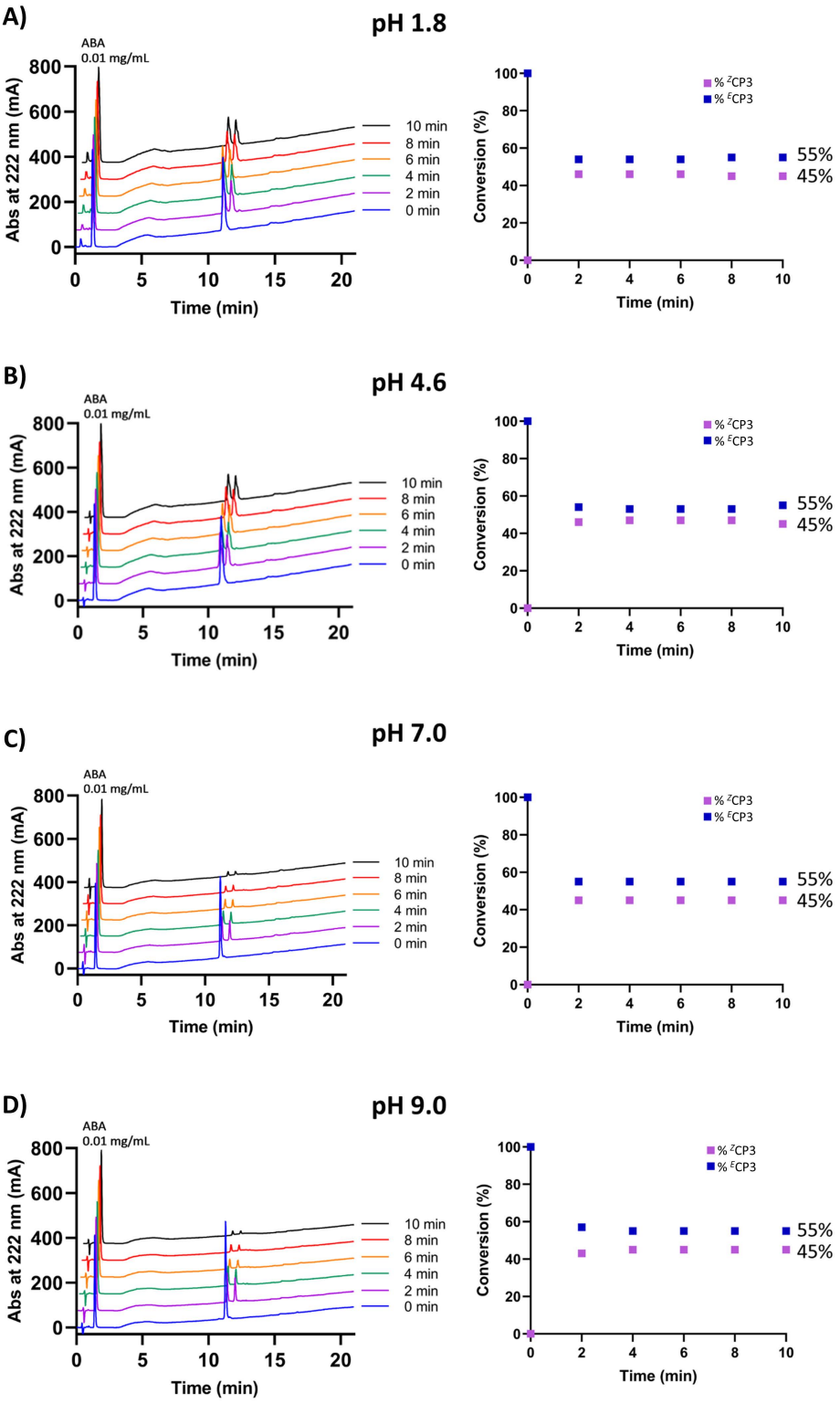

Figure 77. Photoisomerization of **^{E}CP3**. HPLC analysis (HPLC conditions: H_2O (0.1% TFA)/MeCN (0.1% TFA) 100:0 → 80:20 (2 min) and 80:20 → 50:50 (19 min)) and photoisomerization conversion of a solution of **^{E}CP3** (200 µM) irradiated at 254 nm at acidic (A, pH 1.8), native (B, pH 4.6), neutral (C, pH 7.0, 10 mM HEPES) or basic pH (D, pH 9.0, 10 mM Boric acid). An aqueous solution of 4-aminobenzoic acid (ABA, 0.01 mg/mL) was added as an internal standard.

To study if the decrease in the isomerization conversion compared to the examples previously reported with linear peptide by A. Moretto[243,244,245,246] is due to the partial absorption of light by the pyrene moiety, a new peptide with an alkyl chain of six carbons (**^{Z}CP4**/**^{E}CP4**) was prepared and the light-induced isomerization was evaluated (Figure 78). However, isomerization proceeds in both directions with the same conversions as with the pyrene derivatives (**^{Z}CP3**/**^{E}CP3**), suggesting that the conversion reduction is more related to the ring-shaped structure stabilising the *Z*-isomer.

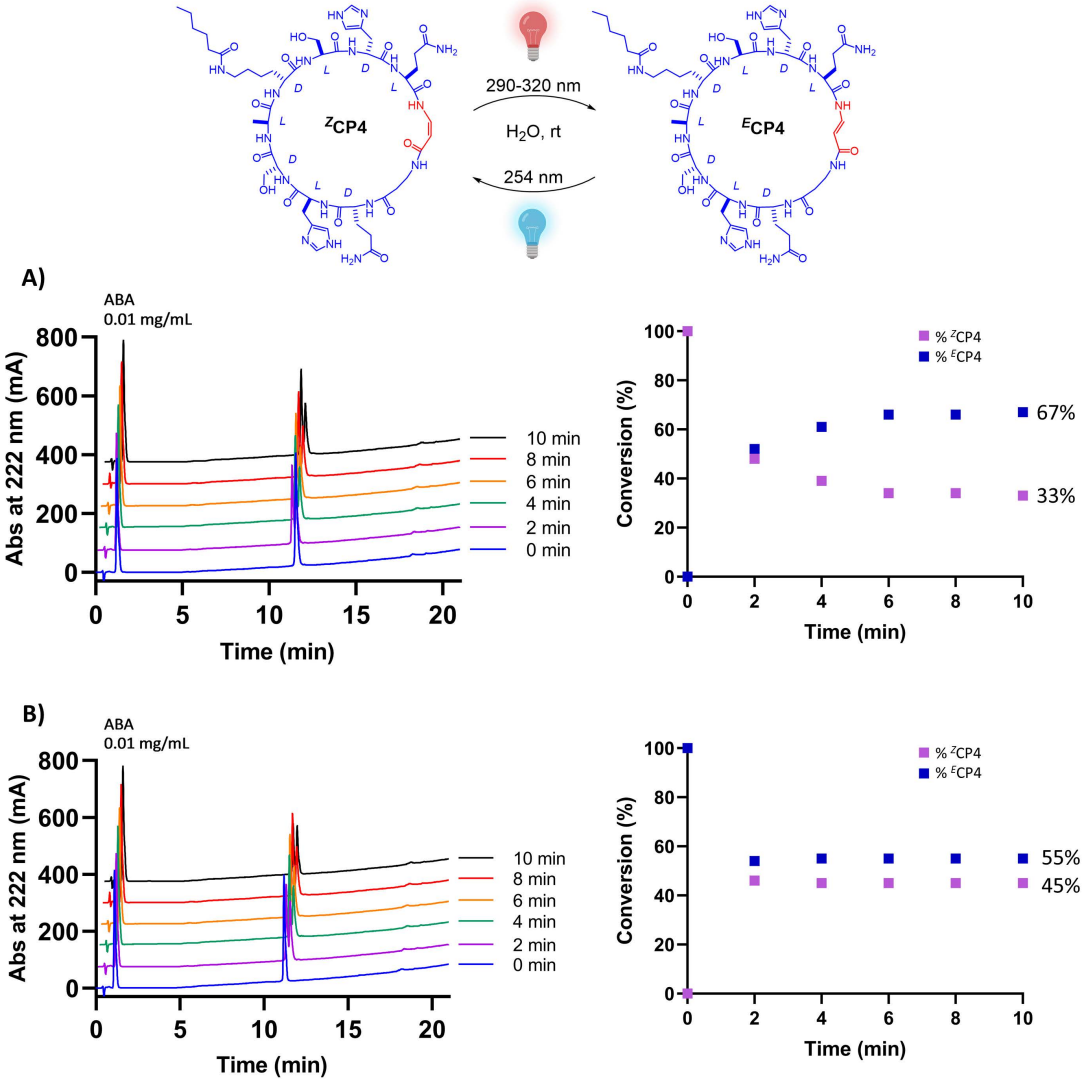

Figure 78. Photoisomerization at native pH (pH 4.5) of 200 µM aqueous solutions of (A) **^{Z}CP4** by irradiation at 290-320 nm or (B) **^{E}CP4** by irradiation at 254 nm. An aqueous solution of 4-aminobenzoic acid (ABA, 0.01 mg/mL) was added as an internal standard. HPLC conditions: H_2O (0.1% TFA)/MeCN (0.1% TFA), 100:0 → 100:0 (2 min) and 100:0 → 50:50 (19 min).

To confirm the stability of the system to the photoisomerization, **CP3** was subjected to several isomerization cycles (Figure 79A) or irradiated for long periods of time (60 min) (Figure 79B-C), and in both cases, no other products were found. Moreover, no isomerization to the thermodynamically more stable *E*-isomer or decomposition was observed when a solution of **^{Z}CP3** was heated at 80°C for 72 h (200 µM) (Figure 79D-E).

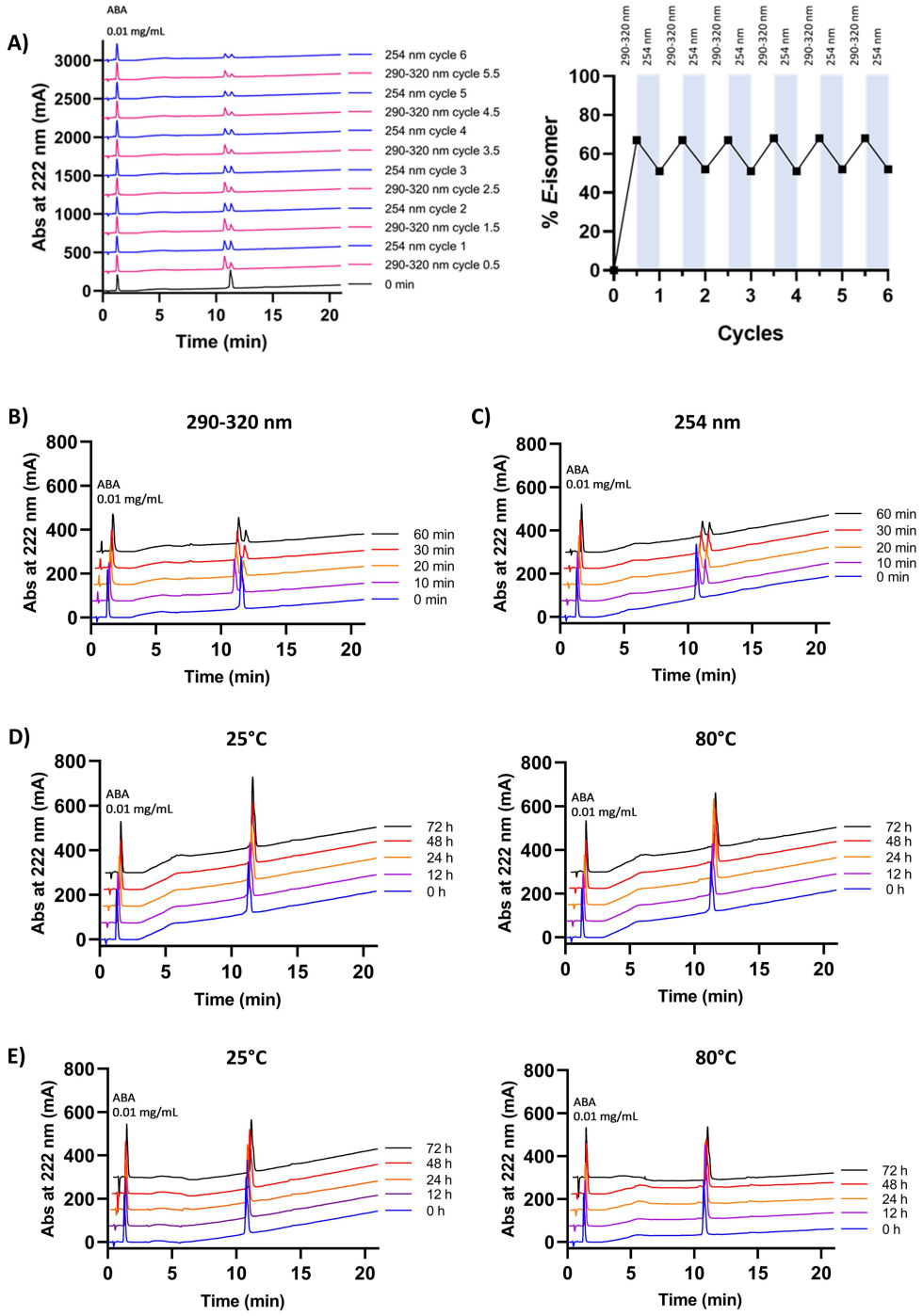

Figure 79. (A) Cycles of irradiation and photoisomerization conversion of a solution of **^{Z}CP3** (200 µM) cyclically irradiated at 290-320 nm (5 min) and 254 nm (2 min) at native pH (pH 5.1). (B) Photostability study of a solution of **^{Z}CP3** (200 µM) irradiated at 290-320 nm at native pH (pH 5.1). (C) Photostability study of a solution of **^{E}CP3** (200 µM) irradiated at 254 nm at native pH (pH 5.1). (D) Thermal stability of a solution of **^{Z}CP3** (200 µM) heated at 25 ℃ or 80 ℃ at native pH (pH 5.1). (E) Thermal stability of a solution of **^{E}CP3** (200 µM) heated at 25 ℃ or 80 ℃ at native pH (pH 5.1). HPLC analysis for all the experiments (HPLC conditions: H_2O (0.1% TFA)/MeCN (0.1% TFA), 100:0 → 80:20 (2 min) and 80:20 → 50:50 (19 min)). An aqueous solution of 4-aminobenzoic acid (ABA, 0.01 mg/mL) was added as an internal standard.

The above-mentioned signal reduction under neutral/basic conditions was also evaluated. For this purpose, the reaction mixtures were lyophilized, subsequently re-dissolved and analysed by HPLC, showing not only the recovery of both peptides

(Figure 80A) but also the appearance of a new oxidized derivative in less than 10%. This suggests that the aforementioned signal reduction is mainly due to precipitation and not due to the decomposition of the CPs as a consequence of the irradiations. In fact, ultracentrifugation of the pH 7.0 reaction mixture after irradiation using the 254 nm wavelength showed the preferential accumulation of **^{E}CP3** (Figure 80B), the precursor of nanotubes, at the bottom of the sample, whereas the ratio of the other isomer is increased in the upper part of the sample. The accumulation of **^{E}CP3** at the bottom fraction suggests that self-assembly and nanotube formation must be the main reason for peptide precipitation.

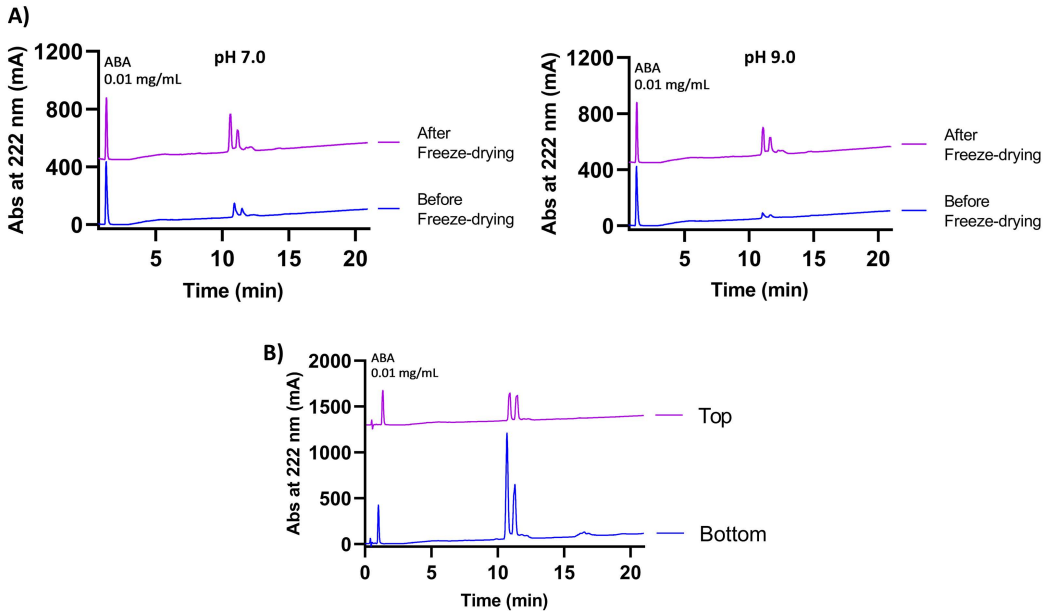

Figure 80. (A) HPLC analysis of a solution of **^{Z}CP3** (200 µM) irradiated at 290-320 nm for 10 minutes at pH 7.0 (10 mM HEPES) or pH 9.0 (10 mM Boric acid 10 mM) before free-drying and after free-drying, followed by re-dissolution. (B) HPLC analysis of a solution of **^{E}CP3** (500 µM) irradiated at 254 nm for 5 minutes at pH 7.0 (10 mM HEPES) and ultracentrifugated for 1 hour (50000 rpm). The upper and lower parts of the sample were separated and analysed independently. HPLC analysis for all the experiments (HPLC conditions: H_2O (0.1% TFA)/MeCN (0.1% TFA), 100:0 → 80:20 (2 min) and 80:20 → 50:50 (19 min)). An aqueous solution of 4-aminobenzoic acid (ABA, 0.01 mg/mL) was added as an internal standard.

6.2.3.3. Self-assembly properties

The self-assembling properties of both isomers were evaluated (Figure 81A), starting with their fluorescence properties. The spectra of **^{E}CP3** in double-distilled water (pH 3-5) showed the characteristic bands of the monomeric pyrene moiety whose emission decreases upon basification (Figure 81B). At pH 6.0, a new band around 475 nm, attributed to the pyrene excimer, started to rise.[260] Subsequent basification did not significantly change the ratio of monomer and excimer emission. Such behaviour can be attributed to the stacking properties of the CP upon deprotonation of the imidazolium rings. At acidic pH, all the imidazole moieties are protonated, preventing the formation of the β-sheet structure because of the repulsion of cationic substituents.

[260] J. Montenegro, C. Vázquez-Vázquez, A. Kalinin, K. E. Geckeler, J. R. Granja, *J. Am. Chem. Soc.* **2014**, *136*, 2484-2491.

Upon neutralization, the formation of hydrogen bonds between peptide backbones facilitates nanotube formation. From this fluorescence experiment, a pKa value of 5.6 was calculated for **^{E}CP3**. In concentration-dependent experiments carried out at neutral pH, the band at 475 nm increased with rising CP concentration, confirming the supramolecular nature of the excimer formation (Figure 81C). Such behaviour was not observed for the *Z*-isomer, whose emission properties did not change with the pH (Figures 81D) or the excimer band was not observed with increasing peptide concentration (Figures 81E).

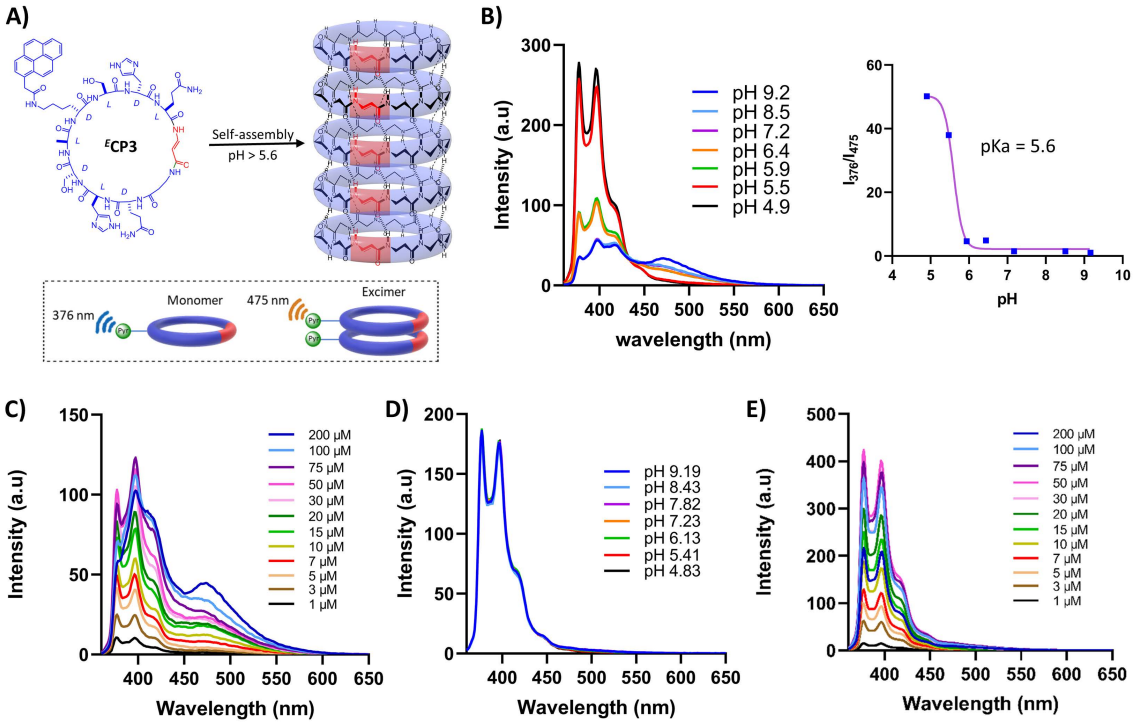

Figure 81. (A) Self-assembly process of **^{E}CP3** and different fluorescence properties of the pyrene monomer and excimer. The amino acid side chains in the nanotube model are omitted for clarity. (B) Fluorescence emission of **^{E}CP3** (100 µM) in water (λ_{exc} = 340 nm, T = 20°C) at different pH by adjusting the media by addition of small aliquots of aqueous NaOH (0.1 M). The data were fitted to obtain a pKa = 5.6. (C) Fluorescence spectra of **^{E}CP3** in HEPES buffer (10 mM, pH 7.0) at different peptide concentrations (λ_{exc} = 340 nm, T = 20°C). (D) Fluorescence spectra of aqueous solutions of **^{Z}CP3** (100 µM) at different pH (λ_{exc} = 340 nm, T = 20°C). The pH was adjusted upon addition of small aliquots of aqueous NaOH (0.1M). (E) Fluorescence spectra of **^{Z}CP3** in HEPES buffer (10 mM, pH 7.0) at different peptide concentrations (λ_{exc} = 340 nm, T = 20°C).

Concentration-dependent experiments in the presence of a β-sheet reporter were also carried out to further confirm that these differences resulted from the opposite assembly properties each CP. To this end, Thioflavin T (ThT), a well-known dye that emits fluorescence upon binding to β-sheet structures, was selected.[231] The experiments were carried out under neutral conditions (10 mM HEPES, pH 7.0, λ_{exc} = 440 nm). Addition of increasing amounts of **^{E}CP3** (1-200 µM) to a solution of ThT (20 µM) gave rise to an evident growth of dye emission that confirms the interaction of the dye with CP assemblies (Figure 82A). From this experiment, we could estimate a critical aggregation concentration (*cac*) at pH 7.0 of around 22 µM. Similar *cac* was obtained at basic pH (9.0) (Figure 82B); although at acidic pH (<4.5), the characteristic

emission band of ThT did not increase. This finding confirms the importance of imidazole protonation/deprotonation in the formation of SCPNs. Under neutral or basic conditions, SCPN formation should bring together the β-sheet reporter (ThT) and the pyrene moieties, consequently fluorescence resonance energy transfer (FRET) between both dyes (pyrene as a donor and ThT as an acceptor) should confirm the spatial proximity between SCPNs and dye.[216] As expected, the FRET effect was only observed for experiments carried out in neutral-alkaline media, which indicated the relation of ThT emission with assembled peptides (λ_{exc} = 340 nm) (Figure 82C). Similar experiments with the *Z*-isomer (**^{Z}CP3**) did not show significant changes in dye emission, confirming the incapability of this isomer to form β-sheet structures (Figure 82D-F).

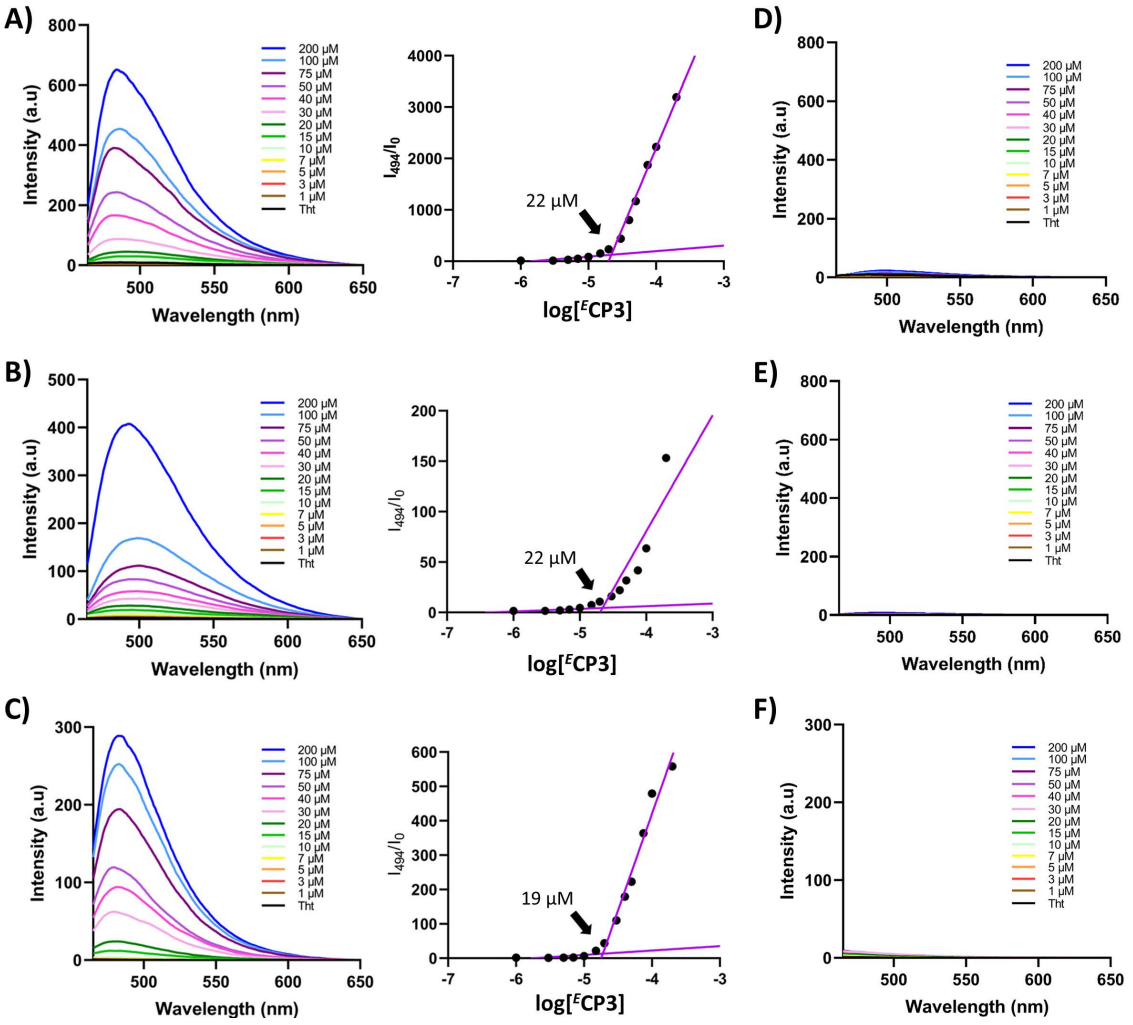

Figure 82. (A) Overlaid ThT (20 µM) fluorescence spectra of solutions of **^{E}CP3** in HEPES (10 mM, pH 7.0) at different concentrations (λ_{exc} = 440 nm) and intensity ratio I_{494}/I_0 versus the logarithm of the concentration of **^{E}CP3** to calculate a *cac* of 22 µM. I_0 is the fluorescence intensity at 494 nm of ThT alone. (B) Overlaid ThT (20 µM) fluorescence spectra of solutions of **^{E}CP3** in Boric acid buffer (10 mM, pH 9.0) at different concentrations (λ_{exc} = 440 nm) and intensity ratio I_{494}/I_0 versus the logarithm of the concentration of **^{E}CP3** to calculate a *cac* of 22 µM. I_0 is the fluorescence intensity at 494 nm of ThT alone. (C) FRET assay of **^{E}CP3** and ThT (20 µM) in HEPES buffer (10 mM, pH 7.0) at different peptide concentrations (λ_{exc} = 340 nm) and intensity ratio I_{494}/I_0 versus the logarithm of the concentration of **^{E}CP3** to calculate a *cac* of 19 µM. (D) ThT (20 µM) assay of **^{Z}CP3** in HEPES buffer (10 mM, pH 7.0) at different peptide concentrations (λ_{exc} = 440 nm). (E) ThT (20 µM) assay of **^{Z}CP3** in Boric acid buffer (10 mM, pH 9.0) at different peptide concentrations (λ_{exc} = 440 nm). (F) FRET assay of **^{Z}CP3** and ThT (20 µM) in HEPES buffer (10 mM, pH 7.0) at different peptide concentrations (λ_{exc} = 340 nm).

To further understand the self-assembly properties of both peptides, circular dichroism (CD) studies were also performed to evaluate the different pH conditions for both isomers (Figure 83). No CD signals corresponding to the pyrene moiety (353 nm) were detected at native pH (4.4) for both peptides at a similar concentration (350 µM). Basification of the solution of **^{Z}CP3** did not induce any change in its CD spectra (Figure 83A). On the contrary, as the pH increases for **^{E}CP3**, a strong CD signal was observed for the pyrene band,[216,261] showing a strong negative band at a pH higher than 5.7 (Figure 83B). This effect suggests transfer of chirality from the peptide backbone to the pyrene unit with the formation of long-range-ordered supramolecular assemblies. These changes take place under similar conditions to the previous fluorescence studies, suggesting that the CD signal must be related to the CP assembly.

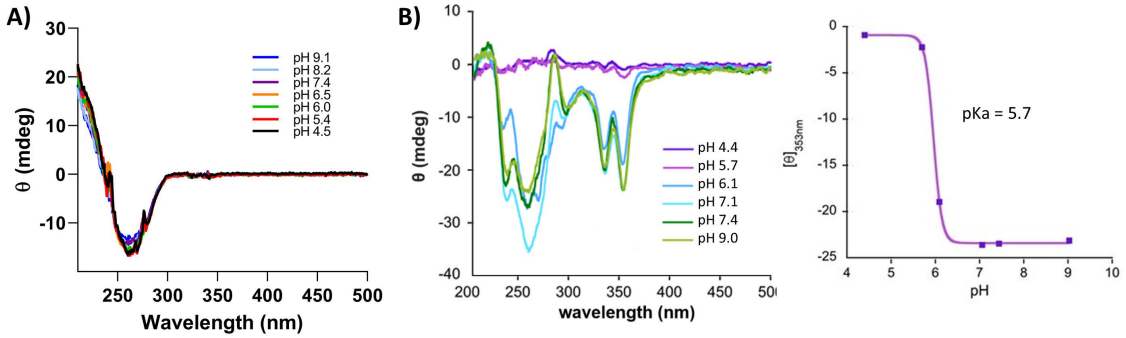

Figure 83. (A) CD spectra of **^{Z}CP3** (350 µM) in water at different pH. The pH was adjusted by adding aqueous NaOH (0.1M). (B) CD spectra of **^{E}CP3** (350 µM) in water at different pH. The pH was adjusted by adding aqueous NaOH (0.1 M). The data were fitted to obtain a pKa = 5.7.

Once the spectroscopic fingerprints highlighting the different assembly properties of both isomers of **CP3** were confirmed, electron microscopy studies were carried out to visualize the structural changes related to the supramolecular properties of these CPs. Scanning transmission electron microscopy (STEM) micrographs confirmed the presence of long linear structures, a few µm long, that can be related to single or bundles of nanotubes of **^{E}CP3** (200 µM) (Figure 84A) over a wide range of pH conditions (pH 5.0-9.0). This outcome confirms the ability of this isomer to stack forming nanotubes especially under neutral or slightly basic conditions. As expected, the length and thickness of these linear supramolecular structures are correlated with CP concentration, as longer and thicker fibres were detected at higher concentrations. Nanotube dissociation can be accomplished by acidification (pH 2.0) without affecting the peptide structure. The assembly and disassembly process can be induced by changing the pH for several cycles without affecting the peptide stability (Figure 84B). In contrast, none of the solutions of **^{Z}CP3** showed these types of structures, as amorphous aggregates were found (Figure 84C).

USC UNIVERSIDADE DE COMPOSTELA

[216] A. Méndez-Ardoy, A. Bayón-Fernández, Z. Yu, C. Abell, J. R. Granja, J. Montenegro, *Angew. Chem. Int. Ed.* **2020**, *59*, 6902-6908.
[261] T. Nishikawa, N. Tajima, M. Kitamatsu, M. Fujiki, Y. Imai, *Org. Biomol. Chem.* **2015**, *13*, 11426-11431.

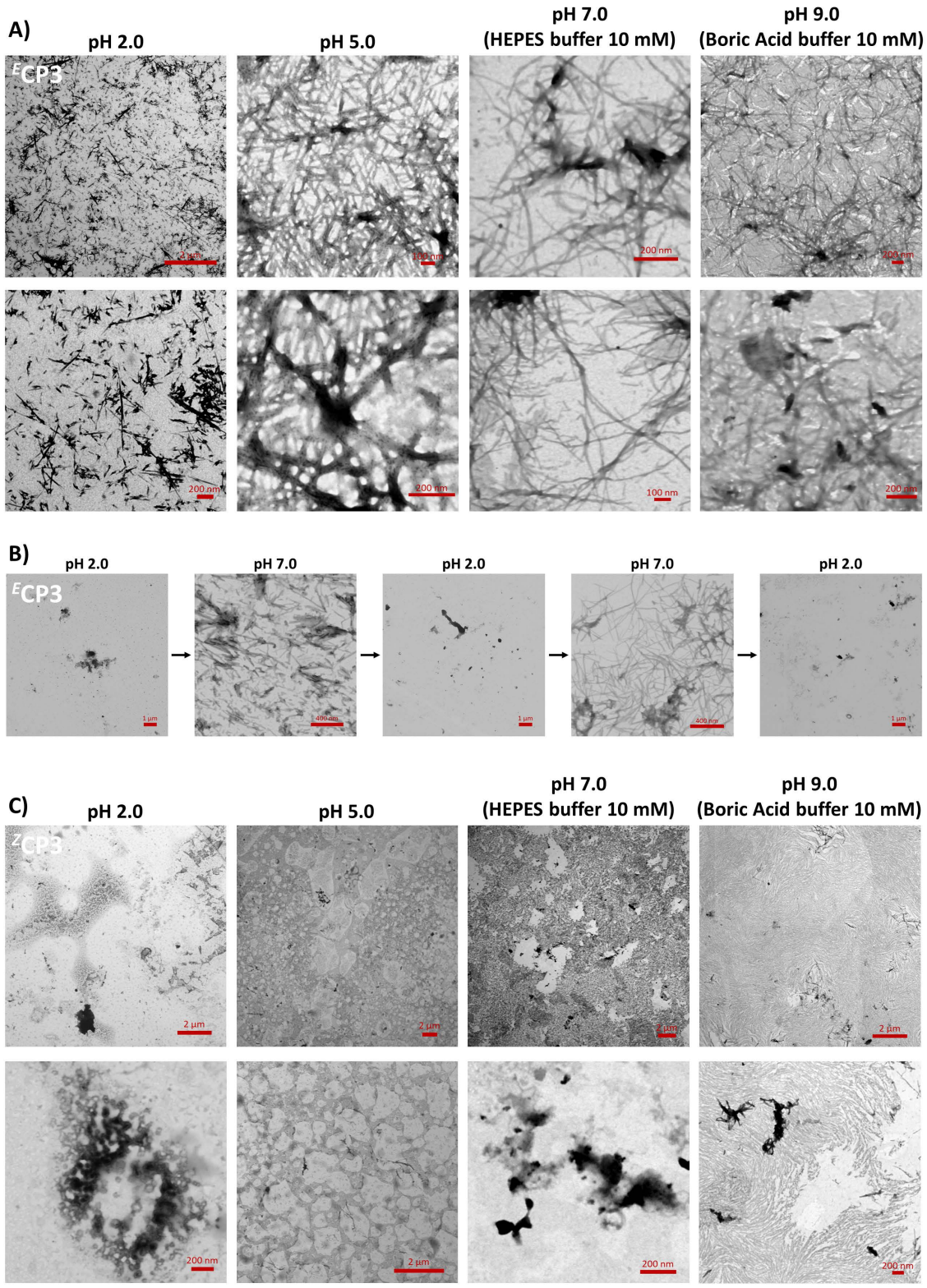

Figure 84. (A) STEM micrographs achieved by deposition of **^{E}CP3** solutions (200 µM) at different pH. (B) STEM micrographs of assembly/disassembly cycles of **^{E}CP3** (200 µM) controlled by pH. The pH was adjusted with aqueous solutions of NaOH (0.1 M) or HCl (0.1 M). (C) STEM micrographs achieved by deposition of **^{Z}CP3** solutions (200 µM) at different pH. Staining in all the images was obtained with 2% w/v phosphotungstic acid (PTA).

USC UNIVERSIDADE DE SANTIAGO DE COMPOSTELA

The SCPN diameter was assessed by atomic force microscopy (AFM) (Figure 85A). The micrographs obtained after drop casting a 200 µM solution at neutral pH of **^{E}CP3** on mica show the presence of polydisperse nanotubes in length that are randomly oriented on the mica surface. The height of individual nanotubes was on the order of 2.95 ± 0.32 nm, which corresponds to the expected for this type of SCPNs. As expected, no tubular structures were found for **^{Z}CP3**. Next, we employed epifluorescence microscopy to study the self-assembly process at the micrometre scale. Analysis of samples containing **^{E}CP3** (350 µM, 10 mM HEPES, pH 7.0) (Figure 85B) showed the hierarchical architecture preserved from the nanotubes to tens of micrometres long fibres. On the other hand, no clear fibrillar structures were observed in samples of **^{Z}CP3** with emissions at shorter wavelengths all over the solution.

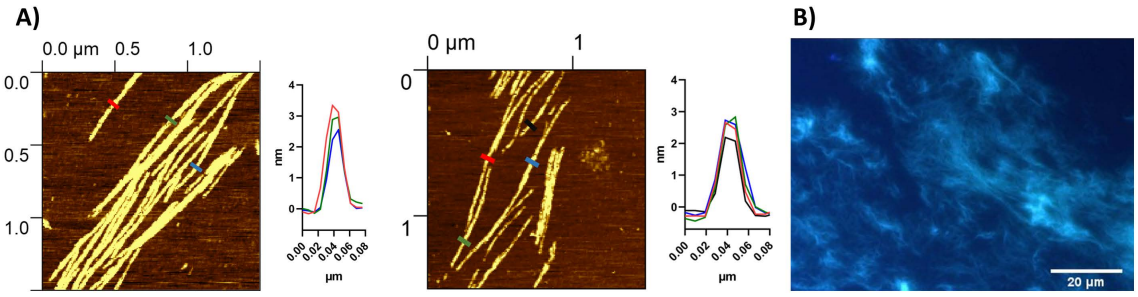

Figure 85. (A) AFM micrographs of **^{E}CP3** (200 µM) in HEPES buffer (10 mM, pH 7.0) on mica surface. The height profiles were achieved along the corresponding colour lines shown in the image. (B) Representative epifluorescence image of SCPNs deposited on a standard glass microscopy slide from a solution of **^{E}CP3** (350 µM) in HEPES (10 mM, pH 7.0).

6.2.3.4. Light-induced assembly/disassembly

To determine if the light-induced isomerization is capable of triggering nanotube disassembly, we performed further irradiation studies on already assembled CPs at neutral pH (Figure 86A). For this purpose, a solution of **^{E}CP3** (200 µM) in HEPES buffer (10 mM, pH 7.0) was irradiated at 254 nm, and aliquots of reaction (400 µL) were taken every minute. These aliquots were mixed with a ThT (40 µM) solution under the same conditions (400 µL, 10 mM HEPES, pH 7.0), and the resulting samples (100 µM irradiated **CP3** and 20 µM ThT) were analysed by fluorescence (Figure 86B). At the initial conditions above the *cac*, most of the **^{E}CP3** should be assembled forming SCPNs, and therefore, the interaction of ThT with the β-sheet structure of SCPN should give rise to its characteristic emission. However, if amino acid isomerization induces CP folding, the ThT emission should change over time. Indeed, immediately after the first irradiation period, the characteristic band derived from the presence of the β-sheet structure starts to shrink. In addition, irradiated samples were taken, deposited on carbon-coated grids, and evaluated by STEM (Figure 86C). Clearly, after 6 min, the STEM micrographs showed amorphous material together with few short persistence SCPNs. These outcomes confirm that isomerization of amino acid double bond can occur in the tubular structure, inducing SCPN disassembly. Likewise, **^{Z}CP3** isomerization under similar conditions (200 µM, 10 mM HEPES, pH 7.0) was also investigated (290-320 nm) and analysed by

fluorescence spectroscopy in a similar manner. In this case, the characteristic emission (494 nm) derived from CP planarization and nanotube formation was growing up (Figure 86D). Moreover, nanotube formation after 2 min of irradiation was corroborated by STEM analysis (Figure 86E). These experiments confirm that either assembly or disassembly of SCPNs can be triggered by light-induced isomerization of one single residue in a CP forming nanotubes. No restrictions on the olefin isomerization were found even if the CP is already assembled.

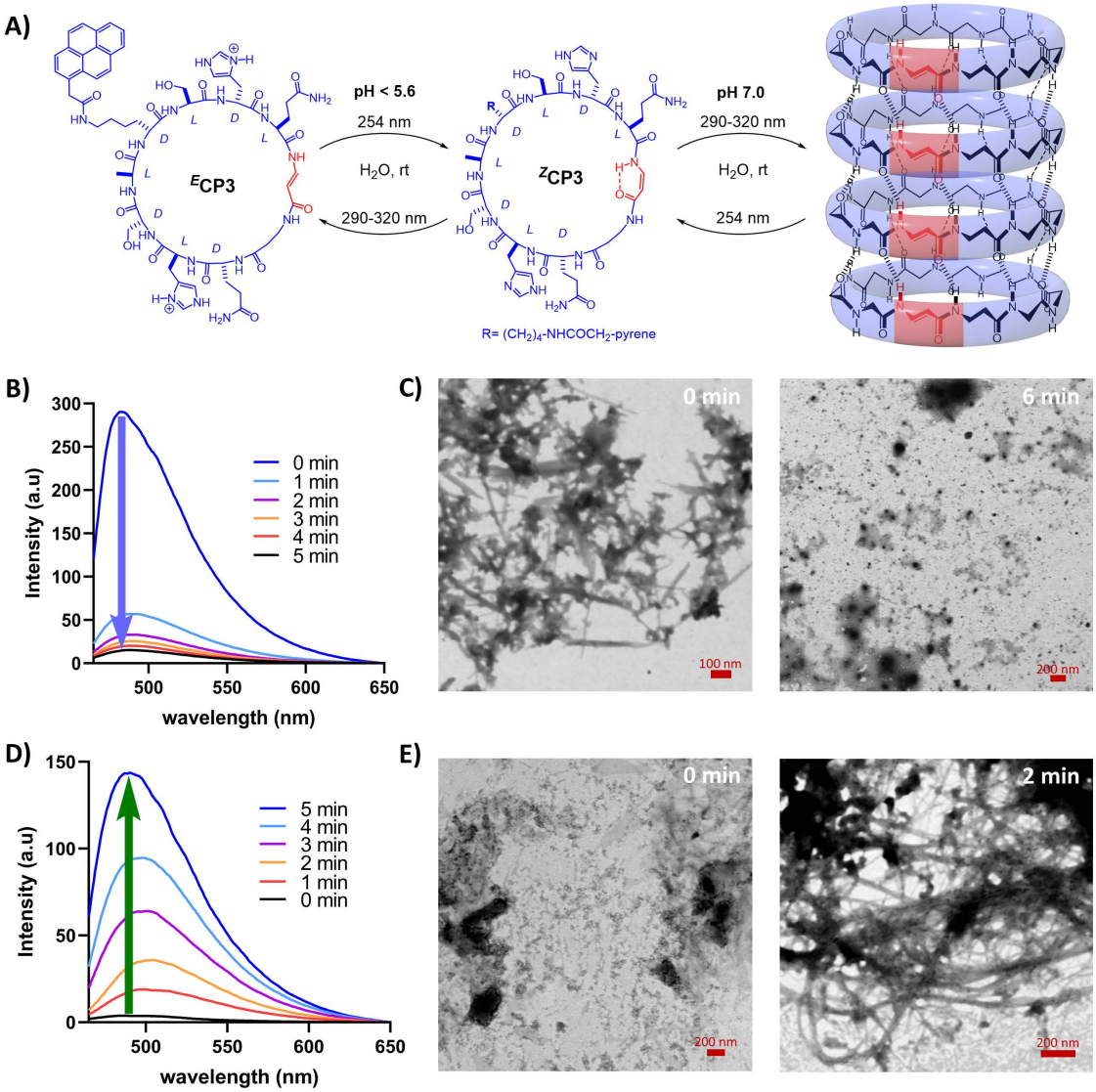

Figure 86. (A) Illustration of the photo-modulated assembly/disassembly process of peptide nanotubes at different pH. The amino acid side chains in the nanotube model are omitted for clarity. (B) Fluorescence analysis (overlaid of ThT [20 µM] fluorescence emission band) of nanotube dissociation of an irradiated solution of **^{E}CP3** (100 µM) with a 254 nm wavelength lamp at pH 7.0 (10 mM HEPES). 400 µL aliquots of CP at 200 µM were taken every minute, mixed with a 40 µM ThT solution (400 µL in 10 mM HEPES, pH 7.0), and then analysed in the fluorimeter. (C) STEM micrographs achieved by deposition of **^{E}CP3** solutions (25 µM) in HEPES buffer (10 mM, pH 7.0) after 0 and 6 minutes of irradiation at 254 nm. Staining was obtained with 2% w/v phosphotungstic acid (PTA). (D) Fluorescence analysis (overlaid of ThT [20 µM] fluorescence emission band) of **^{Z}CP3** (100 µM) irradiated with a 290-320 nm wavelength lamp at pH 7.0 (10 mM HEPES). 400 µL aliquots of CP at 200 µM were taken every minute, mixed with a 40 µM ThT solution (400 µL in 10 mM HEPES, pH 7.0) and then analysed in the fluorimeter. (E) STEM micrographs achieved by deposition of **^{Z}CP3** solutions (200 µM) in HEPES buffer (10 mM, pH 7.0) after 0 and 2 minutes of irradiation at 290-320 nm. Staining was obtained with 2% w/v phosphotungstic acid (PTA).

6.2.3.5. Assembling behaviour in confined spaces

To further understand the process, we decided to evaluate the implications of externally induced isomerization to trigger the supramolecular polymerization in confined spaces using microfluidics techniques.[215,216] Additionally, we could also evaluate the combination of changes in pH or ionic strength with light input on the assembly process. We hypothesized that assembly changes could be monitored by following the different fluorescence properties of the pyrene moiety depending on the assembly state of the CPs. The microfluidic device shown in Figure 87 was employed to control the tandem assembly and droplet confinement of **CP3**. First, we induced peptide assembly in junction J_1 by merging the streams of I_{CP}, containing a slightly acidic aqueous solution of **CP3** (1.0 mM, pH~3.0), and I_T, which contains a second solution responsible for inducing the assembly under the corresponding changes in media conditions. These changes, such as neutralization or increase of ionic strength, should trigger the assembly process. Next, droplet formation was immediately achieved in the J_2 junction by merging the aqueous stream with the oil stream (HFE 7500 3M Novec and 0.5% v/v Pico-Surf as a surfactant, I_{oil}).[262] This setup was employed to adjust the flow rates and the different stimuli.

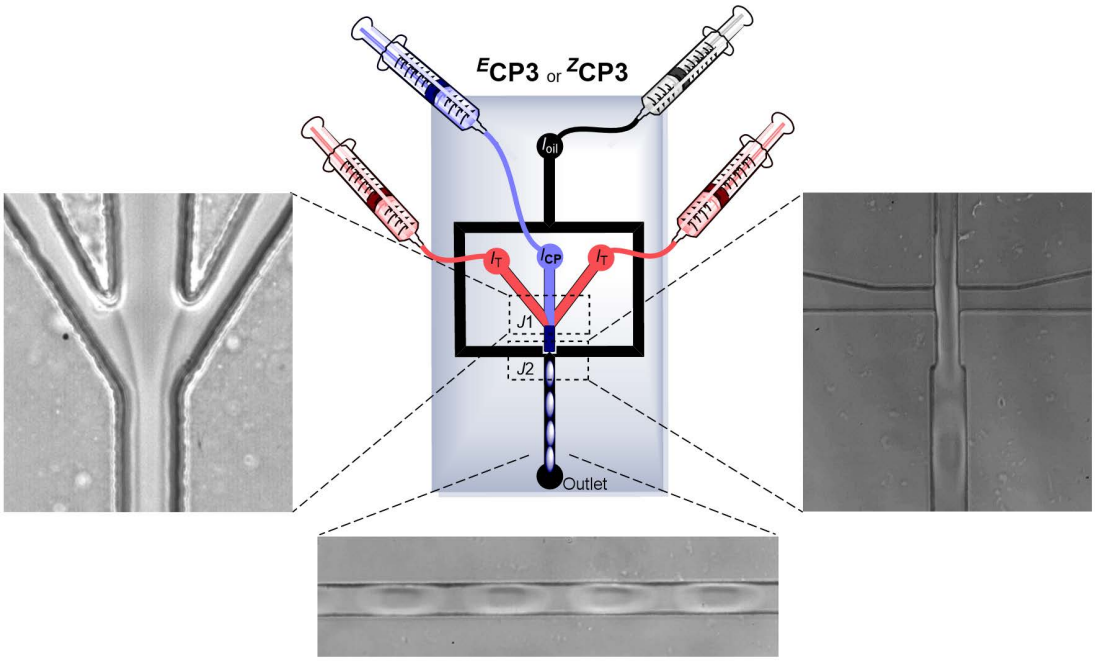

Figure 87. Microfluidic device for *in situ* nanotube formation. Channels dimensions: 35 x 50 µm. CPs (**^{Z}CP3** or **^{E}CP3**) in aqueous media (1.0 mM, milliQ water, pH 2-3) were injected in inlet I_{CP} (blue) at flow rate of 300 µL h^{-1} and assembled upon mixing at J_1 with inlets I_T (red) containing aqueous HEPES (20 mM, pH 7.0) or $CaCl_2$ (1.0 M) at flow rate of 150 µL h^{-1}. The aqueous stream converges in J_2 with the oil phase at inlet I_{oil} (HFE 7500 3M Novec with 0.5% v/v Pico-Surf as surfactant, black) at a flow rate of 500 µL h^{-1} for droplet generation. Droplets are collected in the outlet.

[215] A. Méndez-Ardoy, J. R. Granja, J. Montenegro, *Nanoscale Horiz.* **2018**, *3*, 391-396.
[216] A. Méndez-Ardoy, A. Bayón-Fernández, Z. Yu, C. Abell, J. R. Granja, J. Montenegro, *Angew. Chem. Int. Ed.* **2020**, *59*, 6902-6908.
[262] C. Holtze, A. C. Rowat, J. J. Agresti, J. B. Hutchison, F. E. Angilè, C. H. Schmitz, S. Köster, H. Duan, K. J. Humphry, R. A. Scanga, J. S. Johnson, D. Pisignano, D. A. Weitz, *Lab Chip* **2008**, *8*, 1632-1639.

Initial studies were carried out by merging in J_1 a neutral buffered solution (20 mM HEPES, pH 7.0, I_T) with an aqueous solution of **^{Z}CP3** (1.0 mM, I_{CP}). As expected, the fluorescence microscopy analysis of the resulting droplets showed the typical self-quenched blue fluorescence emission characteristic of highly concentrated monomeric pyrene moieties that belong to dispersed CPs (Figure 88A). For the other isomer (**^{E}CP3**), an acidic aqueous solution (pH 3.0) also provided droplets with the typical quenched emission of monomeric species (Figure 88B). On the other hand, under neutral conditions, obtained by mixing in J_1 the neutral buffered solution (20 mM HEPES, I_T) with the aqueous solution of **^{E}CP3** (1.0 mM, I_{CP}), brighter blue-fluorescent droplets were obtained (Figures 88C) with fibril-like structures preferentially located in contact with the periphery of the droplets (Figure 88D).

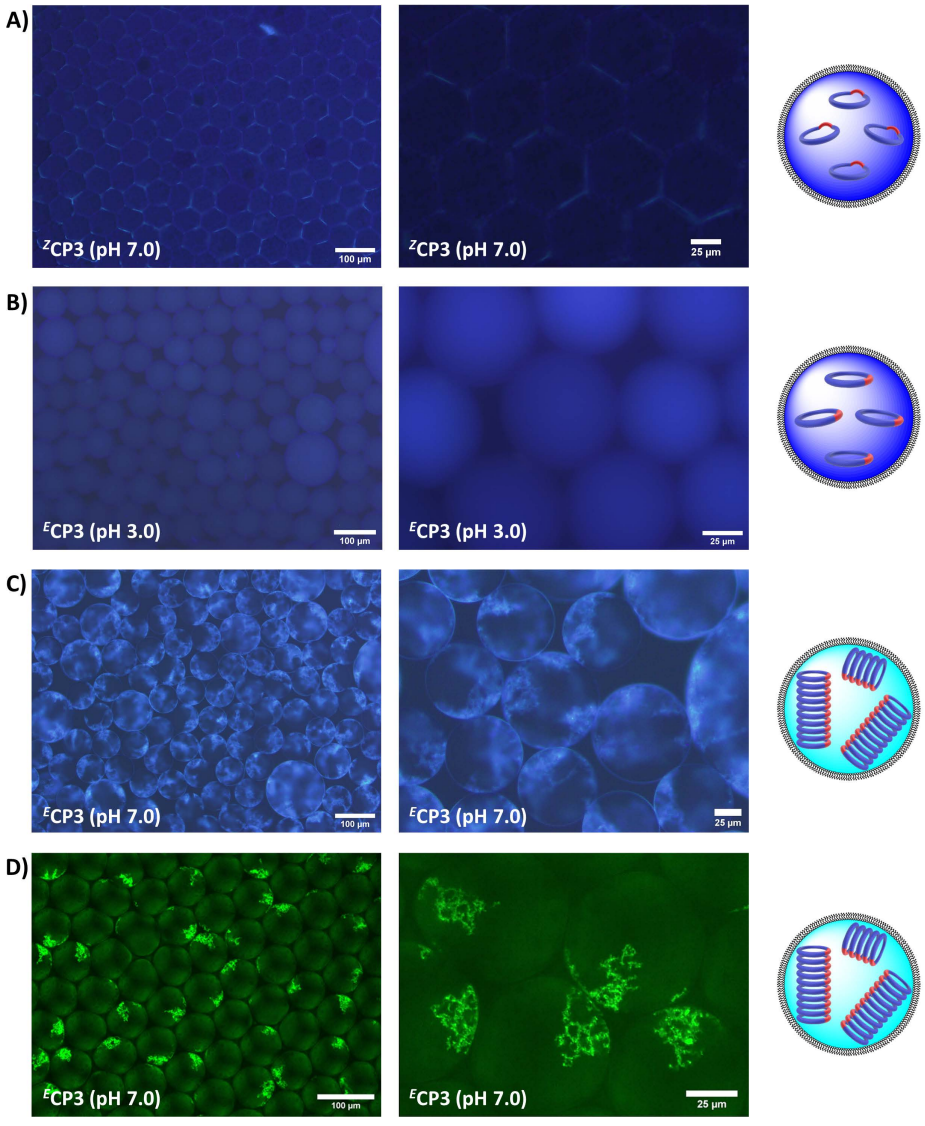

Figure 88. (A) Epifluorescence images of microfluidic droplets (water-in-oil) of **^{Z}CP3** at pH 7.0. I_{CP} is an aqueous solution of **^{Z}CP3** (1.0 mM) and I_T is HEPES (20 mM, pH 7.0). (B) Epifluorescence images of microfluidic droplets (water-in-oil) of **^{E}CP3** at pH 3.0. I_{CP} is an aqueous solution of **^{E}CP3** (1.0 mM) at pH 3.0 and I_T is water. (C) Epifluorescence images of microfluidic droplets (water-in-oil) of **^{E}CP3** at pH 7.0. I_{CP} is an aqueous solution of **^{E}CP3** (1.0 mM) and I_T is HEPES (20 mM, pH 7.0). (D) Confocal planes of microfluidic droplets (water-in-oil) of **^{E}CP3** with ThT at pH 7.0. I_{CP} is an aqueous solution of **^{E}CP3** (1.0 mM) and I_T is aqueous HEPES (20 mM, pH 7.0) containing ThT (40 µM). Flow rates of all experiments: I_{oil} = 500 µL h^{-1}; I_{CP} = 300 µL h^{-1}; I_T = 150 µL h^{-1}.

To our surprise, under the neutral conditions, the droplets containing **^{E}CP3** had different sizes (Figure 88C). Such behaviour could be related to the presence of the SCPNs at the interface and not to the preparation method.[263] Considering the possible fusion of droplets induced by the nanotubes at the vesicle interface, we carried out additional experiments to further understand this process. Therefore, the formation and storage of the vesicles were followed at the microscope (Figure 89). Initially, all the droplets, after leaving the microfluidic tubing, had the same diameter. However, after resting for a few seconds, the fusion of neighbouring vesicles starts to take place all over the media, confirming the fusogenic properties dictated by the nanotubes.

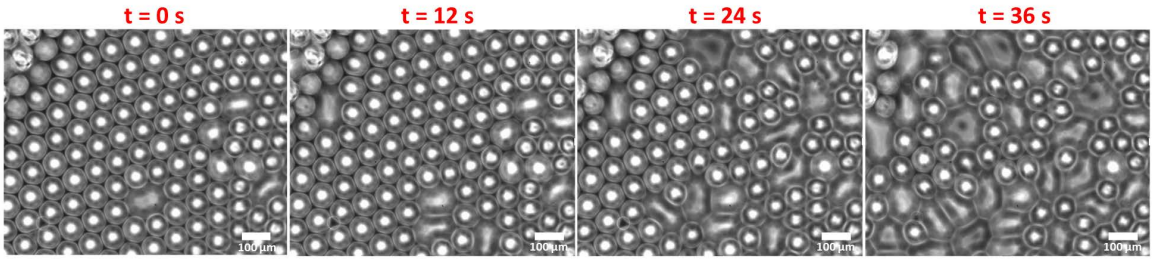

Figure 89. Microscope images at different times after leaving the microfluidic device (0, 12, 24, and 36 s) of droplets containing **^{E}CP3** prepared at neutral pH, showing the vesicles fusogenic properties induced by SCPNs generated at the interface. I_{CP} is an aqueous solution of **^{E}CP3** (1.0 mM) and I_T is HEPES (20 mM, pH 7.0). Flow rates: I_{oil} = 500 µL h^{-1}; I_{CP} = 300 µL h^{-1}; I_T = 150 µL h^{-1}.

To understand these fusion properties, droplets containing either of the two isomers of **CP3** were mixed to evaluate the invasive (parasitic) or self-invasive (narcissistic) properties of the resulting vesicles (Figures 90). To follow the merging process, coloured vesicles containing **^{Z}CP3** (1.0 mM, I_{CP}) were prepared by merging I_{CP} with an aqueous HEPES solution (20 mM, pH 7.0, I_T) containing 5-TAMRA (40 µM). Then, **^{E}CP3** droplets were collected over the **^{Z}CP3** droplets containing 5-TAMRA in a 1:1 ratio. Droplets containing opposite isomers showed no tendency to fuse with each other, while vesicles that contain **^{E}CP3** maintained their self-fusogenic properties. Therefore, it seems that this merging function requires the establishment of an intercommunication between the assembled nanotubes that are deposited at both interfaces of the neighbouring droplets to dictate their fusion.

USC UNIVERSIDADE DE SANTIAGO DE COMPOSTELA

[263] a) R. M. Epand, *Biochim. Biophys. Acta* **2003**, *1614*, 116-121; b) A. B. Theberge, F. Courtois, Y. Schaerli, M. Fischlechner, C. Abell, F. Hollfelder, W. T. S. Huck, *Angew. Chem. Int. Ed.* **2010**, *49*, 5846-5868.

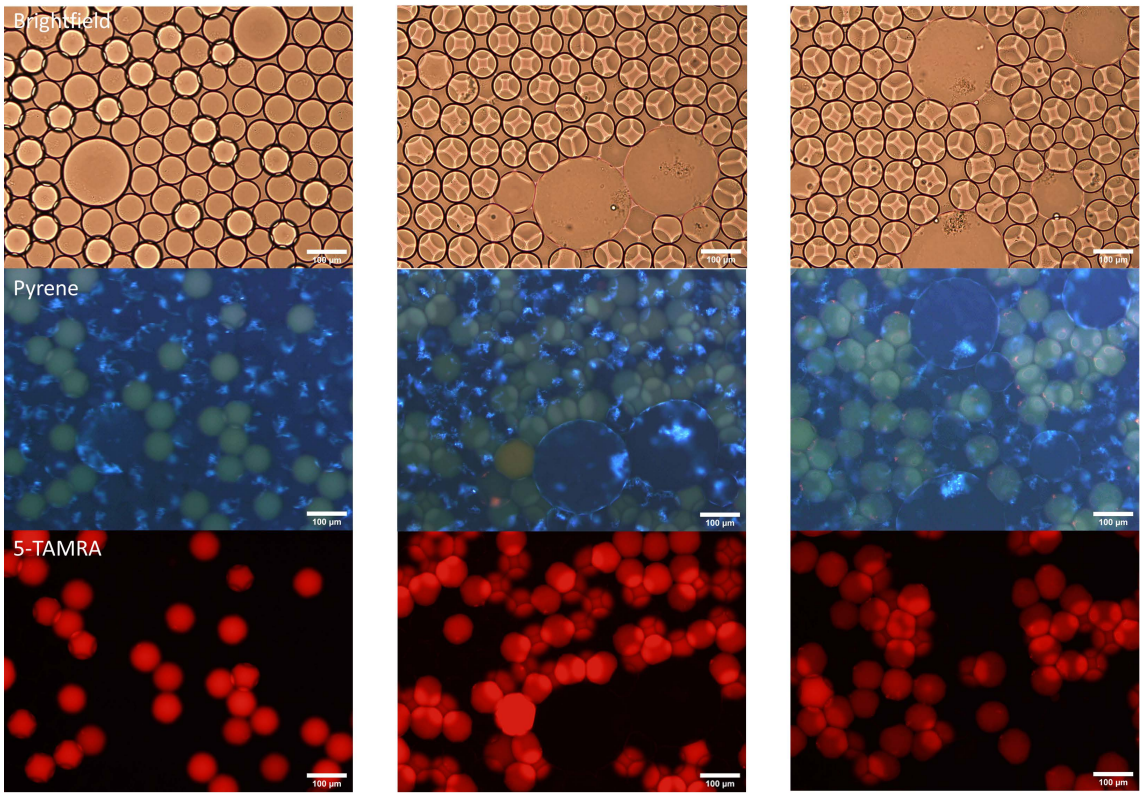

Figure 90. Microfluidic droplets (water-in-oil) of **^{Z}CP3** (red) and **^{E}CP3** (blue) at neutral pH mixed in a 1:1 ratio. For **^{Z}CP3**, I_{CP} is an aqueous peptide solution at 1.0 mM and I_T is a solution of HEPES (20 mM, pH 7.0) containing 5-TAMRA (40 µM). For **^{E}CP3**, I_{CP} is an aqueous peptide solution at 1.0 mM and I_T is a solution of HEPES (20 mM, pH 7.0). Flow rates: I_{oil} = 500 µL h^{-1}; I_{CP} = 300 µL h^{-1}; I_T = 150 µL h^{-1}.

To further understand the mechanism of nanotube-induced droplet fusion, the peptide with an alkyl chain of six carbons (**^{Z}CP4**/**^{E}CP4**) was also studied to evaluate the role of the pyrene moiety in this process. This peptide showed reduced self-assembly properties (Figure 91A-D) compared with **^{E}CP3**, forming nanotubes at higher concentrations, together with a lower propensity to form fibres as indicated by STEM images (Figures 91C-D). Peptide **^{E}CP4** did not show fusogenic properties (Figure 91E-F), despite the microfluidic experiments being carried out at higher concentration (1.5 mM, I_{CP}). This suggests that the π,π-stacking of pyrene moieties not only plays a relevant role in the hierarchical formation of the supramolecular fibres, but also in the induction of droplet fusion.

USC UNIVERSIDADE DE SANTIAGO DE COMPOSTELA

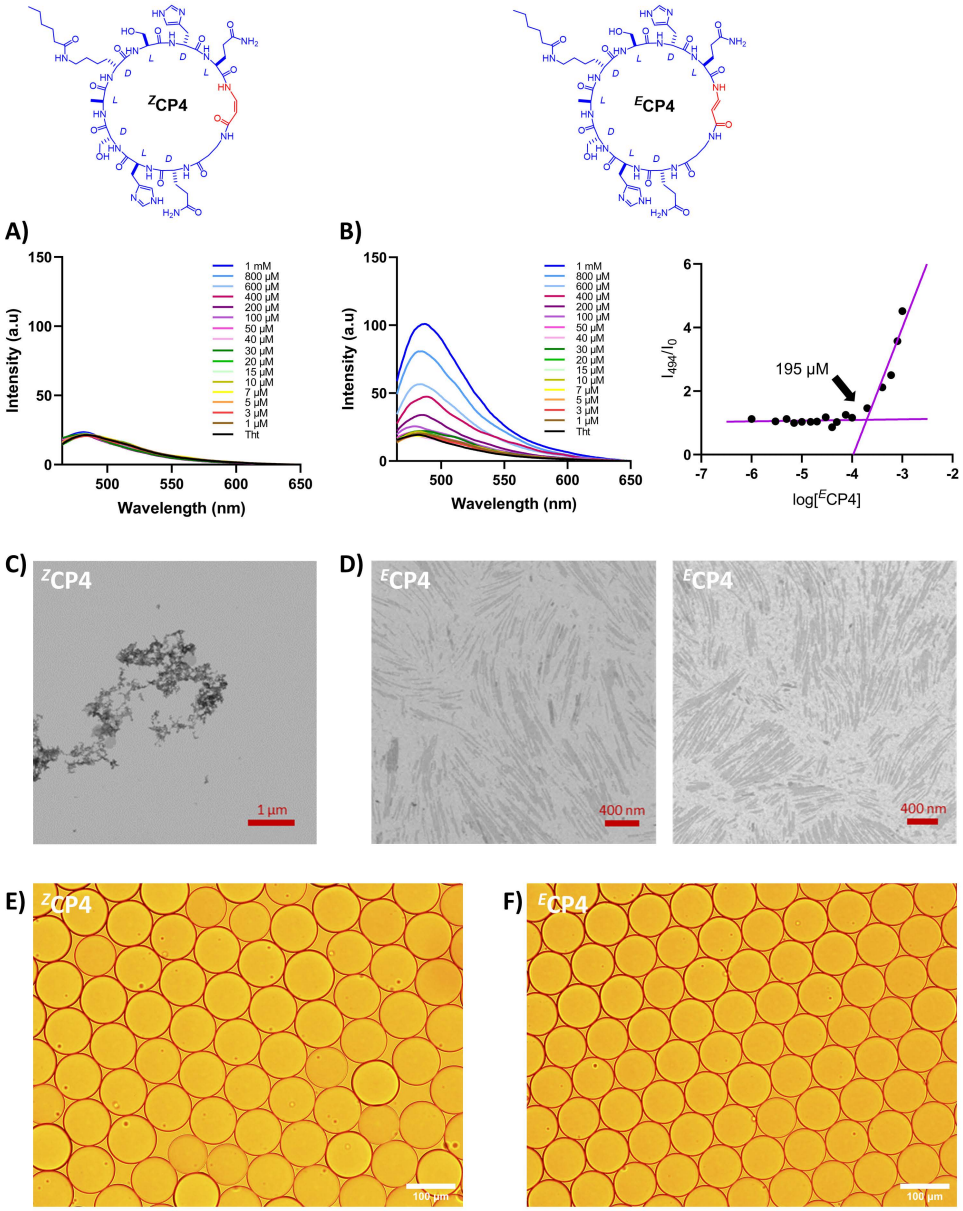

Figure 91. (A) ThT (20 µM) assay in HEPES buffer (10 mM, pH 7.0) of **^{Z}CP4** at different peptide concentrations (λ_{exc} = 440 nm). (B) ThT (20 µM) assay in HEPES buffer (10 mM, pH 7.0) of **^{E}CP4** at different peptide concentrations (λ_{exc} = 440 nm) and intensity ratio I_{494}/I_0 versus the logarithm of the concentration of **^{E}CP4** to calculate a *cac* of 195 µM. I_0 is the fluorescence intensity at 494 nm of ThT alone. (C) STEM micrographs achieved by deposition of a **^{Z}CP4** solution (500 µM) in HEPES buffer (10 mM, pH 7.0). (D) STEM micrographs achieved by deposition of a **^{E}CP4** solution (500 µM) in HEPES buffer (10 mM, pH 7.0). (E) Brightfield of microfluidic droplets (water-in-oil) of **^{Z}CP4** at pH 7.0. I_{CP} is an aqueous solution of **^{Z}CP4** (1.5 mM) and I_T is aqueous HEPES (20 mM, pH 7.0). (F) Brightfield of microfluidic droplets (water-in-oil) of **^{E}CP4** at pH 7.0. I_{CP} is an aqueous solution of **^{E}CP4** (1.5 mM) and I_T is aqueous HEPES (20 mM, pH 7.0). Flow rates of all experiments: I_{oil} = 500 µL h^{-1}; I_{CP} = 300 µL h^{-1}; I_T = 150 µL h^{-1}.

Most likely, under neutral conditions, nanotube assembly in the droplet might induce the formation of a hydrophobic surface that would interact with the droplet interface, exposing the pyrene moieties to the oil media. The contact of two neighbouring droplet interfaces might induce, in the case of **^{E}CP3**, the aggregation of the pyrene moieties, guided by the π,π-stacking,[215,216,217] resulting in vesicle fusion (Figure 92).

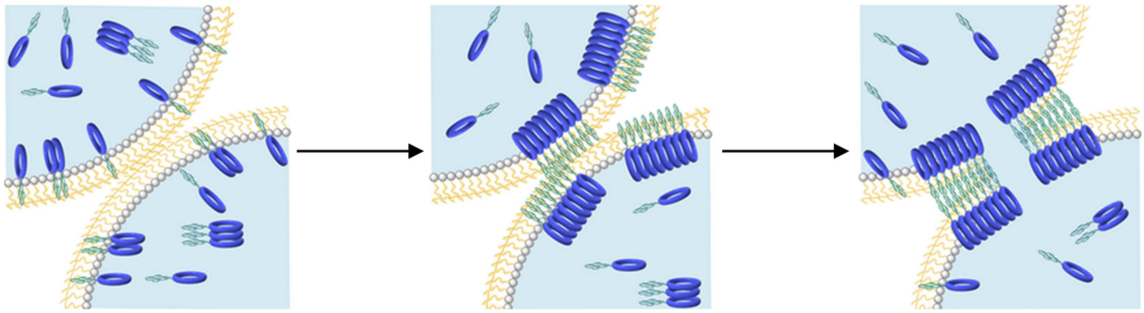

Figure 92. Proposed model of droplet fusion based on the hierarchical process of SCPNs at the interfaces.

The SCPN formation was also evaluated by increasing the ionic strength of the media (Figure 93A-C).[216] Therefore, a $CaCl_2$ (1.0 M, I_T) solution was merged in J_1 with the acidic solution of **^{E}CP3** on I_{CP}. Under these conditions, vesicles with fibre-like structures were also observed, confirming that self-assembly can also be triggered by modulation of the ionic strength of the media (Figure 93D). In this case, the supramolecular fibres seem to be distributed throughout the water droplet internal volume, as already reported with a different peptide,[216] and the resulting droplets presented reduced fusogenic properties, most likely due to the different properties of the resulting nanotubes.

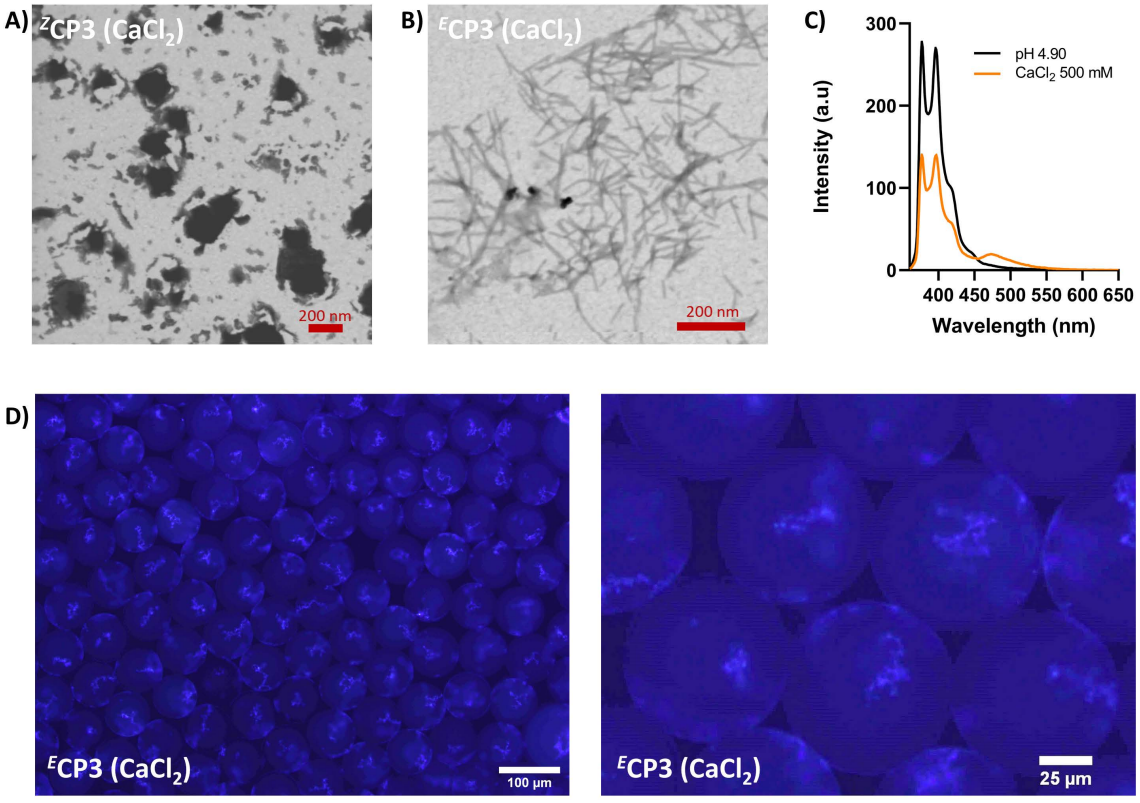

Figure 93. (A) STEM micrograph of **^{Z}CP3** at 200 µM in a solution of $CaCl_2$ (500 mM). (B) STEM micrograph of **^{E}CP3** at 200 µM in a solution of $CaCl_2$ (500 mM). (C) Fluorescence emission of **^{E}CP3** (100 µM) at acidic conditions or in a solution of $CaCl_2$ (500 mM) (λ_{exc} = 340 nm). (D) Self-assembly of **^{E}CP3** in microfluidic droplets (water-in-oil) when I_{CP} is an aqueous peptide solution (1.0 mM) and I_T is an aqueous solution of $CaCl_2$ (1.0 M). Flow rates: I_{oil} = 500 µL h^{-1}; I_{CP} = 300 µL h^{-1}; I_T = 150 µL h^{-1}.

The light-induced assembly inside of the droplet was also assessed. To this end, vesicles were prepared by merging at J_1 an aqueous solution of **^{Z}CP3** (1.0 mM, I_{CP}) with the HEPES solution (20 mM, pH 7.0, I_T). The resulting droplets were stored and analysed by epifluorescence microscopy. The vesicles showed the typical quenched blue fluorescence emission previously mentioned. These vesicles were irradiated using a 290-320 nm lamp for 5 min. After 2 min, clear emissions with fibrillar shape structures were observed at the droplet (Figure 94A), confirming the isomerization-triggered assembly of the CP in the confined environment. The resulting vesicles were lysed by adding a TFA aqueous solution (0.1% v/v) and sonicated for 30 seconds. The supernatant of the resulting aqueous solution was analysed by HPLC showing a similar photostationary state with a 7:3 ratio between **^{E}CP3**:**^{Z}CP3** as found in solution (Figure 94B).

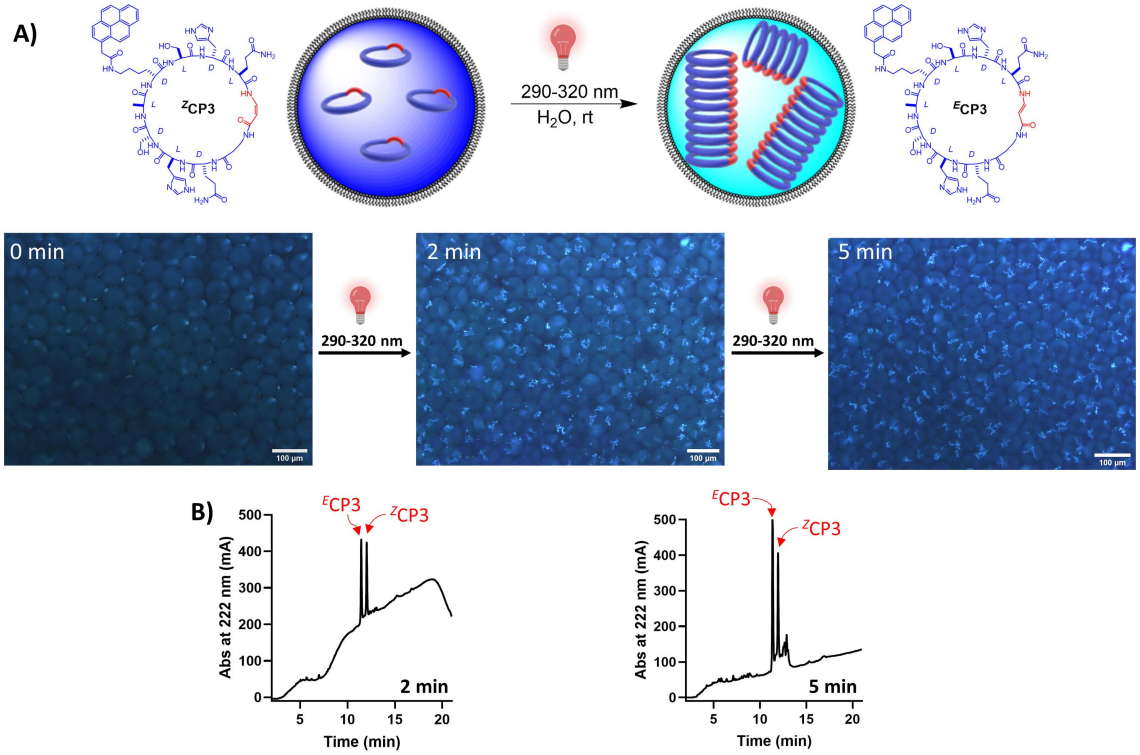

Figure 94. (A) Microfluidic droplets (water-in-oil) of **^{Z}CP3** irradiated at pH 7.0 for 0, 2 or 5 min with a 290-320 nm lamp in which bright fibre-like structures are observed. (B) HPLC analysis of the aqueous interior of droplets containing **^{Z}CP3** irradiated at pH 7.0 for 2 or 5 min with a 290-320 nm lamp. Droplets were lysed prior to analysis. HPLC conditions: H_2O (0.1% TFA)/MeCN (0.1% TFA), 100:0 → 80:20 (2 min) and 80:20 → 50:50 (19 min). For the droplet preparation in all these experiments, I_{CP} is an aqueous **^{Z}CP3** solution (1.0 mM) and I_T is an aqueous solution of HEPES (20 mM, pH 7.0). Flow rates: I_{oil} = 500 µL h^{-1}; I_{CP} = 300 µL h^{-1}; I_T = 150 µL h^{-1}.

6.2.3.6. Cyclic peptide modification

In order to increase the water solubility of the cyclic peptide at high concentrations, a derivative of **CP3** was also studied in which a glutamine residue was replaced by a lysine. Therefore, **CP5** was synthesized following the previously described protocol and the light-induced isomerization was evaluated (Figure 95A). In particular, the isomerization from the *Z* to *E*-isomer process by irradiation at 290-320 nm to obtain again a 7:3 mixture of the two isomers (Figure 95B), while the reverse process is again achieved in almost a 1:1 ratio by irradiation at 254 nm (Figure 95C).

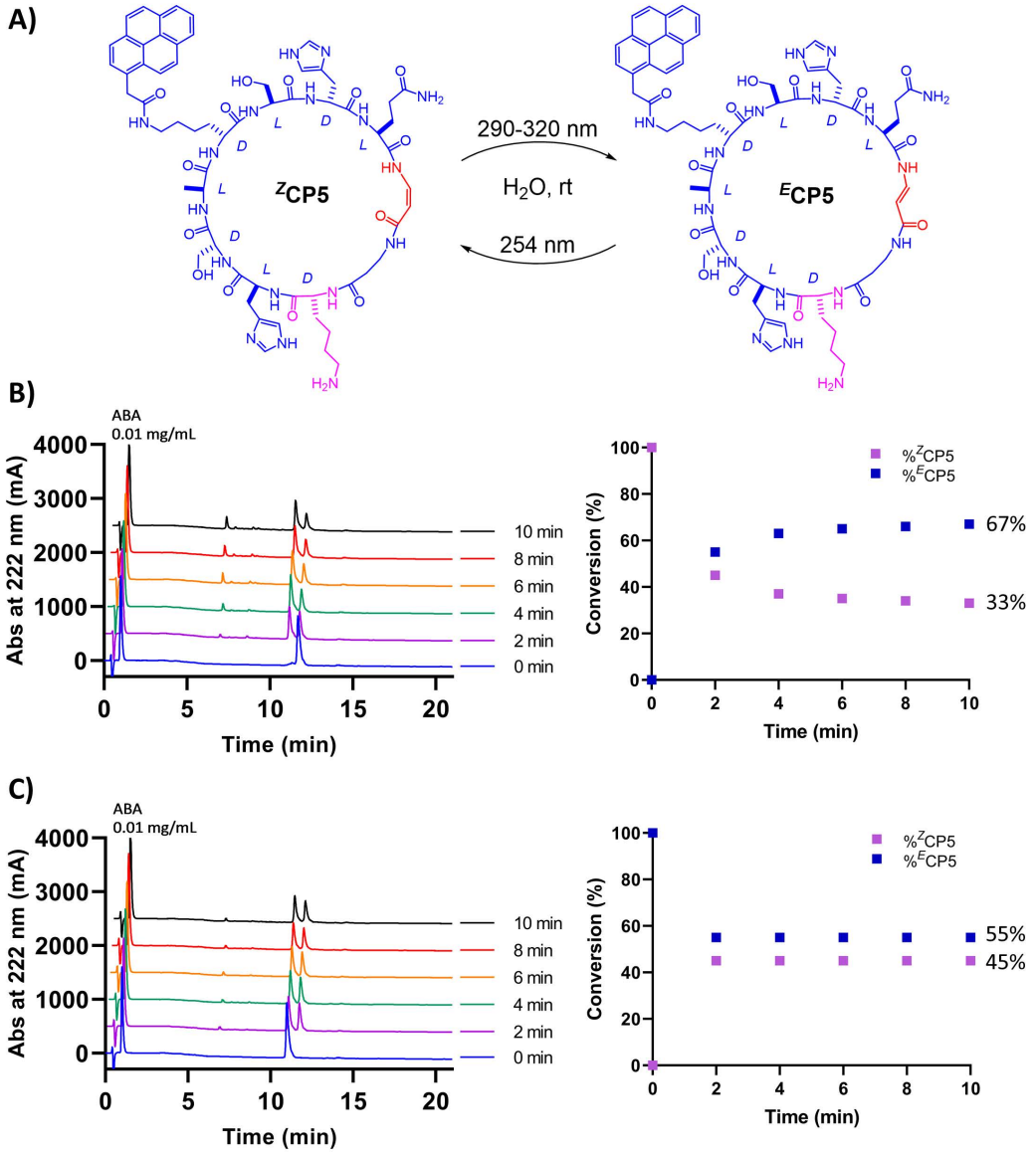

Figure 95. (A) Illustration of the light-induced isomerization between **^{Z}CP5** and **^{E}CP5**. (B) Photoisomerization of **^{Z}CP5**. HPLC analysis (HPLC conditions: H_2O (0.1% TFA)/MeCN (0.1% TFA), 100:0 → 80:20 (2 min) and 80:20 → 50:50 (19 min)) and photoisomerization conversion of a solution of **^{Z}CP5** (200 µM) irradiated at 290-320 nm at pH 5.1. An aqueous solution of 4-aminobenzoic acid (ABA, 0.01 mg/mL) was added as an internal standard. (C) Photoisomerization of **^{E}CP5**. HPLC analysis (HPLC conditions: H_2O (0.1% TFA)/MeCN (0.1% TFA), 100:0 → 80:20 (2 min) and 80:20 → 50:50 (19 min)) and photoisomerization conversion of a solution of **^{E}CP5** (200 µM) irradiated at 254 nm at pH 4.6. An aqueous solution of 4-aminobenzoic acid (ABA, 0.01 mg/mL) was added as an internal standard.

The NMR of **^{Z}CP5** suggests again a folded conformation for this isomer based on the chemical shift (10.55 ppm) of the amide proton of Δ^{Z}βAla due to the formation of the intramolecular hydrogen bond (Figure 96A). In contrast, this signal presents an up-field shift (9.74 ppm) in the NMR of **^{E}CP5** suggesting that this hydrogen bond is not formed in this isomer (Figure 96B).

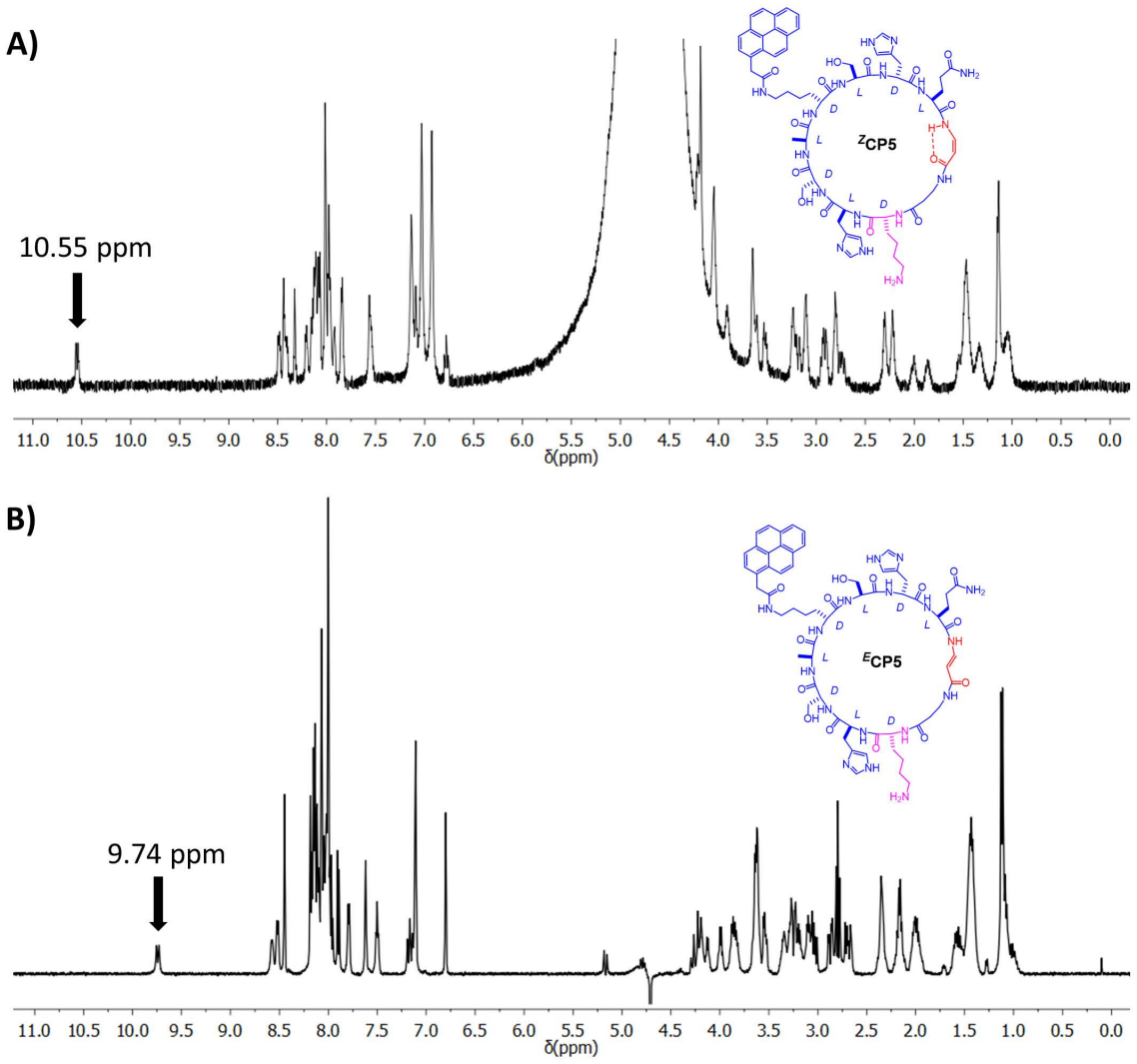

Figure 96. (A) ^{1}H-NMR of **^{Z}CP5** at 4.0 mM (500 MHz, D_2O/H_2O, 298K). (B) ^{1}H-NMR of **^{E}CP5** at 4.2 mM (500 MHz, D_2O/H_2O, 298K).

The differences in the self-assembly properties between the two isomers were also evaluated. The ThT assay[231] at neutral or basic pH revealed an increase of ThT emission with increasing peptide concentration for both isomers (Figure 97A-D). In contrast to what happens with **CP3**, this suggests that both isomers are able to adopt a β-sheet structure. This was confirmed by STEM images, because while **^{Z}CP5** is able to form sheet-like structures (Figure 97E), **^{E}CP5** revealed the formation of nanotubes (Figure 97F).

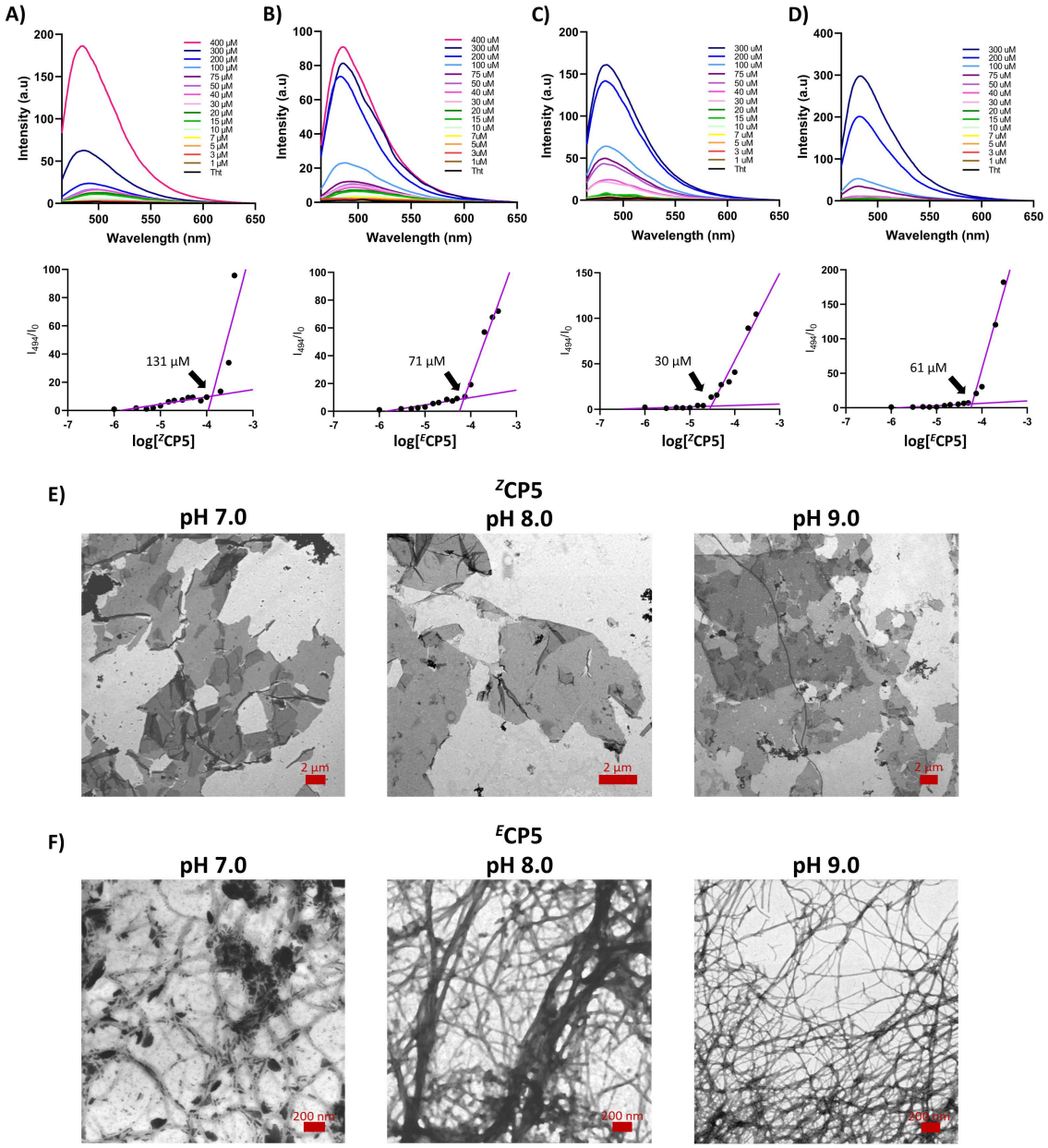

Figure 97. (A-B) Overlaid ThT (20 µM) fluorescence spectra of solutions of **^{Z}CP5** (A) and **^{E}CP5** (B) in HEPES (10 mM, pH 7.0) at different concentrations (λ_{exc} = 440 nm) and intensity ratio I_{494}/I_0 versus the logarithm of the concentration of **CP5** to calculate the *cac*. I_0 is the fluorescence intensity at 494 nm of ThT alone. (C-D) Overlaid ThT (20 µM) fluorescence spectra of solutions of **^{Z}CP5** (C) and **^{E}CP5** (D) in Boric acid buffer (10 mM, pH 9.0) at different concentrations (λ_{exc} = 440 nm) and intensity ratio I_{494}/I_0 versus the logarithm of the concentration of **CP5** to calculate the *cac*. I_0 is the fluorescence intensity at 494 nm of ThT alone. (E) STEM micrographs achieved by deposition of a **^{Z}CP5** solution (200 µM) at different pH. The pH was adjusted by adding small aliquots of aqueous NaOH (0.1 M). (F) STEM micrographs achieved by deposition of a **^{E}CP5** solution (200 µM) at different pH. The pH was adjusted by adding small aliquots of aqueous NaOH (0.1 M).

USC UNIVERSIDADE DE SANTIAGO DE COMPOSTELA

Based on these differences in the type of supramolecular structures obtained depending on the isomer of **CP5**, a preliminary evaluation of the possibility of inducing a transition from sheets to nanotubes by irradiation was studied. However, STEM images suggest a disassembly of the sheet-like structures after 10 minutes of irradiation at 290-320 nm, instead of a transition to nanotubes (Figure 98). Therefore, further experiments are still needed to achieve a photo-conversion between sheets and nanotubes.

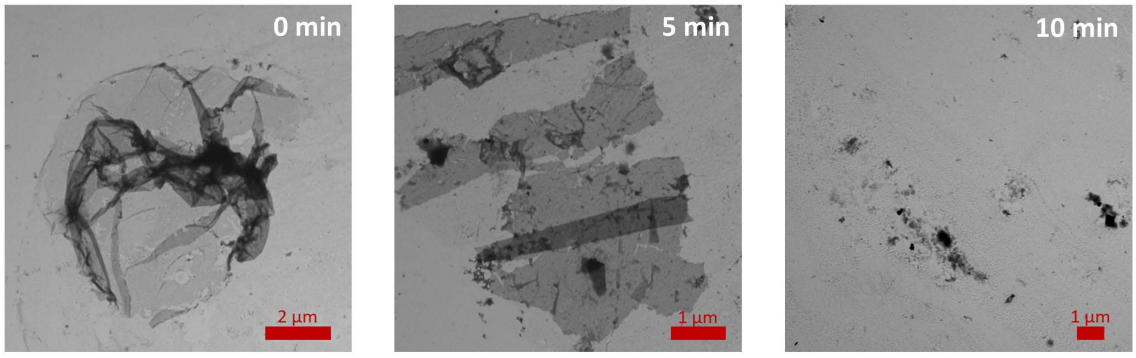

Figure 98. STEM micrographs achieved by deposition of ^{Z}**CP5** solutions (200 µM) in HEPES buffer (10 mM, pH 7.0) after 0, 5 and 10 minutes of irradiation at 290-320 nm. Staining was obtained with 2% w/v phosphotungstic acid (PTA).

USC UNIVERSIDADE DE SANTIAGO DE COMPOSTELA

6.2.4. Conclusions

In this chapter, a switchable structure for the design of novel light-modulated cyclic peptide nanotubes was developed. For this purpose, we have designed a new CP containing an unsaturated β-amino acid, whose irradiation with the appropriate wavelength allowed the isomerization of the aforementioned residue between the *Z*- and the *E*-forms. Although the *Z*-isomer adopts a folded conformation driven by the strong intramolecular hydrogen bonding of the unsaturated residue that constrains its assembly properties, the *E*-isomer adopts a planar conformation that facilitates the stacking and the formation of nanotubes. This assembly process occurs only at appropriate pH (5.6-9.5) due to the selective protonation/deprotonation of basic residues, allowing a dual checkpoint control over nanotube formation. The isomerization and the different properties of both isomers were confirmed by different techniques, such as NMR, fluorescence/CD spectroscopy, STEM or AFM. Finally, the spatially controlled polymerization of CPs to form microfibrillar bundles in confined aqueous droplets was addressed by a microfluidic regulated tandem process. This method allowed not only the visualization of the supramolecular polymerization triggered by light and media, but also the precise preferential localization of fibres at the periphery or into the core of the droplets. The nanotubes generated under neutral conditions, those formed at the interface, exhibit fusogenic properties inducing droplets merging. This work demonstrates the control over the supramolecular polymerization of synthetic fibres based on cyclic peptide nanotubes.

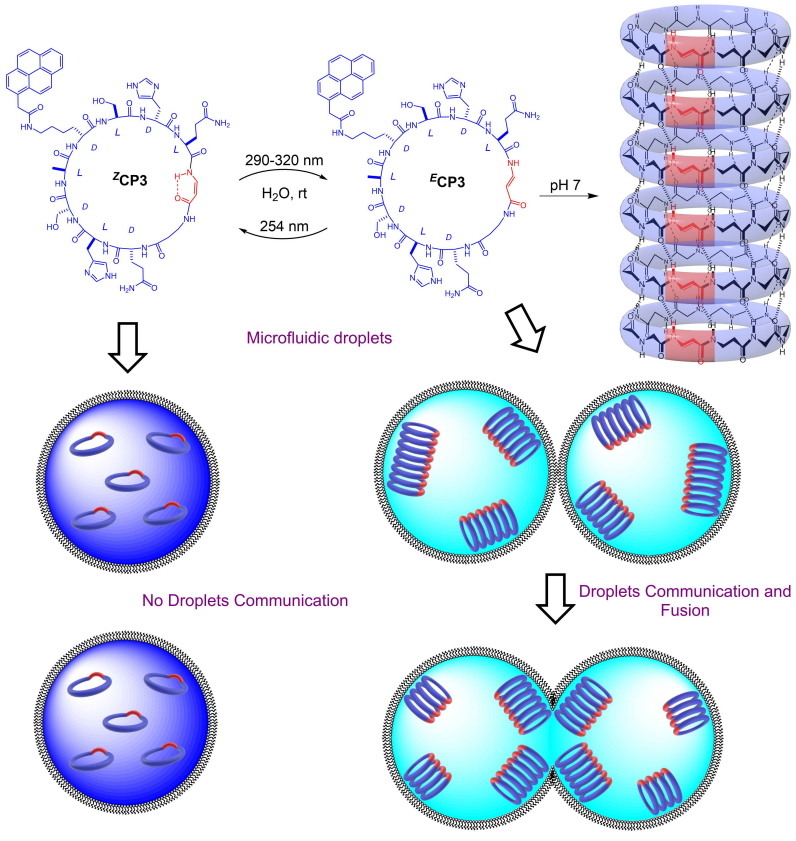

Figure 99. Photo-modulated assembly/disassembly process of cyclic peptide nanotubes and fusion of microfluidic droplets developed in this chapter.

6.3. SELF-ASSEMBLING CYCLIC PEPTIDE NANOTUBES FOR THE TRANSPORT OF DOXORUBICIN INTO CANCER CELLS

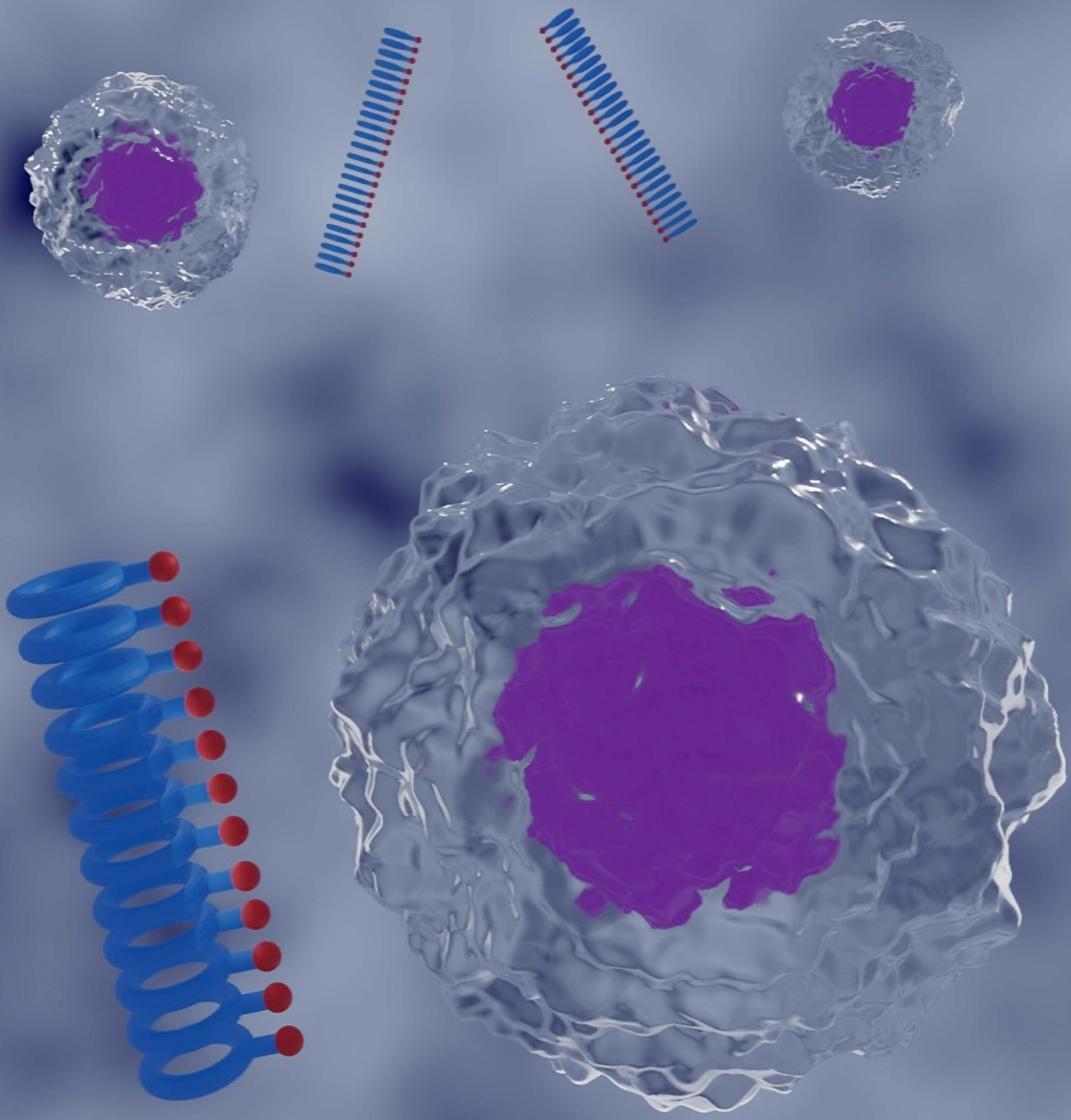

USC
UNIVERSIDADE DE SANTIAGO DE COMPOSTELA

6.3.1. Precedents

Doxorubicin (DOX), also known with the commercial name Adriamycin®, is one of the most potent anticancer drugs approved.[264] It can be used to treat a wide range of cancers, including solid tumours in children, leukaemia and breast, ovarian, stomach or liver tumours, among others. This potency and versatility make it one of the most widely used anticancer drugs. Nevertheless, its clinical application is limited by serious side effects, especially heart problems, and the appearance of drug resistance to the treatment.

In this context, our research group raised the possibility of attaching doxorubicin to cyclic peptide nanotubes previously designed for antimicrobial applications.[265] In particular, it was proposed the binding of doxorubicin to amphipathic cyclic peptides through oxime bond formation (Figure 100A). Since tumour cells have a more acidic pH than healthy cells, the idea was that this dynamic covalent bond would facilitate the selective release of the drug into the membrane or inside the cancer cells in order to reduce its side effects.

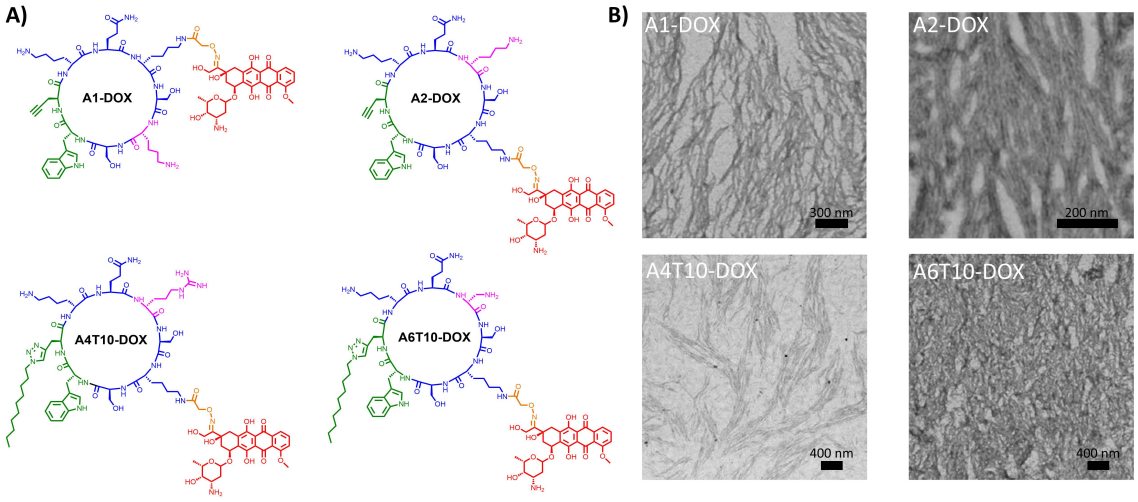

Figure 100. (A) Design of cyclic peptides in which DOX is conjugated with an oxime bond. Adapted with permission from ref. 265. (B) STEM images of aqueous solutions of **A1-DOX** (0.5 mg/mL), **A2-DOX** (0.5 mg/mL), **A4T10-DOX** (5 μg/mL) and **A6T10-DOX** (0.5 mg/mL). Adapted with permission from ref. 265.

Initially, it was demonstrated that these cyclic peptide-doxorubicin conjugates retain the ability to self-assemble into nanotubes (Figure 100B). However, although two of these compounds (**A1-DOX** and **A4T10-DOX**) showed promising activity against a breast cancer cell line (MCF-7), the effect was less pronounced than that obtained with free doxorubicin (Figure 101A). Moreover, none of the designs showed activity against

[264] a) C. Carvalho, R. X. Santos, S. Cardoso, S. Correia, P. J. Oliveira, M. S. Santos, P. I. Moreira, *Curr. Med. Chem.* **2009**, 16, 3267-3285; b) O. Tacar, P. Sriamornsak, C. R. Dass, *J. Pharm. Pharmacol.* **2012**, *65*, 157-170; c) S. Sritharan, N. Sivalingam, *Life Sci.* **2021**, *278*, 119527.

[265] E. González Freire (**2019**), *Application of two orthogonal click-type reactions for the preparation of cyclic peptides with antibacterial and anticancer activity*, PhD Dissertation, University of Santiago de Compostela.

a doxorubicin-resistant ovarian cancer cell line (NCI/ADR-RES). In addition, it was found that incubating the peptide at pH 4.0 for 12 hours did not result in the release of the drug from the cyclic peptide (Figure 101B). Therefore, it was concluded that the low activity of these compounds was due to the high stability of the oxime bond, which prevents the release of the drug and its subsequent therapeutic effect.

A)

	MCF-7 (96 h)		NCI/ADR-RES (48 h)	
Compound	*Emax* (%inhibition)	IC_{50} (μM)	*Emax* (%inhibition)	IC_{50} (μM)
A1-DOX	68 ± 2	4.10 ± 0.17	6 ± 2	-----
A2-DOX	46 ± 2	-----	8 ± 3	-----
A4T10-DOX	91 ± 1	8.33 ± 0.39	48 ± 2	-----
A6T10-DOX	46 ± 2	-----	38 ± 3	-----
DOX	86 ± 1	0.82 ± 0.07	36 ± 4	-----

B)

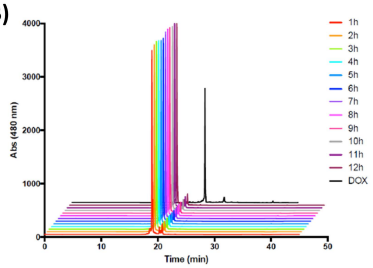

Figure 101. (A) *In vitro* activity in MCF-7 (breast cancer cell line) after 96 hours and NCI/ADR-RES (doxorubicin-resistant ovarian cancer cell line) after 48 hours. *Emax* corresponds to the maximum effect, which is the inhibition obtained at the higher concentration tested (100 μM). IC_{50} is the concentration at which a 50% growth inhibition is obtained. The IC_{50} was only calculated for those compounds with a *Emax* higher than 50%. Adapted with permission from ref. 265. (B) HPLC of **A2-DOX** incubated at pH 4.0 for 12 hours. DOX was used as a control. HPLC conditions: Agilent SB-C18 column, H_2O (0.1% TFA)/MeCN (0.1% TFA), 100:0 → 100:0 (5 min) and 100:0 → 5:95 (30 min). Image adapted with permission from ref. 265.

USC
UNIVERSIDADE DE SANTIAGO DE COMPOSTELA

6.3.2. Objective

In this chapter, we describe the design of a new class of doxorubicin-cyclic peptide conjugates in which the drug is linked using a hydrazone bond. This dynamic covalent bond is more acid-labile than the previously used oxime bond,[265] so it is expected that the drug can now be appropriately released in the more acidic pH environment of tumour cells (Figure 102).[266]

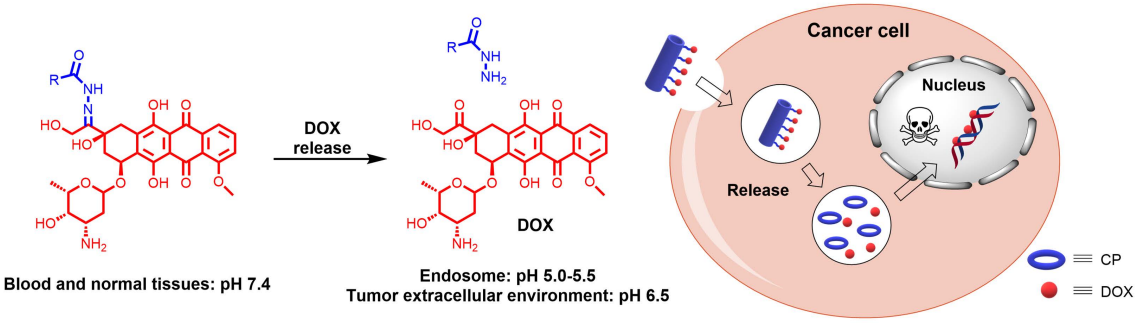

Figure 102. Objective of this chapter: release of doxorubicin inside cancer cells by using cyclic peptide nanotubes.

For this purpose, we designed a collection of cyclic peptides (Figure 103), which will act not only as drug delivery systems, but also as membrane destabilizing compounds. The hydrophobicity of the non-polar region in some cyclic peptides was enhanced by incorporating a hydrocarbon tail following a *click chemistry* strategy previously described in our research group.[183,265] We hypothesise that the cyclic peptides containing the hydrocarbon tail will be able to insert it in the hydrophobic environment of the lipid bilayer, causing membrane disruption. Moreover, we proposed to explore two different positions of drug binding to the cyclic peptide sequence. In this regard, we designed **CP6-DOX** and **CP6Tn-DOX**, which are lysine-containing peptides that represent the hydrazone-based version of the previously tested **A1-DOX**. Also, we proposed **CP6$_{NBD}$-DOX**, which incorporates a tail with a fluorescent nitrobenzoxadiazole (NBD) moiety in order to study the peptide internalization by confocal microscopy. Furthermore, we designed the versions **CP6-SS-DOX** and **CP6Tn-SS-DOX**. These derivatives contain a double reversible binding of the drug. In addition to the acid-labile hydrazone bond, a redox-sensitive disulphide bond is incorporated in the design, which is susceptible to cleavage by glutathione (GSH) inside the cell. On the other hand, we designed **CP7-DOX** and **CP7Tn-DOX**, which contain an arginine residue and are derived from the previous design **A4T10-DOX**.

[183] E. González-Freire, F. Novelli, A. Pérez-Estévez, R. Seoane, M. Amorín, J. R. Granja, *Chem. Eur. J.* **2021**, *27*, 3029-3038.
[265] E. González Freire (**2019**), *Application of two orthogonal click-type reactions for the preparation of cyclic peptides with antibacterial and anticancer activity*, PhD Dissertation, University of Santiago de Compostela.
[266] D. K. Kölmeland, E. T. Kool, *Chem. Rev.* **2017**, *117*, 10358-10376.

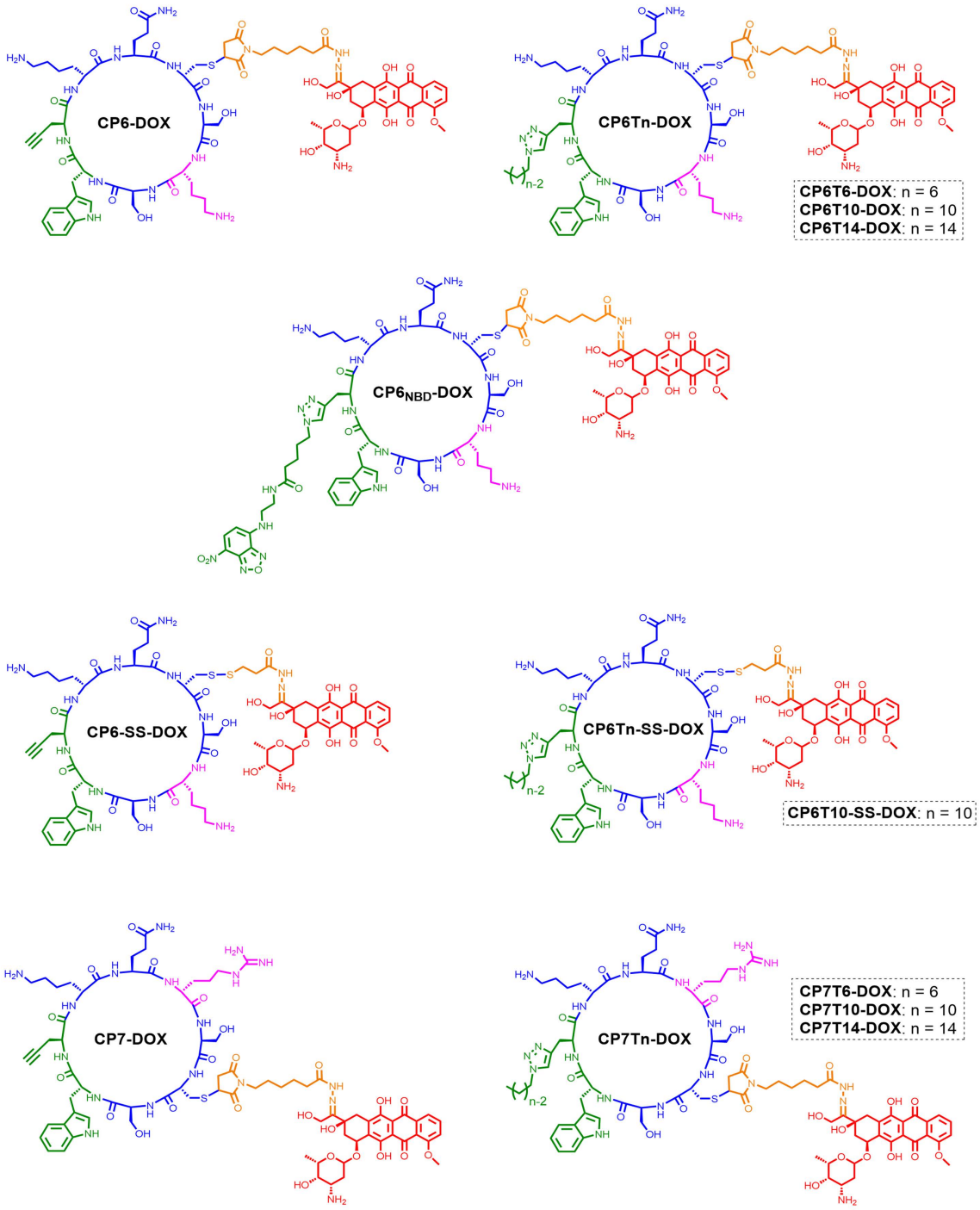

Figure 103. Design of the doxorubicin-cyclic peptide conjugates studied in this chapter.

USC
UNIVERSIDADE
DE SANTIAGO
DE COMPOSTELA

6.3.3. Results and discussion

6.3.3.1. Synthesis of the maleimide-based doxorubicin linker

Considering the first family of cyclic peptides, we performed the synthesis of a maleimide linker with doxorubicin attached by a hydrazone bond (**8**). This compound could be incorporated at a later stage into the cysteine-containing cyclic peptides by a thiol-ene reaction. In particular, the preparation of the (6-maleimidocaproyl)hydrazone derivative of doxorubicin (**8**) was adapted from previously described protocols.[267] The synthesis was performed in four synthetic steps (Figure 104). The first step is the condensation of maleic anhydride and 6-aminocaproic acid, which was carried out at 120°C in acetic acid during 6 hours. After purification, the 6-maleimidocaproic acid (**6**) was obtained as a crystalline white solid in 70% yield. Then, the coupling with *tert*-butyl carbazate was carried out in CH_2Cl_2 by using *N*-HBTU as coupling agent and DIEA as base. The resulting coupling product **7** was obtained after purification in 51% yield. Finally, the incorporation of doxorubicin was performed by the formation of a hydrazone bond. To this end, the *Boc* protecting group was removed by treatment with a mixture of TFA/CH_2Cl_2 (1:1) during 15 minutes. The resulting residue was thoroughly dried, redissolved in MeOH and stirred together with doxorubicin hydrochloride for 24 hours. After precipitation and washing with ethyl acetate, the final linker **8** was obtained as a red solid in 92% yield. This compound was used without further purification.

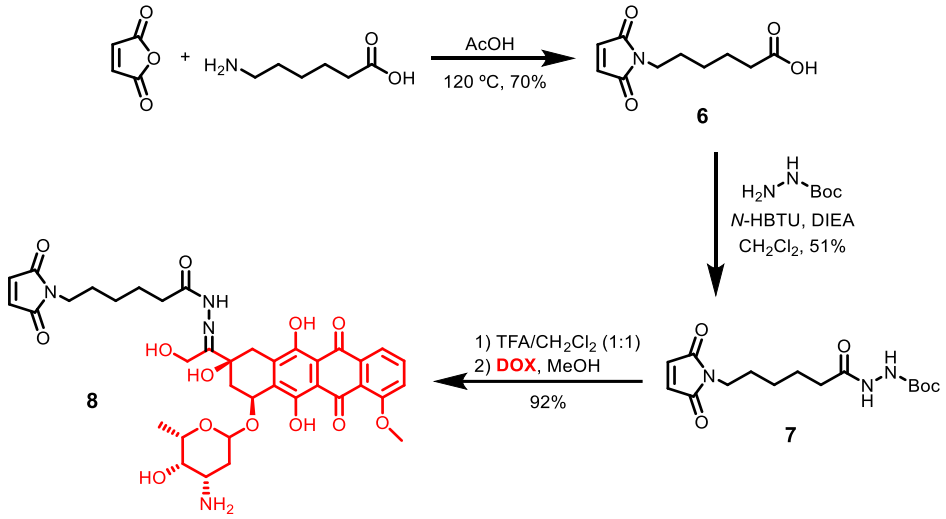

Figure 104. Synthetic strategy to obtain the maleimide-based doxorubicin linker (**8**).

[267] a) D. Willner, P. A. Trail, S. J. Hofstead, H. D. King, S. J. Lasch, G. R. Braslawsky, R. S. Greenfield, T. Kaneko, R. A. Firestone, *Bioconjugate Chem.* **1993**, *4*, 521-527; b) Z. Jia, L. Wong, T. P. Davis, V. Bulmus, *Biomacromolecules* **2008**, *9*, 3106-3113; c) T. Cai, Y. Chen, Y. Wang, H. Wang, X. Liu, Q. Jin, S. Agarwal, J. Ji, *Polym. Chem.* **2014**, *5*, 4061-4068.

6.3.3.2. Synthesis of the disulphide bond-based doxorubicin linker

The synthesis of the disulphide bond-based doxorubicin linker (**11**) was also performed. This compound could be conjugated later to the cyclic peptide scaffold via a thiol-disulphide exchange reaction. The synthetic strategy was designed based on previously reported methods (Figure 105).[268] The first step consisted of a thiol-disulphide exchange reaction between 2,2'-dithiodipyridine and 3-mercaptopropionic acid in 2.5% AcOH/EtOH for 20 hours. After flash chromatography purification, compound **9** was obtained in 78% yield. This compound was coupled with *tert*-butyl carbazate by using HOBt, EDC·HCl and DIEA in MeCN and stirring for 4 hours. The product **10** was obtained in 95% yield after purification. Finally, the *Boc* group was removed by treatment with a mixture of TFA/CH_2Cl_2 (1:1) for 20 minutes and the resulting deprotected residue was condensed with doxorubicin hydrochloride by stirring this mixture in MeOH for 6 days. After precipitation and washing with MeCN, the compound **11** was obtained as a red solid in 74% yield.

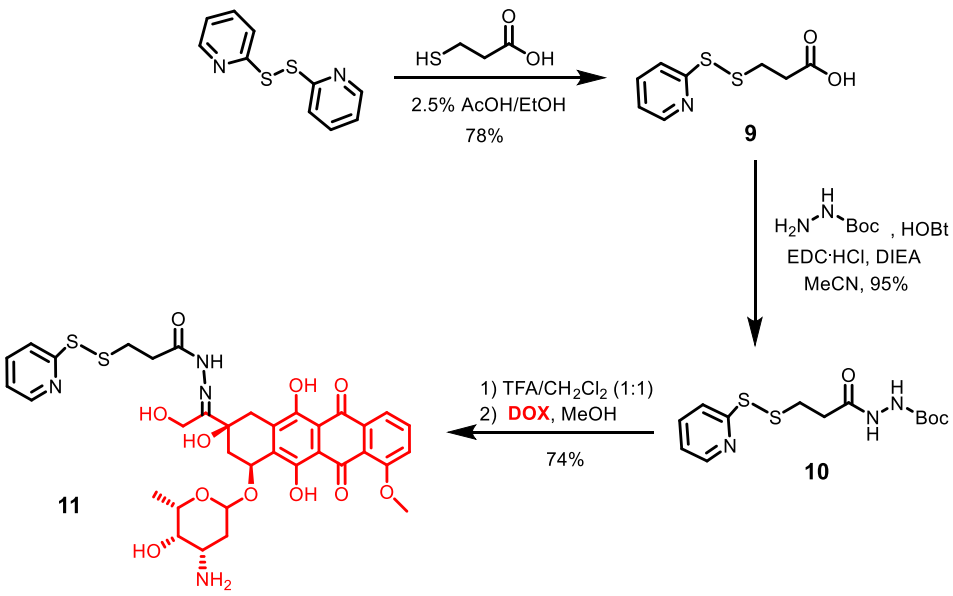

Figure 105. Synthetic strategy to obtain the disulphide bond-based doxorubicin linker (**11**).

USC UNIVERSIDADE DE SANTIAGO DE COMPOSTELA

[268] a) R. S. Greenfield, T. Kaneko, A. Daues, M. A. Edson, K. A. Fitzgerald, L. J. Olech, J. A. Grattan, G. L. Spitalny, G. R. Braslawsky, *Cancer Res.* **1990**, *50*, 6600-6607; b) K. Y. J. Lee, Y. Wang, S. Nie, *RSC Adv.* **2015**, *5*, 65651-65659.

6.3.3.3. Synthesis of the azide-carbon tail containing NBD

For future studies of the mechanism of action by confocal microscopy, a tail containing a fluorescent NBD moiety was also synthesized (Figure 106). This tail was proposed to be incorporated in **CP6$_{NBD}$-DOX** to replace the hydrocarbon tail of the original peptide designs. First, it was performed a nucleophilic aromatic substitution reaction between NBD-Cl and *N*-Boc-ethylenediamine, in CH_2Cl_2 and using Et_3N as a base, for 18 hours under argon atmosphere. The compound **12** was obtained after purification in a 62% yield. Then, the *Boc* group was removed by treatment with TFA/CH_2Cl_2 (1:1) for 15 minutes and a coupling with 5-azidopentanoic was carried out in CH_2Cl_2 and in the presence of *N*-HBTU and DIEA. After 2 hours of reaction under argon atmosphere and subsequent purification, the final product **13** was obtained in 86% yield as an orange solid.

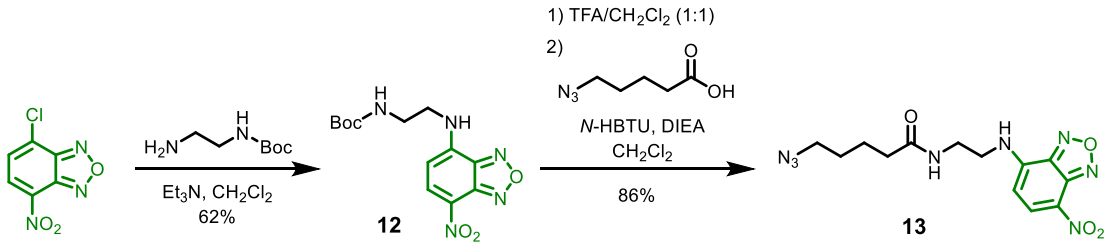

Figure 106. Synthetic strategy to obtain the carbon tail containing a NBD moiety (**13**).

6.3.3.4. Solid-phase peptide synthesis

The synthesis of the cyclic peptide scaffolds was carried out following a Fmoc/tBu solid-phase peptide synthesis using a Rink amide resin (Figure 107).[183,229] First, the linear peptide was synthesized by cycles of deprotection of the Fmoc group with 25% piperidine in DMF and coupling of the next Fmoc-protected amino acid using *N*-HBTU as coupling agent. A propargylglycine residue was used in the sequence to modify the hydrophobicity of the cyclic peptide by introducing different alkyl chains through a *click chemistry* strategy. After the cyclization of the peptide on the solid support, which was performed using PyAOP as coupling agent, the appropriate carbon tail was incorporated on-resin through a Cu(I)-catalysed alkyne-azide cycloaddition (CuAAC), if necessary. Finally, side chain deprotection and release of the CP from the solid support was performed by treating the resin with a cocktail of TFA/DCM/H_2O/EDT (90:5:2.5:2.5). The different peptide scaffolds were purified by reversed-phase HPLC, resulting in a white solid after freeze-drying. In particular, **CP6**, **CP6T6**, **CP6T10**, **CP6T14**, **CP6$_{NBD}$**, **CP7**, **CP7T6**, **CP7T10** and **CP7T14** were prepared following this protocol.

USC UNIVERSIDADE DE SANTIAGO DE COMPOSTELA

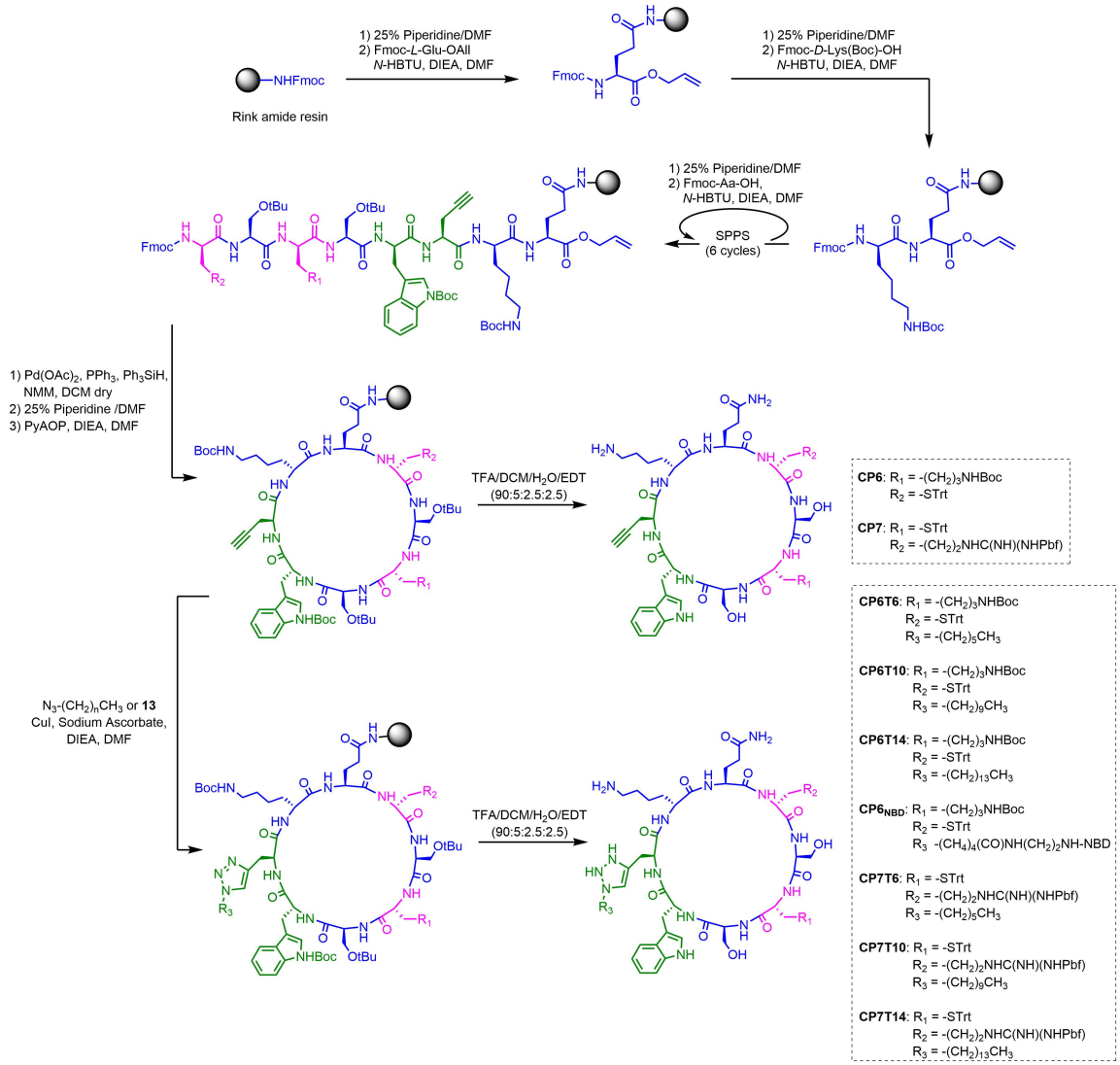

Figure 107. Synthetic strategy to obtain the cyclic peptides scaffolds of this chapter.

6.3.3.5. Conjugation of the maleimide linker to cyclic peptides

The maleimide linker (**8**) was conjugated to the different cyclic peptides via a thiol-ene reaction (Figure 108).[269] Specifically, the corresponding cyclic peptide scaffold and **8** were dissolved in DMF and stirred for 12 hours. The subsequent purification by Sephadex LH-20 column (Eluent: MeOH) and dried under vacuum provided the corresponding final conjugates as a red solid in all cases.

[269] a) B. H. Northrop, S. H. Frayne, U. Choudhary, *Polym. Chem.* **2015**, *6*, 3415-3430; b) S. Li, L. Liu, H. Jia, W. Qiu, L. Rong, H. Cheng, X. Zhang, *Chem. Commun.* **2014**, *50*, 11852-11855; c) J. Wang, M. Chen, S. Li, R. D. Ye, *Mol. Pharmaceutics* **2019**, *16*, 2636-2647.

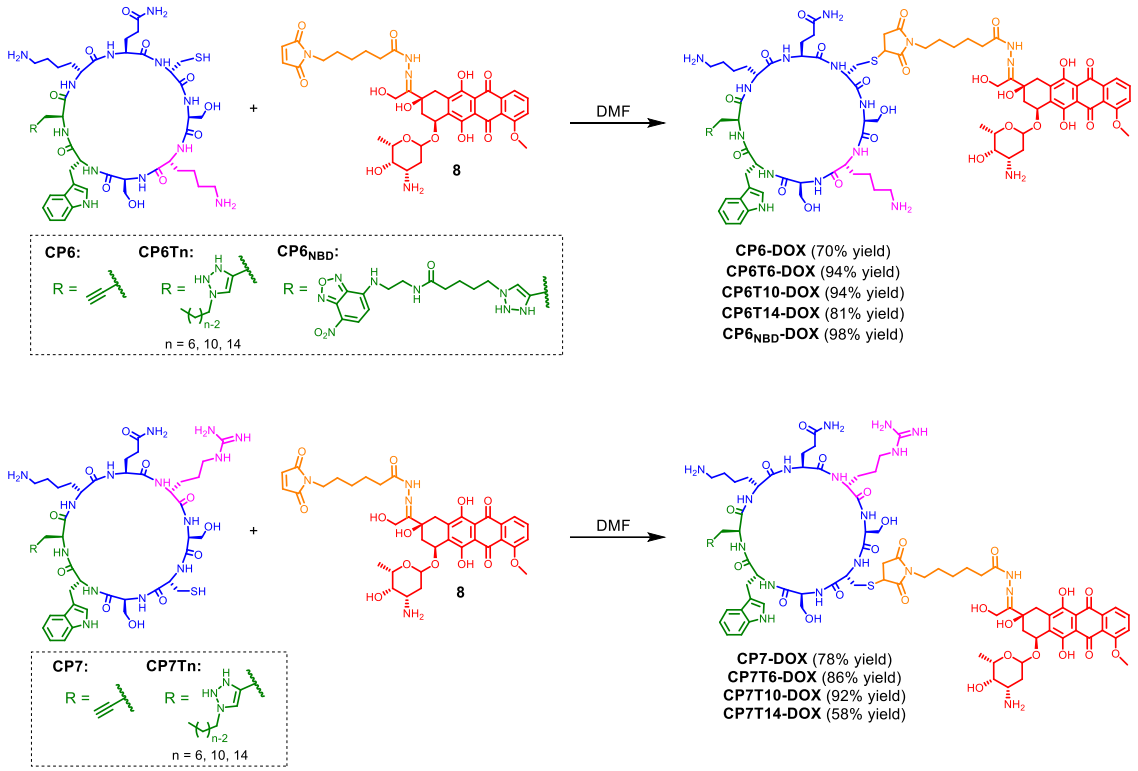

Figure 108. Synthetic scheme to obtain the different cyclic peptide-doxorubicin conjugates with the maleimide linker.

6.3.3.6. Conjugation of the disulphide linker to cyclic peptides

The conjugation of the disulphide linker (**11**) to **CP6** or **CP6T10** was performed with a thiol-disulphide exchange protocol in which both components were stirred in MeOH for 12 hours (Figure 109).[270] After purification by Sephadex LH-20 column (Eluent: MeOH) and dried under vacuum, the final conjugates were obtained as a red solid in both cases.

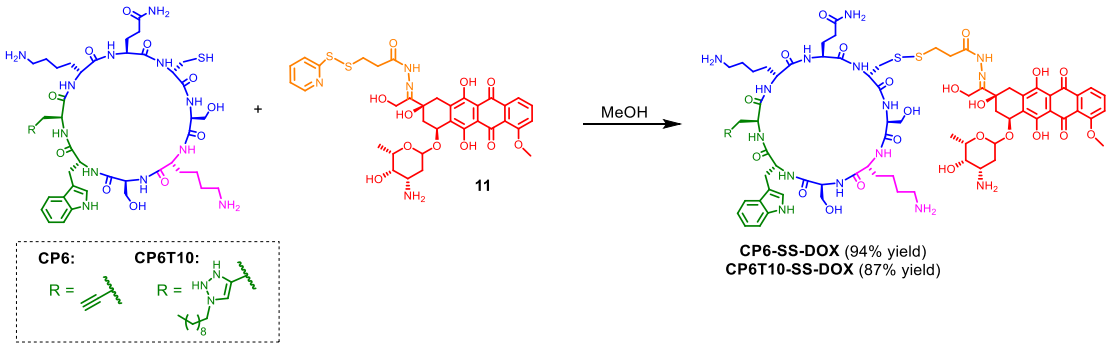

Figure 109. Synthetic scheme to obtain the different cyclic peptide-doxorubicin conjugates with the disulphide linker.

[270] a) I. Altinbasak, M. Arslan, R. Sanyal, A. Sanyal, *Polym. Chem.* **2020**, *11*, 7603-7624; b) S. Darwish, N. Sadeghiani, S. Fong, S. Mozaffari, P. Hamidi, T. Withana, S. Yang, R. K. Tiwari, K. Parang, *Eur. J. Med. Chem.* **2019**, *161*, 594-606.

6.3.3.7. Self-assembly properties

Once the different peptides were synthetized, the self-assembly properties were studied starting with the peptide scaffolds without the drug. To this end, fluorescence experiments were carried out in the presence of ThT (Figure 110A-D).[231] The spectra revealed an increase in ThT emission at neutral pH with increasing peptide concentration, confirming the ability of the peptide scaffolds to form β-sheet structures. As expected, the critical aggregation concentrations (*cac*) were lower for the derivatives that incorporate the carbon tail. The morphology of the peptide scaffolds at 200 µM and pH 7.0 was evaluated by STEM (Figure 110E-H). The images of the peptides **CP6** and **CP7** showed the formation of fibres with lengths of several micrometres long. In contrast, sheet-like structures were obtained for the peptides containing the 10-carbon tail (**CP6T10** and **CP6T10**), suggesting that this tail plays an important role in an additional hierarchical assembly process.

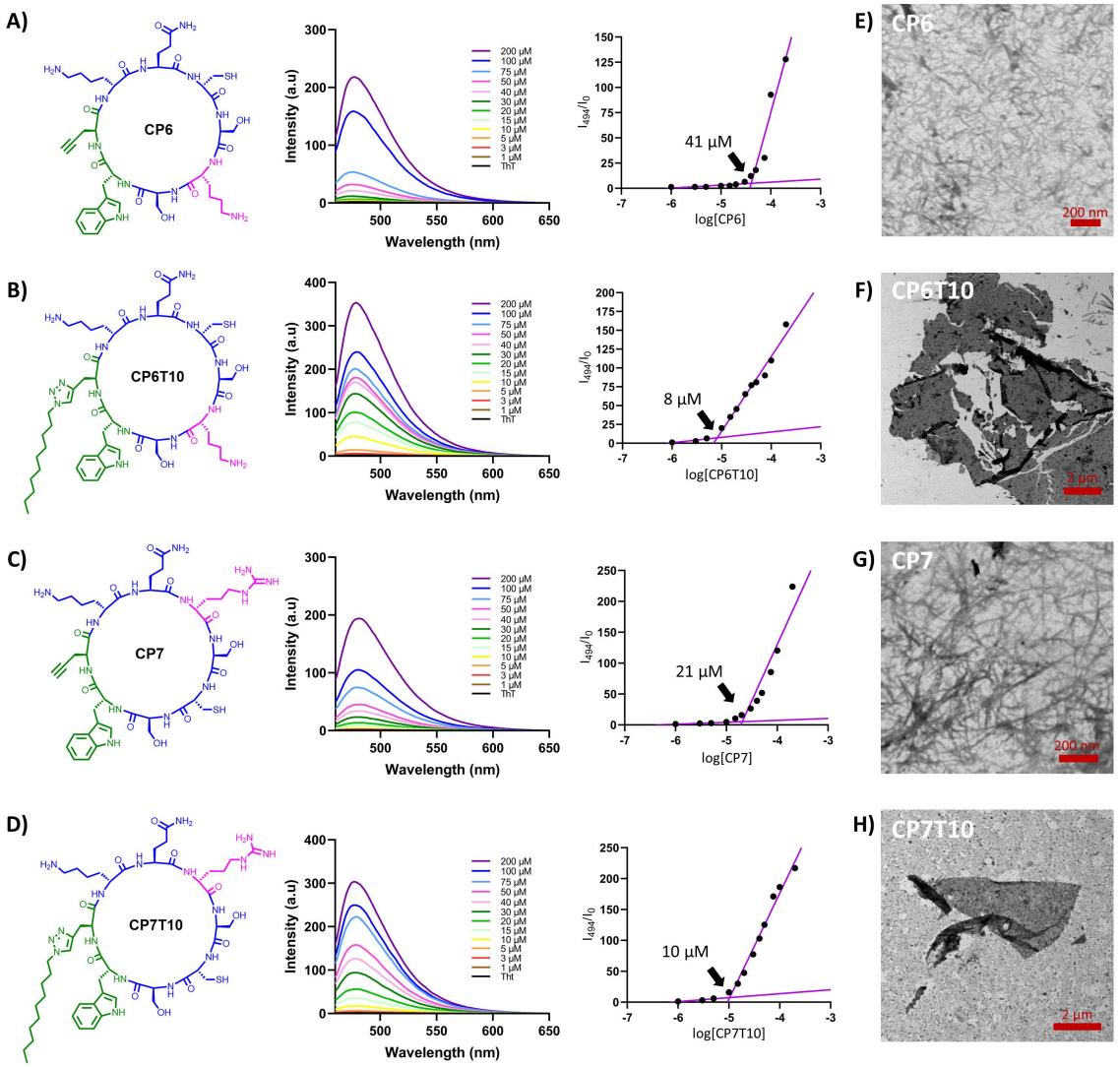

Figure 110. (A-D) ThT (20 µM) fluorescence spectra and critical aggregation concentration (*cac*) of solutions of (A) **CP6**, (B) **CP6T10**, (C) **CP7** or (D) **CP7T10** in PBS buffer (10 mM, 107 mM NaCl, pH 7.4) at different concentrations (λ_{exc} = 440 nm). (E-H) STEM micrographs of (E) **CP6**, (F) **CP6T10**, (G) **CP7** or (H) **CP7T10** at 200 µM and pH 7.0. Staining was obtained with 2% w/v phosphotungstic acid (PTA).

Then, we evaluated if these fibres and sheet-like structures are maintained after the doxorubicin conjugation to the peptides. For that, we calculated the *cac* of the doxorubicin-cyclic peptide conjugates by fluorescence and circular dichroism (CD). First, doxorubicin fluorescence was collected at neutral pH as a function of peptide concentration (Figure 111A-D). In all cases, an increase in fluorescence was observed until a critical concentration, after which the fluorescence started to decrease probably due to peptide self-assembly and aggregation. In addition, concentration-dependent experiments at neutral pH showed an increase in negative CD signals for doxorubicin at 290 nm and 500-550 nm, together with a positive CD signal around 440 nm (Figure 111E-H). This increment with the concentration suggests an assembly with Dox-Dox stacking. In particular, both fluorescence and CD experiments provided again a lower *cac* for the designs with the carbon tail compared with the ones without it.

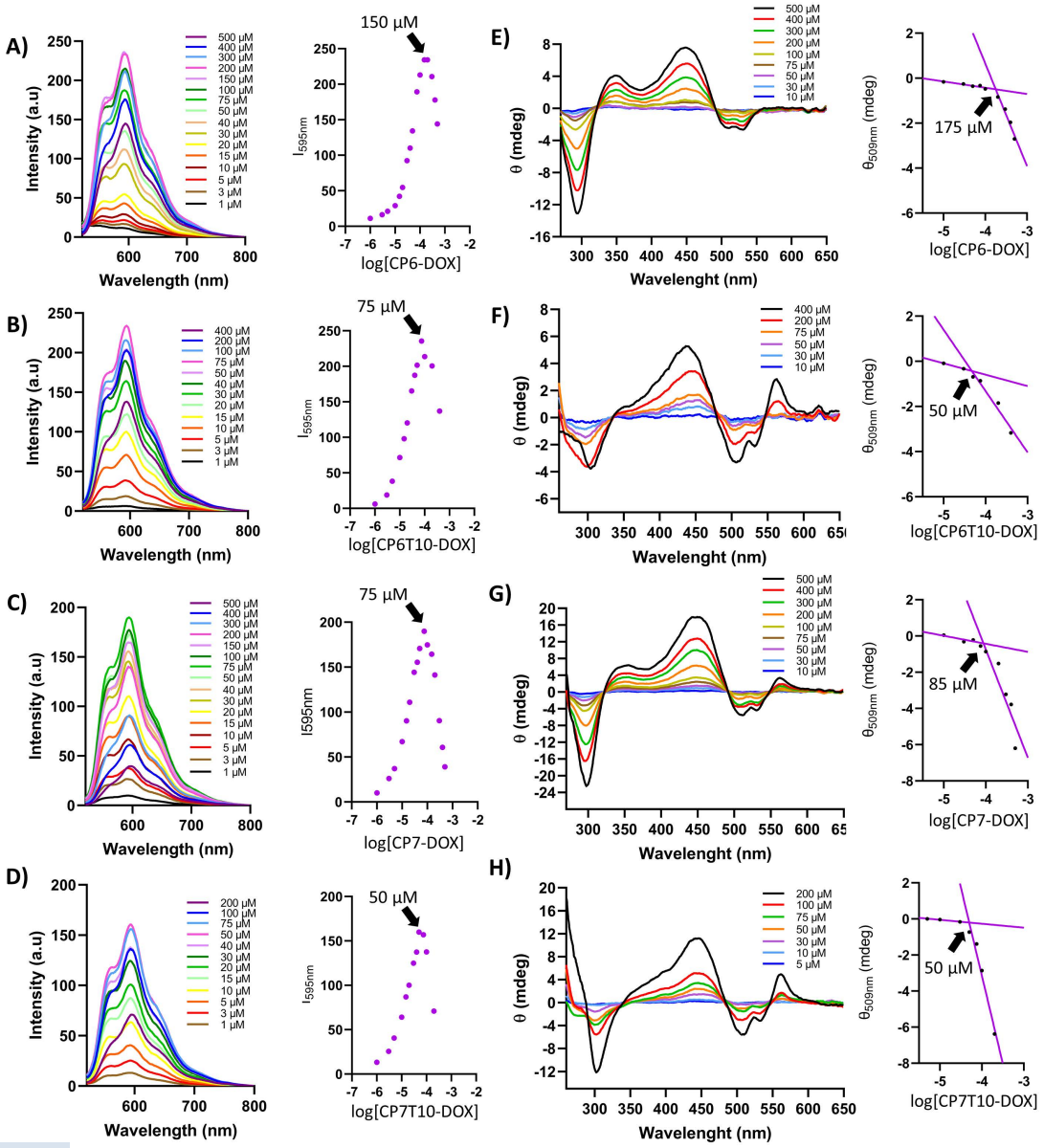

Figure 111. (A-D) Fluorescence spectra and *cac* of solutions of (A) **CP6-DOX**, (B) **CP6T10-DOX**, (C) **CP7-DOX** or (D) **CP7T10-DOX** in PBS buffer (10 mM, 107 mM NaCl, pH 7.4) at different peptide concentrations (λ_{exc} = 480 nm). (E-H) CD spectra and *cac* of (E) **CP6-DOX**, (F) **CP6T10-DOX**, (G) **CP7-DOX** or (H) **CP7T10-DOX** in PBS buffer (10 mM, 107 mM NaCl, pH 7.4) at different concentrations.

In addition, FT-IR spectra of the peptides as a lyophilized powder revealed the amide I band around 1629-1625 cm^{-1} and a shoulder around 1672-1668 cm^{-1} (Table 1). These bands, together with the lack of high-frequency components above 1680 cm^{-1}, suggest the formation of parallel β-sheet structures.[232] In all cases, it was also obtained a strong band for amide A around 3272 cm^{-1} in agreement with the formation of hydrogen bonding interactions.[233]

	Frequency (cm^{-1})			
CP	Amide A	Amide I_a	Amide I_b	Amide II
CP6-DOX	3270.3	1629.4	1670.8	1540.6
CP6T6-DOX	3270.3	1625.4	1670.8	1536.7
CP6T10-DOX	3274.2	1627.4	1672.8	1540.6
CP6T14-DOX	3272.3	1629.4	1670.8	1536.7
CP6T$_{NBD}$-DOX	3274.2	1627.4	1672.8	1536.7
CP7-DOX	3276.2	1627.4	1670.8	1538.7
CP7T6-DOX	3272.3	1627.4	1668.8	1538.7
CP7T10-DOX	3272.3	1625.4	1670.8	1538.7
CP7T14-DOX	3270.3	1629.4	1668.8	1534.7

Table 1. Summary table of doxorubicin-cyclic peptide conjugates FT-IR data.

The nanotube and sheet formation of the doxorubicin-cyclic peptide conjugates was analysed by STEM and TEM (Figure 112). In contrast to what was previously observed with the peptide scaffolds without the drug, the deposition of a **CP6T10-DOX** or **CP7T10-DOX** sample at pH 7.4 in PBS buffer revealed the formation of nanotubes with a length of several nanometres (300-400 nm), while the equivalents without tail **CP6-DOX** or **CP7-DOX** showed the formation of sheet-like structures (Figure 112A-B). In an attempt to dissociate these sheets and visualize the nanotubes that constitute them, depositions were also carried out at neutral pH with 20% acetonitrile or at pH 9.0 (Figure 112C-D). However, under these two conditions, lamellar structures were mainly observed for all the designs, confirming the high tendency of these conjugates to form sheet-like structures. The height of these 2D structures was measured by AFM, obtaining a value of 6.52 ± 0.75 nm (Figure 112E).

USC
UNIVERSIDADE DE SANTIAGO DE COMPOSTELA

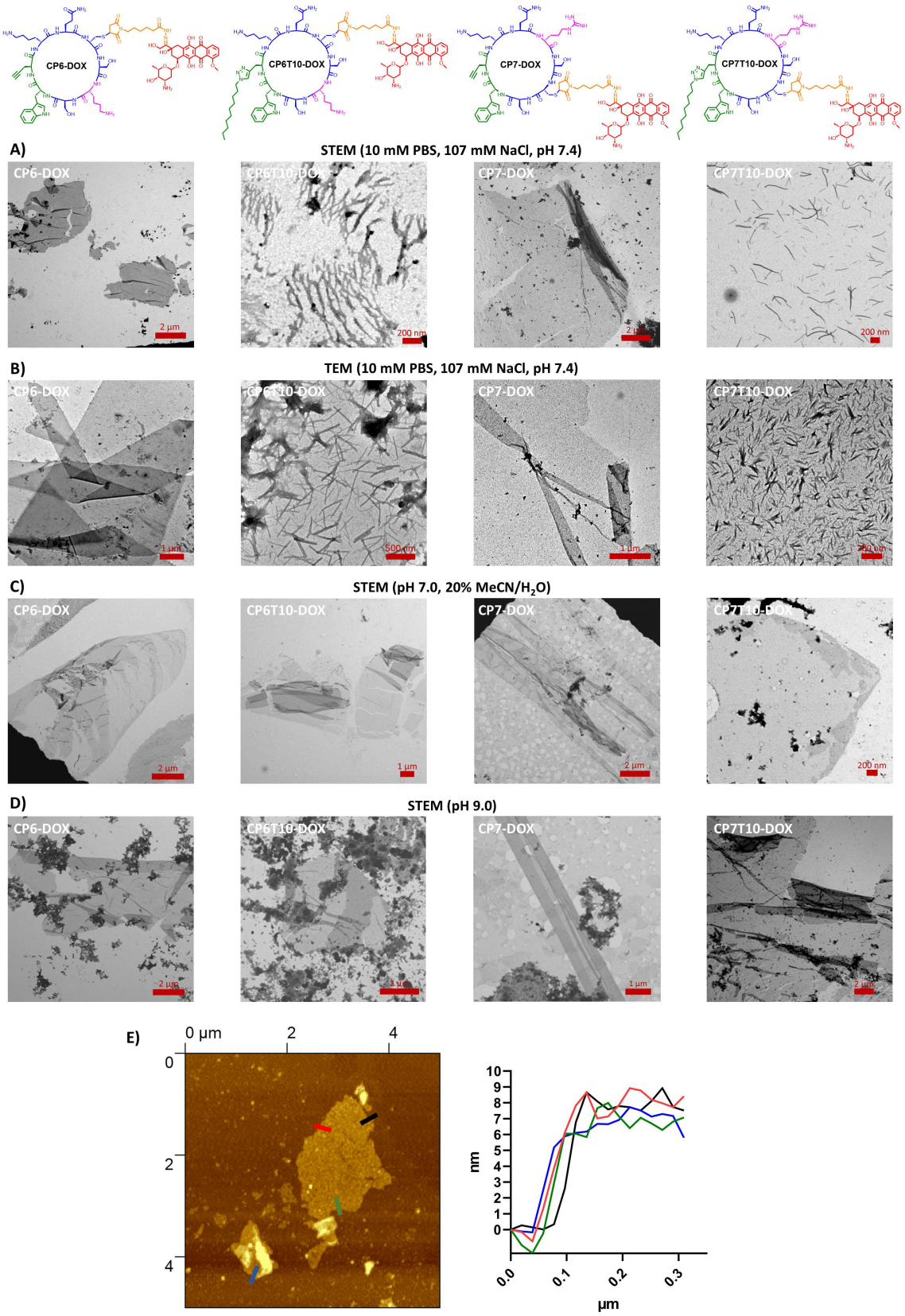

Figure 112. (A-D) STEM or TEM micrographs of 200 µM samples of **CP6-DOX**, **CP6T10-DOX**, **CP7-DOX** and **CP7T10-DOX** in (A and B) PBS buffer (10 mM, 107 mM NaCl) at pH 7.4, (C) pH 7.0 in 20% MeCN/H_2O and (D) pH 9.0. (E) AFM micrographs of **CP7-DOX** (200 µM) in PBS buffer (10 mM, 107 mM NaCl) at pH 7.4 on mica surface. The height profiles were achieved along the corresponding colour lines shown in the image.

6.3.3.8. *In vitro* activity

The anticancer activity of the peptides was evaluated using the MTT (3-[4,5-dimethylthiazol-2-yl]-2,5-diphenyltretrazolium bromid) assay[271] in three different cancer cell lines: a breast cancer cell line (MCF-7),[272] a lung cancer cell line (NCI-H460)[273] and a doxorubicin-resistant ovarian cancer cell line (NCI/ADR-RES).[274] As a control, the maleimide-based doxorubicin linker (**8**) and the antitumour drugs doxorubicin and cisplatin (Table 2) were used.

Initially, all the peptides were tested in the two non-resistant cell lines, MCF-7 and NCI-H460 (Table 2). The peptide scaffolds without the drug showed no activity or a moderate one, with the exception of **CP6** which showed a maximum inhibition of more than 90% in both lines. In contrast, the cyclic peptide-doxorubicin conjugates exhibited a high activity, as shown by their high maximum cell growth inhibition (75-93%) and an IC_{50} within the range of 1-4 µM for all compounds. In fact, these values are comparable or better than those obtained for the controls with the maleimide-based doxorubicin linker (**8**), doxorubicin or cisplatin. No major differences were observed between the derivatives with and without the hydrocarbon tail.

Inspired by these promising results, we decided to evaluate the activity in a doxorubicin-resistant ovarian cancer cell line (NCI/ADR-RES) to study if the conjugation of the drug to the cyclic peptides can help to overcome this resistance (Table 2). In particular, these resistant cells overexpress the P-glycoprotein (P-gp), which is a transporter capable of expelling doxorubicin and avoid its therapeutic action.[274,275] The peptide scaffolds by themselves showed moderate activity, with the exception of **CP7** which showed no toxicity at all. The maximum inhibition observed for these compounds was around 75-90% and their IC_{50} was in the range of 55-69 µM. Moreover, the designs with doxorubicin but lacking a hydrocarbon tail (**CP6-DOX** and **CP7-DOX**) failed to overcome the resistance. In contrast, the derivatives with a 10-hydrocarbon tail (**CP6T10-DOX** and **CP7T10-DOX**) showed maximum cell growth inhibitions of more than 80%. The IC_{50} was around 33-38 µM, which is higher than the one obtained for the control cisplatin, although it represents a promising value considering they are doxorubicin-resistant cells and that the controls with free doxorubicin or the maleimide-based doxorubicin linker (**8**) showed no activity. These findings suggest that the incorporation of a hydrocarbon chain into the design of the cyclic peptides is a crucial strategy for overcoming resistance.

---

[271] a) T. Mossman, *J. Immunol. Methods* **1983**, *65*, 55-63; b) P. Kumar, A. Nagarajan, P. D. Uchil, *Cold Spring Harb. Protoc.* **2018**, *2018*, pdbprot095505.

[272] a) Ş. Comşa, A. M. Cîmpean, M. Raica, *Anticancer Res.* **2015**, *35*, 3147-3154; b) A. V. Lee, S. Oesterreich, N. E. Davidson, *J. Natl. Cancer Inst.* **2015**, *107*, djv073.

[273] a) C. G. Ferreira, S. W. Span, G. J. Peters, F. A. E. Kruyt, G. Giaccone, *Cancer Res.* **2000**, *60*, 7133-7141; b) M. Pesic, J. Z. Markovic, D. Jankovic, S. Kanazir, I. D. Markovic, L. Rakic, S. Ruzdijic, *J. Chemother.* **2006**, *18*, 66-73.

[274] a) M. Liscovitch, D. Ravid, *Cancer Lett.* **2007**, *245*, 350-352; b) W. Ke, P. Yu, J. Wang, R. Wang, C. Guo, L. Zhou, C. Li, K. Li, *Med. Oncol.* **2011**, *28*, 135-141.

[275] Z. E. Sauna, M. M. Smith, M. Müller, K. M. Kerr, S. V. Ambudkar, *J. Bioenerg. Biomembr.* **2001**, *33*, 481-491.

Compound	MCF-7 (96 h)		NCI-H460 (48 h)		NCI/ADR-RES (48 h)	
	Emax (%inhibition)	IC_{50} (μM)	*Emax* (%inhibition)	IC_{50} (μM)	*Emax* (%inhibition)	IC_{50} (μM)
CP6	92 ± 1	17.7 ± 0.3	94 ± 2	37.9 ± 0.4	90 ± 1	55.8 ± 0.7
CP6-DOX	81 ± 1	3.5 ± 0.3	75 ± 1	2.8 ± 0.1	2 ± 2	-----
CP6T10	59 ± 1	78.8 ± 0.1	28 ± 1	-----	70 ± 2	68.9 ± 2.1
CP6T10-DOX	89 ± 1	3.4 ± 0.4	93 ± 1	3.1 ± 0.1	87 ± 2	38.4 ± 0.7
CP7	48 ± 1	-----	8 ± 1	-----	7 ± 3	-----
CP7-DOX	80 ± 1	1.8 ± 0.2	92 ± 1	2.9 ± 0.3	16 ± 3	-----
CP7T10	63 ± 1	50.2 ± 0.6	80 ± 2	> 100	75 ± 2	68.2 ± 4.6
CP7T10-DOX	88 ± 1	2.6 ± 0.3	93 ± 1	1.7 ± 0.1	86 ± 1	33.4 ± 0.3
Linker-DOX (8)	80 ± 1	2.5 ± 0.6	58 ± 1	13.7 ± 0.1	35 ± 3	-----
DOX	86 ± 1	0.82 ± 0.1	56 ± 1	9.3 ± 1.7	36 ± 4	-----
Cisplatin	78 ± 1	7.8 ± 0.6	53 ± 1	5.1 ± 0.6	90 ± 1	11.5 ± 0.6

Table 2. *In vitro* activity in MCF-7 (breast cancer cell line) after incubation for 96 hours, NCI-H460 (lung cancer cell line) after 48 hours and NCI/ADR-RES (doxorubicin-resistant ovarian cancer cell line) after 48 hours. *Emax* corresponds to the maximum effect, which is the inhibition obtained at the higher concentration tested (100 μM). IC_{50} is the concentration at which a 50% growth inhibition is obtained. The IC_{50} was only calculated for those compounds with a *Emax* higher than 50%.

Considering the potential importance of the hydrocarbon tail in overcoming doxorubicin resistance, we evaluated the use of different lengths and incubation times (Table 3). Specifically, an increase in activity was observed when the incubation time was extended from 48 to 72 hours. As indicated in Table 2, only **CP6T10-DOX** and **CP7T10-DOX** showed good cell growth inhibition after 48 hours of incubation. However, good activity was also observed for **CP6T14-DOX**, **$CP6_{NBD}$-DOX** and **CP7T14-DOX** at 72 hours. In particular, **$CP6_{NBD}$-DOX** showed the lowest IC_{50} of all peptides tested (3.7 μM) after 72 hours. Also, **CP6T14-DOX** showed an IC_{50} of 5.7μM and **CP7T14-DOX** one of 8.2 μM. Derivatives lacking the alkyl tail or with the 6-carbon alkyl tail did not show activity even after 72 hours of incubation.

Compound	NCI/ADR-RES (48 h)		NCI/ADR-RES (72 h)	
	Emax (%inhibition)	IC_{50} (μM)	*Emax* (%inhibition)	IC_{50} (μM)
CP6-DOX	2 ± 2	-----	22 ± 4	-----
CP6T6-DOX	26 ± 2	-----	22 ± 3	-----
CP6T10-DOX	87 ± 2	38.4 ± 0.7	84 ± 3	10.8 ± 1.7
CP6T14-DOX	44 ± 4	-----	63 ± 2	5.7 ± 2.7
$CP6_{NBD}$-DOX	30 ± 3	-----	52 ± 2	3.7 ± 0.2
CP7-DOX	16 ± 3	-----	13 ± 1	-----
CP7T6-DOX	22 ± 2	-----	23 ± 0	-----
CP7T10-DOX	86 ± 1	33.4 ± 0.3	64 ± 7	21.8 ± 6.4
CP7T14-DOX	39 ± 9	-----	51 ± 4	8.2 ± 0.8

Table 3. In vitro activity in NCI/ADR-RES (doxorubicin-resistant ovarian cancer cell line) of the derivatives with different alkyl tail lengths after 48 or 72 hours. *Emax* corresponds to the maximum effect, which is the inhibition obtained at the higher concentration tested (100 μM). IC_{50} is the concentration at which a 50% growth inhibition is obtained. The IC_{50} was only calculated for those compounds with a *Emax* higher than 50%.

Moreover, the activity in the NCI/ADR-RES cells of the derivatives with the disulphide linker (**CP6-SS-DOX** and **CP6T10-SS-DOX**) was evaluate to investigate potential differences with respect to the maleimide linker designs (Table 4A). In particular, the trend was the same as the one for derivatives with the maleimide linker. The design without alkyl tail (**CP6-SS-DOX**) showed low inhibition after 72 hours of incubation. However, the derivative with the 10-carbon alkyl tail (**CP6T10-SS-DOX**) exhibited a maximum inhibition of 70% and a IC_{50} of 8.9 µM.

The biocompatibility of the peptides was also evaluated in a non-cancerous cell line (fibroblasts). In particular, the different peptides were incubated in a human embryonic lung cell line (MRC-5) for a period of 7 days (Table 4B). As expected, doxorubicin demonstrated pronounced cytotoxicity in these healthy cells. However, the binding of doxorubicin to the cyclic peptides is able to increase the IC_{50} in all the cases tested. This result suggests that the binding of doxorubicin to a cyclic peptide can increase the efficacy of the drug in cancer cells, while reducing the impact on healthy cells.

A)

	NCI/ADR-RES (72 h)	
Compound	*Emax* (%inhibition)	IC_{50} (µM)
CP6-SS-DOX	46 ± 6	-----
CP6T10-SS-DOX	70 ± 6	8.9 ± 3.9

B)

	MRC-5 (7 days)	
Compound	*Emax* (%inhibition)	IC_{50} (µM)
CP6-DOX	89 ± 3	6.5 ± 0.3
CP6T10-DOX	91 ± 2	2.2 ± 0.1
$CP6_{NBD}$-DOX	93 ± 1	4.7 ± 0.1
CP7-DOX	90 ± 3	3.7 ± 0.2
CP7T10-DOX	92 ± 3	4.3 ± 0.3
Linker-DOX (8)	89 ± 3	2.5 ± 0.2
DOX	87 ± 1	1.5 ± 0.1
Cisplatin	93 ± 3	6.2 ± 0.1

Table 4. (A) In vitro activity in NCI/ADR-RES (doxorubicin-resistant ovarian cancer cell line) after 72 hours of the cyclic peptide-doxorubicin conjugates with a disulphide linker. (B) *In vitro* activity in MRC-5 (human embryonic lung cell line) after 7 days of different cyclic peptide-doxorubicin conjugates. *Emax* corresponds to the maximum effect, which is the inhibition obtained at the higher concentration tested (100 µM). IC_{50} is the concentration at which a 50% growth inhibition is obtained. The IC_{50} was only calculated for those compounds with a *Emax* higher than 50%.

6.3.3.9. Mechanism of action studies

In a non-resistant cancer cell, doxorubicin is able to enter into the cell by diffusion through the membrane (Figure 113A).[264] Once in the cytoplasm, it binds to the proteasome due to its high affinity, specifically to the 20S proteasomal subunit, and is translocated to the nucleus through the nuclear pores. In the nucleus, the drug intercalates into the DNA due to a higher binding affinity than that for the proteasome, inducing the cell apoptosis. This intercalation results in the inhibition of the activity of the Topoisomerase II enzyme and the relaxation of the DNA double helix by causing torsional stress. In addition, it can form DNA-DOX adducts in the presence of formaldehyde by the formation of a covalent bond between the 3'NH_2 of DOX and

the N-2 amino group of guanines. Although the nuclear activity is the main cause of apoptosis, DOX can also bind to inner mitochondrial membrane phospholipids, inhibit the complexes I and II of the electron transport chain (ETC), induce the formation of reactive oxygen species (ROS) or impair mitochondrial and cellular Ca^{2+} hemostasis.[264] In contrast, drug-resistant cells usually overexpress protein transporters in their membrane that are able to expel the drug from the cell interior and prevent its pharmacological action. In particular, the doxorubicin-resistant NCI/ADR-RES cell line overexpresses the P-glycoprotein (P-gp), which is a transporter capable of expelling doxorubicin (Figure 113B).[274,275]

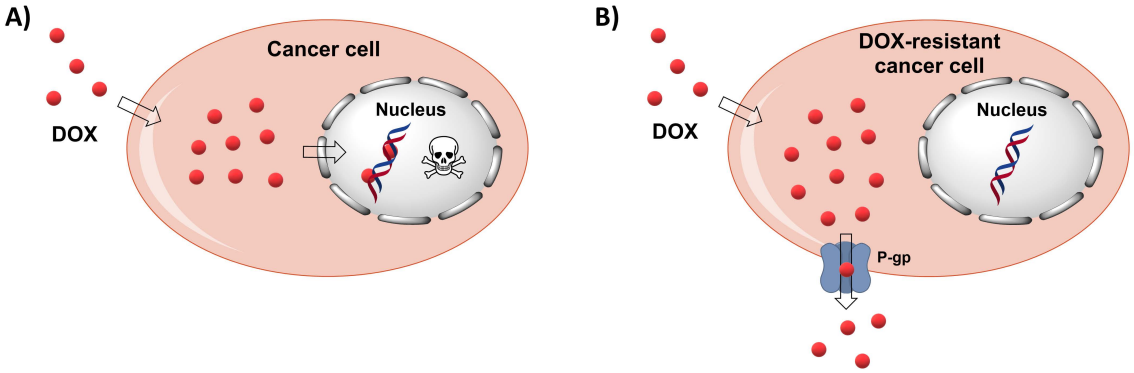

Figure 113. (A) Mechanism of DOX in a cancer cell by membrane diffusion and nuclear DNA intercalation. (B) DOX expulsion by the protein transporter P-gp in a drug-resistant cancer cell.

Therefore, we decided to study the cell internalization of the peptides in the NCI/ADR-RES cancer cells by confocal microscopy to understand the ability of the derivatives with the appropriate tail to overcome resistance. For this purpose, the cells were treated with **DOX**, **CP6-DOX**, **CP6T10-DOX**, **CP7-DOX** or **CP7T10-DOX** at 50 µM for 2 hours (Figure 114). As expected, **DOX** showed practically no internalization in this resistant cell line. In contrast, **CP6-DOX** showed internalization, but it appears to be mainly trapped in lysosomes and endosomes, as evidenced by the observed dotted pattern inside the cell. Also, **CP7-DOX** showed minimal cell internalization after 2 hours of incubation time. These findings are consistent with the observed low cytotoxicity of these two derivatives in this resistant cancer cell line. On the other hand, it was observed for **CP6T10-DOX** and **CP7T10-DOX** that the drug seems to be able to reach the nucleus of the cancer cell. Specifically, a notable accumulation of doxorubicin fluorescence was detected in the nuclear membrane. This ability to reach the nucleus is responsible for the efficacy of these derivatives in exerting their therapeutic effects.

USC
UNIVERSIDADE DE SANTIAGO DE COMPOSTELA

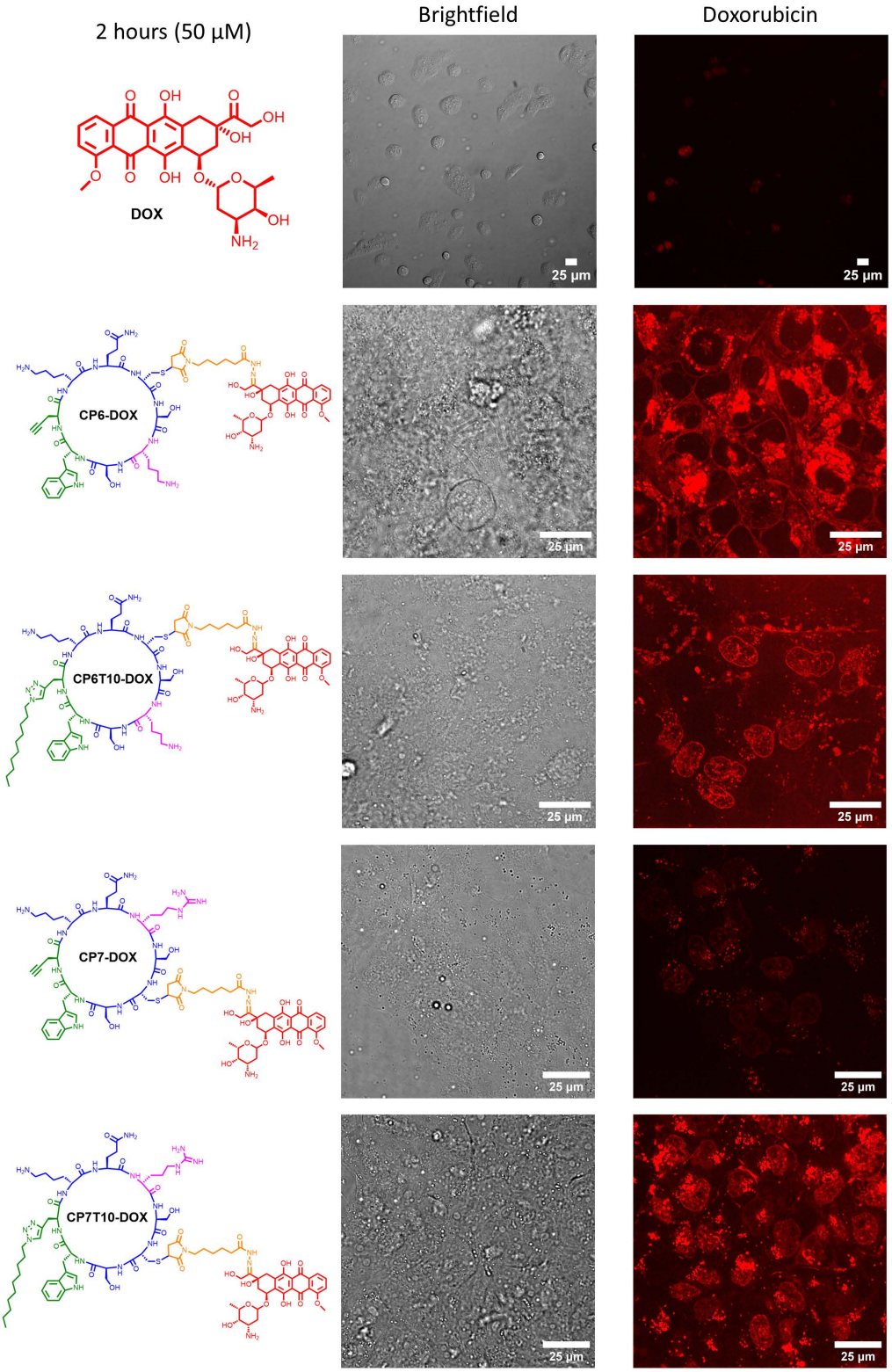

Figure 114. Confocal images of NCI/ADR-RES cells incubated during 2 hours with **DOX**, **CP6-DOX**, **CP6T10-DOX**, **CP7-DOX** or **CP7T10-DOX** at a concentration of 50 µM. Scale bars, 25 µm.

To study if **CP6-DOX** and **CP7-DOX** present a different cell distribution under other experimental conditions, we carried out a screening of concentrations and incubation times (Figure 115). However, in all cases for **CP6-DOX** again a dotted pattern in the cytoplasm was obtained even at high concentration (100 µM) and high incubation

time (48 h) (Figure 115A). This result suggests that this peptide derivative probably enters the cell by endocytosis, but is unable to undergo endosomal escape and remains trapped inside endosomes and lysosomes. Similarly, **CP7-DOX** exhibited enhanced internalization when subjected to a longer incubation period or higher concentration, but also remained predominantly trapped inside endosomes and lysosomes (Figure 115B). Consequently, neither of these two designs reaches the nucleus to induce the death of the cancer cells and they present a low toxicity in this resistant cancer cell line.

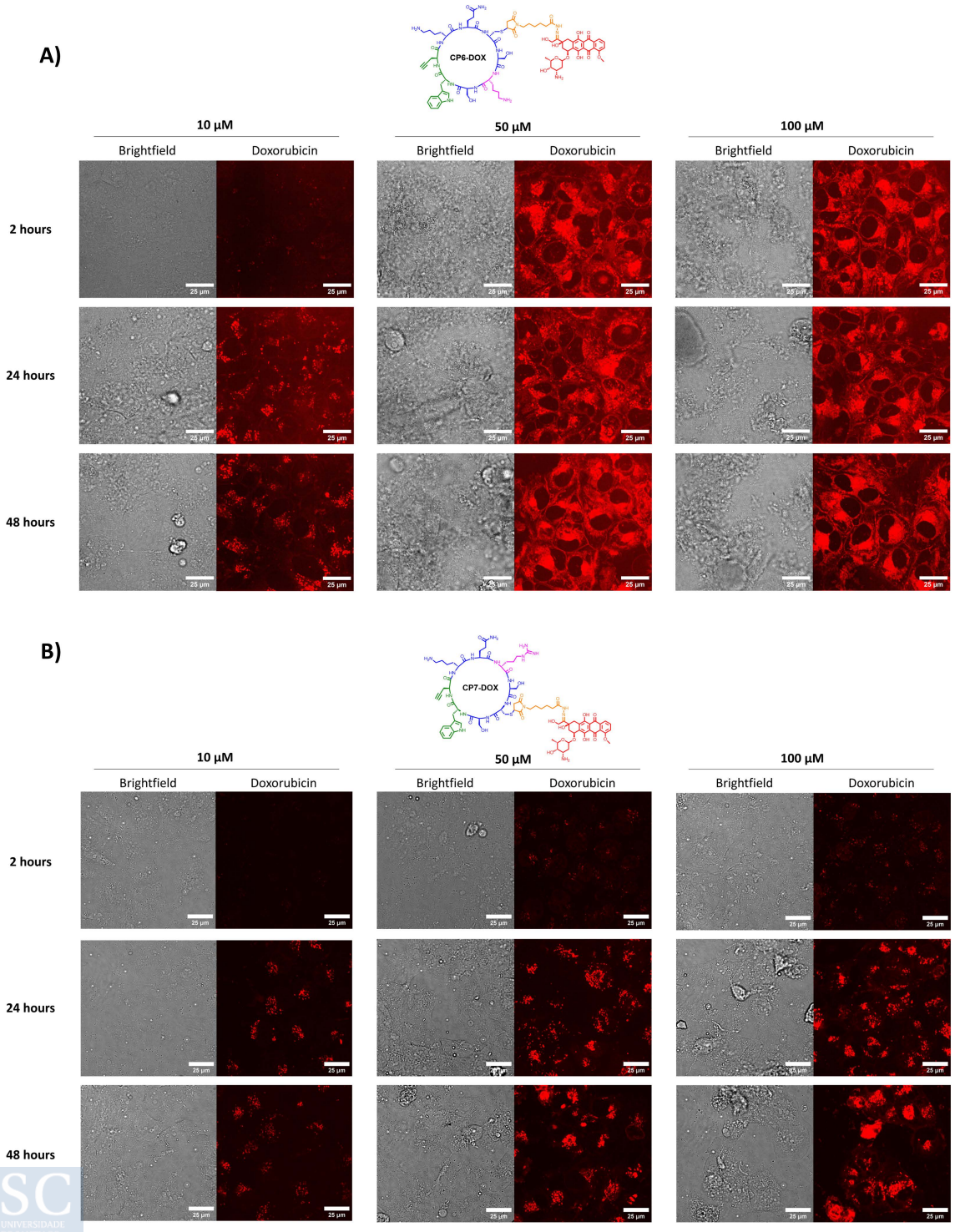

Figure 115. Confocal images of NCI/ADR-RES cells at different times and concentrations of incubation with (A) **CP6-DOX** or (B) **CP7-DOX**. Scale bars, 25 µm.

Next, colocalization experiments were carried out to confirm this different distribution of the drug when the cells were incubated with the different peptide derivatives (Figure 116). To this end, the cells were treated with **CP6-DOX**, **CP6T10-DOX**, **CP6T14-DOX**, **CP7-DOX**, **CP7T10-DOX** or **CP7T14-DOX** for 2 hours, followed by staining of the nuclei with Hoechst 33342. The analysis by confocal microscopy of the cells treated with the 10 or 14-carbon tail derivatives revealed colocalization in the nucleus between doxorubicin and Hoechst 33342 fluorescence. This result corroborates the ability of these cyclic peptides to facilitate the transport of the drug to the nucleus and overcome the resistance of this cell line. In contrast, no nuclear colocalization was observed again for peptides lacking a hydrocarbon tail.

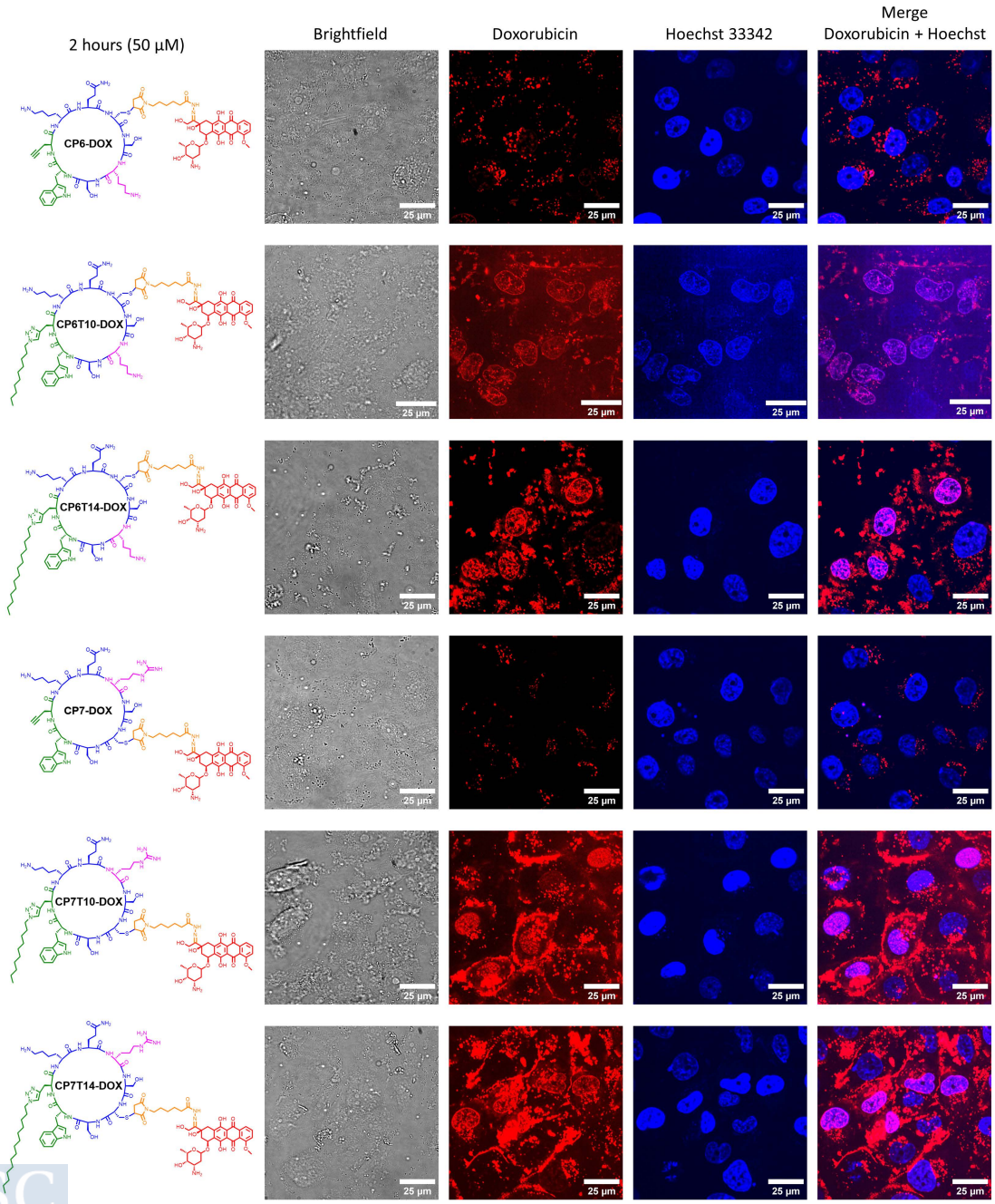

Figure 116. Colocalization by confocal microscopy of **CP6-DOX**, **CP6T10-DOX**, **CP6T14-DOX**, **CP7-DOX**, **CP7T10-DOX** or **CP7T14-DOX** with the NCI/ADR-RES nucleus after incubation for 2 hours at a concentration of 50 µM. The nuclei of the cells were stained with Hoechst 33342. Scale bars, 25 µm.

In order to study in a single experiment if the drug reaches the nucleus conjugated to the cyclic peptide or after hydrolysis of the hydrazone bond, **CP6$_{NBD}$-DOX** was prepared and evaluated (Figure 117). As already mentioned in Table 3, **CP6$_{NBD}$-DOX** showed an excellent activity after incubation for 72 hours, exhibiting the lowest IC_{50} among all peptides tested (3.7 µM). The green fluorescence of NBD allows us to monitor the distribution of the peptide by confocal microscopy, while the drug can be tracked by its red fluorescence. In particular, the fluorescence coincides at all times, which may suggest that the doxorubicin remains bound to the cyclic peptide without being released during all the pathway to the nucleus.

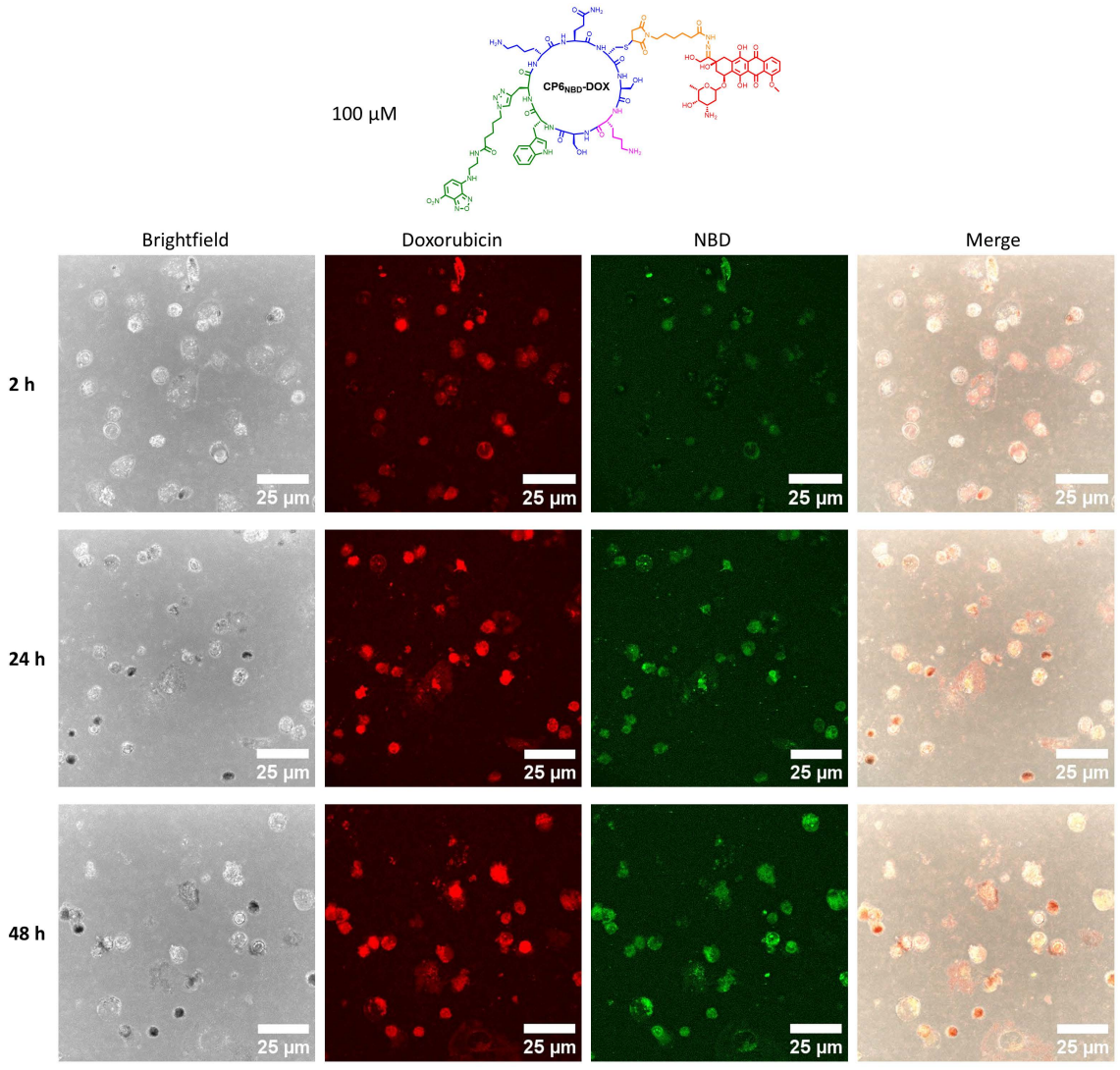

Figure 117. Confocal images of the colocalization of DOX and NBD fluorescence when the cells NCI/ADR-RES are treated with **CP6$_{NBD}$-DOX** at a concentration of 100 µM for 2, 24 or 48 hours. Scale bars, 25 µm.

To confirm if doxorubicin remains bound to the peptide backbone or if it is released under acidic conditions, a solution of **CP6-DOX** or **CP6T10-DOX** at 200 µM and pH 5.0 was prepared. The release was followed by MS for different time intervals (Figure 118). In both cases, a low drug release was observed after 72 hours, especially in

the case of **CP6T10-DOX**. This result suggests that the drug is only partially released and that both drug and peptide remain bound all the pathway to the cell nucleus.

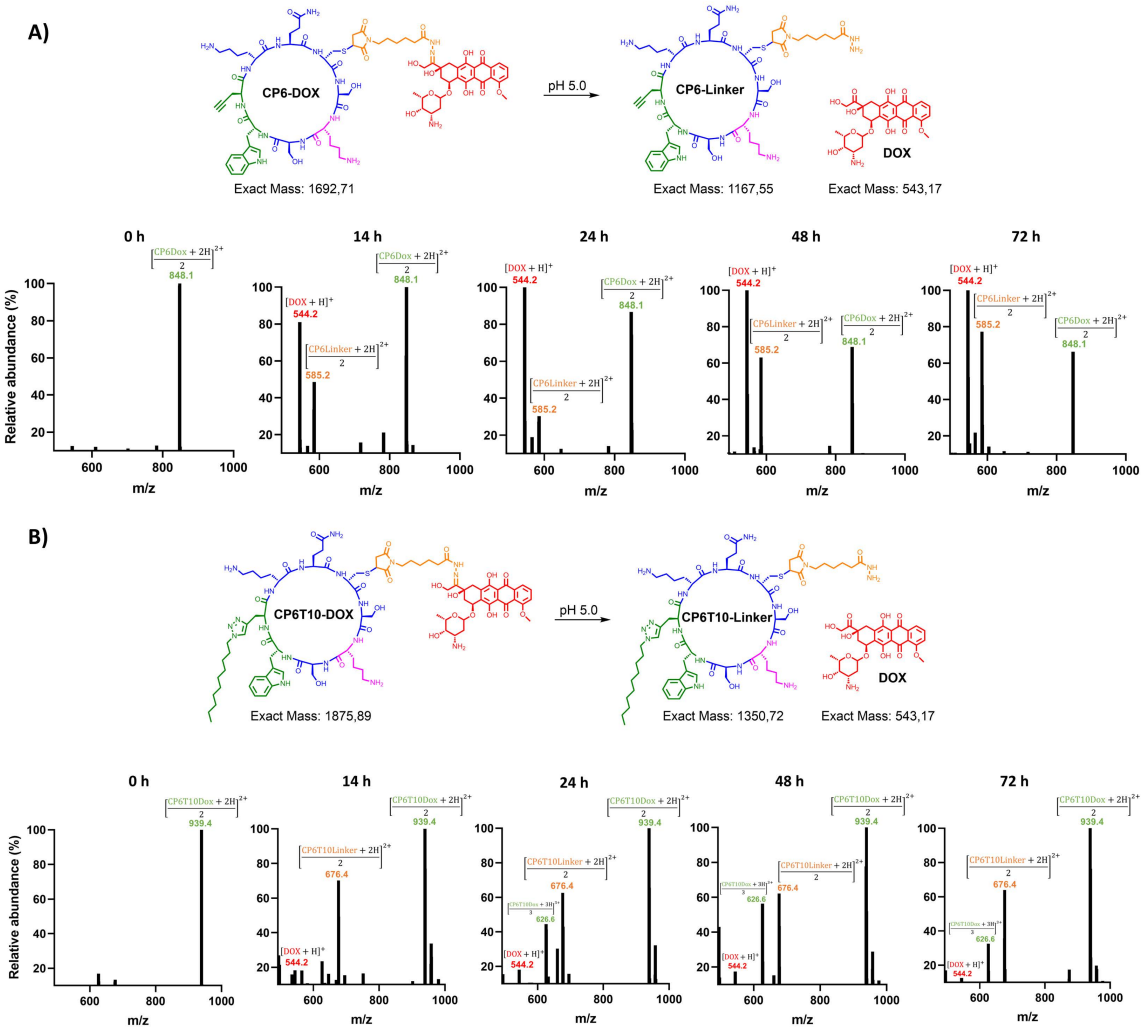

Figure 118. MS analysis of a sample incubated at pH 5.0 of (A) **CP6-DOX** or (B) **CP6T10-DOX** at 200 µM.

Finally, the internalization mechanism was evaluated. For this purpose, cells were incubated for 2 hours with **CP6$_{NBD}$-DOX**, followed by the staining of lysosomes and endosomes with Lysotracker (Figure 119A). In particular, some colocalization of the peptide fluorescence with endosomes and lysosomes was observed as denoted by the yellow dotted colour, which suggests a mechanism of entry by endocytosis. However, after this time much of the peptide is already located in the nucleus. To confirm this mechanism of entry by endocytosis, the internalization was quantified in the presence of endocytosis inhibitors by flow cytometry (Figure 119B). If the peptides enter the cell via endocytosis, a reduction in its internalization should be observed when the cells are treated with these inhibitors. For this purpose, the inhibitors Wortmannin, EIPA, Chlorpromazine and Dynasore were selected. In particular, Wortmannin is an inhibitor of macropinocytosis and clathrin-mediated endocytosis, EIPA inhibits the macropinocytosis, Chlorpromazine inhibits the clathrin-mediated endocytosis and

Dynasore inhibits all the dynamin-dependent pathways.[276] A reduction in the internalization was observed after 1 hour for all inhibitors, especially in the case of Wortmannin and Dynasore. A comparable reduction was observed by flow cytometry in the presence of 1% sodium azide, which blocks cellular energy-dependent processes and causes partial membrane depolarization.[276] These results, together with Lysotracker colocalization and the dotted pattern observed inside cancer cells by confocal microscopy, suggest a mechanism of internalization in which the endocytosis plays a key role. We speculate that this endocytosis pathway must avoid the action of the P-gp protein, which is responsible for doxorubicin resistance (Figure 119C). Furthermore, the incorporation of the hydrocarbon tail in the peptide design enables endosomal escape, facilitating the transport of the drug to the nucleus to treat these resistant cancer cells.

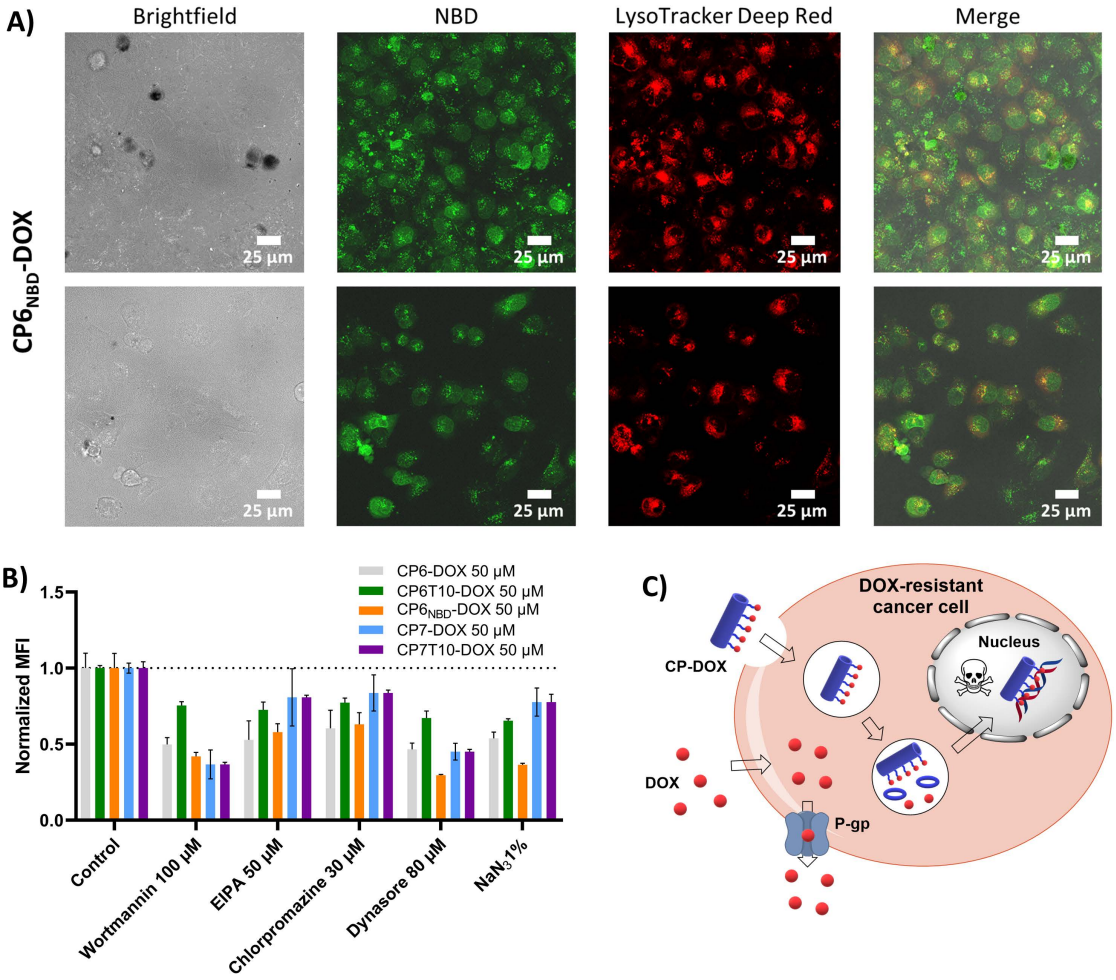

Figure 119. (A) Colocalization confocal images of NBD and LysoTracker Deep Red fluorescence when NCI/ADR-RES cells are treated with **CP6$_{NBD}$-DOX** at a concentration of 100 µM for 2 hours. Scale bars, 25 µm. (B) Internalization of 50 µM peptide samples after incubation for 1 hour when NCI/ADR-RES are treated with endocytosis inhibitors. The quantification was made by flow cytometry. MFI is the median fluorescence intensity. Cells treated only with the peptide and without inhibitors were used as controls. (C) Proposed mechanism of action of the cyclic peptides-doxorubicin conjugates studied in this section, in contrast to the outflow of DOX by the P-gp protein transporter.

[276] a) J. J. Rennick, A. P. R. Johnston, R. G. Parton, *Nat. Nanotechnol.* **2021**, *16*, 266-276; b) P. Lundin, H. Johansson, P. Guterstam, T. Holm, M. Hansen, U. Langel, S. E. Andaloussi, *Bioconjug. Chem.* **2008**, *19*, 2535-2542; c) G. Preta, J. G. Cronin, I. M. Sheldon, *Cell Commun. Signal.* **2015**, *13*, 24.

6.3.4. Conclusions

In this chapter, cyclic peptides capable of transporting the antitumour drug doxorubicin into cancer cells were developed. In particular, a variety of cyclic peptide-DOX conjugates were designed and synthesized using a hydrazone bond to attach the drug. The self-assembly properties were evaluated and, while **CP6-DOX** and **CP7-DOX** mainly form nanosheets at neutral pH, the equivalents with a 10-carbon tail (**CP6T10-DOX** and **CP7T10-DOX**) are able to assemble into nanotubes. All the designs incorporating doxorubicin demonstrated good activity against non-resistant cell lines (MCF-7 and NCI-H460). However, only the designs with the 10-carbon, 14-carbon or NBD tail showed good activity against the resistant cell line (NCI/ADR-RES). Endocytosis seems to be one of the main internalization pathways, but only the peptides with an appropriate tail are able to undergo endosomal escape in this resistant cell line, facilitating the transport of doxorubicin to the nucleus and enabling its therapeutic action.

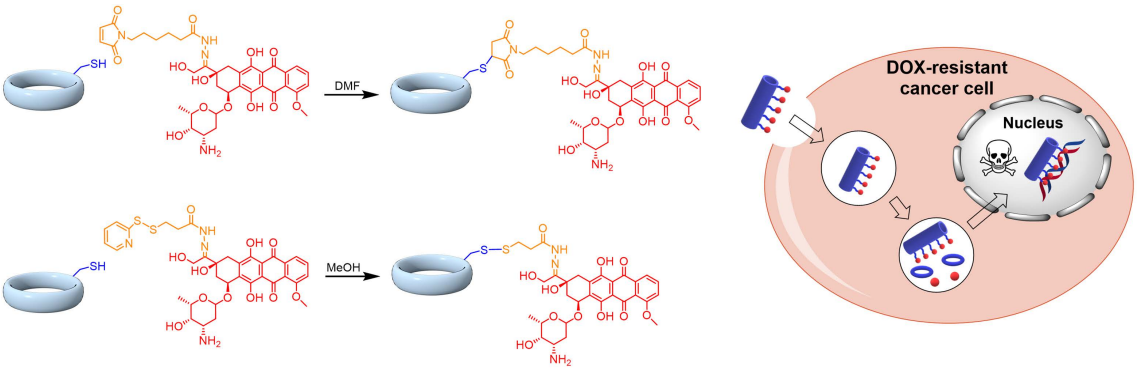

Figure 120. Cyclic peptide-DOX conjugates developed in this chapter for the transport of DOX inside cancer cells.

7. CONCLUSIONS

USC
UNIVERSIDADE
DE SANTIAGO
DE COMPOSTELA

This doctoral thesis has addressed the challenge of developing new strategies to control the assembly process of cyclic peptide nanotubes and to develop drug delivery applications for these supramolecular materials. To this end, different strategies have been proposed to incorporate stimuli-responsive components into peptide nanotubes in order to control their self-assembling properties or to develop new biomedical applications.

Firstly, we found that the orthogonal functionalization of a side chain of a cyclic peptide with an anthracene group can be used to change by light irradiation the shape of the resulting nanotube. In particular, the [4+4] cycloaddition of the anthracene moiety induces changes in the packing that force a bending motion of the nanotube.

Secondly, we proposed the incorporation of a photo-isomerizable unsaturated amino acid into the sequence of a cyclic peptide to control its assembly/disassembly process by appropriate light irradiation. As a consequence of the isomerization between the *Z*- and *E*-isomers, the peptide switches between a folded monomeric conformation and a planar conformation that assembles into nanotubes. The assembly process can be also triggered in the interior of microfluidic aqueous droplets and the nanotubes generated by the *E*-isomer presented fusogenic properties inducing the droplets fusion.

Thirdly, a library of cyclic peptide-doxorubicin conjugates incorporating an acid-labile hydrazone bond were prepared for the transport of doxorubicin into the interior of cancer cells. Interestingly, those designs with a hydrocarbon tail of the appropriate length were even able to overcome resistance and have activity in drug-resistant cells.

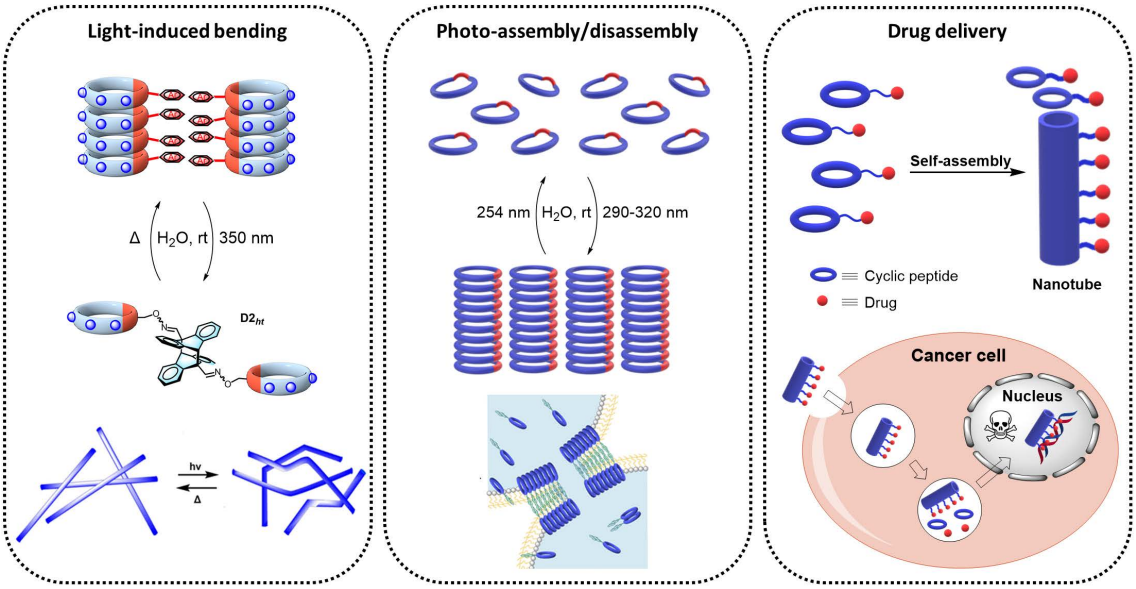

Figure 121. Schematic representation of the main conclusions of this doctoral thesis.

USC UNIVERSIDADE DE SANTIAGO DE COMPOSTELA

8. METHODOLOGY AND EXPERIMENTAL SECTION

USC
UNIVERSIDADE
DE SANTIAGO
DE COMPOSTELA

8.1. General remarks

8.1.1. Materials

Chemical reagents were purchased from Sigma-Aldrich, Iris Biotech, TCI, Alfa Aesar, Fischer Scientific, Carbolution and Sphere Fluidics. All solvents used were HPLC or synthesis grade. In the case of dry CH_2Cl_2, it was distilled over CaH_2.

NMR spectra were performed on a Bruker AVIII 500 MHz or a Varian 300 MHz spectrometer using the specified solvent, concentration and temperature. Chemical shifts (δ) are reported in parts per million (ppm) relative to TMS (δ = 0) or the solvent signals. ^{1}H NMR signals were assigned as singlet (s), doublet (d), triplet (t), multiplet (m), or broad (br). The coupling constants (*J*) are given in Hz. ^{1}H NMR spectra of the peptides were assigned using 2D COSY, TOCSY and ROESY. The water signal was suppressed when required. ^{13}C NMR spectra were assigned using Distortionless Enhancement by Polarization Transfer 135 (DEPT-135), HSQC and HMBC.

Peptide purification was performed on a semi-preparative HPLC Hitachi D-7000 equipped with a Phenomenex Luna 5 µm-C18 column and using H_2O (0.1% TFA) /MeCN (0.1% TFA) gradients as eluents.

Ultrahigh-pressure liquid chromatography coupled with mass spectrometry (uHPLC-MS) analyses were carried out on an Agilent Technologies 1260 Infinity II with a 6120 Quadrupole LC-MS using an Agilent SB-C18 column.

High Resolution Mass Spectrometry (HR-MS) was performed using ESI-MS in a Bruker MicroTof II mass spectrometer. Data are expressed in units of mass per unit of load (m/z).

FT-IR spectra were acquired in a PerkinElmer Spectrum Two ATR by placing the sample as a thin-film on the diamond plate (neat).

Fluorescence experiments were carried out in a Varian Cary Eclipse spectrophotometer equipped with a temperature-controlled cell chamber.

UV-Vis measurements were performed in a Jasco V-630 spectrophotometer or a Varian Cary 500 Scan UV-Vis spectrophotometer.

Circular dichroism measurements were acquired in a Jasco J-1100 CD Spectrometer with a Jasco MCB-100 Mini Circulation Bath.

STEM micrographs were obtained using a ZEISS FESEM ULTRA Plus with EDX operating at an extra high-tension of 20 kV. TEM images were acquired with a JEOL JEM-2010 equipment.

AFM micrographs were obtained using a Park Systems XE-100 in non-contact mode. ACTA tips were used (silicon tips, nominal values: spring constant = 40 N/m, frequency = 300 kHz, ROC less than 10 nm).

USC DE SANTIAGO

Epifluorescence measurements were performed on an Olympus BX51 microscope.

Confocal images were acquired on an Andor DragonFly spinning disc confocal setup mounted on a Nikon Eclipse Ti-E inverted microscope.

8.1.2. General methods

Thioflavin T (ThT) fluorescence assay

Thioflavin T (ThT)[231] fluorescence experiments were performed in a Varian Cary Eclipse spectrophotometer equipped with a temperature-controlled cell chamber. Spectra were recorded at 20°C in a Hellma® fluorescence quartz cuvette (10 x 4 mm) and using an excitation wavelength of 440 nm. Samples containing ThT (20 µM) and the corresponding peptide at the specified concentration range and buffer were prepared. The resulting solutions were allowed to equilibrate for 30 minutes before measuring the fluorescence.

Scanning Transition Electron Microscopy (STEM)

STEM micrographs were obtained using a ZEISS FESEM ULTRA Plus with EDX operating at an extra high-tension of 20 kV. Briefly, samples were prepared by deposition of 10 µL peptide solution at the appropriate pH and concentration over a 400-mesh carbon-coated copper grid (Electron Microscopy Sciences). After a few minutes, excess of sample was removed by blotting with a filter paper. Then, samples were stained with 10 µL of an aqueous solution of phosphotungstic acid (2% w/v) during 3 minutes and washed with 10 µL of Milli-Q H_2O for 1 minute. Samples were allowed to air-dry overnight before imaging.

Fluorescence assay

Fluorescence emission experiments were carried out with a Varian Cary Eclipse spectrophotometer equipped with a temperature-controlled cell chamber and by using a Hellma® fluorescence quartz cell (10 x 2 mm or 10 × 4 mm). Spectra were recorded at 20°C using specified excitation wavelength, pH and concentration. The solutions were allowed to equilibrate 30 minutes before measurements were performed.

To study the influence of pH, an aqueous solution of the CP was prepared at the desired concentration and the spectrum was acquired at native pH (pH∼4). For the rest of the experiment, pH was adjusted by titration with aqueous NaOH (0.1M).

USC UNIVERSIDADE DE SANTIAGO DE COMPOSTELA

For concentration-dependent fluorescence studies, solutions of the CP at the specified pH were prepared in the range of concentrations to be studied.

Circular dichroism

Circular dichroism (CD) measurements were acquired in a Jasco J-1100 CD Spectrometer equipped with a Jasco MCB-100 Mini Circulation Bath for controlling the temperature. Measurements were carried out in a 0.1 cm, 0.2 cm or 0.5 cm quartz cuvette at 20°C and the specified pH and concentration. The equipment was configured for 100 $nm.min^{-1}$ scanning speed, 1 second response time, 1 nm bandwidth and 0.2 nm data pitch. Each spectrum corresponds to the average of 10 scans and the solvent background was corrected.

Epifluorescence microscopy

Epifluorescence measurements were performed on an Olympus BX51 microscope at magnifications of 20x and 40x. Small imaging chambers were achieved by attaching an imaging spacer (Secure-Seal Imaging Spacers, 0.12 mm deep, Grace Bio-Labs) to a clean glass slide. Then, 10 µL of a CP aqueous solution at the appropriate pH and concentration was deposited on the glass, and the whole system was sealed with a second glass slide prior to microscopic visualization. All images were acquired at room temperature and analysed using ImageJ.[277]

Atomic Force Microscopy (AFM)

Atomic force microscopy measurements were performed at room temperature and ambient atmosphere using a Park Systems XE-100 in non-contact mode. ACTA tips were used (silicon tips, nominal values: spring constant = 40 N/m, frequency = 300 kHz, ROC less than 10 nm). Briefly, 10 µL of CP aqueous solutions at the specified pH and concentration were dropped on a silicon wafer or mica substrate. After 5 min, the sample was thoroughly washed with MilliQ-H_2O and dried under argon flow. Image analysis was carried out with Gwyddion.[278]

[277] a) C. A. Schneider, W. S. Rasband, K. W. Eliceiri, *Nat. Methods* **2012**, *9*, 671-675; b) J. Schindelin, I. Arganda-Carreras, E. Frise, V. Kaynig, M. Longair, T. Pietzsch, S. Preibisch, C. Rueden, S. Saalfeld, B. Schmid, J. Tinevez, D. J. White, V. Hartenstein, K. Eliceiri, P. Tomancak, A. Cardona, *Nat. Methods* **2012**, *9*, 676-682.
[278] D. Nečas, P. Klapetek, *Cent. Eur. J. Phys.* **2012**, *10*, 181-188.

8.2. Particular remarks

8.2.1. ANTHRACENE PHOTODIMERIZATION TO BEND SELF-ASSEMBLING CYCLIC PEPTIDE NANOTUBES

8.2.1.1. Methods

Nile red assay

Nile red (NR)[230] fluorescence emission spectra were acquired with a Varian Cary Eclipse fluorescence spectrophotometer provided with a temperature controller and using a Hellma® fluorescence quartz cell (10 × 2 mm). The spectra were collected from 570 to 800 nm using an excitation wavelength of 550 nm. Briefly, CP solutions in HEPES buffer (10 mM) at pH 7.0 and in the specified concentration range, were prepared and NR in MeOH (0.5 mM) was diluted 500-fold into solutions to obtain a final concentration of 1 µM. Therefore, all samples contain 0.2% MeOH content that is not expected to influence the self-assembly process. The solutions were allowed to equilibrate 1 hour before performing the measurements. The maximum emission intensity and the respective wavelength at maximum intensity were both reported as a function of the logarithm of the CP concentration.

Kinetic studies of dimerization

The photodimerization reaction of the anthracene groups was investigated by UV-Vis measurements using a Jasco V-630 spectrophotometer. The spectra were collected from 200 to 500 nm at T = 20°C. Briefly, **CP2** solutions at a concentration of 250 µM at acidic pH (1.85), native pH (4.95), and neutral pH (10 mM HEPES buffer, pH 7.0) were degassed with argon for 5 min and sealed in a quartz cuvette (0.2 cm) under argon atmosphere to avoid the formation of endoperoxide species during the irradiation experiments. After equilibration, the solutions were irradiated at 350 nm with a Xenon Light Source 300W Max-303 through a XUS0350 Shortpass Filter. The photodimerization reaction was monitored by UV-Vis measurements every 5-10 min. During the irradiation, the distance between the sample solutions and the light source was set to be around 5 cm. Product conversion was followed at different time intervals (1, 3, 5, 10, 20, 40 and 90 min) by taking aliquots that were analysed by HPLC. The same methodology was followed to study the photodimerization of **Ant1**.

Irradiation under photo-oxidative conditions

USC

The photodimerization reaction of the anthracene groups was investigated by UV-Vis measurements using a Jasco V-630 spectrophotometer. The spectra were collected from 200 to 500 nm at T = 20°C. An aqueous solution of **CP2** (250 µM) in HEPES

buffer (10 mM, pH 7.0) was degassed by bubbling oxygen for 10 min. Then, the resulting solution was sealed in a quartz cuvette under oxygen atmosphere. After equilibration for 20 min, the solution was irradiated at 350 nm with a Xenon Light Source 300W Max-303 through a XUS0350 Shortpass Filter for 90 min. The distance between the sample solutions and the light source was set to be around 5 cm. The product conversion was followed at different time intervals (1, 3, 5, 10, 20, 40 and 90 min) by taking aliquots that were analysed by HPLC.

Procedure of irradiation-dark cycles

The photodimerization reaction of the anthracene groups was investigated by UV-Vis measurements using a Jasco V-630 spectrophotometer. Aqueous solutions of **CP2** (250 µM) or **Ant1** (250 µM, 1:3 MeOH/aqueous media) in HEPES buffer (10 mM, pH 7.0) were degassed with argon for 10 min. Then, the resulting solutions were sealed in a quartz cuvette under argon atmosphere. After equilibration for 20 min, the solutions were irradiated at 350 nm with a Xenon Light Source 300W Max-303 through a XUS0350 Shortpass Filter for short periods of time. The distance between the sample solutions and the light source was set to be around 5 cm. The samples were initially irradiated for a short time (5-10 min) and after three cycles the irradiation times were doubled (10-20 min). After each irradiation cycle the solutions were maintained at room temperature in the dark at the UV-Vis spectrophotometer chamber for 40 min. The amount of converted material was followed by the disappearance of the absorption band at 386 nm by taking UV spectra every 2 min.

Photodimers thermal dissociation experiments

The thermal reversibility of the photocycloaddition reaction was monitored by UV-Vis measurements using a Varian Cary 500 Scan UV-Vis spectrophotometer equipped with a temperature controller. In these experiments, aqueous solutions of ***E,E*-D2$_{ht}$**, ***Z,Z*-D2$_{ht}$** and ***E,Z*-D2$_{ht}$** derivatives at a concentration of 250 µM were sealed in a 0.2 cm quartz cuvette under argon atmosphere and heated at 80°C for 800 min. Every 5 min, UV-Vis spectra were collected in the 200-500 nm spectral range at T = 80°C to follow the changes in the characteristic absorption bands of anthracene.

Monitoring of the irradiation with ThT

An aqueous solution of the corresponding cyclic peptide [**CP2P** (100 µM), **^{E}CP2azo-ox** (200 µM) or **^{E}CP2azo-am** (200 µM)] at neutral pH (10 mM HEPES, pH 7.0) was prepared and irradiated at 350 nm with a Xenon Light Source 300W Max-303 through a XUS0350 Shortpass Filter. A small irradiated aliquot (400 µL) was taken at different times and a solution of ThT (40 µM, 10 mM HEPES, pH 7.0, 400 µL) was added to each sample to obtain a final ThT concentration of 20 µM. Under these conditions,

the final concentration of CP was 50 µM for **CP2P** and 100 µM for **^{E}CP2azo-ox** or **^{E}CP2azo-am**. The ThT was added after the irradiation to avoid its photodegradation.[279] Finally, the fluorescence spectra were recorded with a Varian Cary Eclipse spectrophotometer by using an excitation wavelength of 440 nm and a Hellma® fluorescence quartz cuvette (10 x 4 mm).

Spontaneous reversibility of azobenzene derivatives

An aqueous solution of the corresponding CP [**^{E}CP2azo-ox** (250 µM) or **^{E}CP2azo-am** (250 µM)] at neutral pH (10 mM HEPES, pH 7.0) was degassed with argon for 10 min. Then, the solutions were sealed in a quartz cuvette under argon atmosphere and irradiated at 350 nm for 10 minutes with a Xenon Light Source 300W Max-303 through a XUS0350 Shortpass Filter. The irradiated samples were allowed to equilibrate in the dark for different hours and the ratio between the *E*- and *Z*-isomer was analysed by HPLC.

8.2.1.2. Solid-phase synthesis of CP1

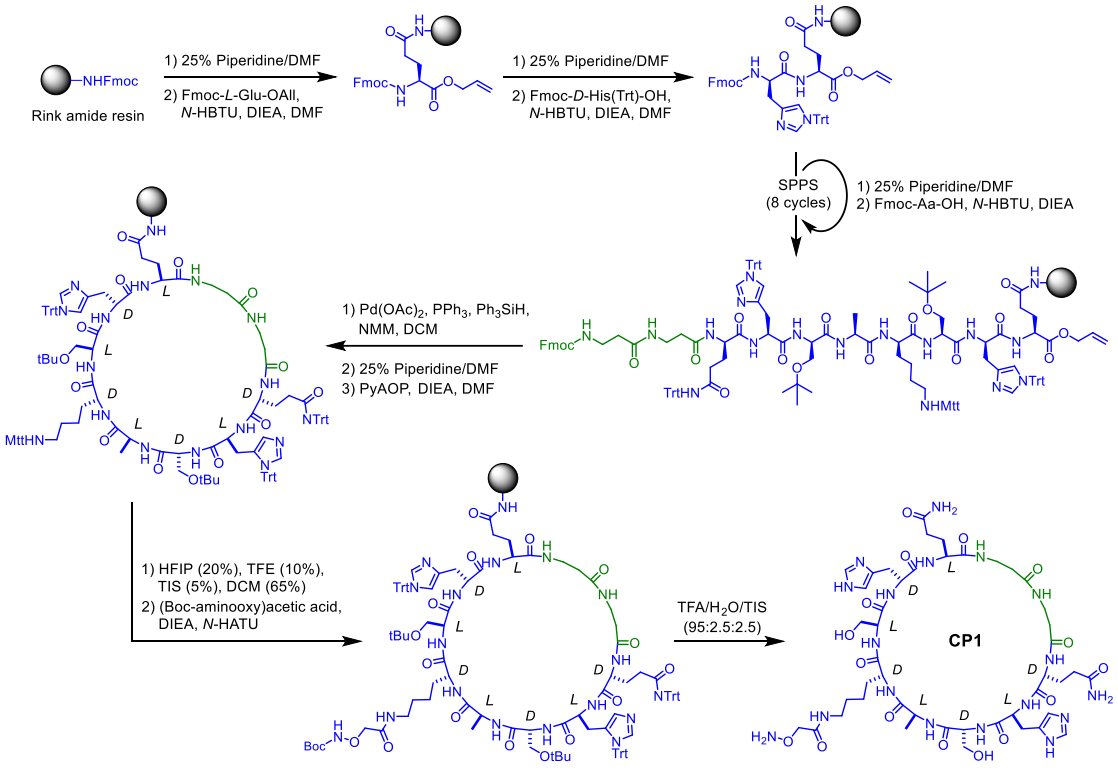

Figure 122. Solid phase peptide synthesis of **CP1**.

USC UNIVERSIDADE DE SANTIAGO DE COMPOSTELA

[279] J. C.-C. Hsu, E. H.-L. Chen, R. C. Snoeberger, F. Y. Luh, T.-S. Lim, C.-P. Hsu, R. P.-Y. Chen, *J. Phys. Chem. B* **2013**, *117*, 3459-3468.

The synthesis of **CP1** was performed on a Rink Amide resin (100-200 mesh; 0.7 mmol·g^{-1}) using manual solid phase synthesis according to the Fmoc-based strategy.[215,216,229] **CP1** was synthesized at a 250 µmol scale. Briefly, Fmoc-Rink Amide resin was swelled in DCM (4 mL) for 30 min in a peptide synthesis vessel and washed with DMF (6 x 4 mL) and DCM (6 x 4 mL). Fmoc group was removed by treating and shaking the resin with piperidine in DMF (25%, 4 mL) for 20 min. After DMF washings (3 x 4 mL), couplings were carried out using a solution of Fmoc-protected amino acid (3 equiv), *N*-HBTU (3 equiv), DIEA (6 equiv) in DMF (4 mL) under orbital shaking for 40 min at room temperature. Once the reaction was completed, the resin was washed with DMF (3 x 4 mL) and DCM (3 x 4 mL). Cycles of deprotection and coupling were repeated using identical conditions until the desired linear peptide was achieved. The last residue was maintained *N*-protected (Fmoc) to prevent side-reactions when deprotecting the *C*-terminal allyl group. The cyclization step started with the deprotection of the allyl protecting group by adding to the resin a degassed mixture of $Pd(OAc)_2$ (0.25 equiv), PPh_3 (1.25 equiv), *N*-methylmorpholine (7 equiv), and phenylsilane (7 equiv) in dry DCM (4 mL) that was previously stirred at room temperature until it took a bright-yellow colour. The reaction was shaken for 3-4 hours at room temperature. Afterwards, the resin was filtered and washed with DCM (3 x 4 mL), DMF (3 x 4 mL), sodium diethyldithiocarbamate in DMF (0.5%, 2 x 4 mL, 15 min), DMF (2 x 4 mL), DIEA in DMF (10%, 2 x 4 mL), DMF (3 x 4 mL). To remove the *N*-terminal Fmoc group, the resin was treated with a solution of piperidine in DMF (25%, 4 mL, 30 min) and, then, washed with DMF (6 x 4 mL), DIEA in DMF (5%, 3 x 4 mL), LiCl in DMF (0.8 M, 3 x 4 mL) and finally DMF (3 x 4 mL). Cyclization was carried out by treatment of the resin with a solution of PyAOP (4 equiv) and DIEA (6 equiv) in DMF (0.4 M, 4 mL) for 3 hours under orbital shaking. After filtration, the resin was washed with DMF (3 x 4 mL) and DCM (3 x 4 mL). This process was repeated twice to ensure complete cyclization.

The lysine side chain functionalization started with the selective deprotection of the 4-methyltrityl group (Mtt). For that, a freshly prepared mixture of DCM, HFIP, TFE and TIS (6.5:2:1:0.5; 3 x 4 mL) was added to the resin and the mixture was stirred for 2 hours. This process was repeated three times. After removal of the reaction mixture, the resin was washed with DCM (3 x 4 mL) and DMF (3 x 4 mL). Subsequently, a solution of (tert-butyloxycarbonylaminoxy)acetic acid (2.5 equiv) and *N*-HATU (2.5 equiv) in DMF (0.3 M, 4 mL) was added to the resin, followed by a dropwise addition of DIEA (5 equiv). The mixture was shaken for 30 min. Finally, the resin was thoroughly washed with DMF (3 x 4 mL).

Deprotection of CP side chains and cleavage was carried out by shaking the resin with a freshly prepared solution of TFA, H_2O and TIS (95:2.5:2.5, 1 mL per 100 mg resin) for 2 hours. The mixture was collected by filtration, concentrated with an argon steam, and added dropwise over an ice/cooled flask containing Et_2O (10 mL of Et_2O per 100 mg of resin). The precipitate was centrifuged (4000 rpm x 10 min) and the supernatant was discarded. After washing with Et_2O, the resulting residue was dried under reduced pressure and solubilized in MilliQ-H_2O with 0.1% TFA (0.1 mL/mg of crude). This solution

was purified by semipreparative RP-HPLC using a Phenomenex Luna C18 (2) 100Å column [gradient: H_2O (0.1% TFA)/MeCN (0.1% TFA), 97:3 → 97:3 (5 min); 97:3 → 85:15 (40 min), R_t = 24.0 min]. After freeze-drying of the proper fractions, **CP1** was obtained as a white solid with an overall yield of 23% (60 mg). The pure product was stored at -20°C until further use.

CP1: ^{1}**H NMR** (500 MHz, H_2O/D_2O) δ: 8.66 (d, *J* = 8.0 Hz, 1H, NH_{His}), 8.54 (s, 2H, CH_{Im}), 8.52 (d, *J* = 7.8 Hz, 1H, NH_{His}), 8.44-8.22 (m, 8H, NH, NH_{Im}), 8.12 (t, *J* = 6.4 Hz, 1H, $^{\varepsilon}NH_{Lys}$), 7.98 (t, *J* = 6.3 Hz, 1H, $NH_{\beta Ala}$), 7.88 (t, *J* = 6.1 Hz, 1H, $NH_{\beta Ala}$), 7.43 (bs, 2H, $NH_{2\text{-}Gln}$), 7.28 (s, 1H, CH_{Im}), 7.14 (s, 1H, CH_{Im}), 6.78 (d, *J* = 14.3 Hz, 2H, $NH_{2\text{-}Gln}$), 4.27 (m, 1H, CH_{Ala}), 4.17 (m, 1H, $^{\alpha}CH_{Gln}$), 3.80-3.68 (m, 6H, $CH_{2\text{-}Ser}$, CH_2ONH), 3.44-3.20 (m, 10H, $CH_{2\text{-}His}$, $^{\beta}CH_{2\text{-}\beta Ala}$), 3.16 (m, 2H, $^{\varepsilon}CH_{2\text{-}Lys}$), 3.08 (m, 1H, $^{\alpha}CH_{His}$), 3.04 (m, 1H, $^{\alpha}CH_{His}$), 2.40 (m, 2H, $^{\alpha}CH_{2\text{-}\beta Ala}$), 2.33 (t, *J* = 6.8 Hz, 2H, $^{\alpha}CH_{2\text{-}\beta Ala}$), 2.22-2.09 (m, 5H, $^{\gamma}CH_{2\text{-}Glu}$), 2.00 (m, 1H, $^{\beta}CH_{2\text{-}Glu}$), 1.89-1.70 (m, 5H, $CH_{2\text{-}Lys}$, $^{\beta}CH_{2\text{-}Glu}$), 1.62 (m, 1H, $CH_{2\text{-}Lys}$), 1.45 (m, 2H, $CH_{2\text{-}Lys}$), 1.32 (d, *J* = 7.3 Hz, $CH_{3\text{-}Ala}$), 1.28 (m, 2H, $CH_{2\text{-}Lys}$). ^{13}**C NMR** (H_2O/D_2O, 75 MHz, δ): 177.8 (CO), 177.6 (CO), 175.0 (CO), 174.2 (CO), 173.8 (CO), 173.6 (CO), 172.9 (CO), 172.1 (CO), 171.7 (CO), 171.4 (CO), 170.1 (CO), 163.1 (CO), 162.8 (CO), 133.9 (CH), 133.8 (CH), 128.6 (C), 117.5 (CH), 117.4 (CH), 115.2 (C), 72.7 (CH_2), 61.5 (CH_2), 61.3 (CH_2), 55.9 (CH), 55.8 (CH), 53.7 (CH), 53.6 (CH), 53.4 (CH), 52.8 (CH), 52.4 (CH), 50.1 (CH), 38.9 (CH_2), 36.2 (CH_2), 35.9 (CH_2), 35.4 (CH_2), 34.9 (CH_2), 31.2 (CH_2), 31.0 (CH_2), 30.7 (CH_2), 27.8 (CH_2), 26.8 (CH_2), 26.7 (CH_2), 26.5 (CH_2), 26.2 (CH_2), 22.4 (CH_2), 17.0 (CH_3). **ESI-MS** *m/z* (%): 1119.5 (47) $[M+H]^+$, 560.3 (100) $[M+2H]^{2+}$, 374.0 (8) $[M+3H]^{3+}$. **HRMS (ESI)** *m/z*: $[M+H]^+$ calculated for $C_{45}H_{71}N_{18}O_{16}$: 1119.5213, found 1119.5290. **FTIR (neat)**: ν = 3279.4 (amide A), 1653.6, 1647.0 (amide I), 1532.8 (amide II) cm^{-1}.

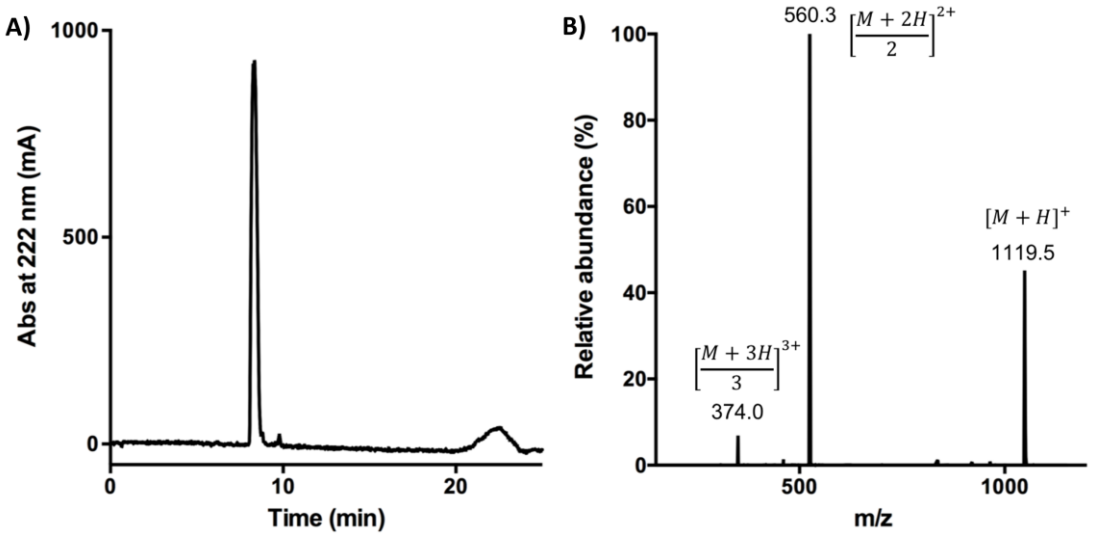

Figure 123. (A) **RP-uHPLC** of **CP1:** [Agilent SB-C18 column, H_20 (0.1% TFA)/MeCN (0.1% TFA), 100:0 → 100:0 (2 min) and 100:0 → 70:30 (19 min)] R_t = 8.4 min. (B) ESI-MS of the main peak.

USC UNIVERSIDADE DE SANTIAGO DE COMPOSTELA

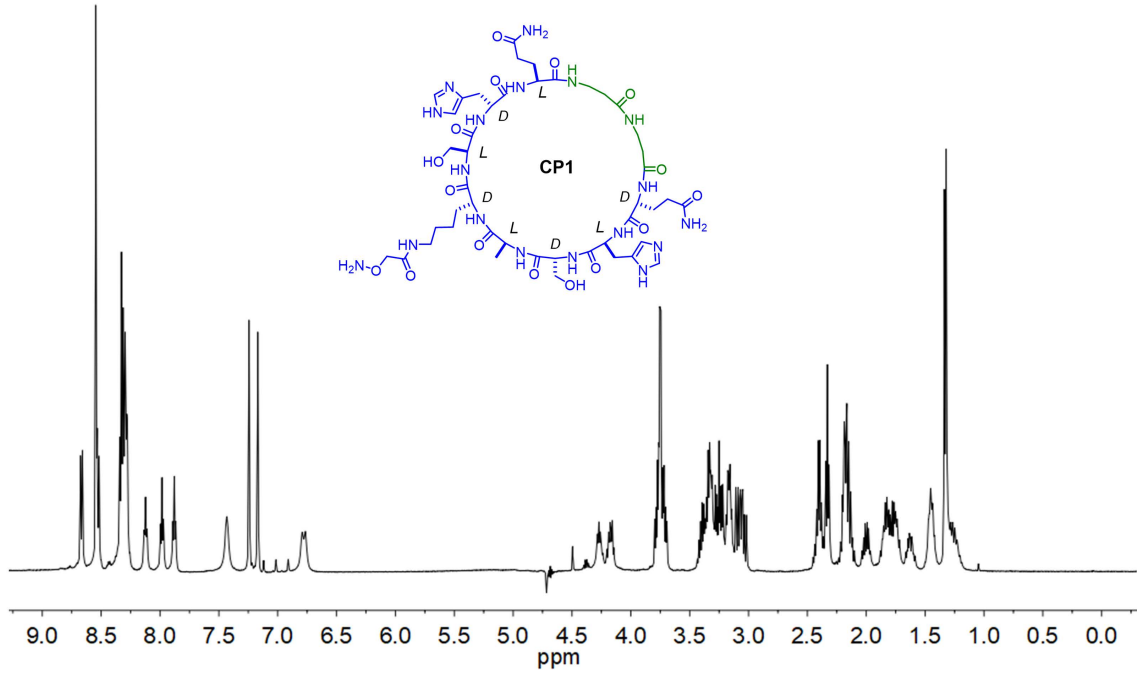

Figure 124. ^{1}H NMR of **CP1** at 3.0 mM (500 MHz, D_2O/H_2O, 298K).

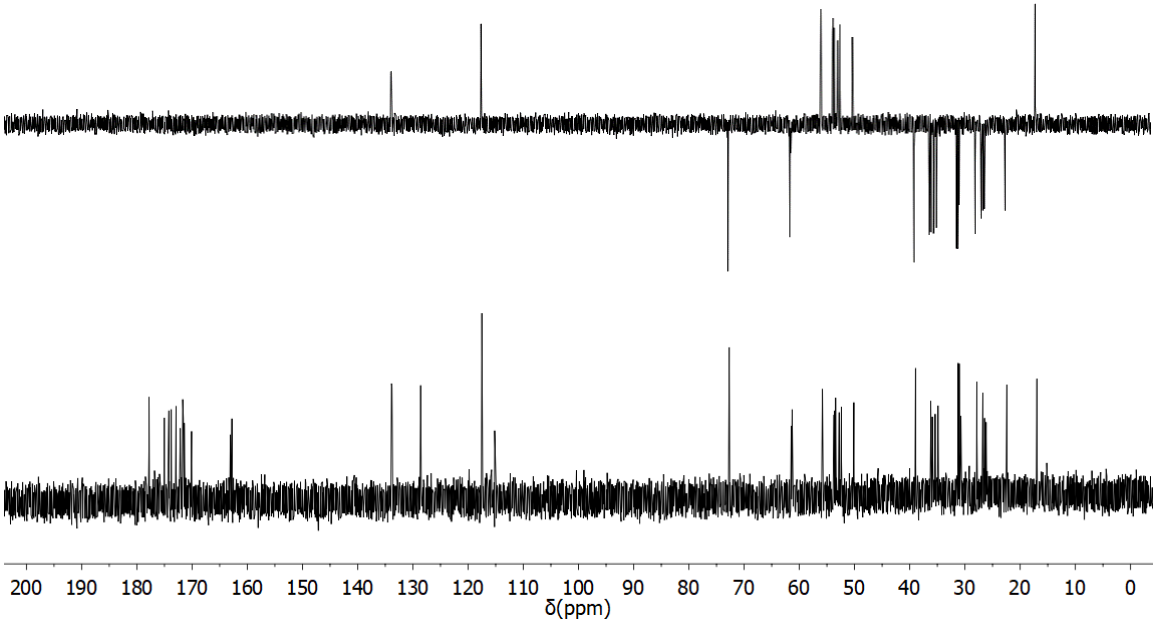

Figure 125. ^{13}C NMR (bottom) and DEPT-135 NMR (top) of **CP1** at 5.5 mM (500 MHz, D_2O/H_2O, 298K).

USC UNIVERSIDADE DE SANTIAGO DE COMPOSTELA

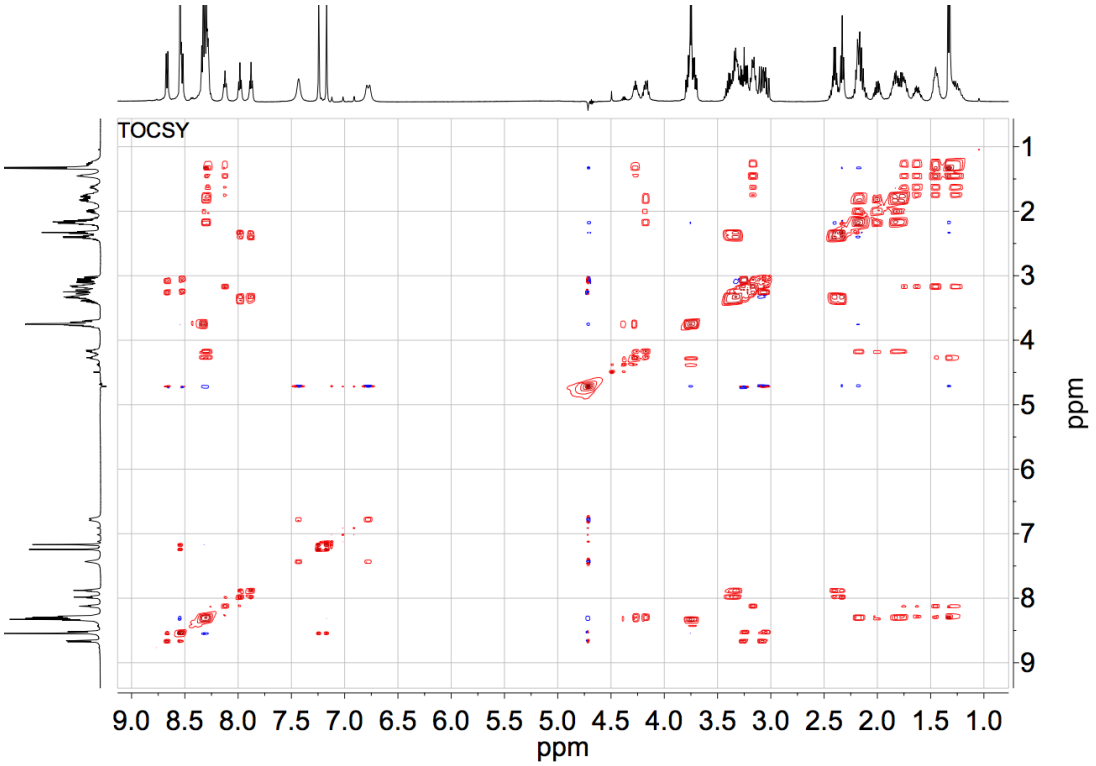

Figure 126. TOCSY of **CP1** at 3.0 mM (500 MHz, D_2O/H_2O, 298K).

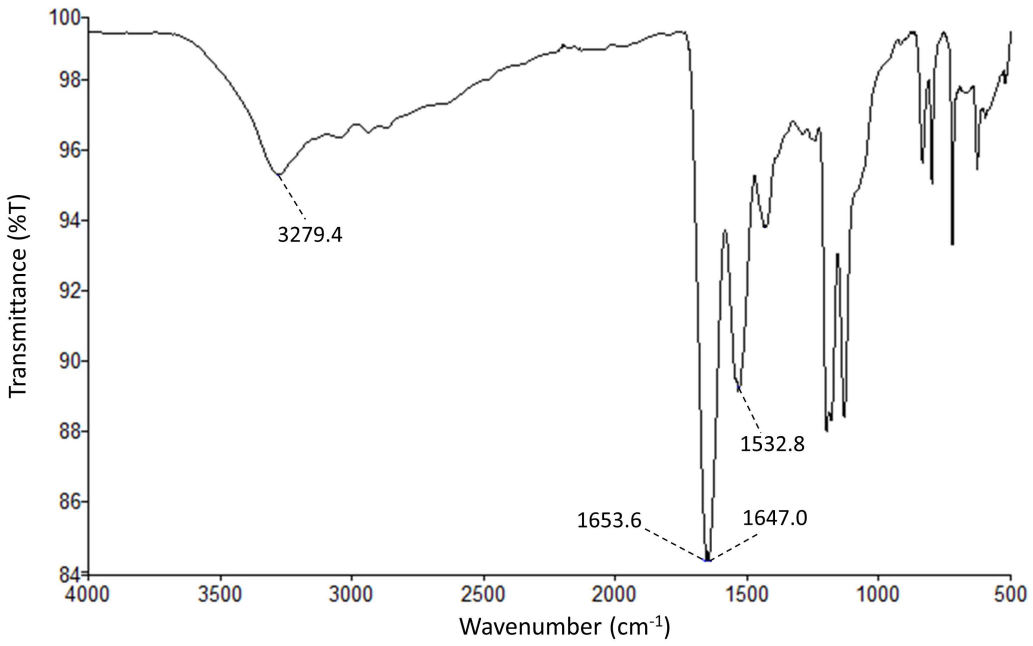

Figure 127. FT-IR spectrum of **CP1** (solid, 298 K).

8.2.1.3. Synthesis of ^{E}CP2

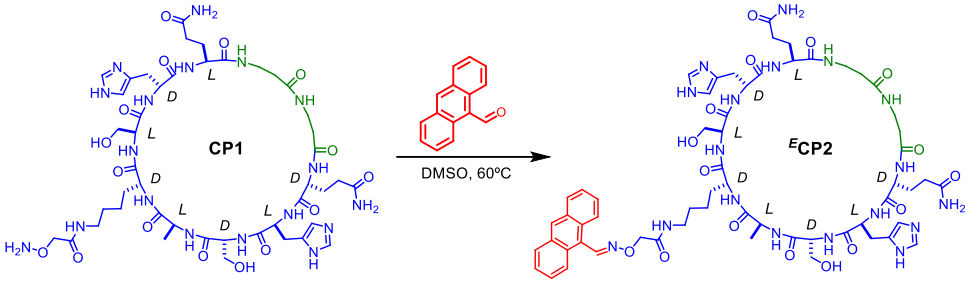

Figure 128. Synthesis of **^{E}CP2**.

CP1 (15.0 mg, 13.4 µmol) was dissolved in a solution of 9-anthracenecarboxaldehyde (3.3 mg, 16.1 µmol) in DMSO (100 µL) and the mixture was heated at 60°C for approximately 2 hours, until no starting substrate was detected by HPLC-MS analysis. The mixture was poured into an eppendorf containing cold diethyl ether (2 mL) and then powerfully shaken to obtain a yellow precipitate. After centrifugation, the organic phase was discarded. The resulting residue was sonicated for 15 minutes with fresh diethyl ether (2 mL), centrifugated and decantated. This step was repeated three times. The product was dried under reduced pressure to provide **^{E}CP2** as a yellow solid (16.2 mg, 93%).

^{E}CP2: **^{1}H NMR** (500 MHz, H_2O/D_2O) δ: 9.31 (s, 1H, CH_{ox}), 8.59 (d, *J* = 8.3 Hz, 1H, NH_{His}), 8.55 (s, 1H, $^{10}H_{Ant}$), 8.45 (s, 1H, CH_{Im}), 8.40 (s, 1H, CH_{Im}), 8.34 (d, *J* = 8.0 Hz, 1H, NH_{His}), 8.30-8.24 (m, 3H, $^{\alpha}NH_{Lys}$ and 2 H_{Ant}), 8.22 (d, *J* = 7.9 Hz, 1H, $^{\alpha}NH_{Gln}$), 8.20 (d, *J* = 6.8 Hz, 2H, NH_{Ser}, $^{\alpha}NH_{Gln}$), 8.16 (d, *J* = 6.2 Hz, 1H, NH_{Ala}), 8.09-8.00 (m, 3H, NH_{Ser}, 2 H_{Ant}), 7.95-7.84 (m, 2H, $^{\varepsilon}NH_{Lys}$, $NH_{\beta Ala}$), 7.74 (t, *J* = 6.2 Hz, 1H, $NH_{\beta Ala}$), 7.58-7.47 (m, 4H, H_{Ant}), 7.38 (brs, 2H, $NH_{2\text{-}Gln}$), 7.08 (s, 1H, CH_{Im}), 7.04 (s, 1H, CH_{Im}), 6.74 (d, *J* = 17.3 Hz, 2H, $NH_{2\text{-}Gln}$), 3.86 (m, 1H, $^{\alpha}CH_{Lys}$), 3.72-3.56 (m, 6H, $CH_{2\text{-}Ser}$, CH_2ONH), 3.34-3.10 (m, 7H, $CH_{2\text{-}Lys}$, $^{\beta}CH_{2\text{-}His}$, $^{\beta}CH_{2\text{-}\beta Ala}$), 3.06 (dd, *J* = 15.8 and 5.4 Hz, 1H, $^{\beta}CH_{2\text{-}His}$), 2.96-2.85 (m, 2H, $^{\beta}CH_{2\text{-}His}$), 2.38-2.18 (m, 2H, $^{\alpha}CH_{2\text{-}\beta Ala}$), 2.16 (t, *J* = 7.0 Hz, 2H, $^{\alpha}CH_{2\text{-}\beta Ala}$), 2.16-2.00 (m, 4H, $^{\gamma}CH_{2\text{-}Glu}$), 1.92 (m, 1H, $^{\beta}CH_{2\text{-}Glu}$), 1.80-1.65 (m, 3H, $^{\beta}CH_{2\text{-}Glu}$), 1.60-1.34 (m, 4H, $CH_{2\text{-}Lys}$), 1.17 (d, *J* = 7.6 Hz, 3H, $CH_{3\text{-}Ala}$), 1.18 (m, 2H, $CH_{2\text{-}Lys}$). **^{13}C NMR** (H_2O/D_2O, 75 MHz, δ): 177.7 (CO), 177.6 (CO), 175.8 (CO), 174.8 (CO), 174.0 (CO), 173.5 (CO), 172.8 (CO), 172.3 (CO), 172.0 (CO), 171.6 (CO), 171.2 (CO), 171.4 (CO), 171.3 (CO), 151.5 (CH), 133.7 (CH), 133.6 (CH), 130.9 (C), 130.0 (CH), 129.6 (C), 129.0 (CH), 128.5 (C), 128.4 (C), 127.4 (CH), 125.9 (CH), 124.5 (CH), 117.5 (C), 117.4 (CH), 117.3 (CH), 72.5 (CH_2), 61.3 (CH_2), 61.2 (CH_2), 55.9 (CH), 55.7 (CH), 53.8 (CH), 53.5 (CH), 53.4 (CH), 52.7 (CH), 52.3 (CH), 50.0 (CH), 38.9 (CH_2), 36.1 (CH_2), 35.7 (CH_2), 35.2 (CH_2), 34.7 (CH_2), 31.2 (CH_2), 30.9 (CH_2), 30.3 (CH_2), 28.2 (CH_2), 26.9 (CH_2), 26.6 (CH_2), 26.2 (CH_2), 26.1 (CH_2), 22.4 (CH_2), 16.9 (CH_3). **ESI-MS** *m/z* (%): 1307.6 (15) $[M+H]^+$, 654.4 (100) $[M+2H]^{2+}$, 436.9 (2) $[M+3H]^{3+}$. **HRMS (ESI)** *m/z*: $[M+H]^+$ calculated for $C_{60}H_{79}N_{18}O_{16}$: 1307.5921, found 1307.5916. **FTIR (neat)**: ν = 3292.5 (amide A), 1664.6, 1633.3 (amide I), 1539.4 (amide II) cm^{-1}.

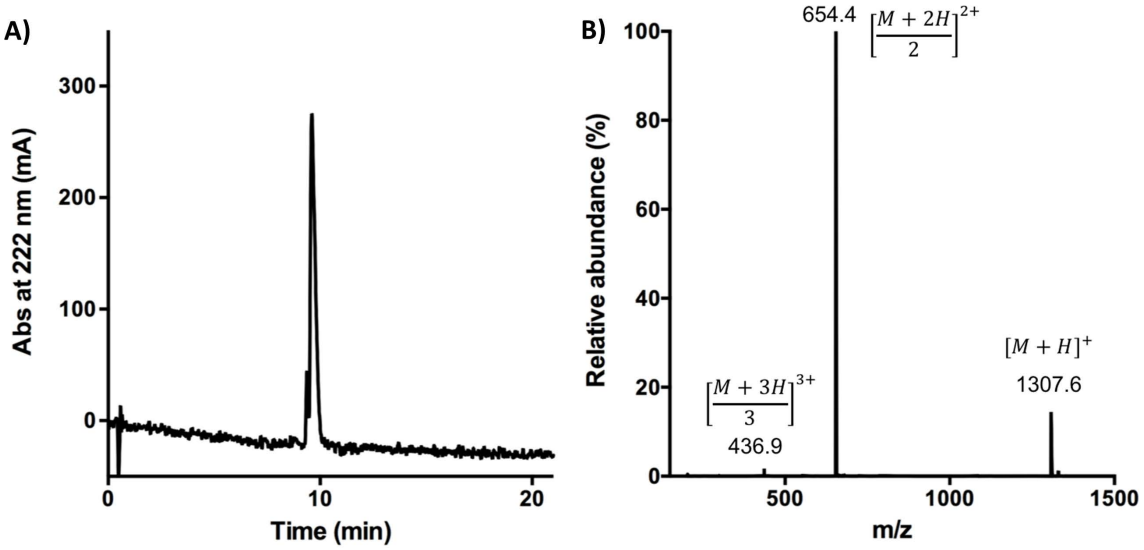

Figure 129. (A) **RP-uHPLC** of **^{E}CP2:** [Agilent SB-C18 column, H_20 (0.1% TFA)/MeCN (0.1% TFA), 80:20 → 80:20 (2 min) and 80:20 → 50:50 (19 min)] R_t = 9.6 min. (B) ESI-MS of the main peak.

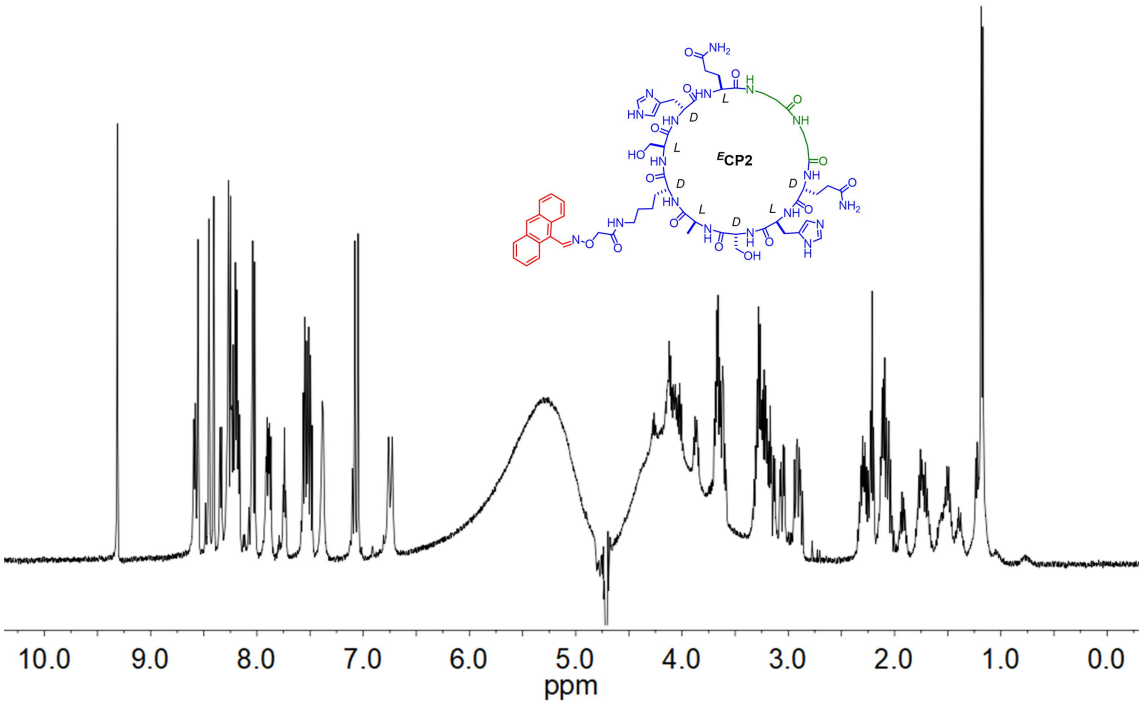

Figure 130. ^{1}H NMR of **^{E}CP2** at 1.3 mM (500 MHz, D_2O/H_2O, 298K).

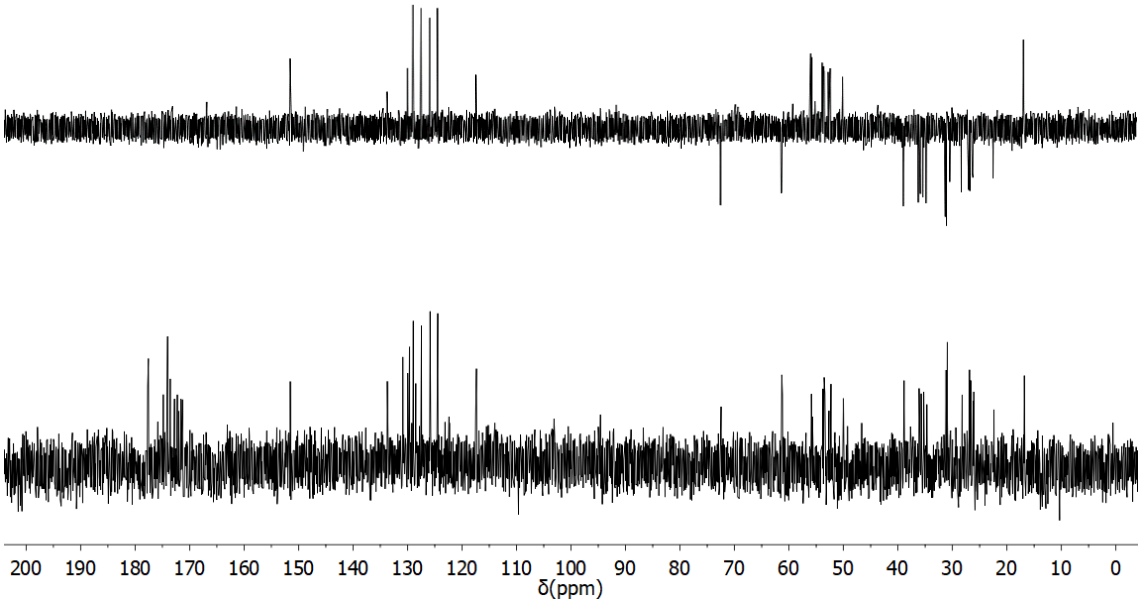

Figure 131. ^{13}C NMR (bottom) and DEPT-135 NMR (top) of **^{E}CP2** at 5.5 mM (500 MHz, D_2O/H_2O, 298K).

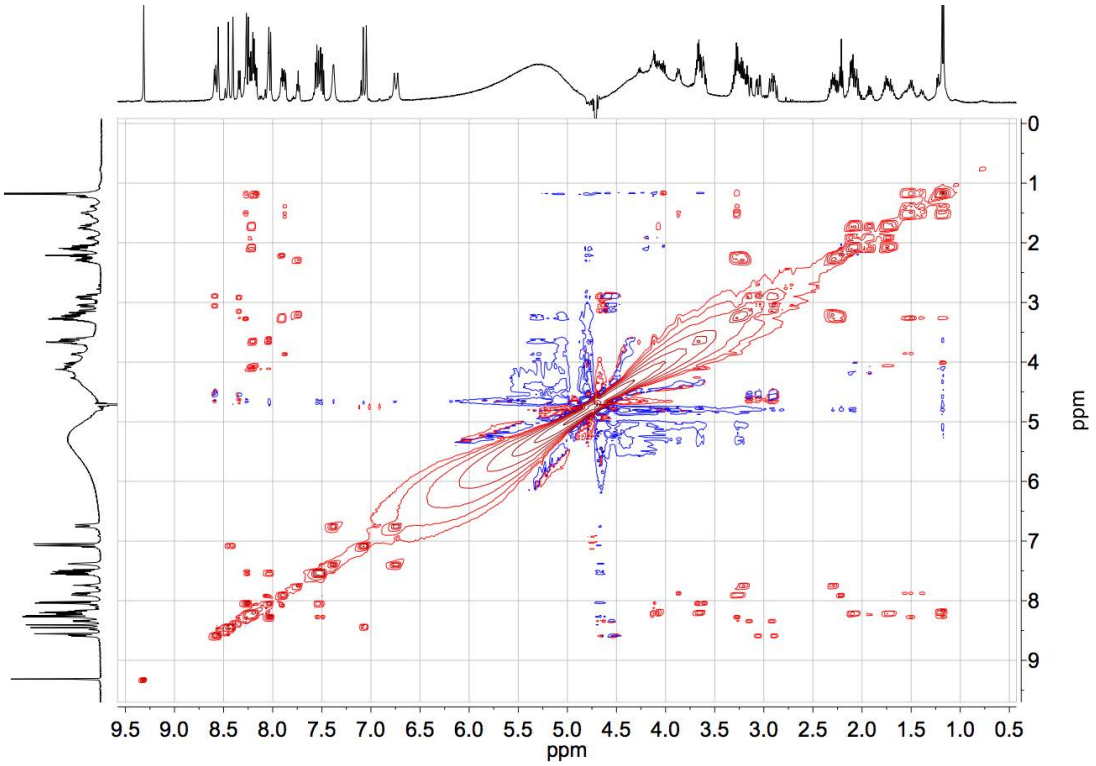

Figure 132. TOCSY of **^{E}CP2** at 1.3 mM (500 MHz, D_2O/H_2O, 298K).

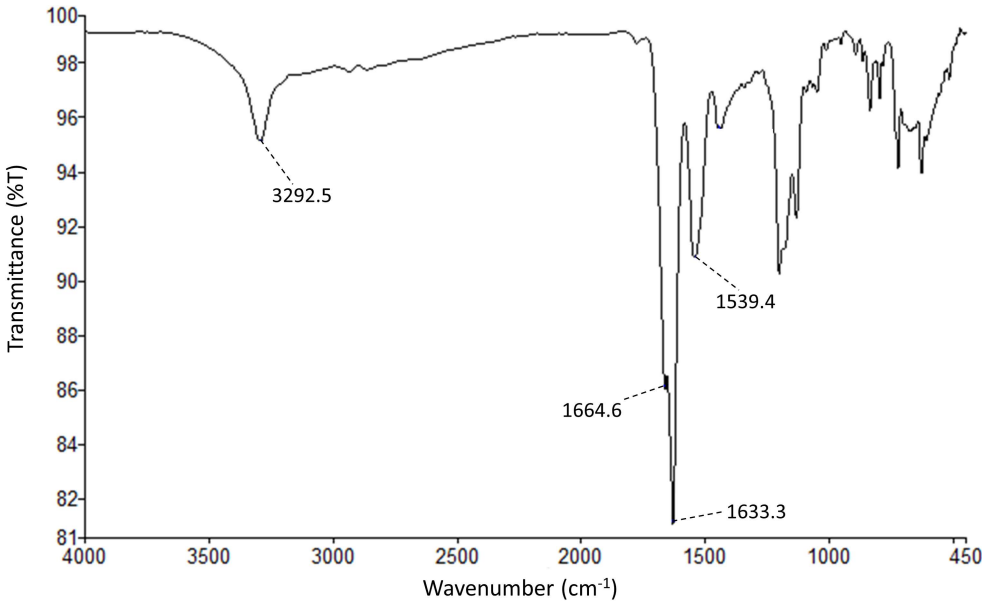

Figure 133. FT-IR spectrum of **^{E}CP2** (solid, 298 K).

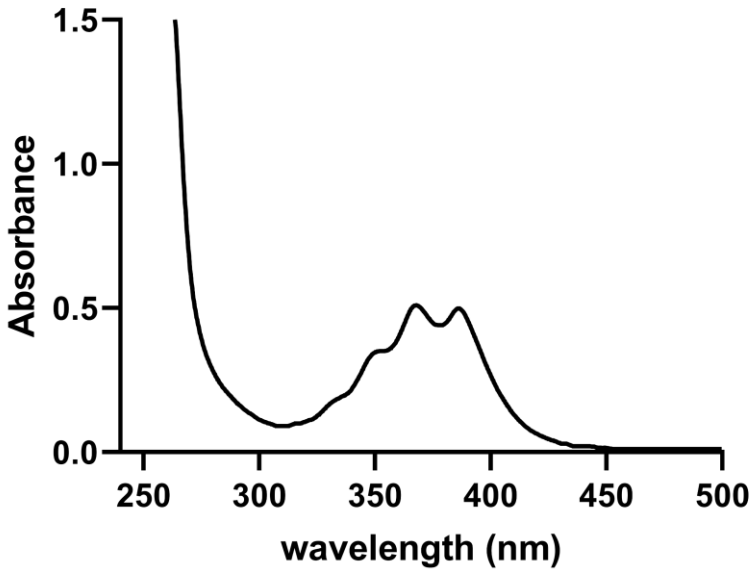

Figure 134. UV-Vis spectrum of an aqueous solution of **^{E}CP2** (100 µM).

USC UNIVERSIDADE DE SANTIAGO DE COMPOSTELA

8.2.1.4. Synthesis of ^{Z}CP2, *E*,*E*-D2$_{ht}$, *Z*,*Z*-D2$_{ht}$, and *E*,*Z*-D2$_{ht}$ derivatives

An aqueous solution of ^{E}**CP2** (400 µM) was neutralized with NaOH (0.1 M) to pH 7-8 and the resulting mixture was degassed with argon for 10 min. Then, the solution was sealed in a quartz cuvette under argon atmosphere to prevent the formation of endoperoxide species during the irradiation experiments. After equilibration for 20 min, the solutions were irradiated at 350 nm with a Xenon Light Source 300W Max-303 through a XUS0350 Shortpass Filter for 40 min. The distance between the sample solutions and the light source was set to be around 5 cm. The resulting mixture was collected and freeze-dried. The solid obtained (20 mg) was solubilized in MilliQ-H_2O with 0.1% TFA (0.05 mL/mg of crude) and purified by semipreparative RP-HPLC using a Phenomenex Luna C18 (2) 100Å column [gradient: H_2O (0.1% TFA)/MeCN (0.1% TFA), 90:10 → 76:24 (10 min); 76:24 → 65:35 (35 min), R_t (***Z*,*Z*-D2$_{ht}$**) = 13.71 min, R_t (***E*,*E*-D2$_{ht}$**) = 17.86 min, R_t (***E*,*E*-D2$_{ht}$**) = 18.43 min, R_t (^{Z}**CP2**) = 25.69 min, R_t (^{E}**CP2**) = 27.50 min]. After freeze-drying of the proper fractions, ***Z*,*Z*-D2$_{ht}$**, ***E*,*E*-D2$_{ht}$**, ***E*,*Z*-D2$_{ht}$**, ^{Z}**CP2** and ^{E}**CP2** were obtained with a yield of 5.5% (white solid, 2.2 mg), 9.6% (white solid, 3.8 mg), 17.1% (white solid, 6.8 mg), 13% (light yellow solid, 2.8 mg) and 14.1% (yellow solid, 3 mg), respectively. The pure products were stored at -20°C until further use.

^{Z}**CP2**: **^{1}H NMR** (500 MHz, H_2O/D_2O) δ: 8.60 (d, *J* = 8.0 Hz, 1H, NH_{His}), 8.48 (s, 1H, CH_{Im}), 8.45 (d, *J* = 8.0 Hz, 1H, NH_{His}), 8.43 (s, 1H, $^{10}H_{Ant}$), 8.42 (s, 1H, CH_{Im}), 8.38 (s, 1H, H_{ox}), 8.26 (d, *J* = 7.5 Hz, 1H, $^{\alpha}NH_{Gln}$), 8.21 ($d_{overlaped}$, *J* = 6.8 Hz, 4H, $^{\alpha}NH_{Gln}$, 2 NH_{Ser}, NH_{Ala}), 8.10 (d, *J* = 7.2 Hz, 1H, $^{\alpha}NH_{Lys}$), 7.97 (d, *J* = 9.3 Hz, 2H, 2 H_{Ant}), 7.92 (t, *J* = 6.3 Hz, 1H, $NH_{\beta Ala}$), 7.82-7.74 (m, 3H, $NH_{\beta Ala}$, 1 H_{Ant}), 7.54-7.44 (m, 4H, H_{Ant}), 7.39 (brs, 2H, $NH_{2\text{-}Gln}$), 7.09 (s, 2H, CH_{Im}), 6.90 (t, *J* = 6.3 Hz, 1H, $^{\varepsilon}NH_{Lys}$), 6.74 (d, *J* = 13.4 Hz, 2H, $NH_{2\text{-}Gln}$), 4.28-4.01 (m, 3H, $^{\alpha}CH_{Gln}$, $^{\alpha}CH_{Lys}$, $^{\alpha}CH_{His}$), 3.72 (m, 1H, $^{\beta}CH_{2\text{-}Ser}$) 3.68-3.58 (m, 3H, $^{\beta}CH_{2\text{-}Ser}$), 3.38-2.84 (m, 10H, $CH_{2\text{-}Lys}$, $CH_{2\text{-}His}$, $^{\beta}CH_{2\text{-}\beta Ala}$), 2.32 (m, 2H, $^{\alpha}CH_{2\text{-}\beta Ala}$), 2.28 (m, 2H, $^{\alpha}CH_{2\text{-}\beta Ala}$), 2.18-2.00 (m, 4H, $CH_{2\text{-}Gln}$), 1.64 (m, 1H, $CH_{2\text{-}Lys}$), 1.48 (m, 1H, $CH_{2\text{-}Lys}$), 1.22 (d, *J* = 7.4 Hz, 3H, $CH_{3\text{-}Ala}$), 1.18 (m, 2H, $^{\delta}CH_{2\text{-}Lys}$), 1.00 (m, 2H, $^{\gamma}CH_{2\text{-}Lys}$). **^{13}C NMR** ($D_2O$, 75 MHz, δ): 177.7 (CO), 177.5 (CO), 175.0 (CO), 174.1 (CO), 174.0 (CO), 173.6 (CO), 172.8 (CO), 172.1 (CO), 171.7 (CO), 171.5 (CO), 171.3 (CO), 163.1 (CO), 162.8 (CO), 150.4 (CH), 133.8 (CH), 130.7 (C), 129.1 (CH), 129.0 (CH), 128.7 (C), 128.6 (C), 127.7 (C), 127.3 (CH), 126.0 (CH), 124.7 (CH), 124.6 (CH), 117.5 (C), 117.4 (CH), 117.3 (CH), 72.4 (CH_2), 61.3 (CH_2), 61.2 (CH_2), 55.9 (CH), 55.7 (CH), 53.8 (CH), 53.6 (CH), 53.5 (CH), 52.7 (CH), 52.3 (CH), 50.1 (CH), 38.6 (CH_2), 36.1 (CH_2), 35.8 (CH_2), 35.3 (CH_2), 34.7 (CH_2), 31.2 (CH_2), 30.9 (CH_2), 30.5 (CH_2), 27.6 (CH_2), 26.8 (CH_2), 26.6 (CH_2), 26.3 (CH_2), 26.1 (CH_2), 22.2 (CH_2), 16.9 (CH_3). **ESI-MS** *m/z* (%): 1307.5 (13) $[M+H]^+$, 654.5 (100) $[M+2H]^{2+}$. **HRMS (ESI)** *m/z*: $[M+H]^+$ calculated for $C_{60}H_{79}N_{18}O_{16}$: 1307.5921, found 1307.5916. **FTIR (neat)**: ν = 3279.7 (amide A), 1638.5 (amide I), 1540.7 (amide II) cm^{-1}.

USC UNIVERSIDADE DE SANTIAGO DE COMPOSTELA

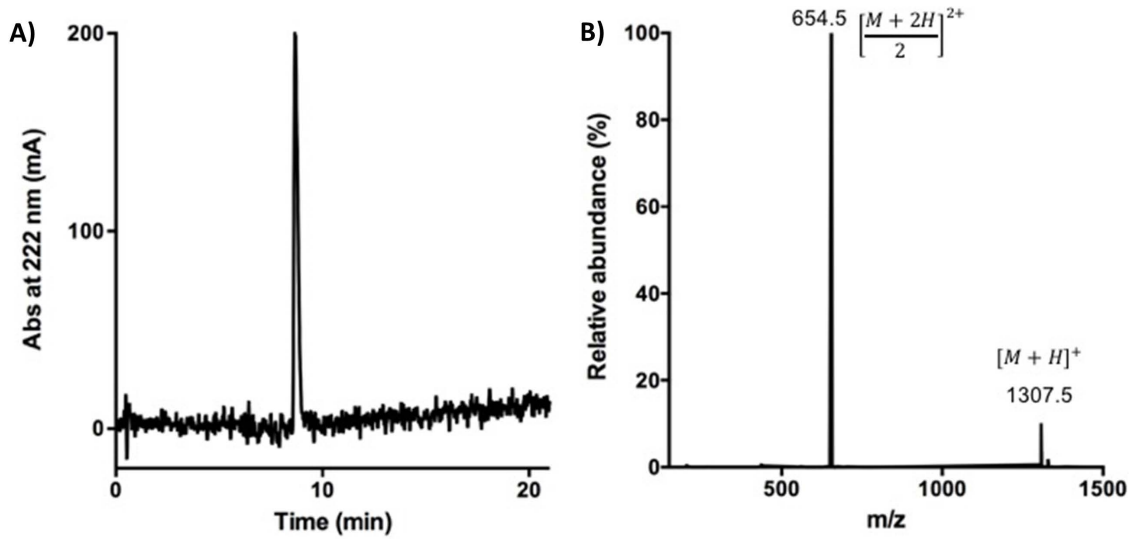

Figure 135. (A) **RP-uHPLC** of **^{z}CP2:** [Agilent SB-C18 column, H_20 (0.1% TFA)/MeCN (0.1% TFA), 80:20 → 80:20 (2 min) and 80:20 → 50:50 (19 min)] R_t = 8.59 min. (B) ESI-MS of the main peak.

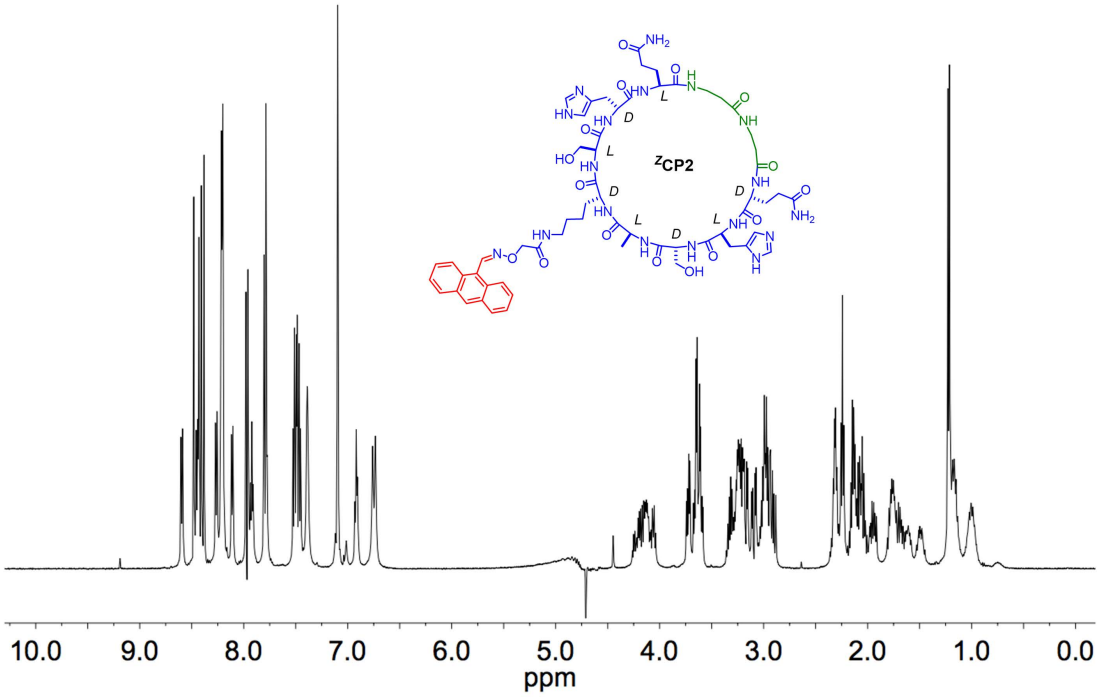

Figure 136. ^{1}H NMR of **^{z}CP2** at 2.5 mM (500 MHz, D_2O/H_2O, 298K).

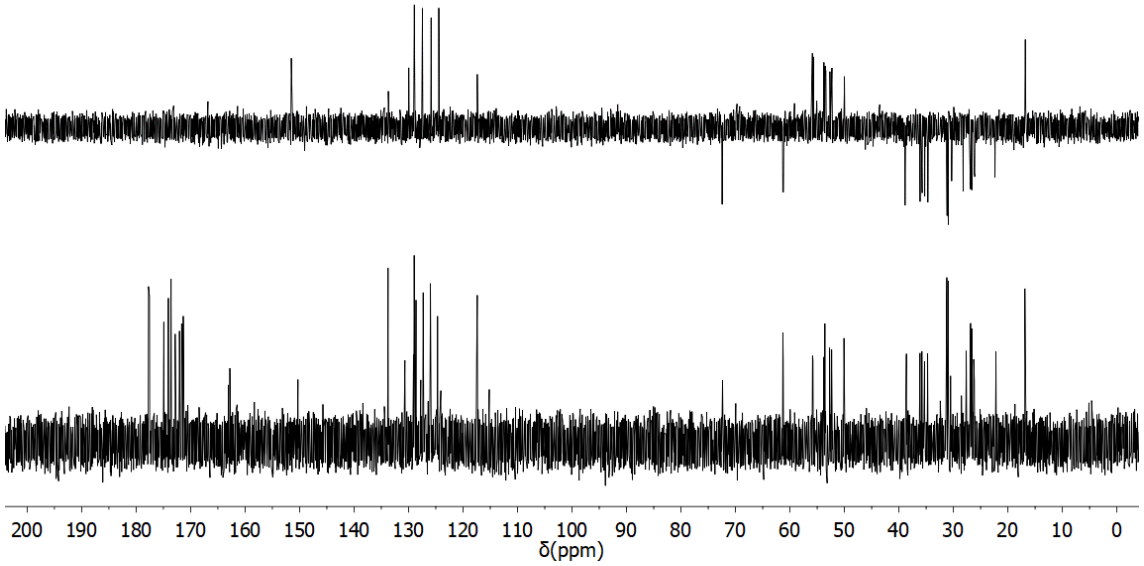

Figure 137. ^{13}C NMR (bottom) and DEPT-135 NMR (top) of **^{Z}CP2** at 2.6 mM (500 MHz, D_2O/H_2O, 298K).

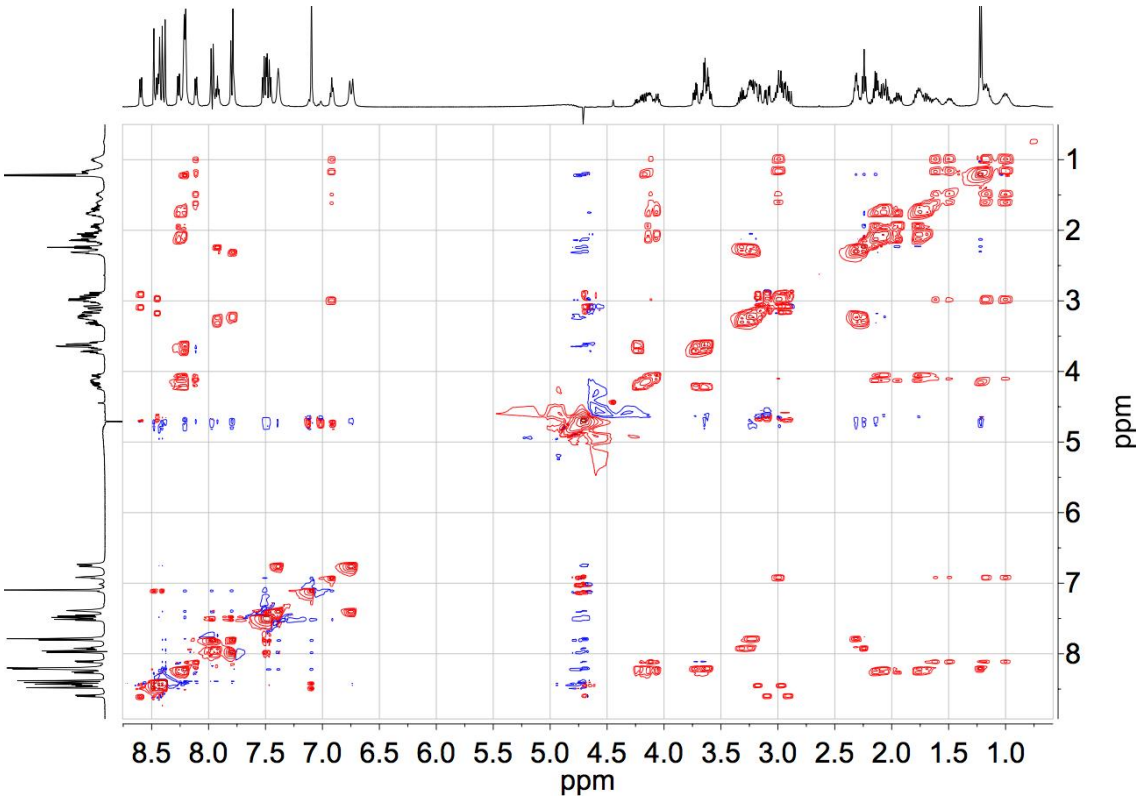

Figure 138. TOCSY of **^{Z}CP2** at 2.5 mM (500 MHz, D_2O/H_2O, 298K).

USC
UNIVERSIDADE DE SANTIAGO DE COMPOSTELA

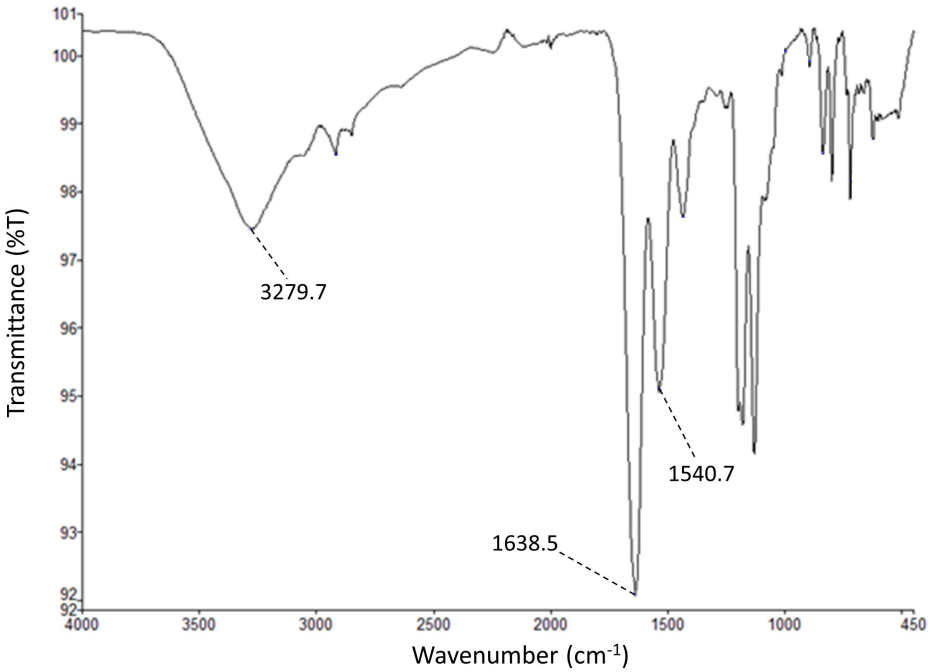

Figure 139. FT-IR spectrum of ^{Z}**CP2** (solid, 298 K).

***Z,Z*-D2$_{ht}$**: **^{1}H NMR** (500 MHz, H_2O/D_2O) δ: 8.68 (d, *J* = 7.9 Hz, 2H, NH_{His}), 8.58-8.45 (m, 6H, NH_{His}, CH_{Im}), 8.34-8.25 ($d_{overlapped}$, 10H, 2 NH_{Ser}, 4 NH_{Gln}, 2 NH_{Ala}, 2 $^{\alpha}NH_{Lys}$), 8.18-8.13 (m, 4H, $NH_{Ser,}$ $^{\varepsilon}NH_{Lys}$), 8.08 (s, 2H, H_{ox}), 7.98 (t, *J* = 6.3 Hz, 2H, $NH_{\beta Ala}$), 7.87 (t, *J* = 6.2 Hz, 2H, $NH_{\beta Ala}$), 7.42 (br, 4H, $NH_{2\text{-}Gln}$), 7.23 (s, 2H, CH_{Im}), 7.16 (s, 2H, CH_{Im}), 7.04 (d, *J* = 7.5 Hz, 4H, H_{Ar}), 6.92-6.69 (m, 14H, H_{Ar} and $NH_{2\text{-}Gln}$), 6.76 (br, 2H, $NH_{2\text{-}Gln}$), 4.28-4.04 (m, 10H, $^{\alpha}CH_{Gln}$, $^{\alpha}CH_{Lys}$, $^{\alpha}CH_{His}$, CH_2ONH), 3.75 (m, 2H, $^{\beta}CH_{2\text{-}Ser}$), 3.72 (d, *J* = 5.1 Hz, 4H, $^{\beta}CH_{2\text{-}Ser}$), 3.66 (m, 2H, $^{\beta}CH_{2\text{-}Ser}$), 3.43-3.20 (m, 12H, $^{\beta}CH_{2\text{-}\beta Ala}$, $^{\beta}CH_{2\text{-}His}$), 3.05 (td, *J* = 16.0 and 9.4 Hz, 4H, $^{\beta}CH_{2\text{-}His}$), 2.74-2.56 (m, 4H, $^{\varepsilon}CH_{2\text{-}Lys}$), 2.39 (m, 4H, $^{\alpha}CH_{2\text{-}\beta Ala}$), 2.31 (t, *J* = 7.0 Hz, 4H, $^{\alpha}CH_{2\text{-}\beta Ala}$), 2.24-2.08 (m, 8H, $CH_{2\text{-}Gln}$), 2.00 (m, 2H, $CH_{2\text{-}Gln}$), 1.54 (m, 2H, $CH_{2\text{-}Lys}$), 1.40 (m, 2H, $CH_{2\text{-}Lys}$), 1.24 (d, *J* = 7.4 Hz, 6H, $CH_{3\text{-}Ala}$), 0.90 (m, 4H, $CH_{2\text{-}Lys}$), 0.77 (m, 2H, $CH_{2\text{-}Lys}$), 0.68 (m, 2H, $CH_{2\text{-}Lys}$). **^{13}C NMR** (H_2O/D_2O, 75 MHz, δ): 177.7 (CO), 177.6 (CO), 175.0 (CO), 174.1 (CO), 174.0 (CO), 173.7 (CO), 172.9 (CO), 172.1 (CO), 171.7 (CO), 171.5 (CO), 171.4 (CO), 163.1 (CO), 162.8 (CO), 157.7 (CH), 140.8 (C), 140.7 (C), 133.9 (CH), 133.8 (CH), 128.7 (C), 128.6 (C), 128.4 (CH), 126.5 (CH), 126.3 (CH), 126.1 (CH), 119.8 (C), 117.5 (CH), 117.4 (CH), 115.2 (C), 71.6 (CH_2), 61.4 (CH_2), 61.2 (CH_2), 61.1 (CH), 60.9 (C), 55.8 (CH), 53.7 (CH), 53.6 (CH), 53.5 (CH), 52.8 (CH), 52.4 (CH), 52.3 (CH), 50.1 (CH), 38.2 (CH_2), 36.2 (CH_2), 35.9 (CH_2), 35.4 (CH_2), 34.8 (CH_2), 31.2 (CH_2), 31.0 (CH_2), 30.4 (CH_2), 27.4 (CH_2), 26.9 (CH_2), 26.7 (CH_2), 26.4 (CH_2), 26.2 (CH_2), 22.0 (CH_2), 16.9 (CH_3). **ESI-MS** *m/z* (%): 1307.9 (14) $[M+2H]^{2+}$, 872.5 (100) $[M+3H]^{3+}$, 654.7 (8) $[M+4H]^{4+}$. **HRMS (ESI)** *m/z*: $[M+2H]^{2+}$ calculated for $C_{120}H_{158}N_{36}O_{32}$, 1307.5921, found 1307.5916. **FTIR (neat)**: ν = 3274.6 (amide A), 1654.0 (amide I), 1540.7 (amide II) cm^{-1}.

USC UNIVERSIDADE DE SANTIAGO DE COMPOSTELA

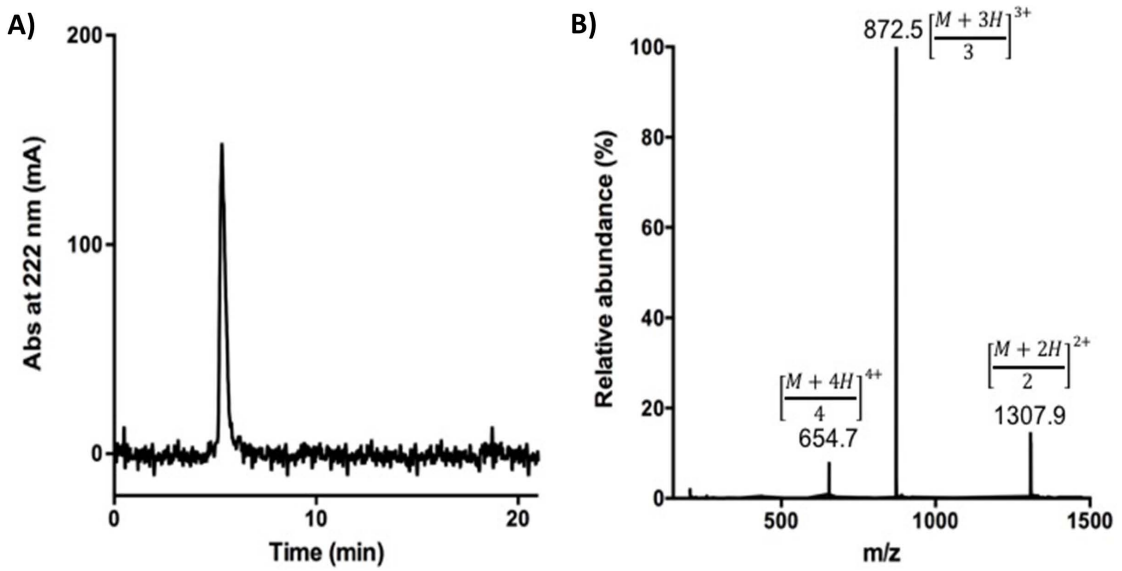

Figure 140. (A) **RP-uHPLC** of ***Z,Z*-D2$_{ht}$:** [Agilent SB-C18 column, H_20 (0.1% TFA)/MeCN (0.1% TFA), 80:20 → 80:20 (2 min) and 80:20 → 50:50 (19 min)] R_t = 5.36 min. (B) ESI-MS of the main peak.

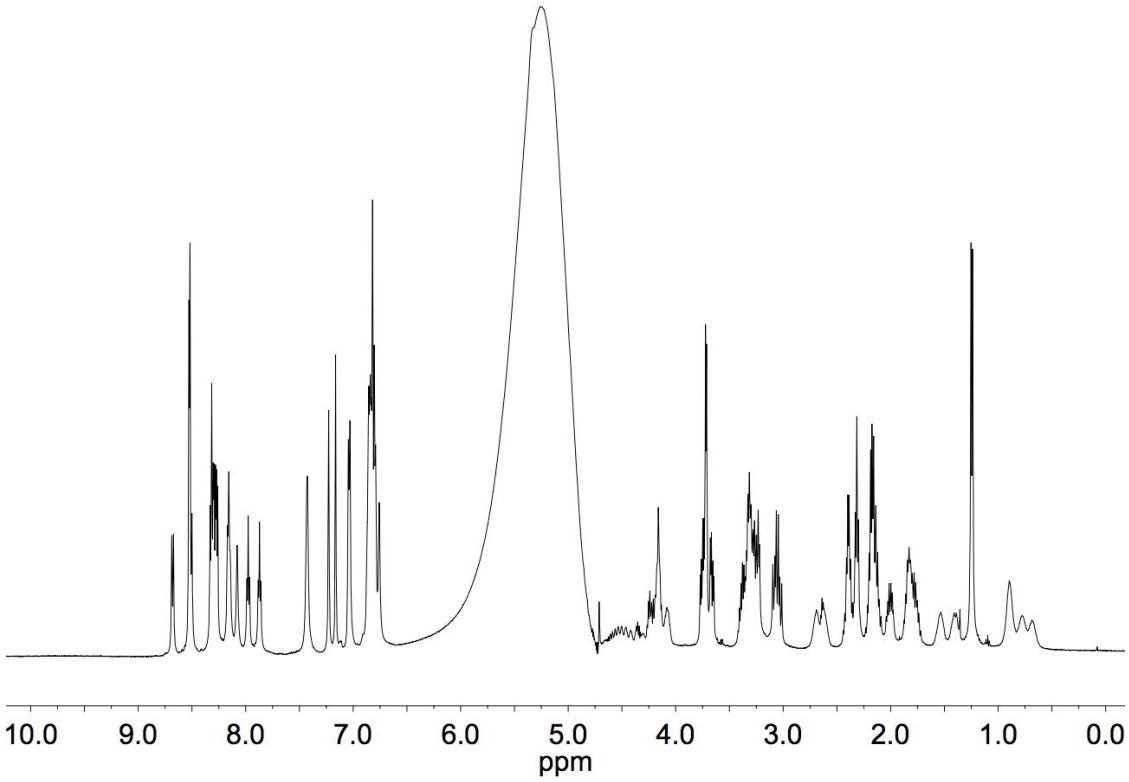

Figure 141. ^{1}H NMR of ***Z,Z*-D2$_{ht}$** at 3.2 mM (500 MHz, D_2O/H_2O, 298K).

USC
UNIVERSIDADE DE SANTIAGO DE COMPOSTELA

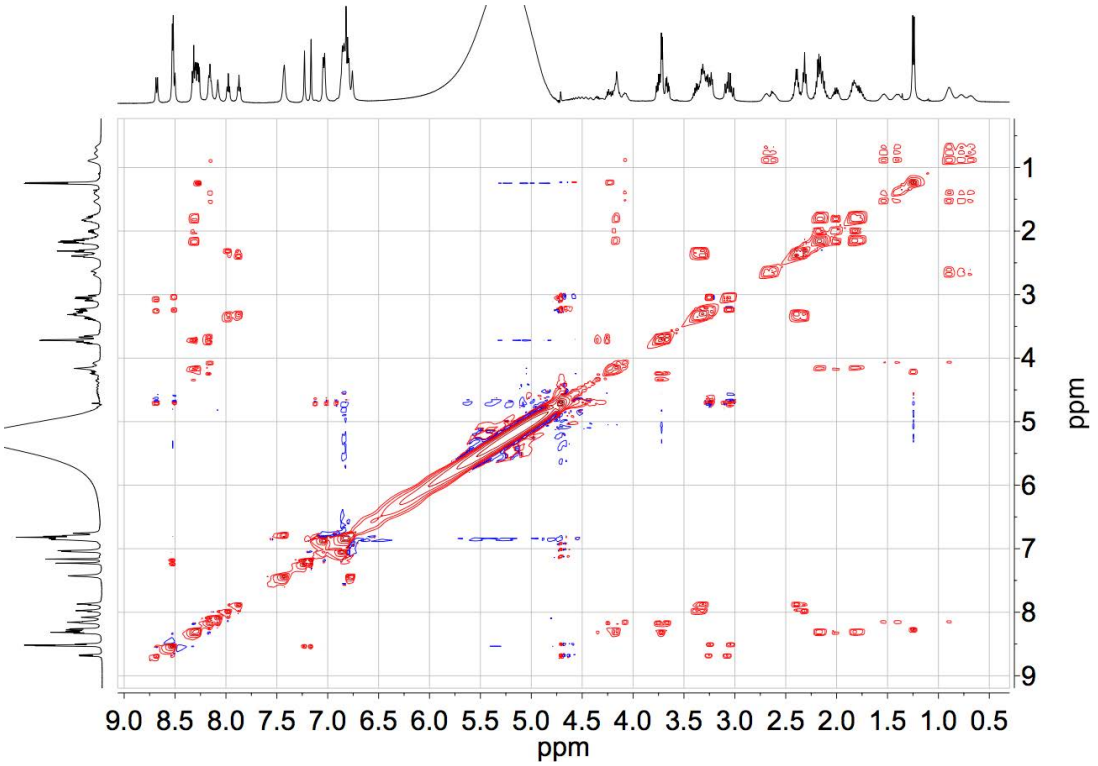

Figure 142. TOCSY of ***Z,Z*-D2$_{ht}$** at 3.2 mM (500 MHz, D_2O/H_2O, 298K).

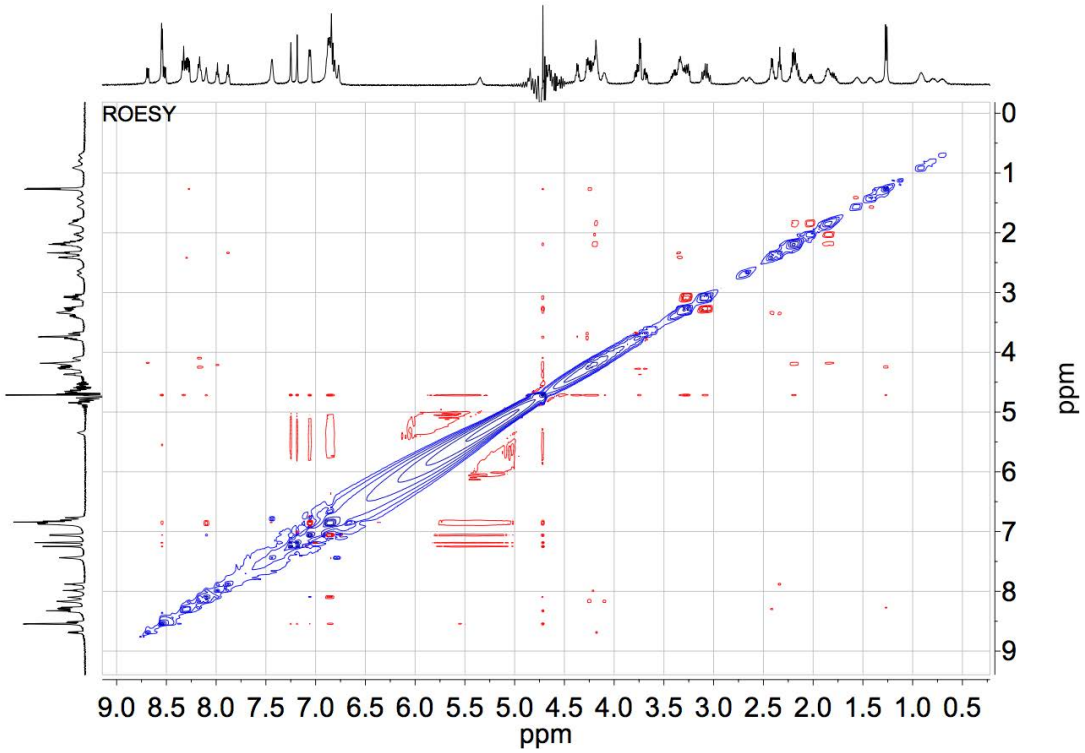

Figure 143. ROESY of ***Z,Z*-D2$_{ht}$** at 3.2 mM (500 MHz, D_2O/H_2O, 298K).

USC
UNIVERSIDADE DE SANTIAGO DE COMPOSTELA

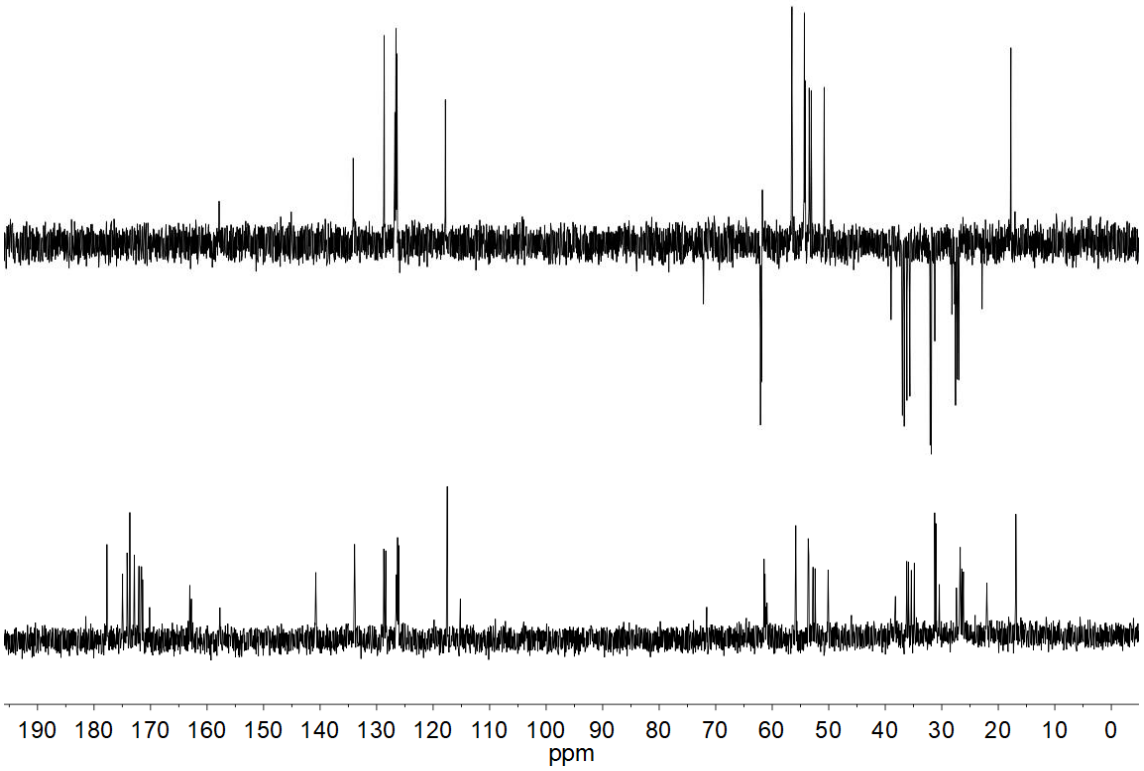

Figure 144. ^{13}C NMR (bottom) and DEPT-135 NMR (top) of ***Z,Z*-D2$_{ht}$** at 3.2 mM (500 MHz, D_2O/H_2O, 298K).

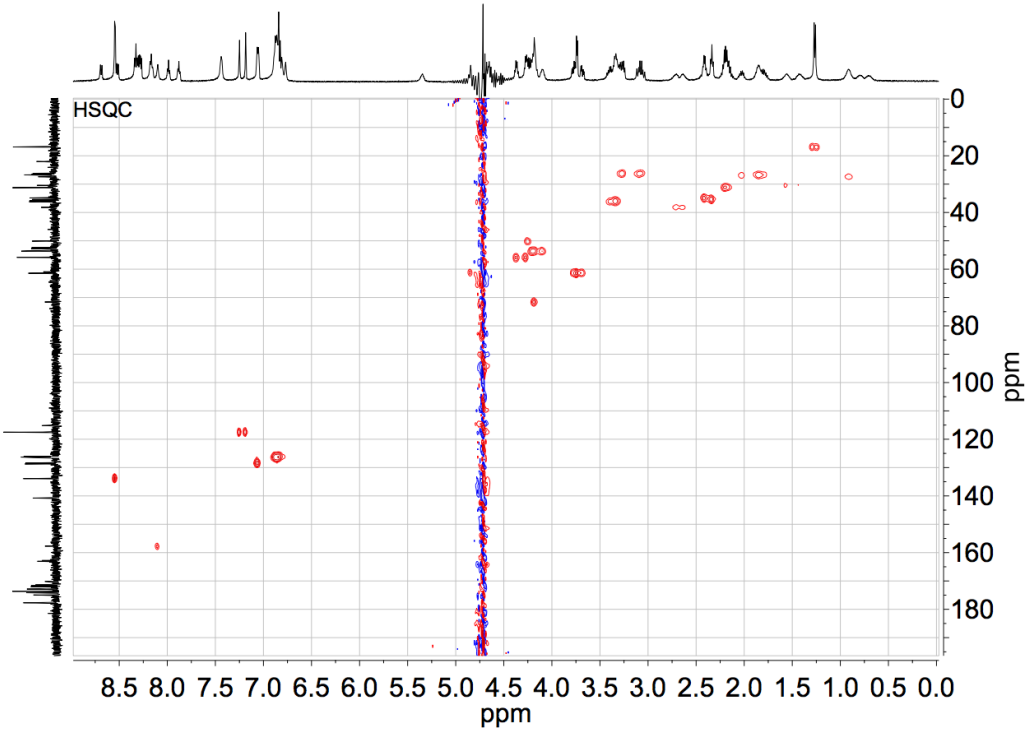

Figure 145. HSQC of ***Z,Z*-D2$_{ht}$** at 3.2 mM (500 MHz, D_2O/H_2O, 298K).

USC
UNIVERSIDADE DE SANTIAGO DE COMPOSTELA

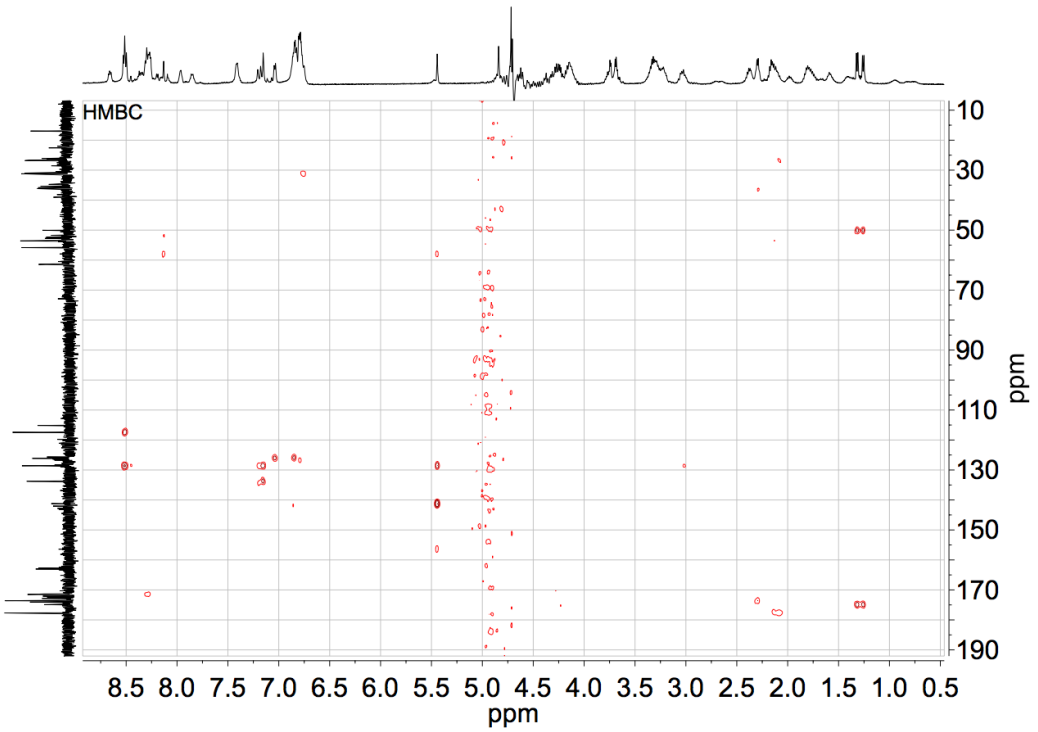

Figure 146. HMBC of ***Z,Z*-D2$_{ht}$** at 3.2 mM (500 MHz, D_2O/H_2O, 298K).

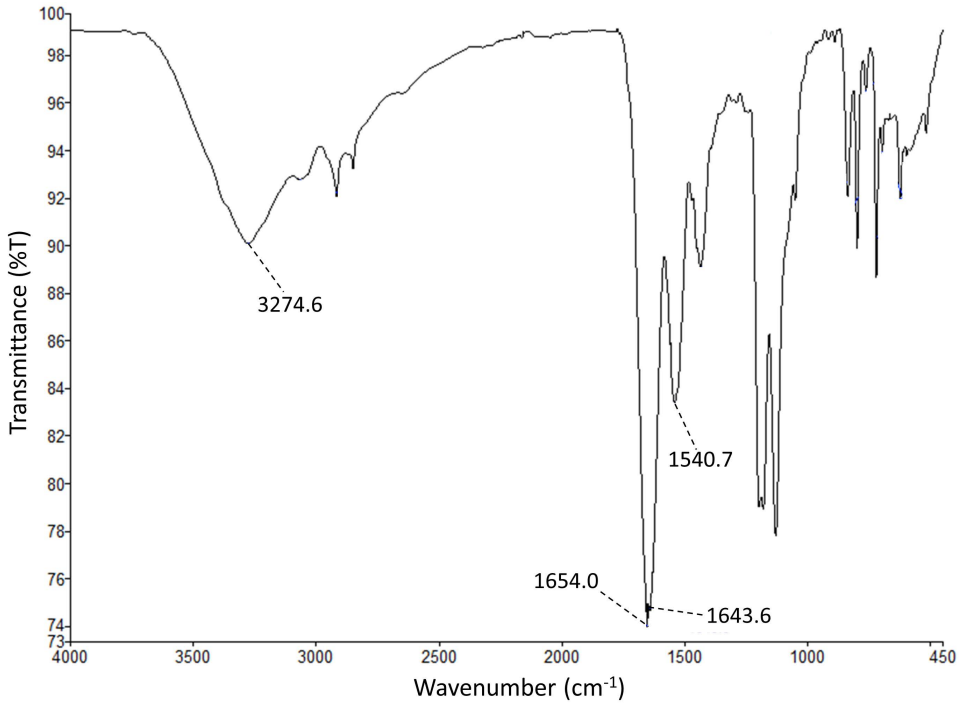

Figure 147. FT-IR spectrum of ***Z,Z*-D2$_{ht}$** (solid, 298 K).

USC
UNIVERSIDADE DE SANTIAGO DE COMPOSTELA

***E,E*-D2$_{ht}$**: **^{1}H NMR** (500 MHz, H_2O/D_2O) δ: 8.64 (d, *J* = 7.9 Hz, 2H, NH_{His}), 8.45 ($s_{overlapped}$, 4H, CH_{Im}), 8.42 (d, *J* = 7.8 Hz, 2H, NH_{His}), 8.40 (m, 2H, $^{\varepsilon}NH_{Lys}$), 8.30-8.18 (m, 12H, NH_{Ser}, $^{\alpha}NH_{Gln}$, NH_{Ala}, $^{\alpha}NH_{Lys}$), 8.09 (s, 2H, H_{ox}), 7.90 (t, *J* = 6.3 Hz, 2H, $NH_{\beta Ala}$), 7.76 (t, *J* = 6.2 Hz, 2H, $NH_{\beta Ala}$), 7.38 (brs, 4H, $NH_{2\text{-}Gln}$), 7.11 (s, 2H, CH_{Im}), 7.06 (s, 2H, CH_{Im}), 6.84-6.70 (m, 20H, H_{Ar}, $NH_{2\text{-}Gln}$), 5.44 (s, 2H, $H_{10\text{-}Ant}$), 4.38-4.02 (m, 6H, $^{\alpha}CH_{Gln}$, $^{\alpha}CH_{Lys}$, $^{\alpha}CH_{His}$), 3.76-3.66 (m, 6H, $CH_{2\text{-}Ser}$), 3.63 (dd, *J* = 11.7 and 4.7 Hz, 2H, $CH_{2\text{-}Ser}$), 3.38-3.10 (m, 16H, $CH_{2\text{-}His}$, $^{\beta}CH_{2\text{-}\beta Ala}$, $^{\varepsilon}CH_{2\text{-}Lys}$), 2.97 (dd, 2H, *J* = 15.8 and 9.4 Hz, $CH_{2\text{-}His}$), 2.91 (dd, 2H, *J* = 15.7 and 9.4 Hz, $CH_{2\text{-}His}$), 2.35-2.26 (m, 4H, $^{\alpha}CH_{2\text{-}\beta Ala}$), 2.22 (t, *J* = 7.1 Hz, 4H, $^{\alpha}CH_{2\text{-}\beta Ala}$), 2.18-1.88 (m, 12H, $CH_{2\text{-}Gln}$), 1.82-1.54 (m, 16H, $CH_{2\text{-}Lys}$, $CH_{2\text{-}Gln}$), 1.38 (m, 4H, $^{\gamma}CH_{2\text{-}Lys}$), 1.28 (d, *J* = 7.4 Hz, 6H, $CH_{3\text{-}Ala}$). **^{13}C NMR** (H_2O/D_2O, 75 MHz, δ): 177.7 (CO), 177.5 (CO), 174.9 (CO), 174.0 (CO), 173.7 (CO), 173.6 (CO), 172.8 (CO), 172.5 (CO), 172.0 (CO), 171.7 (CO), 171.4 (CO), 163.0 (CO), 162.7 (CO), 156.2 (CH), 143.2 (C), 142.5 (C), 133.9 (CH), 133.7 (CH), 128.6 (C), 128.5 (C), 128.4 (CH), 126.6 (CH), 126.0 (CH), 125.7 (CH), 125.6 (CH), 117.5 (C), 117.4 (CH), 115.2 (C), 72.8 (CH_2), 61.4 (CH_2), 61.2 (CH_2), 57.7 (C), 55.8 (CH), 55.7 (CH), 53.8 (CH), 53.6 (CH), 53.5 (CH), 52.8 (CH), 52.4 (CH), 52.0 (CH), 50.1 (CH), 39.0 (CH_2), 36.1 (CH_2), 35.8 (CH_2), 35.3 (CH_2), 34.7 (CH_2), 31.2 (CH_2), 31.0 (CH_2), 30.6 (CH_2), 28.7 (CH_2), 26.8 (CH_2), 26.6 (CH_2), 26.3 (CH_2), 26.0 (CH_2), 22.6 (CH_2), 17.0 (CH_3). **ESI-MS** *m/z* (%): 1307.5 (31) $[M+2H]^{2+}$, 872.5 (100) $[M+3H]^{3+}$, 654.7 (9) $[M+4H]^{4+}$. **HRMS (ESI)** *m/z*: $[M+2H]^{2+}$ calculated for $C_{120}H_{158}N_{36}O_{32}$: 1307.5921, found 1307.5916. **FTIR (neat)**: ν = 3274.6 (amide A), 1659.0 (amide I), 1535.6 (amide II) cm^{-1}.

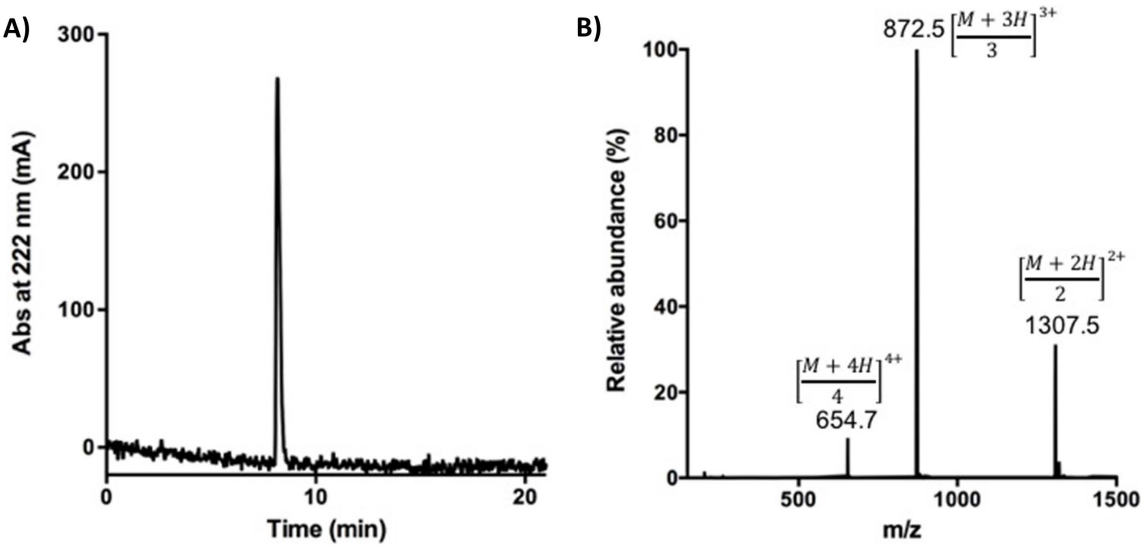

Figure 148. (A) **RP-uHPLC** of ***E,E*-D2$_{ht}$:** [Agilent SB-C18 column, H_20 (0.1% TFA)/MeCN (0.1% TFA), 80:20 → 80:20 (2 min) and 80:20 → 50:50 (19 min)] R_t = 8.19 min. (B) ESI-MS of the main peak.

USC UNIVERSIDADE DE SANTIAGO DE COMPOSTELA

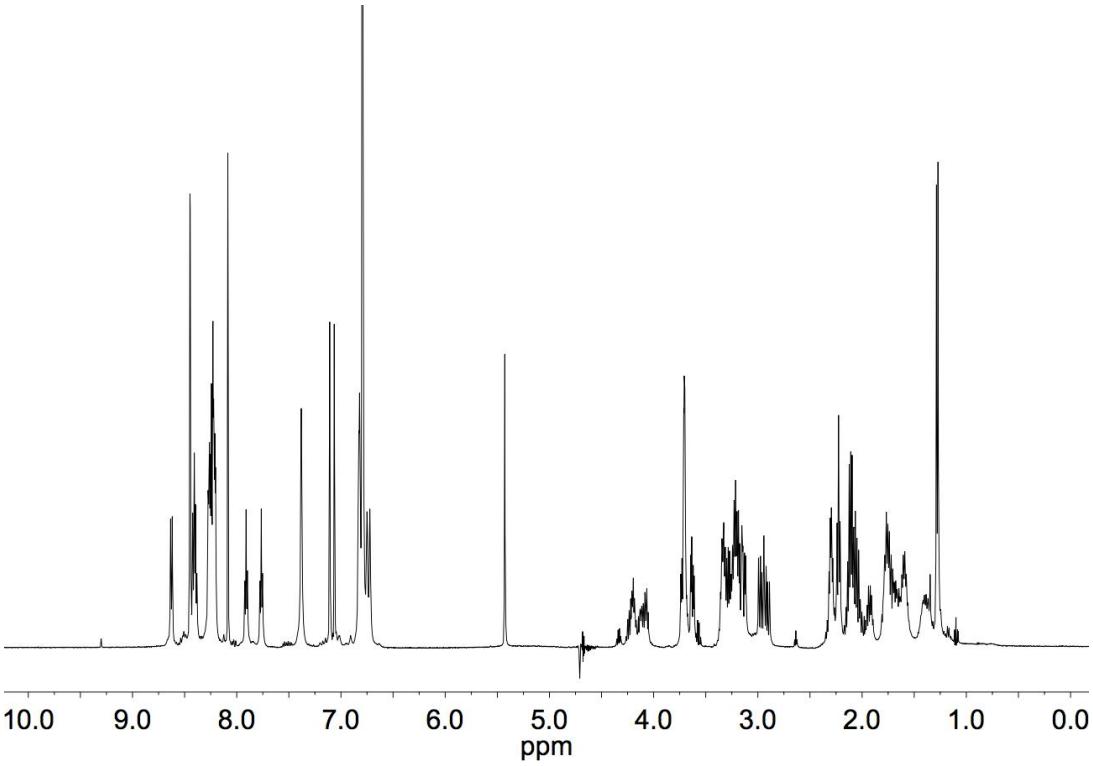

Figure 149. **^{1}H NMR** of ***E,E*-D2$_{ht}$** at 3.4 mM (500 MHz, D_2O/H_2O, 298K).

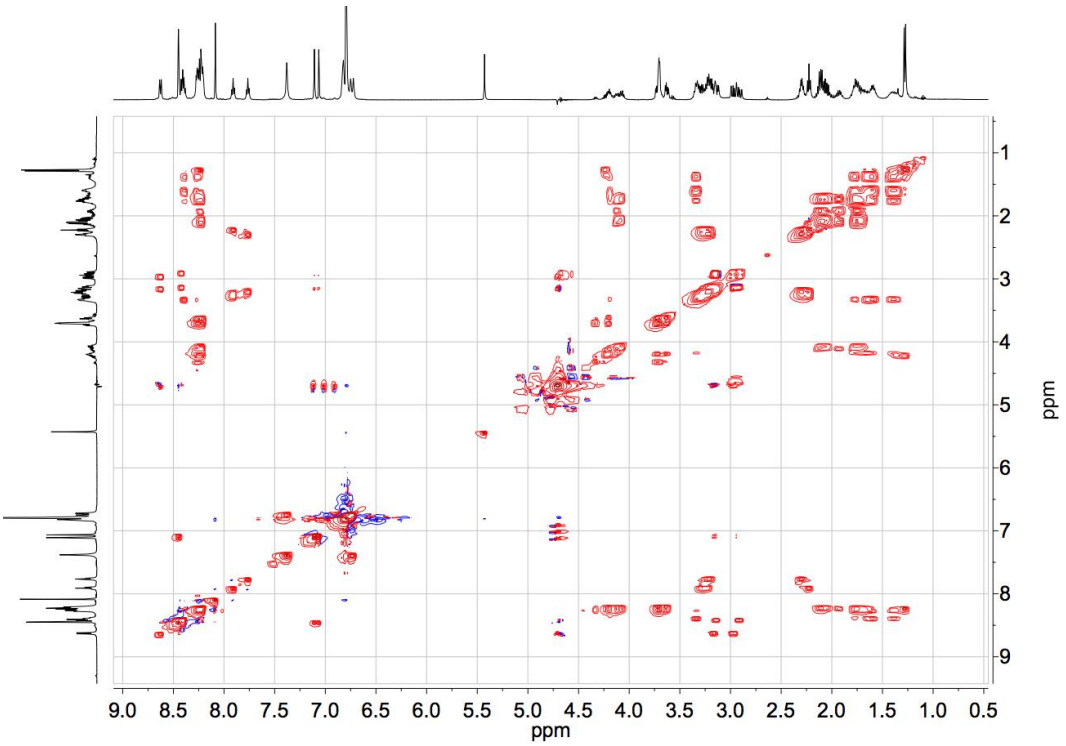

Figure 150. TOCSY of ***E,E*-D2$_{ht}$** at 3.4 mM (500 MHz, D_2O/H_2O, 298K).

USC
UNIVERSIDADE DE SANTIAGO DE COMPOSTELA

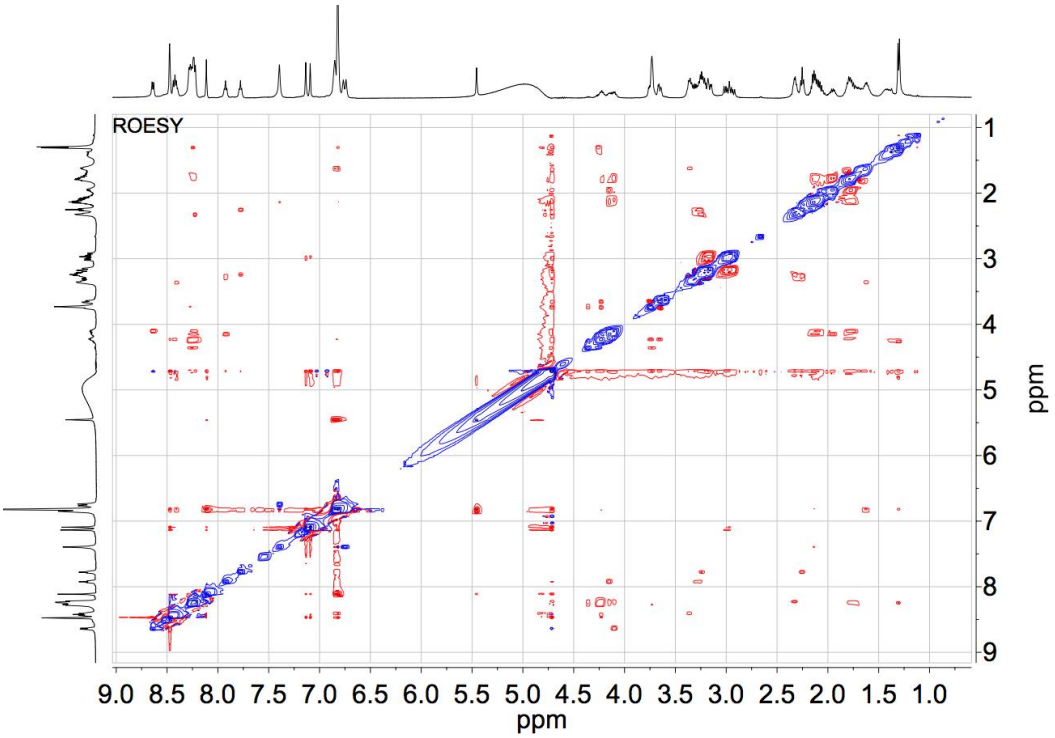

Figure 151. ROESY of ***E,E*-D2$_{ht}$** at 3.4 mM (500 MHz, D_2O/H_2O, 298K).

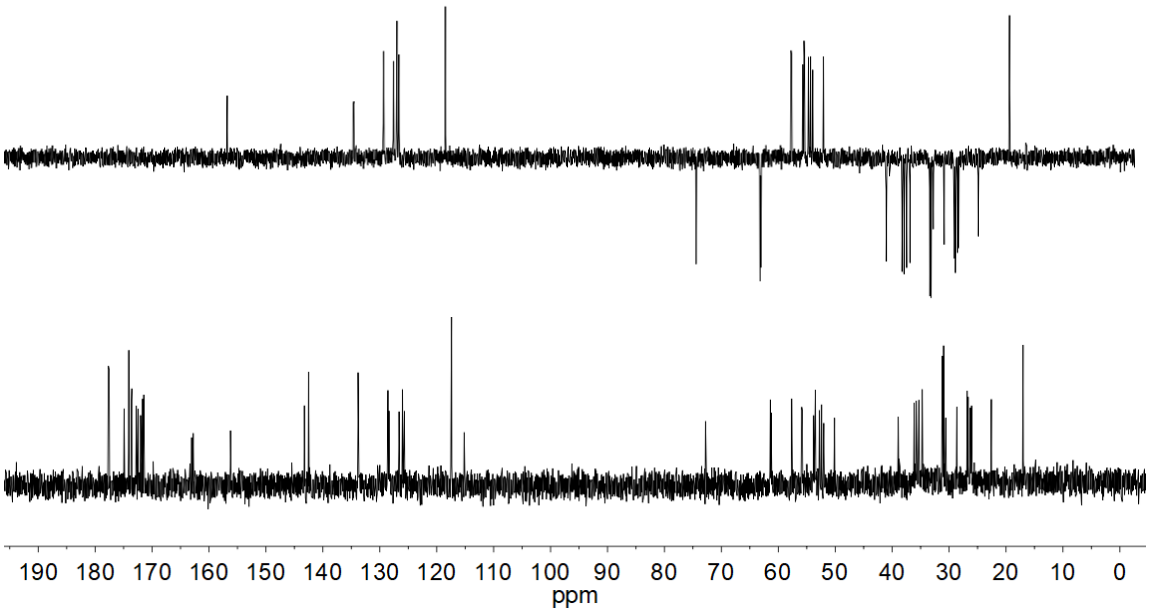

Figure 152. ^{13}C NMR (bottom) and DEPT-135 NMR (top) of ***E,E*-D2$_{ht}$** at 3.7 mM (500 MHz, D_2O/H_2O, 298K).

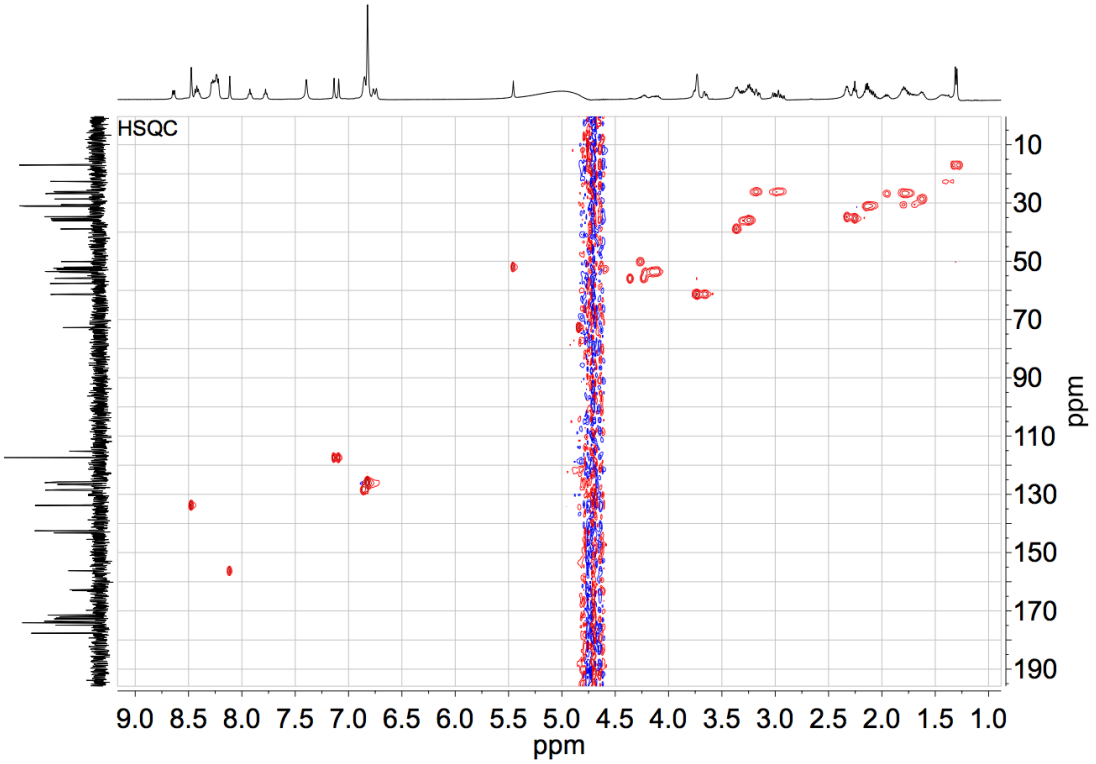

Figure 153. HSQC of ***E,E*-D2$_{ht}$** at 3.7 mM (500 MHz, D_2O/H_2O, 298K).

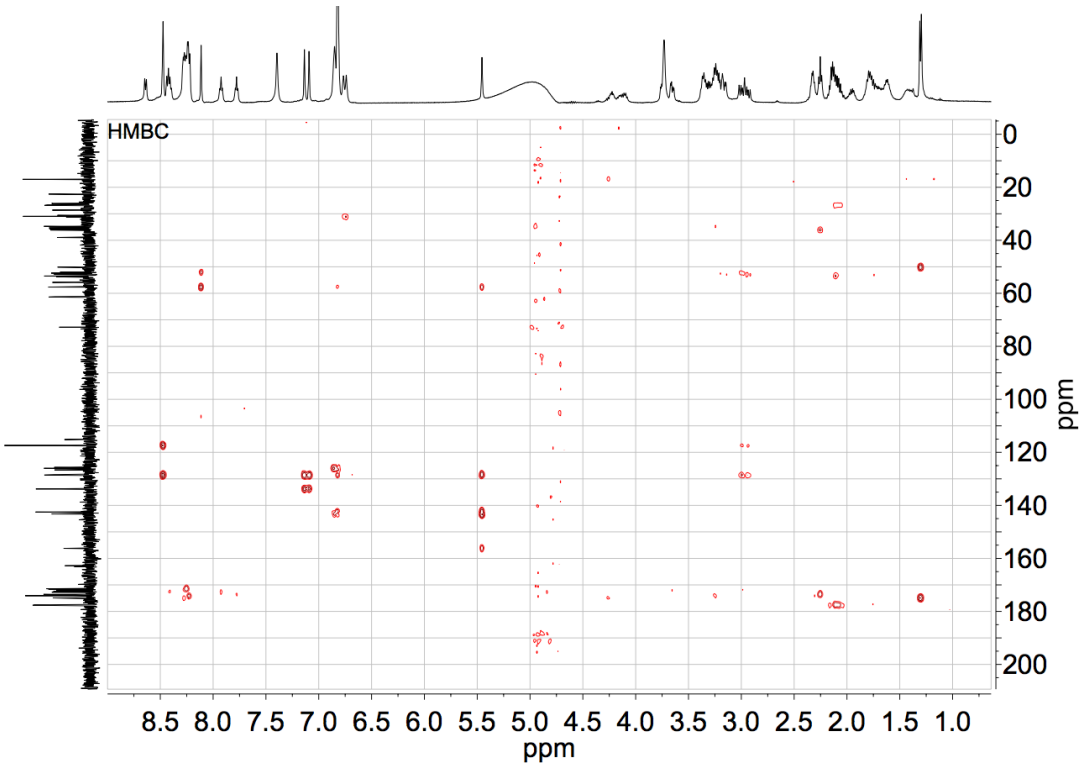

Figure 154. HMBC of ***E,E*-D2$_{ht}$** at 3.7 mM (500 MHz, D_2O/H_2O, 298K).

USC
UNIVERSIDADE DE SANTIAGO DE COMPOSTELA

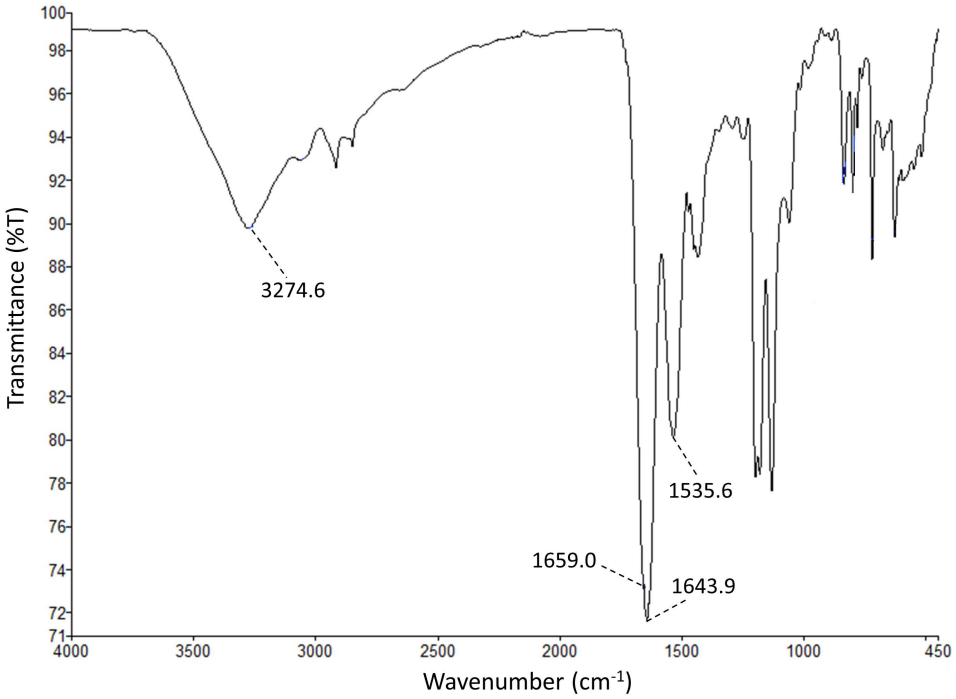

Figure 155. FT-IR spectrum of ***E,E*-D2*ht*** (solid, 298 K).

Z,E*-D2*ht: **^{1}H NMR** (500 MHz, H_2O/D_2O) δ: 8.66 (d, *J* = 7.5 Hz, 1H, NH_{His}), 8.65 (d, *J* = 7.5 Hz, 1H, NH_{His}), 8.54-8.48 (m, 6H, NH_{His}, CH_{Im}), 8.43-8.12 (m, 14H, NH_{Ser}, $^{\alpha}NH_{Gln}$, NH_{Ala}, $^{\alpha}NH_{Lys}$, $^{\varepsilon}NH_{Lys}$), 8.13 (s, 1H, H_{ox}), 8.09 (s, 1H, H_{ox}), 7.96 (m, 2H, $NH_{\beta Ala}$), 7.84 (m, 2H, $NH_{\beta Ala}$), 7.40 (m, 4H, $NH_{2\text{-}Gln}$), 7.20 (s, 1H CH_{Im}), 7.18 (s, 1H CH_{Im}), 7.15 (s, 2H, CH_{Im}), 7.04 (m, 2H, H_{Ar}), 6.90-6.70 (m, 18H, H_{Ar}, $NH_{2\text{-}Gln}$), 5.44 (s, 1H, $^{10}H_{Ar}$), 4.40-4.04 (m, 10H, $^{\alpha}CH_{Gln}$, $^{\alpha}CH_{Lys}$, $^{\alpha}CH_{His}$, CH_2ONH), 3.84-3.64 (m, 10H, $CH_{2\text{-}Ser}$), 3.40-3.16 (m, 14H, $CH_{2\text{-}His}$, $^{\beta}CH_{2\text{-}\beta Ala}$, $^{\varepsilon}CH_{2\text{-}Lys}$), 3.04 (m, 4H, $CH_{2\text{-}His}$), 2.70 (m, 2H, $^{\varepsilon}CH_{2\text{-}Lys}$), 2.45-2.32 (m, 4H, $^{\alpha}CH_{2\text{-}\beta Ala}$), 2.30 (m, 4H, $^{\alpha}CH_{2\text{-}\beta Ala}$), 2.25-2.05 (m, 8H, $CH_{2\text{-}Gln}$), 1.98 (m, 2H, $CH_{2\text{-}Gln}$), 1.84-1.64 (m, 8H, $CH_{2\text{-}Lys}$, $CH_{2\text{-}Gln}$), 1.59 (m, 2H, $CH_{2\text{-}Lys}$), 1.46-1.36 (m, 4H, $CH_{2\text{-}Lys}$), 1.32 (d, *J* = 7.4 Hz, 3H, $CH_{3\text{-}Ala}$), 1.26 (d, *J* = 7.4 Hz, 3H, $CH_{3\text{-}Ala}$), 1.02-0.70 (m, 4H, $CH_{2\text{-}Lys}$). **^{13}C NMR** (H_2O/D_2O, 75 MHz, δ): 117.7 (CO), 117.6 (CO), 177.5 (CO), 177.5 (CO), 175.0 (CO), 174.8 (CO), 174.1 (CO), 174.0 (CO), 173.7 (CO), 173.6 (CO), 172.9 (CO), 172.8 (CO), 172.5 (CO), 172.4 (CO), 172.1 (CO), 172.0 (CO), 171.7 (CO), 171.6 (CO), 171.5 (CO), 171.4 (CO), 171.3 (CO), 171.2 (CO), 163.1 (CO), 163.0 (CO), 162.8 (CO), 162.7 (CO), 156.5 (CH), 156.4 (CH), 143.2 (C), 142.7 (C), 141.9 (C), 141.2 (C), 134.9 (CH), 134.8 (CH), 134.8 (CH), 134.7 (CH), 128.7 (C), 128.6 (C), 128.6 (C), 128.5 (C), 128.5 (CH), 128.3 (CH), 126.7 (CH), 126.6 (CH), 126.5 (CH), 126.4 (CH), 126.3 (CH), 126.1 (CH), 125.9 (CH), 125.7 (CH), 117.5 (C), 117.5 (CH), 117.4 (C), 117.4 (CH), 115.2 (C), 115.1 (C), 72.9 (CH_2), 72.8 (CH_2), 61.5 (CH_2), 61.4 (CH_2), 61.3 (CH_2), 61.2 (CH_2), 60.5 (C), 58.0 (C), 56.0 (CH), 55.9 (CH), 55.8 (CH), 55.7 (CH), 53.8 (CH), 53.7 (CH), 53.6 (CH), 53.6 (CH), 53.5 (CH), 53.4 (CH), 52.8 (CH), 52.7 (CH), 52.4 (CH), 52.3 (CH), 51.7 (CH), 51.6 (CH), 50.1 (CH), 50.0 (CH), 39.1 (CH_2), 38.9 (CH_2), 36.2 (CH_2), 36.1 (CH_2), 35.9 (CH_2), 35.8 (CH_2), 35.4 (CH_2), 35.3 (CH_2), 34.8 (CH_2), 34.7 (CH_2), 31.2 (CH_2), 31.1 (CH_2), 31.0 (CH_2), 30.9 (CH_2), 30.7 (CH_2), 30.5 (CH_2), 28.6 (CH_2), 28.5 (CH_2), 26.8 (CH_2), 26.7 (CH_2), 26.7 (CH_2), 26.6 (CH_2), 26.4 (CH_2), 26.3 (CH_2), 26.1 (CH_2), 26.0 (CH_2), 22.6

(CH_2), 22.5 (CH_2), 17.0 (CH_3), 16.9 (CH_3). **ESI-MS** *m/z* (%): 1307.5 (12) $[M+2H]^{2+}$, 872.5 (100) $[M+3H]^{3+}$, 654.7 (8) $[M+4H]^{4+}$. **HRMS (ESI)** *m/z*: $[M+2H]^{2+}$ calculated for $C_{120}H_{158}N_{36}O_{32}$: 1307.5921, found 1307.5916. **FTIR (neat)**: ν = 3269.4 (amide A), 1643.6 (amide I), 1535.6 (amide II) cm^{-1}.

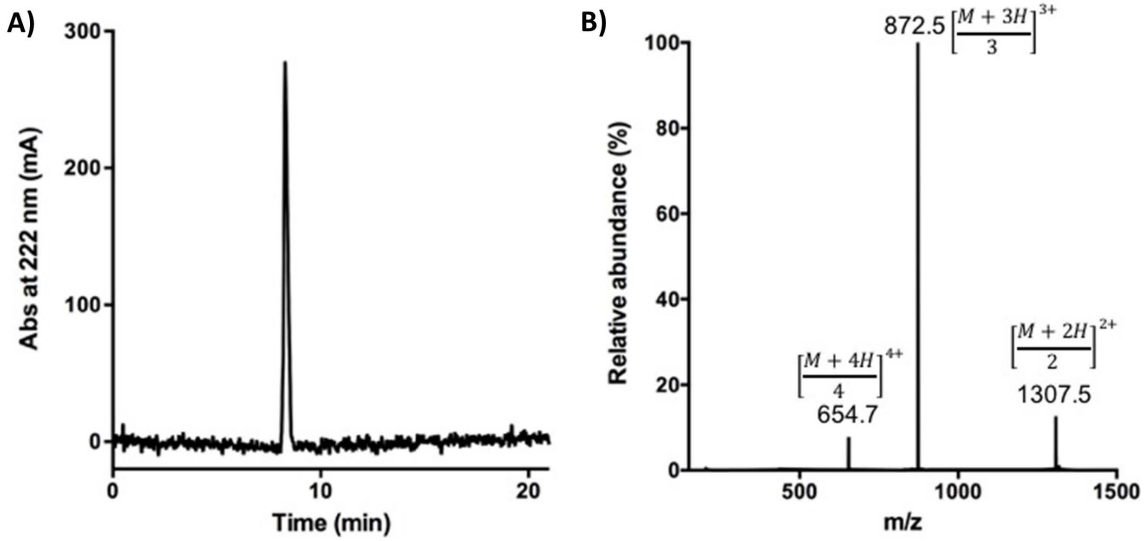

Figure 156. (A) **RP-uHPLC** of ***Z,E*-D2$_{ht}$:** [Agilent SB-C18 column, H_20 (0.1% TFA)/MeCN (0.1% TFA), 80:20 → 80:20 (2 min) and 80:20 → 50:50 (19 min)] R_t = 8.26 min. (B) ESI-MS of the main peak.

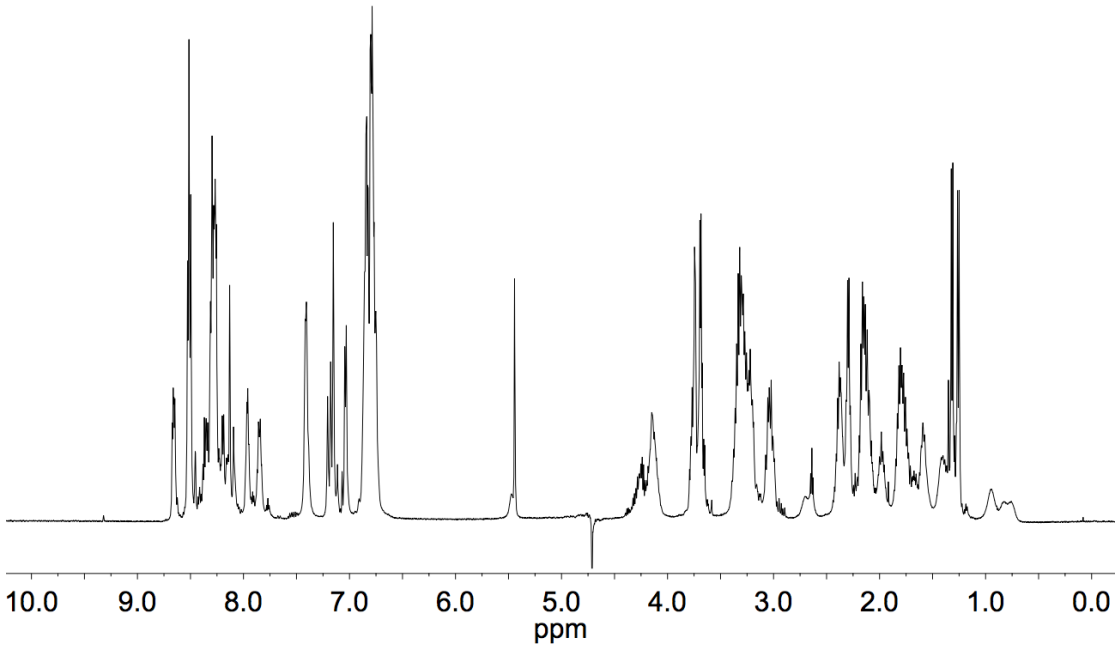

Figure 157. ^{1}H NMR of ***Z,E*-D2$_{ht}$** at 3.4 mM (500 MHz, D_2O/H_2O, 298K).

USC
UNIVERSIDADE DE SANTIAGO DE COMPOSTELA

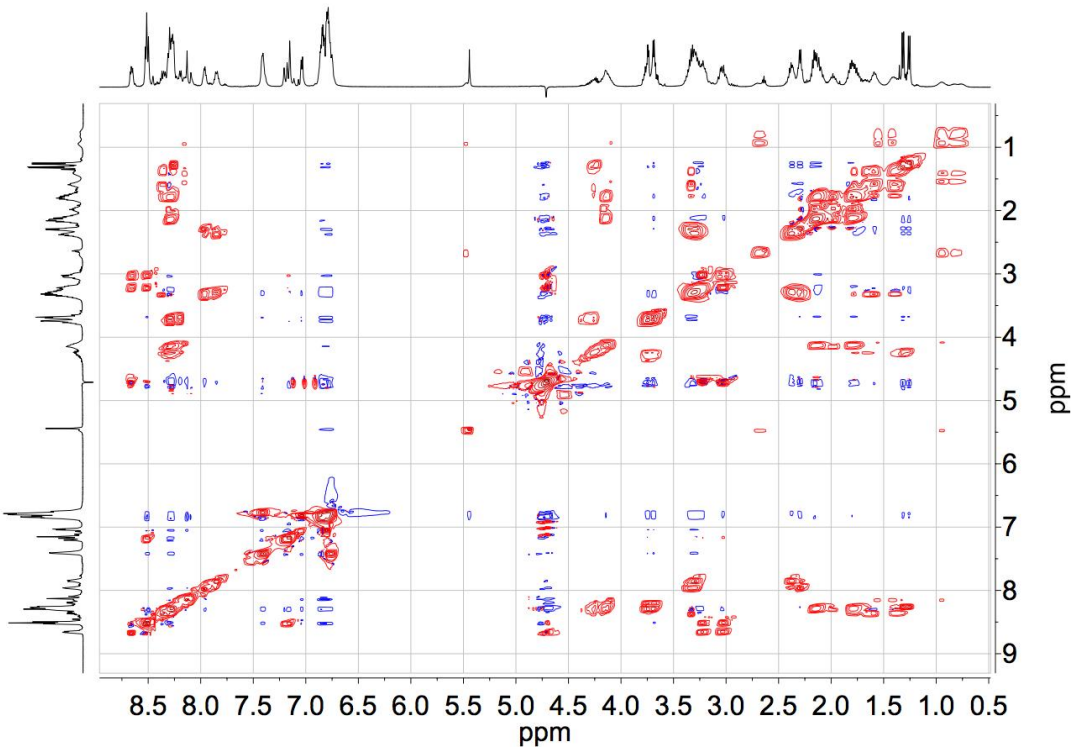

Figure 158. TOCSY of ***Z,E*-D2$_{ht}$** at 3.4 mM (500 MHz, D_2O/H_2O, 298K).

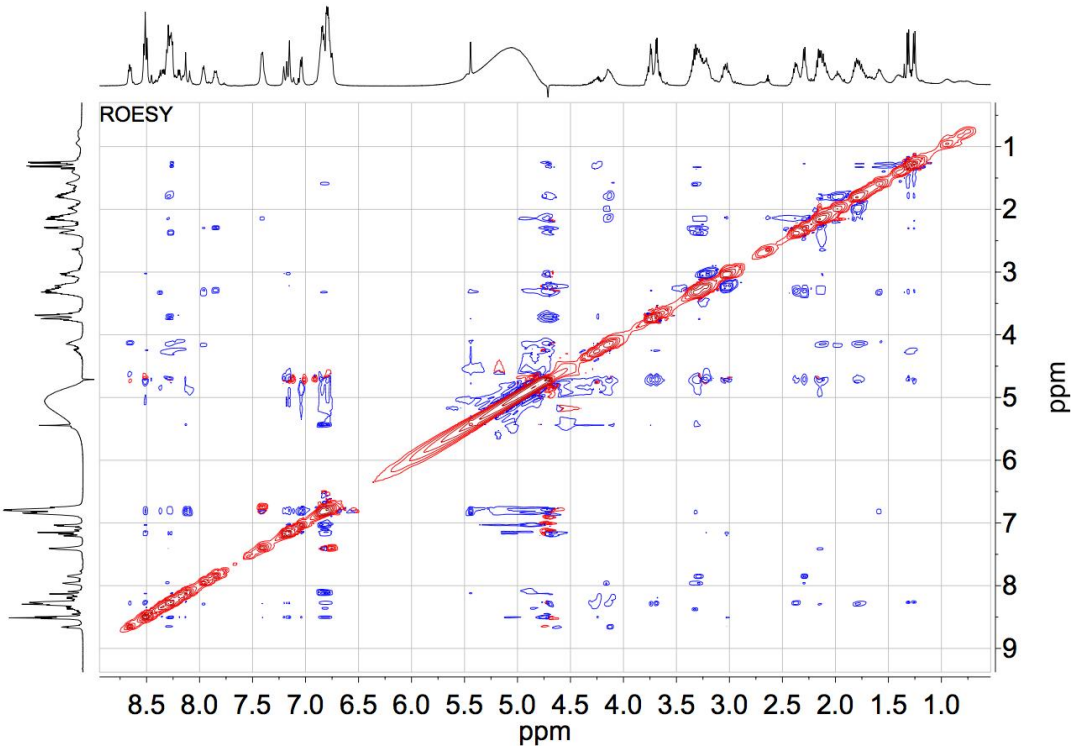

Figure 159. ROESY of ***Z,E*-D2$_{ht}$** at 3.4 mM (500 MHz, D_2O/H_2O, 298K).

USC
UNIVERSIDADE DE SANTIAGO DE COMPOSTELA

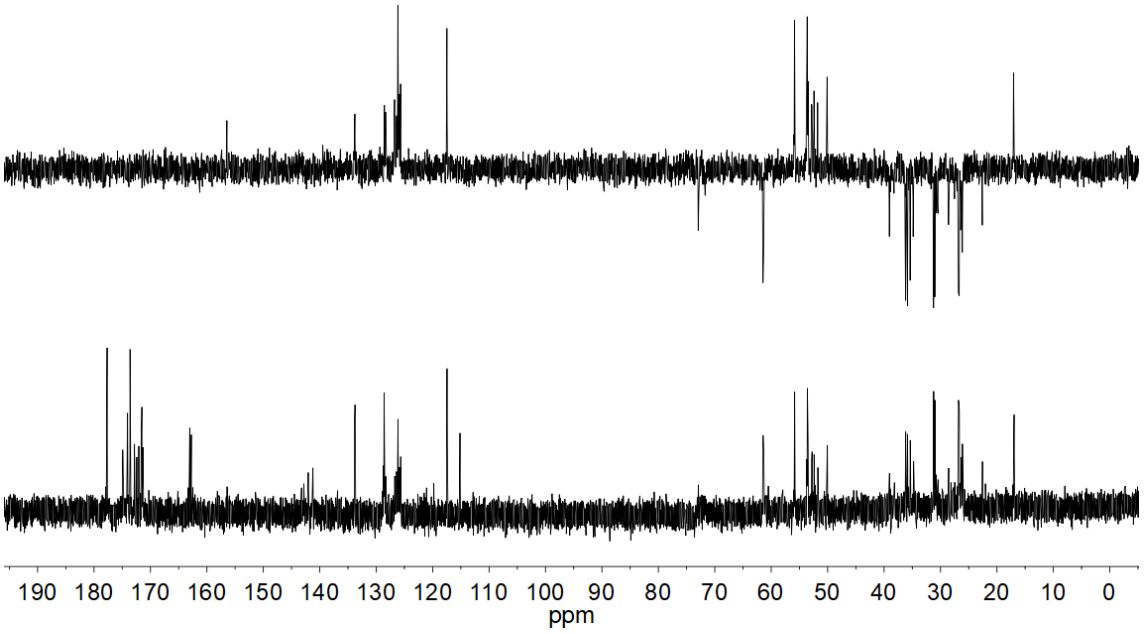

Figure 160. ^{13}C NMR (bottom) and DEPT-135 NMR (top) of ***Z,E*-D2$_{ht}$** at 3.4 mM (500 MHz, D_2O/H_2O, 298K).

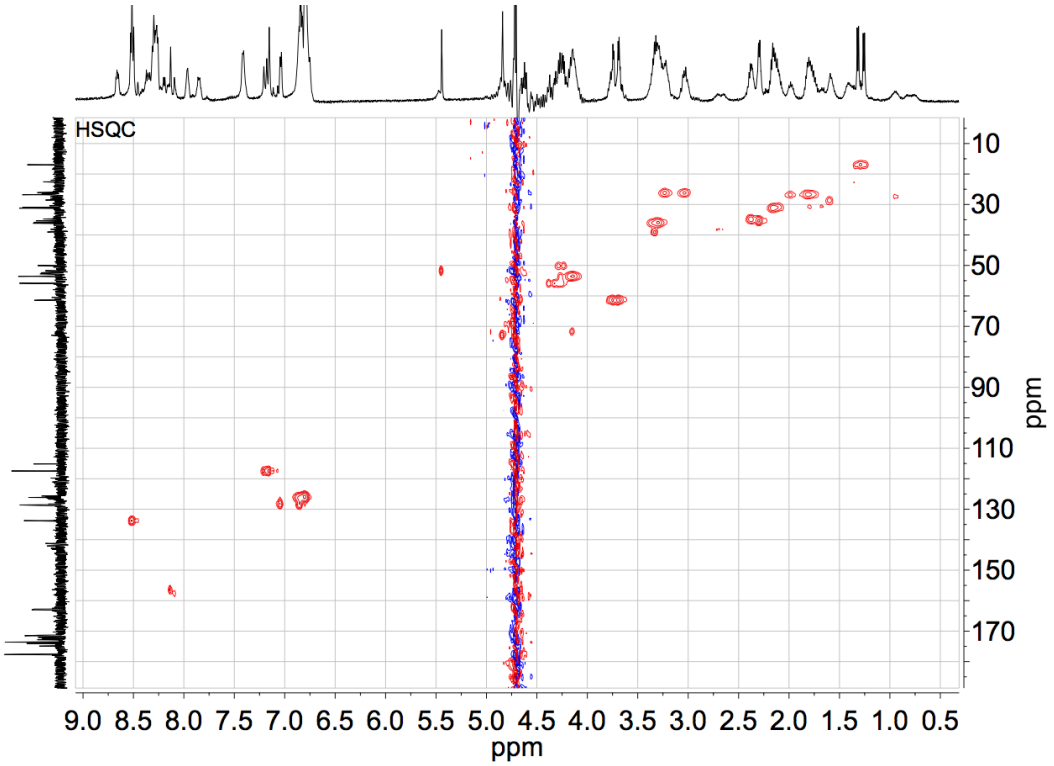

Figure 161. HSQC of ***Z,E*-D2$_{ht}$** at 3.4 mM (500 MHz, D_2O/H_2O, 298K).

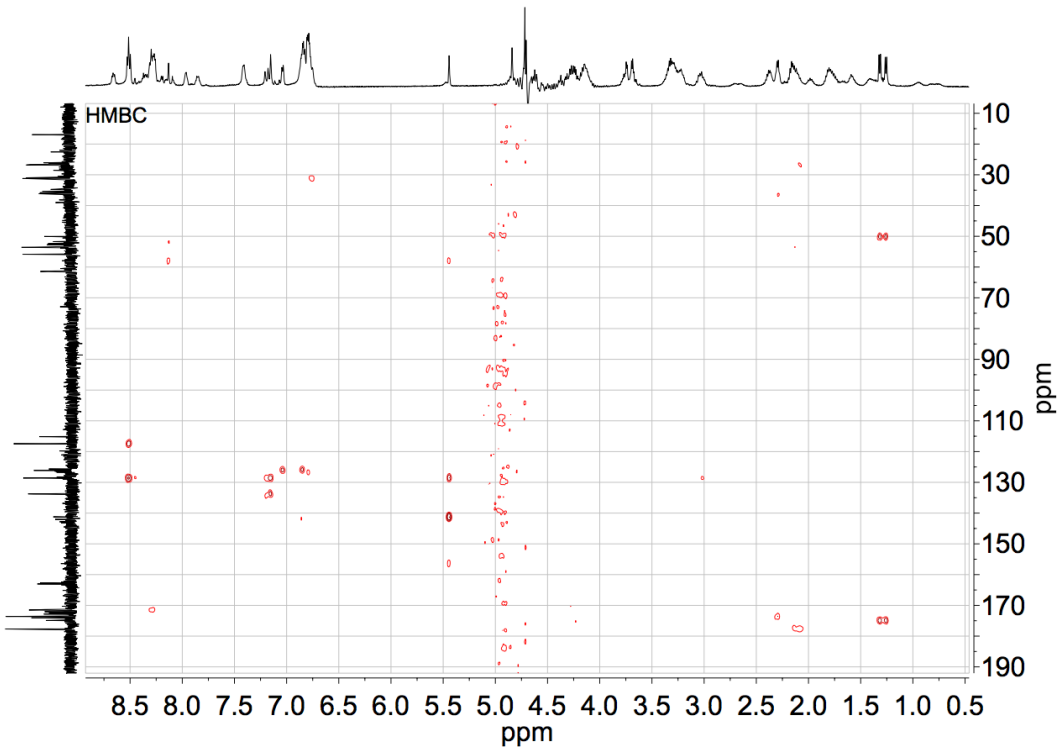

Figure 162. HMBC of ***Z,E*-D2$_{ht}$** at 3.4 mM (500 MHz, D_2O/H_2O, 298K).

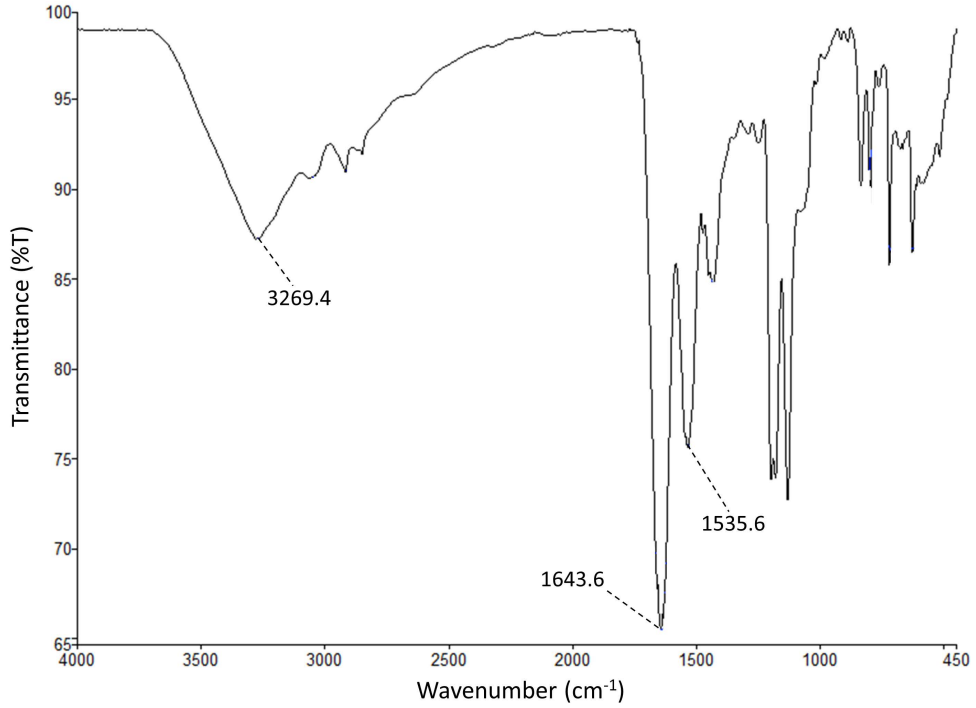

Figure 163. FT-IR spectrum of ***Z,E*-D2$_{ht}$** (solid, 298 K).

8.2.1.5. Synthesis of model anthracene derivative Ant1

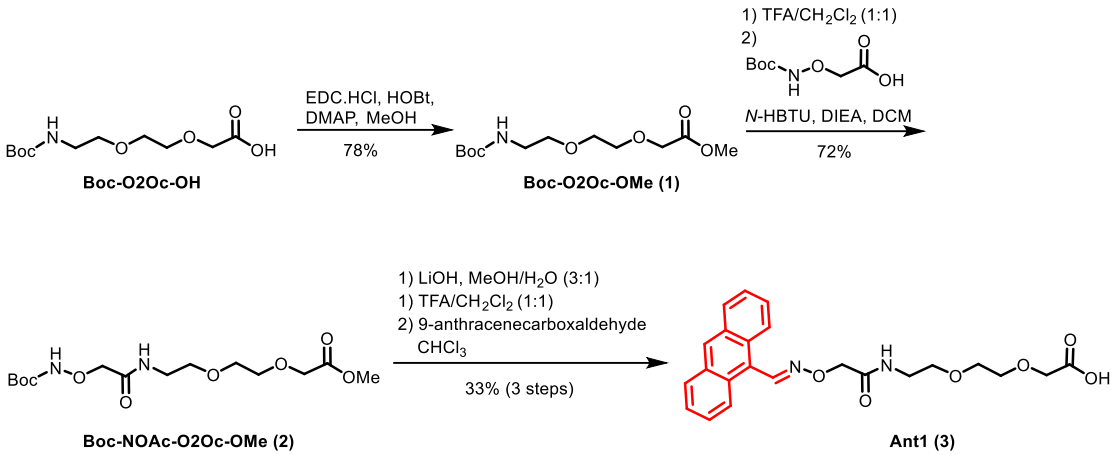

Figure 164. Synthetic strategy for the preparation of **Ant1**.

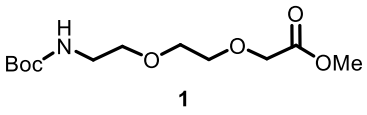

1

Boc-O2Oc-OMe (1). A solution of **Boc-O2Oc-OH** (185 mg, 0.703 mmol) in dry MeOH (7 mL) was treated with EDC·HCl (200 mg, 1.05 mmol), HOBt (142 mg, 1.05 mmol) and DMAP (128 mg, 1.05 mmol). The mixture was stirred for 24 hours at room temperature under argon atmosphere. Then, the solvent was removed under reduced pressure. The resulting residue was redissolved in CH_2Cl_2 and washed with aqueous solutions of HCl (5%, 3 x 5 mL) and $NaHCO_3$ (sat., 3 x 5 mL). The organic phase was dried over anhydrous $MgSO_4$, filtered and concentrated. The product was purified by flash chromatography (0-2% MeOH) to provide **Boc-O2Oc-OMe** as a light-yellow oil [152 mg, 78%, R_f = 0.75 (10% MeOH/CH_2Cl_2)]. **^{1}H NMR** ($CDCl_3$, 300 MHz, δ): 5.02 (br, 1H, NH), 4.14 (s, 2H, CH_2CO), 3.73 (s, 3H, OMe), 3.68 (m, 2H, CH_2), 3.63 (m, 2H, CH_2), 3.52 (m, 2H, CH_2), 3.29 (m, 2H, CH_2), 1.41 (s, 9H, Boc). **^{13}C NMR** ($CDCl_3$, 75 MHz, δ): 170.9 (CO), 156.1 (CO), 79.3 (C), 71.0 (CH_2), 70.4 (CH_2), 70.3 (CH_2), 68.7 (CH_2), 51.9 (CH_3), 40.4 (CH_2), 28.5 (CH_3). **ESI-MS** *m/z* (%): 300.1 (23) $[M+Na]^+$, 278.2 (1) $[M+H]^+$, 178.1 (100) $[M-Boc+H]^+$. **HRMS (ESI)** *m/z*: $[M+H]^+$ calculated for $C_{12}H_{23}NNaO_6$: 300.1418, found 300.1411.

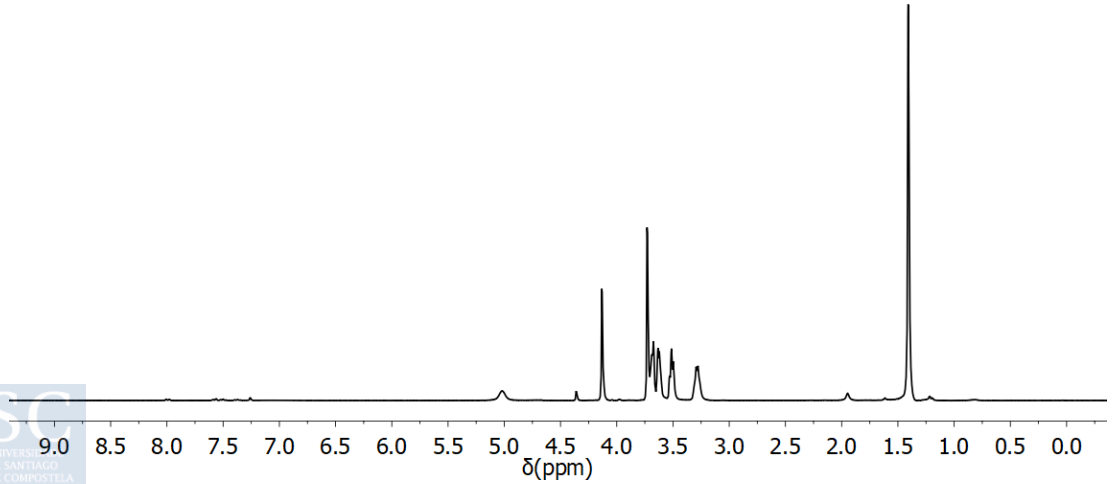

Figure 165. ^{1}H NMR ($CDCl_3$, 300 MHz) of **Boc-O2Oc-OMe** (**1**).

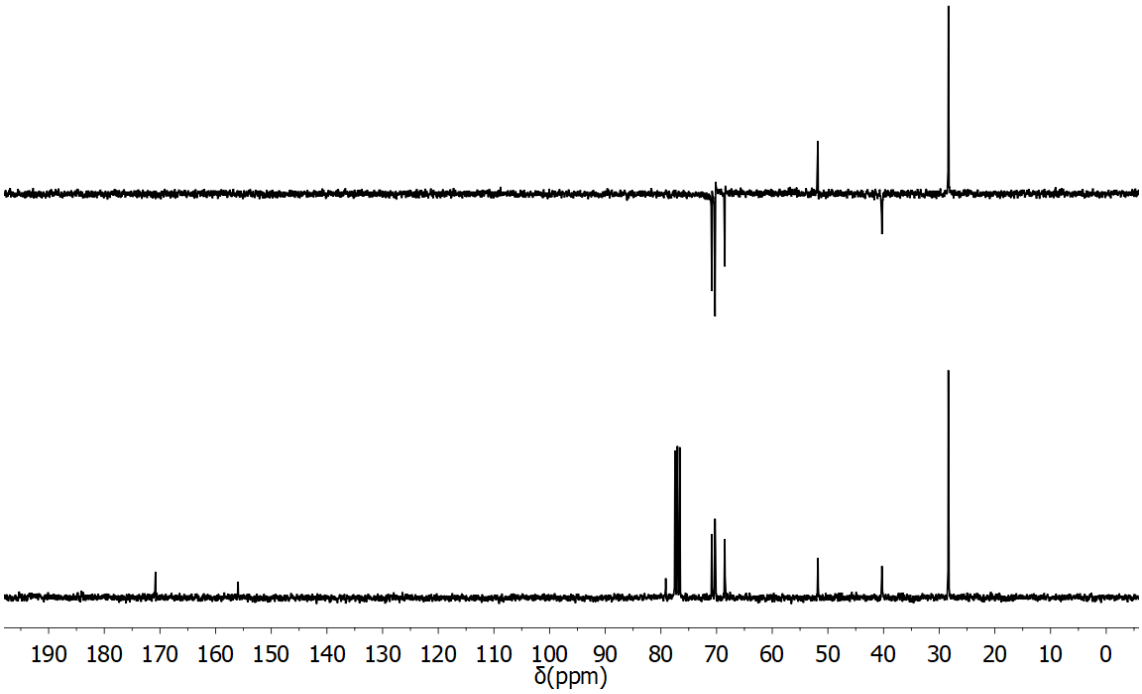

Figure 166. ^{13}C NMR (bottom) and DEPT-135 NMR (top) of **Boc-O2Oc-OMe** (**1**) ($CDCl_3$, 75 MHz).

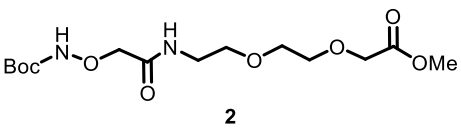

2

Boc-NOAc-O2Oc-OMe (2). A solution of **Boc-O2Oc-OMe** (**1**) (142 mg, 0.512 mmol) in CH_2Cl_2 (2 mL) was treated with TFA (2 mL) and stirred for 15 minutes. The solvent was removed under reduced pressure and the resulting oil was dissolved in CH_2Cl_2 and further evaporated. This process was repeated three times. The resulting residue was dried at high vacuum for 2 hours. Then, it was dissolved in dry CH_2Cl_2 (5 mL) and treated with DIEA (351 µL, 2.05 mmol), *N*-HBTU (243 mg, 0.640 mmol) and (Boc-aminooxy)acetic acid (108 mg, 0.563 mmol). The reaction mixture was stirred for 1.5 hours at room temperature under argon atmosphere and then washed with aqueous solutions of HCl (5%, 3 x 5 mL) and $NaHCO_3$ (sat., 3 x 5 mL). The organic phase was dried over anhydrous $MgSO_4$, filtered and concentrated under vacuum. The resulting residue was purified by flash chromatography (0-3% MeOH/CH_2Cl_2) and the product was obtained as a light-yellow oil [128 mg, 72%, R_f = 0.68 (10% MeOH/CH_2Cl_2)]. **^{1}H NMR** ($CDCl_3$, 300 MHz, δ): 7.99 (br, 1H, NH), 7.86 (br, 1H, NH), 4.32 (s, 2H, $COCH_2O$), 4.15 (s, 2H, $COCH_2ON$), 3.73 (s, 3H, OMe), 3.70 (m, 2H, CH_2), 3.67 (m, 2H, CH_2), 3.57 (m, 2H, CH_2), 3.49 (m, 2H, CH_2), 1.45 (s, 9H, Boc). **^{13}C NMR** ($CDCl_3$, 75 MHz, δ): 171.1 (CO), 169.1 (CO), 157.6 (CO), 82.6 (C), 76.0 (CH_2), 71.0 (CH_2), 70.4 (CH_2), 69.6 (CH_2), 68.6 (CH_2), 52.0 (CH_3), 38.9 (CH_2), 28.2 (CH_3). **ESI-MS** *m/z* (%): 373.2 (51) $[M+Na]^+$, 351.2 (17) $[M+H]^+$, 295.1 (62) $[M-tBu+H]^+$, 251.1 (100) $[M-Boc+H]^+$. **HRMS (ESI)** *m/z*: $[M+H]^+$ calculated for $C_{14}H_{27}N_2O_8$: 351.1762, found 351.1769.

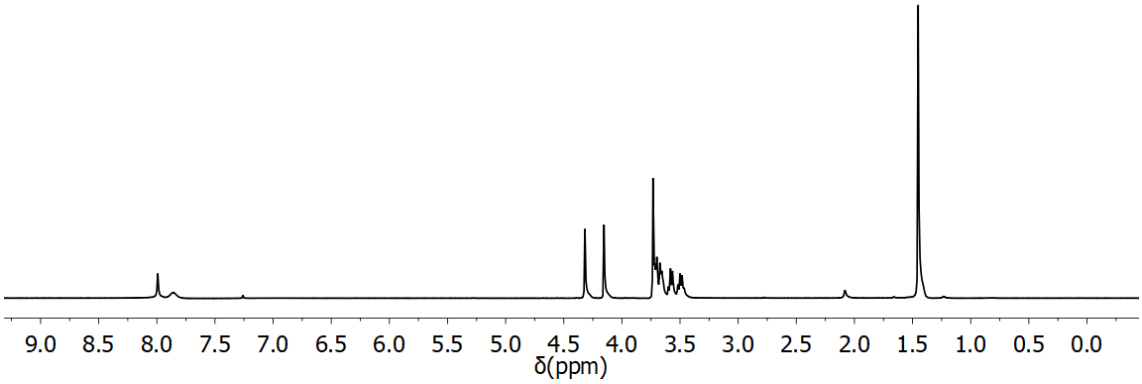

Figure 167. ^{1}H NMR ($CDCl_3$, 300 MHz) of **Boc-NOAc-O2Oc-OMe** (**2**).

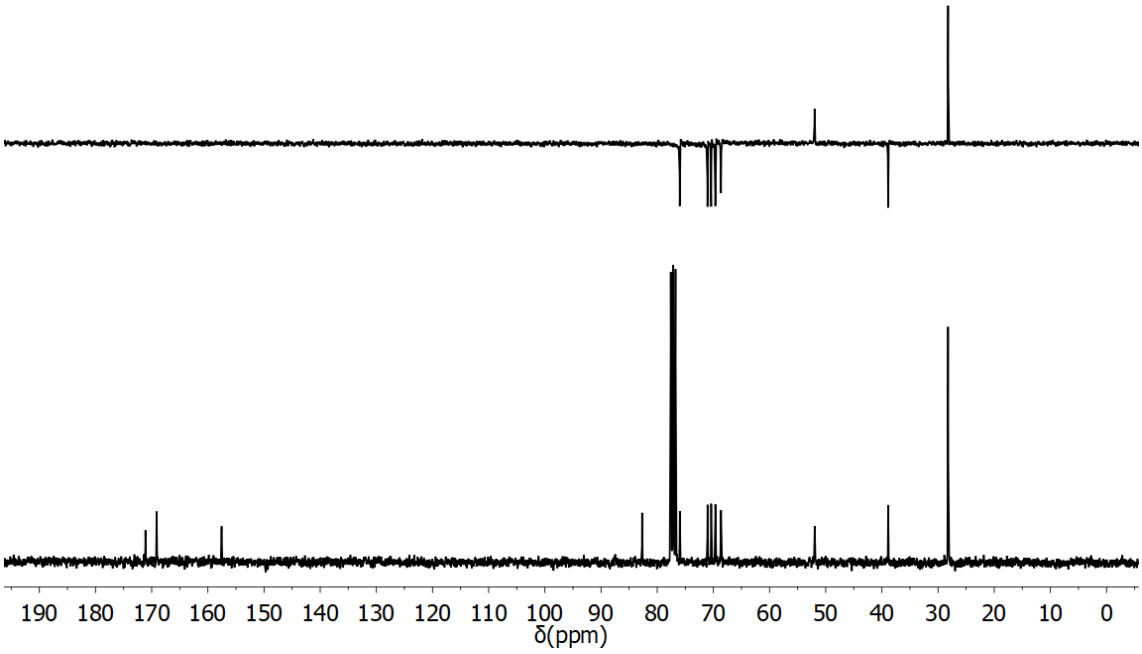

Figure 168. ^{13}C NMR (bottom) and DEPT-135 NMR (top) of **Boc-NOAc-O2Oc-OMe** (**2**) ($CDCl_3$, 75 MHz).

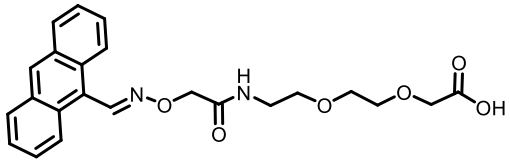

Ant1 (3)

Ant1 (3). A solution of **Boc-NOAc-O2Oc-OMe** (**2**) (99 mg, 0.283 mmol) in MeOH/H_2O (3:1, 6 mL) was treated with LiOH (34 mg, 1.42 mmol). After stirring for 3 hours, the solution was concentrated under reduced pressure to decrease the MeOH content and the aqueous phase was washed with Et_2O (3 x 2 mL). Then, the aqueous phase was acidified with aqueous HCl (5%) to pH 2 and extracted with CH_2Cl_2 (3 x 5 mL). The organic phase was dried over anhydrous $MgSO_4$, filtered and concentrated under vacuum. The resulting light-yellow oil was dissolved in a mixture of TFA/CH_2Cl_2 and stirred for 30 minutes. The mixture was concentrated under reduced pressure, diluted in CH_2Cl_2 and concentrated to dryness; this process was repeated three times. The residue obtained was dried under high vacuum for 2 hours.

After this time, the resulting residue was dissolved in $CHCl_3$ (3 mL) and treated with 9-anthracenecarboxaldehyde (58 mg, 0.283 mmol). The mixture was sonicated for 15 minutes protected from light with aluminium foil. Then, $CHCl_3$ was concentrated under reduced pressure and the residue was solubilized in MeCN/MilliQ-H_2O + 0.1%TFA (1:4). This solution was purified by semipreparative RP-HPLC using a Phenomenex Luna C18 (2) 100Å column [gradient: H_2O (0.1% TFA)/MeCN (0.1% TFA), 80:20 → 80:20 (5 min); 80:20 → 5:95 (40 min), R_t = 24.5 min]. The proper fractions were freeze-dried to provide **Ant1** as a yellow solid with an overall yield of 33% (40 mg). The pure product was stored at -20°C until further use. **^{1}H NMR** (MeOD-d_4, 300 MHz, δ): 9.38 (s, 1H, H_{Ar}), 8.56 (s, 1H, CH_{Ox}), 8.48 (d, J = 8.5 Hz, 2H, 2 H_{Ar}), 8.05 (d, J = 8.2 Hz, 2H, 2 H_{Ar}), 7.51 (m, 4H, 4 H_{Ar}), 4.76 (s, 2H, $COCH_2ON$), 3.92 (s, 2H, $COCH_2O$), 3.58 (m, 2H, CH_2), 3.49 (m, 6H, 3 CH_2). **^{13}C NMR** (MeOD-d_4, 75 MHz, δ): 174.2 (CO), 172.7 (CO), 151.0 (CH), 132.6 (C), 131.3 (C), 130.8 (CH), 129.9 (CH), 128.0 (CH), 126.4 (CH), 126.0 (CH), 124.1 (C), 73.8 (CH_2), 71.4 (CH_2), 71.1 (CH_2), 70.5 (CH_2), 69.0 (CH_2), 40.1 (CH_2). **ESI-MS** *m/z* (%): 447.2 (51) $[M+Na]^+$, 425.2 (100) $[M+H]^+$. **HRMS (ESI)** *m/z*: $[M+H]^+$ calculated for $C_{23}H_{25}N_2O_6$: 425.1707, found 425.1706.

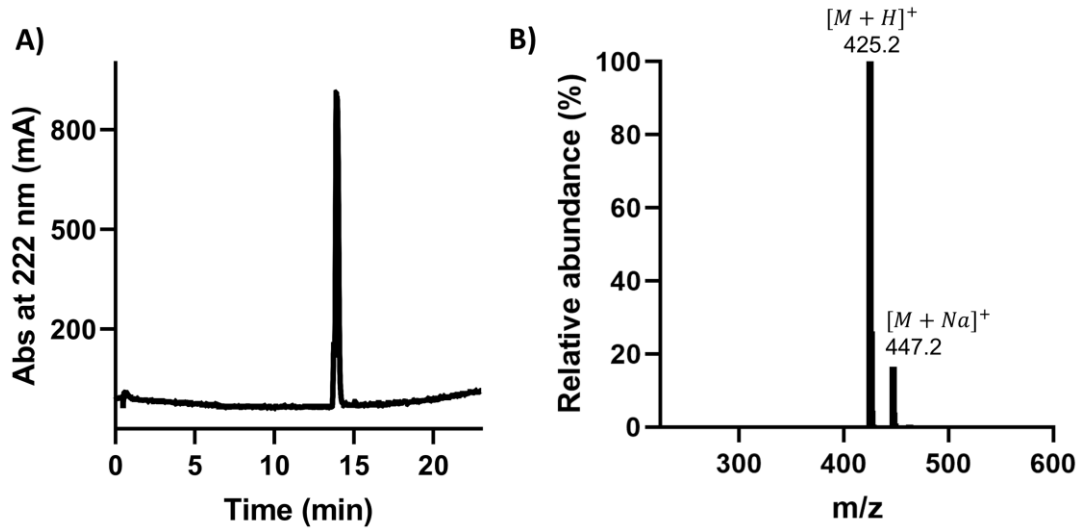

Figure 169. (A) **RP-uHPLC** of **Ant1** (**3**): [Agilent SB-C18 column, H_20 (0.1% TFA)/MeCN (0.1% TFA), 100:0 → 100:0 (2 min) and 100:0 → 25:75 (19 min)] R_t = 13.9 min. (B) ESI-MS of the main peak.

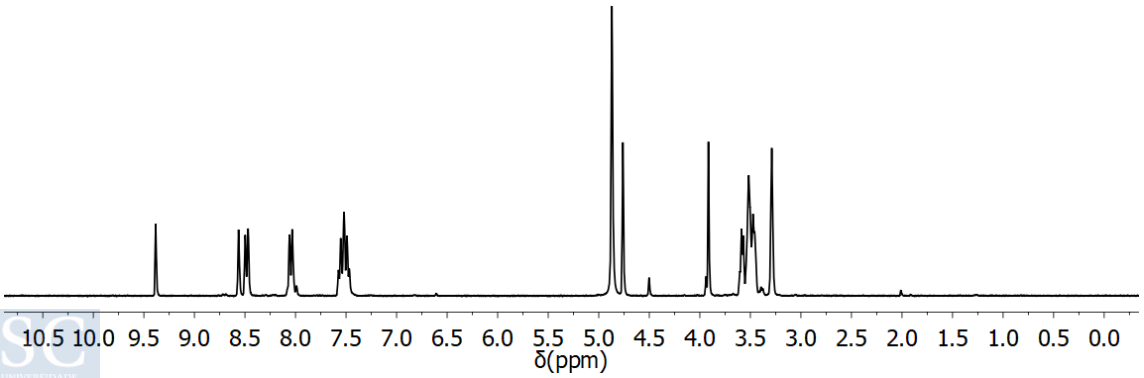

Figure 170. ^{1}H NMR (MeOD-d_4, 300 MHz) of **Ant1** (**3**).

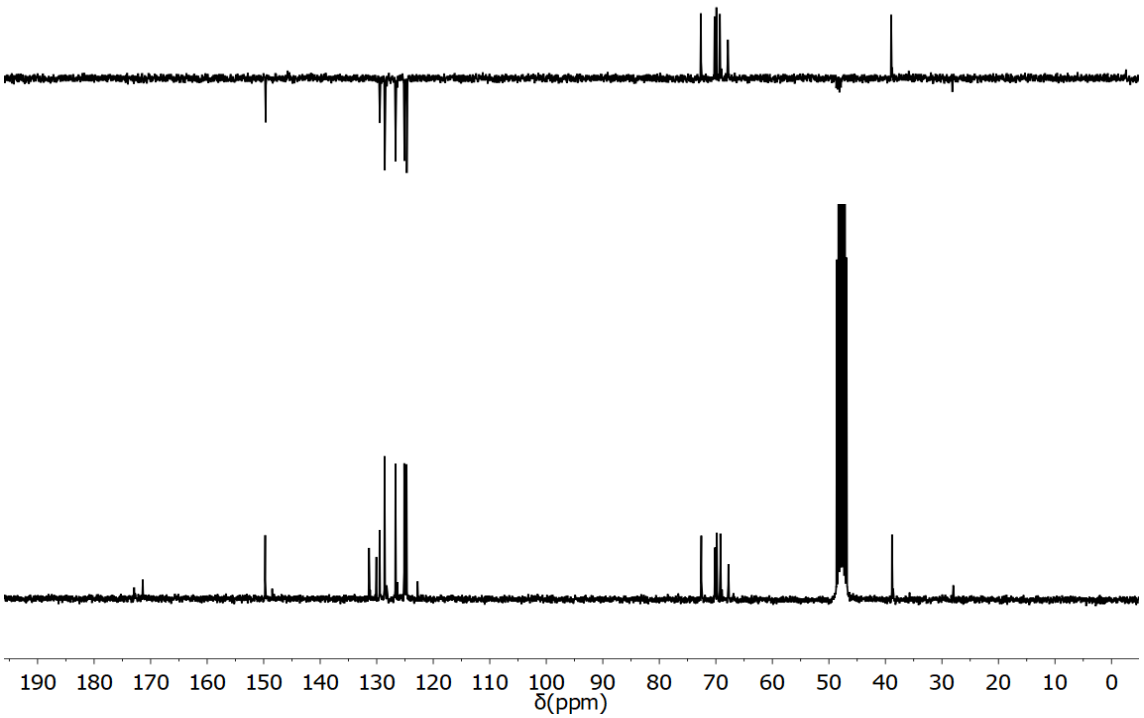

Figure 171. ^{13}C NMR (bottom) and DEPT-135 NMR (top) of **Ant1** (**3**) (MeOD-d_4, 75 MHz).

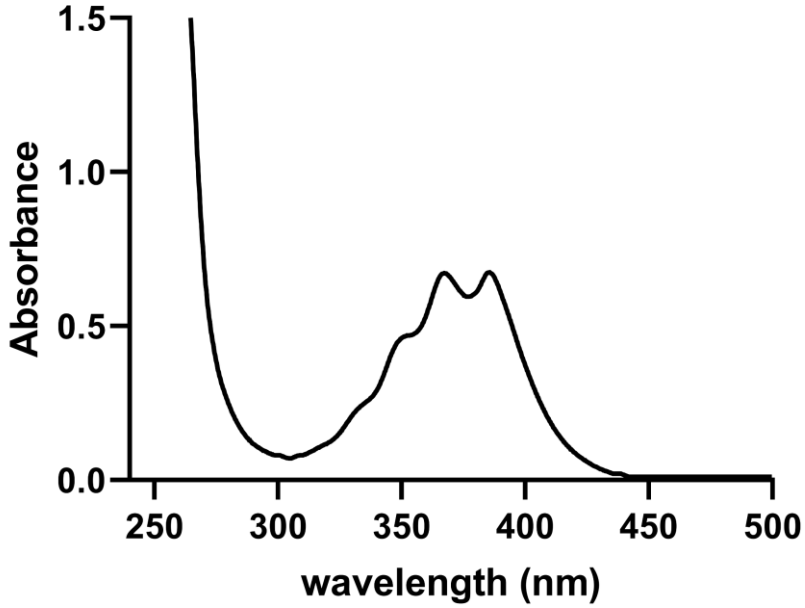

Figure 172. UV-Vis spectrum of an aqueous solution of **Ant1** (**3**) (100 µM).

USC UNIVERSIDADE DE SANTIAGO DE COMPOSTELA

8.2.1.6. Synthesis of the azobenzene aldehyde

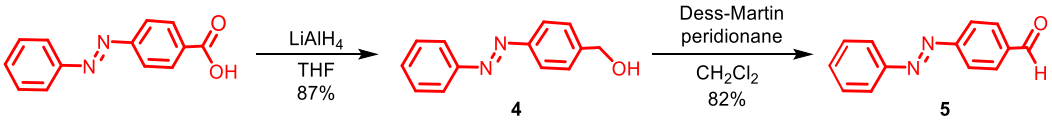

Figure 173. Synthetic scheme to obtain 4-(phenylazo)benzaldehyde (**5**).

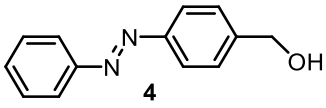

4-(phenylazo)benzyl alcohol (4). A solution of 4-(phenylazo)benzoic acid (404 mg, 1.79 mmol) in dry THF (18 mL) was treated with a solution of $LiAlH_4$ in THF (1.0 M, 5.37 mL, 5.37 mmol) under argon atmosphere. The reaction mixture was stirred under argon atmosphere during 3 hours at room temperature and protected from light using aluminium foil. Then, the reaction was quenched with an aqueous solution of KOH (5 wt%, 10 mL) and diluted with ethyl acetate (10 mL). The resulting mixture was washed with an aqueous solution of NaCl (sat., 3 x 10 mL). The organic phase was dried over anhydrous $MgSO_4$, filtered and concentrated under vacuum. The resulting residue was purified by flash chromatography (5% MeOH/CH_2Cl_2) to obtain the product as an orange solid [332 mg, 87%, R_f = 0.79 (10% MeOH/CH_2Cl_2)]. **^{1}H NMR** ($CDCl_3$, 300 MHz, δ): 7.93 (d, *J* = 8.5 Hz, 4H, H_{Ar}), 7.52 (d, *J* = 7.9 Hz, 5H, H_{Ar}), 4.79 (s, 2H, CH_2), 1.64 (bs, 1H, OH). **^{13}C NMR** ($CDCl_3$, 75 MHz, δ): 152.7 (C), 152.2 (C), 143.8 (C), 131.0 (CH), 129.1 (CH), 127.4 (CH), 123.1 (CH), 122.8 (CH), 64.9 (CH_2). **ESI-MS** *m/z* (%): 213.1 (100) $[M+H]^+$. **HRMS (ESI)** *m/z*: $[M+H]^+$ calculated for $C_{13}H_{13}N_2O$: 213.1022, found 213.1018. The characterization data are consistent with those reported in the literature.[280]

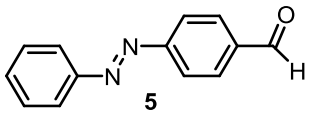

4-(phenylazo)benzaldehyde (5). A solution of 4-(phenylazo)benzyl alcohol (**4**) (304 mg, 1.43 mmol) in dry CH_2Cl_2 (17 mL) was treated with Dess-Martin peridionane (729 mg, 1.72 mmol). The reaction mixture was stirred for 1.5 hours at room temperature and protected from light with aluminium foil. After this time, the mixture was washed with an aqueous solution of $NaHCO_3$ (sat., 3 x 5 mL) and an aqueous solution of NaCl (sat., 3 x 5 mL). The organic phase was dried over anhydrous $MgSO_4$, filtered and concentrated under vacuum. The resulting residue was purified by flash chromatography (2% MeOH/CH_2Cl_2) to obtain the product as an orange solid [247 mg, 82%, R_f = 0.85 (5% MeOH/CH_2Cl_2)]. **^{1}H NMR** ($CDCl_3$, 300 MHz, δ): 10.09 (s, 1H, CHO), 8.02 (br s, 4H, H_{Ar}), 7.96 (m, 2H, H_{Ar}), 7.53 (m, 3H, H_{Ar}). **^{13}C NMR** ($CDCl_3$, 75 MHz, δ): 191.5 (CHO), 155.9 (C), 152.6 (C), 137.5 (C), 132.0 (CH), 130.7 (CH), 129.2 (CH), 123.3 (CH), 123.2 (CH). **ESI-MS** *m/z* (%): 211.1 (100) $[M+H]^+$. **HRMS (ESI)** *m/z*: $[M+H]^+$ calculated for $C_{13}H_{11}N_2O$: 211.0866, found 211.0858. The characterization data are consistent with those reported in the literature.[280]

[280] a) Y. Kim, M. Koh, D. K. Kim, H. S. Choi, S. B. Park, *J. Comb. Chem.* **2009**, *11*, 928-937; b) C. Freeman, J. S. Vyle, F. Heaney, *RSC Adv.* **2013**, *3*, 1652-1655; c) A. Samanta, B. J. Ravoo, *Chem. Eur. J.* **2014**, *20*, 4966-4973.

8.2.1.7. Condensation reaction for the preparation of CP2N, CP2P and CP2azo-ox

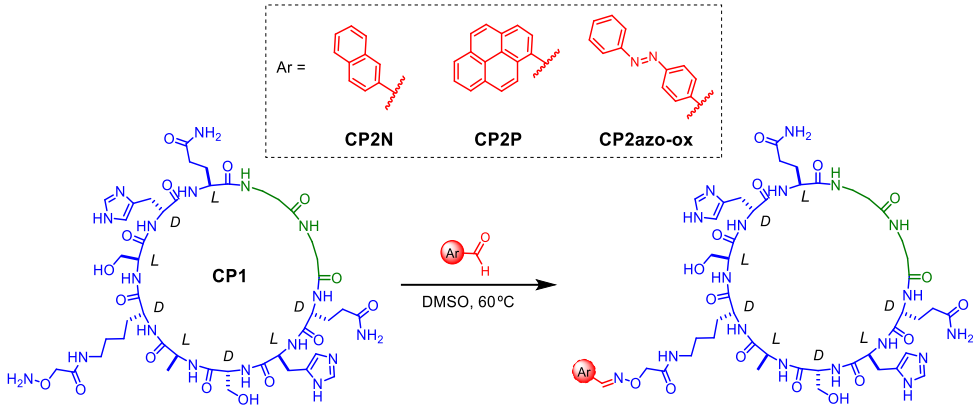

Figure 174. Synthesis of **CP2N**, **CP2P** and **CP2azo-ox**.

General procedure: **CP1** (1 equiv) was dissolved in a solution of the corresponding aldehyde (1.2 equiv) in DMSO (100 µL) and the mixture was heated at 60°C for approximately 2 hours, until no starting substrate was detected by HPLC-MS analysis. The mixture was poured into an eppendorf containing cold diethyl ether (2 mL) and then powerfully shaken to obtain a precipitate. After centrifugation, the organic phase was discarded. The residue was sonicated for 15 minutes with fresh diethyl ether (2 mL), centrifugated and decantated. This step was repeated three times. The product was dried under reduced pressure to provide **CP2N**, **CP2P** or **CP2azo-ox**.

CP2N: The general procedure described above was carried out with **CP1** (7.1 mg, 6.3 µmol) and 2-naphthaldehyde (1.2 mg, 7.7 µmol) to obtain the product as a white solid in 63% yield (5.0 mg). **ESI-MS** *m/z* (%): 1257.6 (7) $[M+H]^+$, 629.4 (100) $[M+2H]^{2+}$, 420.1 (2) $[M+3H]^{3+}$. **HRMS (ESI)** *m/z*: $[M+H]^+$ calculated for $C_{56}H_{77}N_{18}O_{16}$: 1257.5759, found 1257.5748. **FTIR (neat)**: ν = 3288.0 (amide A), 1643.2 (amide I), 1538.7 (amide II) cm^{-1}.

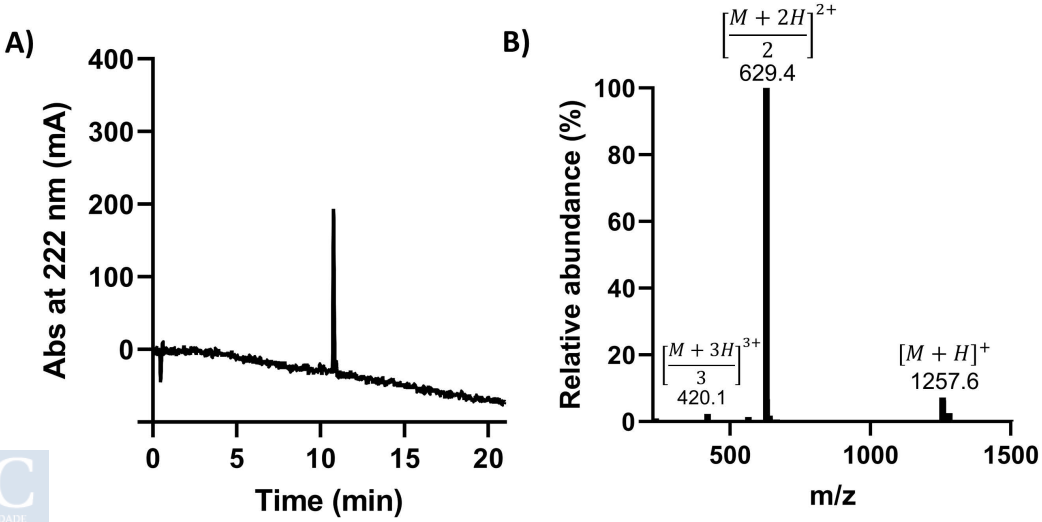

Figure 175. (A) **RP-uHPLC** of **CP2N**: [Agilent SB-C18 column, H_20 (0.1% TFA)/MeCN (0.1% TFA), 100:0 → 100:0 (2 min) and 100:0 → 25:75 (19 min)] R_t = 10.3 min. (B) ESI-MS of the main peak.

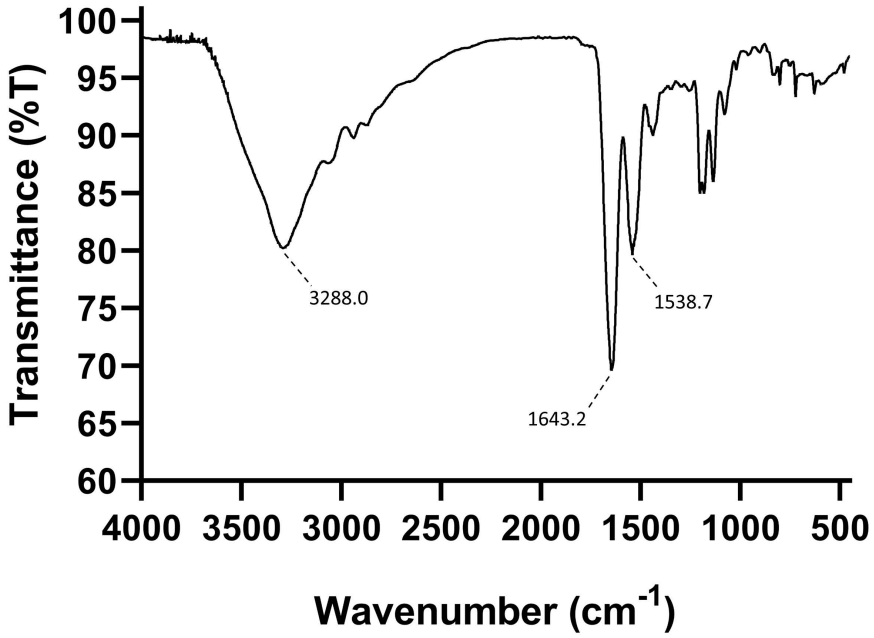

Figure 176. FT-IR spectrum of **CP2N** (solid, 298 K).

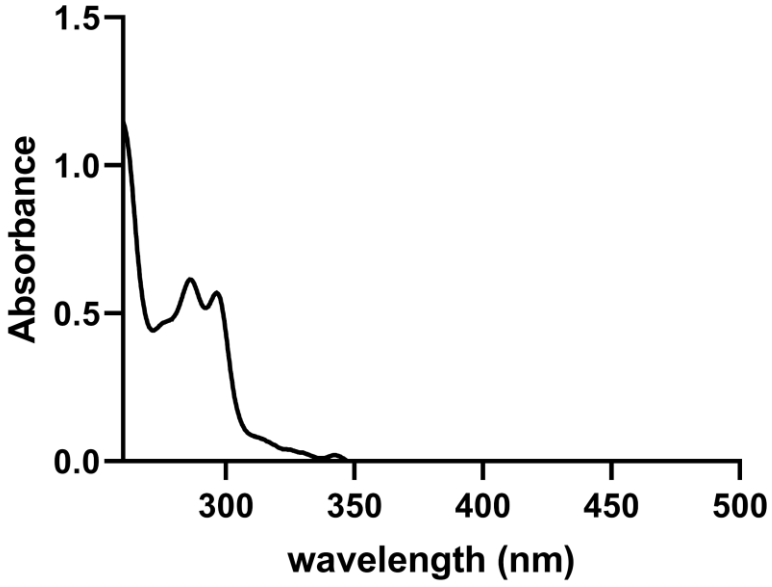

Figure 177. UV-Vis spectrum of an aqueous solution of **CP2N** (50 µM).

USC
UNIVERSIDADE DE SANTIAGO DE COMPOSTELA

CP2P: The general procedure described above was carried out with **CP1** (8.5 mg, 7.6 µmol) and 1-pyrenecarboxaldehyde (2.1 mg, 9.1 µmol) to obtain the product as a white solid in 86% yield (8.7 mg). **ESI-MS** *m/z* (%): 1331.6 (13) $[M+H]^+$, 666.4 (100) $[M+2H]^{2+}$, 445.4 (2) $[M+3H]^{3+}$. **HRMS (ESI)** *m/z*: $[M+H]^+$ calculated for $C_{62}H_{79}N_{18}O_{16}$: 1331.5916, found 1331.5933. **FTIR (neat)**: ν = 3286.1 (amide A), 1651.1 (amide I), 1544.6 (amide II) cm^{-1}.

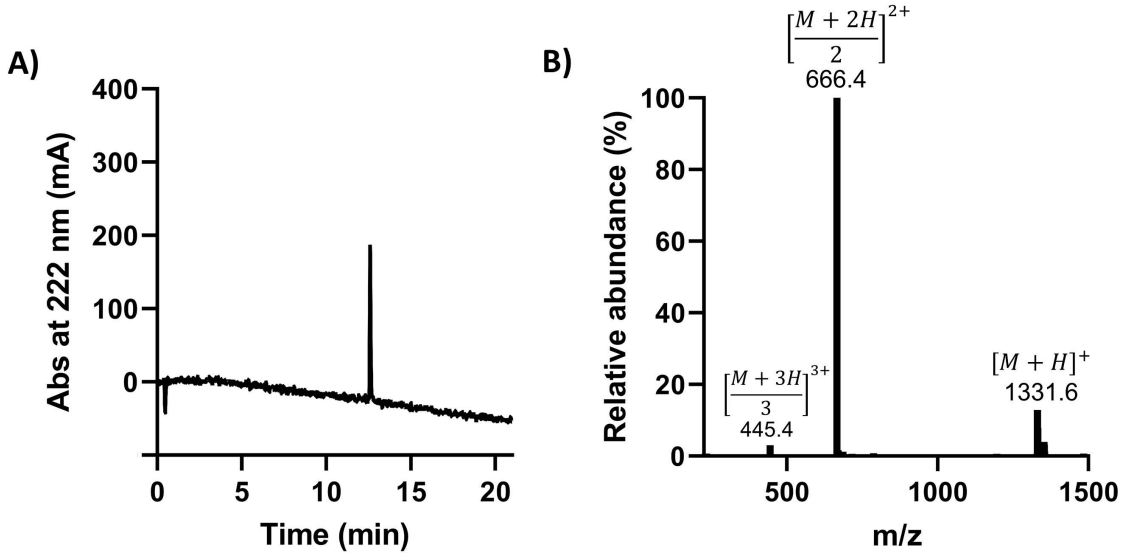

Figure 178. (A) **RP-uHPLC** of **CP2P**: [Agilent SB-C18 column, H_20 (0.1% TFA)/MeCN (0.1% TFA), 100:0 → 100:0 (2 min) and 100:0 → 25:75 (19 min)] R_t = 12.7 min. (B) ESI-MS of the main peak.

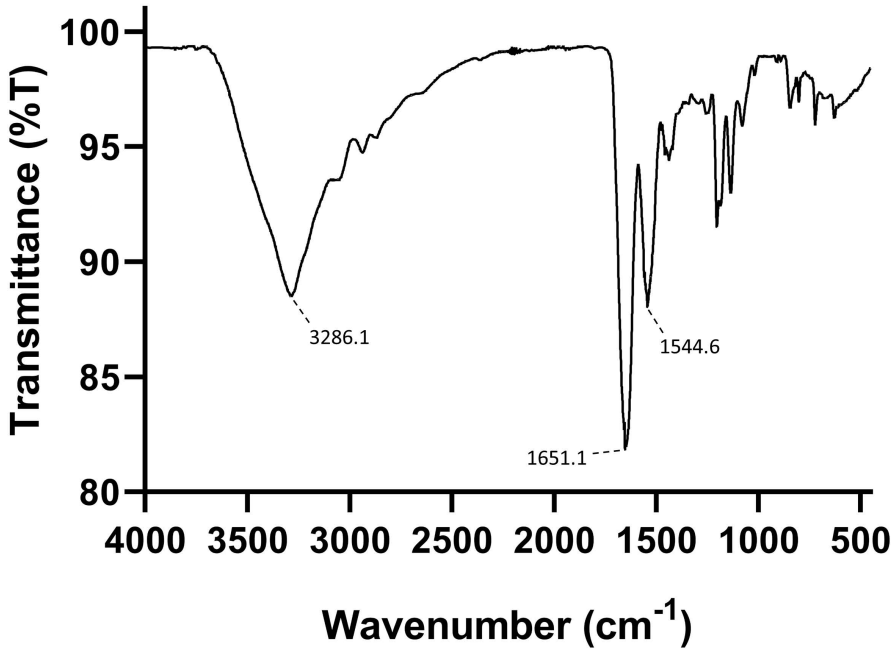

Figure 179. FT-IR spectrum of **CP2P** (solid, 298 K).

USC UNIVERSIDADE DE SANTIAGO DE COMPOSTELA

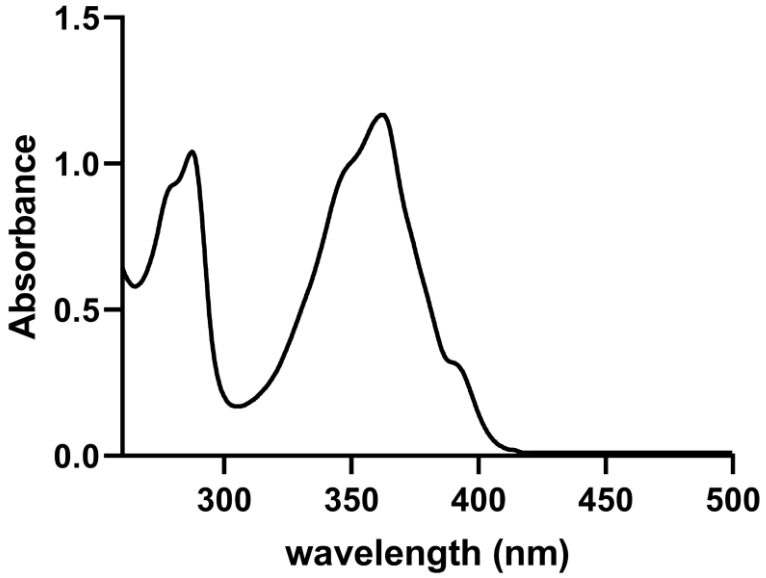

Figure 180. UV-Vis spectrum of an aqueous solution of **CP2P** (50 µM).

CP2azo-ox: The general procedure described above was carried out with **CP1** (6.2 mg, 5.5 µmol) and 4-(phenylazo)benzaldehyde (**5**) (1.4 mg, 6.7 µmol) to obtain the product as an orange solid in 41% yield (3.0 mg). **ESI-MS** *m/z* (%): 1311.6 (6) $[M+H]^+$, 656.2 (100) $[M+2H]^{2+}$, 437.8 (4) $[M+3H]^{3+}$. **HRMS (ESI)** *m/z*: $[M+H]^+$ calculated for $C_{58}H_{79}N_{20}O_{16}$: 1311.5977, found 1311.5971. **FTIR (neat)**: ν = 3280.1 (amide A), 1651.1 (amide I), 1538.7 (amide II) cm^{-1}.

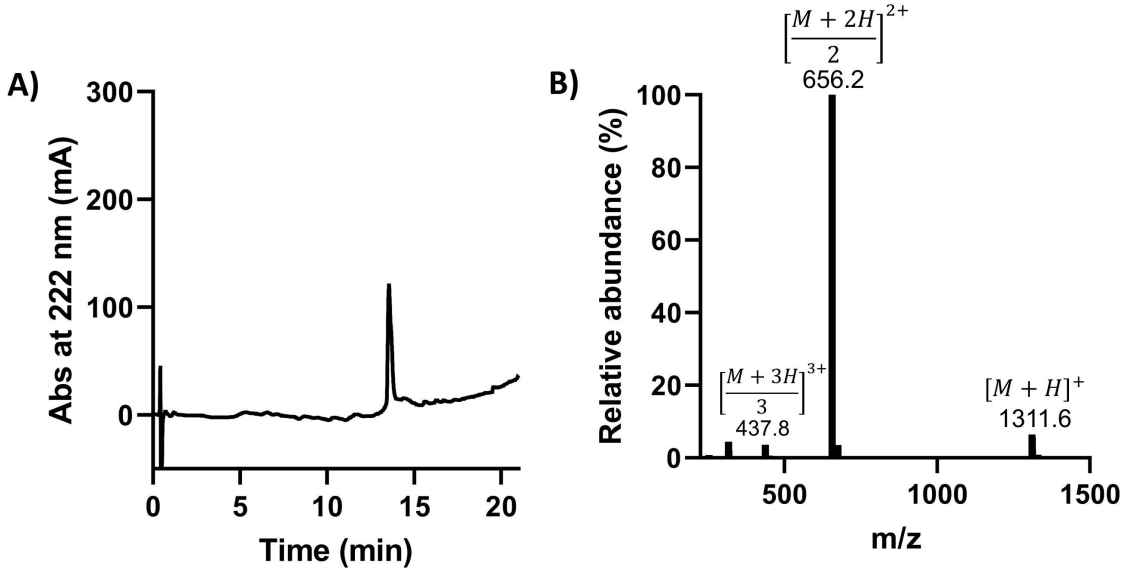

Figure 181. (A) **RP-uHPLC** of **CP2azo-ox**: [Agilent SB-C18 column, H_20 (0.1% TFA)/MeCN (0.1% TFA), 90:10 → 90:10 (2 min) and 90:10 → 40:60 (19 min)] R_t = 13.6 min. (B) ESI-MS of the main peak.

USC
UNIVERSIDADE DE SANTIAGO DE COMPOSTELA

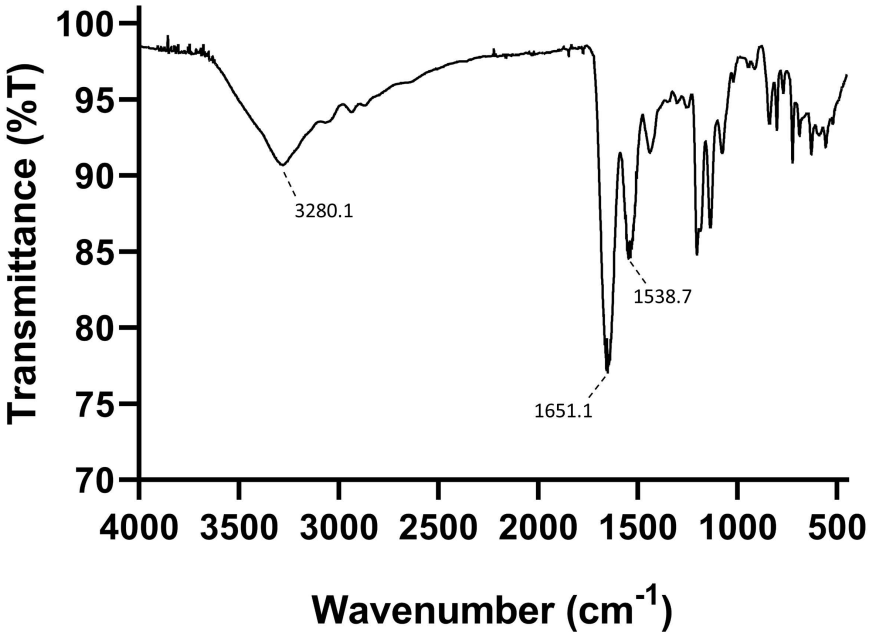

Figure 182. FT-IR spectrum of **CP2azo-ox** (solid, 298 K).

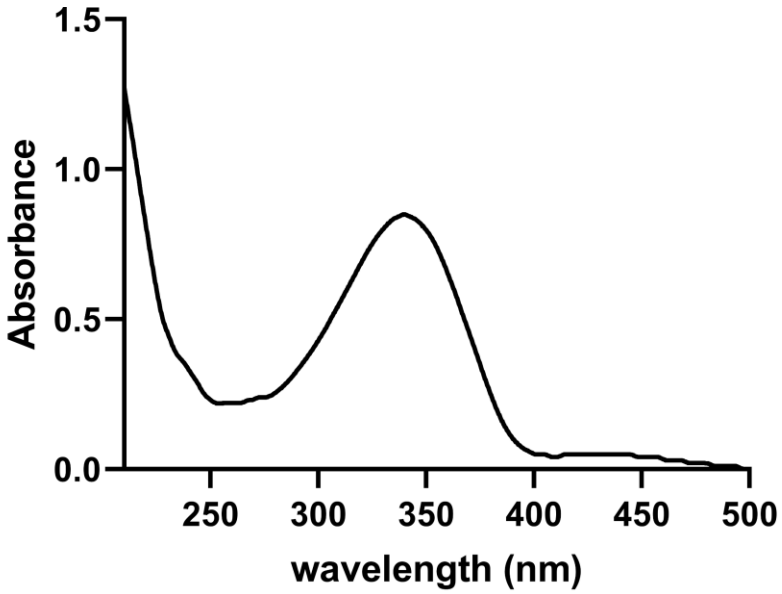

Figure 183. UV-Vis spectrum of an aqueous solution of **CP2azo-ox** (50 μM).

USC
UNIVERSIDADE DE SANTIAGO DE COMPOSTELA

8.2.1.8. Solid-phase synthesis of CP2azo-am derivative

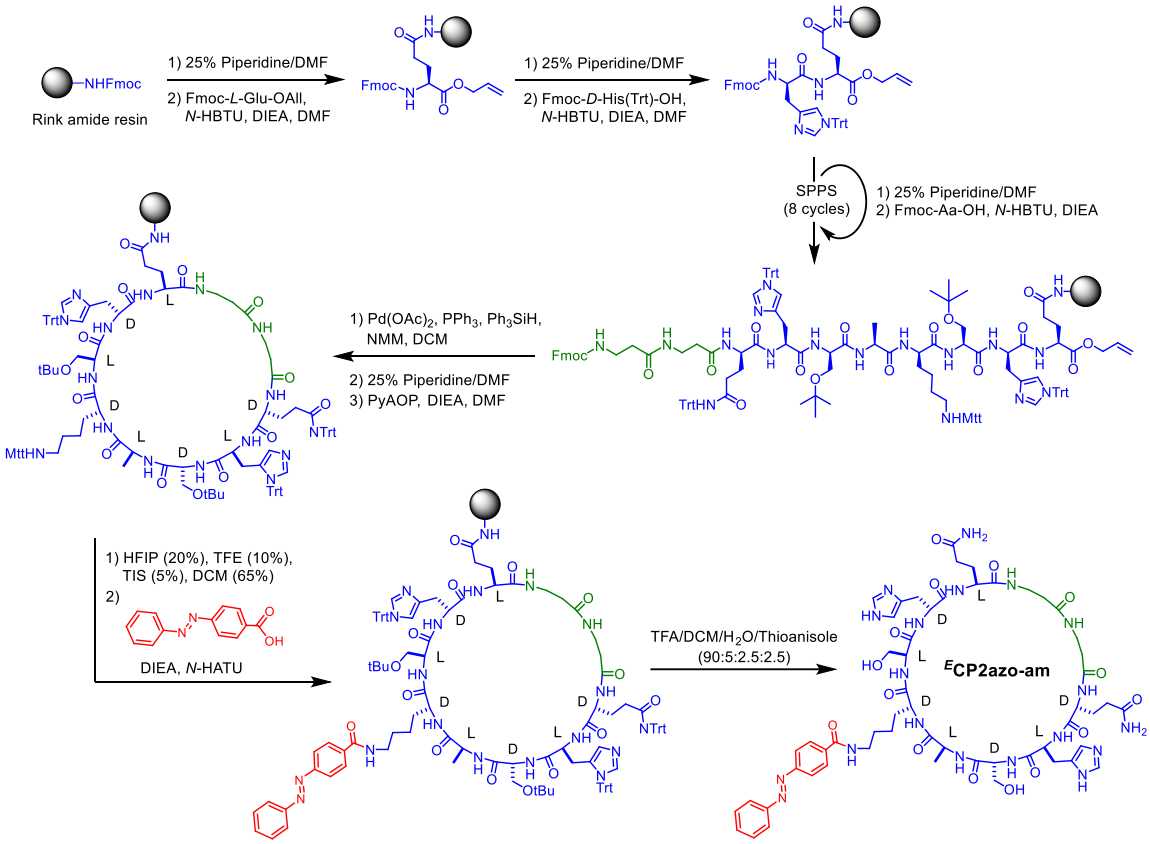

Figure 184. Solid-phase synthesis of **^{E}CP2azo-am**.

The synthesis of the linear peptide and the cyclization reaction were performed in solid-phase following the protocol previously described for **CP1**. Then, the 4-methyltrityl group (Mtt) of the lysine side chain was removed by treating the resin with a freshly prepared mixture of DCM, HFIP, TFE and TIS (6.5:2:1:0.5, 4 mL) for 2 hours. This process was repeated three times. After removal of this mixture, the resin was washed with DCM (3 x 4 mL) and DMF (3 x 4 mL). Subsequently, a solution of 4-(phenylazo)benzoic acid (3 equiv), *N*-HATU (3 equiv) and DIEA (6 equiv) in DMF (4 mL) was added to the resin. After shaking the mixture for 30 min, the resin was thoroughly washed with DMF (3 x 4 mL). Deprotection of CP side chains and cleavage was carried out by shaking the resin with a freshly prepared solution of TFA, DCM, H_2O and Thioanisole (90:5:2.5:2.5, 10 mL/g of resin) for 2 hours. The mixture was collected by filtration, concentrated with an argon steam, and added dropwise over a flask containing cold Et_2O (10 mL of Et_2O per 100 mg of initial resin). The precipitate was centrifuged (4000 rpm x 10 min) and the supernatant discarded. After washing with diethyl ether, the resulting residue was dried under reduced pressure and solubilized in MilliQ-H_2O with 0.1% TFA (0.1 mL/mg of crude). The resulting solution was purified by semipreparative RP-HPLC using a Phenomenex Luna C18 (2) 100Å column [gradient: H_2O (0.1% TFA)/MeCN (0.1% TFA), 80:20 → 80:20 (5 min); 80:20 → 40:60 (40 min), R_t = 16.5 min]. After freeze-drying of the proper fractions, **CP2azo-am** was obtained as

an orange solid with an overall yield of 7% (25.1 mg). The pure product was stored at -20°C until further use. **ESI-MS** *m/z* (%): 1254.8 (11) $[M+H]^+$, 627.6 (100) $[M+2H]^{2+}$, 418.9 (3) $[M+3H]^{3+}$. **HRMS (ESI)** *m/z*: $[M+H]^+$ calculated for $C_{56}H_{76}N_{19}O_{15}$: 1254.5763, found 1254.5765. **FTIR (neat)**: ν = 3288.0 (amide A), 1635.2 (amide I), 1536.7 (amide II) cm^{-1}.

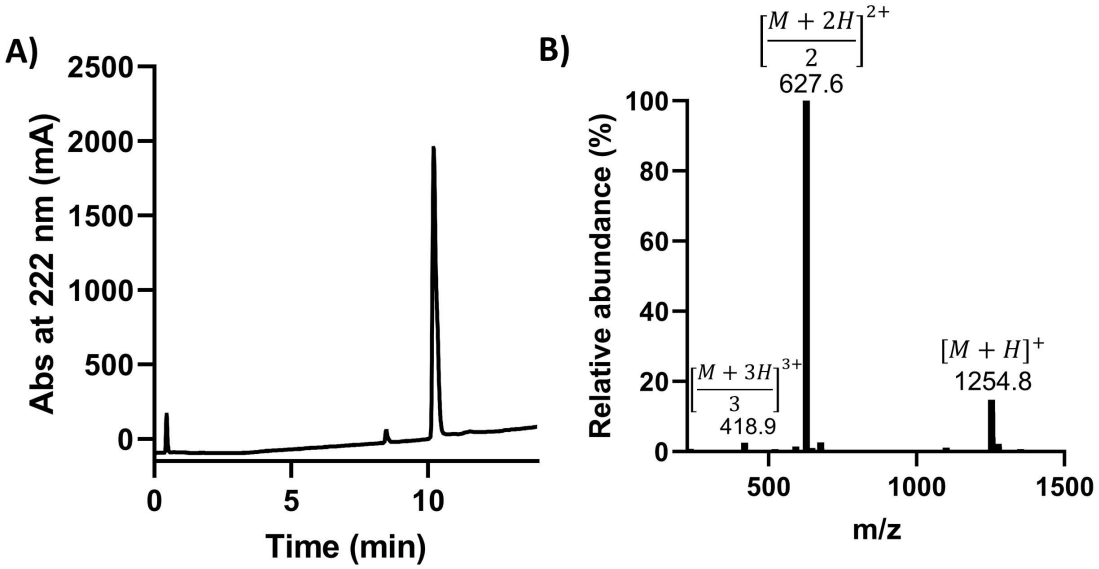

Figure 185. (A) **RP-uHPLC** of **CP2azo-am**: [Agilent SB-C18 column, H_20 (0.1% TFA)/MeCN (0.1% TFA), 100:0 → 100:0 (2 min) and 100:0 → 50:50 (12 min)] R_t = 10.2 min. (B) ESI-MS of the main peak.

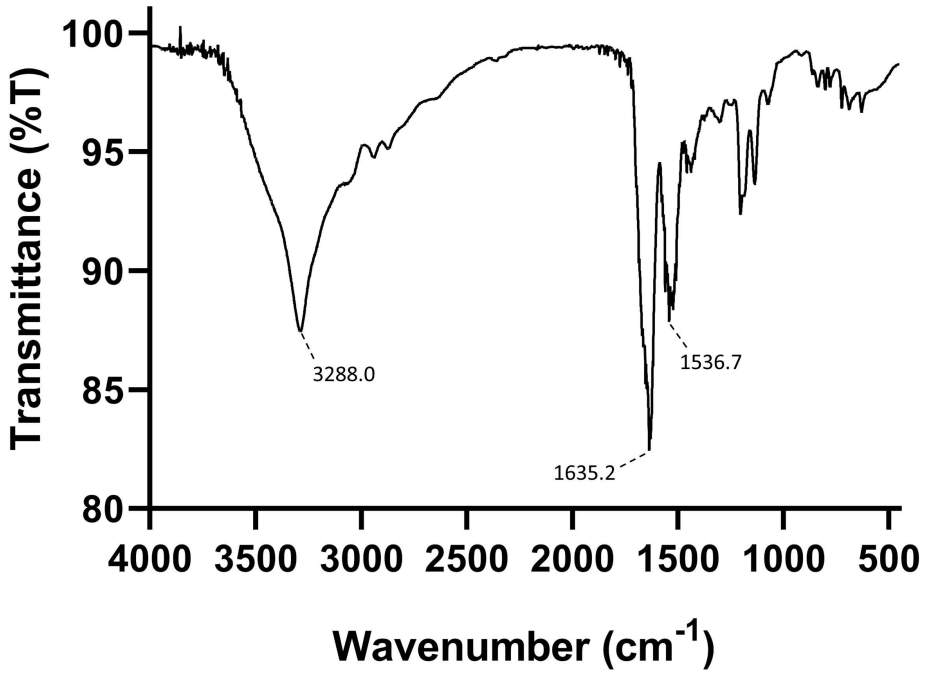

Figure 186. FT-IR spectrum of **CP2azo-am** (solid, 298 K).

USC UNIVERSIDADE DE SANTIAGO DE COMPOSTELA

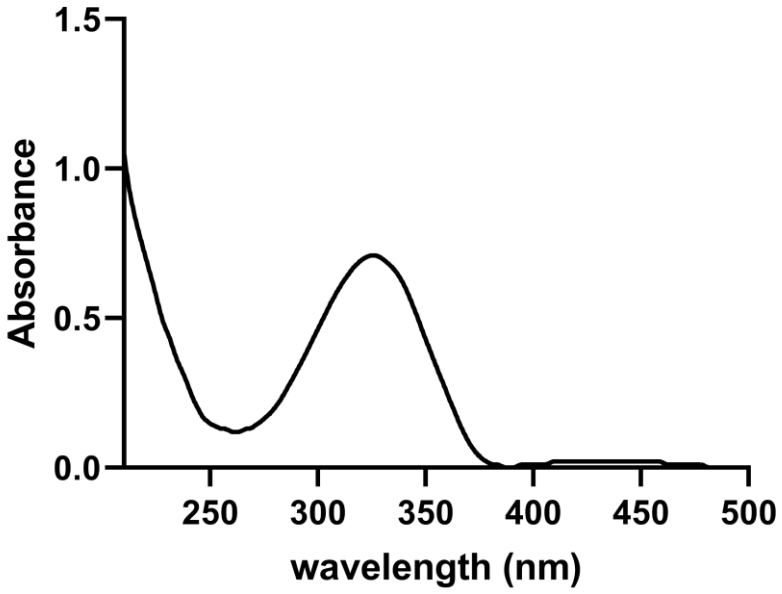

Figure 187. UV-Vis spectrum of an aqueous solution of **CP2azo-am** (50 µM).

USC
UNIVERSIDADE DE SANTIAGO DE COMPOSTELA

8.2.2. PHOTO-ASSEMBLING CYCLIC PEPTIDES FOR DYNAMIC LIGHT-DRIVEN PEPTIDE NANOTUBES

8.2.2.1. Methods

Kinetic studies of the isomerization, photostability and irradiation cycles

Solutions of **^{Z}CP3**, **^{E}CP3, ^{Z}CP4**, **^{E}CP4, ^{Z}CP5** or **^{E}CP5** (200 µM) at acidic (pH 1.8), native (pH 4.0-5.1), neutral (pH 7.0, 10 mM HEPES buffer) or basic conditions (pH 9.0, 10 mM Boric acid buffer) were degassed by bubbling argon for 5 min and sealed in a quartz cuvette under a micro-hood with argon. The samples were allowed to equilibrate for 5 minutes before the irradiation. Then, the solutions were irradiated at the appropriate wavelength: 290-320 nm (Phillips TL 20W/12 RS lamp) or 254 nm (Phillips TUV 15W/G15 T8 lamp). The distance between the lamp and the sample was around 5 cm. At each specific time, a small aliquot (20 µL) of the irradiated solution was collected and diluted with milli-Q water + 0.1% TFA (20 µL) and an aqueous solution of 4-aminobenzoic acid (ABA, 0.03 mg/mL, 20 µL). The final ABA concentration in the solution was 0.01 mg/mL and it was used as an internal standard. The resulting samples were evaluated by uHPLC-MS (Agilent Technologies 1260 Infinity II with a 6120 Quadrupole LC-MS and an Agilent SB-C18 column) using the method specified in each case.

Thermal stability studies

Aqueous solutions of **^{Z}CP3** or **^{E}CP3** (200 µM) were heated at 25°C or 80°C in a thermoshaker. Sample aliquots (20 µL) were collected at each specific time. These aliquots were diluted with milli-Q water + 0.1% TFA (20 µL) and an aqueous solution of 4-aminobenzoic acid (ABA, 0.03 mg/mL, 20 µL). The final ABA concentration in the solution was 0.01 mg/mL and it was used as an internal standard. The samples were analysed by uHPLC-MS (Agilent Technologies 1260 Infinity II with a 6120 Quadrupole LC-MS and an Agilent SB-C18 column) using the method specified in each case.

Monitoring of the irradiation with ThT

In the experiments performed to monitor the isomerization process, the ThT was added after the irradiation to avoid its photodegradation.[279] Specifically, **^{Z}CP3** or **^{E}CP3** solutions (200 µM) in HEPES buffer (10 mM, pH 7.0) were prepared and irradiated at the appropriate wavelength: 290-320 nm (Phillips TL 20W/12 RS lamp) or 254 nm (Phillips TUV 15W/G15 T8 lamp). A small irradiated aliquot (400 µL) was taken every minute. Then, a ThT solution (40 µM, HEPES 10 mM, pH 7.0, 400 µL) was added to each sample aliquot to obtain a final CP concentration of 100 µM and a ThT concentration of 20 µM. Finally, the fluorescence spectra were recorded in a Varian Cary Eclipse

spectrophotometer by using an excitation wavelength of 440 nm and a Hellma® fluorescence quartz cuvette (10 x 4 mm).

Microfluidic experiments

The microfluidic device (channels size: 35 × 50 µm) was produced as previously reported (Figure 87).[216,241] For the generation of cyclic peptide droplets, an aqueous solution of **^{Z}CP3** (1.0 mM), **^{E}CP3** (1.0 mM), **^{Z}CP4** (1.5 mM) or **^{E}CP4** (1.5 mM) was sonicated for 60 min. Then, the oil phase was obtained by diluting to 0.5% v/v the commercial PicoSurf™ solution with HFE-7500 3M™ Novec™. The oil was injected into the device at a flow rate of 500 µL/h (I_{oil}), the triggering solutions at 150 µL/h (I_T) and the peptide solution at 300 µL/h (I_{CP}). The formation of the droplets was monitored with a high-speed Fastcam Mini camera equipped to a Nikon Eclipse Ti2. Droplets were collected at the outlet over HFE-7500 3M™ Novec™ containing 0.5% v/v Pico-Surf™ and analysed by epifluorescence (Olympus BX51 microscope) or confocal microscopy (Andor DragonFly spinning disc confocal setup mounted on a Nikon Eclipse Ti-E inverted microscope).

For droplet irradiation, a sample containing **^{Z}CP3** droplets at neutral pH (HEPES buffer) was sealed in a quartz cuvette and irradiated at 290-320 nm (Phillips TL 20W/12 RS lamp). The distance between the lamp and the sample was around 5 cm. The process was followed at different times on an Olympus BX51 microscope by deposition on a clean glass slide. All images were acquired at room temperature and analysed using ImageJ.[277] The interior of the irradiated droplets was analysed by uHPLC-MS, after lysing the vesicles by adding an aqueous solution of TFA (0.1% v/v) and sonicating for 30 seconds. This sample was centrifuged, decanted and the aqueous phase was analysed by uHPLC-MS (Agilent Technologies 1260 Infinity II with a 6120 Quadrupole LC-MS and an Agilent SB-C18 column).

USC UNIVERSIDADE DE SANTIAGO DE COMPOSTELA

8.2.2.2. Solid-phase synthesis of ^{P}CP3, ^{P}CP4 and ^{P}CP5

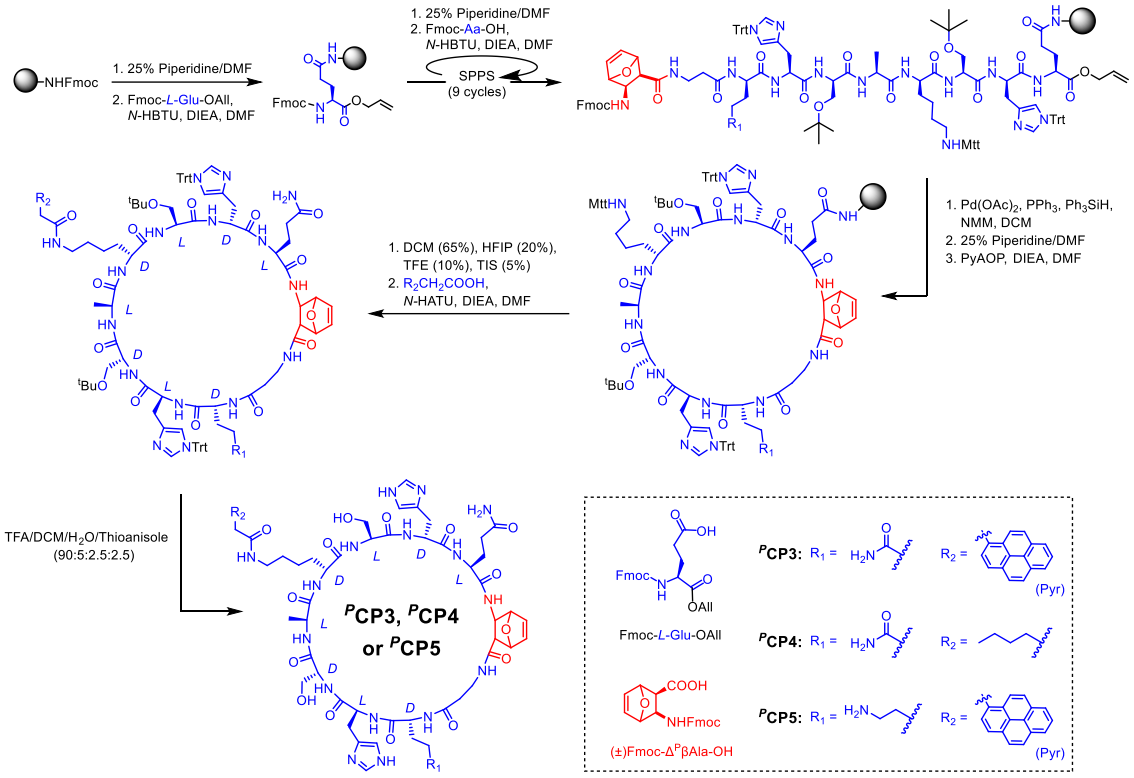

Figure 188. Solid-phase peptide synthesis to obtain **^{P}CP3**, **^{P}CP4** or **^{P}CP5**.

The synthesis of **^{P}CP3**, **^{P}CP4** or **^{P}CP5** was performed on a Rink Amide resin (100-200 mesh, 0.64 mmol/g) using manual Fmoc solid phase peptide synthesis.[215,216,229] Briefly, Fmoc-Rink Amide resin (400 mg, 256 µmol) was swelled in DCM (4 mL) for 30 minutes in a peptide synthesis vessel and washed with DMF (3 x 4 mL) and DCM (3 x 4 mL). Fmoc group was removed by treating the resin with a solution of piperidine in DMF (25%, 4 mL) for 20 min. After washing with DMF (3 x 4 mL) and DCM (3 x 4 mL), couplings were carried out under orbital shaking for 40 min at room temperature using a solution of Fmoc-protected amino acid (3 equiv), *N*-HBTU (3 equiv), DIEA (6 equiv) in DMF (4 mL). Finally, the resin was washed with DMF (3 x 4 mL). Cycles of deprotection and coupling were repeated until the fully-protected linear peptide was obtained. Interestingly, the number of equivalents was reduced for the coupling of the last amino acid by using a solution of (±)Fmoc-Δ^{P}βAla-OH (1.5 equiv), *N*-HBTU (1.5 equiv) and DIEA (3 equiv) in DMF (4 mL). Allyl protecting group deprotection was achieved by adding to the resin a degassed solution of $Pd(OAc)_2$ (0.25 equiv), PPh_3 (1.25 equiv), *N*-methylmorpholine (6 equiv), and phenylsilane (6 equiv) in dry DCM (4 mL). The mixture was shaken for 2 hours at room temperature. Then, the resin was filtered and washed with DCM (3 x 4 mL), DMF (3 x 4 mL), sodium diethyldithiocarbamate in DMF (0.5% v/v, 2 x 4 mL, 15 min), DMF (2 x 4 mL), a solution of DIEA in DMF (10% v/v, 2 x 4 mL) and DMF (3 x 4 mL). To remove the *N*-terminal Fmoc group, the resin was treated with a solution of piperidine in DMF (25%, 4 mL) for 30 min and, after filtration, the resin was washed with DMF (3 x 4 mL), DCM (3 x 4 mL), DIEA in DMF (5%, 3 x 4 mL),

LiCl in DMF (0.8 M, 3 x 4 mL) and DMF (3 x 4 mL). Cyclization was performed by treating the resin with a solution of PyAOP (3 equiv) and DIEA (6 equiv) in DMF (4 mL) for 2 hours under orbital shaking. After filtration, the resin was washed with DMF (3 x 4 mL) and DCM (3 x 4 mL).

For the lysine functionalization, the 4-methyltrityl group (Mtt) was selectively deprotected by treatment with a freshly prepared mixture of DCM, HFIP, TFE and TIS (65:20:10:5, 4 mL) for 2 hours. This process was repeated three times. After each cycle, washes were performed with DCM (3 x 3 mL). Then, a solution of 1-pyreneacetic acid (for **^{P}CP3 and ^{P}CP5**, 3 equiv) or hexanoic acid (for **^{P}CP4**, 3 equiv), *N*-HATU (3 equiv) and DIEA (6 equiv) in DMF (4 mL) was added to the resin and the mixture was shaken for 40 min. Finally, the resin was washed with DMF (3 x 4 mL) and DCM (3 x 4 mL).

The removal of CP protecting groups and cleavage from the resin was performed by treating the resin at room temperature with a freshly prepared cocktail of Thioanisole, H_2O, DCM in TFA (2.5:2.5:5:90, 1 mL per 100 mg resin) for 2 hours. The mixture was collected by filtration, concentrated by bubbling argon and added dropwise to cold Et_2O (10 mL of Et_2O per 100 mg of resin). The resulting precipitate was centrifuged (4000 rpm x 10 min) and the supernatant was discarded. After washing with diethyl ether, the precipitate was dried under vacuum, dissolved in MilliQ-H_2O with 0.1% TFA and purified by reverse phase semipreparative high-performance liquid chromatography (RP-HPLC) using a Phenomenex Luna C18 (2) 100Å column. Finally, the proper fractions were collected and lyophilized to afford the pure peptide.

^{P}CP3: The peptide was purified by reverse phase semipreparative HPLC [gradient: H_2O (0.1% TFA)/MeCN (0.1% TFA), 80:20 → 80:20 (5 min); 80:20 → 50:50 (40 min), R_t = 25.6 min]. The pure fractions were lyophilized to obtain the peptide as a white solid with and overall yield of 18% (61.2 mg), which was stored at -20°C until further use. **^{1}H RMN** (500 MHz, H_2O/D_2O) δ: 8.54 (d, *J* = 7.4 Hz, 1H, NH_{His}), 8.47 (d, *J* = 7.5 Hz, 1H, NH_{His}), 8.43 (s, 1H, CH_{Im}), 8.41 (s, 1H, CH_{Im}), 8.39 (d, *J* = 8.4 Hz, 1H, NH_{His}), 8.33 (s, 1H, CH_{Im}), 8.31 (s, 1H, CH_{Im}), 8.26 (d, *J* = 8.1 Hz, 1H, NH_{His}), 8.19 (m, 3H, NH_{Ala}, NH_{Ser}), 8.17-8.07 (m, 10H, H_{Pyr}, NH_{Ala}, NH_{Ser}, NH_{Gln}), 8.03 (m, 3H, $^{\alpha}NH_{Lys,}$ H_{Pyr}), 8.00-7.92 (m, 12H, $^{\alpha}NH_{Lys}$, H_{Pyr}), 7.90 (m, 2H, $^{\varepsilon}NH_{Lys}$, $NH_{P\text{-}\Delta\beta Ala}$), 7.85 (t, *J* = 7.4 Hz, 1H, $^{\varepsilon}NH_{Lys}$), 7.80 (m, 2H, H_{Pyr}), 7.67 (d, *J* = 9.1 Hz, 1H, $NH_{P\text{-}\Delta\beta Ala}$), 7.56 (t, *J* = 6.0 Hz, 1H, $NH_{\beta Ala}$), 7.38 (m, 5H, $NH_{\beta Ala}$, $NH_{2\text{-}Gln}$), 7.00 (s, 1H, CH_{Im}), 6.94 (s, 2H, CH_{Im}), 6.92 (s, 1H, CH_{Im}), 6.74 (m, 4H, $NH_{2\text{-}Gln}$), 6.33 (s, 2H, $CH{=}CH_{P\text{-}\Delta\beta Ala}$), 6.28 (s, 1H, $CH{=}CH_{P\text{-}\Delta\beta Ala}$), 6.21 (s, 1H, $CH{=}CH_{P\text{-}\Delta\beta Ala}$), 4.29 (m, 1H, $^{\alpha}CH_{Ser}$), 4.20 (m, 2H, $^{\alpha}CH_{Gln}$), 4.13 (m, 8H, $^{\alpha}CH_{Gln}$, $^{\alpha}CH_{Ala}$,$CH_{P\text{-}\Delta\beta Ala}$), 4.03 (m, 2H, $^{\alpha}CH_{Lys}$), 3.64 (m, 8H, $CH_{2\text{-}Pyr}$, $CH_{2\text{-}Ser}$), 3.51 (m, 4H, $CH_{2\text{-}Ser}$), 3.25 (m, 2H, $^{\beta}CH_{2\text{-}\beta Ala}$), 3.11 (m, 8H, $^{\beta}CH_{2\text{-}\beta Ala}$, $CH_{2\text{-}Lys}$, $^{\beta}CH_{2\text{-}His}$), 2.90 (m, 4H, $^{\beta}CH_{2\text{-}His}$), 2.70 (m, 2H, $^{\beta}CH_{2\text{-}His}$), 2.53 (d, *J* = 8.1 Hz, 1H, $CH_{P\text{-}\Delta\beta Ala}$), 2.42 (d, *J* = 8.1 Hz, 1H, $CH_{P\text{-}\Delta\beta Ala}$), 2.26 (m, 4H, $^{\alpha}CH_{2\text{-}\beta Ala}$), 2.10 (m, 8H, $CH_{2\text{-}Gln}$), 1.92 (m, 2H, $CH_{2\text{-}Gln}$), 1.79 (m, 2H, $CH_{2\text{-}Gln}$), 1.71 (m, 4H, $CH_{2\text{-}Gln}$), 1.54 (m, 4H, $CH_{2\text{-}Lys}$), 1.36 (m, 4H, $CH_{2\text{-}Lys}$), 1.17 (m, 6H, $CH_{3\text{-}Ala}$), 1.10 (m, 4H, $CH_{2\text{-}Lys}$). **^{13}C NMR** (H_2O/D_2O, 75 MHz, δ): 176.6 (CO), 176.6 (CO), 173.8 (CO), 173.6 (CO), 173.4 (CO), 173.4 (CO), 173.1 (CO), 173.0 (CO), 172.9 (CO), 172.6 (CO), 172.3 (CO), 172.2 (CO), 171.8 (CO),

171.7 (CO), 171.7 (CO), 171.5 (CO), 171.4 (CO), 170.9 (CO), 170.9 (CO), 170.5 (CO), 170.4 (CO), 170.1 (CO), 170.0 (CO), 169.9 (CO), 162.0 (CO), 161.8 (CO), 137.0 (CH), 136.9 (CH), 134.0 (CH), 133.9 (CH), 132.6 (CH), 132.5 (CH), 132.5 (CH), 132.4 (CH), 129.8 (C), 129.7 (C), 129.3 (C), 129.2 (C), 127.9 (C), 127.8 (CH), 127.8 (CH), 127.7 (C), 127.5 (C), 127.4 (C), 127.3 (C), 127.1 (C), 126.8 (CH), 126.7 (CH), 126.4 (CH), 126.3 (CH), 126.2 (CH), 126.2 (CH), 125.5 (CH), 125.4 (CH), 124.5 (CH), 124.4 (CH), 124.3 (CH), 124.2 (CH), 124.0 (CH), 123.9 (CH), 123.0 (C), 122.9 (C), 122.7 (C), 122.6 (C), 121.9 (CH), 121.8 (CH), 116.5 (C), 116.4 (C), 116.3 (CH), 116.2 (CH), 116.1 (CH), 116.0 (CH), 114.2 (C), 114.1 (C), 81.5 (CH), 81.4 (CH), 79.4 (CH), 79.3 (CH), 60.3 (CH_2), 60.2 (CH_2), 60.2 (CH_2), 60.1 (CH_2), 54.8 (CH), 54.7 (CH), 54.5 (CH), 54.4 (CH), 52.9 (CH), 52.6 (CH), 52.2 (CH), 52.1 (CH), 52.0 (CH), 52.0 (CH), 51.6 (CH), 51.3 (CH), 51.2 (CH), 51.1 (CH), 50.4 (CH), 50.3 (CH), 48.9 (CH), 48.8 (CH), 46.3 (CH), 46.2 (CH), 39.5 (CH_2), 39.4 (CH_2), 38.2 (CH_2), 38.1 (CH_2), 34.8 (CH_2), 34.7 (CH_2), 33.8 (CH_2), 33.7 (CH_2), 30.2 (CH_2), 30.1 (CH_2), 30.0 (CH_2), 29.9 (CH_2), 26.8 (CH_2), 26.3 (CH_2), 26.1 (CH_2), 26.0 (CH_2), 25.8 (CH_2), 25.7 (CH_2), 25.3 (CH_2), 25.2 (CH_2), 25.0 (CH_2), 24.9 (CH_2), 24.9 (CH_2), 24.8 (CH_2), 21.2 (CH_2), 21.1 (CH_2), 16.0 (CH_3), 15.8 (CH_3). **ESI-MS** *m/z* (%): 1354.6 (14) $[M+H]^+$, 677.9 (100) $[M+2H]^{2+}$, 452.4 (3) $[M+3H]^{3+}$. **HRMS (ESI)** *m/z*: $[M+2H]^{2+}$ calculated for $C_{65}H_{81}N_{17}O_{16}$, 677.8018, found 677.8019. **FTIR (neat)**: ν = 3278.2 (amide A), 1647.1 (amide I), 1534.7 (amide II) cm^{-1}.

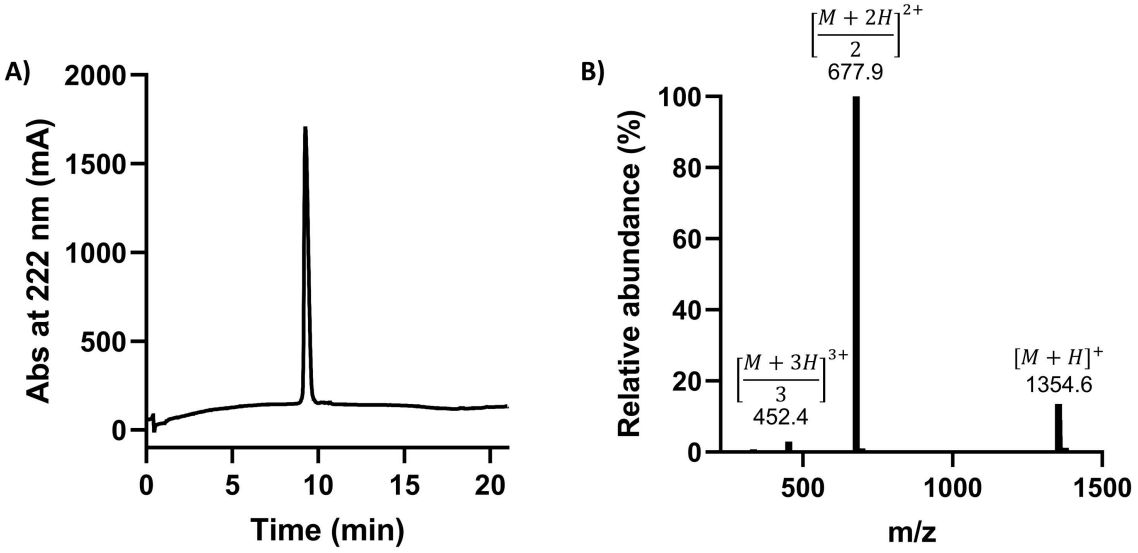

Figure 189. (A) **RP-uHPLC** of **^{P}CP3:** [Agilent SB-C18 column, H_20 (0.1% TFA)/MeCN (0.1% TFA), 80:20 → 80:20 (2 min) and 80:20 → 50:50 (19 min)] R_t = 9.3 min. (B) ESI-MS of the main peak.

USC UNIVERSIDADE DE SANTIAGO DE COMPOSTELA

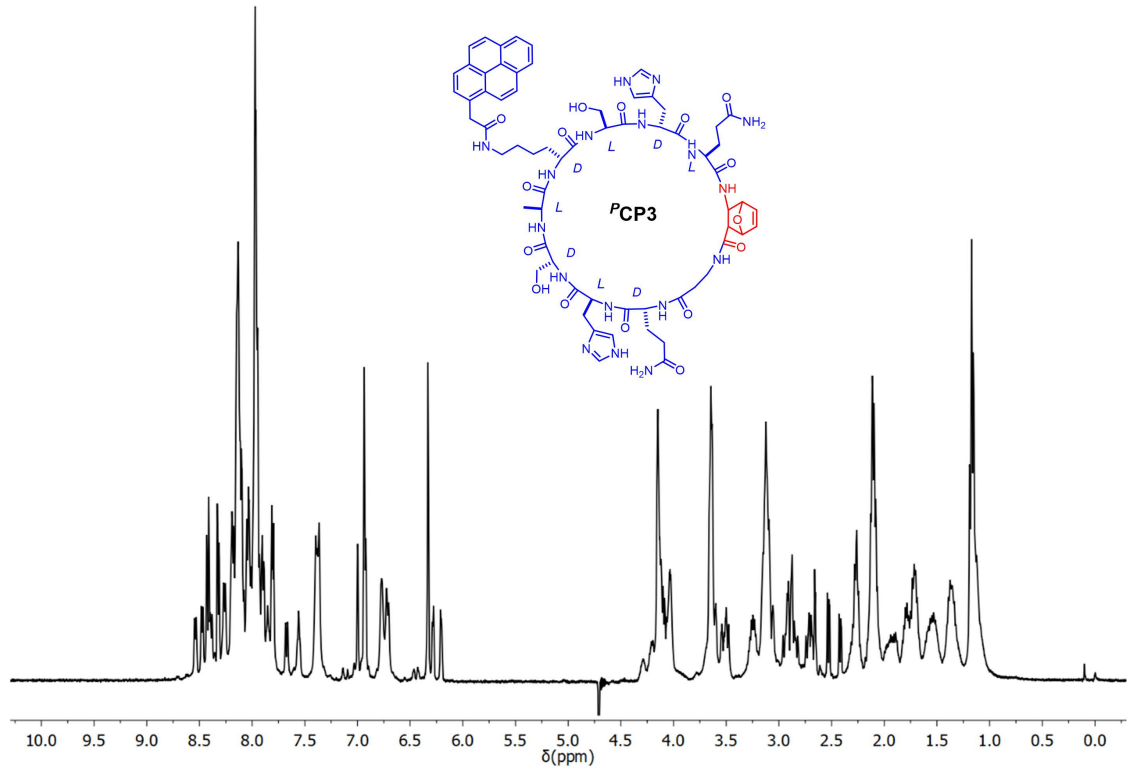

Figure 190. ^{1}H-NMR of **ᴰCP3** at 4.5 mM (500 MHz, D_2O/H_2O, 298K).

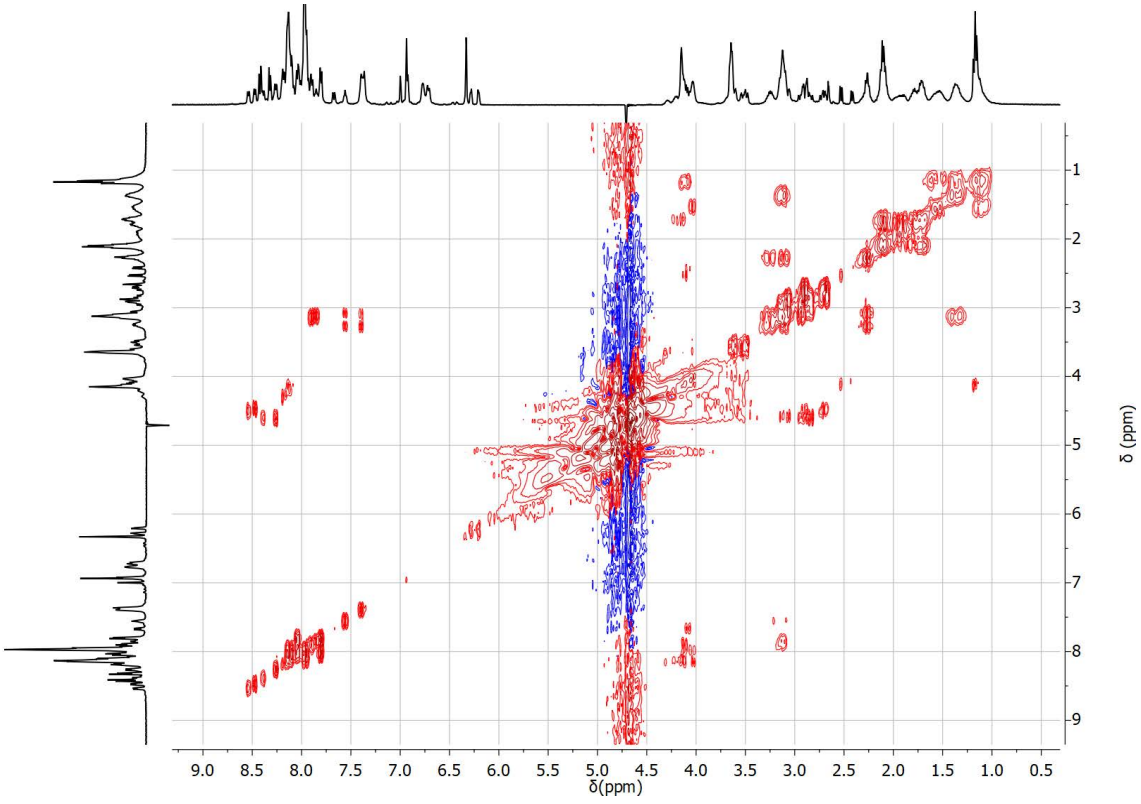

Figure 191. COSY of **ᴰCP3** at 4.5 mM (500 MHz, D_2O/H_2O, 298K).

UNIVERSIDADE DE SANTIAGO DE COMPOSTELA

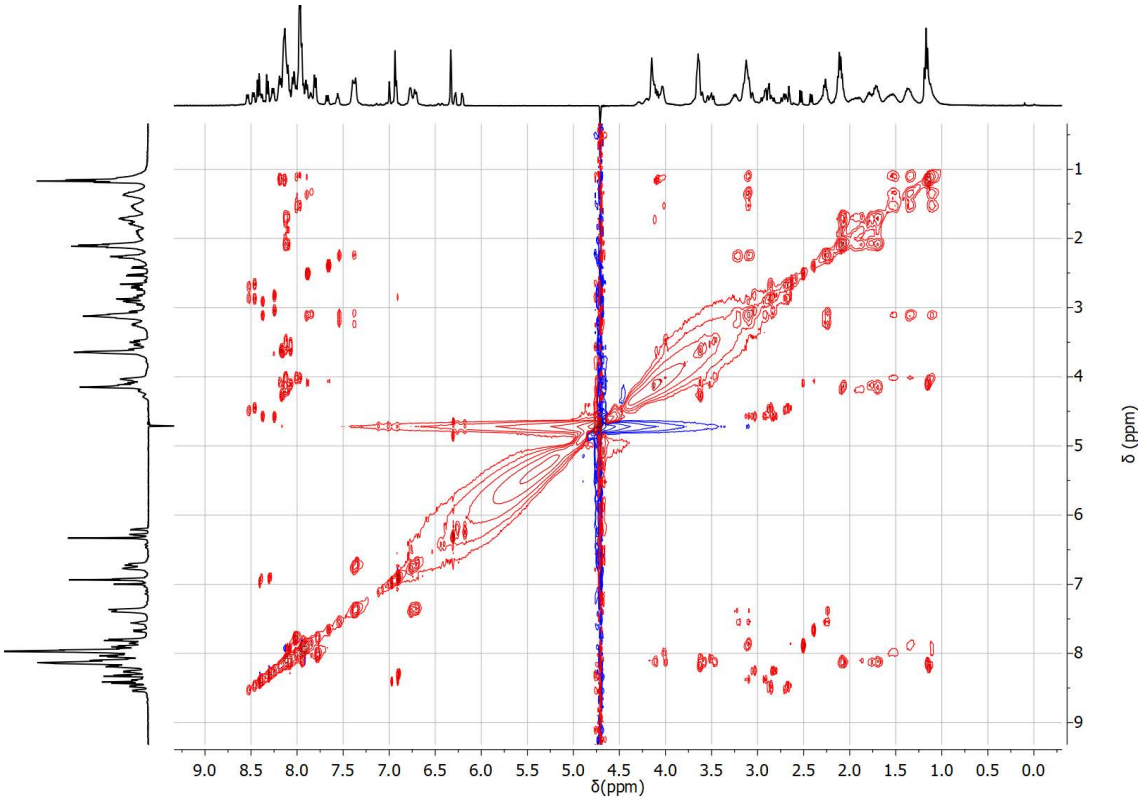

Figure 192. TOCSY of **^{P}CP3** at 4.5 mM (500 MHz, D_2O/H_2O, 298K).

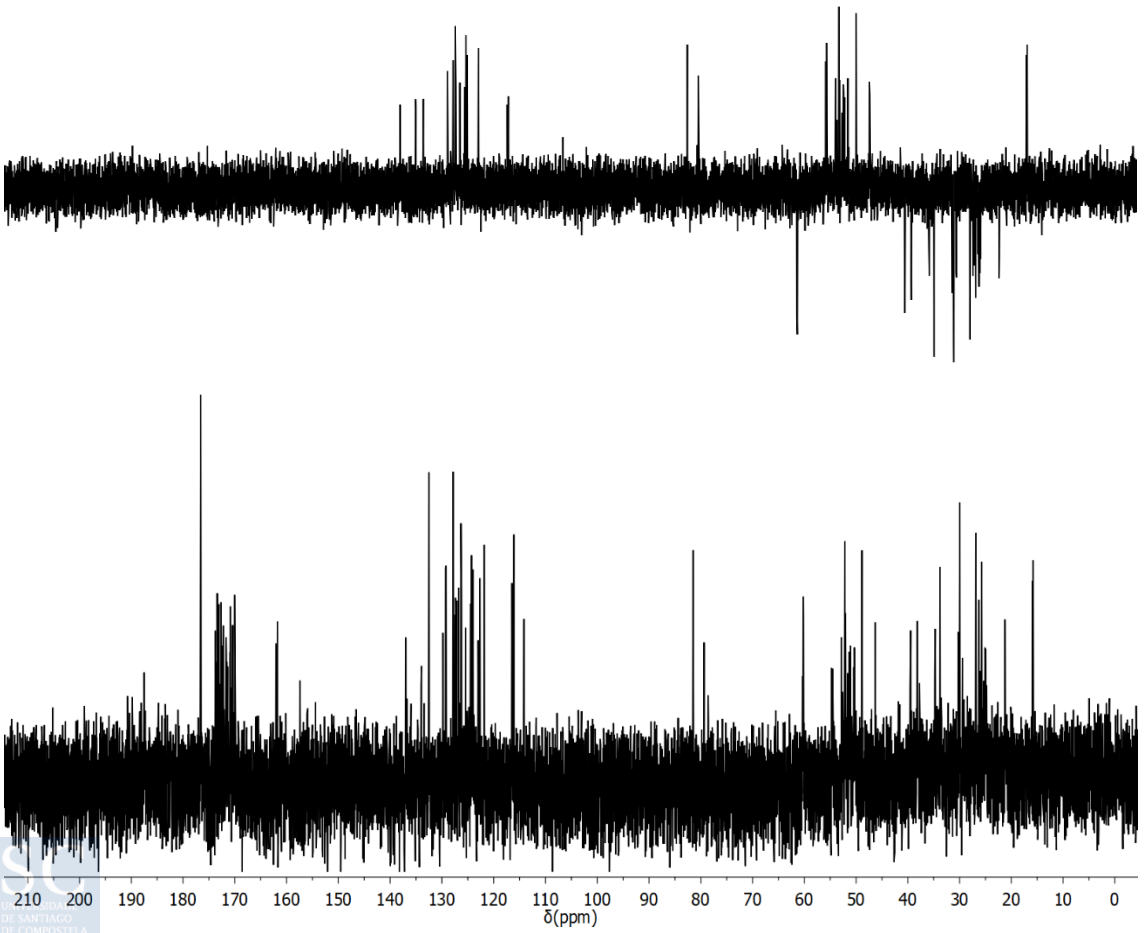

Figure 193. ^{13}C NMR (bottom) and DEPT-135 NMR (top) of **^{P}CP3** at 4.5 mM (75 MHz, D_2O/H_2O, 298K).

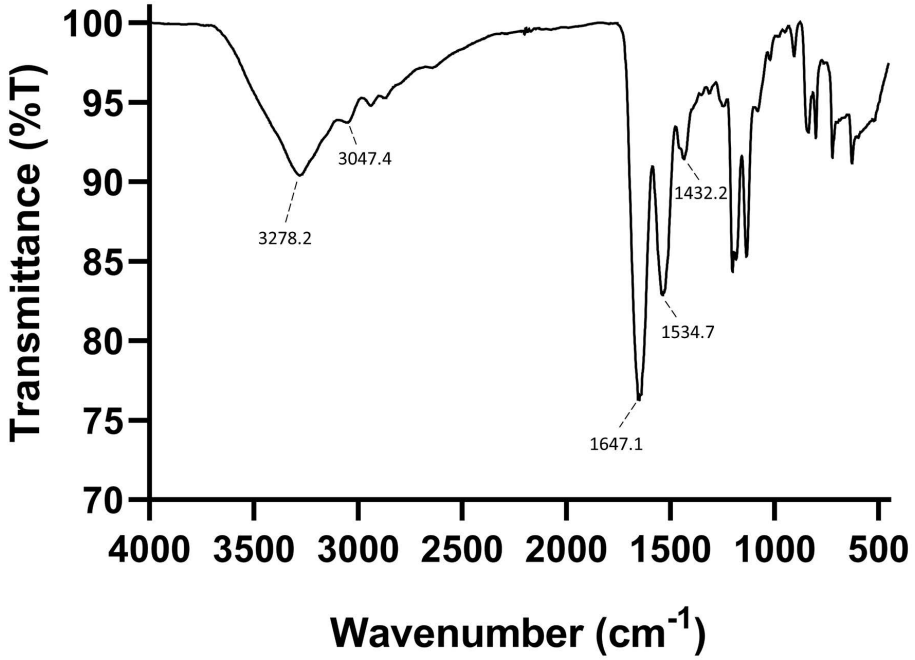

Figure 194. FT-IR spectrum of **^{P}CP3** (solid, 298 K).

^{P}CP4: The peptide was purified by reverse phase semipreparative HPLC [gradient: H_2O (0.1% TFA)/MeCN (0.1% TFA), 100:0 → 100:0 (5 min); 100:0 → 50:50 (40 min), R_t = 24.0 min]. The pure fractions were lyophilized to obtain the peptide as a white solid with and overall yield of 14% (43.0 mg), which was stored at -20°C until further use. **ESI-MS** *m/z* (%): 1210.6 (16) $[M+H]^+$, 605.9 (100) $[M+2H]^{2+}$, 404.3 (6) $[M+3H]^{3+}$. **HRMS (ESI)** *m/z*: $[M+H]^+$ calculated for $C_{53}H_{80}N_{17}O_{16}$: 1210.5963, found 1210.5962. **FTIR (neat)**: ν = 3292.0 (amide A), 1629.4 (amide I), 1538.7 (amide II) cm^{-1}.

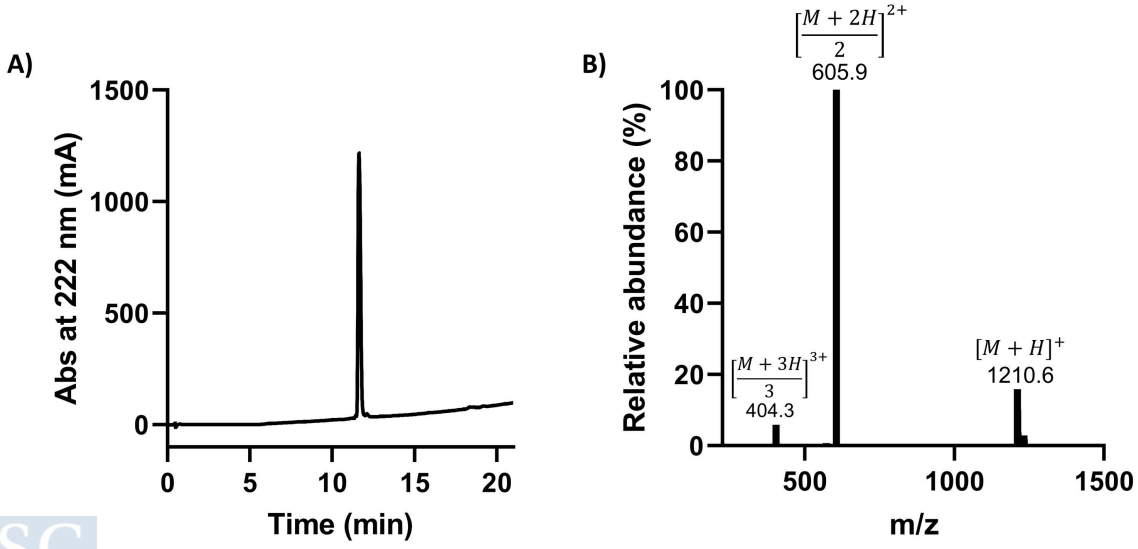

Figure 195. (A) **RP-uHPLC** of **^{P}CP4:** [Agilent SB-C18 column, H_20 (0.1% TFA)/MeCN (0.1% TFA), 100:00 → 100:0 (2 min) and 80:20 → 50:50 (19 min)] R_t = 11.6 min. (B) ESI-MS of the main peak.

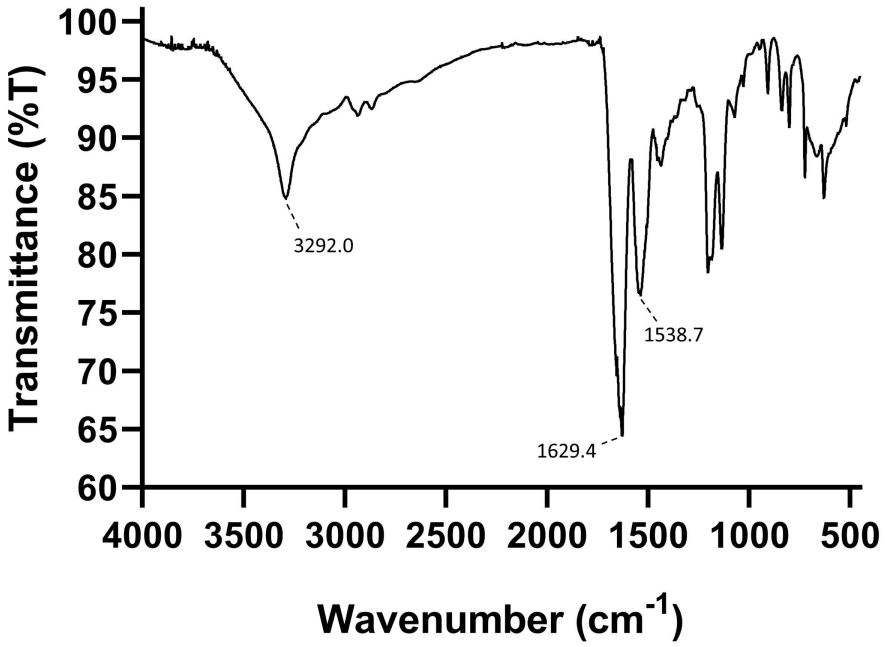

Figure 196. FT-IR spectrum of **^{P}CP4** (solid, 298 K).

^{P}CP5: The peptide was purified by reverse phase semipreparative HPLC [gradient: H_2O (0.1% TFA)/MeCN (0.1% TFA), 80:20 → 80:20 (5 min); 80:20 → 50:50 (40 min), R_t = 24.6 min]. The pure fractions were lyophilized to obtain the peptide as a white solid with and overall yield of 5% (19.0 mg), which was stored at -20°C until further use. **ESI-MS** *m/z* (%): 1354.6 (6) $[M+H]^+$, 677.9 (100) $[M+2H]^{2+}$, 452.4 (10) $[M+3H]^{3+}$. **HRMS (ESI)** *m/z*: $[M+H]^+$ calculated for $C_{66}H_{84}N_{17}O_{15}$: 1354.6327, found 1354.6290. **FTIR (neat)**: ν = 3282.1 (amide A), 1641.2 (amide I), 1540.6 (amide II) cm^{-1}.

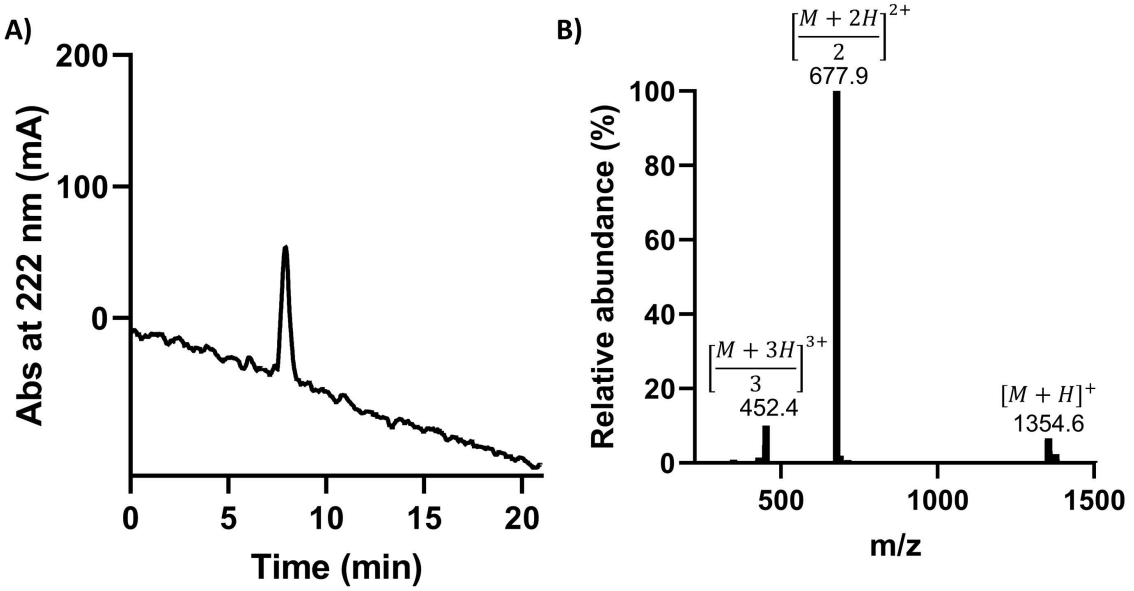

Figure 197. (A) **RP-uHPLC** of **^{P}CP5:** [Agilent SB-C18 column, H_20 (0.1% TFA)/MeCN (0.1% TFA), 80:20 → 80:20 (2 min) and 80:20 → 50:50 (19 min)] R_t = 7.8 min. (B) ESI-MS of the main peak.

USC UNIVERSIDADE DE SANTIAGO DE COMPOSTELA

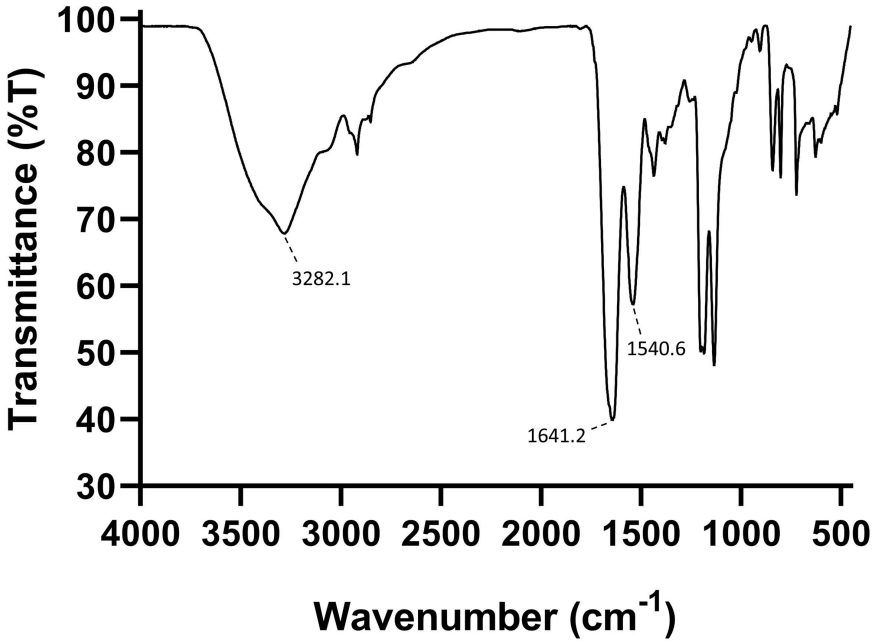

Figure 198. FT-IR spectrum of **^{P}CP5** (solid, 298 K).

8.2.2.3. Synthesis of ^{Z}CP3, ^{Z}CP4 and ^{Z}CP5

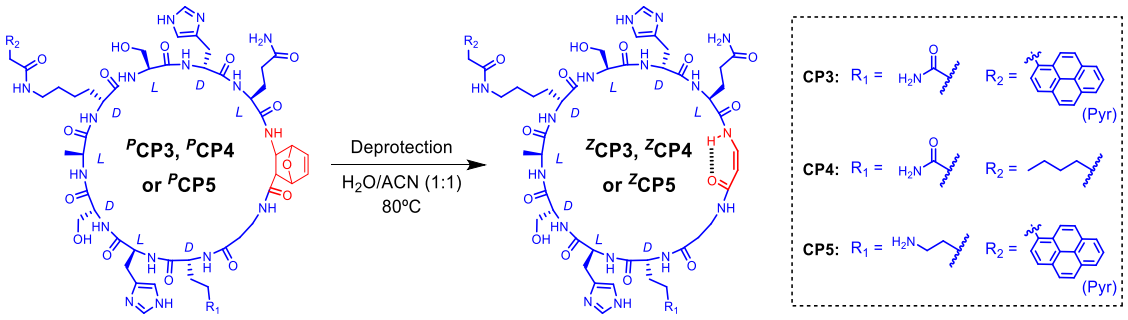

Figure 199. Retro-Diels-Alder reaction to obtain **^{Z}CP3, ^{Z}CP4** and **^{Z}CP5**.

A solution of the protected CP (**^{P}CP3**, **^{P}CP4** or **^{P}CP5**) in H_2O/MeCN (1:1, 1.5 mM) was shaken for 24 hours at 80°C. The resulting mixture was purified by semipreparative RP-HPLC using a Phenomenex Luna C18 (2) 100Å column. The proper fractions were freeze-dried to afford in all cases the pure **^{Z}CP** as a white solid. The product was stored at -20°C until further use.

^{Z}CP3: The general procedure described above was carried out with 13.3 mg (9.8 µmol) of **^{P}CP3**. After HPLC purification [gradient: H_2O (0.1% TFA)/MeCN (0.1% TFA), 80:20 → 80:20 (5 min); 80:20 → 50:50 (40 min), R_t = 25.8 min] and freeze-drying, the pure peptide **^{Z}CP3** was obtained as a white solid in a 91% yield (11.5 mg). **^{1}H RMN** (500 MHz, H_2O/D_2O) δ: 11.28 (d, J = 11.0 Hz, 1H, $NH_{Z\text{-}\Delta\beta Ala}$), 8.54 (d, J = 11.0 Hz, 1H, NH_{His}),

8.41 (s, 1H, CH_{Im}), 8.36 (s, 1H, CH_{Im}), 8.26 (m, 3H, NH_{Ser}, NH_{His}, NH_{Gln}), 8.15 (m, 2H, NH_{Gln}, NH_{Ala}), 8.00 (m, 3H, $^{\alpha}NH_{Lys}$, NH_{Ser}, H_{Pyr}), 7.95 (m, 2H, H_{Pyr}), 7.84 (m, 6H, H_{Pyr}), 7.72 (m, 2H, $NH_{\beta Ala}$, $^{\varepsilon}NH_{Lys}$), 7.29 (m, 2H, $NH_{2\text{-}Gln}$), 6.99 (s, 1H, CH_{Im}), 6.98 (s, 1H, CH_{Im}), 6.94 (d, *J* = 10.4 Hz, 1H, $CH_{Z\text{-}\Delta\beta Ala}$), 6.70 (m, 2H, $NH_{2\text{-}Gln}$), 5.03 (d, *J* = 8.9 Hz, 1H, $CH_{Z\text{-}\Delta\beta Ala}$), 4.30 (m, 1H, $^{\alpha}CH_{Ser}$), 4.20 (m, 1H, $^{\alpha}CH_{Gln}$), 4.09 (m, 1H, $^{\alpha}CH_{Gln}$), 4.07 (s, 2H, $CH_{2\text{-}Pyr}$), 4.02 (m, 1H, $^{\alpha}CH_{Ala}$), 3.78 (m, 1H, $^{\alpha}CH_{Lys}$), 3.70-3.54 (m, 4H, $CH_{2\text{-}Ser}$), 3.31 (m, 1H, $^{\beta}CH_{2\text{-}\beta Ala}$), 3.09 (m, 4H, $^{\beta}CH_{2\text{-}His}$, $CH_{2\text{-}Lys}$, $^{\beta}CH_{2\text{-}\beta Ala}$), 3.01 (dd, *J* = 15.6 and 8.0 Hz, 1H, $^{\beta}CH_{2\text{-}His}$), 2.94 (dd, *J* = 15.7 and 5.9 Hz, 1H, $^{\beta}CH_{2\text{-}His}$), 2.79 (dd, *J* = 15.6 and 8.7 Hz, 1H, $^{\beta}CH_{2\text{-}His}$), 2.29 (m, 2H, $^{\alpha}CH_{2\text{-}\beta Ala}$), 2.06 (m, 4H, $CH_{2\text{-}Gln}$), 1.92 (m, 1H, $CH_{2\text{-}Gln}$), 1.75 (m, 1H, $CH_{2\text{-}Gln}$), 1.66 (m, 2H, $CH_{2\text{-}Gln}$), 1.46 (m, 2H, $CH_{2\text{-}Lys}$), 1.29 (p, *J* = 7.3 Hz, 2H, $CH_{2\text{-}Lys}$), 1.12 (d, *J* = 7.5 Hz, 3H, $CH_{3\text{-}Ala}$), 1.00 (m, 2H, $CH_{2\text{-}Lys}$). **^{13}C NMR** (H_2O/D_2O, 75 MHz, δ): 176.5 (CO), 173.8 (CO), 173.3 (CO), 173.0 (CO), 172.5 (CO), 172.3 (CO), 171.2 (CO), 171.0 (CO), 170.6 (CO), 170.3 (CO), 169.9 (CO), 167.9 (CO), 162.1 (CO), 132.6 (CH), 132.5 (CH), 132.3 (CH), 129.7 (C), 129.3 (C), 129.1 (C), 127.7 (CH), 127.4 (C), 127.3 (C), 126.7 (CH), 126.2 (CH), 126.1 (CH), 125.3 (CH), 124.4 (CH), 124.2 (CH), 123.9 (CH), 123.0 (C), 122.6 (C), 121.7 (CH), 116.6 (CH), 116.5 (C), 116.1 (CH), 114.2 (C), 100.8 (CH), 60.2 (CH_2), 59.9 (CH_2), 55.1 (CH), 54.6 (CH), 53.0 (CH), 52.7 (CH), 52.2 (CH), 51.3 (CH), 51.1 (CH), 49.1 (CH), 39.6 (CH_2), 38.2 (CH_2), 34.3 (CH_2), 33.8 (CH_2), 30.1 (CH_2), 30.0 (CH_2), 28.9 (CH_2), 26.9 (CH_2), 25.8 (CH_2), 25.2 (CH_2), 24.8 (CH_2), 24.7 (CH_2), 21.2 (CH_2), 15.3 (CH_3). **ESI-MS** *m/z* (%): 1286.6 (20) $[M+H]^+$, 643.8 (100) $[M+2H]^{2+}$, 429.8 (3) $[M+3H]^{3+}$. **HRMS (ESI)** *m/z*: $[M+H]^+$ calculated for $C_{61}H_{76}N_{17}O_{15}$, 1286.5701, found 1286.5680. **FTIR (neat)**: ν = 3276.2 (amide A), 1655.0 (amide I), 1548.5 (amide II) cm^{-1}.

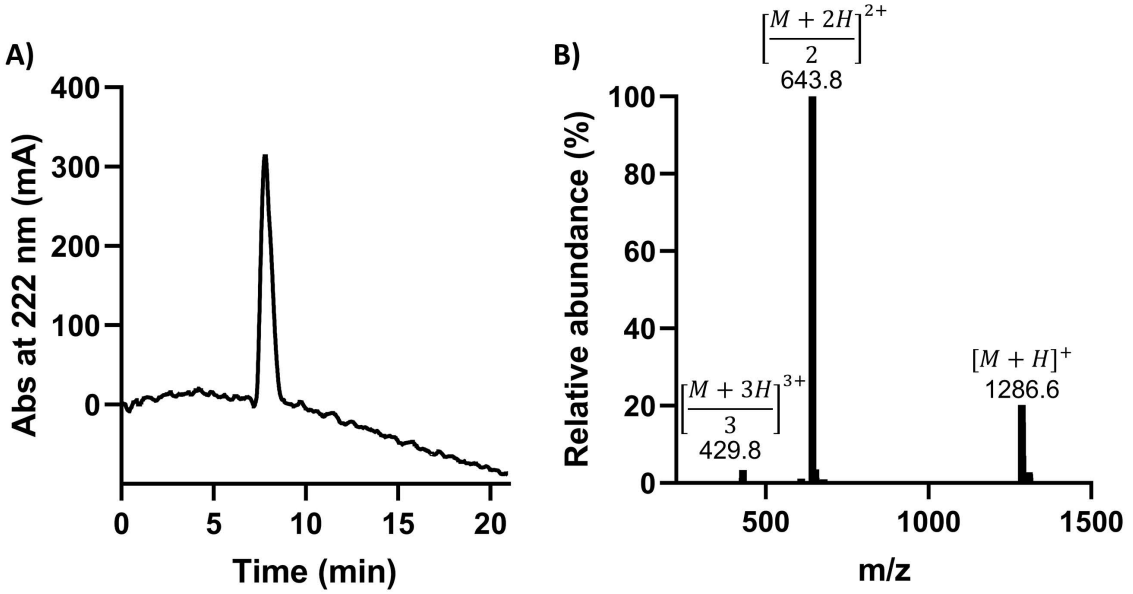

Figure 200. (A) **RP-uHPLC of ^{Z}CP3:** [Agilent SB-C18 column, H_20 (0.1% TFA)/MeCN (0.1% TFA), 80:20 → 80:20 (2 min) and 80:20 → 50:50 (19 min)] R_t = 7.7 min. (B) ESI-MS of the main peak.

USC UNIVERSIDADE DE SANTIAGO DE COMPOSTELA

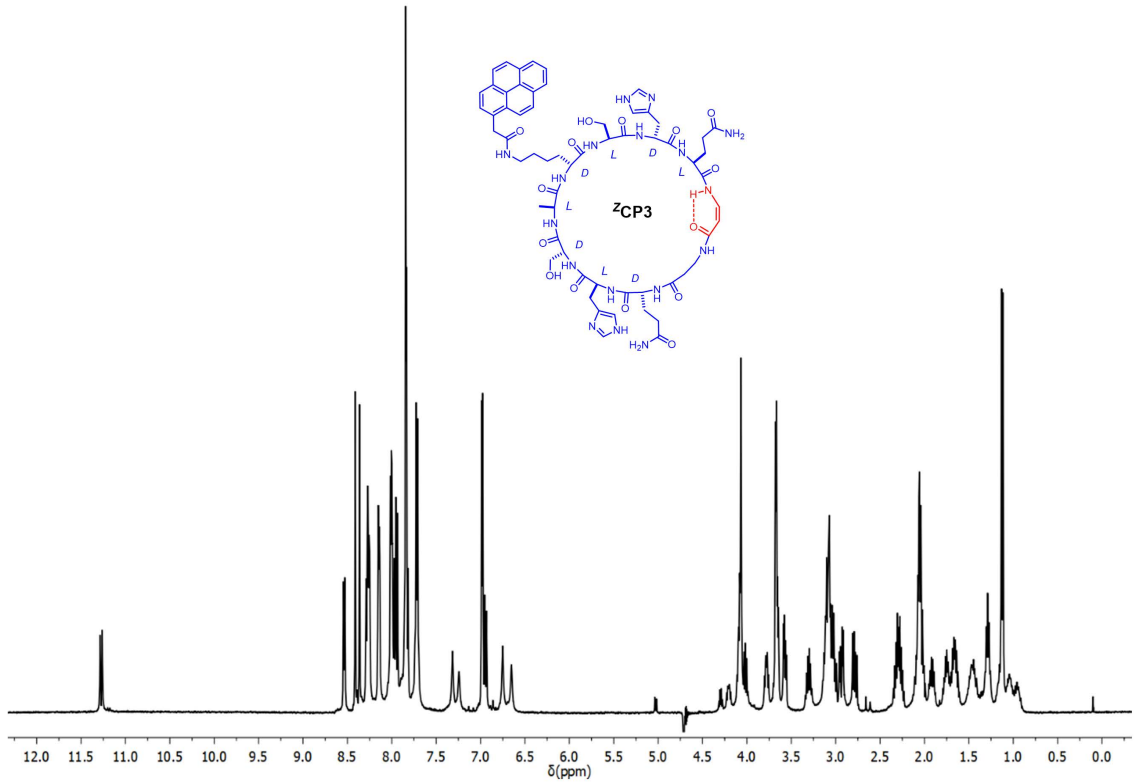

Figure 201. ^{1}H-NMR of **^{Z}CP3** at 4.4 mM (500 MHz, D_2O/H_2O, 298K).

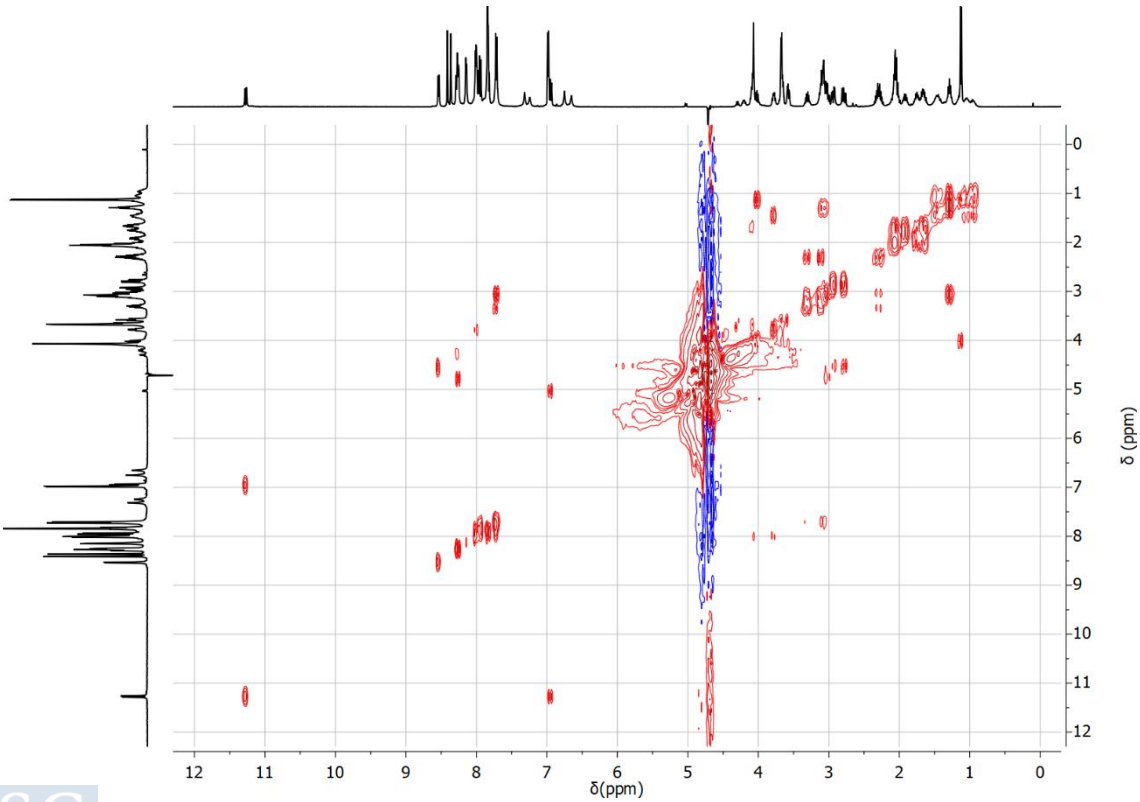

Figure 202. COSY of **^{Z}CP3** at 4.4 mM (500 MHz, D_2O/H_2O, 298K).

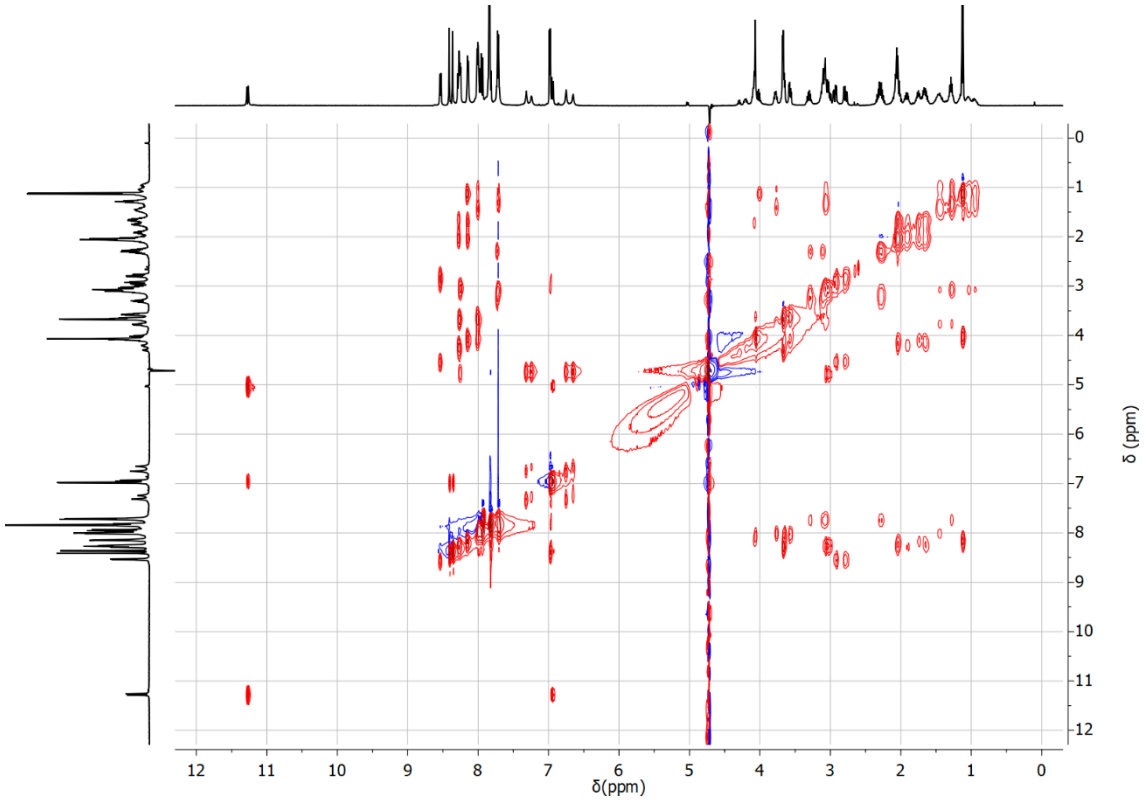

Figure 203. TOCSY of **^{Z}CP3** at 4.4 mM (500 MHz, D_2O/H_2O, 298K).

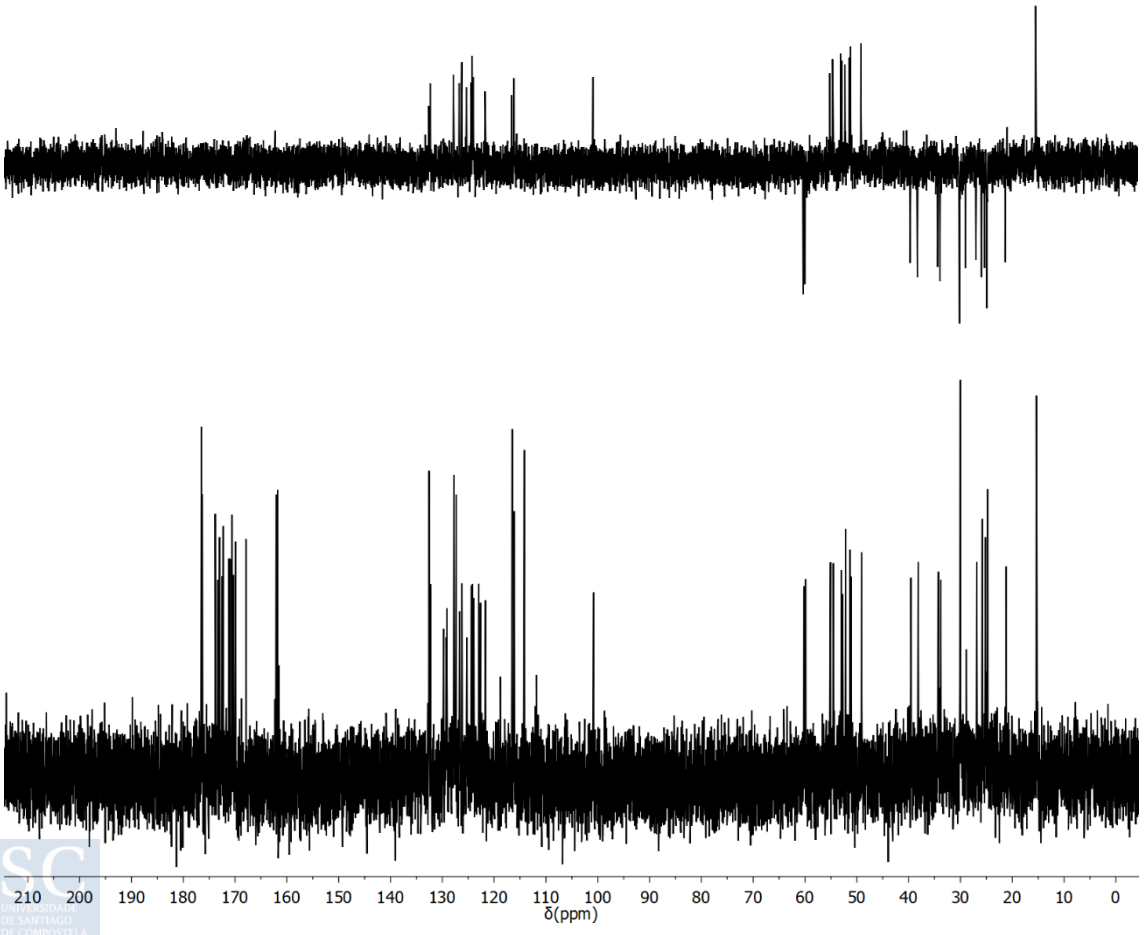

Figure 204. ^{13}C NMR (bottom) and DEPT-135 NMR (top) of **^{Z}CP3** at 4.4 mM (75 MHz, D_2O/H_2O, 298K).

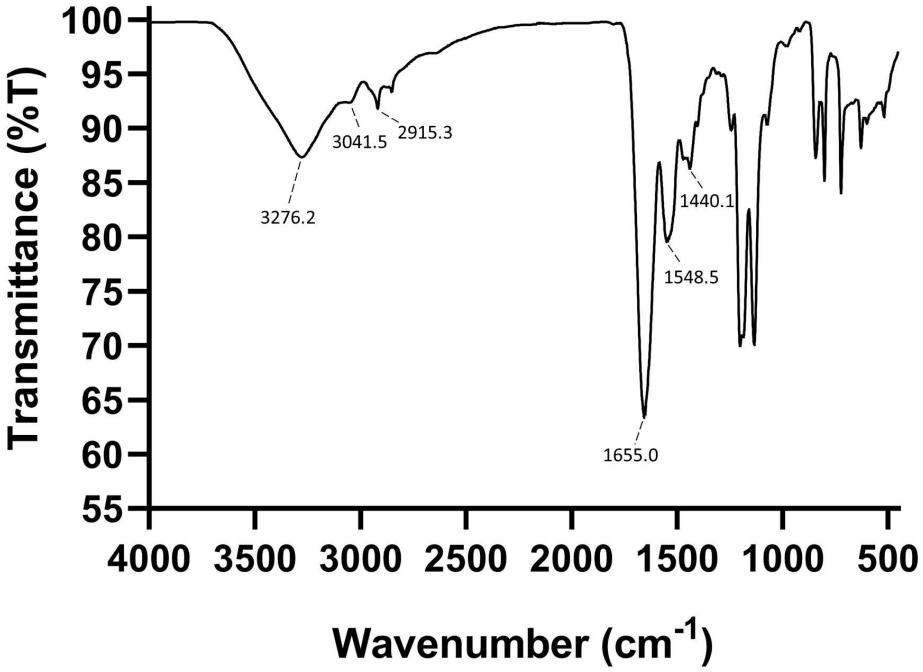

Figure 205. FT-IR spectrum of **^{Z}CP3** (solid, 298 K).

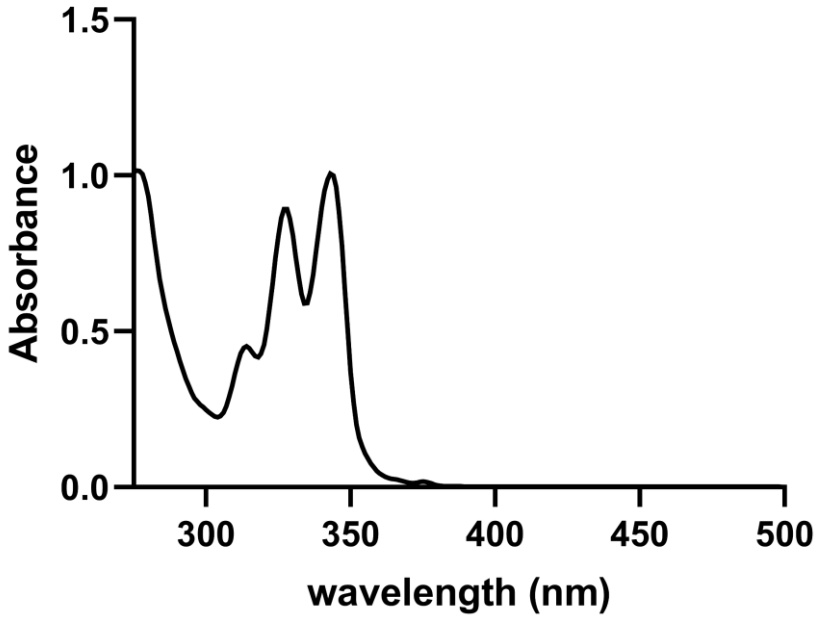

Figure 206. UV-Vis spectrum of an aqueous solution of **^{Z}CP3** (100 µM).

USC
UNIVERSIDADE DE SANTIAGO DE COMPOSTELA

^{Z}CP4: The general procedure described above was carried out with 19.1 mg (15.8 µmol) of **^{P}CP4**. After HPLC purification [gradient: H_2O (0.1% TFA)/MeCN (0.1% TFA), 100:0 → 100:0 (5 min); 100:0 → 50:50 (40 min), R_t = 24.0 min] and freeze-drying, the pure peptide **^{Z}CP4** was obtained as a white solid in a 26% yield (4.7 mg). **ESI-MS** *m/z* (%): 1142.6 (15) $[M+H]^+$, 571.9 (100) $[M+2H]^{2+}$, 381.6 (8) $[M+3H]^{3+}$. **HRMS (ESI)** *m/z*: $[M+H]^+$ calculated for $C_{49}H_{76}N_{17}O_{15}$: 1142.5701, found 1142.5694. **FTIR (neat)**: ν = 3274.2 (amide A), 1649.1 (amide I), 1542.6 (amide II) cm^{-1}.

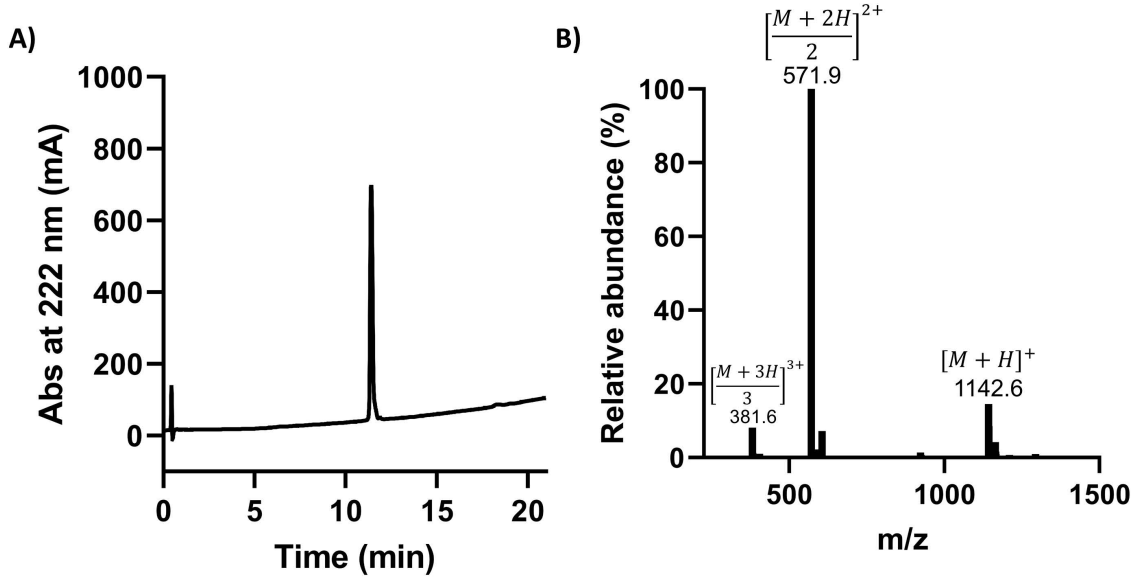

Figure 207. (A) RP-uHPLC of **^{Z}CP4**: [Agilent SB-C18 column, H_20 (0.1% TFA)/MeCN (0.1% TFA), 100:0 → 100:0 (2 min) and 100:0 → 50:50 (19 min)] R_t = 11.4 min. (B) ESI-MS of the main peak.

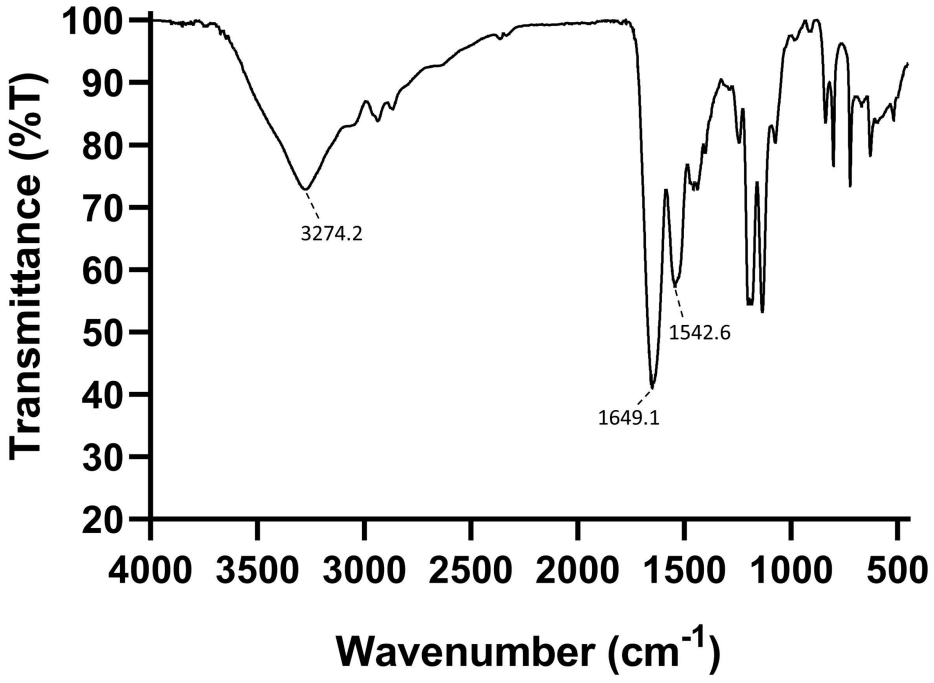

USC UNIVERSIDADE DE SANTIAGO DE COMPOSTELA

Figure 208. FT-IR spectrum of **^{Z}CP4** (solid, 298 K).

^{Z}CP5: The general procedure described above was carried out with 4.0 mg (3.0 µmol) of **^{P}CP5**. After HPLC purification [gradient: H_2O (0.1% TFA)/MeCN (0.1% TFA), 80:20 → 80:20 (5 min); 80:20 → 50:50 (40 min), R_t = 24.0 min] and freeze-drying, the pure peptide **^{Z}CP5** was obtained as a white solid in a 87% yield (3.3 mg). **ESI-MS** *m/z* (%): 1286.6 (21) $[M+H]^+$, 644.0 (100) $[M+2H]^{2+}$, 429.8 (13) $[M+3H]^{3+}$. **HRMS (ESI)** *m/z*: $[M+H]^+$ calculated for $C_{62}H_{80}N_{17}O_{14}$: 1286.6065, found 1286.6017. **FTIR (neat)**: ν = 3282.1 (amide A), 1651.1 (amide I), 1540.6 (amide II) cm^{-1}.

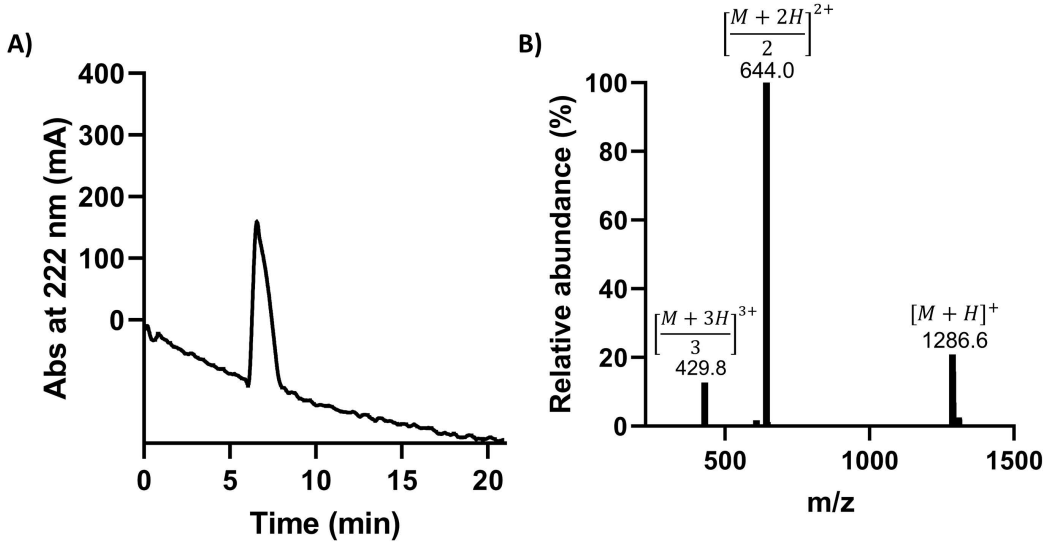

Figure 209. (A) RP-uHPLC of **^{Z}CP5**: [Agilent SB-C18 column, H_20 (0.1% TFA)/MeCN (0.1% TFA), 80:20 → 80:20 (2 min) and 80:20 → 50:50 (19 min)] R_t = 6.4 min. (B) ESI-MS of the main peak.

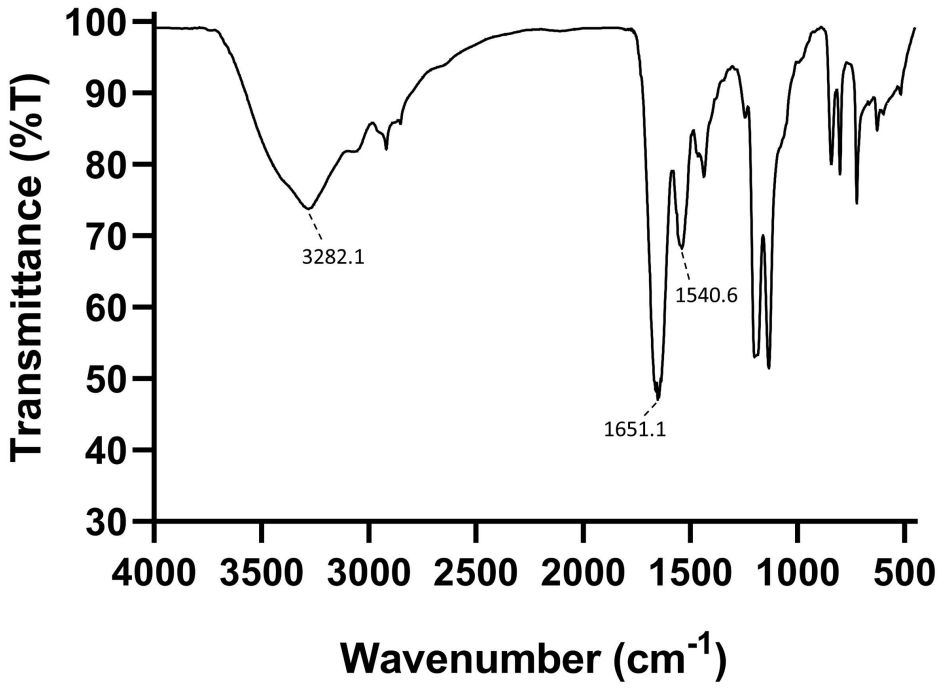

Figure 210. FT-IR spectrum of **^{Z}CP5** (solid, 298 K).

UdC UNIVERSIDADE DE SANTIAGO DE COMPOSTELA

8.2.2.4. Synthesis of ^{E}CP3, ^{E}CP4 and ^{E}CP5

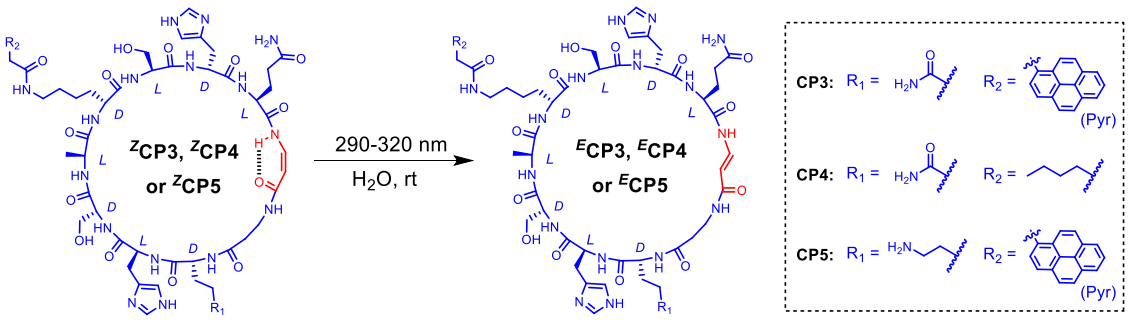

Figure 211. Light-induced isomerization to obtain **^{E}CP3**, **^{E}CP4** and **^{E}CP5**.

A solution of the *Z*-isomer of the corresponding CP (**^{Z}CP3**, **^{Z}CP4** or **^{Z}CP5**, 400 µM) in MilliQ-H_2O with TFA (0.1%) was prepared and degassed by bubbling argon for 5 minutes. The resulting solution was sealed in a quartz cuvette under argon atmosphere and irradiated for 10 minutes at 290-320 nm (Phillips TL 20W/12 RS lamp). The distance between the light source and the sample was around 5 cm. Then, the products were separated by semipreparative RP-HPLC using a Phenomenex Luna C18 (2) 100Å column. After freeze-drying, the products were stored at -20°C until further use.

^{E}CP3: The general procedure described above was carried out with 4.9 mg (3.8 µmol) of **^{Z}CP3**. After HPLC purification [gradient: H_2O (0.1% TFA)/MeCN (0.1% TFA), 80:20 → 80:20 (5 min); 80:20 → 50:50 (40 min), R_t (**^{E}CP3**) = 24.7 min, R_t (**^{Z}CP3**) = 25.8 min] and freeze-drying, **^{E}CP3** was obtained with a yield of 61% (white solid, 3.0 mg) and **^{Z}CP3** was partially recovered in a 27% (white solid, 1.3 mg). **^{1}H RMN** (500 MHz, H_2O/D_2O) δ: 9.79 (d, *J* = 11.8 Hz, 1H, $NH_{E\text{-}\Delta\beta Ala}$), 8.57 (d, *J* = 7.0 Hz, 1H, NH_{His}), 8.39 (s, 1H, CH_{Im}), 8.28 (bs, 3H, CH_{Im}, NH_{His}, NH_{Gln}), 8.12 (m, 4H, NH_{Gln}, NH_{Ser}, $^{\alpha}NH_{Lys}$, NH_{Ala}), 7.99 (m, 2H, NH_{Ser}, H_{Pyr}), 7.96-7.69 (m, 9H, $^{\varepsilon}NH_{Lys}$, H_{Pyr}), 7.55 (bs, 1H, $NH_{\beta Ala}$), 7.34 (m, 3H, $CH_{E\text{-}\Delta\beta Ala}$, $NH_{2\text{-}Gln}$), 6.97 (s, 1H, CH_{Im}), 6.86 (s, 1H, CH_{Im}), 6.72 (m, 2H, $NH_{2\text{-}Gln}$), 5.52 (d, *J* = 15.6 Hz, 1H, $CH_{E\text{-}\Delta\beta Ala}$), 4.21 (m, 1H, $^{\alpha}CH_{Ser}$), 4.09 (m, 2H, $^{\alpha}CH_{Ser}$, $^{\alpha}CH_{Gln}$), 3.93 (m, 3H, $^{\alpha}CH_{Ala}$, $CH_{2\text{-}Pyr}$), 3.81 (s, 1H, $^{\alpha}CH_{Lys}$), 3.73-3.54 (m, 4H, $CH_{2\text{-}Ser}$), 3.36 (bs, 1H, $^{\beta}CH_{2\text{-}\beta Ala}$), 3.17 (bs, 1H, $^{\beta}CH_{2\text{-}\beta Ala}$), 3.09 (m, 3H, $^{\beta}CH_{2\text{-}His}$, $CH_{2\text{-}Lys}$), 2.84 (m, 3H, $^{\beta}CH_{2\text{-}His}$), 2.32 (bs, 2H, $^{\alpha}CH_{2\text{-}\beta Ala}$), 2.13 (m, 3H, $CH_{2\text{-}Gln}$), 1.96 (m, 3H, $CH_{2\text{-}Gln}$), 1.70 (m, 2H, $CH_{2\text{-}Gln}$), 1.64-1.43 (m, 2H, $CH_{2\text{-}Lys}$), 1.36 (m, 2H, $CH_{2\text{-}Lys}$), 1.13 (d, *J* = 7.1 Hz, 3H, $CH_{3\text{-}Ala}$), 1.05 (m, 2H, $CH_{2\text{-}Lys}$). **^{13}C NMR** (DMSO-d_6, 75 MHz, δ): 173.1 (CO), 172.9 (CO), 171.8 (CO), 171.4 (CO), 171.3 (CO), 171.2 (CO), 170.2 (CO), 169.7 (CO), 169.4 (CO), 169.4 (CO), 168.9 (CO), 165.3 (CO), 157.5 (CO), 133.2 (CH), 133.1 (CH), 132.3 (CH), 130.5 (C), 130.3 (C), 129.8 (C), 129.2 (C), 128.9 (C), 128.7 (C), 128.4 (C), 128.0 (CH), 126.8 (CH), 126.6 (CH), 126.3 (CH), 125.7 (CH), 124.6 (CH), 124.4 (CH), 124.2 (CH), 123.6 (C), 124.4 (CH), 123.4 (C), 116.5 (CH), 116.4 (CH), 105.4 (CH), 61.4 (CH_2), 61.0 (CH_2), 55.2 (CH), 54.0 (CH), 52.6 (CH), 52.3 (CH), 51.7 (CH), 51.5 (CH), 51.0 (CH), 47.9 (CH), 39.5 (CH_2), 38.2 (CH_2), 34.6 (CH_2), 34.5 (CH_2), 31.3 (CH_2), 30.7 (CH_2), 30.6 (CH_2), 28.2 (CH_2), 26.5 (CH_2), 26.2 (CH_2), 26.0 (CH_2), 25.9 (CH_2),

22.1 (CH_2), 18.0 (CH_3). **ESI-MS** *m/z* (%): 1286.6 (14) $[M+H]^+$, 643.9 (100) $[M+2H]^{2+}$, 429.7 (1) $[M+3H]^{3+}$. **HRMS (ESI)** *m/z*: $[M+H]^+$ calculated for $C_{61}H_{76}N_{17}O_{15}$: 1286.5701, found 1286.5695. **FTIR (neat)**: ν = 3293.9 (amide A), 1655.0 (amide I), 1633.3 (amide I), 1530.8 (amide II) cm^{-1}.

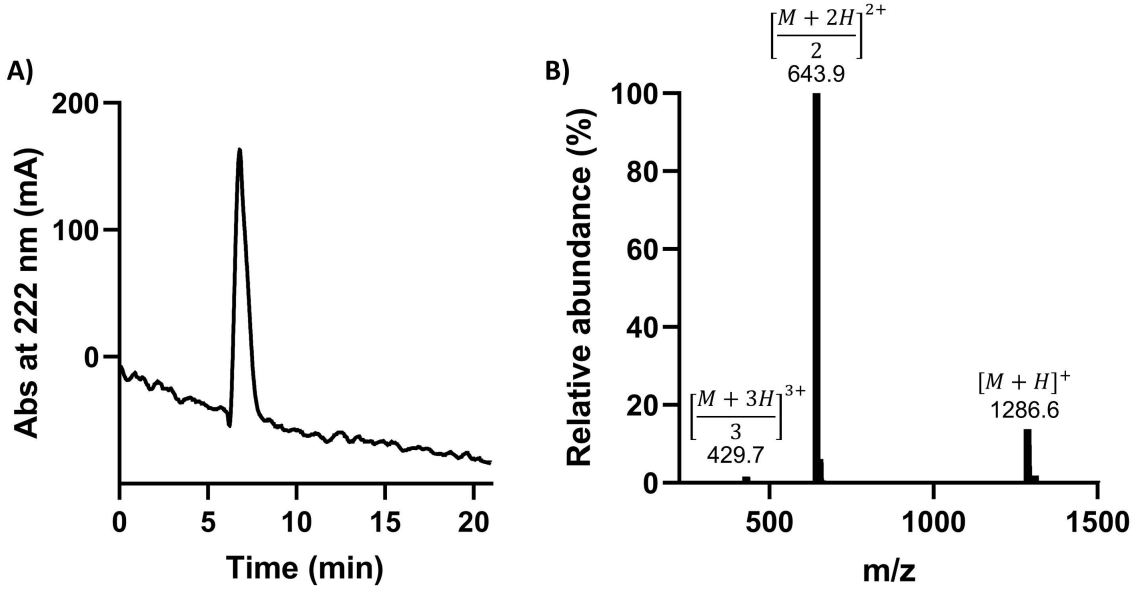

Figure 212. (A) **RP-uHPLC** of **^{E}CP3:** [Agilent SB-C18 column, H_20 (0.1% TFA)/MeCN (0.1% TFA), 80:20 → 80:20 (2 min) and 80:20 → 50:50 (19 min)] R_t = 6.6 min. (B) ESI-MS of the main peak.

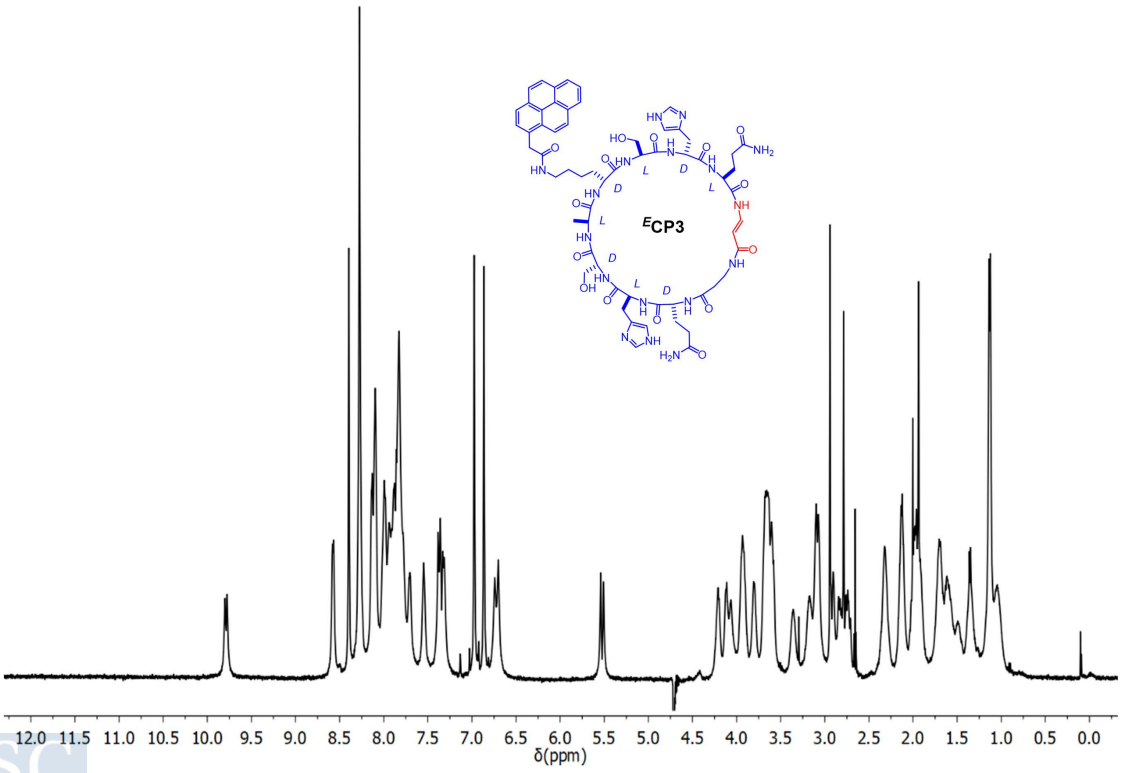

Figure 213. ^{1}H-NMR of **^{E}CP3** at 3.5 mM (500 MHz, D_2O/H_2O, 298K).

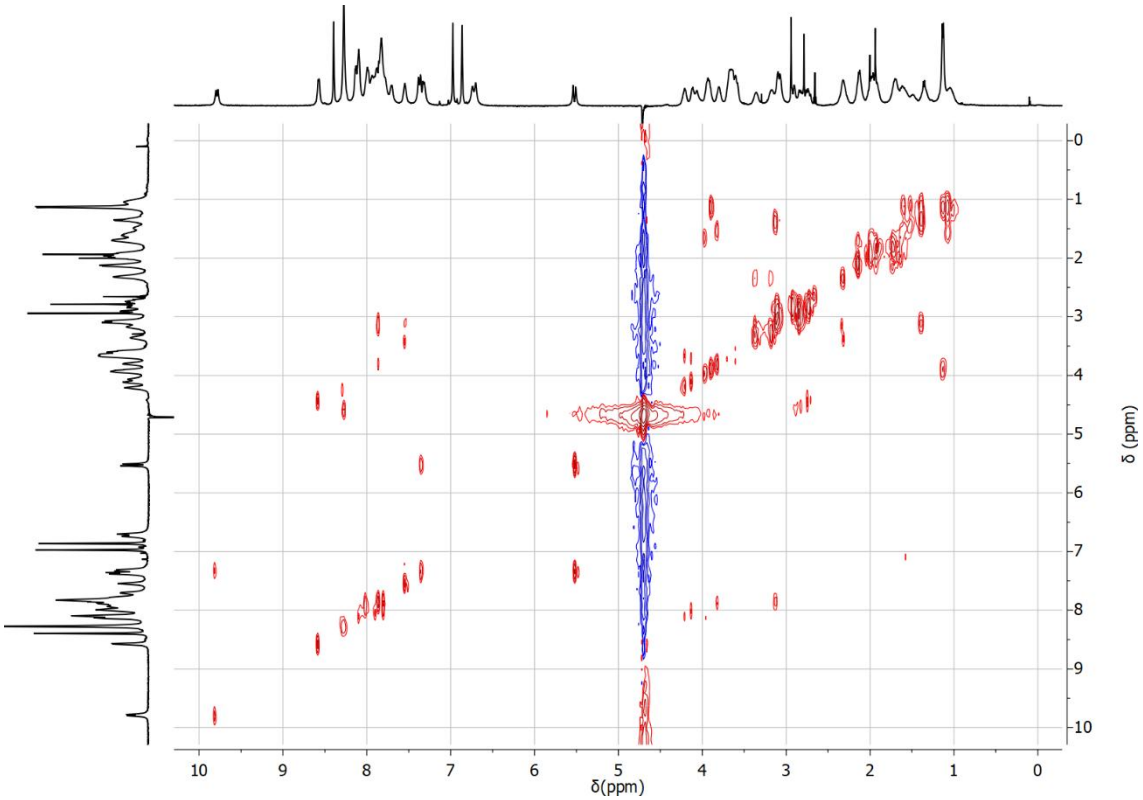

Figure 214. COSY of ^{E}**CP3** at 3.5 mM (500 MHz, D_2O/H_2O, 298K).

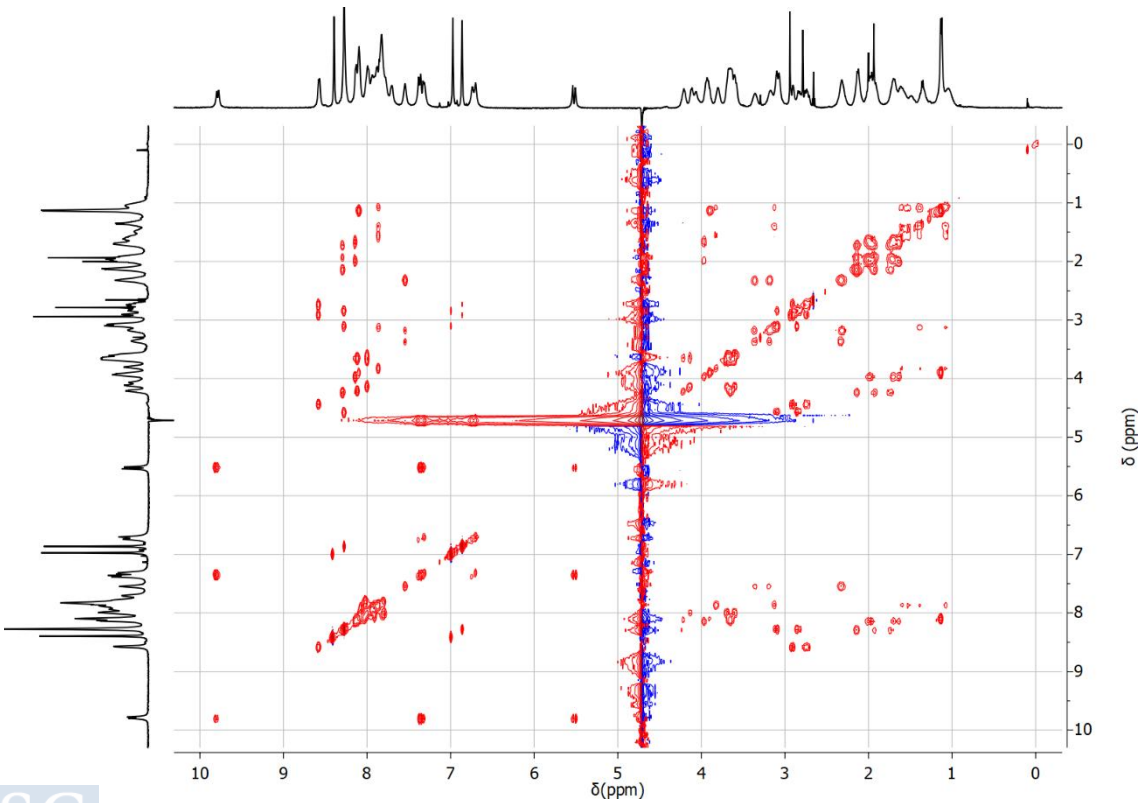

Figure 215. TOCSY of ^{E}**CP3** at 3.5 mM (500 MHz, D_2O/H_2O, 298K).

USC
UNIVERSIDADE DE SANTIAGO DE COMPOSTELA

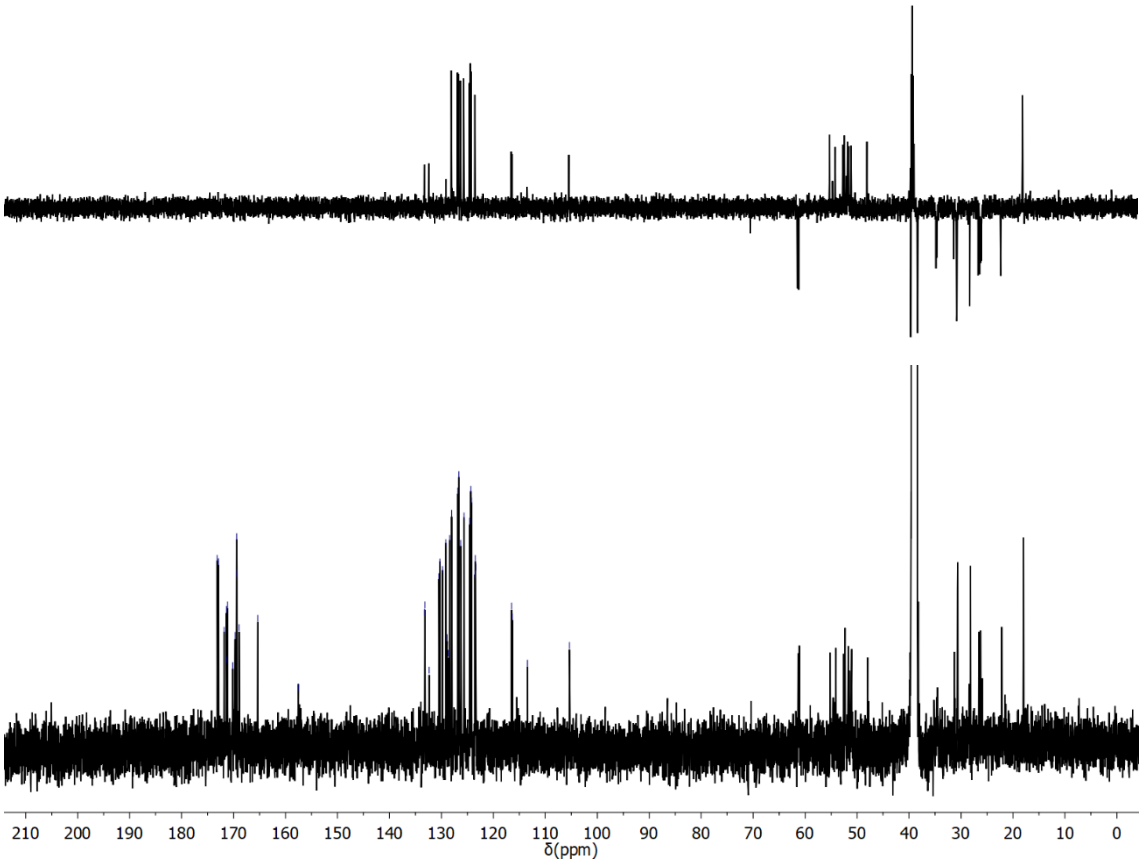

Figure 216. ^{13}C NMR (bottom) and DEPT-135 NMR (top) of **^{E}CP3** at 6.7 mM (75 MHz, DMSO-d_6, 298K).

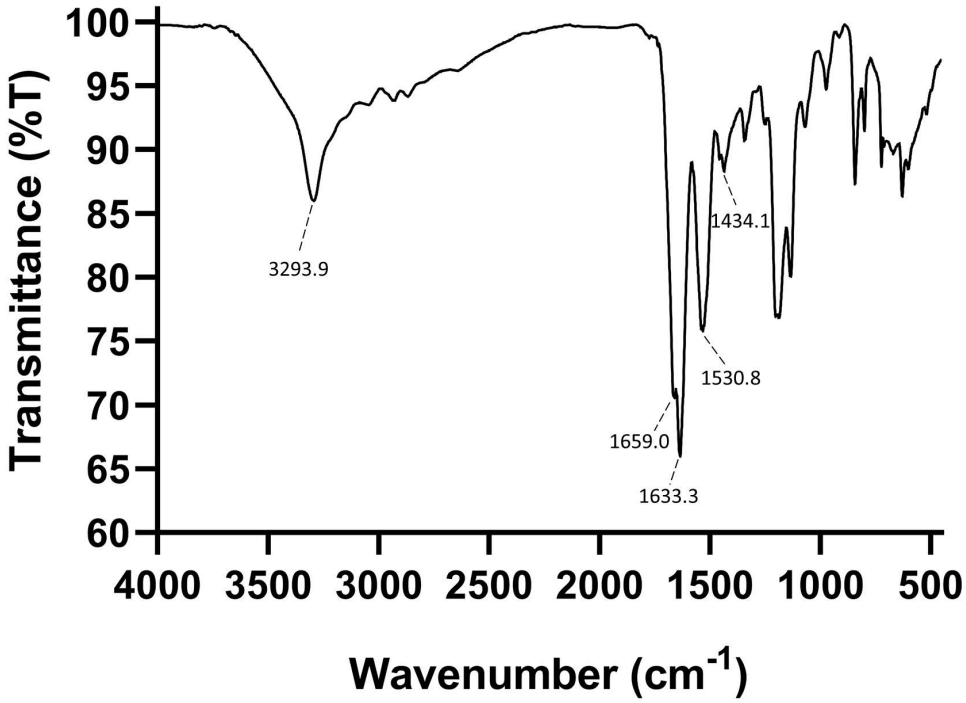

Figure 217. FT-IR spectrum of **^{E}CP3** (solid, 298 K).

UdC UNIVERSIDADE DE SANTIAGO DE COMPOSTELA

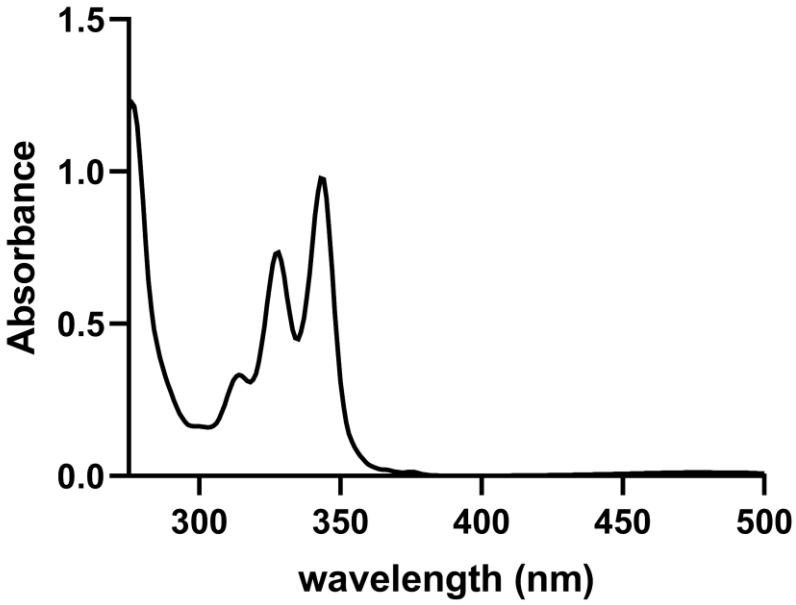

Figure 218. UV-Vis spectrum of an aqueous solution of **^{E}CP3** (100 µM).

^{E}CP4: The general procedure described above was carried out with 2.8 mg (2.5 µmol) of **^{Z}CP4**. After HPLC purification [gradient: H_2O (0.1% TFA)/MeCN (0.1% TFA), 100:0 → 100:0 (5 min); 100:0 → 50:50 (40 min), R_t (**^{E}CP4**) = 23.5 min, R_t (**^{Z}CP4**) = 24.0 min] and freeze-drying, **^{E}CP4** was obtained with a yield of 36% (white solid, 1.0 mg) and **^{Z}CP4** was partially recovered in a 14% (white solid, 0.4 mg). **ESI-MS** m/z (%): 1142.6 (8) $[M+H]^+$, 571.9 (100) $[M+2H]^{2+}$, 381.6 (6) $[M+3H]^{3+}$. **HRMS (ESI)** *m/z*: $[M+H]^+$ calculated for $C_{49}H_{76}N_{17}O_{15}$: 1142.5701, found 1142.5693. **FTIR (neat)**: ν = 3276.2 (amide A), 1653.1 (amide I), 1538.7 (amide II) cm^{-1}.

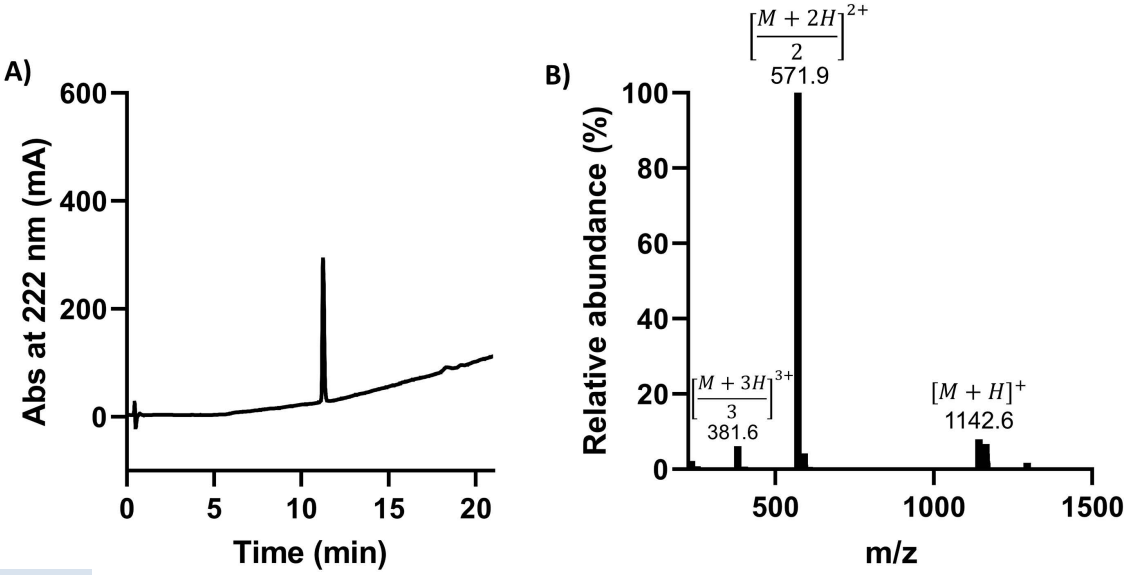

Figure 219. (A) **RP-uHPLC** of **^{E}CP4:** [Agilent SB-C18 column, H_20 (0.1% TFA)/MeCN (0.1% TFA), 100:0 → 100:0 (2 min) and 100:0 → 50:50 (19 min)] R_t = 11.2 min. (B) ESI-MS of the main peak.

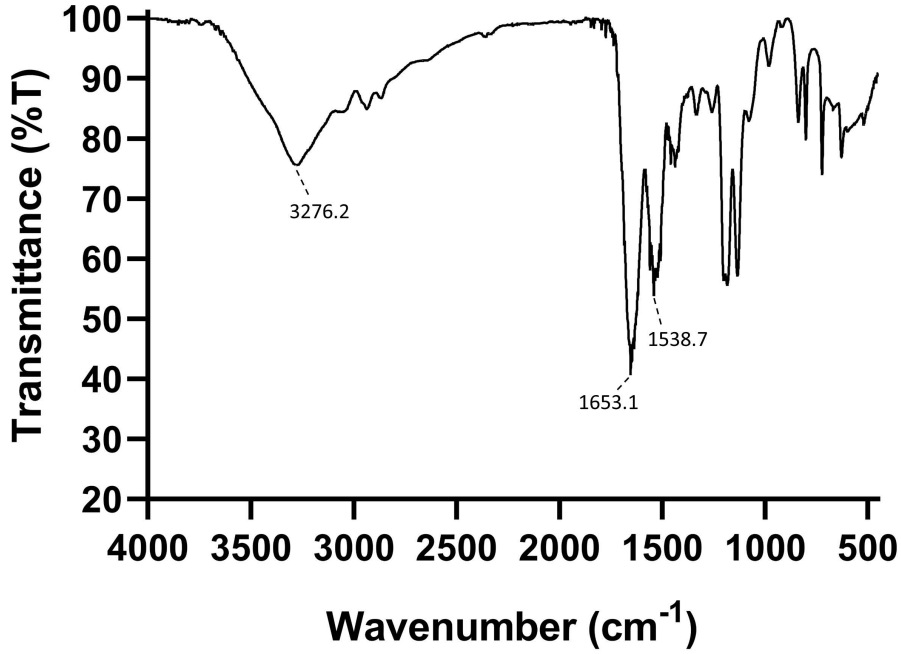

Figure 220. FT-IR spectrum of **^{E}CP4** (solid, 298 K).

^{E}CP5: The general procedure described above was carried out with 2.6 mg (2.0 µmol) of **^{Z}CP5**. After HPLC purification [gradient: H_2O (0.1% TFA)/MeCN (0.1% TFA), 80:20 → 80:20 (5 min); 80:20 → 50:50 (40 min), R_t (**^{E}CP5**) = 23.3 min, R_t (**^{Z}CP5**) = 24.0 min] and freeze-drying, **^{E}CP5** was obtained with a yield of 58% (white solid, 1.5 mg) and **^{Z}CP5** was partially recovered in a 23% (white solid, 0.6 mg). **ESI-MS** m/z (%): 1286.6 (9) $[M+H]^+$, 643.9 (100) $[M+2H]^{2+}$, 429.7 (10) $[M+3H]^{3+}$. **HRMS (ESI)** *m/z*: $[M+H]^+$ calculated for $C_{62}H_{80}N_{17}O_{14}$: 1286.6065, found 1286.6064. **FTIR (neat)**: ν = 3303.8 (amide A), 1653.1 (amide I), 1544.6 (amide II) cm^{-1}.

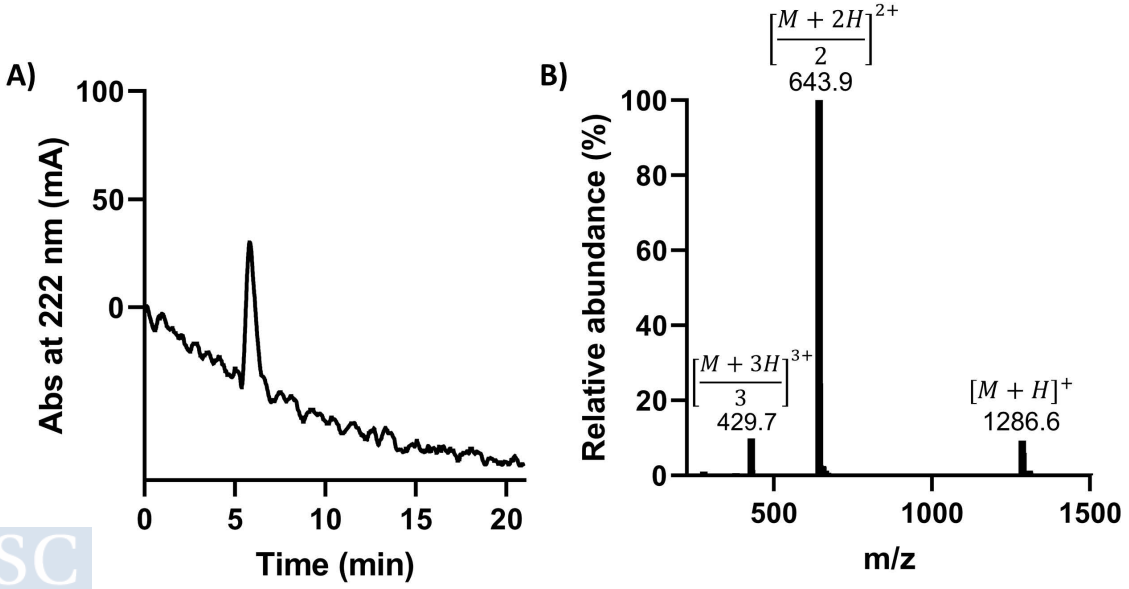

Figure 221. (A) RP-uHPLC of **^{E}CP5**: [Agilent SB-C18 column, H_20 (0.1% TFA)/MeCN (0.1% TFA), 80:20 → 80:20 (2 min) and 80:20 → 50:50 (19 min)] R_t = 5.7 min. (B) ESI-MS of the main peak.

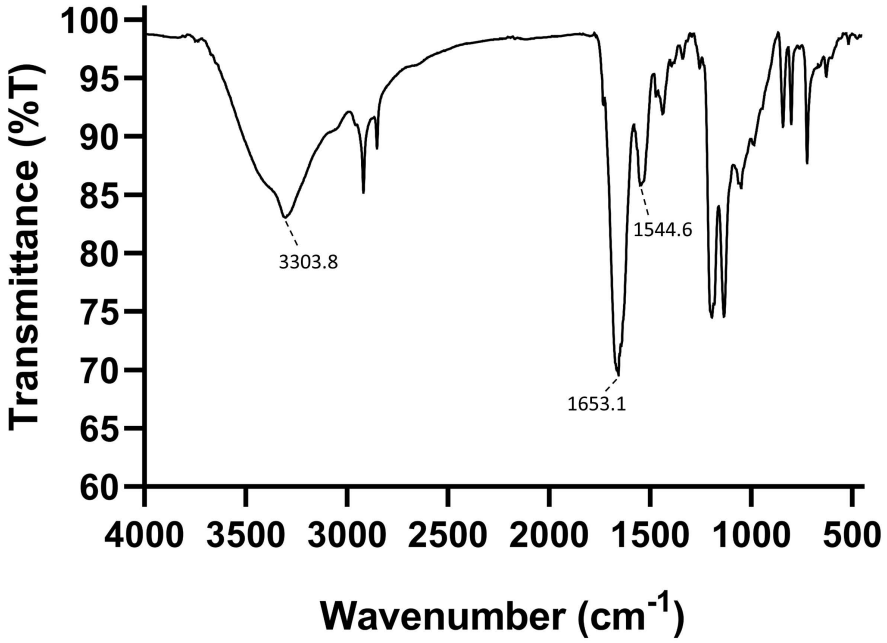

Figure 222. FT-IR spectrum of **^{E}CP5** (solid, 298 K).

USC
UNIVERSIDADE DE SANTIAGO DE COMPOSTELA

8.2.3. SELF-ASSEMBLING CYCLIC PEPTIDE NANOTUBES FOR THE TRANSPORT OF DOXORUBICIN INTO CANCER CELLS

8.2.3.1. Methods

Transition Electron Microscopy (TEM)

TEM images were acquired with a JEOL JEM-2010 equipment. Samples were prepared by deposition of a peptide solution (200 µM, 10 µL) in PBS buffer (10 mM, 107 mM NaCl, pH 7.4) over a 400-mesh carbon-coated copper grid (Electron Microscopy Sciences). After 10 minutes, excess of the sample was removed with a filter paper. Then, samples were stained with an aqueous solution of phosphotungstic acid (2% w/v, 10 µL) during 3 minutes and washed with Milli-Q H_2O (10 µL) for 1 minute. Samples were allowed to air-dry overnight before imaging.

Cell viability assays

The cell growth inhibition of each compound was evaluated using the MTT (3-[4,5-dimethylthiazol-2-yl]-2,5-diphenyltretrazolium bromid) assay.[271] MCF-7 and MRC-5 cells were grown on Minimum Essential Medium Eagle, while NCI-H460 and NCI/ADR-RES cells were grown on culture medium RPMI 1640. All culture mediums were supplemented with 10% FBS (Fetal Bovine Serum) and 1% penicillin-streptomycin-glutamine mix. The incubation conditions were an atmosphere of 95% air and 5% CO_2 at 37°C.

MCF-7 (100000 cells/mL), NCI-H460 (150000 cells/mL), NCI/ADR-RES (150000 cells/mL) or MRC-5 (100000 cells/mL) cells were seeded the day before in sterile 96-well plates (100 µL/well). Then, cells were incubated with each concentration of the compound (100 µL/well) during the specified time for each cell line. The compounds were previously dissolved in DMSO and diluted at the time of the experiment with complete medium to the concentration to be tested. The DMSO content of each well was maintained less than 1%. All concentrations were carried out with triplicates points and controls with DMSO at the same proportion in which the compounds were dissolved were included in all experiments. After the incubation time, the samples were removed and 100 µL of complete medium with 0.5 mg/ml MTT were added to each well. Cells were incubated for 4 hours and the medium was removed. The resulting formazan crystal were dissolved in DMSO (100 µL/well). The absorbance of each well at 595 nm was acquired with a Tecan Infinite F200Pro plate reader. A blank subtraction was performed (cells treated with Triton X-100) and the data was normalized to the value of the untreated cells (100% viability). Data were analysed with GraphPad Prism software.[281]

USC UNIVERSIDADE DE COMPOSTELA

[271] a) T. Mossman, *J. Immunol. Methods* **1983**, *65*, 55-63; b) P. Kumar, A. Nagarajan, P. D. Uchil, *Cold Spring Harb. Protoc.* **2018**, *2018* (6), pdbprot095505.
[281] M. L. Swift, *J. Chem. Inf. Comput. Sci.* **1997**, *37*, 411-412.

Confocal microscopy experiments

NCI/ADR-RES cells were seeded at 150000 cells/mL in a 96-well plate (100 µL/well) the day before. The medium was RPMI 1640 with 10% FBS and 1% penicillin-streptomycin-glutamine mix. Then, medium from cells was eliminated and peptide solutions at the desired concentration in complete medium were added (100 µL/well). Cells were incubated with the compound during the specified time in an atmosphere of 95% air and 5% CO_2 at 37°C.

When nuclear staining was required, medium from cells was removed after incubation with the peptide and 50µL/well of a solution of Hoechst 33342 (1 µM) in cell medium was added. The cells were incubated for 30 minutes and then the medium was replaced with 100 µL/well of complete medium.

When staining with Lysotracker Deep Red was required, medium from cells was removed after incubation with the peptide and 50µL/well of a solution of Lysotracker Deep Red (50 nM) in cell medium was added. The cells were incubated for 30 minutes and then the medium was replaced with 100 µL/well of complete medium.

Cells were analysed with an Andor DragonFly spinning disc confocal setup mounted on a Nikon Eclipse Ti-E inverted microscope. Images were analysed using ImageJ.[277]

Endocytosis inhibition experiments

NCI/ADRR-RES cells were seeded the day before on a 96-well plate (150000 cells/mL). The next day, cells were treated with Wortmannin (100 µM), Dynasore (80 µM), EIPA (50 µM), Chlorpromazine (30 µM) or sodium azide (1 %) (100 µL/well) diluted in complete RPMI 1640 medium. These inhibitors were incubated for 30 min at 37°C in an atmosphere of 95% air and 5% CO_2. Then, these solutions were replaced by a sample of 50 µM **CP6-DOX**, **CP6T10-DOX**, **CP6$_{NBD}$-DOX**, **CP7-DOX** or **CP7T10-DOX** (100 µL/well) and the same amount of the corresponding inhibitor in RPMI 1640 without serum. After incubation for 1 hour, cells were washed twice with PBS and detached with Trypsin (100 µL/well, incubated for 10 min). Once the cells were in suspension, Trypsin was neutralized with PBS containing 2 % FBS and 5 mM EDTA (100 µL/well). The cell uptake was quantified with a Guava easyCyte BG HT flow cytometer. DOX was excited at 488 nm (blue laser) and the emission was collected at 580 nm (yellow channel). The median fluorescence intensity (MFI) was calculated for each sample. Each condition was measured in triplicate and data were normalized to untreated controls. Data were analysed with the InCyte analysis mode included in GuavaSoft 3.2 software.

Doxorubicin release by mass spectrometry

An aqueous solution of **CP6-DOX** or **CP6T10-DOX** (200 µM) at pH 5.0 was prepared. The release was followed by direct analysis after 0, 14, 24, 48 and 72 hours with an Agilent Technologies 1260 Infinity II with a 6120 Quadrupole LC-MS.

USC UNIVERSIDADE DE SANTIAGO

8.2.3.2. Synthesis of the maleimide-based doxorubicin linker

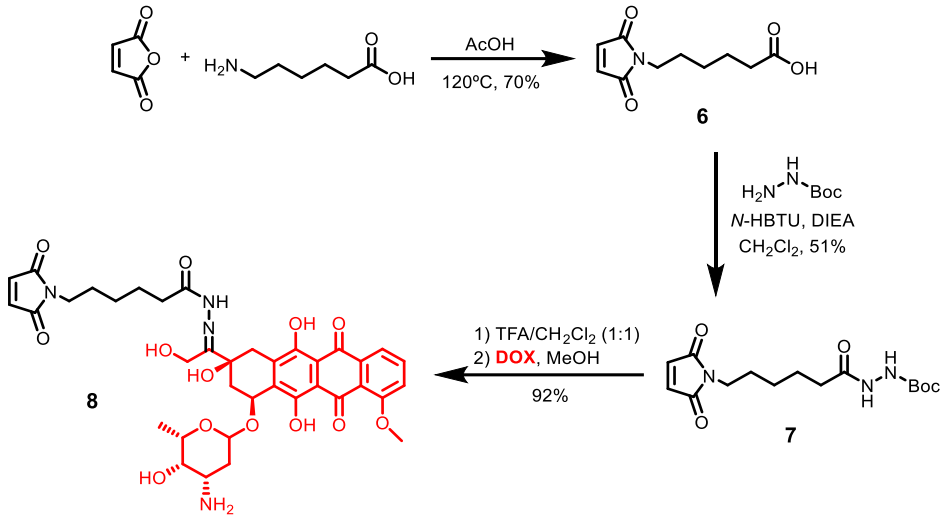

Figure 223. Synthetic route to obtain **8**.

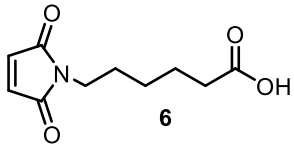

6-(2,5-dihydro-2,5-dioxo-1*H*-pyrrol-1-yl)hexanoic acid (6-maleimidocaproic acid) (6). A solution of maleic anhydride (1.44 g, 14.64 mmol) and 6-aminocaproic acid (1.60 g, 12.20 mmol) in acetic acid glacial (40 mL) was refluxed for 6 hours at 120ºC. Then, the reaction mixture was diluted with H_2O and extracted with AcOEt (3 x 20 mL). The organic phase was dried over anhydrous $MgSO_4$, filtered and concentrated under reduced pressure. The resulting residue was purified by flash chromatography (5-10% MeOH/CH_2Cl_2) to afford the product as a crystalline white solid [1.88 g, 70%, R_f = 0.61 (10% MeOH/CH_2Cl_2)]. **^{1}H NMR** ($CDCl_3$, 300 MHz, δ): 11.30 (br, 1H, COOH), 6.65 (s, 2H, CH=CH), 3.46 (t, *J* = 7.2 Hz, 2H, N-CH_2), 2.29 (t, *J* = 7.4 Hz, 2H, CH_2-CO), 1.57 (m, 4H, 2 CH_2), 1.29 (m, 2H, CH_2). **^{13}C NMR** ($CDCl_3$, 75 MHz, δ): 179.7 (CO), 170.9 (CO), 134.1 (CH), 37.6 (CH_2), 33.8 (CH_2), 28.1 (CH_2), 26.1 (CH_2), 24.1 (CH_2). **ESI-MS** *m/z* (%): 234.1 (100) $[M+Na]^+$, 212.1 (46) $[M+H]^+$. **HRMS (ESI)** *m/z*: $[M+Na]^+$ calculated for $C_{10}H_{13}NNaO_4$: 234.0737, found 234.0736. The characterization data are consistent with those reported in the literature.[267,282]

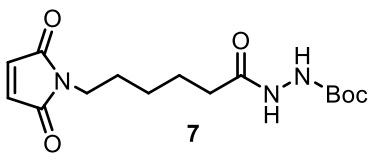

tert-butyl 2-(6-(2,5-dihydro-2,5-dioxo-1*H*-pyrrol-1-yl)hexanoyl)hydrazinecarboxylate (7). A solution of 6-maleimidocaproic acid (**6**) (826 mg, 3.91 mmol) in CH_2Cl_2 (40 mL) was treated with *N*-HBTU (1.85 g, 4.89 mmol), DIEA (2.7 mL, 15.64 mmol) and *tert*-butyl carbazate (517 mg, 3.91 mmol).

[267] a) D. Willner, P. A. Trail, S. J. Hofstead, H. D. King, S. J. Lasch, G. R. Braslawsky, R. S. Greenfield, T. Kaneko, R. A. Firestone, *Bioconjugate Chem.* **1993**, *4*, 521-527; b) Z. Jia, L. Wong, T. P. Davis, V. Bulmus, *Biomacromolecules* **2008**, *9*, 3106-3113; c) T. Cai, Y. Chen, Y. Wang, H. Wang, X. Liu, Q. Jin, S. Agarwal, J. Ji, *Polym. Chem.* **2014**, *5*, 4061-4068.
[282] D. Xiao, L. Luo, J. Li, Z. Wang, L. Liu, F. Xie, J. Feng, X. Zhou, *Bioorg. Chem.* **2021**, *116*, 105366.

The reaction mixture was stirred for 1.5 hours under argon atmosphere and then washed with aqueous solutions of HCl (5%, 3 x 20 mL) and $NaHCO_3$ (sat., 3 x 20 mL). Then, the organic phase was dried over anhydrous $MgSO_4$, filtered and concentrated under vacuum. The residue was purified by flash chromatography (1-3% MeOH/CH_2Cl_2) to afford the product as a light-yellow oil [645 mg, 51%, R_f = 0.53 (5% MeOH/CH_2Cl_2)]. **^{1}H NMR** ($CDCl_3$, 300 MHz, δ): 7.56 (br, 1H, NH), 6.67 (s, 2H, CH=CH), 6.58 (br, 1H, NH), 3.50 (t, *J* = 7.2 Hz, 2H, N-CH_2), 2.20 (t, *J* = 7.5 Hz, 2H, CH_2-CO), 1.76-1.51 (m, 4H, 2 CH_2), 1.45 (s, 9H, Boc), 1.30 (m, 2H, CH_2). **^{13}C NMR** ($CDCl_3$, 75 MHz, δ): 172.4 (CO), 170.5 (CO), 155.5 (CO), 133.7 (CH), 80.7 (C), 38.2 (CH_2), 37.1 (CH_2), 33.1 (CH_2), 27.7 (CH_3), 25.8 (CH_2), 24.3 (CH_2). **ESI-MS** *m/z* (%): 348.2 (100) $[M+Na]^+$, 226.2 (23) $[M+H\text{-Boc}]^+$. **HRMS (ESI)** *m/z*: $[M+H]^+$ calculated for $C_{15}H_{24}N_3O_5$: 326.1710, found 326.1710. The characterization data are consistent with those reported in the literature.[267]

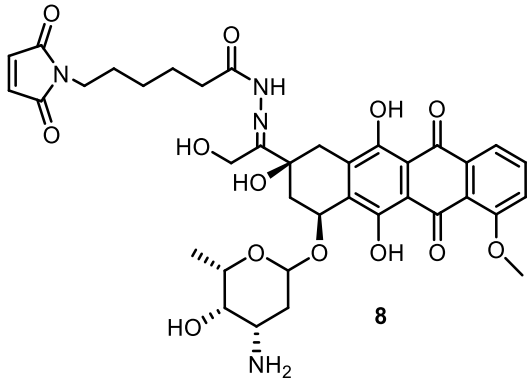

8

(6-maleimidocaproyl)hydrazone derivative of doxorubicin (8). A solution of **7** (411 mg, 1.26 mmol) in CH_2Cl_2 (10 mL) was treated with TFA (10 mL) and stirred for 15 minutes. After this time, the solvent was removed under reduced pressure and the resulting oil was redissolved in CH_2Cl_2 and further evaporated, this process was repeated three times. Then, Et_2O was added three times, concentrating after each time, and dried at high vacuum for 2 hours. The residue was dissolved in dry MeOH (140 mL) and treated with doxorubicin hydrochloride (244 mg, 0.420 mmol). The reaction mixture was stirred for 24 hours under argon atmosphere, room temperature and protected from light using aluminium foil. Once the reaction was completed, the volume was reduced at the rotary evaporator to approximately 1-2 mL and poured over ethyl acetate (40 mL). The red precipitate obtained was collected by centrifugation and washed with ethyl acetate (3 x 40 mL), centrifuging after each time. Finally, it was dried under high vacuum to obtain the product as a red solid [290 mg, 92%]. **^{1}H NMR** (DMSO-d_6, 500 MHz, δ): 14.08 (s, 1H, OH), 13.31 (s, 1H, OH), 10.29 (s, 1H, -N-NH-CO), 7.91 (m, 2H, H_{Ar}), 7.81 (bs, 2H, NH_2), 7.66 (m, 1H, H_{Ar}), 6.97 (s, 2H, CH=CH), 5.75 (t, *J* = 4.8 Hz, 1H, -O-CH-O- of sugar), 5.48 (s, 2H, CH_2-N=), 4.98 (m, 1H, CH), 4.42 (m, 2H, CH_2 sugar), 4.24-4.02 (m, 1H, CH sugar), 4.00 (s, 3H, OCH_3), 3.58 (m, 1H, CH sugar), 3.40 (m, 2H, CH_2 aliphatic ring), 3.31 (m, 1H, CH sugar), 3.25 (m, 2H, CH_2 aliphatic chain), 2.30-1.85 (m, 4H, CH_2 aliphatic chain and CH_2 aliphatic ring), 1.80-1.45 (m, 2H, CH_2 aliphatic chain), 1.32 (m, 2H, CH_2 aliphatic chain), 1.18 (m, 3H, CH_3 sugar), 1.04 (m, 2H, CH_2 aliphatic chain). **ESI-MS** *m/z* (%): 773.3 (10) $[M+Na]^+$, 751.3 (100) $[M+H]^+$. **HRMS (ESI)** *m/z*: $[M+H]^+$ calculated for $C_{37}H_{43}N_4O_{13}$: 751.2821, found 751.2821. The characterization data are consistent with those reported in the literature.[267]

UCC UNIVERSIDADE DE SANTIAGO DE COMPOSTELA

8.2.3.3. Synthesis of the disulphide bond-based doxorubicin linker

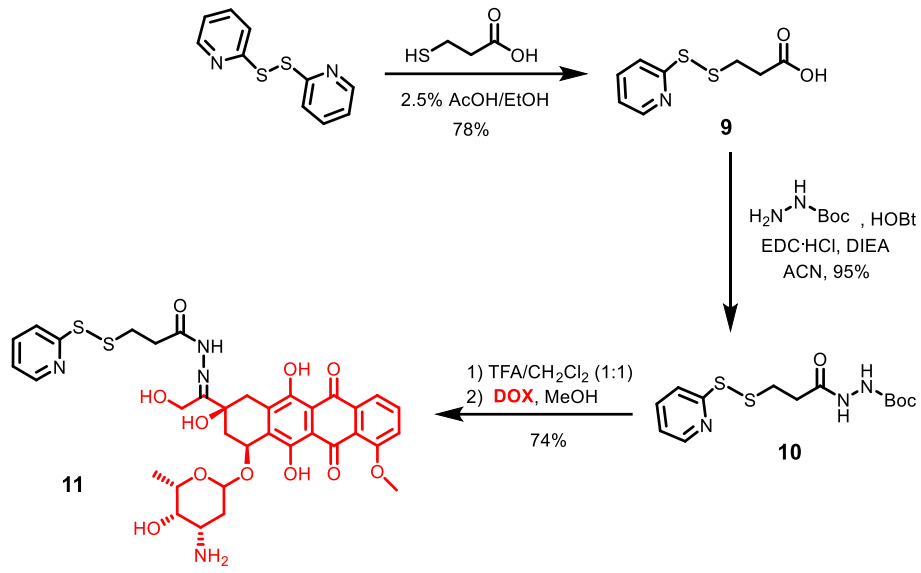

Figure 224. Synthetic strategy to obtain **11**.

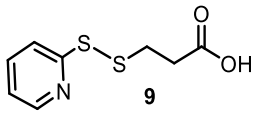

3-(pyridin-2-yldisulfanyl)propanoic acid (9). A solution of 2,2'-dithiodipyridine (1.23 g, 5.59 mmol) in EtOH (5 mL) was treated with acetic acid (132 µL) and 3-mercaptopropionic acid (297 mg, 2.80 mmol). The reaction mixture was stirred for 20 hours and concentrated under vacuum. Purification was carried out via Al_2O_3 chromatography (20% EtOH/CH_2Cl_2 and 20% EtOH/CH_2Cl_2 + 2% AcOH) and the product was obtained as a yellow oil [467 mg, 78%, R_f = 0.27 (5% MeOH/CH_2Cl_2)]. **^{1}H NMR** ($CDCl_3$, 300 MHz, δ): 12.30 (br, 1H, COOH), 8.40 (m, 1H, H_{Ar}), 7.63 (m, 2H, H_{Ar}), 7.05 (m, 1H, H_{Ar}), 2.86 (m, 4H, 2 CH_2). **^{13}C NMR** ($CDCl_3$, 75 MHz, δ): 175.5 (C), 159.4 (C), 149.1 (CH), 137.7 (CH), 121.0 (CH), 120.1 (CH), 33.9 (CH_2), 33.6 (CH_2). **ESI-MS** *m/z* (%): 238.0 (5) $[M+Na]^+$, 216.0 (100) $[M+H]^+$. **HRMS (ESI)** *m/z*: $[M+H]^+$ calculated for $C_8H_{10}NO_2S_2$: 216.0147, found 216.0148. The characterization data are consistent with those reported in the literature.[283]

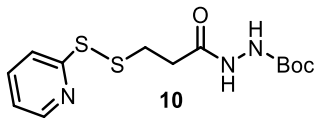

***tert*-butyl 2-(3-(pyridin-2-yldisulfaneyl)propanoyl)hydrazine-1-carboxylate (10).** A solution of **9** (179 mg, 0.83 mmol) in dry acetonitrile (9 mL) under argon atmosphere was cooled in an ice-water bath and treated with HOBt (449 mg, 3.32 mmol), *tert*-butyl carbazate (219 mg, 1.66 mmol), DIEA (426 µL, 2.49 mmol) and EDC·HCl (318 mg, 1.66 mmol). The reaction mixture was stirred for 4 hours at room temperature and concentrated under vacuum. The obtained residue was dissolved in CH_2Cl_2 (5 mL) and washed with H_2O (3 x 10 mL). The organic phase was dried over anhydrous $MgSO_4$, filtered and concentrated under vacuum. The resulting residue was purified by flash chromatography (2% MeOH/CH_2Cl_2) and the product was

[283] a) J. Carlsson, H. Drevin, R. Axén, *Biochem J.* **1978**, *173*, 723-737; b) S. Y. Tan, C. Y. Ang, Z. Luo, P. Li, K. T. Nguyen, Y. Zhao, *Chem. Eur. J.* **2015**, *21*, 6123-6131.

obtained as a colourless oil [258 mg, 95%, R_f = 0.40 (5% MeOH/CH_2Cl_2)]. **^{1}H NMR** ($CDCl_3$, 300 MHz, δ): 9.43 (br, 1H, NH), 8.49 (m, 1H, H_{Ar}), 7.59 (m, 2H, 2 H_{Ar}), 7.09 (m, 1H, H_{Ar}), 6.23 (br, 1H, NH), 3.05 (t, *J* = 6.8 Hz, 2H, CH_2), 2.65 (t, *J* = 6.7 Hz, 2H, CH_2), 1.44 (s, 3H, CH_3). **^{13}C NMR** ($CDCl_3$, 75 MHz, δ): 170.5 (CO), 159.2 (C), 155.6 (CO), 149.7 (CH), 137.3 (CH), 121.3 (CH), 120.6 (CH), 81.7 (C), 34.9 (CH_2), 33.7 (CH_2), 28.2 (CH_3). **ESI-MS** *m/z* (%): 352.1 (26) $[M+Na]^+$, 330.1 (100) $[M+H]^+$. **HRMS (ESI)** *m/z*: $[M+H]^+$ calculated for $C_{13}H_{20}N_3O_3S_2$: 330.0941, found 330.0943.

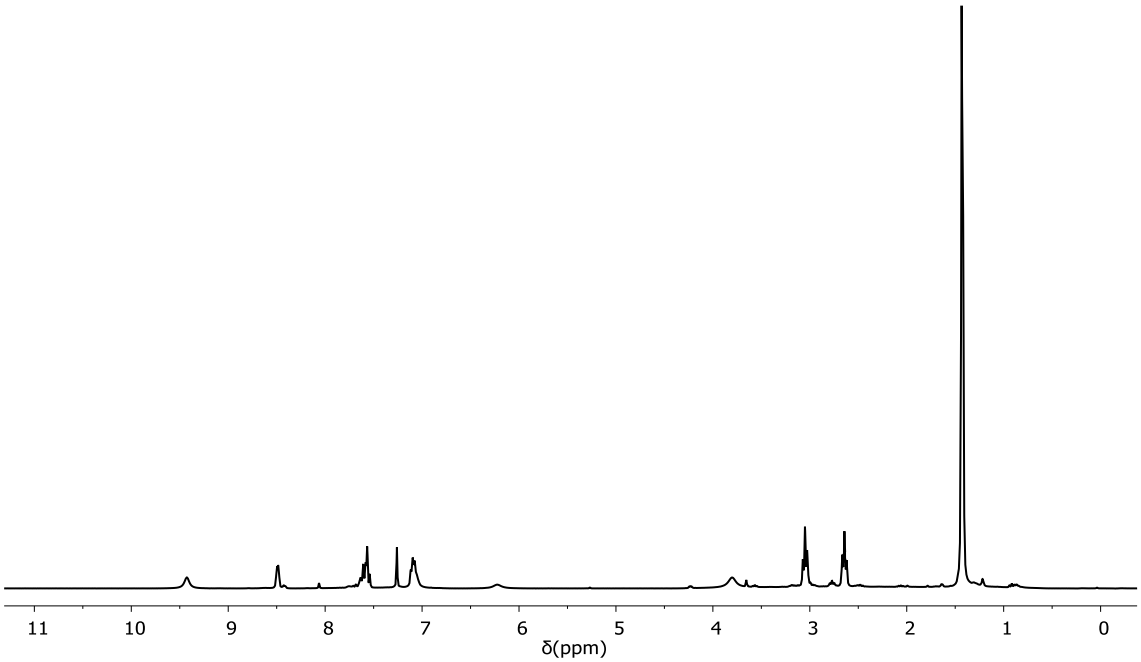

Figure 225. ^{1}H NMR ($CDCl_3$, 300 MHz) of **10**.

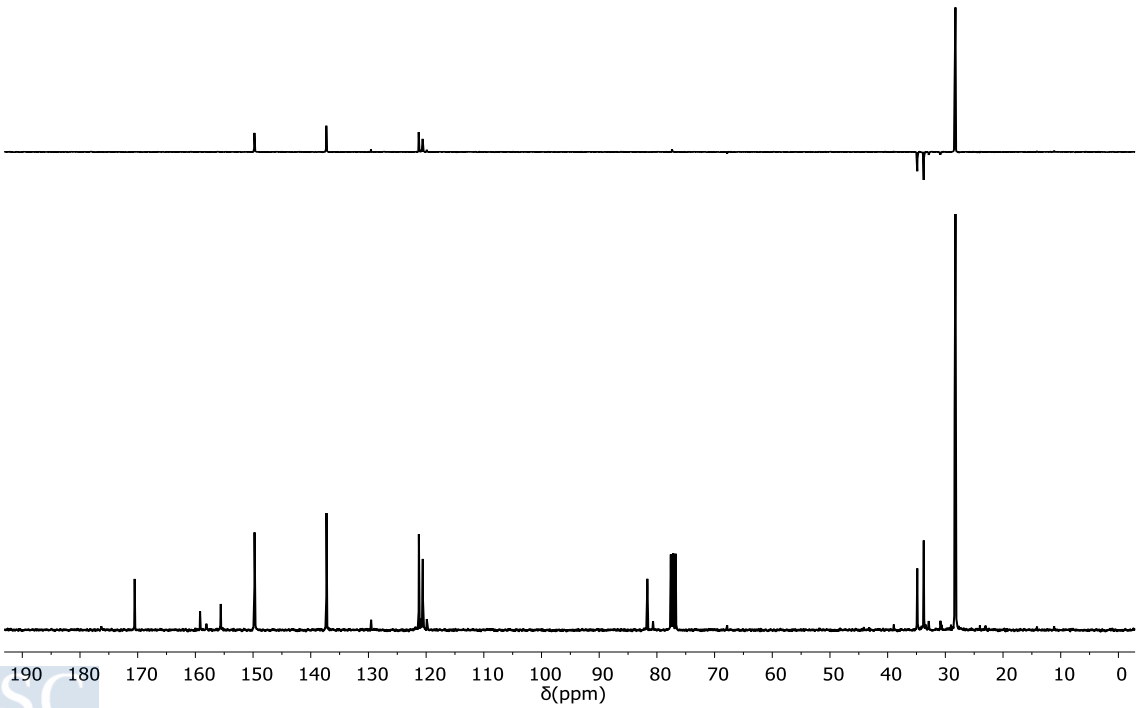

Figure 226. ^{13}C NMR (bottom) and DEPT-135 NMR (top) of **10** ($CDCl_3$, 75 MHz).

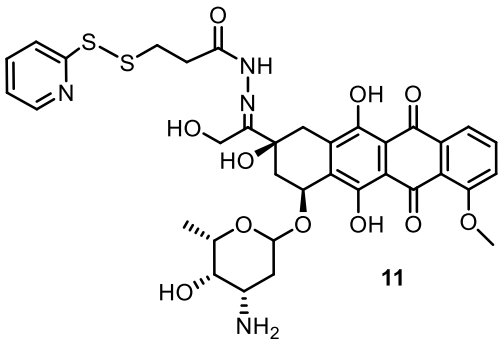

(3-(pyridin-2-yldisulfaneyl)propanoyl)hydrazone derivative of doxorubicin (11). A solution of **10** (34 mg, 103 µmol) was stirred in a mixture of TFA/CH_2Cl_2 (1:1, 3 mL) for 20 min. The solvent was then removed under reduced pressure and the resulting oil was redissolved in CH_2Cl_2 and evaporated three times. The same process was repeated three times with Et_2O and dried at high vacuum for 2 hours. The resulting residue was dissolved in dry MeOH (12 mL), treated with doxorubicin hydrochloride (24 mg, 41.2 µmol) and stirred for 6 days under argon atmosphere at room temperature and protected from light using aluminium foil. Then, the volume was reduced at the rotary evaporator to approximately 1-2 mL and added over acetonitrile (40 mL). The red precipitate obtained was collected by centrifugation, washed with acetonitrile (3 x 40 mL) and dried under high vacuum to obtain the product as a red solid [23 mg, 74%]. **^{1}H NMR** (DMSO-d_6, 500 MHz, δ): 14.11 (s, 1H, OH), 13.34 (s, 1H, OH), 10.51 (s, 1H, -N-NH-CO), 8.52-7.14 (m, 7H, H_{Ar}), 5.80 (t, *J* = 4.7 Hz, 1H, -O-CH-O- of sugar), 5.47 (s, 2H, CH_2-N=), 5.33 (m, 1H, CH), 4.45 (m, 2H, CH_2 sugar), 4.01 (m, 2H, 2 CH sugar), 3.99 (s, 3H, OCH_3), 3.58 (m, 1H, CH sugar), 2.92-2.63 (m, 4H, 2 CH_2 aliphatic ring), 2.24-1.46 (m, 4H, 2 CH_2 aliphatic chain), 1.19 (d, *J* = 6.5 Hz, 3H, CH_3 sugar). **ESI-MS** *m/z* (%): 777.3 (33) $[M+Na]^+$, 755.3 (100) $[M+H]^+$, 626.2 (92) $[M+H\text{-sugar}]^+$. **HRMS (ESI)** *m/z*: $[M+H]^+$ calculated for $C_{35}H_{39}N_4O_{11}S_2$: 755.2051, found 755.2053. The characterization data are consistent with those reported in the literature.[268]

8.2.3.4. Synthesis of the azide-carbon tail containing NBD

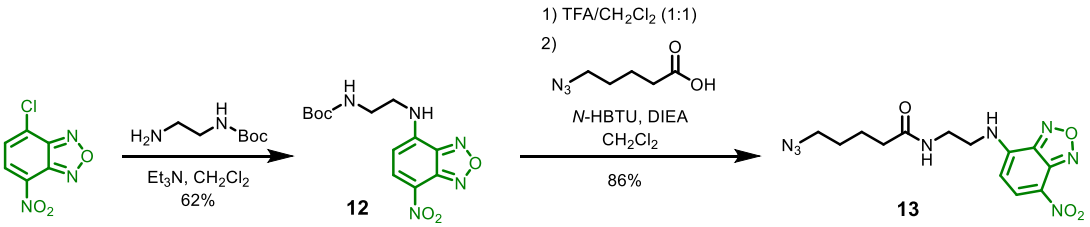

Figure 227. Synthetic route to obtain **13**.

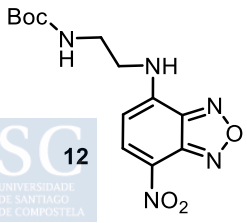

tert-butyl *N*-[2-(7-nitrobenzofuran-4-ylamino)ethyl]carbamate (12). A solution of *N*-Boc-ethylenediamine (194 mg, 1.21 mmol) and Et_3N (168 µL, 1.21 mmol) in CH_2Cl_2 (2 mL) was added to a solution of 4-chloro-7-nitrobenzofuran (219 mg, 1.10 mmol) in CH_2Cl_2 (6 mL). The reaction mixture was protected from light using aluminium foil and stirred for 18 hours under argon atmosphere. Then, the mixture was diluted with CH_2Cl_2 and washed with $NaHCO_3$ (sat., 3x20 mL). The

organic phase was dried over anhydrous $MgSO_4$, filtered and concentrated under reduced pressure. The resulting residue was purified by flash chromatography (1-2% $MeOH/CH_2Cl_2$) and the product was obtained as a brown foam [221 mg, 62%, R_f = 0.55 (5% $MeOH/ CH_2Cl_2$)]. **^{1}H NMR** ($CDCl_3$, 300 MHz, δ): 8.43 (d, *J* = 8.7 Hz, 1H, H_{Ar}), 7.78 (br, 1H, NH), 6.15 (d, *J* = 8.7 Hz, 1H, H_{Ar}), 5.26 (br, 1H, NH), 3.61 (m, 4H, 2 CH_2), 1.44 (s, 9H, Boc). **^{13}C NMR** ($CDCl_3$, 75 MHz, δ): 157.8 (CO), 144.5 (C), 144.4 (C), 144.3 (C), 144.1 (C), 136.4 (CH), 98.6 (CH), 81.1 (C), 46.1 (CH_2), 39.4 (CH_2), 28.4 (CH_3). **ESI-MS** *m/z* (%): 346.1 (100) $[M+Na]^+$, 324.1 (44) $[M+H]^+$. **HRMS (ESI)** *m/z*: $[M+H]^+$ calculated for $C_{13}H_{18}N_5O_5$: 324.1302, found 324.1304. The characterization data are consistent with those reported in the literature.[284]

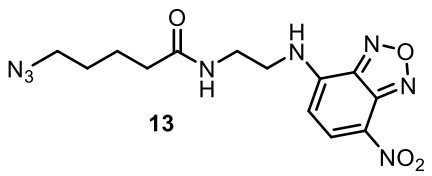

13

5-azido-N-(2-((7-nitrobenzo[c][1,2,5]oxadiazol-4-yl)amino)ethyl)pentanamide (13). A solution of **12** (96 mg, 0.297 mmol) in CH_2Cl_2 (2.5 mL) was treated with TFA (2.5 mL) and stirred for 15 min. After the solvent was removed under reduced pressure, the oil obtained was redissolved in CH_2Cl_2 and further evaporated, the process was repeated three times. The residue was dried at high vacuum for 2 hours. The resulting TFA salt was dissolved under argon atmosphere in dry CH_2Cl_2 (10 mL) and treated with DIEA (204 µL, 1.19 mmol), *N*-HBTU (141 mg, 0.371 mmol) and 5-azidopentanoic acid (47 mg, 0.327 mmol). The reaction mixture was stirred for 2 hours under argon atmosphere. Then, it was washed with aqueous solutions of HCl (5%, 3 x 5 mL) and $NaHCO_3$ (sat., 3 x 5 mL). The organic phase was dried over anhydrous $MgSO_4$, filtered and concentrated under vacuum. The resulting residue was purified by flash chromatography (1-2% $MeOH/CH_2Cl_2$) and the product was obtained as an orange solid [89 mg, 86%, R_f = 0.77 (10% $MeOH/CH_2Cl_2$)]. **^{1}H NMR** ($CDCl_3$, 300 MHz, δ): 8.40 (d, *J* = 8.5 Hz, 1H, H_{Ar}), 7.80 (br, 1H, NH), 6.41 (br, 1H, NH), 6.15 (d, *J* = 8.5 Hz, 1H, H_{Ar}), 3.70 (m, 2H, CH_2), 3.29 (t, *J* = 6.4 Hz, 2H, CH_2), 2.34 (t, *J* = 7.1 Hz, 2H, CH_2), 1.76 (m, 2H, CH_2), 1.63 (m, 2H, CH_2), 1.30 (m, 2H, CH_2). **^{13}C NMR** ($CDCl_3$, 75 MHz, δ): 175.3 (CO), 144.7 (C), 144.4 (C), 144.3 (C), 144.0 (C), 136.7 (CH), 98.8 (CH), 51.2 (CH_2), 38.8 (CH_2), 36.0 (CH_2), 35.8 (CH_2), 28.3 (CH_2), 22.7 (CH_2). **ESI-MS** *m/z* (%): 387.1 (32) $[M+K]^+$, 372.1 (100) $[M+Na]^+$, 349.1 (81) $[M+H]^+$. **HRMS (ESI)** *m/z*: $[M+H]^+$ calculated for $C_{13}H_{17}N_8O_4$: 349.1367, found 349.1355.

[284] a) S. Otake, K. Okuro, D. Bochicchio, G. M. Pavan, T. Aida, *Bioconjug. Chem.* **2018**, *29*, 2068-2073; b) S. Taliani, F. Simorini, V. Sergianni, C. La Motta, F. Da Settimo, B. Cosimelli, E. Abignente, G. Greco, E. Novellino, L. Rossi, V. Gremigni, F. Spinetti, B. Chelli, C. Martini, *J. Med. Chem.* **2007,** *50*, 404-407; c) X. Xu, Z. Kuang, J. Han, Y. Meng, L. Li, H. Luan, P. Xu, J. Wang, C. Luo, H. Ding, Z. Li, J. Bian, *J. Med. Chem.* **2019**, *62*, 9642-9657; d) M. Ciba, B. Dibnah, B. D. Hudson, E. R. Ulven, *J. Med. Chem.* **2023**, *66*, 8951-8974.

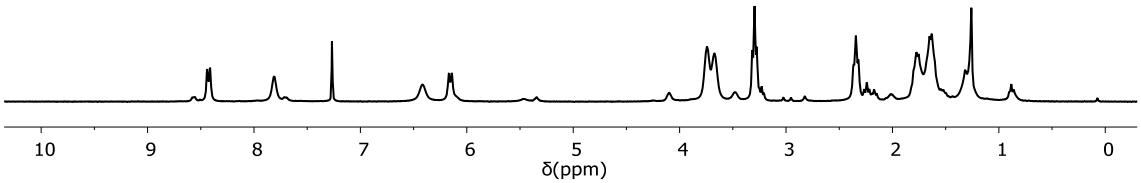

Figure 228. ^{1}H NMR ($CDCl_3$, 300 MHz) of **13**.

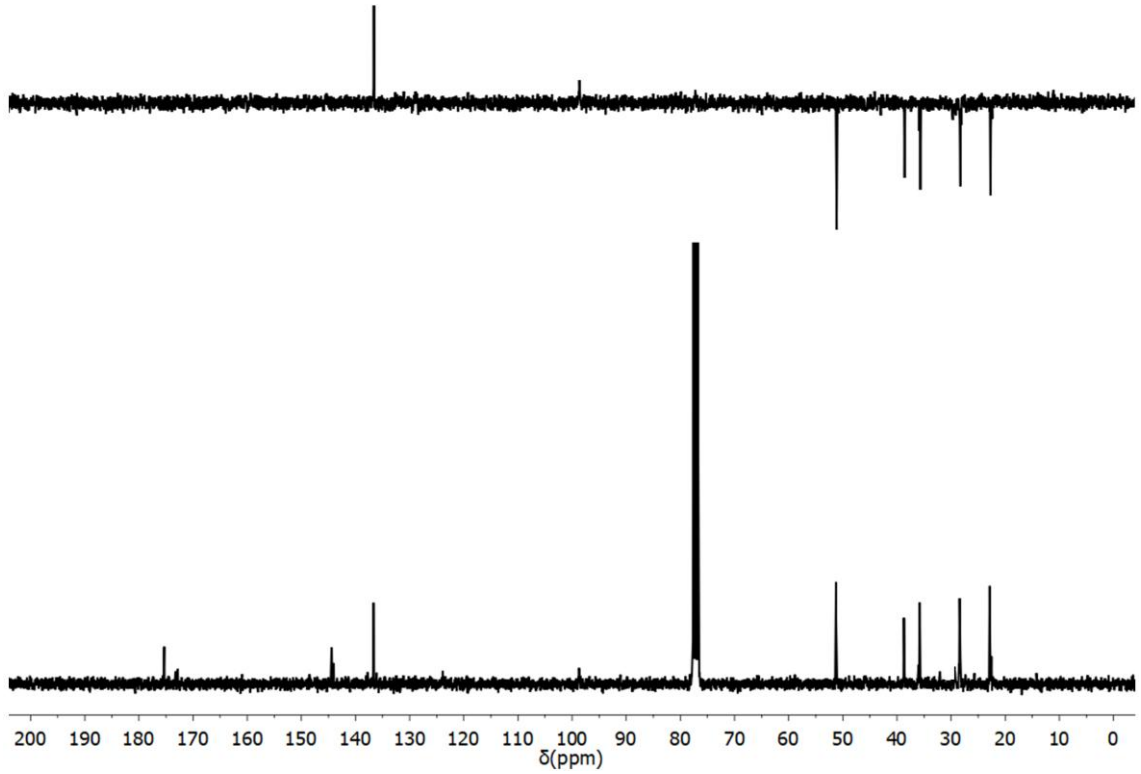

Figure 229. ^{13}C NMR (bottom) and DEPT-135 NMR (top) of **13** ($CDCl_3$, 75 MHz).

USC
UNIVERSIDADE DE SANTIAGO DE COMPOSTELA

8.2.3.5. Solid-phase peptide synthesis

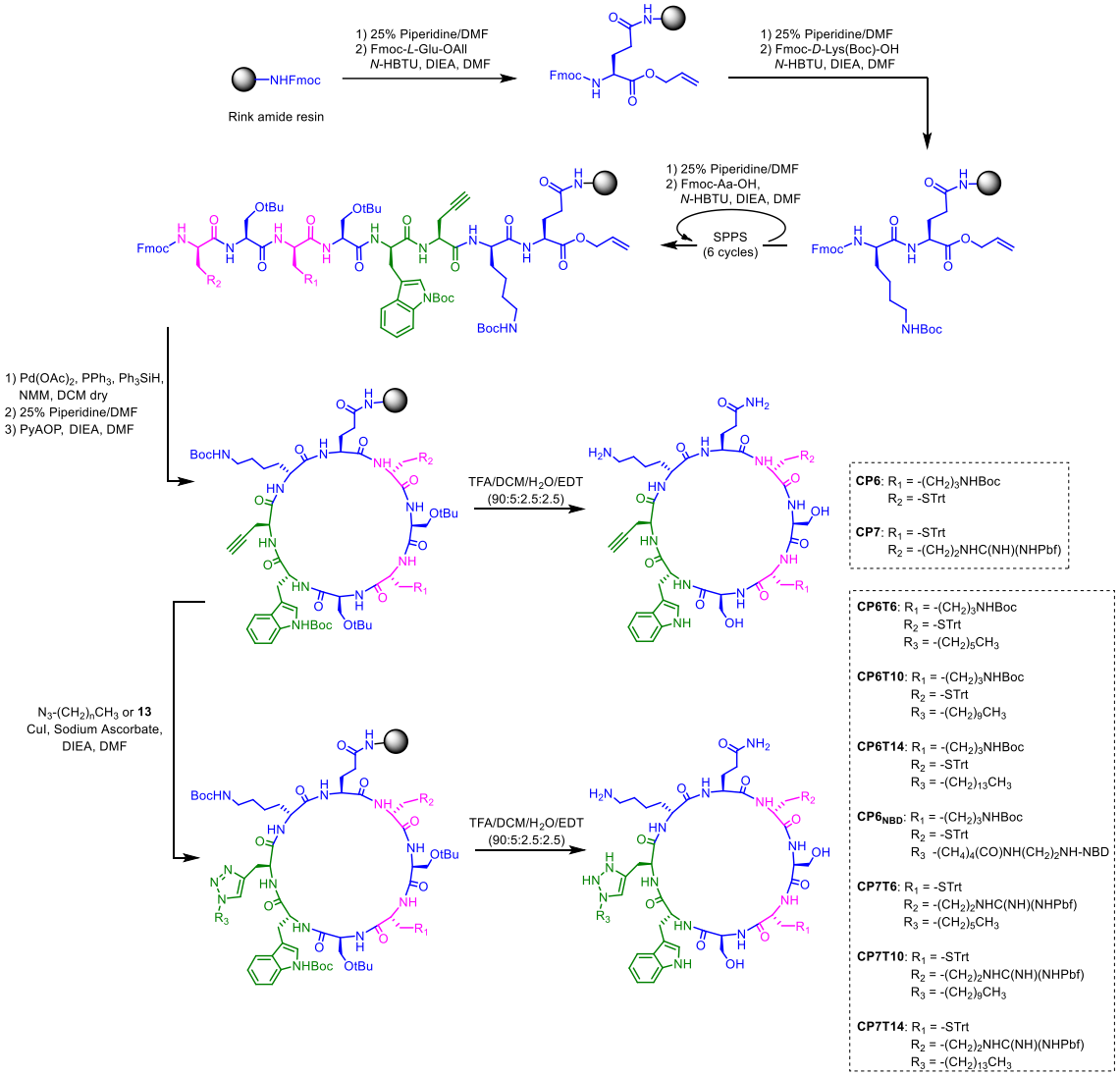

Figure 230. Synthetic strategy to obtain the cyclic peptides scaffolds.

General protocol of solid-phase synthesis: The synthesis of CPs was performed on a Rink Amide resin (100-200 mesh; 0.64 mmol·g^{-1}) using manual solid phase synthesis according to the Fmoc-based strategy.[183,229] Briefly, Fmoc-Rink Amide resin (400 mg, 256 µmol) was swelled in DCM (3 mL) for 30 min in a peptide synthesis vessel and washed with DMF (6 x 4 mL) and DCM (6 x 4 mL). Fmoc group was removed by treating the resin with a solution of piperidine in DMF (25%, 4 mL) for 20 min. After DMF washings (3 x 4 mL), the coupling of the next amino acid was carried out using a solution of Fmoc-protected amino acid (3 equiv), *N*-HBTU (3 equiv), DIEA (6 equiv) in DMF (4 mL) under orbital shaking for 40 min at room temperature. Once the reaction was completed, the resin was washed with DMF (3 x 4 mL) and DCM (3 x 4 mL). Cycles of deprotection and coupling were repeated until the desired linear peptide was achieved. Deprotection of the allyl protecting group was performed by adding to the resin a degassed mixture of $Pd(OAc)_2$ (0.25 equiv), PPh_3 (1.25 equiv), *N*-methylmorpholine

(6 equiv), and phenylsilane (6 equiv) in dry DCM (4 mL). The reaction was shaken for 2 hours at room temperature. Then, the resin was filtered and washed with DCM (3 x 4 mL), DMF (3 x 4 mL), sodium diethyldithiocarbamate in DMF (0.5%, 2 x 4 mL, 20 min), DMF (2 x 4 mL), DIEA in DMF (10%, 2 x 4 mL), DMF (3 x 4 mL). To remove the *N*-terminal Fmoc group, the resin was treated with a solution of piperidine in DMF (25%, 4 mL, 30 min) and, then, washed with DMF (6 x 4 mL), DIEA in DMF (5%, 3 x 4 mL), LiCl in DMF (0.8 M, 3 x 4 mL) and DMF (3 x 4 mL). Cyclization was carried out by treating the resin with a solution of PyAOP (4 equiv) and DIEA (6 equiv) in DMF (4 mL) for 2 hours under orbital shaking. After filtration, the resin was washed with DMF (3 x 4 mL) and DCM (3 x 4 mL).

Click chemistry reaction: The functionalization with an alkyl chain was carried out when necessary. For this purpose, azide derivatives were prepared previously. A solution of the corresponding bromoalkane (6 equiv) and NaN_3 (6 equiv) in DMF (1 mL) was stirred for 24 hours at 80°C. The resulting azide derivative was used in the following reaction without further purification. The compound **13** was synthesized as previously described.

Then, DMF (0.2 mL), piperidine (0.3 mL), the resulting azido derivative (6 equiv), CuI (5 equiv), sodium ascorbate (5 equiv), and DIEA (10 equiv) were added to a vial containing the resin with the CP and the mixture was purged with argon for 5 min. The reaction mixture was shaken at room temperature for 48 hours under orbital shaking. After filtration, the resin was washed with DCM (3 x 4 mL), DMF (3 x 4 mL), piperidine in DMF (25%, 2 x 4 mL, 15 min), DMF (3 x 4 mL), MilliQ H_2O (2 x 4 mL, 10 min), DMF (3 x 4 mL), and DCM (3 x 4 mL).

Cleavage and purification: The CPs were cleaved from the resin and side-chain deprotected by shaking with a freshly prepared solution of TFA/DCM/H_2O/EDT (90:5:2.5:2.5, 1 mL per 100 mg resin) for 2 hours. The mixture was collected by filtration, concentrated with an argon steam and added dropwise to cold Et_2O (10 mL of Et_2O per 100 mg of resin). The precipitate was centrifuged (4000 rpm x 5 min) and the supernatant was discarded. After washings with diethyl ether (x3), the residue was dried under vacuum and solubilized in MilliQ-H_2O with 0.1% TFA. This solution was purified by semipreparative RP-HPLC using a Phenomenex Luna C18 (2) 100Å column. The proper fractions were freeze-dried to provide the desired CP. The pure product was stored at -20°C until further use.

USC UNIVERSIDADE DE SANTIAGO DE COMPOSTELA

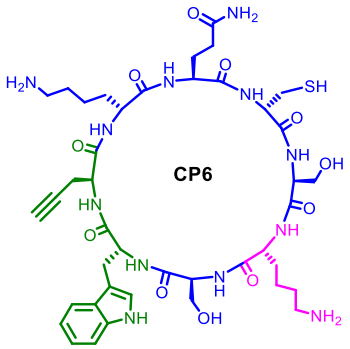

CP6: The peptide was synthesized according to the general protocol for solid-phase synthesis (400 mg of resin, 0.64 mmol·g^{-1}). Then, it was cleaved from the resin and purified by semipreparative RP-HPLC using a Phenomenex Luna C18 (2) 100Å column. [gradient: H_2O (0.1% TFA)/MeCN (0.1% TFA), 100:0 → 100:0 (5 min); 100:0 → 60:40 (40 min), R_t = 31 min]. The proper fractions were freeze-dried to provide **CP6** as a white solid with an overall yield of 14% (34 mg). **^{1}H NMR** (500 MHz, D_2O/H_2O): 10.18 (s, 1H, NH_{Indole}), 8.60 (d, *J* = 7.1 Hz, 1H, NH_{Gln}), 8.46 (d, *J* = 6.6 Hz, 1H, NH_{Ser}), 8.41 (d, *J* = 7.0 Hz, 1H, NH_{Cys}), 8.33 (d, *J* = 7.6 Hz, 1H, NH_{Lys}), 8.28 (d, *J* = 6.6 Hz, 1H, NH_{Trp}), 8.20 (d, *J* = 8.0 Hz, 1H, NH_{Prg}), 8.18 (d, *J* = 8.2 Hz, 1H, NH_{Lys}), 8.07 (d, *J* = 7.8 Hz, 1H, NH_{Ser}), 7.63 (d, *J* = 8.0 Hz, 1H, H_{Ar}), 7.58-7.42 (m, 5H, H_{Ar} and 2 $NH_{2\text{-}Lys}$), 7.25 (m, 1H, H_{Ar}), 7.23 (s, 1H, CH_{Indole}), 7.18 (m, 1H, H_{Ar}), 6.80 (br, 2H, $NH_{2\text{-}Gln}$), 4.72-4.24 (8 αCH), 3.89 (m, 2H, $CH_{2\text{-}Ser}$), 3.73 (m, 2H, $CH_{2\text{-}Ser}$), 3.30 (m, 2H, $CH_{2\text{-}Trp}$), 2.96 (m, 6H, 2 $CH_{2\text{-}Lys}$ and $CH_{2\text{-}Gln}$), 2.41 (m, 2H, $CH_{2\text{-}Cys}$), 2.30 (t, *J* = 8.0 Hz, 1H, CH_{Prg}), 2.18-1.88 (m, 2H, $CH_{2\text{-}Prg}$), 1.88-1.55 (m, 10 H, 4 $CH_{2\text{-}Lys}$ and $CH_{2\text{-}Gln}$), 1.36 (m, 4H, 2 $CH_{2\text{-}Lys}$). **ESI-MS** *m/z* (%): 943.5 (31) $[M+H]^+$, 472.4 (100) $[M+2H]^{2+}$. **HRMS (ESI)** *m/z*: $[M+H]^+$ calculated for $C_{42}H_{63}N_{12}O_{11}S$: 943.4454, found 943.4450. **FTIR (neat)**: v = 3276.2 (amide A), 1666.9 (amide I_b), 1623.5 (amide I_a), 1534.7 (amide II) cm^{-1}.

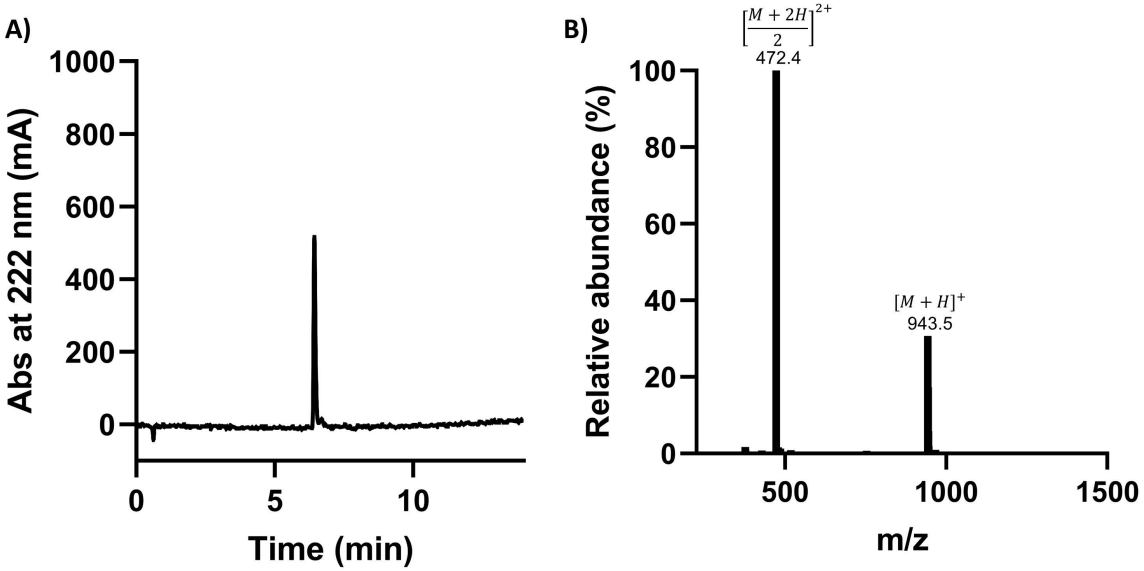

Figure 231. (A) **RP-uHPLC** of **CP6:** [Agilent SB-C18 column, H_20 (0.1% TFA)/MeCN (0.1% TFA), 100:0 →100:0 (2 min) and 100:0 → 50:50 (12 min)] R_t = 6.5 min. (B) ESI-MS of the main peak.

UNIVERSIDADE DE SANTIAGO DE COMPOSTELA

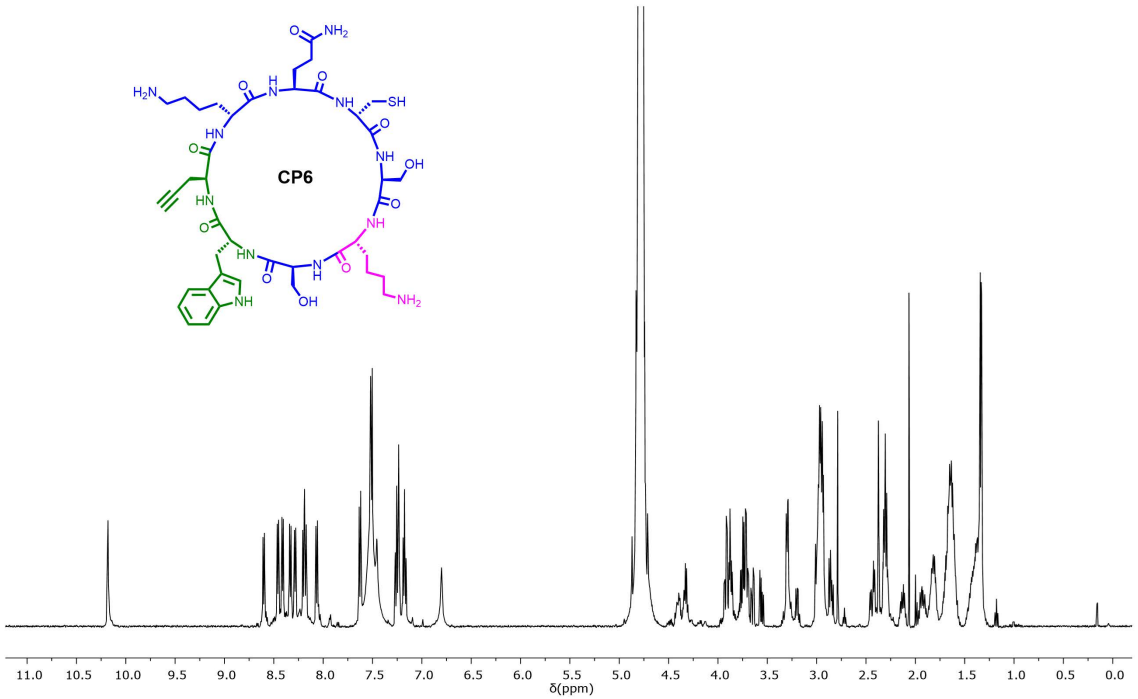

Figure 232. ^{1}H NMR of **CP6** at 5.1 mM (500 MHz, D_2O/H_2O, 298 K).

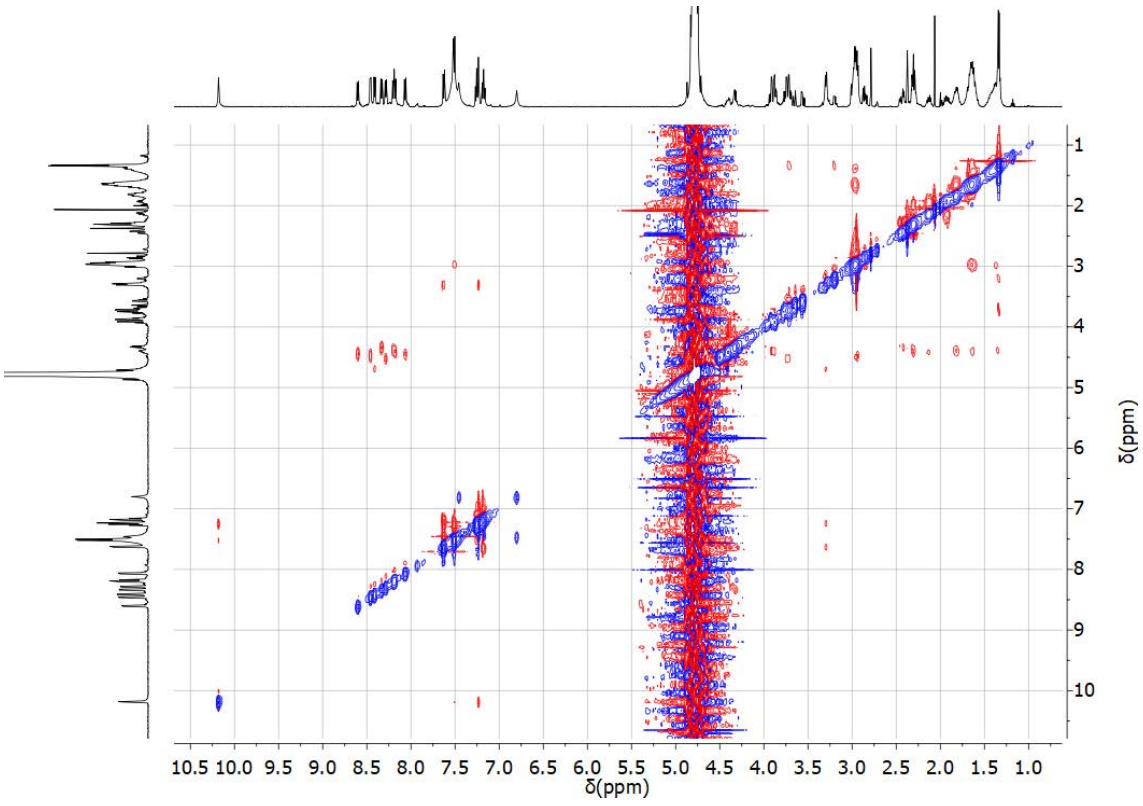

Figure 233. COSY of **CP6** at 5.1 mM (500 MHz, D_2O/H_2O, 298 K).

USC
UNIVERSIDADE DE SANTIAGO DE COMPOSTELA

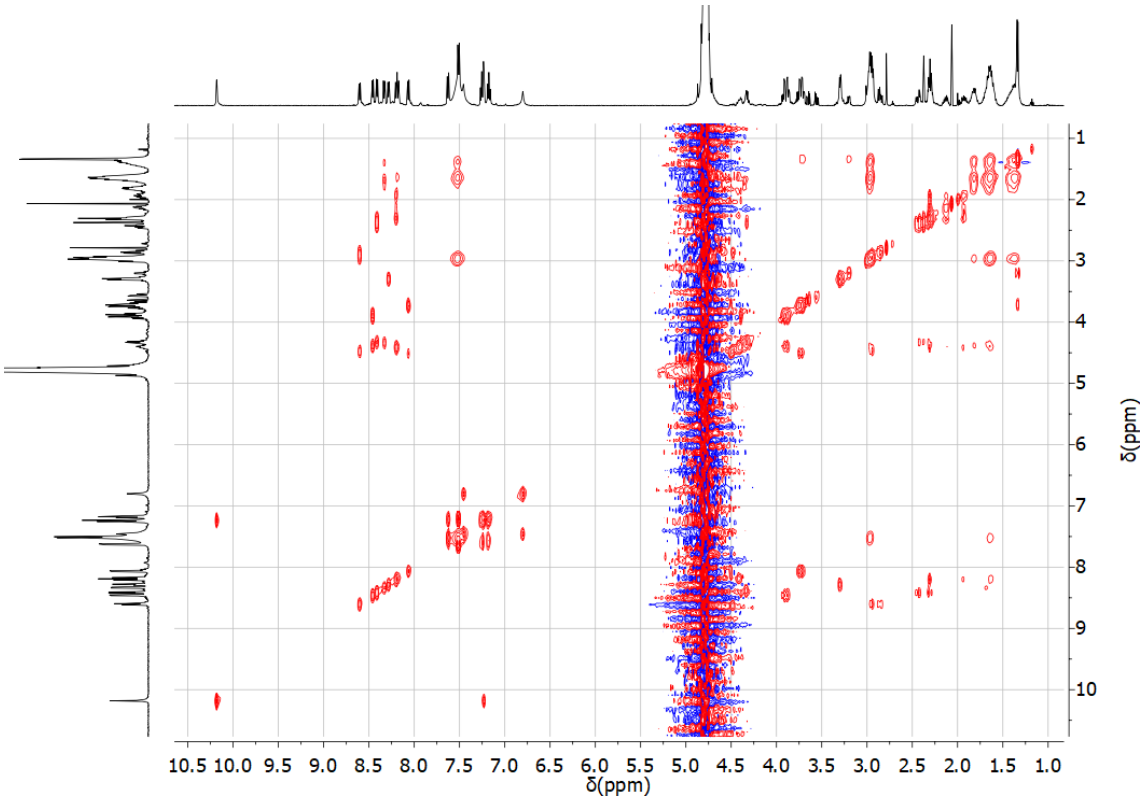

Figure 234. TOCSY of **CP6** at 5.1 mM (500 MHz, D_2O/H_2O, 298 K).

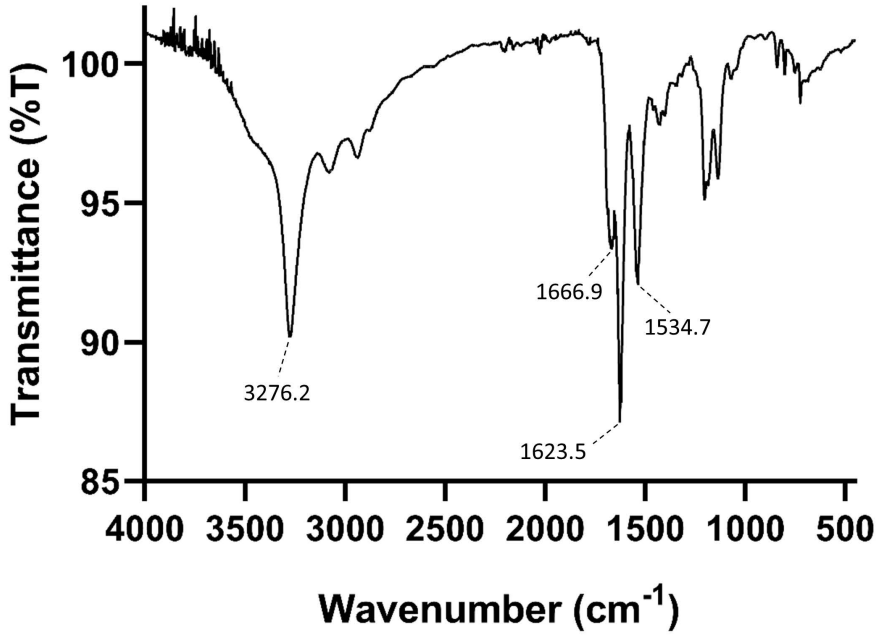

Figure 235. FT-IR spectrum of **CP6** (solid, 298 K).

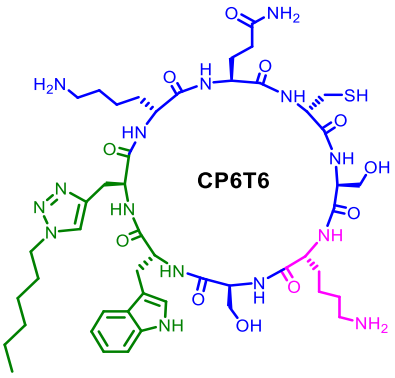

CP6T6: The peptide was synthesized according to the general protocol for solid-phase synthesis (150 mg of resin, 0.64 mmol·g^{-1}). Then, the click chemistry reaction was performed and the peptide was cleaved and purified by semipreparative RP-HPLC using a Phenomenex Luna C18 (2) 100Å column. [gradient: H_2O (0.1% TFA)/MeCN (0.1% TFA), 90:10 → 90:10 (2 min); 40:60 → 40:60 (40 min), R_t = 26.5 min]. The proper fractions were freeze-dried to provide **CP6T6** as a white solid with an overall yield of 4% (4.4 mg). **ESI-MS** *m/z* (%): 1070.5 (12) $[M+H]^+$, 535.9 (100) $[M+2H]^{2+}$, 357.6 (5) $[M+3H]^{3+}$. **HRMS (ESI)** *m/z*: $[M+H]^+$ calculated for $C_{48}H_{76}N_{15}O_{11}S$: 1070.5569, found 1070.5495. **FTIR (neat)**: ν = 3274.2 (amide A), 1662.9 (amide I_b), 1629.4 (amide I_a), 1534.7 (amide II) cm^{-1}.

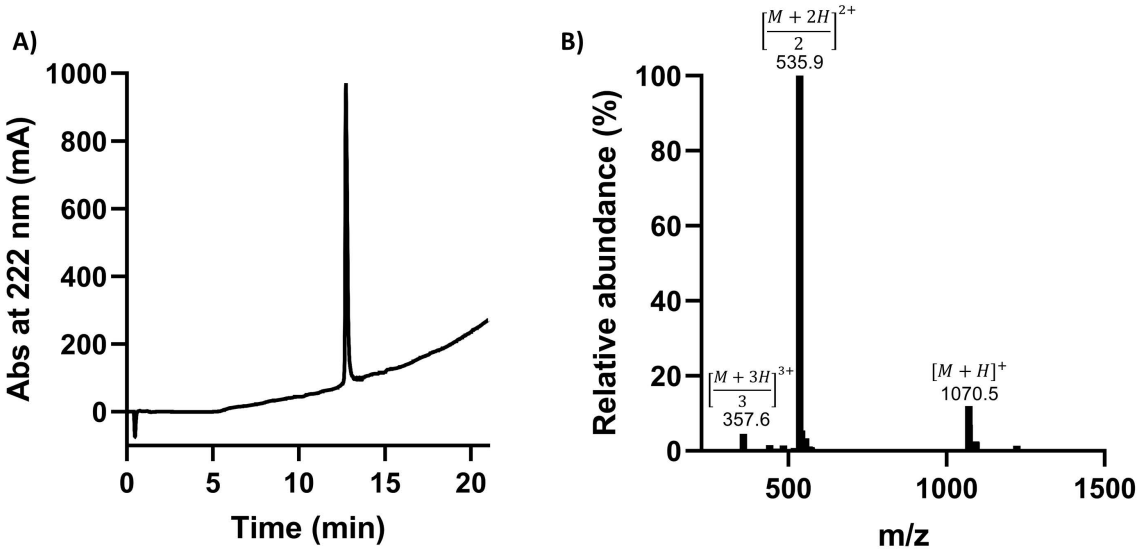

Figure 236. (A) **RP-uHPLC** of **CP6T6:** [Agilent SB-C18 column, H_2O (0.1% TFA)/MeCN (0.1% TFA), 100:0 → 100:2 (2 min) and 100:0 → 25:75 (19 min)] R_t = 12.8 min. (B) ESI-MS of the main peak.

USC UNIVERSIDADE DE SANTIAGO DE COMPOSTELA

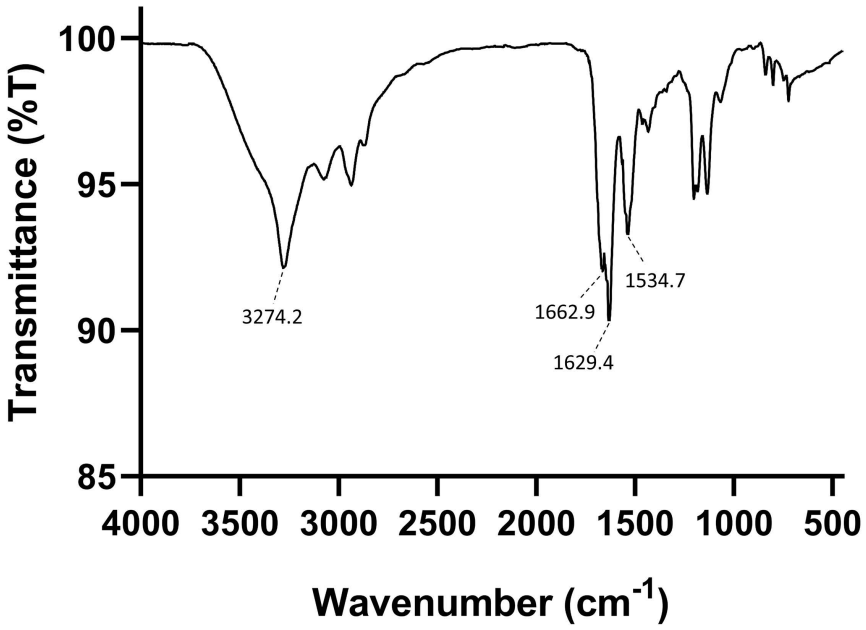

Figure 237. FT-IR spectrum of **CP6T6** (solid, 298 K).

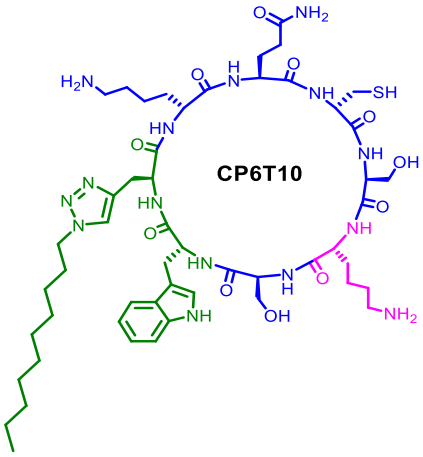

CP6T10: The peptide was synthesized according to the general protocol for solid-phase synthesis (150 mg of resin, 0.64 mmol·g^{-1}). Then, the click chemistry reaction was performed and the peptide was cleaved and purified by semipreparative RP-HPLC using a Phenomenex Luna C18 (2) 100Å column. [gradient: H_2O (0.1% TFA)/MeCN (0.1% TFA), 85:15 → 85:15 (5 min); 85:15 → 25:75 (40 min), R_t = 28.5 min]. The proper fractions were freeze-dried to provide **CP6T10** as a white solid with an overall yield of 20% (22.1 mg). **ESI-MS** *m/z* (%): 1126.7 (11) $[M+H]^+$, 564.0 (100) $[M+2H]^{2+}$, 376.3 (3) $[M+3H]^{3+}$. **HRMS (ESI)** *m/z*: $[M+2H]^{2+}$ calculated for $C_{52}H_{85}N_{15}O_{11}S$: 563.8131, found 563.8139. **FTIR (neat)**: ν = 3276.2 (amide A), 1670.8 (amide I_b), 1627.4 (amide I_a), 1540.6 (amide II) cm^{-1}.

USC UNIVERSIDADE DE SANTIAGO DE COMPOSTELA

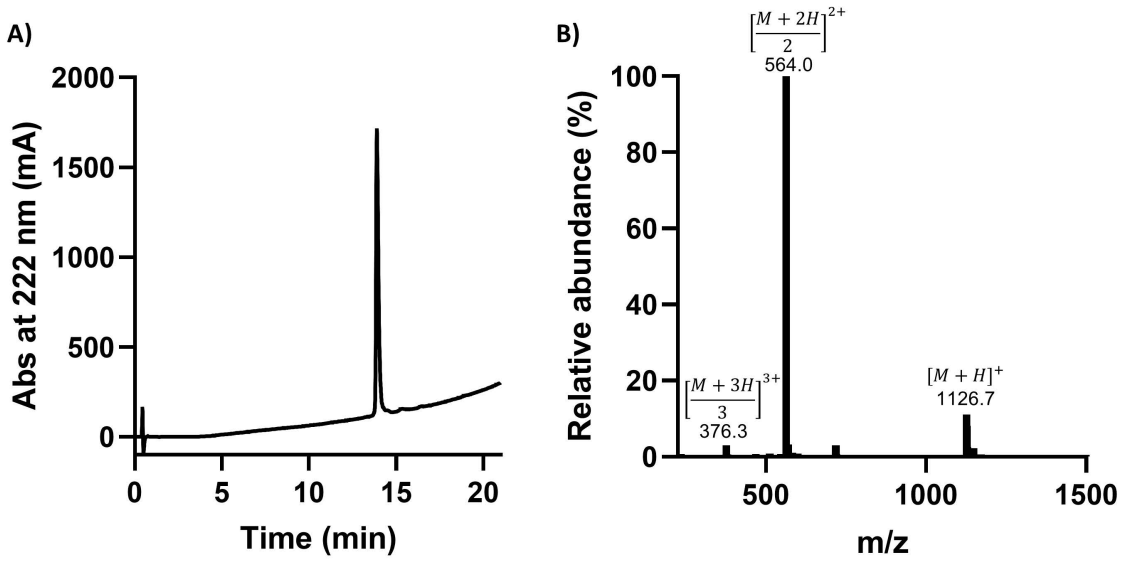

Figure 238. (A) **RP-uHPLC** of **CP6T10:** [Agilent SB-C18 column, H_2O (0.1% TFA)/MeCN (0.1% TFA), 100:0 → 100:2 (2 min) and 100:0 → 25:75 (19 min)] R_t = 13.8 min. (B) ESI-MS of the main peak.

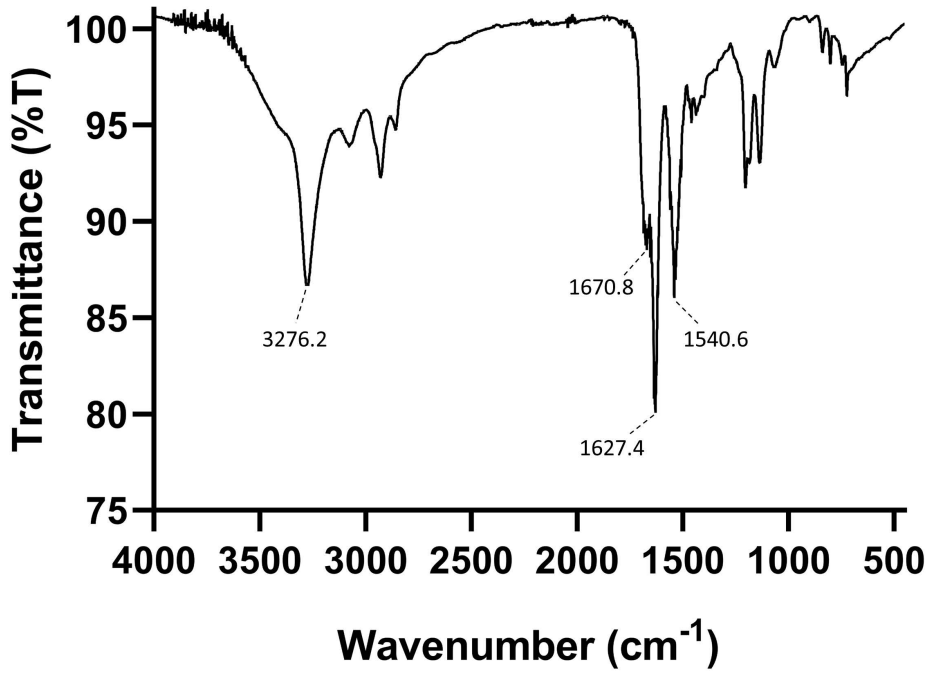

Figure 239. FT-IR spectrum of **CP6T10** (solid, 298 K).

USC
UNIVERSIDADE DE SANTIAGO DE COMPOSTELA

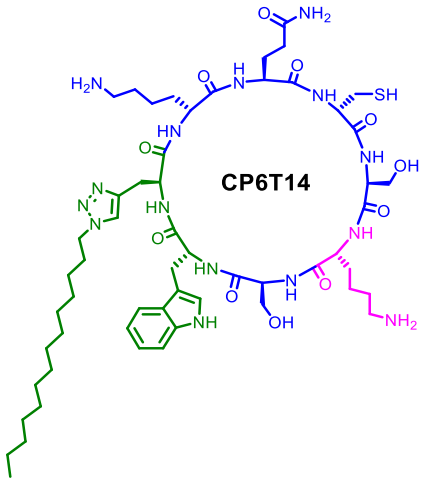

CP6T14: The peptide was synthesized according to the general protocol for solid-phase synthesis (150 mg of resin, 0.64 mmol·g^{-1}). Then, the click chemistry reaction was performed and the peptide was cleaved and purified by semipreparative RP-HPLC using a Phenomenex Luna C18 (2) 100Å column. [gradient: H_2O (0.1% TFA)/MeCN (0.1% TFA), 90:10 → 90:10 (5 min); 90:10 → 25:75 (40 min), R_t = 35.0 min]. The proper fractions were freeze-dried to provide **CP6T14** as a white solid with an overall yield of 5% (6.1 mg). **ESI-MS** *m/z* (%): 1182.7 (6) $[M+H]^+$, 591.9 (100) $[M+2H]^{2+}$, 394.9 (4) $[M+3H]^{3+}$. **HRMS (ESI)** *m/z*: $[M+H]^+$ calculated for $C_{56}H_{92}N_{15}O_{11}S$: 1182.6816, found 1182.6789. **FTIR (neat)**: ν = 3274.2 (amide A), 1670.8 (amide I_b), 1627.4 (amide I_a), 1538.7 (amide II) cm^{-1}.

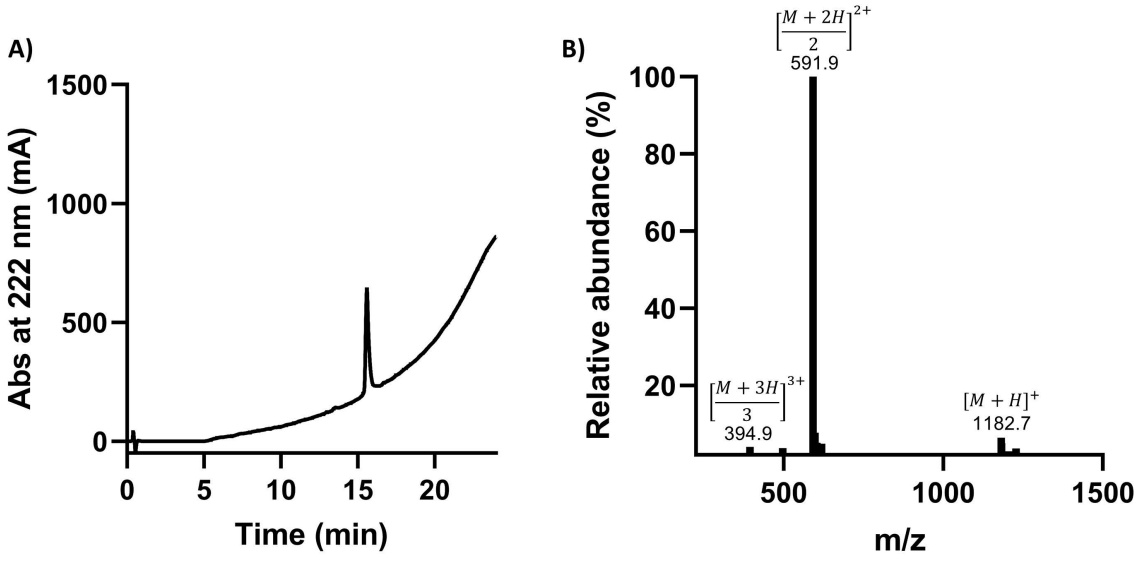

Figure 240. (A) **RP-uHPLC** of **CP6T14:** [Agilent SB-C18 column, H_2O (0.1% TFA)/MeCN (0.1% TFA), 100:0 → 100:2 (2 min) and 100:0 → 5:95 (19 min)] R_t = 15.6 min. (B) ESI-MS of the main peak.

USC UNIVERSIDADE DE SANTIAGO DE COMPOSTELA

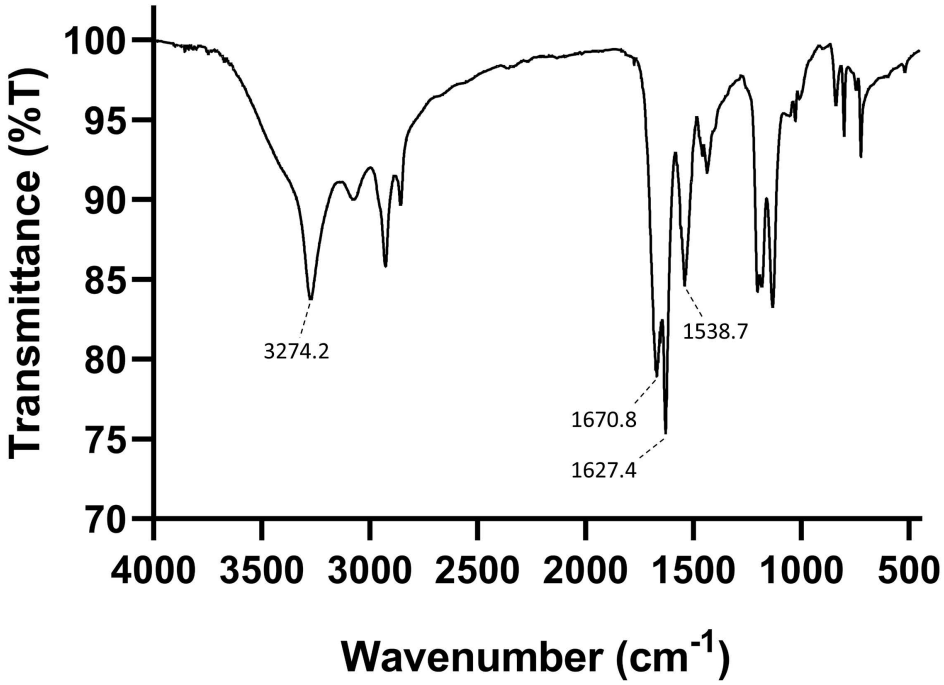

Figure 241. FT-IR spectrum of **CP6T14** (solid, 298 K).

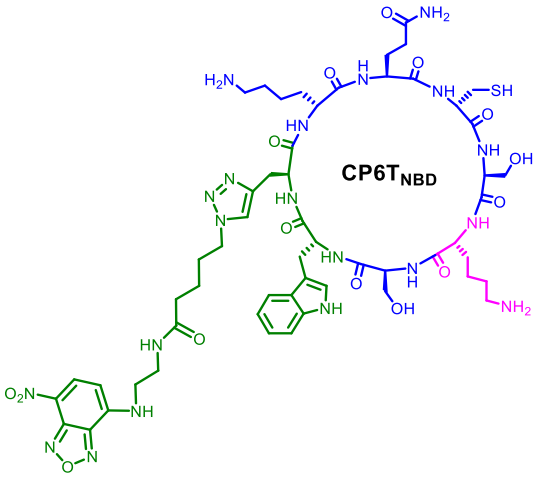

$CP6T_{NBD}$: The peptide was synthesized according to the general protocol for solid-phase synthesis (75 mg of resin, 0.64 mmol·g^{-1}). Then, the click chemistry reaction was performed and the peptide was cleaved and purified by semipreparative RP-HPLC using a Phenomenex Luna C18 (2) 100Å column. [gradient: H_2O (0.1% TFA)/MeCN (0.1% TFA), 100:0 → 100:0 (5 min); 100:0 → 50:50 (40 min), R_t = 25.0 min]. The proper fractions were freeze-dried to provide **$CP6T_{NBD}$** as an orange solid with an overall yield of 7% (4.3 mg). **ESI-MS** *m/z* (%): 1291.6 (5) $[M+H]^+$, 646.3 (100) $[M+2H]^{2+}$, 431.5 (7) $[M+3H]^{3+}$. **HRMS (ESI)** *m/z*: $[M+H]^+$ calculated for $C_{55}H_{79}N_{20}O_{15}S$: 1291.5749, found 1291.5741. **FTIR (neat)**: ν = 3272.3 (amide A), 1672.8 (amide I_b), 1623.5 (amide I_a), 1538.7 (amide II) cm^{-1}.

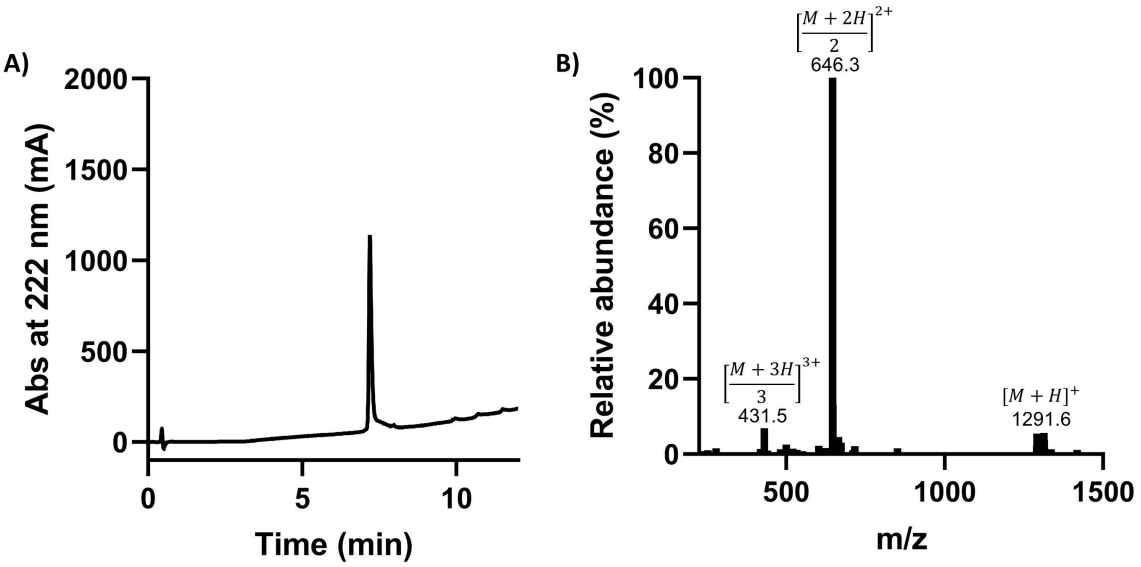

Figure 242. (A) **RP-uHPLC** of **CP6T$_{NBD}$:** [Agilent SB-C18 column, H_20 (0.1% TFA)/MeCN (0.1% TFA), 100:0 →100:0 (2 min) and 100:0 → 50:50 (12 min)], R_t = 7.2 min. (B) ESI-MS of the main peak.

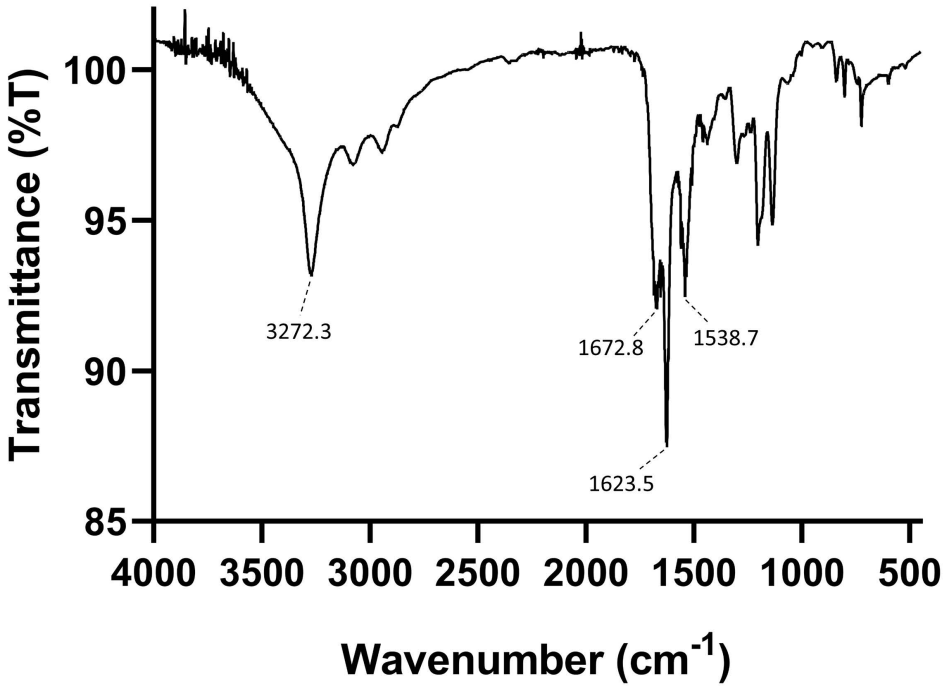

Figure 243. FT-IR spectrum of **CP6T$_{NBD}$** (solid, 298 K).

USC
UNIVERSIDADE DE SANTIAGO DE COMPOSTELA

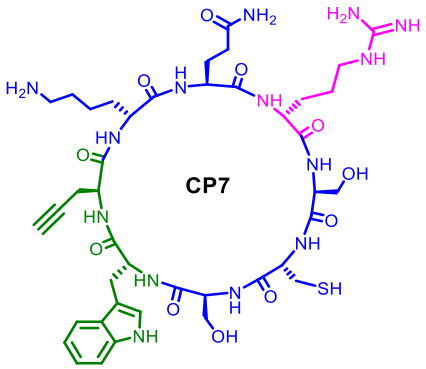

CP7: The peptide was synthesized according to the general protocol for solid-phase synthesis (400 mg of resin, 0.64 mmol·g^{-1}). Then, it was cleaved from the resin and purified by semipreparative RP-HPLC using a Phenomenex Luna C18 (2) 100Å column. [gradient: H_2O (0.1% TFA)/MeCN (0.1% TFA), 90:10 → 90:10 (5 min); 90:10 → 60:40 (40 min), R_t = 25.9 min]. The proper fractions were freeze-dried to provide **CP7** as a white solid with an overall yield of 3 % (8 mg). **^{1}H NMR** (500 MHz, D_2O/H_2O): 10.09 (s, 1H, NH_{Indole}), 8.39 (m, 2H, NH_{Gln} and NH_{Ser}), 8.35 (d, *J* = 7.4 Hz, 1H, NH_{Cys}), 8.26 (m, 3H, NH_{Prg}, NH_{Lys} and NH_{Trp}), 8.22 (d, *J* = 7.4 Hz, 1H, NH_{Arg}), 8.17 (d, *J* = 7.5 Hz, 1H, NH_{Ser}), 7.56 (d, *J* = 8.0 Hz, 1H, H_{Ar}), 7.44 (m, 3H, $H_{Ar,}$ $NH_{2\text{-}Lys}$), 7.20 (m, 1H, H_{Ar}), 7.17 (s, 1H, CH_{Indole}), 7.11 (m, 1H, H_{Ar}), 7.07-6.70 (m, 2H, $NH_{2\text{-}Gln}$), 4.46-4.17 (8 αCH), 3.83 (m, 2H, $CH_{2\text{-}Ser}$), 3.71 (m, 2H, $CH_{2\text{-}Ser}$), 3.21 (m, 4H, $CH_{2\text{-}Arg}$ and $CH_{2\text{-}Trp}$), 3.05 (m, 2H, $CH_{2\text{-}Gln}$), 2.92 (m, 2H, $CH_{2\text{-}Lys}$), 2.82 (m, 2H, $CH_{2\text{-}Cys}$), 2.34 (m, 1H, CH_{Prg}), 2.24 (m, 4H, $CH_{2\text{-}Arg}$ and $CH_{2\text{-}Prg}$), 2.09-1.81 (m, 2H, $CH_{2\text{-}Arg}$), 1.70-1.44 (m, 6H, 2 $CH_{2\text{-}Lys}$ and $CH_{2\text{-}Gln}$), 1.34 (m, 2H, $CH_{2\text{-}Lys}$). **ESI-MS** *m/z* (%): 971.5 (21) $[M+H]^+$, 486.3 (100) $[M+2H]^{2+}$. **HRMS (ESI)** *m/z*: $[M+2H]^{2+}$ calculated for $C_{42}H_{64}N_{14}O_{11}S$: 486.2294, found 486.2296. **FTIR (neat)**: ν = 3270.3 (amide A), 1664.9 (amide I_b), 1625.4 (amide I_a), 1536.7 (amide II) cm^{-1}.

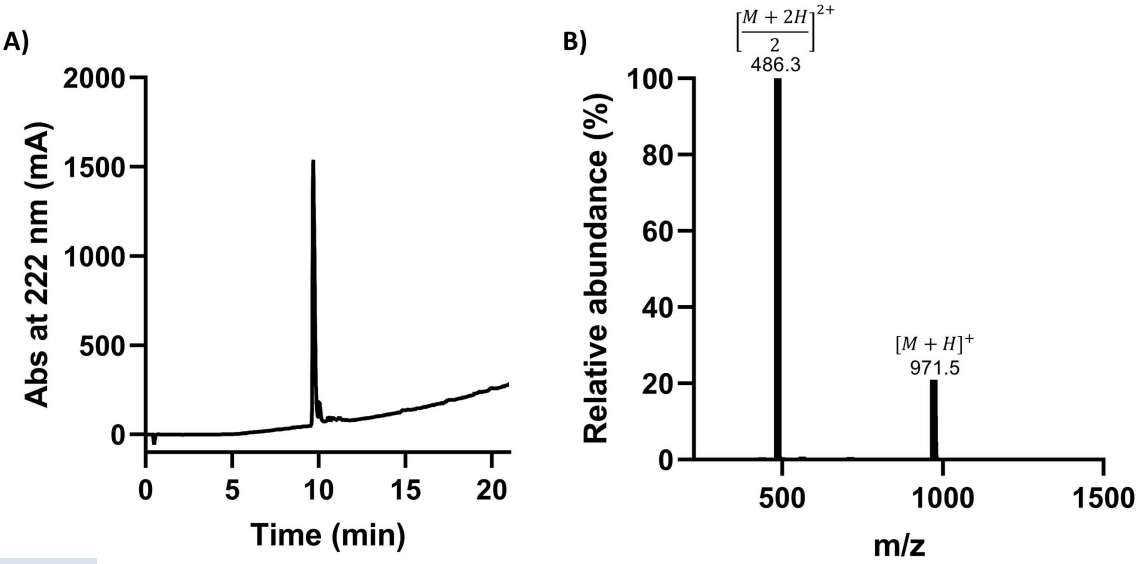

Figure 244. (A) **RP-uHPLC** of **CP7:** [Agilent SB-C18 column, H_2O (0.1% TFA)/MeCN (0.1% TFA), 100:0 → 100:2 (2 min) and 100:0 → 25:75 (19 min)], R_t = 9.6 min. (B) ESI-MS of the main peak.

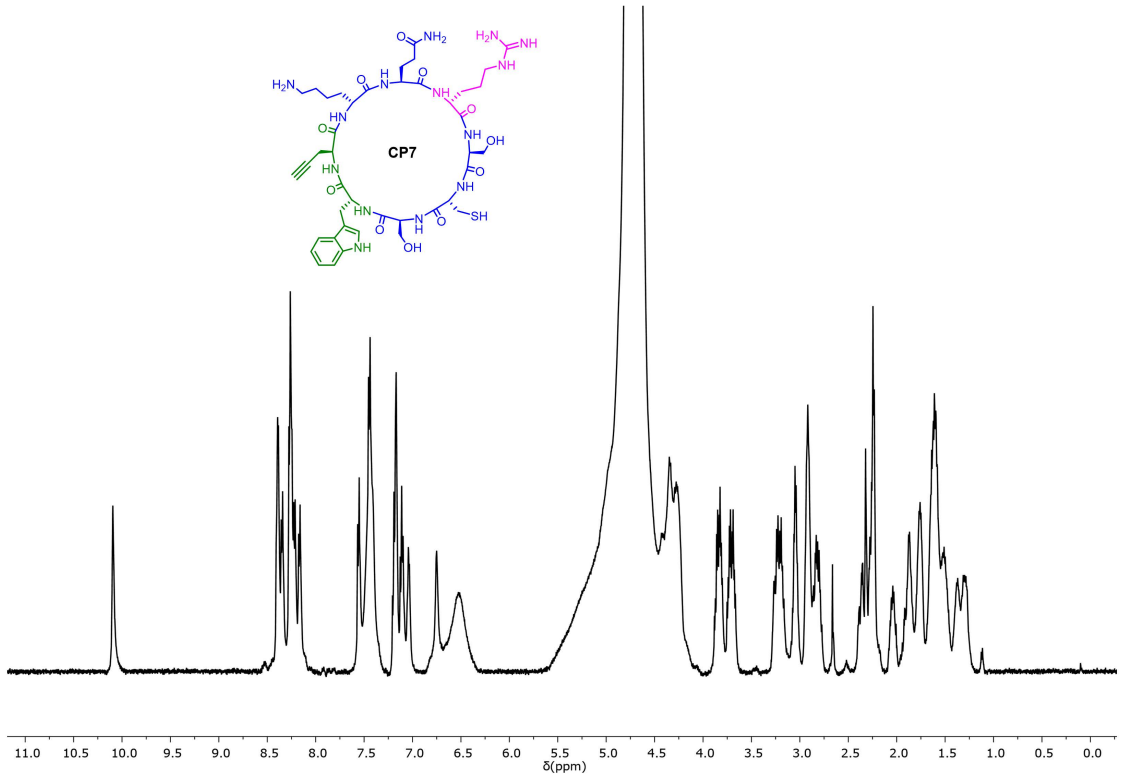

Figure 245. ^{1}H NMR of **CP7** at 5.5 mM (500 MHz, D_2O/H_2O, 298 K).

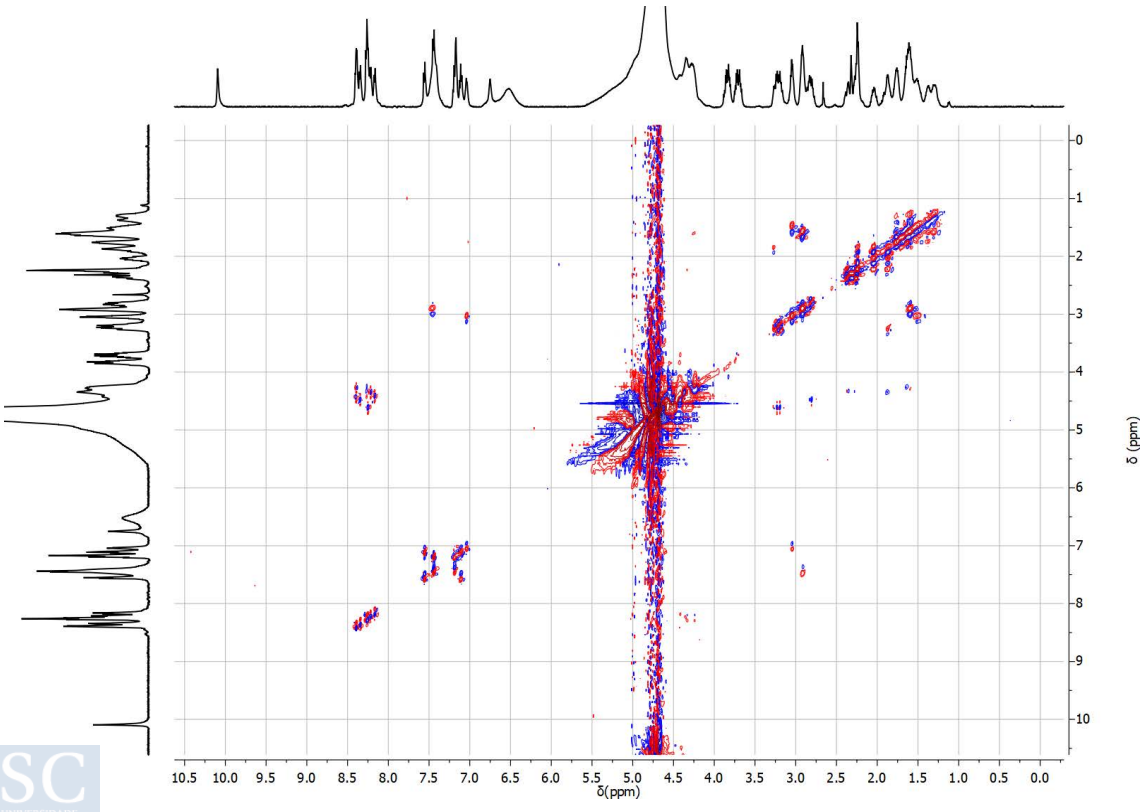

Figure 246. COSY of **CP7** at 5.5 mM (500 MHz, D_2O/H_2O, 298 K).

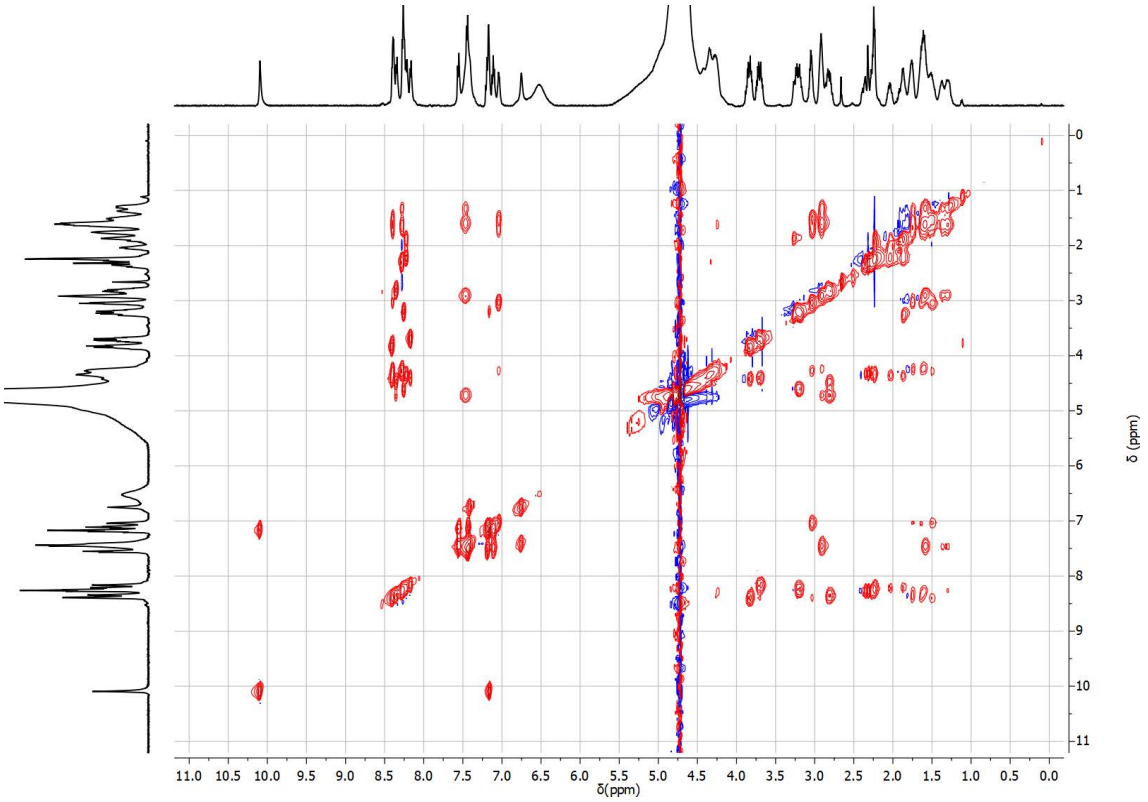

Figure 247. TOCSY of **CP7** at 5.5 mM (500 MHz, D_2O/H_2O, 298 K).

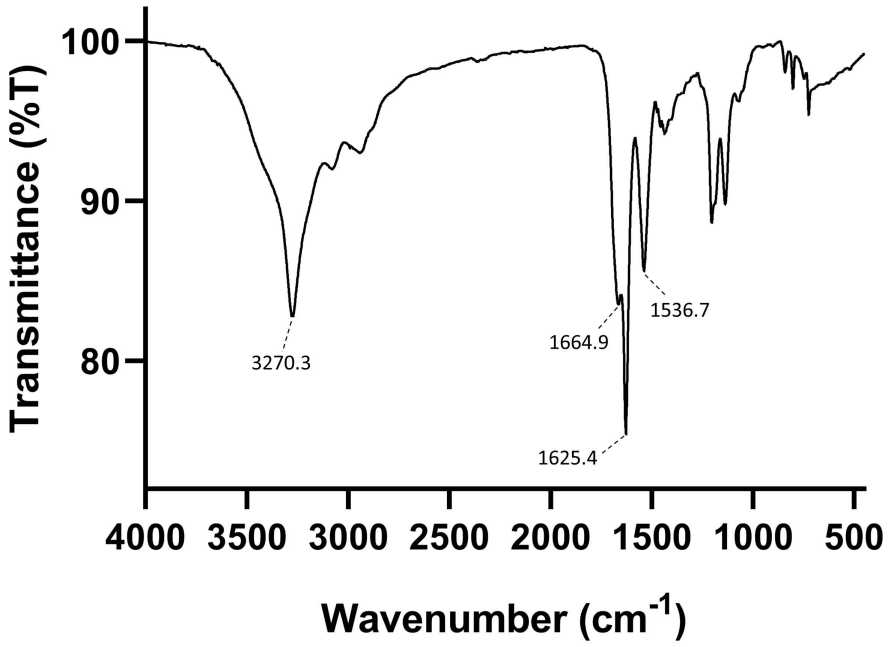

Figure 248. FT-IR spectrum of **CP7** (solid, 298 K).

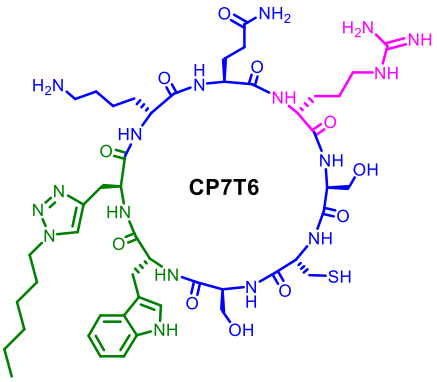

CP7T6: The peptide was synthesized according to the general protocol for solid-phase synthesis (188 mg of resin, 0.64 mmol·g^{-1}). Then, the click chemistry reaction was performed and the peptide was cleaved and purified by semipreparative RP-HPLC using a Phenomenex Luna C18 (2) 100Å column. [gradient: H_2O (0.1% TFA)/MeCN (0.1% TFA), 90:10 → 90:10 (5 min); 90:10 → 40:60 (40 min), R_t = 27.4 min]. The proper fractions were freeze-dried to provide **CP7T6** as a white solid with an overall yield of 4% (5.6 mg). **ESI-MS** *m/z* (%): 1098.6 (16) $[M+H]^+$, 549.9 (100) $[M+2H]^{2+}$, 366.9 (5) $[M+3H]^{3+}$. **HRMS (ESI)** *m/z*: $[M+2H]^{2+}$ calculated for $C_{48}H_{77}N_{17}O_{11}S$: 549.7849, found 549.7851. **FTIR (neat)**: ν = 3274.2 (amide A), 1660.9 (amide Ib), 1625.4 (amide Ia), 1538.7 (amide II) cm^{-1}.

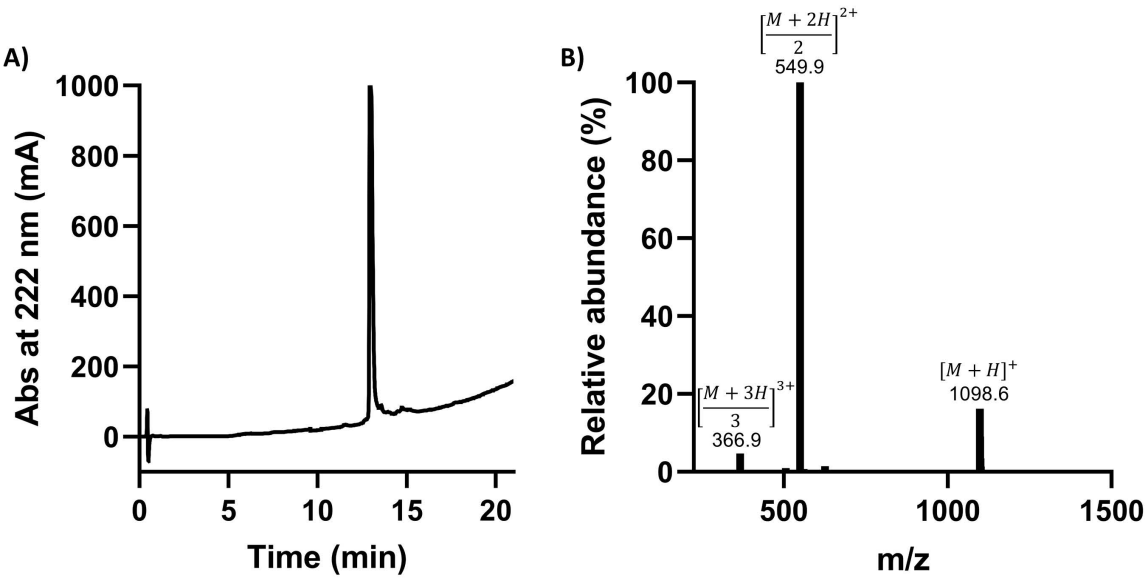

Figure 249. (A) **RP-uHPLC** of **CP7T6:** [Agilent SB-C18 column, H_2O (0.1% TFA)/MeCN (0.1% TFA), 100:0 → 100:2 (2 min) and 100:0 → 25:75 (19 min)], R_t = 12.3 min. (B) ESI-MS of the main peak.

USC UNIVERSIDADE DE SANTIAGO DE COMPOSTELA

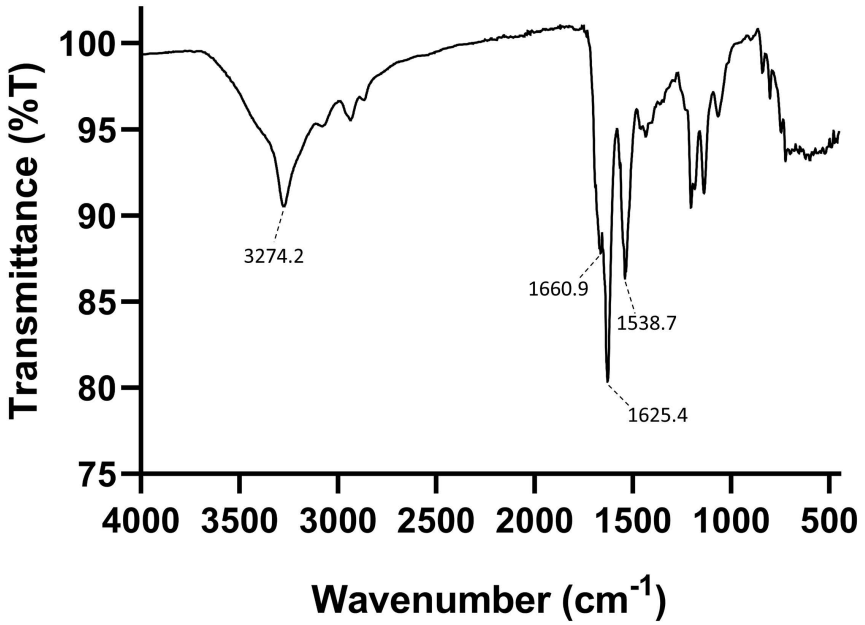

Figure 250. FT-IR spectrum of **CP7T6** (solid, 298 K).

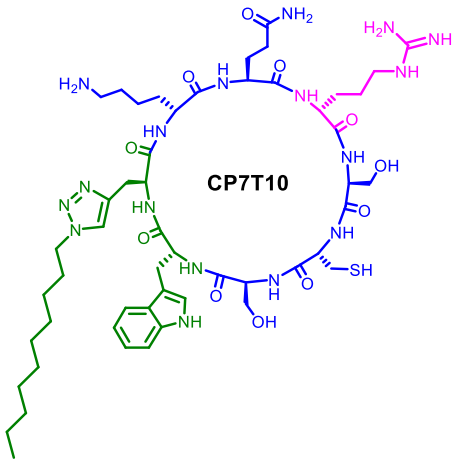

CP7T10: The peptide was synthesized according to the general protocol for solid-phase synthesis (100 mg of resin, 0.64 mmol·g^{-1}). Then, the click chemistry reaction was performed and the peptide was cleaved and purified by semipreparative RP-HPLC using a Phenomenex Luna C18 (2) 100Å column. [gradient: H_2O (0.1% TFA)/MeCN (0.1% TFA), 85:15 → 85:15 (5 min); 85:15 → 25:75 (40 min), R_t = 29.2 min]. The proper fractions were freeze-dried to provide **CP7T10** as a white solid with an overall yield of 12% (8.5 mg). **ESI-MS** *m/z* (%): 1154.6 (13) $[M+H]^+$, 578.0 (100) $[M+2H]^{2+}$, 385.8 (5) $[M+3H]^{3+}$. **HRMS (ESI)** *m/z*: $[M+2H]^{2+}$ calculated for $C_{52}H_{85}N_{17}O_{11}S$: 577.8162, found 577.8163. **FTIR (neat)**: ν = 3274.2 (amide A), 1668.8 (amide I_b), 1627.4 (amide I_a), 1538.7 (amide II) cm^{-1}.

USC UNIVERSIDADE DE SANTIAGO DE COMPOSTELA

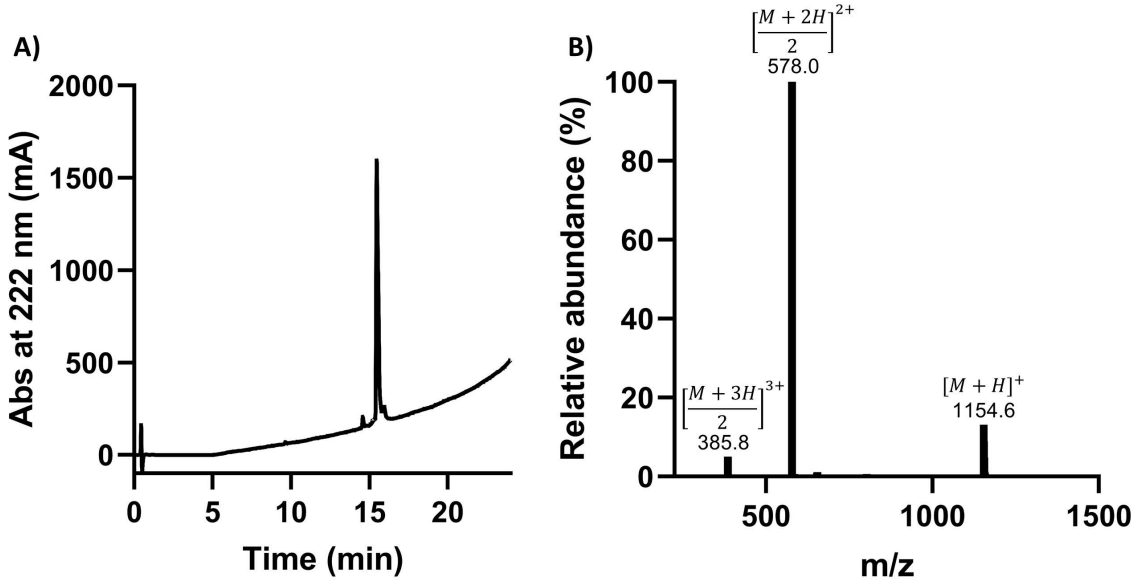

Figure 251. (A) **RP-uHPLC** of **CP7T10:** [Agilent SB-C18 column, H_2O (0.1% TFA)/MeCN (0.1% TFA), 100:0 → 100:2 (2 min) and 100:0 → 25:75 (19 min)], R_t = 15.4 min. (B) ESI-MS of the main peak.

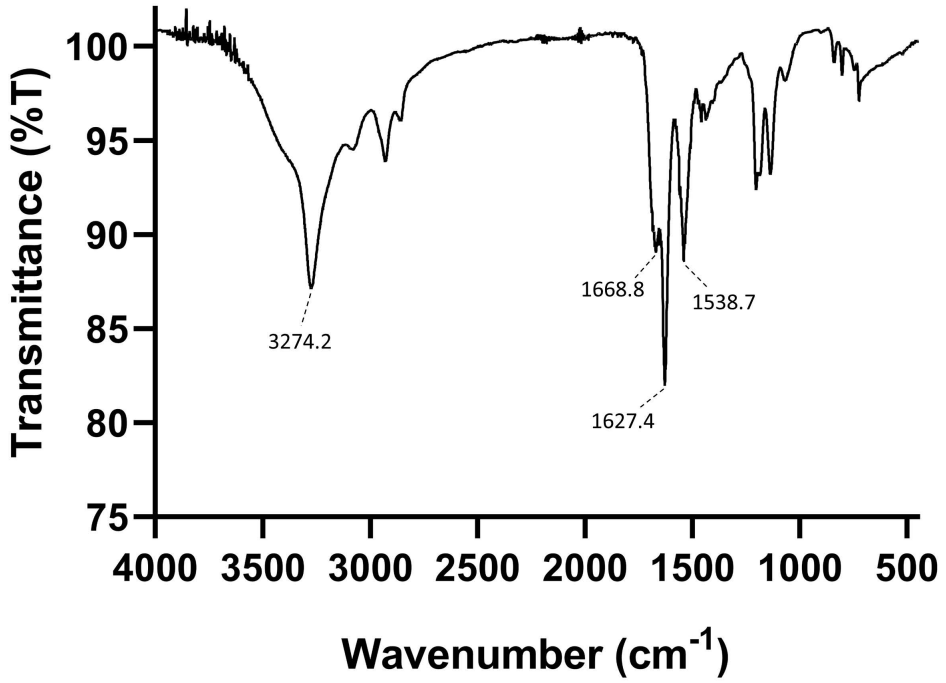

Figure 252. FT-IR spectrum of **CP7T10** (solid, 298 K).

USC
UNIVERSIDADE DE SANTIAGO DE COMPOSTELA

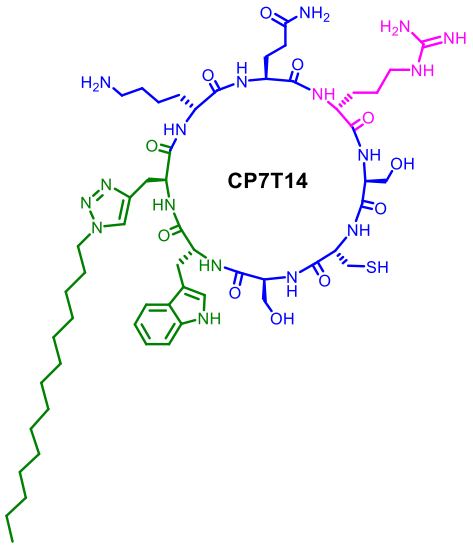

CP7T14: The peptide was synthesized according to the general protocol for solid-phase synthesis (145 mg of resin, 0.64 mmol·g^{-1}). Then, the click chemistry reaction was performed and the peptide was cleaved and purified by semipreparative RP-HPLC using a Phenomenex Luna C18 (2) 100Å column. [gradient: H_2O (0.1% TFA)/MeCN (0.1% TFA), 70:30 → 70:30 (5 min); 70:30 → 15:85 (40 min), R_t = 24.9 min]. The proper fractions were freeze-dried to provide **CP7T14** as a white solid with an overall yield of 2% (2.5 mg). **ESI-MS** *m/z* (%): 1210.7 (13) $[M+H]^+$, 605.6 (100) $[M+2H]^{2+}$, 404.2 (4) $[M+3H]^{3+}$. **HRMS (ESI)** *m/z*: $[M+H]^+$ calculated for $C_{56}H_{92}N_{17}O_{11}S$: 1210.6877, found 1210.6901. **FTIR (neat)**: ν = 3268.3 (amide A), 1668.8 (amide I_b), 1627.4 (amide I_a), 1538.7 (amide II) cm^{-1}.

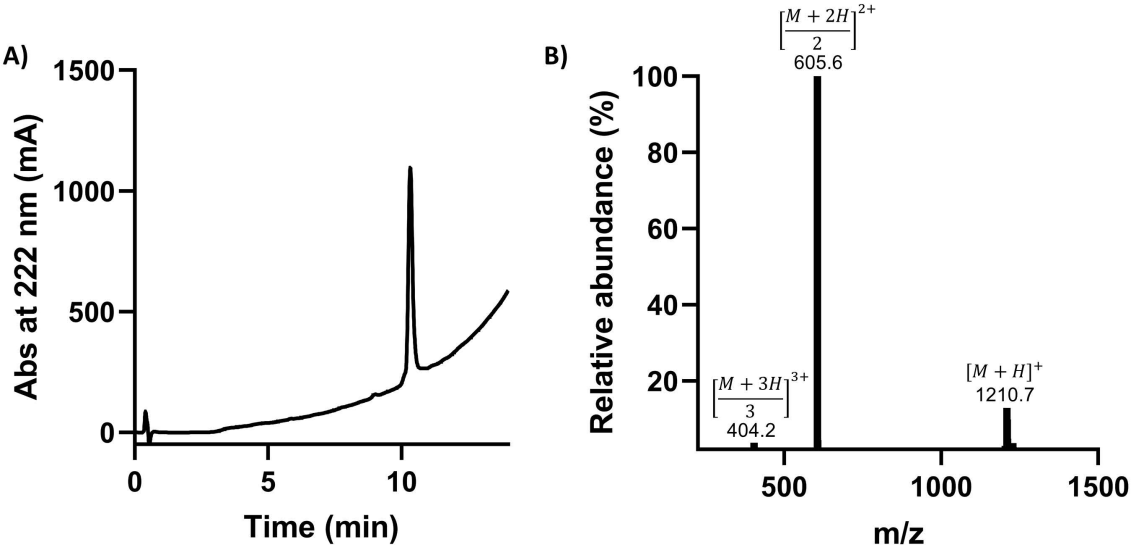

Figure 253. (A) **RP-uHPLC** of **CP7T14:** [Agilent SB-C18 column, H_2O (0.1% TFA)/MeCN (0.1% TFA), 100:0 → 100:2 (2 min) and 100:0 → 25:75 (12 min)], R_t = 10.3 min. (B) ESI-MS of the main peak.

USC UNIVERSIDADE DE SANTIAGO DE COMPOSTELA

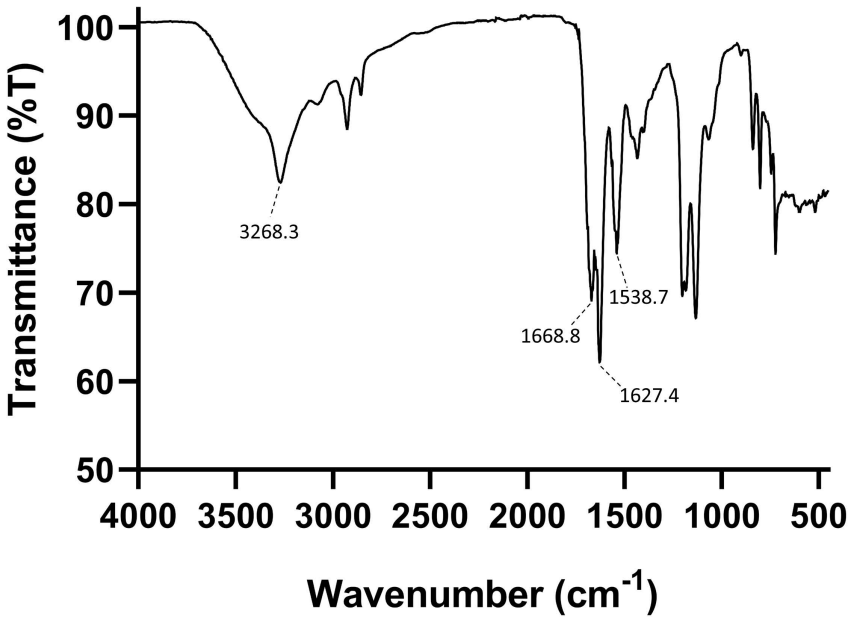

Figure 254. FT-IR spectrum of **CP7T14** (solid, 298 K).

8.2.3.6. Maleimide-thiol doxorubicin conjugation

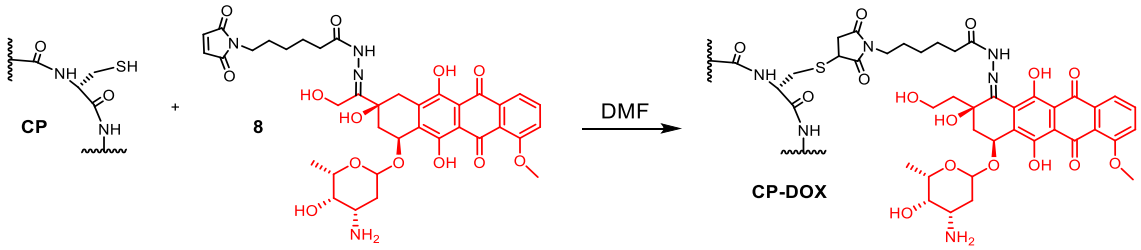

Figure 255. Thiol-ene reaction to obtain **CP-DOX** conjugates.

General protocol:

The corresponding CP (1 equiv.) and **8** (1 equiv.) were dissolved in 1 mL of DMF (dry). The resulting solution was stirred for 12 hours at room temperature and protected from light using aluminium foil. Then, the reaction mixture was poured over cold Et_2O (40 mL) and the red solid formed was collected by centrifugation (4000 rpm x 10 min). The product was purified by Sephadex LH-20 column (Eluent: MeOH). The pure fractions with the product were concentrated without reaching dryness, poured over cold Et_2O (40 mL), centrifuged (4000 rpm x 10 min) and dried under vacuum. The product was obtained as a red solid in all cases.

USC UNIVERSIDADE DE SANTIAGO DE COMPOSTELA

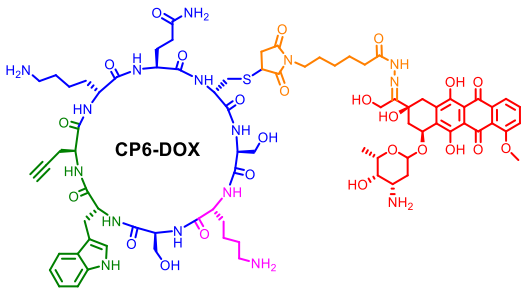

CP6-DOX: The thiol-ene reaction between **CP6** (6.0 mg, 6.4 µmol) and **8** (4.8 mg, 6.4 µmol) was performed according to the general protocol. **CP6-DOX** was obtained as a red solid with an overall yield of 70% (7.6 mg). **ESI-MS** *m/z* (%): 847.4 (100) $[M+2H]^{2+}$. **HRMS (ESI)** *m/z*: $[M+2H]^{2+}$ calculated for $C_{79}H_{106}N_{16}O_{24}S$: 847.3638, found 847.3637. **FTIR (neat)**: ν = 3270.3 (amide A), 1670.8 (amide I_b), 1629.4 (amide I_a), 1540.6 (amide II) cm^{-1}.

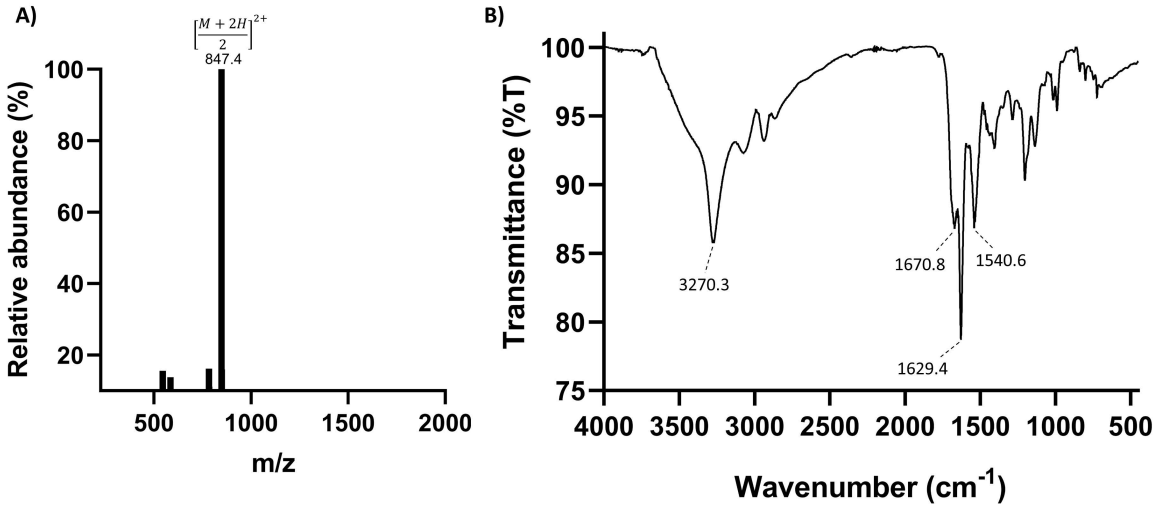

Figure 256. (A) ESI-MS of **CP6-DOX**. (B) FT-IR spectrum of **CP6-DOX** (solid, 298 K).

USC UNIVERSIDADE DE SANTIAGO DE COMPOSTELA

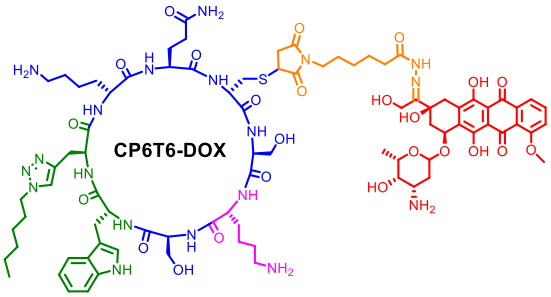

CP6T6-DOX: The thiol-ene reaction between **CP6T6** (2.1 mg, 2.0 µmol) and **8** (1.5 mg, 2.0 µmol) was performed according to the general protocol. **CP6T6-DOX** was obtained as a red solid with an overall yield of 94% (3.4 mg). **ESI-MS** *m/z* (%): 911.2 (100) $[M+2H]^{2+}$, 608.0 (25) $[M+3H]^{3+}$. **HRMS (ESI)** *m/z*: $[M+H]^{+}$ calculated for $C_{85}H_{118}N_{19}O_{24}S$: 1820.8312, found 1820.8312. **FTIR (neat)**: ν = 3270.3 (amide A), 1670.8 (amide I_b), 1625.4 (amide I_a), 1536.7 (amide II) cm^{-1}.

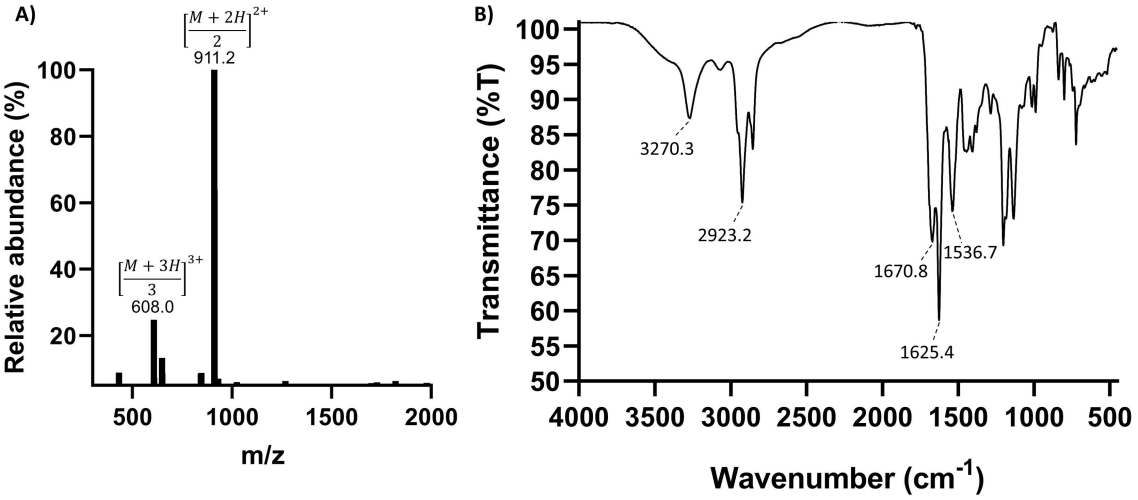

Figure 257. (A) ESI-MS of **CP6T6-DOX**. (B) FT-IR spectrum of **CP6T6-DOX** (solid, 298 K).

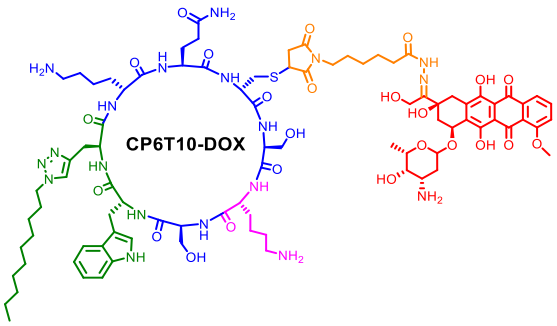

CP6T10-DOX: The thiol-ene reaction between **CP6T10** (3.0 mg, 2.7 µmol) and **8** (2.0 mg, 2.7 µmol) was performed according to the general protocol. **CP6T10-DOX** was obtained as a red solid with an overall yield of 94% (4.7 mg). **ESI-MS** *m/z* (%): 939.4 (100) $[M+2H]^{2+}$, 626.5 (36) $[M+3H]^{3+}$. **HRMS (ESI)** *m/z*: $[M+2H]^{2+}$ calculated for $C_{89}H_{127}N_{19}O_{24}S$: 938.9506, found 938.9500. **FTIR (neat)**: ν = 3274.2 (amide A), 1672.8 (amide I_b), 1627.4 (amide I_a), 1540.6 (amide II) cm^{-1}.

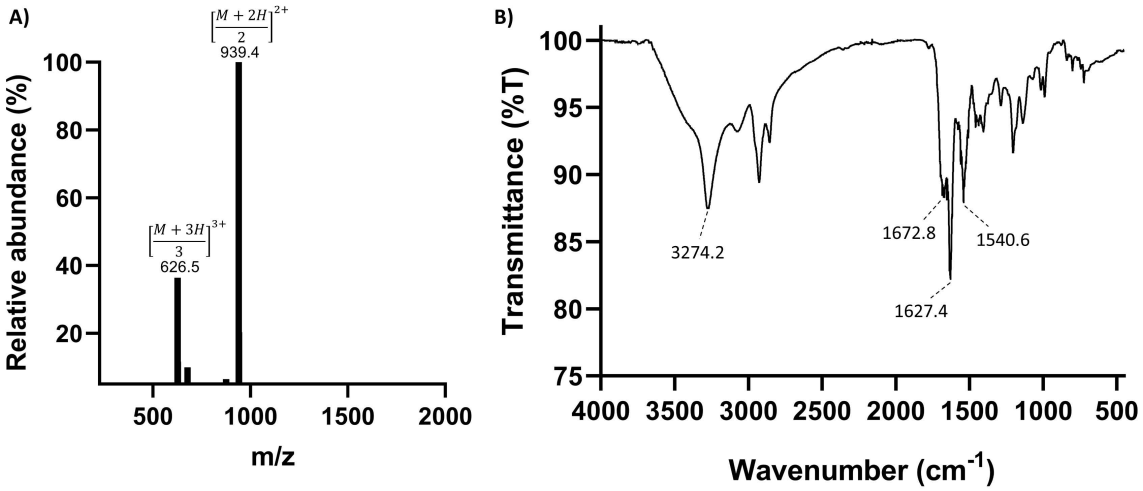

Figure 258. (A) ESI-MS of **CP6T10-DOX**. (B) FT-IR spectrum of **CP6T10-DOX** (solid, 298 K).

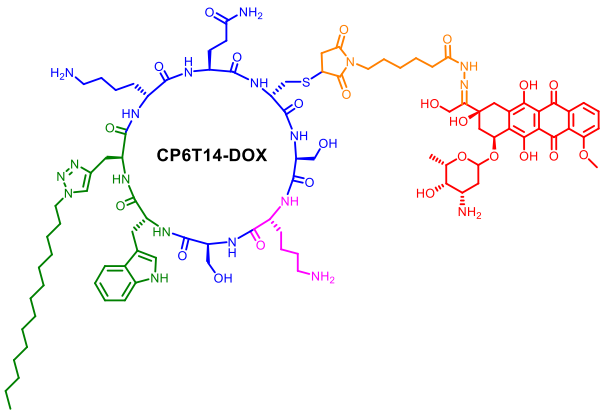

CP6T14-DOX: The thiol-ene reaction between **CP6T14** (3.5 mg, 3.0 µmol) and **8** (2.2 mg, 3.0 µmol) was performed according to the general protocol. **CP6T14-DOX** was obtained as a red solid with an overall yield of 81% (4.6 mg). **ESI-MS** *m/z* (%): 967.4 (100) $[M+2H]^{2+}$, 645.0 (26) $[M+3H]^{3+}$. **HRMS (ESI)** *m/z*: $[M+2H]^{2+}$ calculated for $C_{93}H_{135}N_{19}O_{24}S$: 966.9819, found 966.9822. **FTIR (neat)**: ν = 3274.2 (amide A), 1670.8 (amide I_b), 1629.4 (amide I_a), 1536.7 (amide II) cm^{-1}.

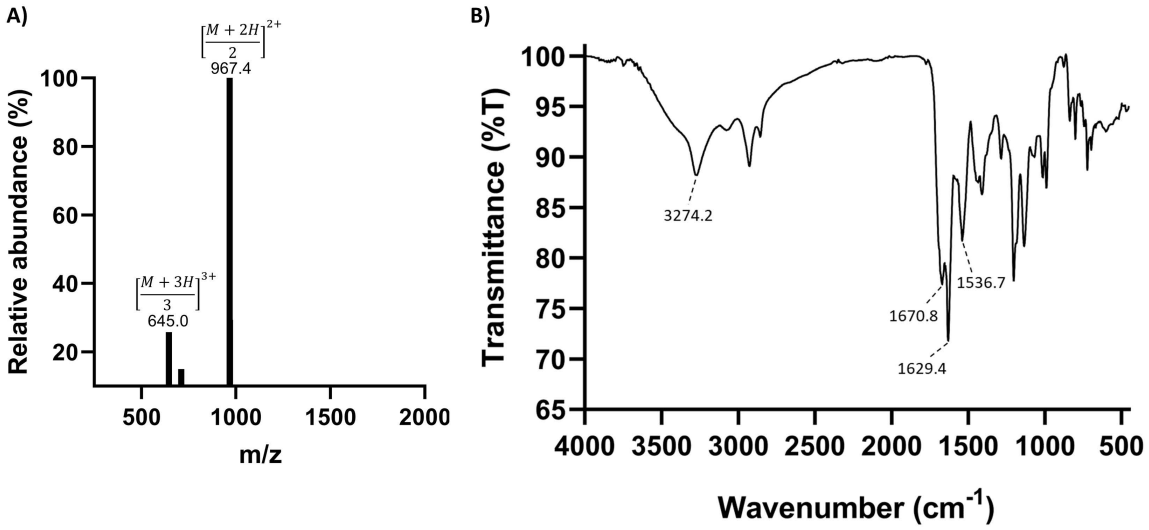

Figure 259. (A) ESI-MS of **CP6T14-DOX**. (B) FT-IR spectrum of **CP6T14-DOX** (solid, 298 K).

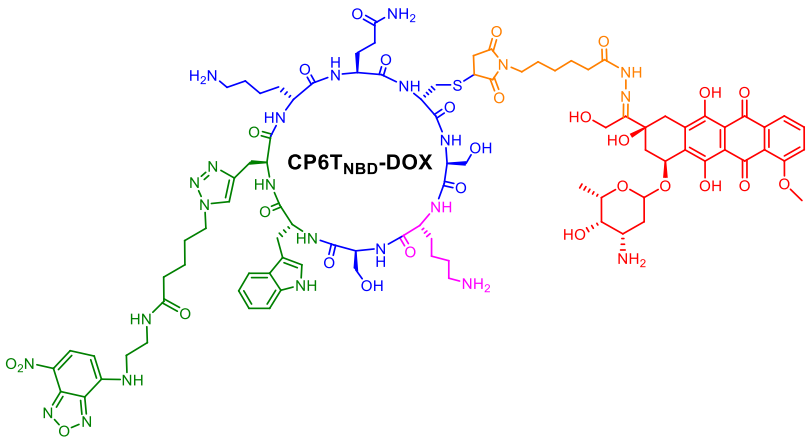

CP6T$_{NBD}$-DOX: The thiol-ene reaction between **CP6T$_{NBD}$** (3.3 mg, 2.6 µmol) and **8** (1.9 mg, 2.6 µmol) was performed according to the general protocol. **CP6T$_{NBD}$-DOX** was obtained as a red solid with an overall yield of 98% (5.1 mg). **ESI-MS** *m/z* (%): 1021.5 (100) $[M+2H]^{2+}$, 681.8 (68) $[M+3H]^{3+}$. **HRMS (ESI)** *m/z*: $[M+2H]^{2+}$ calculated for $C_{92}H_{122}N_{24}O_{28}S$: 1021.4285, found 1021.4303. **FTIR (neat)**: ν = 3274.2 (amide A), 1672.8 (amide I_b), 1627.4 (amide I_a), 1536.7 (amide II) cm^{-1}.

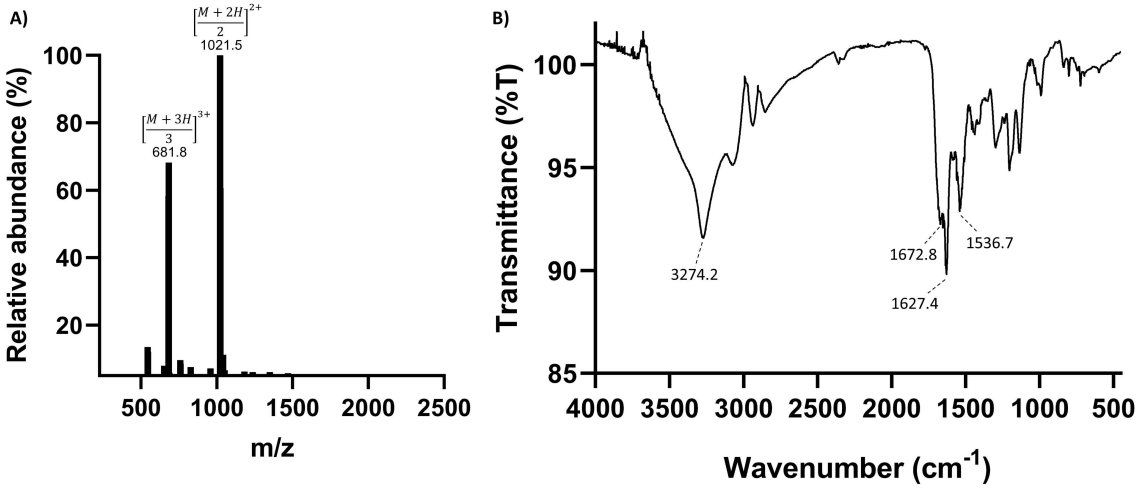

Figure 260. (A) ESI-MS of **CP6T$_{NBD}$-DOX**. (B) FT-IR spectrum of **CP6T$_{NBD}$-DOX** (solid, 298 K).

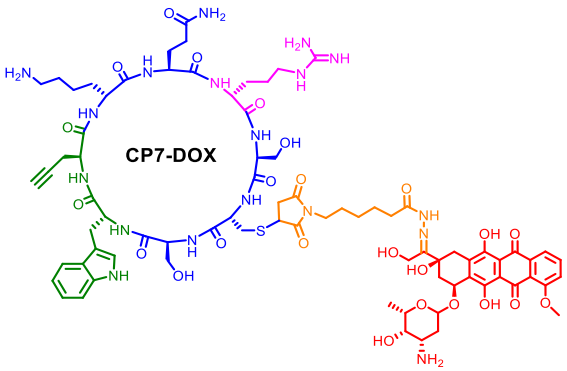

CP7-DOX: The thiol-ene reaction between **CP7** (2.6 mg, 2.7 µmol) and **8** (2.0 mg, 2.7 µmol) was performed according to the general protocol. **CP7-DOX** was obtained as a red solid with an overall yield of 78% (3.6 mg). **ESI-MS** *m/z* (%): 861.5 (100) $[M+2H]^{2+}$. **HRMS (ESI)** *m/z*: $[M+2H]^{2+}$ calculated for $C_{79}H_{106}N_{18}O_{24}S$: 861.3669, found 861.3666. **FTIR (neat)**: ν = 3276.2 (amide A), 1670.8 (amide I_b), 1627.4 (amide I_a), 1538.7 (amide II) cm^{-1}.

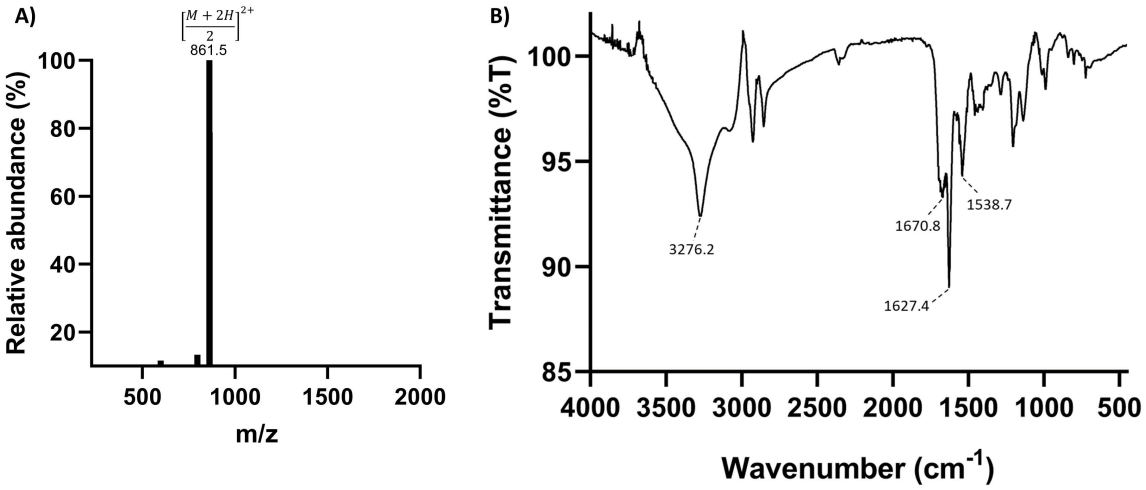

Figure 261. (A) ESI-MS of **CP7-DOX**. (B) FT-IR spectrum of **CP7-DOX** (solid, 298 K).

USC UNIVERSIDADE DE SANTIAGO DE COMPOSTELA

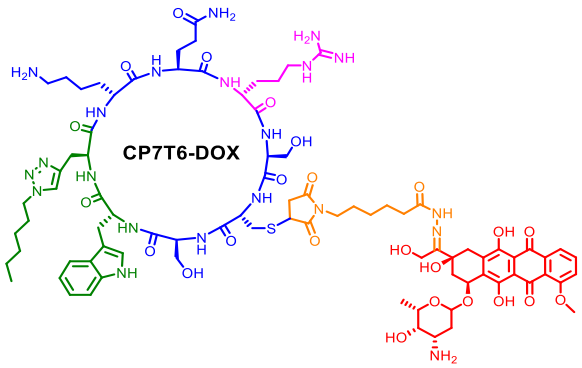

CP7T6-DOX: The thiol-ene reaction between **CP7T6** (2.5 mg, 2.3 µmol) and **8** (1.7 mg, 2.3 µmol) was performed according to the general protocol. **CP7T6-DOX** was obtained as a red solid with an overall yield of 86% (3.6 mg). **ESI-MS** *m/z* (%): 1848.6 (4) $[M+H]^+$, 925.3 (100) $[M+2H]^{2+}$, 617.1 (35) $[M+3H]^{3+}$. **HRMS (ESI)** *m/z*: $[M+2H]^{2+}$ calculated for $C_{85}H_{119}N_{21}O_{24}S$: 924.9223, found 924.9225. **FTIR (neat)**: ν = 3272.3 (amide A), 1668.8 (amide I_b), 1627.4 (amide I_a), 1538.7 (amide II) cm^{-1}.

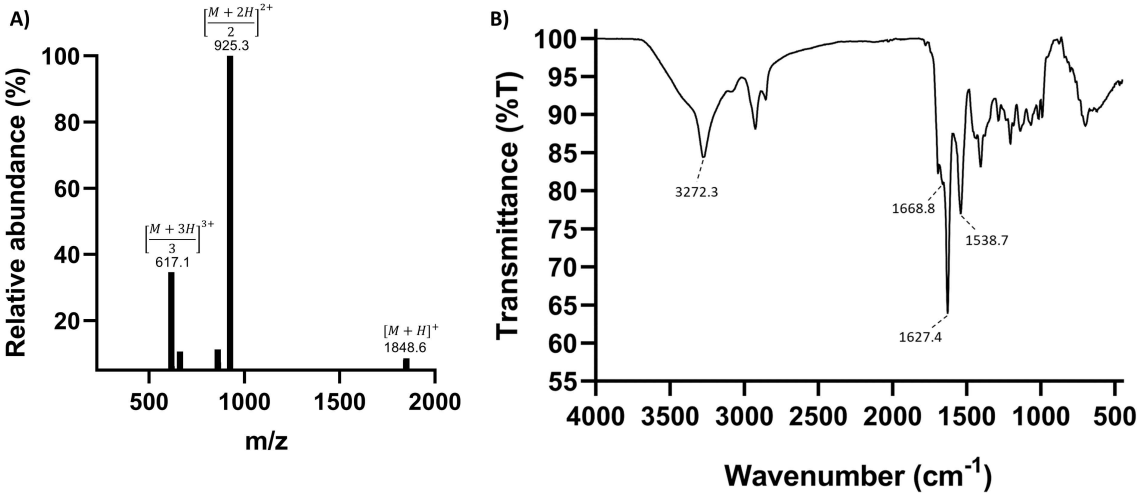

Figure 262. (A) ESI-MS of **CP7T6-DOX**. (B) FT-IR spectrum of **CP7T6-DOX** (solid, 298 K).

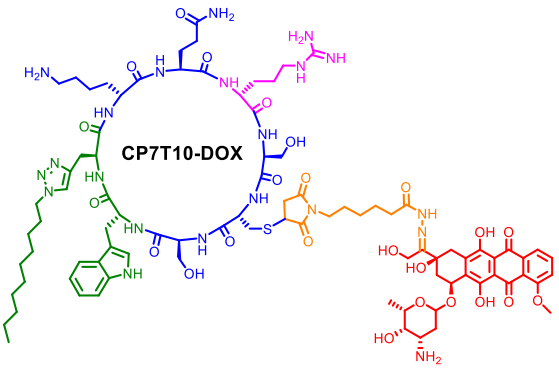

CP2T10-DOX: The thiol-ene reaction between **CP7T10** (3.0 mg, 2.6 µmol) and **8** (2.0 mg, 2.6 µmol) was performed according to the general protocol. **CP7T10-DOX** was obtained as a red solid with an overall yield of 92% (4.6 mg). **ESI-MS** *m/z* (%): 953.0 (100) $[M+2H]^{2+}$, 636.0 (50) $[M+3H]^{3+}$. **HRMS (ESI)** *m/z*: $[M+2H]^{2+}$ calculated for $C_{89}H_{127}N_{21}O_{24}S$: 952.9536, found 952.9538. **FTIR (neat)**: ν = 3272.3 (amide A), 1670.8 (amide I_b), 1625.4 (amide I_a), 1538.7 (amide II) cm^{-1}.

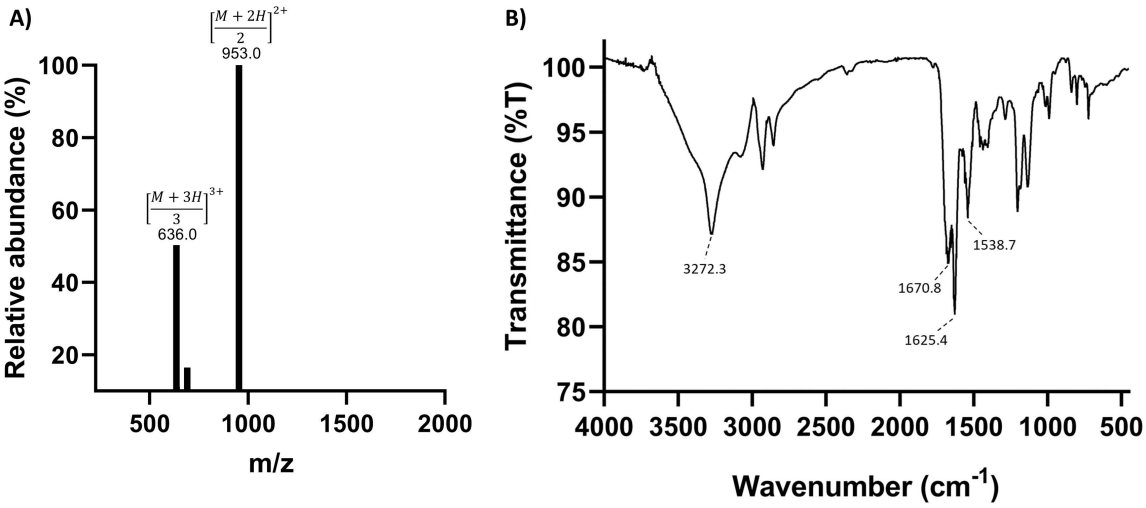

Figure 263. (A) ESI-MS of **CP7T10-DOX**. (B) FT-IR spectrum of **CP7T10-DOX** (solid, 298 K).

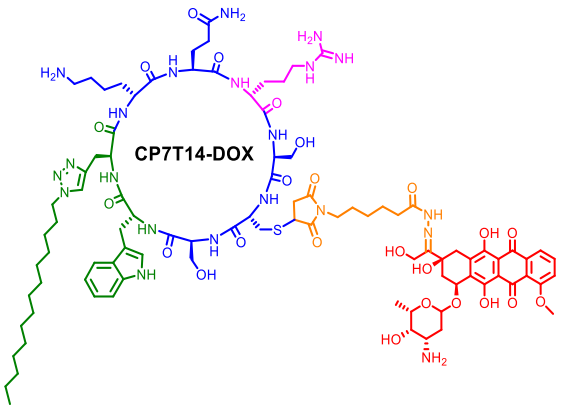

CP7T14-DOX: The thiol-ene reaction between **CP7T14** (1.5 mg, 1.2 µmol) and **8** (0.9 mg, 1.2 µmol) was performed according to the general protocol. **CP7T14-DOX** was obtained as a red solid with an overall yield of 58% (1.4 mg). **ESI-MS** *m/z* (%): 980.8 (100) $[M+2H]^{2+}$. **HRMS (ESI)** *m/z*: $[M+2H]^{2+}$ calculated for $C_{93}H_{135}N_{21}O_{24}S$: 980.9849, found 980.9850. **FTIR (neat)**: ν = 3270.3 (amide A), 1668.8 (amide I_b), 1629.4 (amide I_a), 1534.7 (amide II) cm^{-1}.

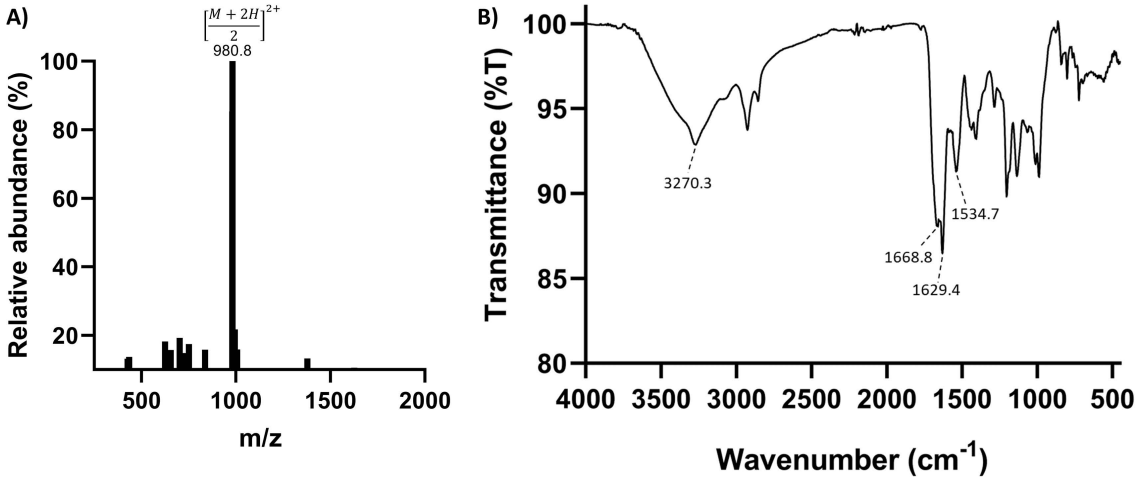

Figure 264. (A) ESI-MS of **CP7T14-DOX**. (B) FT-IR spectrum of **CP7T14-DOX** (solid, 298 K).

8.2.3.7. Thiol-disulphide exchange doxorubicin conjugation

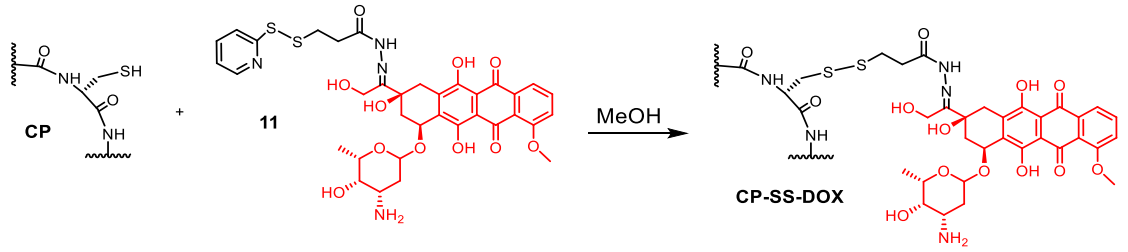

Figure 265. Thiol-disulphide exchange reaction to obtain **CP-SS-DOX** conjugates.

General protocol:

The corresponding CP (1 equiv.) and **11** (1 equiv.) were dissolved in 1 mL of MeOH (dry). The resulting solution was stirred for 12 hours at room temperature and protected from light using aluminium foil. Then, the reaction mixture was poured over cold Et_2O (40 mL) and the red solid formed was collected by centrifugation (4000 rpm x 10 min). The product was purified by Sephadex LH-20 column (Eluent: MeOH). The pure fractions with the product were concentrated without reaching dryness, poured over cold Et_2O (40 mL), centrifuged (4000 rpm x 10 min) and dried under vacuum. The product was obtained as a red solid in all cases.

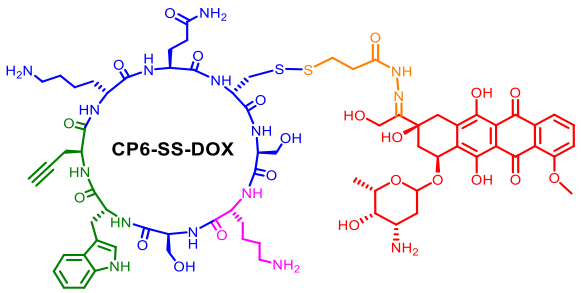

CP6-SS-DOX: The thiol-disulphide exchange reaction between **CP6** (2.1 mg, 2.3 µmol) and **11** (1.7 mg, 2.3 µmol) was performed according to the general protocol. **CP6-SS-DOX** was obtained as a red solid with an overall yield of 94% (3.3 mg). **ESI-MS** *m/z* (%): 1586.6 (16) $[M+H]^+$, 793.9 (100) $[M+2H]^{2+}$. **HRMS (ESI)** *m/z*: $[M+2H]^{2+}$ calculated for $C_{72}H_{97}N_{15}O_{22}S_2$: 793.8182, found: 793.8188. **FTIR (neat)**: ν = 3268.3 (amide A), 1670.8 (amide I_b), 1625.4 (amide I_a), 1538.7 (amide II) cm^{-1}.

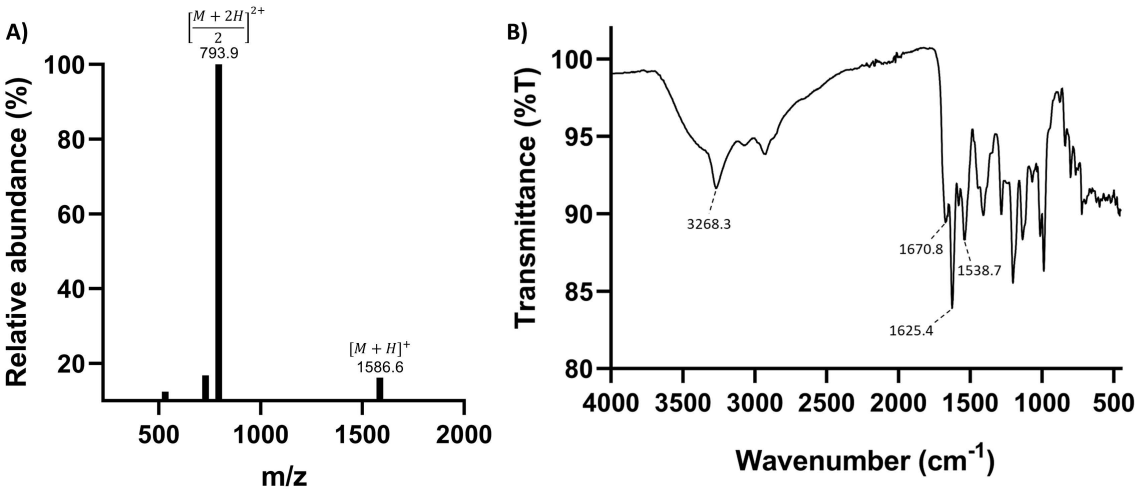

Figure 266. (A) ESI-MS of **CP6-SS-DOX**. (B) FT-IR spectrum of **CP6-SS-DOX** (solid, 298 K).

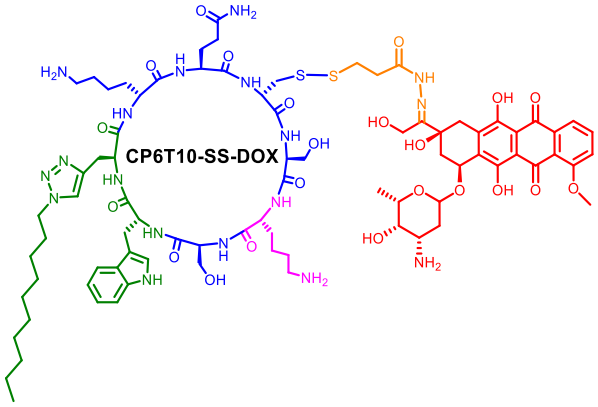

CP6T10-SS-DOX: The thiol-disulphide exchange reaction between **CP6T10** (15.7 mg, 13.9 µmol) and **11** (10.5 mg, 13.9 µmol) was performed according to the general protocol. **CP6T10-SS-DOX** was obtained as a red solid with an overall yield of 87% (21.5 mg). **ESI-MS** *m/z* (%): 885.6 (100) $[M+2H]^{2+}$, 590.9 (19) $[M+3H]^{3+}$. **HRMS (ESI)** *m/z*: $[M+H]^{+}$ calculated for $C_{82}H_{118}N_{18}O_{22}S_2$: 1769.8026, found: 1769.8040. **FTIR (neat)**: ν = 3274.2 (amide A), 1664.9 (amide I_b), 1625.4 (amide I_a), 1538.7 (amide II) cm^{-1}.

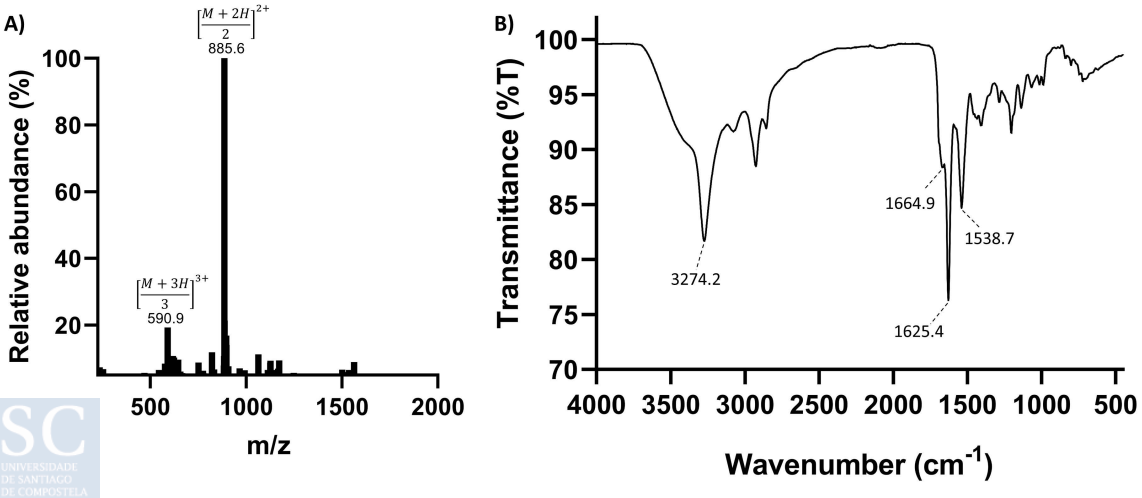

USC UNIVERSIDADE DE SANTIAGO DE COMPOSTELA

Figure 267. (A) ESI-MS of **CP6T10-SS-DOX**. (B) FT-IR spectrum of **CP6T10-SS-DOX** (solid, 298 K).

9. REFERENCES

USC
UNIVERSIDADE
DE SANTIAGO
DE COMPOSTELA

1. J. W. Steed, J. L. Atwood. *Supramolecular Chemistry*, 3rd Edition. John Wiley & Sons Ltd, Chichester, UK, **2022**.
2. J. D. van der Waals, *On the Continuity of the Gaseous and Liquid States*, University of Leiden, Leiden, **1873**.
3. E. Fischer, *Ber. Dtsch. Chem. Ges.* **1894**, *27*, 2985-2993.
4. W. M. Latimer, W. H. Rodebush, *J. Am. Chem. Soc.* **1920**, *42*, 1419-1433.
5. J. M. Lehn, *Science* **1993**, *260*, 1762-1763.
6. a) J. D. Watson, F. H. C. Crick, *Nature* **1953**, *171*, 737-738; b) M. H. F. Wilkins, A. R. Strokes, H. R. Wilson, *Nature* **1953**, *171*, 738-740; c) R. E. Franklin, R. G. Gosling, *Nature* **1953**, *172*, 156-157.
7. S. Neidle, *J. Biol. Chem.* **2021**, *296*, 100553.
8. a) D. B. Amabilino, D. K. Smith, J. W. Steed, *Chem. Soc. Rev.* **2017**, *46*, 2404-2420; b) M. J. Webber, E. A. Appel, E. W. Meijer, R. Langer, *Nat. Mater.* **2016**, *15*, 13-26.
9. a) C. J. Pedersen, *Science* **1988**, *241*, 536-540; b) J. M. Lehn, *Acc. Chem. Res.* **1978**, *11*, 49-57; c) J. M. Lehn, *Angew. Chem. Int. Ed. Engl.* **1988**, *27*, 89-112; d) D. J. Cram, *Angew. Chem. Int. Ed. Engl.* **1988**, *27*, 1009-1020; e) C. J. Pedersen, *Angew. Chem. Int. Ed. Engl.* **1988**, *27*, 1021-1027.
10. a) J.-P. Sauvage, *Angew. Chem. Int. Ed.* **2017**, *56*, 11080-11093; b) J. F. Stoddart, *Angew. Chem. Int. Ed.* **2017**, *56*, 11094-11125; c) B. L. Feringa, *Angew. Chem. Int. Ed.* **2017**, *56*, 11060-11078; d) D. A. Leigh, *Angew. Chem. Int. Ed.* **2016**, *55*, 14506-14508; e) V. Balzani, A. Credi, F. M. Raymo, J. F. Stoddart, *Angew. Chem. Int. Ed.* **2000**, *39*, 3348-3391; f) S. Erbas-Cakmak, D. A. Leigh, C. T. McTernan, A. L. Nussbaumer, *Chem. Rev.* **2015**, *115*, 10081-10206.
11. S. Kassem, T. van Leeuwen, A. S. Lubbe, M. R. Wilson, B. L. Feringa, D. A. Leigh, *Chem. Soc. Rev.* **2017**, *46*, 2592-2621.
12. D. Kumar, D. Sharma, G. Singh, M. Singh, M. S. Rathore, *ISRN Pharm* **2012**, *2012*, 474830.
13. a) L. Brunsveld, B. J. B. Folmer, E. W. Meijer, R. P. Sijbesma, *Chem. Rev.* **2001**, *101*, 4071-4097; b) T. Aida, E. W. Meijer, S. I. Stupp, *Science* **2012**, 335, 813-817; c) E. Krieg, M. M. C. Bastings, P. Besenius, B. Rybtchinski, *Chem. Rev.* **2016**, *116*, 2414-2477.
14. a) T. D. Pollard, G. G. Borisy, *Cell* **2003**, *112*, 453-465; b) A. Akhmanova, M. O. Steinmetz, *Nat. Rev. Mol. Cell Biol.* **2015**, *16*, 711-726.
15. C. Conde, A. Cáceres, *Nat. Rev. Neurosci.* **2009**, *10*, 319-332.
16. a) L. Albertazzi, F. J. Martinez-Veracoechea, C. M. A. Leenders, I. K. Voets, D. Frenkel, E. W. Meijer, *Proc. Natl. Acad. Sci. U.S.A.* **2013**, *110*, 12203-12208; b) L. Albertazzi, D. van der Zwaag, C. M. A. Leenders, R. Fitzner, R. W. van der Hofstad, E. W. Meijer, *Science* **2014**, *344*, 491-495.
17. S. Cantekin, T. F. A. de Greef, A. R. A. Palmans, *Chem. Soc. Rev.* **2012**, *41*, 6125-6137.
18. R. P. Sijbesma, F. H. Beijer, L. Brunsveld, B. J. B. Folmer, J. H. K. K. Hirschberg, R. F. M. Lange, J. K. L. Lowe, E. W. Meijer, *Science* **1997**, *278*, 1601-1604.
19. P. Y. W. Dankers, T. M. Hermans, T. W. Baughman, Y. Kamikawa, R. E. Kieltyka, M. M. C. Bastings, H. M. Janssen, N. A. J. M. Sommerdijk, A. Larsen, M. J. A. van Luyn, A. W. Bosman, E. R. Popa, G. Fytas, E. W. Meijer, *Adv. Mater.* **2012**, *24*, 2703-2709.
20. X. Zhang, D. Görl, V. Stepanenko, F. Würthner, *Angew. Chem. Int. Ed.* **2014**, *53*, 1270-1274.
21. D. Görl, X. Zhang, V. Stepanenko, F. Würthner, *Nat. Commun.* **2015**, *6*, 7009.
22. J. P. Hill, W. Jin, A. Kosaka, T. Fukushima, H. Ichihara, T. Shimomura, K. Ito, T. Hashizume, N. Ishii, T. Aida, *Science* **2004**, *304*, 1481-1483.
23. G. Zhang, W. Jin, T. Fukushima, A. Kosaka, N. Ishii, T. Aida, *J. Am. Chem. Soc.* **2007**, *129*, 719-722.
24. a) J. D. Hartgerink, E. Beniash, S. I. Stupp, *Science* **2001**, *294*, 1684-1688; b) Z. Álvarez, A. Kolberg-Edelbrock, I. Sasselli, J. Ortega, R. Qiu, Z. Syrgiannis, P. Mirau, F. Chen, S. Chin, S. Weigand, E. Kiskinis, S. I. Stupp, *Science* **2021**, *374*, 848-856.
25. C. S. Smith, Z. Álvarez, R. Qiu, I. R. Sasselli, T. Clemons, J. A. Ortega, M. Vilela-Picos, H. Wellman, E. Kiskinis, S. I. Stupp, *ACS Nano* **2023**, *17*, 19887-19902.
26. a) X. Yan, F. Wang, B. Zheng, F. Huang, *Chem. Soc. Rev.* **2012**, *41*, 6042-6065; b) X. Ma, H. Tian, *Acc. Chem. Res.* **2014**, *47*, 1971-1981.
27. a) X. Yao, T. Li, J. Wang, X. Ma, H. Tian, *Adv. Optical Mater.* **2016**, *4*, 1322-1349; b) M. Baroncini, J. Groppi, S. Corra, S. Silvi, A. Credi, *Adv. Optical Mater.* **2019**, *7*, 1900392; c) F. Xu, B. L. Feringa, *Adv. Mater.* **2023**, *35*, 2204413.
28. a) A. K. Miller, Z. Li, K. A. Streletzky, A. M. Jamieson, S. J. Rowan, *Polym. Chem.* **2012**, *3*, 3132-3138; b) Q. Yan, A. Feng, H. Zhang, Y. Yin, J. Yuan, *Polym. Chem.* **2013**, *4*, 1216-1220.
29. a) J. Hu, G. Zhang, S. Liu, *Chem. Soc. Rev.* **2012**, *41*, 5933-5949; b) Y. Ding, Y. Kang, X. Zhang, *Chem. Commun.* **2015**, *51*, 996-1003; c) X. Xiao, J. Huang, *Langmuir* **2024**, *40*, 15407-15420.

30. a) K. C. Leung, C. Chak, C. Lo, W. Wong, S. Xuan, C. H. K. Cheng, *Chem. Asian J.* **2009**, *4*, 364-381; b) H. Frisch, P. Besenius, *Macromol. Rapid Commun.* **2015**, *36*, 346-363.
31. H. Takala, P. Edlund, J. A. Ihalainen, S. Westenhoff, *Photochem. Photobiol. Sci.* **2020**, *19*, 1488-1510.
32. a) P. W. Kim, N. C. Rockwell, L. H. Freer, C. Chang, S. S. Martin, J. C. Lagarias, D. S. Larsen, *J. Phys. Chem. Lett.* **2013**, *4*, 2605-2609; b) D. Morozov, V. Modi, V. Mironov, G. Groenhof, *J. Phys. Chem. Lett.* **2022**, *13*, 4538-4542.
33. a) R. Hubbard, A. Kropf, *Proc. Natl. Acad. Sci. U S A*. **1958**, *44*, 130-139; b) K. Palczewski, *J. Biol. Chem.* **2012**, *287*, 1612-1619.
34. P. Nogly, T. Weinert, D. James, S. Carbajo, D. Ozerov, A. Furrer, D. Gashi, V. Borin, P. Skopintsev, K. Jaeger, K. Nass, P. Båtch, R. Bosman, J. Koglin, M. Seaberg, T. Lane, D. Kekilli, S. Brünle, T. Tanaya, W. Wu, C. Milne, T. White, A. Barty, U. Weierstall, V. Panneels, E. Nango, S. Iwata, M. Hunter, I. Schapiro, G. Schertler, R. Neutze, J. Standfuss, *Science* **2018**, *361*, eaat0094.
35. O. P. Ernst, D. T. Lodowski, M. Elstner, P. Hegemann, L. S. Brown, H. Kandori, *Chem. Rev.* **2014**, *114*, 126-163.
36. Z. L. Pianowski, *Chem. Eur. J.* **2019**, *25*, 5128-5144.
37. J. Volarić, W. Szymanski, N. A. Simeth, B. L. Feringa, *Chem. Soc. Rev.* **2021**, *50*, 12377-12449.
38. a) M. Russew, S. Hecht, *Adv. Mater.* **2010**, *22*, 3348-3360; b) J. Boelke, S. Hech, *Adv. Optical Mater.* **2019**, *7*, 1900404; c) B. L. Feringa. *Molecular Photoswitches: Chemistry, Properties, and Applications*, *2 Volume Set.* John Wiley & Sons Ltd, Chichester, UK, **2022**.
39. a) A. A. Beharry, G. A. Woolley, *Chem. Soc. Rev.* **2011**, *40*, 4422-4437; b) H. M. D. Bandarab, S. C. Burdette, *Chem. Soc. Rev.* **2012**, *41*, 1809-1825; c) F. A. Jerca, V. V. Jerca, R. Hoogenboom, *Nat. Rev. Chem.* **2022**, *6*, 51-69.
40. M. Dong, A. Babalhavaeji, S. Samanta, A. A. Beharry, G. A. Woolley, *Acc. Chem. Res.* **2015**, *48*, 2662-2670.
41. O. Sadovski, A. A. Beharry, F. Zhang, G. A. Woolley, *Angew. Chem. Int. Ed.* **2009**, *48*, 1484-1486.
42. a) A. A. Beharry, O. Sadovski, G. A. Woolley, *J. Am. Chem. Soc.* **2011**, *133*, 19684-19687; b) S. Samanta, A. A. Beharry, O. Sadovski, T. M. McCormick, A. Babalhavaeji, V. Tropepe, G. A. Woolley, *J. Am. Chem. Soc.* **2013**, *135*, 9777-9784.
43. a) S. Kobayashi, H. Yokoyama, H. Kamei, *Chem. Phys. Lett.* **1987**, *138*, 333-338; b) F. Aleotti, A. Nenov, L. Salvigni, M. Bonfanti, M. M. El-Tahawy, A. Giunchi, M. Gentile, C. Spallacci, A. Ventimiglia, G. Cirillo, L. Montali, S. Scurti, M. Garavelli, I. Conti, *J. Phys. Chem. A* **2020**, *124*, 9513-9523.
44. a) D. Bléger, J. Schwarz, A. M. Brouwer, S. Hecht, *J. Am. Chem. Soc.* **2012**, *134*, 20597-20600; b) C. Knie, M. Utecht, F. Zhao, H. Kulla, S. Kovalenko, A. M. Brouwer, P, Saalfrank, S. Hecht, D. Bléger, *Chem. Eur. J.* **2014**, *20*, 16492-16501; c) S. Axelrod, E. Shakhnovich, R. Gómez-Bombarelli, *ACS Cent. Sci.* **2023**, *9*, 166-176.
45. Y. Wang, N. Ma, Z. Wang, X. Zhang, *Angew. Chem. Int. Ed.* **2007**, *46*, 2823-2826.
46. J. W. Fredya, A. Méndez-Ardoy, S. Kwangmettatama, D. Bochicchio, B. Matt, M. C. A. Stuart, J. Huskens, N. Katsonis, G. M. Pavan, T. Kudernac, *Proc. Natl. Acad. Sci. USA* **2017**, *114*, 11850-11855.
47. a) L. Albert, O. Vázquez, *Chem. Commun.* **2019**, *55*, 10192-10213; b) C. Renner, L. Moroder, *ChemBioChem* **2006**, *7*, 868-878; c) R. J. Mart, R. K. Allemann, *Chem. Commun.* **2016**, *52*, 12262-12277.
48. J. Rodríguez, J. Mosquera, S. Learte-Aymamí, M. Eugenio Vázquez, J. L. Mascareñas, *Acc. Chem. Res.* **2020**, *53*, 2286-2298.
49. A. M. Caamaño, M. E. Vázquez, J. Martínez-Costas, L. Castedo, J. L. Mascareñas, *Angew. Chem. Int. Ed.* **2000**, 39, 3104-3107.
50. a) G. A. Woolley, A. S. I. Jaikaran, M. Berezovski, J. P. Calarco, S. N. Krylov, *Biochemistry* **2006**, *45*, 6075-6084; b) F. Zhang, K. A. Timm, K. M. Arndt, G. A. Woolley, *Angew. Chem. Int. Ed*. **2010**, *49*, 3943-3946.
51. G. M. Murawska, C. Poloni, N. A. Simeth, W. Skymanski, B. L. Feringa, *Chem. Eur. J.* **2019**, *25*, 4965-4973.
52. S. Kneissl, E. J. Loveridge, C. Williams, M. P. Crump, R. K. Allemann, *ChemBioChem. **2008**, 9, 3046-3054.*
53. R. J. Mart, R. J. Errington, C. L. Watkins, S. C. Chappell, M. Wiltshire, A. T. Jones, P. J. Smith, R. K. Allemann, *Mol. BioSyst.* **2013**, *9*, 2597-2603.
54. C. Hoppmann, S. Seedorff, A. Richter, H. Fabian, P. Schmieder, K. Rück-Braun, M. Beyermann, *Angew. Chem. Int. Ed.* **2009**, *48*, 6636-6639.
55. C. Hoppmann, P. Schmieder, P. Domaing, G. Vogelreiter, J. Eichhorst, B. Wiesner, I. Morano, K. Rück-Braun, M. Beyermann, *Angew. Chem. Int. Ed.* **2011**, *50*, 7699-7702.
56. J. Auernheimer, C. Dahmen, U. Hersel, A. Bausch, H. Kessler, *J. Am. Chem. Soc.* **2005**, *127*, 16107-16110.
57. T. Podewin, J. Broichhagen, C. Frost, D. Groneberg, J. Ast, H. Meyer-Berg, N. H. F. Fine, A. Friebe, M. Zacharias, D. J. Hodson, D. Trauner, A. Hoffmann-Roder, *Chem. Sci.* **2017**, *8*, 4644-4653.

58. a) A. Prestela, H. M. Mölle, *Chem. Commun.* **2016**, *52*, 701-704; b) Y. Q. Yeoh, J. Yu, S. W. Polyak, J. R. Horsley, A. D. Abell, *ChemBioChem* **2018**, *19*, 2591-2597; c) X. Just-Baringo, A. Yeste-Vázquez, J. Moreno-Morales, C. Ballesté-Delpierre, P. J. Vila, E. Giralt, *Chem. Eur. J.* **2021**, *27*, 12987-12991.
59. a) S. Crespi, N. A. Simeth, B. König, *Nat. Rev. Chem.* **2019**, *3*, 133-146; b) C. E. Weston, R. D. Richardson, P. R. Haycock, A. J. P. White, M. J. Fuchter, *J. Am. Chem. Soc.* **2014**, *136*, 11878-11881; c) L. Stricker, E. Fritz, M. Peterlechner, N. L. Doltsinis, B. J. Ravoo, *J. Am. Chem. Soc.* **2016**, *138*, 4547-4554.
60. a) D. H. Waldeck, *Chem. Rev.* **1991**, *91*, 415-436; b) W. Fuß, C. Kosmidis, W. E. Schmid, S. A. Trushin, *Angew. Chem. Int. Ed.* **2004**, *43*, 4178-4182.
61. a) D. Villarón, S. J. Wezenberg, *Angew. Chem. Int. Ed.* **2020**, *59*, 13192-13202; b) F. Xu, J. Sheng, C. N. Stindt, S. Crespi, W. Danowski, M. F. Hilbers, W. J. Buma, B. L. Feringa, *Chem. Sci.* **2024**, *15*, 6763-6769.
62. a) C. Petermayer, H. Dube, *Acc. Chem. Res.* **2018**, *51*, 1153-1163; b) C. Petermayer, S. Thumser, F. Kink, P. Mayer, H. Dube, *J. Am. Chem. Soc.* **2017**, *139*, 15060-15067; c) S. Wiedbrauk, H. Dube, *Tetrahedron Lett.* **2015**, *56*, 4266-4274.
63. a) N. Koumura, R. W. J. Zijlstra, R. A. van Delden, N. Harada, B. L. Feringa, *Nature* **1999**, *401*, 152-155; b) N. Koumura, E. M. Geertsema, M. B. van Gelder, A. Meetsma, B. L. Feringa, *J. Am. Chem. Soc.* **2002**, *124*, 5037-5051; c) J. C. M. Kistemaker, P. Štacko, D. Roke, A. T. Wolters, G. H. Heideman, M. Chang, P. van der Meulen, J. Visser, E. Otten, B. L. Feringa, *J. Am. Chem. Soc.* **2017**, *139*, 9650-9661; d) D. R. S. Pooler, A. S. Lubbe, S. Crespi, B. L. Feringa, *Chem. Sci.* **2021**, *12*, 14964-14986.
64. a) H. Qian, S. Pramanik, I. Aprahamian, *J. Am. Chem. Soc.* **2017**, *139*, 9140-9143; b) M. Jeong, J. Park, Y. Seo, K. Lee, S. Pramanik, S. Ahn, S. Kwon, *Chem. Eur. J.* **2022**, *28*, e202103972; c) A. Ryabchun, Q. Li, F. Lancia, I. Aprahamian, N. Katsonis, *J. Am. Chem. Soc.* **2019**, *141*, 1196-1200.
65. P. Kuad, A. Miyawaki, Y. Takashima, H. Yamaguchi, A. Harada, *J. Am. Chem. Soc.* **2007**, *129*, 12630-12631.
66. F. Xu, L. Pfeifer, S. Crespi, F. King-Chi Leung, M. C. A. Stuart, S. J. Wezenberg, B. L. Feringa, *J. Am. Chem. Soc.* **2021**, *143*, 5990-5997.
67. J. Chen, F. K.-C. Leung, M. C. A. Stuart, T. Kajitani, T. Fukushima, E. van der Giessen, B. L. Feringa, *Nat. Chem.* **2018**, *10*, 132-138.
68. E. Weyandt, G. M. ter Huurne, G. Vantomme, A. J. Markvoort, A. R. A. Palmans, E. W. Meijer, *J. Am. Chem. Soc.* **2020**, *142*, 6295-6303.
69. a) H. Tian, S. Yang, *Chem. Soc. Rev.* **2004**, *33*, 85-97; b) J. Zhang, H. Tian, *Adv. Optical Mater.* **2018**, 1701278; c) H. Cheng, S. Zhang, E. Bai, X. Cao, J. Wang, J. Qi, J. Liu, J. Zhao, L. Zhang, J. Yoon, *Adv. Mater.* **2022**, *34*, 2108289.
70. Y. Cai, Z. Guo, J. Chen, W. Li, L. Zhong, Y. Gao, L. Jiang, L. Chi, H. Tian, W. Zhu, *J. Am. Chem. Soc.* **2016**, *138*, 2219-2224.
71. T. Li, X. Li, J. Wang, H. Ågren, X. Ma, H. Tian, *Adv. Optical Mater.* **2016**, *4*, 840-847.
72. a) R. Klajn, *Chem. Soc. Rev.* **2014**, *43*, 148-184; b) L. Kortekaas, W. R. Browne, *Chem. Soc. Rev.* **2019**, *48*, 3406-3424; c) J. K. Rad, Z. Balzade, A. R. Mahdavian, *J. Photochem. Photobiol. C.* **2022**, *51*, 100487.
73. C. Li, A. Iscen, L. C. Palmer, G. C. Scharz, S. I. Stupp, *J. Am. Chem. Soc.* **2020**, *142*, 8447-8453.
74. C. Li, Q. Xiong, T. D. Clemons, H. Sai, Y. Yang, M. H. Sangji, A. Iscen, L. C. Palmer, G. C. Schatz, S. I. Stupp, *Chem. Sci.* **2023**, *14*, 6095-6104.
75. T. Sendai, S. Biswas, T. Aida, *J. Am. Chem. Soc.* **2013**, *135*, 11509-11512.
76. Y. Xiao, S. Zarghami, K. Wagner, P. Wagner, K. C. Gordon, L. Florea, D. Diamond, D. L. Officer, *Adv. Mater.* **2018**, *30*, 1801821.
77. R. Matsushima, H. Sakaguchi, *J. Photochem. Photobiol.* A, **1997**, *108*, 239-245.
78. a) M. Vlajić, W. Unger, J. Bruns, K. Rueck-Braun, *Appl. Surf. Sci.* **2019**, *465*, 686-692; b) S. Klaes, C. Henry-de-Villeneuve, F. Ozanam, C. Barta, K. Rück-Braun, R. Métivier, P. Allongue, *J. Phys. Chem. C* **2019**, *123*, 12223-12233; c) Y. Jiao, R. Yang, Y. Luo, L. Liu, B. Xu, W. Tian, *CCS Chem.* **2022**, *4*, 132-140.
79. E. Weiderpass, B. W. Stewart, World Cancer Report, **2020** (IARC Press, Lyon, 2020).
80. N. Vasan, J. Baselga, D. M. Hyman, *Nature* **2019**, *575*, 299-309.
81. M. M. Gottesman, T. Fojo, S. E. Bates, *Nat. Rev. Cancer* **2002**, *2*, 48-58.
82. a) D. Peer, J. Karp, S. Hong, O. Farokhzard, R. Margalit, R. Langer, *Nat. Nanotechnol.* **2007**, *2*, 751-760; b) S. Senapati, A. K. Mahanta, S. Kumar, P. Maiti, *Sig. Transduct. Target. Ther.* **2018**, *3*, 7; c) A. M. Vargason, A. C. Anselmo, S. Mitragotri, *Nat. Biomed. Eng.* **2021**, *5*, 951-967; d) W. Li, J. Tang, D. Lee, T. R. Tice, S. P. Schwendeman, M. R. Prausnitz, *Nat. Rev. Mater.* **2022**, *7*, 406-420; e) J. Gao, J. M. Karp, R. Langer, N. Joshi, *Chem. Mater.* **2023**, *35*, 359-363.
83. K. K. Jain, *Drug Delivery Systems-An Overview* in *Drug Delivery Systems*. Eds. K. K. Jain. Humana Press: Totowa, **2008**, pp. 1-50.

84. a) R.H. Blythe (1956). *Sympathomimetic Preparation* (U.S. Patent No. US2738303A). United States Patent Office; b) K. Park, *J. Control. Release* **2014**, *190*, 3-8; c) H. Park, A. Otte, K. Park, *J. Control Release* **2022**, *342*, 53-65.
85. a) T. M. Allen, P. R. Cullis, *Adv. Drug Deliv. Rev.* **2013**, *65*, 36-48; b) S. Saraf, A. Jain, A. Tiwari, A. Verma, P. K. Panda, S. K. Jain, *Drug Deliv. Sci. Technol.* **2020**, *56*, 101549; c) D. Guimarães, A. Cavaco-Paulo, E. Nogueira, *Int. J. Pharm.* **2021**, *601*, 120571.
86. Y. Barenholz*, J. Control Release* **2012**, *160*, 117-134.
87. a) Z. Ahmad, A. Shah, M. Siddiq, H. Kraatz, *RSC Adv.* **2014**, *4*, 17028-17038; b) D. Hwang, J. D. Ramsey, A. V. Kabanov, *Adv. Drug Deliv. Rev.* **2020**, *156*, 80-118.
88. a) P. Kesharwani, K. Jain, N. K. Jain, *Prog. Polym. Sci.* **2014**, *39*, 268-307; b) A. Caminade, C. Turrin, *J. Mater. Chem. B* **2014**, *2*, 4055-4066; c) H. Wang, Q. Huang, H. Chang, J. Xiao, Y. Cheng, *Biomater. Sci.* **2016**, *4*, 375-390.
89. a) J. Li, D. J. Mooney, *Nat. Rev. Mater.* **2016**, 16071; b) Z. Sun, C. Song, C. Wang, Y. Hu, J. Wu, *Mol. Pharmaceutics* **2020**, *17*, 373-391.
90. a) D. Bobo, K. J. Robinson, J. Islam, K. J. Thurecht, S. R. Corrie, *Pharm. Res.* **2016**, *33*, 2373-2387; b) M. J. Mitchell, M. M. Billingsley, R. M. Haley, M. E. Wechsler, N. A. Peppas, R. Langer, *Nat. Rev. Drug Discov.* **2021**, *20*, 101-124; c) M. A. Beach, U. Nayanathara, Y. Gao, C. Zhang, Y. Xiong, Y. Wang, G. K. Such, *Chem. Rev.* **2024**, *124*, 5505-5616.
91. W. Zhang, Z. Zhang, Y. Zhang, *Nanoscale Res. Lett.* **2011**, *6*, 555.
92. a) Z. Song, X. Chen, X. You, K. Huang, A. Dhinakar, Z. Gu, J. Wu, *Biomater. Sci.* **2017**, *5*, 2369-2380; b) Z. Lian, T. Ji, *J. Mater. Chem. B* **2020**, *8*, 6517-6529; c) J. Yang, H. An, H. Wang, *ACS Appl. Bio Mater.* **2021**, *4*, 24-46; d) Y. Zhu, K. Tang, J. Lv, *Trends Pharmacol. Sci*. **2021**, *42*, 857-869.
93. T. Christian Ezike, U. S. Okpala, U. L. Onoja, C. P. Nwike, E. C. Ezeako, O. J. Okpara, C. C. Okoroafor, S. C. Eze, O. L. Kalu, E. C. Odoh, U. G. Nwadike, J. O. Ogbodo, B. U. Umeh, E. C. Ossai, B. C. Nwangumaa, *Heliyon* **2023**, *9*, e17488.
94. M. T. Manzari, Y. Shamay, H. Kiguchi, N. Rosen, M. Scaltriti, D. A. Heller, *Nat. Rev. Mater.* **2021,** *6*, 351-370.
95. J. Di, F. Xie, Y. Xu, *Adv. Drug Deliv. Rev*. **2020**, *154-155*, 151-162.
96. G. Mondal, S. Almawash, A. K. Chaudhary, R. I. Mahoto, *Mol. Pharmaceutics* **2017**, *14*, 3121-3133.
97. a) J. Sudimack, R. J. Lee, *Adv Drug Deliv Rev.* **2000**, *41*, 147-162; b) M. Ahmadi, C. A. Ritter, T. von Woedtke, S. Bekeschus, K. Wende, *Chem. Sci.* **2024**, *15*, 1966-2006.
98. a) Y. Sun, C. Kang, F. Liu, Y. Zhou, L. Luo, H. Qiao, *Drug Dev. Res.* **2017**, *78*, 283-291; b) Y. Cheng, Y. Ji, *Eur. J. Pharm. Sci.* **2019**, *128*, 8-17.
99. S. Mura, J. Nicolas, P. Couvreur, *Nat. Mater.* **2013**, *12*, 991-1003.
100. a) C. Álvarez-Lorenzo, A. Concheiro, *Chem. Commun.* **2014**, *50*, 7743-7765; b) V. P. Torchilin, *Fundamentals of Stimuli-responsive Drug and Gene Delivery Systems* in *Stimuli-responsive Drug Delivery Systems*. Eds. A. Singh, M. M. Amiji. Royal Society of Chemistry, **2018**, 1-32.
101. a) B. A. Webb, M. Chimenti, M. P. Jacobson, D. L. Barber, *Nat. Rev. Cancer* **2011**, *11*, 671-677; b) J. Liu, Y. Huang, A. Kumar, A. Tan, S. Jin, A. Mozhi, X. Liang, *Biotechnol. Adv.* **2014**, *32*, 693-710.
102. a) I. Mellman, R. Fuchs, A. Helenius, *Ann. Rev. Biochem.* **1986**, *55*, 663-670; b) X. He, J. Li, S. An, C. Jiang, *Ther. Deliv.* **2013**, *4*, 1499-1510; c) Z. Kaźmierczak, K. Szostak-Paluch, M. Przybyło, M. Langner, W. Witkiewicz, N. Jędruchniewicz, K. Dąbrowska, *Bioorg. Med. Chem.* **2020**, *28*, 115556.
103. a) D. Kim, E. S. Lee, K. T. Oh, Z. G. Gao, Y. H. Bae, *Small* **2008**, *4*, 2043-2050; b) B. Zhao, Y. Zhao, Y. Huang, L. Luo, P. Song, X. Wang, S. Chen, K. Yu, X. Zhang, Q. Zhang, *Biomaterials* **2012**, *33*, 2508-2520; c) W. Hao, D. Liu, Y. Shang, J. Zhang, S. Xu, H. Liu, *RSC Adv.* **2016,** *6***,** 29149-29158.
104. H. Wu, L. Zhu, V. P. Torchilin, *Biomaterials* **2013**, 34, 1213-1222.
105. a) J. Shin, P. Shum, D. H. Thompson, *J. Control Release* **2003**, *91*, 187-200; b) J. A. Boomer, M. M. Qualls, H. D. Inerowicz, R. H. Haynes, V. S. Patri, J. Kim, D. H. Thompson, *Bioconjugate Chem.* **2009**, *20*, 47-59; c) H. Kim, J. Van den Bossche, S. Hyun, D. H. Thompson, *Bioconjugate Chem.* **2012**, *23*, 2071-2077; d) J. Shin, P. Shum, J. Grey, S. Fujiwara, G. S. Malhotra, A. González-Bonet, S. Hyun, E. Moase, T. M. Allen, D. H. Thompson, *Mol. Pharmaceutics* **2012**, *9*, 3266-3276.
106. a) C. Ding, J. Gu, X. Qu, Z. Yang, *Bioconjugate Chem.* **2009**, *20*, 1163-1170; b) X. Qu, Z. Yang, *Chem. Asian J.* **2016**, *11*, 2633-2641; c) X. Zeng, G. Liu, W. Tao, Y. Ma, X. Zhang, F. He, J. Pan, L. Mei, G. Pan, *Adv. Funct. Mater.* **2017**, *27*, 1605985.
107. Y. Jin, L. Song, Y. Su, L. Zhu, Y. Pang, F. Qiu, G. Tong, D. Yan, B. Zhu, X. Zhu, *Biomacromolecules* **2011**, *12*, 3460-3468.

108. a) J. B. Matson, S. I. Stupp, *Chem. Commun.* **2011**, *47*, 7962-7964; b) S. J. Sonawane, R. S. Kalhapure, T. Govender, *Eur. J. Pharm. Sci.* **2017**, *99*, 45-65; c) J. Wahbeh, S. Milkowski, *SLAS Technol.* **2019**, *24*, 161-168.
109. a) L. Li, K. Knickelbein, L. Zhang, J. Wang, M. Obrinske, G. Z. Ma, L. Zhang, L. Bitterman, W. Du, *Chem. Commun.* **2015**, *51*, 13078-13081; c) G. Yan, J. Wang, P. Zhang, L. Hu, X. Wang, G. Yang, S. Fu, X. Cheng, R. Tang, *Polym. Chem.* **2017**, *8*, 2063-2073; c) M. Sun, D. Li, X. Wang, L. He, X. Lv, Y. Xu, R. Tang, *J. Mater. Chem. B* **2019**, *7*, 3692-3703.
110. a) Z. Shi, Q. Li, L. Mei, *Chin. Chem. Lett.* **2020**, *31*, 1345-1356; b) H. Ding, P. Tan, S. Fu, X. Tian, H. Zhang, X. Ma, Z. Gu, K. Luo, *J. Control Release* **2022**, *348*, 206-238.
111. a) C. Lee, S. Cheng, I. Huang, J. S. Souris, C. Yang, C. Mou, L. Lo, *Angew. Chem. Int. Ed.* **2010**, *49*, 8214-8219; b) D. Ren, F. Kratz, S. Wang, *Small* **2011**, *7*, 1051-1560; c) V. Rao N, S. R. Mane, A. Kishore, J. D. Sarma, R. Shunmugam, *Biomacromolecules* **2012**, *13*, 221-230; d) J. D. Wallat, J. K. Harrison, J. K. Pokorski, *Mol. Pharmaceutics* **2018**, *15*, 2954-2962; e) H. Cai, P. Tan, X. Chen, M. Kopytynski, D. Pan, X. Zheng, L. Gu, Q. Gong, X. Tian, Z. Gu, H. Zhang, R. Chen, K. Luo, *Adv. Mater.* **2022**, *34*, 2108049.
112. J. Du, X. Du, X. Mao, J. Wang, *J. Am. Chem. Soc.* **2011**, *133*, 17560-17563.
113. F. Wang, Y. Wang, S. Dou, M. Xiong, T. Sun, J. Wang, *ACS Nano* **2011**, *5*, 3679-3692.
114. Y. Jin, Y. Huang, H. Yang, G. Liu, R. Zhao, *Chem. Commun.* **2015**, *51*, 14454-14457.
115. X. Duan, J. Xiao, Q. Yin, Z. Zhang, H. Yu, S. Mao, Y. Li, *ACS Nano* **2013**, *7*, 5858-5869.
116. R. Cheng, F. Feng, F. Meng, C. Deng, J. Feijen, Z. Zhong, *J. Control. Release* **2011**, *152*, 2-12.
117. a) J. Wu, L. Zhao, X. Xu, N. Bertrand, W. Choi, B. Yammen, J. Shi, V. Shah, M. Mulvale, J. L. MacLean, O. C. Farokhzad, *Angew. Chem. Int. Ed.* **2015**, *54*, 9218-9223; b) N. Liu, Y. Tan, Y. Hu, T. Meng, L. Wen, J. Liu, B. Cheng, H. Yuan, X. Huang, F. Hu, *ACS Appl. Mater. Interfaces* **2016**, *8*, 33148-33156; c) X. He, K. Cai, Y. Zhang, Y. Lu, Q. Guo, Y. Zhang, L. Liu, C. Ruan, Q. Chen, X. Chen, C. Li, T. Sun, J. Cheng, C. Jiang, *ACS Appl. Mater. Interfaces* **2018**, *10*, 39455-39467.
118. A. G. Cheetham, P. Zhang, Y. Lin, L. L. Lock, H. Cui, *J. Am. Chem. Soc.* **2013**, *135*, 2907-2910.
119. J. Shen, Q. Wang, J. Fang, W. Shen, D. Wu, G. Tang, J. Yang, *RSC Adv.* **2019**, *9*, 37232-37240.
120. S. Wang, H. Wang, Z. Liu, L. Wang, X. Wang, L. Su, J. Chang, *Nanoscale*, **2014**, *6*, 7635-7642.
121. Y. Wang, L. Zhang, X. Zhang, X. Wei, Z. Tang, S. Zhou, *ACS Appl. Mater. Interfaces* **2016**, *8*, 5833-5846.
122. a) Q. Hu, P. S. Katti, Z. Gu, *Nanoscale*, **2014**, *6*, 12273-12286; b) M. Shahriari, M. Zahiri, K. Abnous, S. M. Taghdisi, M. Ramezani, M. Aliboland, *J. Control. Release* **2019**, *308,* 172-189.
123. Q. Yao, L. Kou, Y. Tu, L. Zhu, *Trends Pharmacol. Sci.* **2018**, *39*,766-781.
124. M. Cao, S. Lu, N. Wang, H. Xu, H. Cox, R. Li, T. Waigh, Y. Han, Y. Wang, J. R. Lu, *ACS Appl. Mater. Interfaces* **2019**, *11*, 16357-16366.
125. a) L. Zhu, P. Kate, V. P. Torchilin, *ACS Nano* **2012**, *6*, 3491-3498; b) X. Gao, J. Zhang, Z. Huang, T. Zuo, Q. Lu, G. Wu, Q. Shen, *ACS Appl. Mater. Interfaces* **2017**, *9*, 29457-29468.
126. V. S. Egorova, E. P. Kolesova, M. Lopus, N. Yan, A. Parodi, A. A. Zamyatnin, *Pharmaceutics* **2023**, *15*, 1848-1868.
127. M. J. Webber, C. J. Newcomb, R. Bitton, S. I. Stupp, *Soft Matter* **2011**, *7*, 9665-9672.
128. Y. Li, Y. Chen, H. Dong, C. Dong, *Med. Chem. Commun.* **2015**, *6*, 1874-1881.
129. R. Barat, T. Legigan, I. Tranoy-Opalinski, B. Renoux, E. Péraudeau, J. Clarhaut, P. Poinot, A. E. Fernandes, V. Aucagne, D. A. Leigh, S. Papot, *Chem. Sci.* **2015**, *6*, 2608-2613.
130. Y. Li, X. Xu, X. Zhang, Y. Li, Z. Zhang, Z. Gu, *ACS Nano* **2017**, *11*, 416-429.
131. a) J. Dobson, *Drug. Dev. Res.* **2006**, *67*, 55-60; b) A. Grillone, G. Ciofani, *Chem. Eur. J.* **2017**, *23*, 16109-16114; c) Y. Liu, M. Li, F. Yang, N. Gu, *Sci. China Mater.* **2017**, *60*, 471-486; d) G. M. Ziarani, M. Malmir, N. Lashgari, A. Badiei, *RSC Adv.* **2019**, *9*, 25094-25106.
132. H. Arami, A. Khandhar, D. Liggitt, K. M. Krishnan, *Chem. Soc. Rev.* **2015**, *44*, 8576-8607.
133. A. Quarta, M. Amorín, M. J. Aldegunde, L. Blasi, A. Ragusa. S. Nitti, G. Pugliese, G. Gigli, J. R. Granja, T. Pellegrino, *Nanoscale* **2019**, *11*, 23482-23497.
134. A. Ito, M. Shinkai, H. Honda, T. Kobayashi, *J. Biosci. Bioeng.* **2005**, *100*, 1-11.
135. C. R. Thomas, D. P. Ferris, J. Lee, E. Choi, M. H. Cho, E. S. Kim, J. F. Stoddart, J. Shin, J. Cheon, J. I. Zink, *J. Am. Chem. Soc.* **2010**, *132*, 10623-10625.
136. W. Zhao, Y. Zhao, Q. Wang, T. Liu, J. Sun, R. Zhang, *Small* **2019**, *15*, 1903060.
137. C. Álvarez-Lorenzo, L. Bromberg, A. Concheiro, *Photochem. Photobiol.* **2009**, *85*, 848-860.
138. C. S. Linsley, B. M. Wu, *Ther. Deliv.* **2017**, *8*, 89-107.
139. A. P. Pelliccioli, J. Wirz, *Photochem. Photobiol. Sci.* **2002**, *1*, 441-458.
140. H. Zhao, E. S. Sterner, E. B. Coughlin, P. Theato, *Macromolecules* **2012**, *45*, 1723-1736.

141. X. Tan, B. B. Li, X. Lu, F. Jia, C. Santori, P. Menon, H. Lui, B. Zhang, J. J. Zhao, K. Zhang, *J. Am. Chem. Soc.* **2015**, *137*, 6112-6115.
142. J. Zhu, T. Guo, Z. Wang, Y. Zhao, *J. Control. Release* **2022**, *345*, 475-493.
143. D. Wang, S. Wu, *Langmuir* **2016**, *32*, 632-636.
144. A. Fagan, M. Bartkowski, S. Giordani, *Front. Chem.* **2021**, *9*, 720087.
145. S. Jia, W. Fong, B. Graham, B. J. Boyd, *Chem. Mater.* **2018**, *30*, 2873-2887.
146. a) N. S. Abadeer, C. J. Murphy, *J. Phys. Chem. C* **2016**, *120*, 4691-4716; b) K. Sztandera, M. Gorzkiewicz, B. Klajnert-Maculewicz, *Mol. Pharmaceutics* **2019**, *16*, 1-23.
147. H. Ke, X. Yue, J. Wang, S. Xing, Q. Zhang, Z. Dai, J. Tian, Sh. Wang, Y. Jin, *Small* **2014**, *10*, 1220-1227.
148. a) X. Huang, I. H. El-Sayed, W. Qian, M. A. El-Sayed, *J. Am. Chem. Soc.* **2006**, *128*, 2115-2120; b) W. I. Choi, A. Sahu, Y. H. Kim, G. Tae, *Ann. Biomed. Eng.* **2012**, *40*, 534-546.
149. a) H. Yuan, A. M. Fales, T. Vo-Dinh, *J. Am. Chem. Soc.* **2012**, *134*, 11358-11361; b) Y. Liu, H. Yuan, A. M. Fales, J. K. Register, T. Vo-Dinh, *Front. Chem.* **2015**, *3*, 51.
150. J. An, X. Yang, K. Cheng, X. Song, L. Zhang, C. Li, X. Zhang, Y. Xuan, Y. Song, B. Fang, X. Hou, Y. Zhao, B. Liu, *ACS Appl. Mater. Interfaces* **2017**, *9*, 41748-41759.
151. a) S. R. Sirsi, M. A. Borden, *Adv. Drug Deliv. Rev.* **2014**, *72*, 3-14; b) X. Cai, Y. Jiang, M. Lin, J. Zhang, H. Guo, F. Yang, W. Leung, C. Xu, *Front. Pharmacol*. **2020**, *10*, 1650; c) P. Wei, E. J. Cornel, J. Du, *Drug Deliv. Transl. Res.* **2021**, *11*, 1323-1339.
152. a) M. C. Cochran, J. Eisenbrey, R. O. Ouma, M. Soulen, M. A. Wheatley, *Int. J. Pharm.* **2011**, *414*, 161-170; b) C. Niu, Z. Wang, G. Lu, T. M. Krupka, Y. Sun, Y. You, W. Song, H. Ran, P. Li, Y. Zheng, *Biomaterials* **2013**, *34*, 2307-2317; c) C. McEwan, C. Fowley, N. Nomikou, B. McCaughan, A. P. McHale, J. F. Callan, *Langmuir* **2014**, *30*, 14926-14930.
153. a) T. Yin, P. Wang, J. Li, Y. Wang, B. Zheng, R. Zheng, D. Cheng, X. Shuai, *Biomaterials* **2014**, *35*, 5932-5943; b) C. Hernandez, S. Gulati, G. Fioravanti, P. L. Stewart, A. A. Exner, *Sci. Rep.* **2017**, *7*, 13517.
154. a) W. Tang, Z. Yang, S. Wang, Z. Wang, J. Song, G. Yu, W. Fan, Y. Dai, J. Wang, L. Shan, G. Niu, Q. Fan, X. Chen, *ACS Nano* **2018**, *12*, 2610-2622; b) L. Zhang, T. Yin, B. Li, R. Zheng, C. Qiu, K. S. Lam, Q. Zhang, X. Shuai, *ACS Nano* **2018**, *12*, 3449-3460.
155. a) N. Rapoport, K. Nam, R. Gupta, Z. Gao, P. Mohan, A. Payne, N. Todd, X. Liu, T. Kim, J. Shea, C. Scaife, D. L. Parker, E. Jeong, A. M Kennedy, *J. Control Release* **2011**, *153*, 4-15; b) M. Javadi, W. G. Pitt, D. M. Belnap, N. H. Tsosie, J. M. Hartley, *Langmuir* **2012**, *28*, 14720-14729.
156. a) Z. Gao, H. D. Fain, N. Rapoport, *Mol. Pharm.* **2004**, *1*, 317-330; b) P. Wu, Y. Jia, F. Qu, Y. Sun, P. Wang, K. Zhang, C. Xu, Q. Liu, X. Wang, *ACS Appl. Mater. Interfaces* **2017**, *9*, 25706-25716.
157. a) N. Huebsch, C. J. Kearney, X. Zhao, J. Kim, C. A. Cezar, Z. Suo, D. J. Mooney, *Proc. Natl. Acad. Sci. U. S. A.* **2014**, *111*, 9762-9767; b) Y. Zhou, G. Liu, S. Guo, *J. Mater. Chem. B* **2022**, *10*, 3947-3958.
158. N. Y. Rapoport, A. M. Kennedy, J. E. Shea, C. L. Scaife, K. Nam, *J. Control. Release* **2009**, *138*, 268-276.
159. P. Wei, M. Sun, B. Yang, J. Xiao, J. Du, *J. Control. Release* **2020**, 322, 81-94.
160. P. De Santis, S. Morosetti, R. Rizzo, *Macromolecules* **1974**, *7*, 52-58.
161. L. Tomasic, G. P. Lorenzi, *Helv. Chim. Acta* **1987**, *70*, 1012-1016.
162. M. R. Ghadiri, J. R. Granja, R. A. Milligan, D. E. McRee, N. Khazanovich, *Nature*, **1993**, *366*, 324-327.
163. a) D. Seebach, J. L. Matthews, A. Meden, T. Wessels, C. Baerlocher, L. B. McCusker, *Helv. Chim. Acta* **1997**, *80*, 173-182; b) T. D. Clark, L. K. Buehler, M. R. Ghadiri, *J. Am. Chem. Soc.* **1998**, *120*, 651-656; c) F. Fujimura, T. Hirata, T. Morita, S. Kimura, *Biomacromolecules* **2006**, *7*, 2394-2400; d) F. Fujimura, Y. Horikawa, T. Morita, J. Sugiyama, S. Kimura, *Biomacromolecules* **2007**, *8*, 611-616; e) Y. Ishihara, S. Kimura, *J. Pept. Sci.* **2010**, *16*, 110-114.
164. a) M. Amorín, L. Castedo, J. R. Granja, *J. Am. Chem. Soc.* **2003**, *125*, 2844-2845; b) C. Reiriz, R. J. Brea, R. Arranz, J. L. Carrascosa, A. Garibotti, B. Manning, J. M. Valpuesta, R. Eritja, L. Castedo, J. R. Granja, *J. Am. Chem. Soc.* **2009**, *131*, 11335-11337; c) R. Hourani, C. Zhang, R. van der Weegen, L. Ruiz, C. Li, S. Keten, B. A. Helms, T. Xu, *J. Am. Chem. Soc.* **2011**, *133*, 15296-15299.
165. a) M. Calvelo, A. Lamas, A. Guerra, M. Amorín, R. Garcia-Fandino, J. R. Granja, *Chem. Eur. J.* **2020**, *26*, 5846-5858; b) A. Blanco-González, M. Calvelo, P. F. Garrido, M. Amorín, J. R. Granja, Á. Piñeiro, R. Garcia-Fandino, *Front. Chem.* **2021**, *9*, 704160.
166. a) W. S. Horne, C. D. Stout, M. R. Ghadiri, *J. Am. Chem. Soc.* **2003**, *125*, 9372-9376; b) S. M. Darnall, C. Li, M. Dunbar, M. Alsina, S. Keten, B. A. Helms, T. Xu, *J. Am. Chem. Soc.* **2019**, *141*, 10953-10957.
167. a) R. J. Brea, C. Reiriz, J. R. Granja, *Chem. Soc. Rev.* **2010**, *39*, 1448-1456; b) R. Chapman, M. Danial, M. L. Koh, K. A. Jolliffe, S. Perrier, *Chem. Soc. Rev.* **2012**, *41*, 6023-6041.
168. Q. Song, Z. Cheng, M. Kariuki, S. C. L. Hall, S. K. Hill, J. Y. Rho, S. Perrier, *Chem. Rev.* **2021**, *121*, 13936-13995.

169. N. Khazanovich, J. R. Granja, D. E. McRee, R. A. Milligan, M. R. Ghadiri, *J. Am. Chem. Soc.* **1994**, *116*, 6011-6012.
170. N. Rodríguez-Vázquez, M. Amorín, J. R. Granja, *Org. Biomol. Chem.* **2017**, *15*, 4490-4505.
171. a) M. R. Ghadiri, K. Kobayashi, J. R. Granja, R. K. Chadha, D. E. McRee, *Angew. Chem. Int. Ed. Engl.* **1995**, *34*, 93-95; b) T. D. Clark, J. M. Buriak, K. Kobayashi, M. P. Isler, D. E. McRee, M. R. Ghadiri, *J. Am. Chem. Soc.* **1998**, *120*, 8949-8962.
172. K. Kobayashi, J. R. Granja, M. R. Ghadiri, *Angew. Chem. Int. Ed. Engl.* **1995**, *34*, 95-98.
173. A. Fuertes, M. Amorín, J. R. Granja, *Chem. Commun.* **2020**, *56*, 46-49.
174. a) A. Fuertes, M. Amorín, J. R. Granja, *Supramol. Chem.* **2020**, *32*, 239-246; b) V. López-Corbalán, A. Fuertes, A. L. Llamas-Saiz, M. Amorín, J. R. Granja, *Nat. Commun.* **2024**, *15*, 6055.
175. A. Fuertes, H. L. Ozores, M. Amorín, J. R. Granja, *Nanoscale*, **2017**, *9*, 748-753.
176. H. L. Ozores, M. Amorín, J. R. Granja, *J. Am. Chem. Soc.* **2017**, *139*, 776-784.
177. a) N. Rodríguez-Vázquez, R. García-Fandiño, M. J. Aldegunde, J. Brea, M. Isabel Loza, M. Amorín, J. R. Granja, *Org. Lett.* **2017**, *19*, 2560-2563; b) A. Pizzi, H. L. Ozores, M. Calvelo, R. García-Fandiño, M. Amorín, N. Demitri, G. Terraneo, S. Bracco, A. Comotti, P. Sozzani, C. X, Bezuidenhout, P. Metrangolo, J. R. Granja, *Angew. Chem. Int. Ed.* **2019**, *58*, 14472-14476.
178. M. S. Vollmer, T. D. Clark, C. Steinem, M. R. Ghadiri, *Angew. Chem. Int. Ed.* **1999**, *38*, 1598-1601.
179. C. Steinem, A. Janshoff, M. S. Vollmer, M. R. Ghadiri, *Langmuir* **1999**, *15*, 3956-3964.
180. I. Insua, J. Montenegro, *J. Am. Chem. Soc.* **2020**, *142*, 300-307.
181. S. Díaz, I. Insua, G. Bhak, J. Montenegro, *Chem. Eur. J.* **2020**, 26, 14765-14770.
182. I. Insua, A. Cardellini, S. Díaz, J. Bergueiro, R. Capelli, G. M. Pavan and J. Montenegro, *Chem. Sci.* **2023**, *14*, 14074–14081.
183. E. González-Freire, F. Novelli, A. Pérez-Estévez, R. Seoane, M. Amorín, J. R. Granja, *Chem. Eur. J.* **2021**, *27*, 3029-3038.
184. R. Chapman, K. A. Jolliffe, S. Perrier, *Polym. Chem.* **2011**, *2*, 1956-1963.
185. J. C. Brendel, J. Sanchis, S. Catrouillet, E. Czuba, M. Z. Chen, B. M. Long, C. Nowell, A. Johnston, K. A. Jolliffe, S. Perrier, *Angew. Chem. Int. Ed.* **2018**, *57*, 16678-16682.
186. A. Bayón-Fernández, A. Méndez-Ardoy, C. Alvarez-Lorenzo, J. R. Granja, J. Montenegro, *J. Mater. Chem. B* **2023**, *11*, 606-617.
187. A. Lamas, A. Guerra, M. Amorín, J. R. Granja, *Chem. Sci.* **2018**, *9*, 8228-8233.
188. N. Rodríguez-Vázquez, H. L. Ozores, A. Guerra, E. González-Freire, A. Fuertes, M. Panciera, J. M. Priegue, J. Outeiral, J. Montenegro, R. García-Fandino, M. Amorín, J. R. Granja, *Curr. Top. Med. Chem.* **2014**, *14*, 2647-2661.
189. J. Montenegro, M. R. Ghadiri, J. R. Granja, *Acc. Chem. Res.* **2013**, *46*, 2955-2965.
190. T. M. Fyles, *Chem. Soc. Rev.* **2007**, *36*, 335-347.
191. M. R. Ghadiri, J. R. Granja, L. K. Buehler, *Nature* **1994**, *369*, 301-304.
192. H. S. Kim, J. D. Hartgerink, M. R. Ghadiri, *J. Am. Chem. Soc.* **1998**, *120*, 4417-4424.
193. J. R. Granja, M. R. Ghadiri, *J. Am. Chem. Soc.* **1994**, *116*, 10785-10786.
194. J. Sánchez-Quesada, H. S. Kim, M. R. Ghadiri, *Angew. Chem. Int. Ed.* **2001**, *40*, 2503-2506.
195. a) J. Sánchez-Quesada, M. P. Isler, M. R. Ghadiri, *J. Am. Chem. Soc.* **2002**, *124*, 10004-10005; b) K. Motesharei, M. R. Ghadiri, *J. Am. Chem. Soc.* **1997**, *119*, 11306-11312.
196. a) R. García-Fandiño, J. R. Granja, M. D'Abramo, M. Orozco, *J. Am. Chem. Soc.* **2009**, *131*, 15678-15686; b) R. García-Fandiño, M. Amorín, L. Castedo, J. R. Granja, *Chem. Sci.* **2012**, *3*, 3280-3285; c) L. Ruiz, A. Benjamin, M. Sullivan, S. Keten, *J. Phys. Chem. Lett.* **2015**, *6*, 1514-1520; d) M. Calvelo, C. I. Lynch, J. R. Granja, M. S. P. Sansom, R. Garcia-Fandiño, *ACS Nano* **2021**, *15*, 7053-7064.
197. M. Danial, C. M.-N. Tran, K. A. Jolliffe, S. Perrier, *J. Am. Chem. Soc.* **2014**, *136*, 8018-8026.
198. a) A. H. Holmes, L. S. P. Moore, A. Sundsfjord, M. Steinbakk, S. Regmi, A. Karkey, P. J Guerin, L. J. V. Piddock, *Lancet.* **2016**, *387*, 176-187; b) T. Pulingam, T. Parumasivam, A. M. Gazzali, A. M. Sulaiman, J. Y. Chee, M. Lakshmanan, C. F. Chin, K. Sudesh, *Eur. J. Pharm. Sci.* **2022**, 170, 106103.
199. S. Fernandez-Lopez, H.-S. Kim, E. C. Choi, M. Delgado, J. R. Granja, A. Khasanov, K. Kraehenbuehl, G. Long, D. A. Weinberger, K. M. Wilcoxen, M. R. Ghadiri, *Nature* **2001**, *412*, 452-455.
200. V. Dartois, J. Sanchez-Quesada, E. Cabezas, E. Chi, C. Dubbelde, C. Dunn, J. Granja, C. Gritzen, D. Weinberger, M. R. Ghadiri, T. R. Parr, *Antimicrob. Agents Chemother*. **2005**, *49*, 3302-3310.
201. B. Claro, E. González-Freire, M. Calvelo, L. J. Bessa, E. Goormaghtigh, M. Amorín, J. R. Granja, R. Garcia-Fandiño, M. Bastos, *Colloids Surf. B Biointerfaces*. **2020**, *196*, 111349.
202. L. Motiei, S. Rahimipour, D. A. Thayer, C. Wong, M. R. Ghadiri, *Chem. Commun.* **2009**, *25*, 3693-3695.
203. H. Liu, J. Chen, Q. Shen, W. Fu, W. Wu, *Mol. Pharmaceutics* **2010**, *7*, 1985-1994.

204. R. Vijayaraj, S. V. Damme, P. Bultinck, V. Subramanian, *Phys. Chem. Chem. Phys.* **2013**, *15*, 1260-1270.
205. J. Chen, B. Zhang, F. Xia, Y. Xie, S. Jiang, R. Su, Y. Lua, W. Wu, *Nanoscale*, **2016**, *8*, 7127-7136.
206. Y. Wang, S. Yi, L. Sun, Y. Huang, S. C. Lenaghan, M. Zhang, *J. Biomed. Nanotechnol.* **2014**, *10*, 445-454.
207. a) B. M. Blunden, R. Chapman, M. Danial, H. Lu, K. A. Jolliffe, S. Perrier, M. H. Stenzel, *Chem. Eur. J.* **2014**, *20*, 12745-12749; b) S. C. Larnaudie, J. C. Brendel, I. Romero-Canelón, C. Sanchez-Cano, S. Catrouillet, J. Sanchis, J. P. C. Coverdale, J. Song, A. Habtemariam, P. J. Sadler, K. A. Jolliffe, S. Perrier, *Biomacromolecules* **2018**, *19*, 239-247.
208. S. K. Hill, R. M. England, S. Perrier, *J. Control Release* **2024**, *367*, 687-696.
209. J. Yang, J. Song, Q. Song, J. Y. Rho, E. D. H. Mansfield, S. C. L. Hall, M. Sambrook, F. Huang, S. Perrier, *Angew. Chem. Int. Ed.* **2020**, *59*, 8860-8863.
210. S. C. Larnaudie, J. C. Brendel, K. A. Jolliffe, S. Perrier, *ACS Macro Lett.* **2017**, *6*, 1347-1351.
211. Q. Song, J. Yang, S. C. L. Hall, P. Gurnani, S. Perrier, *ACS Macro Lett.* **2019**, *8*, 1347-1352.
212. M. Hartlieb, S. Catrouillet, A. Kuroki, C. Sanchez-Cano, R. Peltier, S. Perrier, *Chem. Sci.* **2019**, *10*, 5476-5483.
213. Q. Song, J. Yang, J. Y. Rho, S. Perrier, *Chem. Commun.* **2019**, *55*, 5291-5294.
214. N. Cissé, T. Kudernac, *ChemSystemsChem*, **2020**, *2*, e2000012.
215. A. Méndez-Ardoy, J. R. Granja, J. Montenegro, *Nanoscale Horiz.* **2018**, *3*, 391-396.
216. A. Méndez-Ardoy, A. Bayón-Fernández, Z. Yu, C. Abell, J. R. Granja, J. Montenegro, *Angew. Chem. Int. Ed.* **2020**, *59*, 6902-6908.
217. F. Novelli, M. Vilela, A. Pazó, M. Amorín, J. R. Granja. *Angew. Chem. Int. Ed.* **2021**, *60*, 18838-18844.
218. a) D. Greene, S. L. Misrock, J. R. Wolfe, *J. Am. Chem. Soc.* **1955**, *77*, 3852-3855; b) D. E. Applequist, R. L. Litle, E. C. Friedrich, R. E. Wall, *J. Am. Chem. Soc.* **1959**, *81*, 452-456; c) H. Becker, *Chem. Rev.* **1993**, *93*, 145-172; d) H. Bouas-Laurent, A. Castellan, J.-P. Desvergnea, R. Lapouyadec, *Chem. Soc. Rev.* **2000**, *29*, 43-55; e) H. Bouas-Laurent, A. Castellan, J.-P. Desvergnea, R. Lapouyadec, *Chem. Soc. Rev.* **2001**, *30*, 248-263; f) M. Yoshizawa, J. K. Klosterman, *Chem. Soc. Rev.* **2014**, *43*, 1885-1898.
219. a) Z. Hou, W. M. Nau, R. Hoogenboom, *Polym. Chem.* **2021**, *12*, 307-315; b) J. Bai, Z. Shi, J. Yin, M. Tian, R. Qu, *Adv. Funct. Mater.* **2018**, *28*, 1800939; c) Z. Wang, L. Guo, H. Xiao, H. Cong, S. Wang, *Mater. Horiz.* **2020**, *7*, 282-288; d) M. C. Paderes, M. J. Diaz, C. Angelo Pagtalunan, D. A. Bruzon, G. A Tapang, *Chem Asian J.* **2022**, *17*, e202200193.
220. A. Saruwatari, R. Tamate, H. Kokubo, M. Watanabe, *Chem. Commun.* **2018**, *54*, 13371-13374.
221. Z. Jiang, M. L. Tan, M. Taheri, Q. Yan, T. Tsuzuki, M. G. Gardiner, B. Diggle, L. A. Connal, *Angew. Chem. Int. Ed.* **2020**, *59*, 7049-7056.
222. J. Xu, Y. Chen, L. Wu, C. Tung, Q. Yang, *Org. Lett.* **2013**, *15*, 6148-6151.
223. P. R. A. Chivers, R. S. Dookie, J. E. Gough, S. J. Webb, *Chem. Commun.* **2020**, *56*, 13792-13795.
224. T. Kim, L. Zhu, L. J. Mueller, C. J. Bardeen, *J. Am. Chem. Soc.* **2014**, *136*, 6617-6625.
225. a) J. Y. Rho, S. Perrier, *ACS Macro Lett.* **2021**, *10*, 258-271; b) S. Catrouillet, J. C. Brendel, S. Larnaudie, T. Barlow, K. A. Jolliffe, S. Perrier, *ACS Macro Lett.* **2016**, *5*, 1119-1123; c) R. Chapman, M. L. Koh, G. G. Warr, K. A. Jolliffe, S. Perrier, *Chem. Sci.* **2013**, *4*, 2581-2589; d) J. Y. Rho, J. C. Brendel, L. R. MacFarlane, E. D. H. Mansfield, R. Peltier, S. Rogers, M. Hartlieb, S. Perrier, *Adv. Funct. Mater.* **2017**, *27*, 201704569.
226. M. R. Silk, J. Newman, J. C. Ratcliffe, J. F. White, T. Caradoc-Davies, J. R. Price, S. Perrier, P. E. Thompson, D. K. Chalmers, *Chem. Commun.* **2017**, *53*, 6613-6616.
227. R. P. Cheng, S. H. Gellman, W. F. DeGrado, *Chem. Rev.* **2001**, *101*, 3219-3232.
228. a) M. R. Silk, J. Newman, J. C. Ratcliffe, J. F. White, T. Caradoc-Davies, J. R. Price, S. Perrier, P. E. Thompson, D. K. Chalmers, *Chem. Commun.* **2017**, *53*, 6613-6616; b) T. D. Clark, L. K. Buehler, M. R. Ghadiri, *J. Am. Chem. Soc.* **1998**, *120*, 651-656; c) D. Seebach, J. L. Matthew, T. W. A. Meden, C. Baerlocher, L. B. McCusker, *Helv. Chim. Acta* **1997**, *80*, 173-182; d) T. Marmin, Y. L. Dory, *Chem. Eur. J.* **2019**, *25*, 6707-6711; e) S. Leclair, P. Baillargeon, R. Skouta, D. Gauthier, Y. Zhao, Y. L. Dory, *Angew. Chem. Int. Ed.* **2004**, *43*, 349-353; f) Y. Tabata, Y. Kamano, H. Uji, T. Imai, S. Kimura, *Chem. Lett.* **2019**, *48*, 322-324.
229. a) J. M. Palomo, *RSC Adv.* **2014**, *4*, 32658-32672; b) P. Rovero, L. Quartara, G. Fabbri, *Tetrahedron Lett.* **1991**, *32*, 2639-2642; c) A. El-Faham, F. Albericio, *Chem. Rev.* **2011**, *111*, 6557-6602; d) F. Albericio, *Biopolymers* **2000**, *55*, 123-139.
230. a) R. M. P. Da Silva, D. Van Der Zwaag, L. Albertazzi, S. S. Lee, E. W. Meijer, S. I. Stupp, *Nat. Commun.* **2016**, *7*, 11561; b) R. Mishra, D. Sjölander, P. Hammarström, *Mol. BioSyst.* **2011**, *7*, 1232-1240; c) M. C. A. Stuart, J. C. van de Pas, J. B. F. N. Engberts, *J. Phys. Org. Chem.* **2005**, *18*, 929-934.
231. a) H. Naiki, K. Higuchi, M. Hosokawa, T. Takeda, *Anal. Biochem.* **1989**, *177*, 244-249; b) M. Girych, G. Gorbenko, I. Maliyov, V. Trusova, C. Mizuguchi, H. Saito, P. Kinnunen, *Methods Appl. Fluoresc.* **2016**, *4*, 034010; c) M. J. Groenning, *J. Chem. Biol.* **2010**, *3*, 1-18.

232. a) J. Kubelka, T. A. Keiderling, *J. Am. Chem. Soc.* **2001**, *123*, 12048-12058; b) Y. Zou, Y. Li, W. Hao, X. Hu, G. Ma, *J. Phys. Chem. B* **2013**, *117*, 4003-4013.
233. S. Krimm, J. Bandekar in Advances in Protein Chemistry, *Vol. 38* (Eds.: C. B. Anfinsen, J. T. Edsall, F. M. Richards), Elsevier, Amsterdam, **1986**, pp. 181-364.
234. C.-H. Tung, J.-Q. Guan, *J. Org. Chem.* **1998**, *63*, 5857-5862.
235. a) W. Fudickar, T. Linker, *Chem. Eur. J.* **2011**, *17*, 13661-13664; b) W. Fudickar, T. Linker, *J. Am. Chem. Soc.* **2012**, *134*, 15071-15082; c) Y. Han, M. Liu, R. Zhong, Z. Gao, Z. Chen, M. Zhang, F. Wang, *Inorg. Chem.* **2019**, *58*, 12407-12414.
236. a) H. D. Roth, *Light-Induced Chemistry of Oximes and Derivatives*, John Wiley & Sons Ltd, Chichester, UK, **2010**; b) S. Mondal, P. Chakraborty, P. Bairi, D. P. Chatterjee, A. K. Nandi, *Chem. Commun.* **2015**, *51*, 10680-10683; c) B. Bai, M. Zhang, N. Ji, J. Wei, H. Wang, M. Li, *Chem. Commun.* **2017**, *53*, 2693-2696.
237. A. Castellan, R. Lapouyade, H. Boutas-Laurent, J. Y. Lallemand, *Tetrahedron Lett.* **1975**, *29*, 2467-2470.
238. A. Tron, P. J. Thornton, C. Lincheneau, J.-P. Desvergne, N. Spencer, J. H. R. Tucker, N. D. McClenaghan, *J. Org. Chem.* **2015**, *80*, 988-996.
239. a) M. Fréneau, P. de Sainte Claire, N. Hoffmann, J. Vors, J. Geist, M. Euvrardd, C. Richard, *RSC Adv.* **2016**, *6*, 5512-5522. b) B. Sevilla-Morán, P. Sandín-España, M. J. Vicente-Arana, J. L. Alonso-Prados, J. M. García-Baudín, *J. Photochem. Photobiol. A Chem.* **2008**, *198*, 162-168.
240. M. Vilela-Picos, F. Novelli, A. Pazó, A. Méndez-Ardoy, G. Marafon, M. Amorín, A. Moretto, J. R. Granja. *Chem* **2023**, *9*, 3365-3378.
241. M. Vilela-Picos, F. Novelli, A. Méndez-Ardoy, A. Moretto, J. R. Granja. *STAR Protocols* **2024**, *5*, 103031.
242. Q. Zhang, D. Qu, H. Tian, *Adv. Opt. Mater.* **2019**, *7*, 1900033.
243. G. Marafon, M. Crisma, A. Moretto, *Angew. Chem. Int. Ed.* **2018**, *57*, 10217-10220.
244. G. Marafon, M. Crisma, A. Moretto, *Org. Lett.* **2019**, *21*, 4182-4186.
245. G. Marafon, M. Crisma, A. Masato, N. Plotegher, L. Bubacco, A. Moretto, *Angew. Chem. Int. Ed.* **2021**, *60*, 5173-5178.
246. M. Pollastrini, G. Marafon, J. Clayden, A. Moretto, *Chem. Commun.* **2021**, *57*, 2269-2272.
247. a) G. M. Whitesides, *Nature*, **2006**, *442*, 368-373; b) L. Shang, Y. Cheng, Y. Zhao, *Chem. Rev.* **2017**, *117*, 7964-8040; c) D. Khoeini, T. F. Scott, A. Neild, *Lab Chip*, **2021**, *21*, 1661-1675; d) P. Zhu, L. Wang, *Lab Chip* **2016**, *17*, 34-75.
248. a) B. Zheng, L. S. Roach, R. F. Ismagilov, *J. Am. Chem. Soc.* **2003**, *125*, 11170-11171; b) Y. Zhu, L. Zhu, R. Guo, H. Cui, S. Ye, Q. Fang, *Sci. Rep.* **2014**, *4*, 5046.
249. a) M. N. Hsu, R. Luo, K. Z. Kwek, Y. C. Por, Y. Zhang, C. Chen, *Biomicrofluidics* **2015**, *9*, 052601; b) M. Windbergs, Y. Zhao, J. Heyman, D. A. Weitz, *J. Am. Chem. Soc.* **2013**, *135*, 7933-7937.
250. a) S. Köster, F. E. Angilè, H. Duan, J. J. Agresti, A. Wintner, C. Schmitz, A. C. Rowat, C. A. Merten, D. Pisignano, A. D. Griffiths, D. A. Weitz, *Lab Chip*, **2008**, *8*, 1110-1115; b) J. Clausell-Tormos, D. Lieber, J. C. Baret, A. El-Harrak, O. J. Miller, L. Frenz, J. Blouwolff, K. J. Humphry, S. Köster, H. Duan, C. Holtze, D. A. Weitz, A. D. Griffiths, C. A. Merten, *ACS Chem. Biol.* **2008**, *15*, 427-437; c) E. Brouzes, M. Medkova, N. Savenelli, D. Marran, M. Twardowski, J. B. Hutchison, J. M. Rothberg, D. R. Link, N. Perrimon, M. L. Samuels, *Proc. Natl. Acad. Sci. U. S. A.* **2009**, *106* , 14195-14200; d) S. Sart, G. Ronteix, S. Jain, G. Amselem, C. N. Baroud, *Chem. Rev.* **2022**, *122*, 7061-7096.
251. a) H. Lin, L. Zhou, F. Mei, W. Dou, L. Hu, H. Yang, L. Xu, *Angew. Chem. Int. Ed.* **2023**, *62*, e202301900; b) S. Bai, S. Debnath, K. Gibson, B. Schlicht, L. Bayne, M. Zagnoni, R. V. Ulijn, *Small* **2014**, *10*, 285-293; c) A. Levin, T. C. T. Michaels, T. O. Mason, T. Müller, L. Adler-Abramovich, L. Mahadevan, M. E. Cates, E. Gazit, T. P. J. Knowles, *ACS Appl. Mater. Interfaces* **2018**, *10*, 27578-27583.
252. J. Liu, Y. Lan, Z. Yu, C. S.Y. Tan, R. M. Parker, C. Abell, O. A. Scherman, *Acc. Chem. Res.* **2017**, *50*, 208-217.
253. J. Zhang, R. J. Coulston, S. T. Jones, J. Geng, O. A. Scherman, C. Abell, *Science* **2012**, *335*, 690-694.
254. a) Y. Zheng, Z. Yu, R. M. Parker, Y. Wu, C. Abell, O. A. Scherman, *Nat. Commun.* **2014**, 5, 5772; b) X. Xu, E. A. Appel, X. Liu, R. M. Parker, O. A. Scherman, C. Abell, *Biomacromolecules* **2015**, *16*, 2743-2749; c) Z. Yu, J. Zhang, R. J. Coulston, R. M. Parker, F. Biedermann, X. Liu, O. A. Scherman, C. Abell, *Chem. Sci.* **2015**, *6*, 4929-4933; d) Z. Yu, Y. Zheng, R. M. Parker, Y. Lan, Y. Wu, R. J. Coulston, J. Zhang, O. A. Scherman, C. Abell, *ACS Appl. Mater. Interfaces* **2016**, *8*, 8811-8820.
255. a) C. Martino, A. J. deMello, *Interface Focus* **2016**, *6*, 20160011; b) S. Tan, Y. Ai, X. Yin, Z. Xue, X. Fang, Q. Liang, X. Gong, X. Dai, *Adv. Funct. Mater.* **2023**, *33*, 2305071; c) S. Fasciano, S. Wang, *SLAS Technol.* **2024**, *29*, 100090.
256. N. Deng, M. Yelleswarapu, L. Zheng, W. T. S. Huck, *J. Am. Chem. Soc.* **2017**, *139*, 587-590.

USC DE SANTIAGO DE COMPOSTELA

257. M. Weiss, J. P. Frohnmayer, L. T. Benk, B. Haller, J. Janiesch, T. Heitkamp, M. Börsch, R. B. Lira, R. Dimova, R. Lipowsky, E. Bodenschatz, J.Baret, T. Vidakovic-Koch, K. Sundmacher, I. Platzman, J. P. Spatz, *Nat. Mater.* **2018**, *17*, 89-96.
258. P. Zhan, K. Jahnke, N. Liu, K. Göpfrich, *Nat. Chem.* **2022**, *14*, 958-963.
259. Z. Li, H. Wang, Y. Gao, J. Chen, G. Gu, J. Liu, Y. Chen, X. Guo, Y. Wang, *Small* **2024**, 2403085.
260. J. Montenegro, C. Vázquez-Vázquez, A. Kalinin, K. E. Geckeler, J. R. Granja, *J. Am. Chem. Soc.* **2014**, *136*, 2484-2491.
261. T. Nishikawa, N. Tajima, M. Kitamatsu, M. Fujiki, Y. Imai, *Org. Biomol. Chem.* **2015**, *13*, 11426-11431.
262. C. Holtze, A. C. Rowat, J. J. Agresti, J. B. Hutchison, F. E. Angilè, C. H. Schmitz, S. Köster, H. Duan, K. J. Humphry, R. A. Scanga, J. S. Johnson, D. Pisignano, D. A. Weitz, *Lab Chip* **2008**, *8*, 1632-1639.
263. a) R. M. Epand, *Biochim. Biophys. Acta* **2003**, *1614*, 116-121; b) A. B. Theberge, F. Courtois, Y. Schaerli, M. Fischlechner, C. Abell, F. Hollfelder, W. T. S. Huck, *Angew. Chem. Int. Ed.* **2010**, *49*, 5846-5868.
264. a) C. Carvalho, R. X. Santos, S. Cardoso, S. Correia, P. J. Oliveira, M. S. Santos, P. I. Moreira, *Curr. Med. Chem.* **2009**, 16, 3267-3285; b) O. Tacar, P. Sriamornsak, C. R. Dass, *J. Pharm. Pharmacol.* **2012**, *65*, 157-170; c) S. Sritharan, N. Sivalingam, *Life Sci.* **2021**, *278*, 119527.
265. E. González Freire (**2019**), *Application of two orthogonal click-type reactions for the preparation of cyclic peptides with antibacterial and anticancer activity*, PhD Dissertation, University of Santiago de Compostela.
266. D. K. Kölmeland, E. T. Kool, *Chem. Rev.* **2017**, *117*, 10358-10376.
267. a) D. Willner, P. A. Trail, S. J. Hofstead, H. D. King, S. J. Lasch, G. R. Braslawsky, R. S. Greenfield, T. Kaneko, R. A. Firestone, *Bioconjugate Chem.* **1993**, *4*, 521-527; b) Z. Jia, L. Wong, T. P. Davis, V. Bulmus, *Biomacromolecules* **2008**, *9*, 3106-3113; c) T. Cai, Y. Chen, Y. Wang, H. Wang, X. Liu, Q. Jin, S. Agarwal, J. Ji, *Polym. Chem.* **2014**, *5*, 4061-4068.
268. a) R. S. Greenfield, T. Kaneko, A. Daues, M. A. Edson, K. A. Fitzgerald, L. J. Olech, J. A. Grattan, G. L. Spitalny, G. R. Braslawsky, *Cancer Res.* **1990**, *50*, 6600-6607; b) K. Y. J. Lee, Y. Wang, S. Nie, *RSC Adv.* **2015**, *5*, 65651-65659.
269. a) B. H. Northrop, S. H. Frayne, U. Choudhary, *Polym. Chem.* **2015**, *6*, 3415-3430; b) S. Li, L. Liu, H. Jia, W. Qiu, L. Rong, H. Cheng, X. Zhang, *Chem. Commun.* **2014**, *50*, 11852-11855; c) J. Wang, M. Chen, S. Li, R. D. Ye, *Mol. Pharmaceutics* **2019**, *16*, 2636-2647.
270. a) I. Altinbasak, M. Arslan, R. Sanyal, A. Sanyal, *Polym. Chem.* **2020**, *11*, 7603-7624; b) S. Darwish, N. Sadeghiani, S. Fong, S. Mozaffari, P. Hamidi, T. Withana, S. Yang, R. K. Tiwari, K. Parang, *Eur. J. Med. Chem.* **2019**, *161*, 594-606.
271. a) T. Mossman, *J. Immunol. Methods* **1983**, *65*, 55-63; b) P. Kumar, A. Nagarajan, P. D. Uchil, *Cold Spring Harb. Protoc.* **2018**, *2018*, pdbprot095505.
272. a) Ş. Comşa, A. M. Cîmpean, M. Raica, *Anticancer Res.* **2015**, *35*, 3147-3154; b) A. V. Lee, S. Oesterreich, N. E. Davidson, *J. Natl. Cancer Inst.* **2015**, *107*, djv073.
273. a) C. G. Ferreira, S. W. Span, G. J. Peters, F. A. E. Kruyt, G. Giaccone, *Cancer Res.* **2000**, *60*, 7133-7141; b) M. Pesic, J. Z. Markovic, D. Jankovic, S. Kanazir, I. D. Markovic, L. Rakic, S. Ruzdijic, *J. Chemother.* **2006**, *18*, 66-73.
274. a) M. Liscovitch, D. Ravid, *Cancer Lett.* **2007**, *245*, 350-352; b) W. Ke, P. Yu, J. Wang, R. Wang, C. Guo, L. Zhou, C. Li, K. Li, *Med. Oncol.* **2011**, *28*, 135-141.
275. Z. E. Sauna, M. M. Smith, M. Müller, K. M. Kerr, S. V. Ambudkar, *J. Bioenerg. Biomembr.* **2001**, *33*, 481-491.
276. a) J. J. Rennick, A. P. R. Johnston, R. G. Parton, *Nat. Nanotechnol.* **2021**, *16*, 266-276; b) P. Lundin, H. Johansson, P. Guterstam, T. Holm, M. Hansen, U. Langel, S. E. Andaloussi, *Bioconjug. Chem.* **2008**, *19*, 2535-2542; c) G. Preta, J. G. Cronin, I. M. Sheldon, *Cell Commun. Signal.* **2015**, *13*, 24.
277. a) C. A. Schneider, W. S. Rasband, K. W. Eliceiri, *Nat. Methods* **2012**, *9*, 671-675; b) J. Schindelin, I. Arganda-Carreras, E. Frise, V. Kaynig, M. Longair, T. Pietzsch, S. Preibisch, C. Rueden, S. Saalfeld, B. Schmid, J. Tinevez, D. J. White, V. Hartenstein, K. Eliceiri, P. Tomancak, A. Cardona, *Nat. Methods* **2012**, *9*, 676-682.
278. D. Nečas, P. Klapetek, *Cent. Eur. J. Phys.* **2012**, *10*, 181-188.
279. J. C.-C. Hsu, E. H.-L. Chen, R. C. Snoeberger, F. Y. Luh, T.-S. Lim, C.-P. Hsu, R. P.-Y. Chen, *J. Phys. Chem. B* **2013**, *117*, 3459-3468.
280. a) Y. Kim, M. Koh, D. K. Kim, H. S. Choi, S. B. Park, *J. Comb. Chem.* **2009**, *11*, 928-937; b) C. Freeman, J. S. Vyle, F. Heaney, *RSC Adv.* **2013**, *3*, 1652-1655; c) A. Samanta, B. J. Ravoo, *Chem. Eur. J.* **2014**, *20*, 4966-4973.
281. M. L. Swift, *J. Chem. Inf. Comput. Sci.* **1997**, *37*, 411-412.

282. D. Xiao, L. Luo, J. Li, Z. Wang, L. Liu, F. Xie, J. Feng, X. Zhou, *Bioorg. Chem.* **2021**, *116*, 105366.
283. a) J. Carlsson, H. Drevin, R. Axén, *Biochem J.* **1978**, *173*, 723-737; b) S. Y. Tan, C. Y. Ang, Z. Luo, P. Li, K. T. Nguyen, Y. Zhao, *Chem. Eur. J.* **2015**, *21*, 6123-6131.
284. a) S. Otake, K. Okuro, D. Bochicchio, G. M. Pavan, T. Aida, *Bioconjug. Chem.* **2018**, *29*, 2068-2073; b) S. Taliani, F. Simorini, V. Sergianni, C. La Motta, F. Da Settimo, B. Cosimelli, E. Abignente, G. Greco, E. Novellino, L. Rossi, V. Gremigni, F. Spinetti, B. Chelli, C. Martini, *J. Med. Chem.* **2007,** *50*, 404-407; c) X. Xu, Z. Kuang, J. Han, Y. Meng, L. Li, H. Luan, P. Xu, J. Wang, C. Luo, H. Ding, Z. Li, J. Bian, *J. Med. Chem.* **2019**, *62*, 9642-9657; d) M. Ciba, B. Dibnah, B. D. Hudson, E. R. Ulven, *J. Med. Chem.* **2023**, *66*, 8951-8974.

USC
UNIVERSIDADE DE SANTIAGO DE COMPOSTELA

10. ANNEXES

USC
UNIVERSIDADE
DE SANTIAGO
DE COMPOSTELA

10.1. Annex I: List of publications

Title: Molecular Plumbing to Bend Self-Assembling Peptide Nanotubes

Authors: F. Novelli, M. Vilela, A. Pazó, M. Amorín, J. R. Granja

Year: 2021

Journal: Angewandte Chemie International Edition

Volume and pages: 60, 18838-18844

DOI: 10.1002/anie.202107034

Impact factor: 16.1 (2023 Journal Citation Reports)

PhD student contribution: Synthesis and characterization of the molecular structures, study of the photodimerization reaction and evaluation of the nanotube bending motion.

Authorization of the journal:

Thank you for your order!

Dear Mr. Marcos Vilela Picos,

Thank you for placing your order through Copyright Clearance Center's RightsLink® service.

Order Summary

Licensee:	Mr. Marcos Vilela Picos
Order Date:	Oct 2, 2024
Order Number:	5880890318626
Publication:	Angewandte Chemie International Edition
Title:	Molecular Plumbing to Bend Self-Assembling Peptide Nanotubes
Type of Use:	Dissertation/Thesis
Order Total:	0.00 EUR

View or print complete details of your order and the publisher's terms and conditions.

Sincerely,

Copyright Clearance Center

USC UNIVERSIDADE DE SANTIAGO DE COMPOSTELA

Title: Photo-assembling Cyclic Peptides for Dynamic Light-driven Peptide Nanotubes

Authors: M. Vilela-Picos, F. Novelli, A. Pazó, A. Méndez-Ardoy, G. Marafon, M. Amorín, A. Moretto, J. R. Granja

Year: 2023

Journal: Chem

Volume and pages: *9*, 3365-3378

DOI: 10.1016/j.chempr.2023.10.005

Impact factor: 19.1 (2023 Journal Citation Reports)

PhD student contribution: Design, synthesis and characterization of the molecular structures. Studies of the isomerization, the self-assembly properties and the light-induced assembly/disassembly. Evaluation of the self-assembly by microfluidic experiments.

Authorization of the journal:

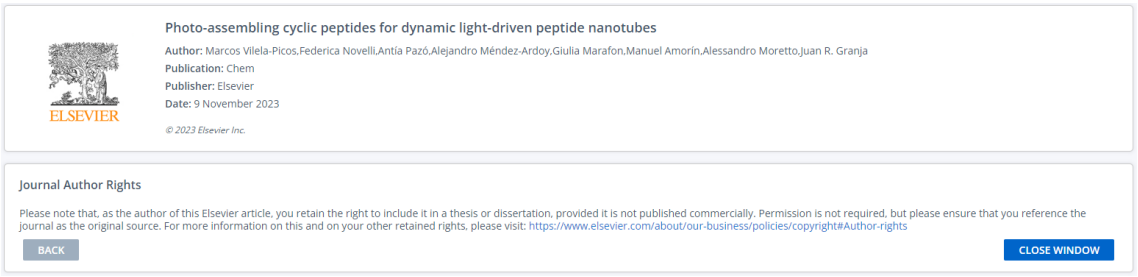

USC UNIVERSIDADE DE SANTIAGO DE COMPOSTELA

Title: Protocol for Photo-controlling the Assembly of Cyclic Peptide Nanotubes in Solution and Inside Microfluidic Droplets

Authors: M. Vilela-Picos, F. Novelli, A. Méndez-Ardoy, A. Moretto, J. R. Granja

Year: 2024

Journal: STAR Protocols

Volume and pages: 5, 103031

DOI: 10.1016/j.xpro.2024.103031

Impact factor: 1.3 (2023 Journal Citation Reports)

PhD student contribution: Design, synthesis and characterization of the molecular structures. Studies of the isomerization, the self-assembly properties and the light-induced assembly/disassembly. Evaluation of the self-assembly by microfluidic experiments.

Authorization of the journal:

CCC Marketplace

This is a License Agreement between Marcos Vilela Picos ("User") and Copyright Clearance Center, Inc. ("CCC") on behalf of the Rightsholder identified in the order details below. The license consists of the order details, the Marketplace Permissions General Terms and Conditions below, and any Rightsholder Terms and Conditions which are included below.

All payments must be made in full to CCC in accordance with the Marketplace Permissions General Terms and Conditions below.

Order Date	04-Oct-2024	Type of Use	Republish in a thesis/dissertation
Order License ID	1532813-1	Publisher	Elsevier Inc
ISSN	2666-1667	Portion	Chapter/article

LICENSED CONTENT

Publication Title	STAR Protocols	Publication Type	e-Journal
Article Title	Protocol for photo-controlling the assembly of cyclic peptide nanotubes in solution and inside microfluidic droplets	Start Page	103031
		Issue	2
		Volume	5
Date	01/01/2020		
Rightsholder	Elsevier Science & Technology Journals		

USC UNIVERSIDADE DE SANTIAGO DE COMPOSTELA

10.2. Annex II: Conflict of interest

The PhD candidate Marcos Vilela Picos declares no conflict of interest in relation to this doctoral thesis.

Santiago de Compostela, December 2nd 2024.

10.3. Annex III: Rights and permissions of the images

Figure 1A

Lipoidal soft hybrid biocarriers of supramolecular construction for drug delivery.

Kumar, Dinesh; Sharma, Deepak; Singh, Gurmeet; Singh, Mankaran; Rathore, ...More *ISRN Pharmaceutics (Print)*, 19 Jul 2012, Vol. 2012, pages 474830 - ...

ISSN: 20906145
DOI: 10.5402/2012/474830
PMID: 22888455
PMCID: PMC3409530

Publisher: Hindawi Publishing Corporation; Hindawi Limited; Hindawi Pub. Corp
Language: English
Country: Egypt
URL: https://www.hindawi.com/journals/isrn/2012/474830/

Details >

Request Reprints/ePrints | Request Single Copy | Request Permission | Open Access - Creative Commons CC BY 3.0

Figure 1C

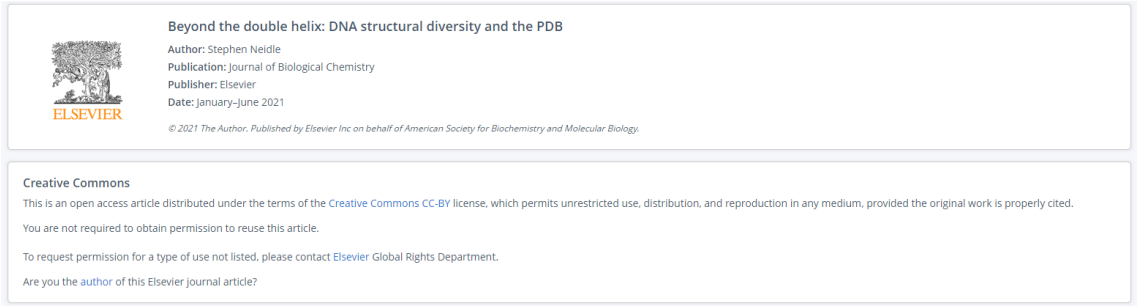

Beyond the double helix: DNA structural diversity and the PDB

Author: Stephen Neidle
Publication: Journal of Biological Chemistry
Publisher: Elsevier
Date: January–June 2021

© 2021 The Author. Published by Elsevier Inc on behalf of American Society for Biochemistry and Molecular Biology.

Creative Commons

This is an open access article distributed under the terms of the Creative Commons CC-BY license, which permits unrestricted use, distribution, and reproduction in any medium, provided the original work is properly cited.

You are not required to obtain permission to reuse this article.

To request permission for a type of use not listed, please contact Elsevier Global Rights Department.

Are you the author of this Elsevier journal article?

Figure 1F

CCC Marketplace

This is a License Agreement between Marcos Vilela Picos ("User") and Copyright Clearance Center, Inc. ("CCC") on behalf of the Rightsholder identified in the order details below. The license consists of the order details, the Marketplace Permissions General Terms and Conditions below, and any Rightsholder Terms and Conditions which are included below.

All payments must be made in full to CCC in accordance with the Marketplace Permissions General Terms and Conditions below.

Order Date	03-Sep-2024	Type of Use	Republish in a thesis/dissertation
Order License ID	1521952-1	Publisher	ROYAL SOCIETY OF CHEMISTRY
ISSN	1460-4744	Portion	Chart/graph/table/figure

LICENSED CONTENT

Publication Title	Chemical Society reviews	Publication Type	e-Journal
Article Title	Artificial molecular motors.	Start Page	2592
Author / Editor	Royal Society of Chemistry (Great Britain)	End Page	2621
Date	01/01/1972	Issue	9
Language	English	Volume	46
Country	United Kingdom of Great Britain and Northern Ireland	URL	http://www.rsc.org/csr
Rightsholder	Royal Society of Chemistry		

USC UNIVERSIDADE DE SANTIAGO DE COMPOSTELA

Figure 2A

Order Summary

Licensee:	Mr. Marcos Vilela Picos
Order Date:	Aug 30, 2024
Order Number:	5858741008201
Publication:	Nature Reviews Neuroscience
Title:	Microtubule assembly, organization and dynamics in axons and dendrites
Type of Use:	Thesis/Dissertation
Order Total:	0.00 EUR

Figure 2B

CCC Marketplace

This is a License Agreement between Marcos Vilela Picos ("User") and Copyright Clearance Center, Inc. ("CCC") on behalf of the Rightsholder identified in the order details below. The license consists of the order details, the Marketplace Permissions General Terms and Conditions below, and any Rightsholder Terms and Conditions which are included below.

All payments must be made in full to CCC in accordance with the Marketplace Permissions General Terms and Conditions below.

Order Date	02-Sep-2024	Type of Use	Republish in a thesis/dissertation
Order License ID	1521556-1	Publisher	ROYAL SOCIETY OF CHEMISTRY
ISSN	1460-4744	Portion	Chart/graph/table/figure

LICENSED CONTENT

Publication Title	Chemical Society reviews	Rightsholder	Royal Society of Chemistry
Article Title	Benzene-1,3,5-tricarboxamide: a versatile ordering moiety for supramolecular chemistry.	Publication Type	e-Journal
		Start Page	6125
Author / Editor	Royal Society of Chemistry (Great Britain)	Issue	18
Date	01/01/1972	Volume	41
Language	English	URL	http://www.rsc.org/csr
Country	United Kingdom of Great Britain and Northern Ireland		

Figure 2C

Order Summary

Licensee:	Mr. Marcos Vilela Picos
Order Date:	Sep 2, 2024
Order Number:	5860700446843
Publication:	Advanced Materials
Title:	Hierarchical Formation of Supramolecular Transient Networks in Water: A Modular Injectable Delivery System
Type of Use:	Dissertation/Thesis
Order Total:	0.00 EUR

Figure 3A

SPRINGER NATURE

Supramolecular block copolymers by kinetically controlled co-self-assembly of planar and core-twisted perylene bisimides

Author: Daniel Görl et al
Publication: Nature Communications
Publisher: Springer Nature
Date: May 11, 2015

Copyright © 2015, The Author(s)

Creative Commons

This is an open access article distributed under the terms of the Creative Commons CC BY license, which permits unrestricted use, distribution, and reproduction in any medium, provided the original work is properly cited.

You are not required to obtain permission to reuse this article.

To request permission for a type of use not listed, please contact Springer Nature

USAL UNIVERSIDAD DE SALAMANCA

Figure 3B

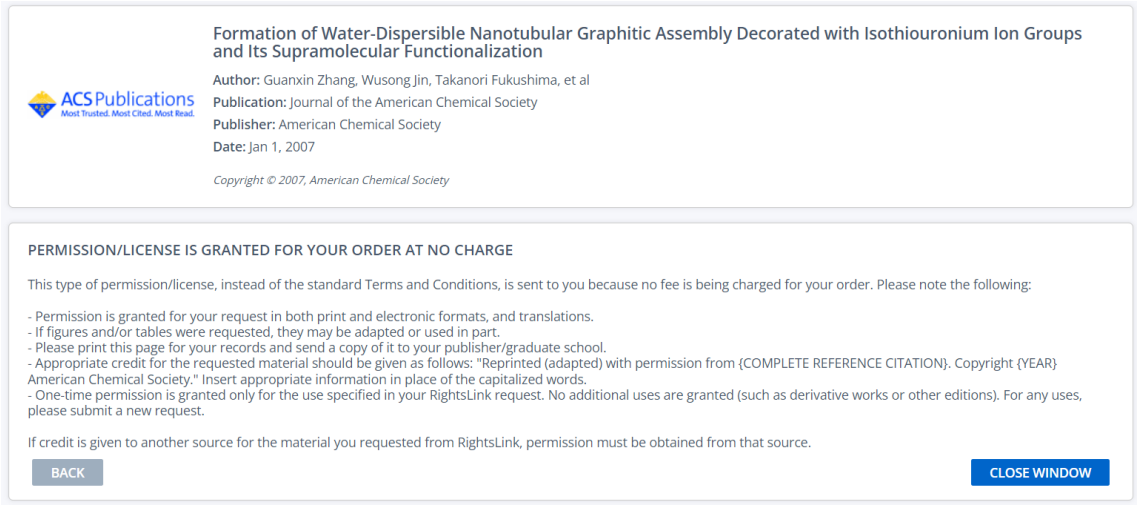

ACS Publications
Most Trusted. Most Cited. Most Read.

Formation of Water-Dispersible Nanotubular Graphitic Assembly Decorated with Isothiouronium Ion Groups and Its Supramolecular Functionalization

Author: Guanxin Zhang, Wusong Jin, Takanori Fukushima, et al
Publication: Journal of the American Chemical Society
Publisher: American Chemical Society
Date: Jan 1, 2007

Copyright © 2007, American Chemical Society

PERMISSION/LICENSE IS GRANTED FOR YOUR ORDER AT NO CHARGE

This type of permission/license, instead of the standard Terms and Conditions, is sent to you because no fee is being charged for your order. Please note the following:

- Permission is granted for your request in both print and electronic formats, and translations.
- If figures and/or tables were requested, they may be adapted or used in part.
- Please print this page for your records and send a copy of it to your publisher/graduate school.
- Appropriate credit for the requested material should be given as follows: "Reprinted (adapted) with permission from {COMPLETE REFERENCE CITATION}. Copyright {YEAR} American Chemical Society." Insert appropriate information in place of the capitalized words.
- One-time permission is granted only for the use specified in your RightsLink request. No additional uses are granted (such as derivative works or other editions). For any uses, please submit a new request.

If credit is given to another source for the material you requested from RightsLink, permission must be obtained from that source.

BACK CLOSE WINDOW

Figure 3C

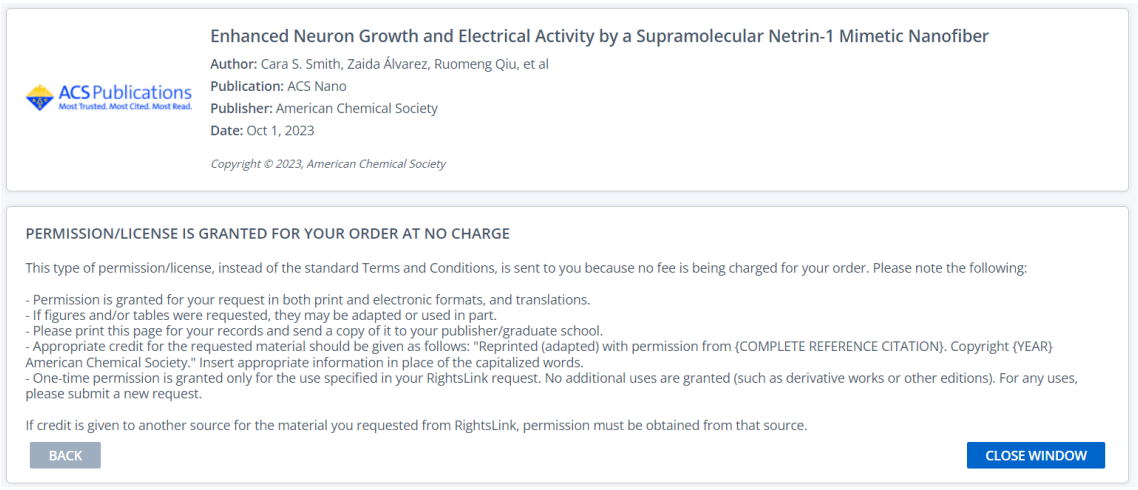

ACS Publications
Most Trusted. Most Cited. Most Read.

Enhanced Neuron Growth and Electrical Activity by a Supramolecular Netrin-1 Mimetic Nanofiber

Author: Cara S. Smith, Zaida Álvarez, Ruomeng Qiu, et al
Publication: ACS Nano
Publisher: American Chemical Society
Date: Oct 1, 2023

Copyright © 2023, American Chemical Society

PERMISSION/LICENSE IS GRANTED FOR YOUR ORDER AT NO CHARGE

This type of permission/license, instead of the standard Terms and Conditions, is sent to you because no fee is being charged for your order. Please note the following:

- Permission is granted for your request in both print and electronic formats, and translations.
- If figures and/or tables were requested, they may be adapted or used in part.
- Please print this page for your records and send a copy of it to your publisher/graduate school.
- Appropriate credit for the requested material should be given as follows: "Reprinted (adapted) with permission from {COMPLETE REFERENCE CITATION}. Copyright {YEAR} American Chemical Society." Insert appropriate information in place of the capitalized words.
- One-time permission is granted only for the use specified in your RightsLink request. No additional uses are granted (such as derivative works or other editions). For any uses, please submit a new request.

If credit is given to another source for the material you requested from RightsLink, permission must be obtained from that source.

BACK CLOSE WINDOW

Figure 4A

Tips and turns of bacteriophytochrome photoactivation

H. Takala, P. Edlund, J. A. Ihalainen and S. Westenhoff, *Photochem. Photobiol. Sci.*, 2020, **19**, 1488 **DOI:** 10.1039/D0PP00117A

This article is licensed under a Creative Commons Attribution-NonCommercial 3.0 Unported Licence. **You can use material from this article in other publications, without requesting further permission** from the RSC, provided that the correct acknowledgement is given and it is not used for commercial purposes.

USC UNIVERSIDADE DE SANTIAGO DE COMPOSTELA

Figure 4B

Can I use AAAS material in a thesis or dissertation?

Yes, different criteria apply depending upon whether you are the author of the AAAS article being reproduced.

Authors:

If you are the author of the AAAS article being reproduced, please refer to your License to Publish for rules on reproducing your paper in a dissertation or thesis.

Others:

AAAS permits the use of content published in its journals *Science*, *Science Immunology*, *Science Robotics*, *Science Signaling*, and *Science Translational Medicine* to be used in a thesis or dissertation, but only provided the following criteria are met:

1. If you are using figure(s)/table(s), permission is granted for use in print and electronic versions of your dissertation or thesis.
2. A full-text article may be used only in print versions of a dissertation or thesis. AAAS does not permit the reproduction of full-text articles in electronic versions of theses or dissertations.
3. The following credit line must be printed along with the AAAS material: "From [Full Reference Citation]. Reprinted with permission from AAAS."
4. All required credit lines and notices must be visible any time a user accesses any part of the AAAS material and must appear on any printed copies that an authorized user might make.
5. The AAAS material may not be modified or altered, with the exception that figures and tables may be modified with permission from the author. Author permission for any such changes must be secured prior to your use.
6. AAAS must publish the full paper prior to your use of any of its text or figures.
7. If the AAAS material covered by this permission was published in *Science* during the years 1974–1994, you must also obtain permission from the author, who may grant or withhold permission, and who may or may not charge a fee if permission is granted. See original article for author's address. This condition does not apply to news articles.
8. If you are an original author of the AAAS article being reproduced, please refer to your License to Publish for rules on reproducing your paper in a dissertation or thesis.
9. Permission covers the distribution of your dissertation or thesis on demand by a third-party distributor (e.g., ProQuest/UMI), provided the AAAS material covered by this permission remains in situ and is not distributed by that third party outside of the context of your thesis/dissertation.
10. Permission does not apply to figures/photos/artwork or any other content or materials included in your work that are credited to non-AAAS sources. If the requested material is sourced to or references non-AAAS sources, you must obtain authorization from that source as well before using that material. You agree to hold harmless and indemnify AAAS against any claims arising from your use of any content in your work that is credited to non-AAAS sources.
11. By using the AAAS material identified in your request, you agree to abide by all the terms and conditions herein.
12. AAAS makes no representations or warranties as to the accuracy of any information contained in the AAAS material covered by this permission, including any warranties of merchantability or fitness for a particular purpose.

Figure 5A

Molecular photoswitches in aqueous environments

J. Volarić, W. Szymanski, N. A. Simeth and B. L. Feringa, *Chem. Soc. Rev.*, 2021, **50**, 12377 **DOI:** 10.1039/D0CS00547A

This article is licensed under a Creative Commons Attribution-NonCommercial 3.0 Unported Licence. **You can use material from this article in other publications, without requesting further permission** from the RSC, provided that the correct acknowledgement is given and it is not used for commercial purposes.

USC UNIVERSIDADE DE SANTIAGO DE COMPOSTELA

Figure 6A

Order Summary

Licensee:	Mr. Marcos Vilela Picos
Order Date:	Sep 4, 2024
Order Number:	5861890719259
Publication:	Angewandte Chemie International Edition
Title:	Photocontrolled Reversible Supramolecular Assemblies of an Azobenzene-Containing Surfactant with α-Cyclodextrin
Type of Use:	Dissertation/Thesis
Order Total:	0.00 EUR

Figure 6B

Dear Marcos,

Thank you for your message. Permission is granted for your use of the material as described in your request. Please include a complete citation for the original PNAS article when reusing the material. Because this material published after 2008, a copyright note is not needed. There is no charge for this material, either. Let us know if you have any questions.

Best regards,
William Choi for
Diane Sullenberger
PNAS Executive Editor

Figure 7A

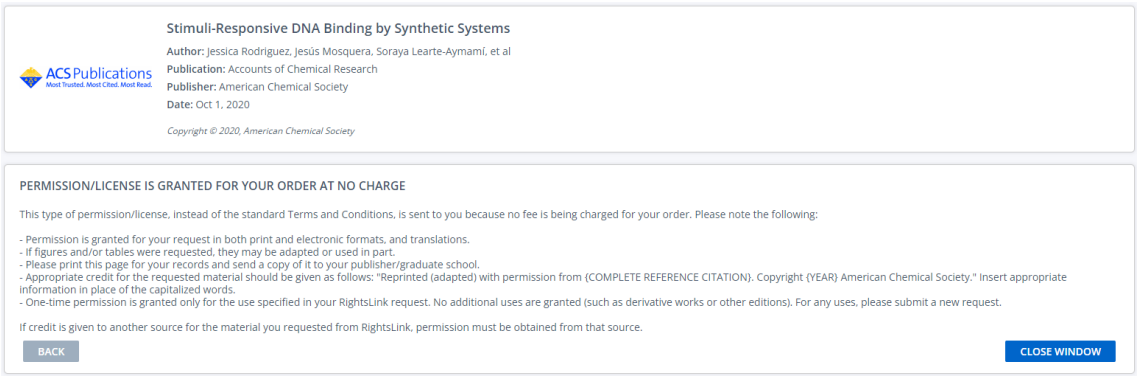

ACS Publications
Most Trusted. Most Cited. Most Read.

Stimuli-Responsive DNA Binding by Synthetic Systems

Author: Jessica Rodríguez, Jesús Mosquera, Soraya Learte-Aymamí, et al
Publication: Accounts of Chemical Research
Publisher: American Chemical Society
Date: Oct 1, 2020

Copyright © 2020, American Chemical Society

PERMISSION/LICENSE IS GRANTED FOR YOUR ORDER AT NO CHARGE

This type of permission/license, instead of the standard Terms and Conditions, is sent to you because no fee is being charged for your order. Please note the following:

- Permission is granted for your request in both print and electronic formats, and translations.
- If figures and/or tables were requested, they may be adapted or used in part.
- Please print this page for your records and send a copy of it to your publisher/graduate school.
- Appropriate credit for the requested material should be given as follows: "Reprinted (adapted) with permission from {COMPLETE REFERENCE CITATION}. Copyright {YEAR} American Chemical Society." Insert appropriate information in place of the capitalized words.
- One-time permission is granted only for the use specified in your RightsLink request. No additional uses are granted (such as derivative works or other editions). For any uses, please submit a new request.

If credit is given to another source for the material you requested from RightsLink, permission must be obtained from that source.

BACK CLOSE WINDOW

Figure 7B

Order Summary

Licensee:	Mr. Marcos Vilela Picos
Order Date:	Sep 4, 2024
Order Number:	5861951019511
Publication:	ChemBioChem
Title:	Photocontrollable Peptide-Based Switches Target the Anti-Apoptotic Protein Bcl-xL
Type of Use:	Dissertation/Thesis
Order Total:	0.00 EUR

USC UNIVERSIDADE DE SANTIAGO DE COMPOSTELA

Figure 7C

Order Summary

Licensee:	Mr. Marcos Vilela Picos
Order Date:	Sep 4, 2024
Order Number:	5861960693169
Publication:	Angewandte Chemie International Edition
Title:	Light-Directed Protein Binding of a Biologically Relevant β-Sheet
Type of Use:	Dissertation/Thesis
Order Total:	0.00 EUR

Figure 7D

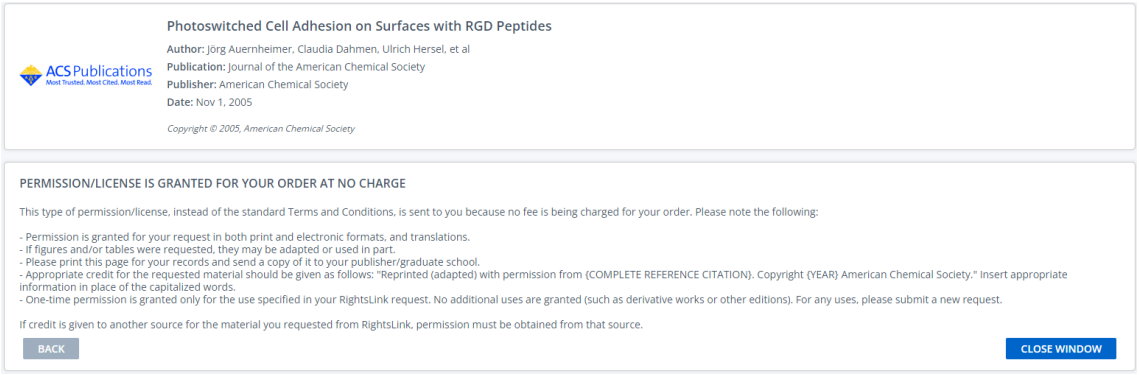

ACS Publications
Most Trusted. Most Cited. Most Read.

Photoswitched Cell Adhesion on Surfaces with RGD Peptides

Author: Jörg Auernheimer, Claudia Dahmen, Ulrich Hersel, et al
Publication: Journal of the American Chemical Society
Publisher: American Chemical Society
Date: Nov 1, 2005

Copyright © 2005, American Chemical Society

PERMISSION/LICENSE IS GRANTED FOR YOUR ORDER AT NO CHARGE

This type of permission/license, instead of the standard Terms and Conditions, is sent to you because no fee is being charged for your order. Please note the following:

- Permission is granted for your request in both print and electronic formats, and translations.
- If figures and/or tables were requested, they may be adapted or used in part.
- Please print this page for your records and send a copy of it to your publisher/graduate school.
- Appropriate credit for the requested material should be given as follows: "Reprinted (adapted) with permission from {COMPLETE REFERENCE CITATION}. Copyright {YEAR} American Chemical Society." Insert appropriate information in place of the capitalized words.
- One-time permission is granted only for the use specified in your RightsLink request. No additional uses are granted (such as derivative works or other editions). For any uses, please submit a new request.

If credit is given to another source for the material you requested from RightsLink, permission must be obtained from that source.

BACK CLOSE WINDOW

Figure 8A

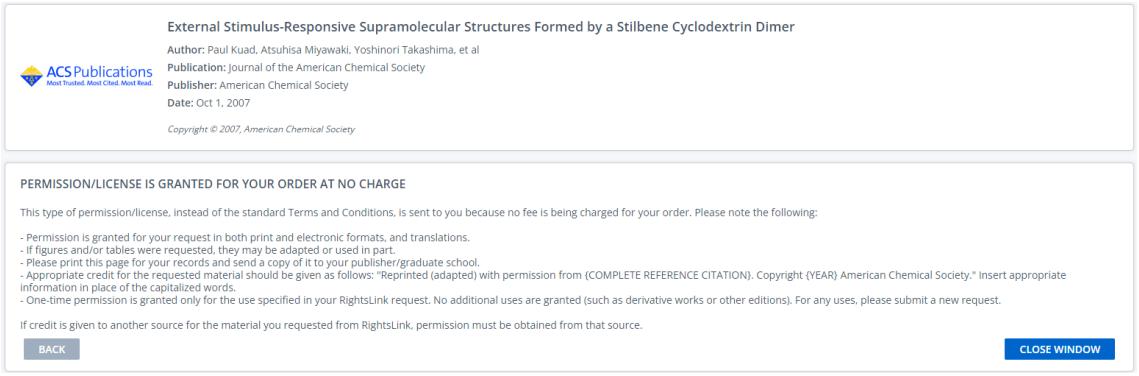

ACS Publications
Most Trusted. Most Cited. Most Read.

External Stimulus-Responsive Supramolecular Structures Formed by a Stilbene Cyclodextrin Dimer

Author: Paul Kuad, Atsuhisa Miyawaki, Yoshinori Takashima, et al
Publication: Journal of the American Chemical Society
Publisher: American Chemical Society
Date: Oct 1, 2007

Copyright © 2007, American Chemical Society

PERMISSION/LICENSE IS GRANTED FOR YOUR ORDER AT NO CHARGE

This type of permission/license, instead of the standard Terms and Conditions, is sent to you because no fee is being charged for your order. Please note the following:

- Permission is granted for your request in both print and electronic formats, and translations.
- If figures and/or tables were requested, they may be adapted or used in part.
- Please print this page for your records and send a copy of it to your publisher/graduate school.
- Appropriate credit for the requested material should be given as follows: "Reprinted (adapted) with permission from {COMPLETE REFERENCE CITATION}. Copyright {YEAR} American Chemical Society." Insert appropriate information in place of the capitalized words.
- One-time permission is granted only for the use specified in your RightsLink request. No additional uses are granted (such as derivative works or other editions). For any uses, please submit a new request.

If credit is given to another source for the material you requested from RightsLink, permission must be obtained from that source.

BACK CLOSE WINDOW

Figure 8B

From Photoinduced Supramolecular Polymerization to Responsive Organogels.

Xu, Fan; Pfeifer, Lukas; Crespi, Stefano; Leung, Franco King-Chi; ...More *Journal of the American Chemical Society*, 21 Apr 2021, Vol. 143, Issue 15, pages 5990 - 5997

ISSN: 00027863
DOI: 10.1021/jacs.1c01802
PMID: 33830767
PMCID: PMC8154511

Publisher: AMERICAN CHEMICAL SOCIETY]; American Chemical Society; Oxford University Press ...view all
Language: English
Country: United States of America
URL: https://pubs.acs.org/doi/10.1021/jacs.1c01802

Details >

Request Reprints/ePrints | Request Single Copy | Request Permission | Open Access - Creative Commons CC BY-NC-ND 4.0

Figure 9A

Order Summary

Licensee:	Mr. Marcos Vilela Picos
Order Date:	Sep 4, 2024
Order Number:	5862090744031
Publication:	Nature Chemistry
Title:	Artificial muscle-like function from hierarchical supramolecular assembly of photoresponsive molecular motors
Type of Use:	Thesis/Dissertation
Order Total:	0.00 EUR

Figure 9B

Photodynamic Control of the Chain Length in Supramolecular Polymers: Switching an Intercalator into a Chain Capper.

Weyandt, Elisabeth; ter Huurne, Gijs M.; Vantomme, Ghislaine; Markvoort, Albert J.; Palmans, Anja R.A.; Meijer, Egbert Willem Less *Journal of the American Chemical Society*, 01 Apr 2020, Vol. 142, Issue 13, pages 6295 - 6303

ISSN: 00027863
DOI: 10.1021/jacs.0c00858
PMID: 32167302
PMCID: PMC7118707

Publisher: AMERICAN CHEMICAL SOCIETY]; American Chemical Society; Oxford University Press ...view all
Language: English
Country: United States of America
URL: https://pubs.acs.org/doi/10.1021/jacs.0c00858

Details >

Request Reprints/ePrints | Request Single Copy | Request Permission | Open Access - Creative Commons CC BY-NC-ND 4.0

Figure 10A

ACS Publications
Most Trusted. Most Cited. Most Read.

Enabling Light Work in Helical Self-Assembly for Dynamic Amplification of Chirality with Photoreversibility

Author: Yunsong Cai, Zhiqian Guo, Jianmei Chen, et al
Publication: Journal of the American Chemical Society
Publisher: American Chemical Society
Date: Feb 1, 2016

Copyright © 2016, American Chemical Society

PERMISSION/LICENSE IS GRANTED FOR YOUR ORDER AT NO CHARGE

This type of permission/license, instead of the standard Terms and Conditions, is sent to you because no fee is being charged for your order. Please note the following:

- Permission is granted for your request in both print and electronic formats, and translations.
- If figures and/or tables were requested, they may be adapted or used in part.
- Please print this page for your records and send a copy of it to your publisher/graduate school.
- Appropriate credit for the requested material should be given as follows: "Reprinted (adapted) with permission from {COMPLETE REFERENCE CITATION}. Copyright {YEAR} American Chemical Society." Insert appropriate information in place of the capitalized words.
- One-time permission is granted only for the use specified in your RightsLink request. No additional uses are granted (such as derivative works or other editions). For any uses, please submit a new request.

If credit is given to another source for the material you requested from RightsLink, permission must be obtained from that source.

BACK CLOSE WINDOW

Figure 10B

Order Summary

Licensee:	Mr. Marcos Vilela Picos
Order Date:	Sep 5, 2024
Order Number:	5862401272681
Publication:	Advanced Optical Materials
Title:	Supramolecular Assemblies: Photoresponsive Supramolecular Assemblies Based on a C3-Symmetric Benzene-1,3,5-tricarboxamide-Anchored Diarylethene (Advanced Optical Materials 6/2016)
Type of Use:	Dissertation/Thesis
Order Total:	0.00 EUR

USC UNIVERSIDADE DE SANTIAGO DE COMPOSTELA

Figure 11A

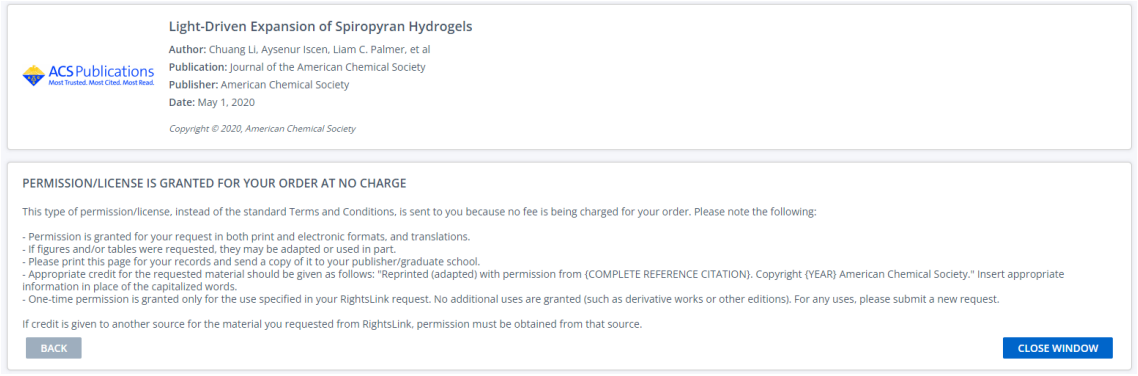

Light-Driven Expansion of Spiropyran Hydrogels

Author: Chuang Li, Aysenur Iscen, Liam C. Palmer, et al
Publication: Journal of the American Chemical Society
Publisher: American Chemical Society
Date: May 1, 2020

Copyright © 2020, American Chemical Society

PERMISSION/LICENSE IS GRANTED FOR YOUR ORDER AT NO CHARGE

This type of permission/license, instead of the standard Terms and Conditions, is sent to you because no fee is being charged for your order. Please note the following:

- Permission is granted for your request in both print and electronic formats, and translations.
- If figures and/or tables were requested, they may be adapted or used in part.
- Please print this page for your records and send a copy of it to your publisher/graduate school.
- Appropriate credit for the requested material should be given as follows: "Reprinted (adapted) with permission from {COMPLETE REFERENCE CITATION}. Copyright {YEAR} American Chemical Society." Insert appropriate information in place of the capitalized words.
- One-time permission is granted only for the use specified in your RightsLink request. No additional uses are granted (such as derivative works or other editions). For any uses, please submit a new request.

If credit is given to another source for the material you requested from RightsLink, permission must be obtained from that source.

BACK CLOSE WINDOW

Figure 11B

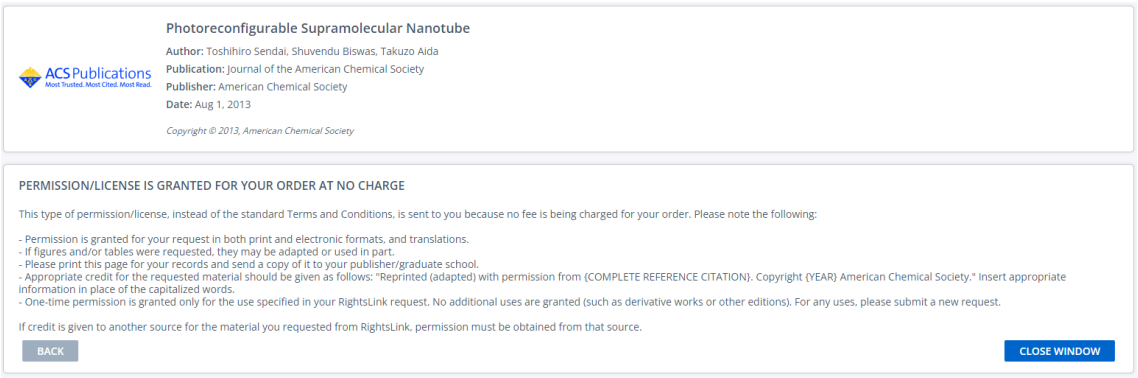

Photoreconfigurable Supramolecular Nanotube

Author: Toshihiro Sendai, Shuvendu Biswas, Takuzo Aida
Publication: Journal of the American Chemical Society
Publisher: American Chemical Society
Date: Aug 1, 2013

Copyright © 2013, American Chemical Society

PERMISSION/LICENSE IS GRANTED FOR YOUR ORDER AT NO CHARGE

This type of permission/license, instead of the standard Terms and Conditions, is sent to you because no fee is being charged for your order. Please note the following:

- Permission is granted for your request in both print and electronic formats, and translations.
- If figures and/or tables were requested, they may be adapted or used in part.
- Please print this page for your records and send a copy of it to your publisher/graduate school.
- Appropriate credit for the requested material should be given as follows: "Reprinted (adapted) with permission from {COMPLETE REFERENCE CITATION}. Copyright {YEAR} American Chemical Society." Insert appropriate information in place of the capitalized words.
- One-time permission is granted only for the use specified in your RightsLink request. No additional uses are granted (such as derivative works or other editions). For any uses, please submit a new request.

If credit is given to another source for the material you requested from RightsLink, permission must be obtained from that source.

BACK CLOSE WINDOW

Figure 11C

Order Summary

Licensee:	Mr. Marcos Vilela Picos
Order Date:	Sep 5, 2024
Order Number:	5862470284451
Publication:	Advanced Materials
Title:	Moving Droplets in 3D Using Light
Type of Use:	Dissertation/Thesis
Order Total:	0.00 EUR

Figure 15

Order Summary

Licensee:	Mr. Marcos Vilela Picos
Order Date:	Sep 6, 2024
Order Number:	5863140275690
Publication:	Biomaterials
Title:	pH-sensitive poly(histidine)-PEG/DSPE-PEG co-polymer micelles for cytosolic drug delivery
Type of Use:	reuse in a thesis/dissertation
Order Total:	0.00 EUR

USC UNIVERSIDADE DE SANTIAGO DE COMPOSTELA

Figure 16A

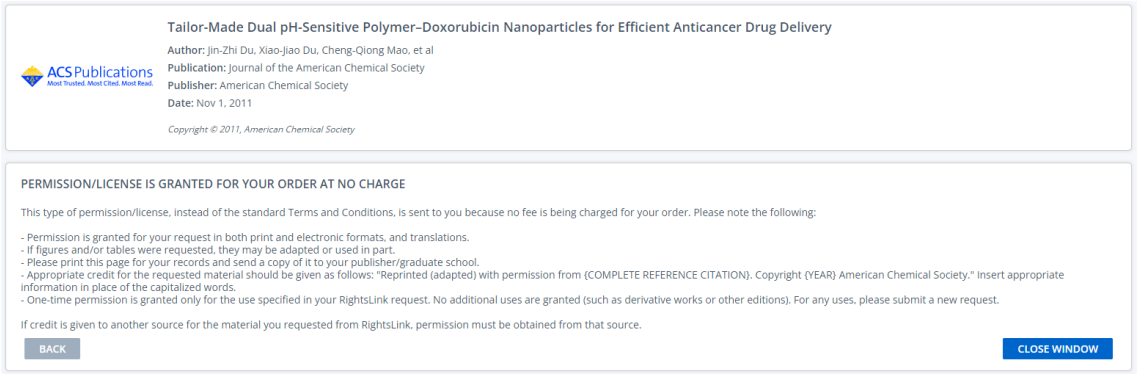

Tailor-Made Dual pH-Sensitive Polymer–Doxorubicin Nanoparticles for Efficient Anticancer Drug Delivery

Author: Jin-Zhi Du, Xiao-Jiao Du, Cheng-Qiong Mao, et al
Publication: Journal of the American Chemical Society
Publisher: American Chemical Society
Date: Nov 1, 2011

Copyright © 2011, American Chemical Society

PERMISSION/LICENSE IS GRANTED FOR YOUR ORDER AT NO CHARGE

This type of permission/license, instead of the standard Terms and Conditions, is sent to you because no fee is being charged for your order. Please note the following:

- Permission is granted for your request in both print and electronic formats, and translations.
- If figures and/or tables were requested, they may be adapted or used in part.
- Please print this page for your records and send a copy of it to your publisher/graduate school.
- Appropriate credit for the requested material should be given as follows: "Reprinted (adapted) with permission from {COMPLETE REFERENCE CITATION}. Copyright {YEAR} American Chemical Society." Insert appropriate information in place of the capitalized words.
- One-time permission is granted only for the use specified in your RightsLink request. No additional uses are granted (such as derivative works or other editions). For any uses, please submit a new request.

If credit is given to another source for the material you requested from RightsLink, permission must be obtained from that source.

BACK CLOSE WINDOW

Figure 16B

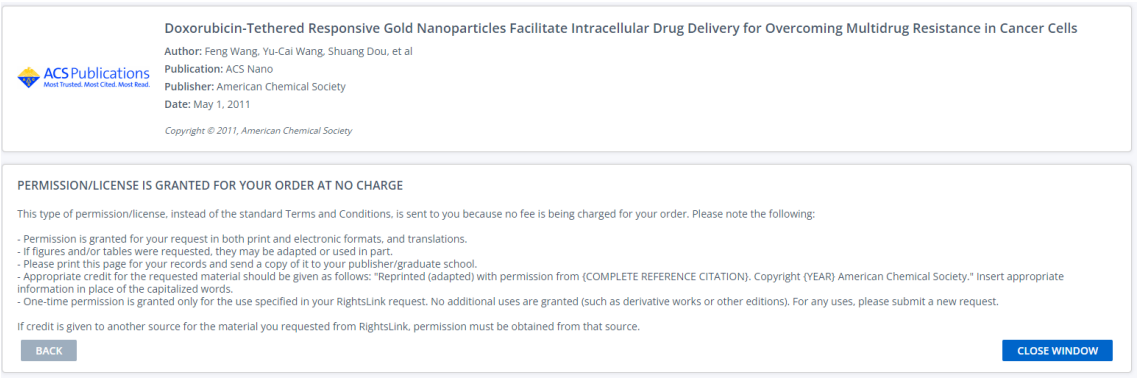

Doxorubicin-Tethered Responsive Gold Nanoparticles Facilitate Intracellular Drug Delivery for Overcoming Multidrug Resistance in Cancer Cells

Author: Feng Wang, Yu-Cai Wang, Shuang Dou, et al
Publication: ACS Nano
Publisher: American Chemical Society
Date: May 1, 2011

Copyright © 2011, American Chemical Society

PERMISSION/LICENSE IS GRANTED FOR YOUR ORDER AT NO CHARGE

This type of permission/license, instead of the standard Terms and Conditions, is sent to you because no fee is being charged for your order. Please note the following:

- Permission is granted for your request in both print and electronic formats, and translations.
- If figures and/or tables were requested, they may be adapted or used in part.
- Please print this page for your records and send a copy of it to your publisher/graduate school.
- Appropriate credit for the requested material should be given as follows: "Reprinted (adapted) with permission from {COMPLETE REFERENCE CITATION}. Copyright {YEAR} American Chemical Society." Insert appropriate information in place of the capitalized words.
- One-time permission is granted only for the use specified in your RightsLink request. No additional uses are granted (such as derivative works or other editions). For any uses, please submit a new request.

If credit is given to another source for the material you requested from RightsLink, permission must be obtained from that source.

BACK CLOSE WINDOW

Figure 16C

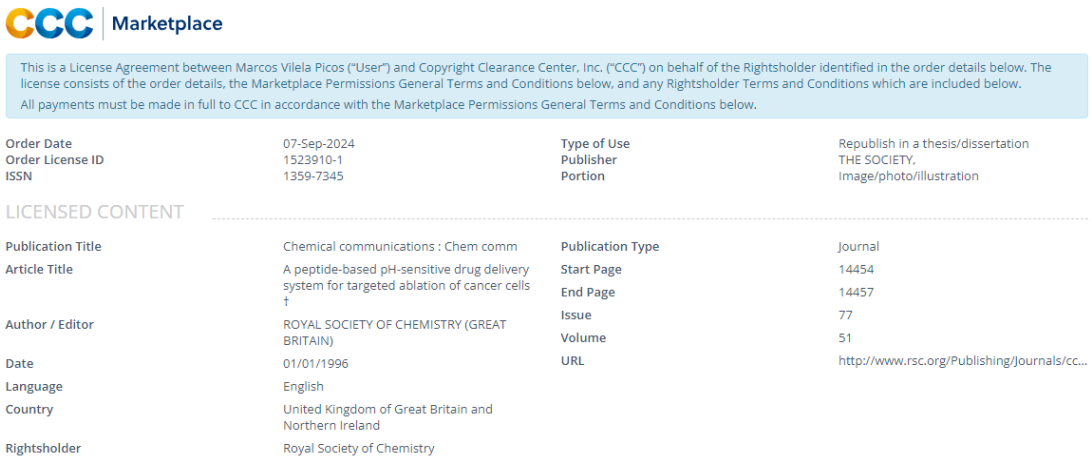

CCC Marketplace

This is a License Agreement between Marcos Vilela Picos ("User") and Copyright Clearance Center, Inc. ("CCC") on behalf of the Rightsholder identified in the order details below. The license consists of the order details, the Marketplace Permissions General Terms and Conditions below, and any Rightsholder Terms and Conditions which are included below.

All payments must be made in full to CCC in accordance with the Marketplace Permissions General Terms and Conditions below.

Order Date	07-Sep-2024	Type of Use	Republish in a thesis/dissertation
Order License ID	1523910-1	Publisher	THE SOCIETY,
ISSN	1359-7345	Portion	Image/photo/illustration

LICENSED CONTENT

Publication Title	Chemical communications : Chem comm	Publication Type	Journal
Article Title	A peptide-based pH-sensitive drug delivery system for targeted ablation of cancer cells †	Start Page	14454
		End Page	14457
Author / Editor	ROYAL SOCIETY OF CHEMISTRY (GREAT BRITAIN)	Issue	77
		Volume	51
Date	01/01/1996	URL	http://www.rsc.org/Publishing/Journals/cc...
Language	English		
Country	United Kingdom of Great Britain and Northern Ireland		
Rightsholder	Royal Society of Chemistry		

USC UNIVERSIDADE DE SANTIAGO DE COMPOSTELA

Figure 17

Smart pH-Sensitive and Temporal-Controlled Polymeric Micelles for Effective Combination Therapy of Doxorubicin and Disulfiram

Author: Xiaopin Duan, Jisheng Xiao, Qi Yin, et al
Publication: ACS Nano
Publisher: American Chemical Society
Date: Jul 1, 2013

Copyright © 2013, American Chemical Society

PERMISSION/LICENSE IS GRANTED FOR YOUR ORDER AT NO CHARGE

This type of permission/license, instead of the standard Terms and Conditions, is sent to you because no fee is being charged for your order. Please note the following:

- Permission is granted for your request in both print and electronic formats, and translations.
- If figures and/or tables were requested, they may be adapted or used in part.
- Please print this page for your records and send a copy of it to your publisher/graduate school.
- Appropriate credit for the requested material should be given as follows: "Reprinted (adapted) with permission from {COMPLETE REFERENCE CITATION}. Copyright {YEAR} American Chemical Society." Insert appropriate information in place of the capitalized words.
- One-time permission is granted only for the use specified in your RightsLink request. No additional uses are granted (such as derivative works or other editions). For any uses, please submit a new request.

If credit is given to another source for the material you requested from RightsLink, permission must be obtained from that source.

BACK CLOSE WINDOW

Figure 18A

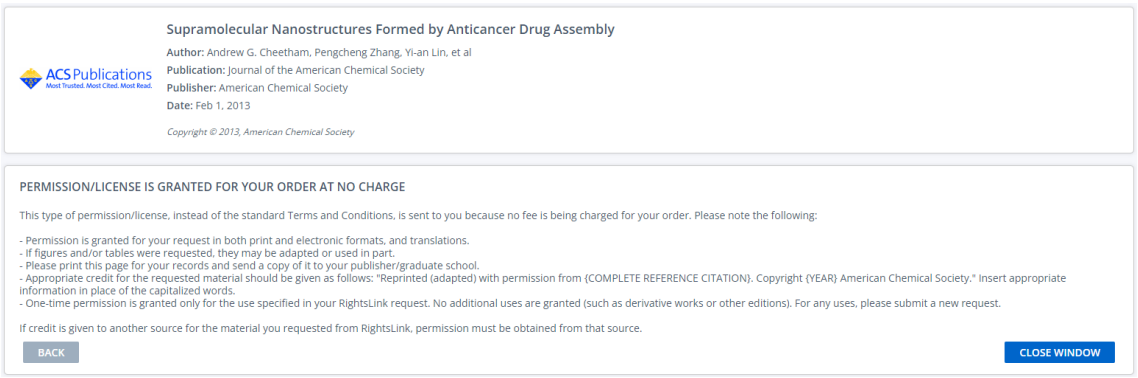

Supramolecular Nanostructures Formed by Anticancer Drug Assembly

Author: Andrew G. Cheetham, Pengcheng Zhang, Yi-an Lin, et al
Publication: Journal of the American Chemical Society
Publisher: American Chemical Society
Date: Feb 1, 2013

Copyright © 2013, American Chemical Society

PERMISSION/LICENSE IS GRANTED FOR YOUR ORDER AT NO CHARGE

This type of permission/license, instead of the standard Terms and Conditions, is sent to you because no fee is being charged for your order. Please note the following:

- Permission is granted for your request in both print and electronic formats, and translations.
- If figures and/or tables were requested, they may be adapted or used in part.
- Please print this page for your records and send a copy of it to your publisher/graduate school.
- Appropriate credit for the requested material should be given as follows: "Reprinted (adapted) with permission from {COMPLETE REFERENCE CITATION}. Copyright {YEAR} American Chemical Society." Insert appropriate information in place of the capitalized words.
- One-time permission is granted only for the use specified in your RightsLink request. No additional uses are granted (such as derivative works or other editions). For any uses, please submit a new request.

If credit is given to another source for the material you requested from RightsLink, permission must be obtained from that source.

BACK CLOSE WINDOW

Figure 18B

Therapeutic polymeric nanomedicine: GSH-responsive release promotes drug release for cancer synergistic chemotherapy

J. Shen, Q. Wang, J. Fang, W. Shen, D. Wu, G. Tang and J. Yang, *RSC Adv.*, 2019, **9**, 37232 **DOI:** 10.1039/C9RA07051F

This article is licensed under a Creative Commons Attribution-NonCommercial 3.0 Unported Licence. **You can use material from this article in other publications, without requesting further permission** from the RSC, provided that the correct acknowledgement is given and it is not used for commercial purposes.

USC UNIVERSIDADE DE SANTIAGO DE COMPOSTELA

Figure 19A

CCC Marketplace

This is a License Agreement between Marcos Vilela Picos ("User") and Copyright Clearance Center, Inc. ("CCC") on behalf of the Rightsholder identified in the order details below. The license consists of the order details, the Marketplace Permissions General Terms and Conditions below, and any Rightsholder Terms and Conditions which are included below.

All payments must be made in full to CCC in accordance with the Marketplace Permissions General Terms and Conditions below.

Order Date	07-Sep-2024	Type of Use	Republish in a thesis/dissertation
Order License ID	1523920-1	Publisher	RSC Pub
ISSN	2040-3372	Portion	Image/photo/illustration

LICENSED CONTENT

Publication Title	Nanoscale	Rightsholder	Royal Society of Chemistry
Article Title	Smart pH- and reduction-dual-responsive folate-PEG-coated polymeric lipid vesicles for tumor-triggered targeted drug delivery.	Publication Type	e-Journal
		Start Page	7635
Author / Editor	Royal Society of Chemistry (Great Britain), National Center for Nanoscience and Technology.	Issue	13
		Volume	6
Date	01/01/2009	URL	http://www.rsc.org/Publishing/Journals/N...
Language	English		
Country	United Kingdom of Great Britain and Northern Ireland		

Figure 19B

ACS Publications
Most Trusted. Most Cited. Most Read.

Precise Polymerization of a Highly Tumor Microenvironment-Responsive Nanoplatform for Strongly Enhanced Intracellular Drug Release

Author: Yi Wang, Lei Zhang, Xiaobin Zhang, et al
Publication: Applied Materials
Publisher: American Chemical Society
Date: Mar 1, 2016

Copyright © 2016, American Chemical Society

PERMISSION/LICENSE IS GRANTED FOR YOUR ORDER AT NO CHARGE

This type of permission/license, instead of the standard Terms and Conditions, is sent to you because no fee is being charged for your order. Please note the following:

- Permission is granted for your request in both print and electronic formats, and translations.
- If figures and/or tables were requested, they may be adapted or used in part.
- Please print this page for your records and send a copy of it to your publisher/graduate school.
- Appropriate credit for the requested material should be given as follows: "Reprinted (adapted) with permission from {COMPLETE REFERENCE CITATION}. Copyright {YEAR} American Chemical Society." Insert appropriate information in place of the capitalized words.
- One-time permission is granted only for the use specified in your RightsLink request. No additional uses are granted (such as derivative works or other editions). For any uses, please submit a new request.

If credit is given to another source for the material you requested from RightsLink, permission must be obtained from that source.

BACK CLOSE WINDOW

Figure 20A

ACS Publications
Most Trusted. Most Cited. Most Read.

Enzyme-Triggered Morphological Transition of Peptide Nanostructures for Tumor-Targeted Drug Delivery and Enhanced Cancer Therapy

Author: Meiwen Cao, Sha Lu, Ningning Wang, et al
Publication: Applied Materials
Publisher: American Chemical Society
Date: May 1, 2019

Copyright © 2019, American Chemical Society

PERMISSION/LICENSE IS GRANTED FOR YOUR ORDER AT NO CHARGE

This type of permission/license, instead of the standard Terms and Conditions, is sent to you because no fee is being charged for your order. Please note the following:

- Permission is granted for your request in both print and electronic formats, and translations.
- If figures and/or tables were requested, they may be adapted or used in part.
- Please print this page for your records and send a copy of it to your publisher/graduate school.
- Appropriate credit for the requested material should be given as follows: "Reprinted (adapted) with permission from {COMPLETE REFERENCE CITATION}. Copyright {YEAR} American Chemical Society." Insert appropriate information in place of the capitalized words.
- One-time permission is granted only for the use specified in your RightsLink request. No additional uses are granted (such as derivative works or other editions). For any uses, please submit a new request.

If credit is given to another source for the material you requested from RightsLink, permission must be obtained from that source.

BACK CLOSE WINDOW

USC UNIVERSIDADE DE SANTIAGO DE COMPOSTELA

Figure 20B

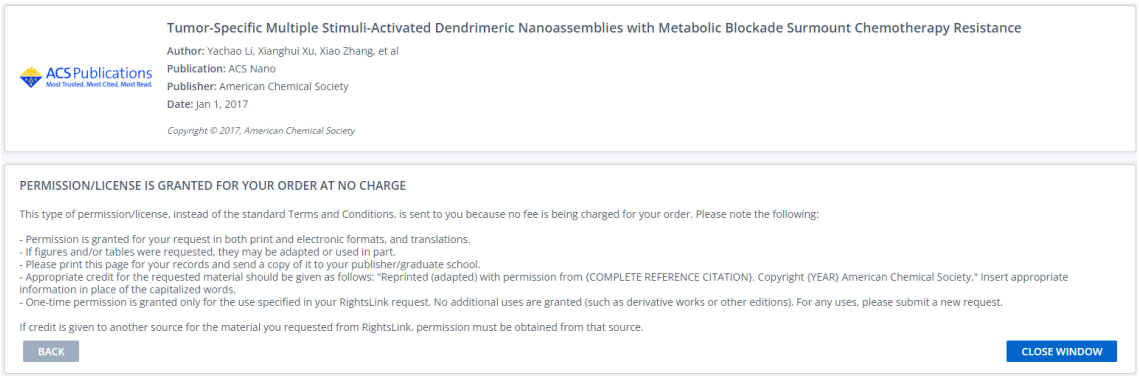

Tumor-Specific Multiple Stimuli-Activated Dendrimeric Nanoassemblies with Metabolic Blockade Surmount Chemotherapy Resistance

Author: Yachao Li, Xianghui Xu, Xiao Zhang, et al
Publication: ACS Nano
Publisher: American Chemical Society
Date: Jan 1, 2017

Copyright © 2017, American Chemical Society

PERMISSION/LICENSE IS GRANTED FOR YOUR ORDER AT NO CHARGE

This type of permission/license, instead of the standard Terms and Conditions, is sent to you because no fee is being charged for your order. Please note the following:

- Permission is granted for your request in both print and electronic formats, and translations.
- If figures and/or tables were requested, they may be adapted or used in part.
- Please print this page for your records and send a copy of it to your publisher/graduate school.
- Appropriate credit for the requested material should be given as follows: "Reprinted (adapted) with permission from {COMPLETE REFERENCE CITATION}. Copyright {YEAR} American Chemical Society." Insert appropriate information in place of the capitalized words.
- One-time permission is granted only for the use specified in your RightsLink request. No additional uses are granted (such as derivative works or other editions). For any uses, please submit a new request.

If credit is given to another source for the material you requested from RightsLink, permission must be obtained from that source.

BACK CLOSE WINDOW

Figure 21A

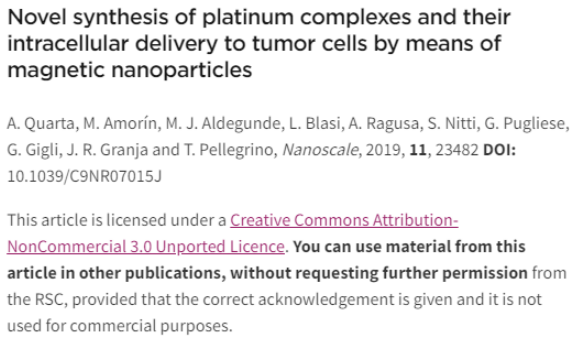

Novel synthesis of platinum complexes and their intracellular delivery to tumor cells by means of magnetic nanoparticles

A. Quarta, M. Amorín, M. J. Aldegunde, L. Blasi, A. Ragusa, S. Nitti, G. Pugliese, G. Gigli, J. R. Granja and T. Pellegrino, *Nanoscale*, 2019, **11**, 23482 **DOI:** 10.1039/C9NR07015J

This article is licensed under a Creative Commons Attribution-NonCommercial 3.0 Unported Licence. **You can use material from this article in other publications, without requesting further permission** from the RSC, provided that the correct acknowledgement is given and it is not used for commercial purposes.

Figure 21B

Noninvasive Remote-Controlled Release of Drug Molecules in Vitro Using Magnetic Actuation of Mechanized Nanoparticles

Author: Courtney R. Thomas, Daniel P. Ferris, Jae-Hyun Lee, et al
Publication: Journal of the American Chemical Society
Publisher: American Chemical Society
Date: Aug 1, 2010

Copyright © 2010, American Chemical Society

PERMISSION/LICENSE IS GRANTED FOR YOUR ORDER AT NO CHARGE

This type of permission/license, instead of the standard Terms and Conditions, is sent to you because no fee is being charged for your order. Please note the following:

- Permission is granted for your request in both print and electronic formats, and translations.
- If figures and/or tables were requested, they may be adapted or used in part.
- Please print this page for your records and send a copy of it to your publisher/graduate school.
- Appropriate credit for the requested material should be given as follows: "Reprinted (adapted) with permission from {COMPLETE REFERENCE CITATION}. Copyright {YEAR} American Chemical Society." Insert appropriate information in place of the capitalized words.
- One-time permission is granted only for the use specified in your RightsLink request. No additional uses are granted (such as derivative works or other editions). For any uses, please submit a new request.

If credit is given to another source for the material you requested from RightsLink, permission must be obtained from that source.

BACK CLOSE WINDOW

USC UNIVERSIDADE DE SANTIAGO DE COMPOSTELA

Figure 22A

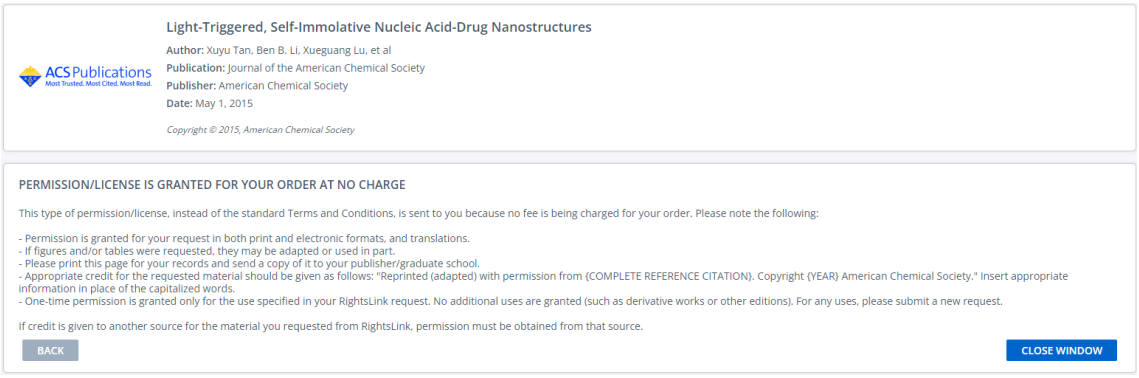

ACS Publications
Most Trusted. Most Cited. Most Read.

Light-Triggered, Self-Immolative Nucleic Acid-Drug Nanostructures

Author: Xuyu Tan, Ben B. Li, Xueguang Lu, et al
Publication: Journal of the American Chemical Society
Publisher: American Chemical Society
Date: May 1, 2015

Copyright © 2015, American Chemical Society

PERMISSION/LICENSE IS GRANTED FOR YOUR ORDER AT NO CHARGE

This type of permission/license, instead of the standard Terms and Conditions, is sent to you because no fee is being charged for your order. Please note the following:

- Permission is granted for your request in both print and electronic formats, and translations.
- If figures and/or tables were requested, they may be adapted or used in part.
- Please print this page for your records and send a copy of it to your publisher/graduate school.
- Appropriate credit for the requested material should be given as follows: "Reprinted (adapted) with permission from {COMPLETE REFERENCE CITATION}. Copyright {YEAR} American Chemical Society." Insert appropriate information in place of the capitalized words.
- One-time permission is granted only for the use specified in your RightsLink request. No additional uses are granted (such as derivative works or other editions). For any uses, please submit a new request.

If credit is given to another source for the material you requested from RightsLink, permission must be obtained from that source.

BACK CLOSE WINDOW

Figure 22B

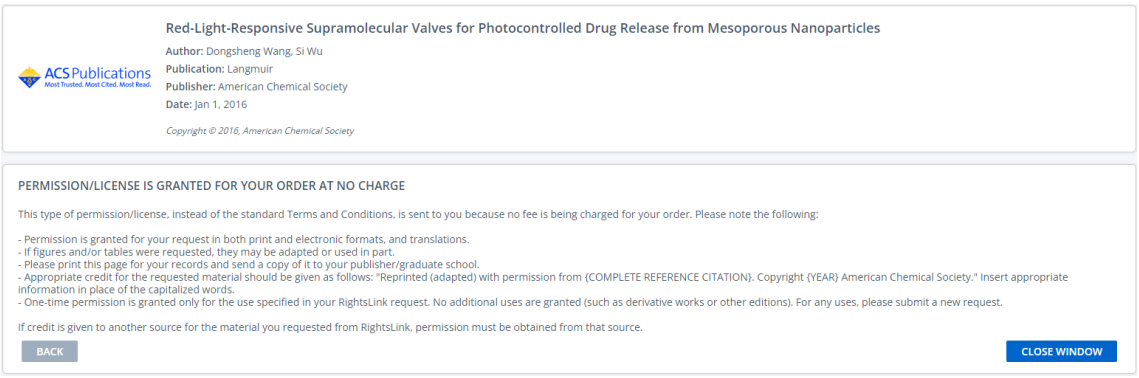

ACS Publications
Most Trusted. Most Cited. Most Read.

Red-Light-Responsive Supramolecular Valves for Photocontrolled Drug Release from Mesoporous Nanoparticles

Author: Dongsheng Wang, Si Wu
Publication: Langmuir
Publisher: American Chemical Society
Date: Jan 1, 2016

Copyright © 2016, American Chemical Society

PERMISSION/LICENSE IS GRANTED FOR YOUR ORDER AT NO CHARGE

This type of permission/license, instead of the standard Terms and Conditions, is sent to you because no fee is being charged for your order. Please note the following:

- Permission is granted for your request in both print and electronic formats, and translations.
- If figures and/or tables were requested, they may be adapted or used in part.
- Please print this page for your records and send a copy of it to your publisher/graduate school.
- Appropriate credit for the requested material should be given as follows: "Reprinted (adapted) with permission from {COMPLETE REFERENCE CITATION}. Copyright {YEAR} American Chemical Society." Insert appropriate information in place of the capitalized words.
- One-time permission is granted only for the use specified in your RightsLink request. No additional uses are granted (such as derivative works or other editions). For any uses, please submit a new request.

If credit is given to another source for the material you requested from RightsLink, permission must be obtained from that source.

BACK CLOSE WINDOW

Figure 22C

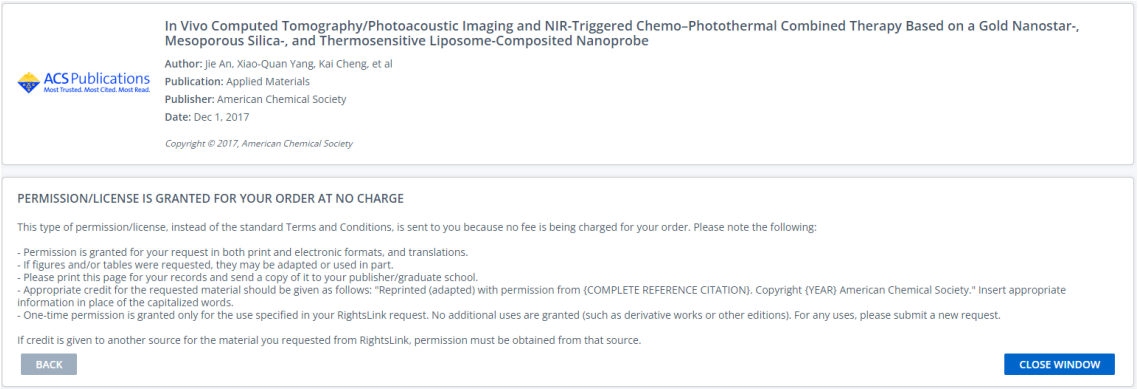

ACS Publications
Most Trusted. Most Cited. Most Read.

In Vivo Computed Tomography/Photoacoustic Imaging and NIR-Triggered Chemo–Photothermal Combined Therapy Based on a Gold Nanostar-, Mesoporous Silica-, and Thermosensitive Liposome-Composited Nanoprobe

Author: Jie An, Xiao-Quan Yang, Kai Cheng, et al
Publication: Applied Materials
Publisher: American Chemical Society
Date: Dec 1, 2017

Copyright © 2017, American Chemical Society

PERMISSION/LICENSE IS GRANTED FOR YOUR ORDER AT NO CHARGE

This type of permission/license, instead of the standard Terms and Conditions, is sent to you because no fee is being charged for your order. Please note the following:

- Permission is granted for your request in both print and electronic formats, and translations.
- If figures and/or tables were requested, they may be adapted or used in part.
- Please print this page for your records and send a copy of it to your publisher/graduate school.
- Appropriate credit for the requested material should be given as follows: "Reprinted (adapted) with permission from {COMPLETE REFERENCE CITATION}. Copyright {YEAR} American Chemical Society." Insert appropriate information in place of the capitalized words.
- One-time permission is granted only for the use specified in your RightsLink request. No additional uses are granted (such as derivative works or other editions). For any uses, please submit a new request.

If credit is given to another source for the material you requested from RightsLink, permission must be obtained from that source.

BACK CLOSE WINDOW

USC UNIVERSIDADE DE SANTIAGO DE COMPOSTELA

Figure 23A

Order Summary

Licensee:	Mr. Marcos Vilela Picos
Order Date:	Sep 8, 2024
Order Number:	5864290934463
Publication:	Nature Materials
Title:	Stimuli-responsive nanocarriers for drug delivery
Type of Use:	Thesis/Dissertation
Order Total:	0.00 EUR

CCC Marketplace

This is a License Agreement between Marcos Vilela Picos ("User") and Copyright Clearance Center, Inc. ("CCC") on behalf of the Rightsholder identified in the order details below. The license consists of the order details, the Marketplace Permissions General Terms and Conditions below, and any Rightsholder Terms and Conditions which are included below.

All payments must be made in full to CCC in accordance with the Marketplace Permissions General Terms and Conditions below.

Order Date	08-Sep-2024	Type of Use	Republish in a thesis/dissertation
Order License ID	1524083-1	Publisher	ELSEVIER BV
ISSN	1873-4995	Portion	Chart/graph/table/figure

LICENSED CONTENT

Publication Title	Journal of controlled release	Publication Type	e-Journal
Article Title	Controlled and targeted tumor chemotherapy by ultrasound-activated nanoemulsions/microbubbles	Start Page	268
		End Page	276
Author / Editor	Controlled Release Society, Japanese Society of Drug Delivery Systems	Issue	3
		Volume	138
Date	01/01/1984	URL	http://www.sciencedirect.com/science/jo...
Language	English		
Country	Netherlands		
Rightsholder	Elsevier Science & Technology Journals		

Figure 23B

CCC Marketplace

This is a License Agreement between Marcos Vilela Picos ("User") and Copyright Clearance Center, Inc. ("CCC") on behalf of the Rightsholder identified in the order details below. The license consists of the order details, the Marketplace Permissions General Terms and Conditions below, and any Rightsholder Terms and Conditions which are included below.

All payments must be made in full to CCC in accordance with the Marketplace Permissions General Terms and Conditions below.

Order Date	08-Sep-2024	Type of Use	Republish in a thesis/dissertation
Order License ID	1524084-1	Publisher	ELSEVIER BV
ISSN	1873-4995	Portion	Chart/graph/table/figure

LICENSED CONTENT

Publication Title	Journal of controlled release	Rightsholder	Elsevier Science & Technology Journals
Article Title	Ultrasound-responsive polymersomes capable of endosomal escape for efficient cancer therapy	Publication Type	e-Journal
		Start Page	81
Author / Editor	Controlled Release Society, Japanese Society of Drug Delivery Systems	End Page	94
		Volume	322
Date	01/01/1984	URL	http://www.sciencedirect.com/science/jo...
Language	English		
Country	Netherlands		

USC UNIVERSIDADE DE SANTIAGO DE COMPOSTELA

Figure 24A

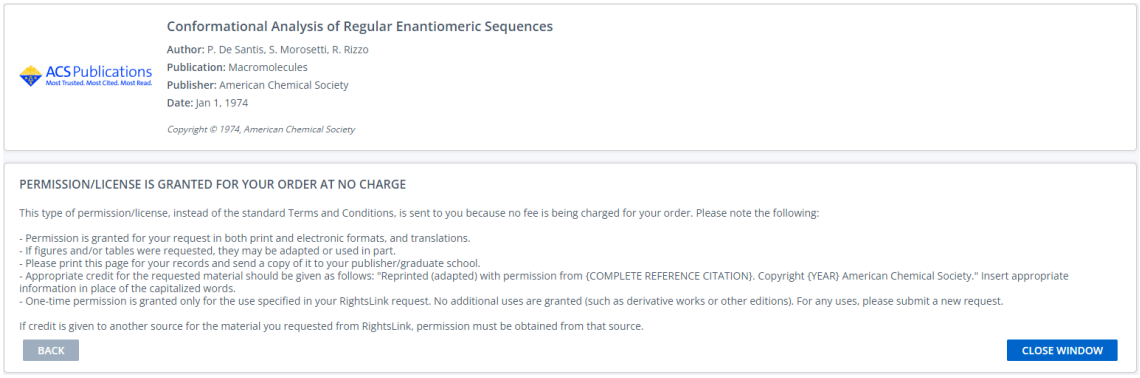

Conformational Analysis of Regular Enantiomeric Sequences

Author: P. De Santis, S. Morosetti, R. Rizzo
Publication: Macromolecules
Publisher: American Chemical Society
Date: Jan 1, 1974

Copyright © 1974, American Chemical Society

PERMISSION/LICENSE IS GRANTED FOR YOUR ORDER AT NO CHARGE

This type of permission/license, instead of the standard Terms and Conditions, is sent to you because no fee is being charged for your order. Please note the following:

- Permission is granted for your request in both print and electronic formats, and translations.
- If figures and/or tables were requested, they may be adapted or used in part.
- Please print this page for your records and send a copy of it to your publisher/graduate school.
- Appropriate credit for the requested material should be given as follows: "Reprinted (adapted) with permission from {COMPLETE REFERENCE CITATION}. Copyright {YEAR} American Chemical Society." Insert appropriate information in place of the capitalized words.
- One-time permission is granted only for the use specified in your RightsLink request. No additional uses are granted (such as derivative works or other editions). For any uses, please submit a new request.

If credit is given to another source for the material you requested from RightsLink, permission must be obtained from that source.

BACK CLOSE WINDOW

Figure 24B

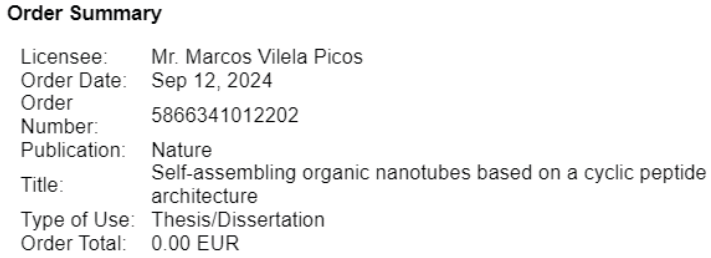

Order Summary

Licensee:	Mr. Marcos Vilela Picos
Order Date:	Sep 12, 2024
Order Number:	5866341012202
Publication:	Nature
Title:	Self-assembling organic nanotubes based on a cyclic peptide architecture
Type of Use:	Thesis/Dissertation
Order Total:	0.00 EUR

Figure 24C

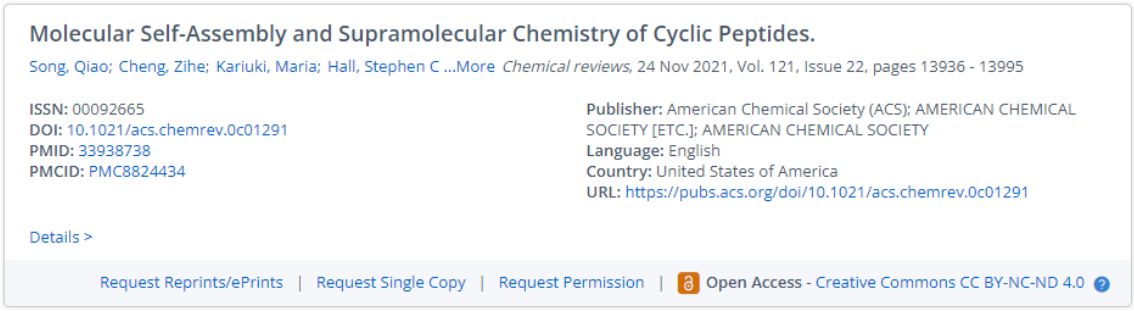

Molecular Self-Assembly and Supramolecular Chemistry of Cyclic Peptides.

Song, Qiao; Cheng, Zihe; Kariuki, Maria; Hall, Stephen C ...More *Chemical reviews*, 24 Nov 2021, Vol. 121, Issue 22, pages 13936 - 13995

ISSN: 00092665
DOI: 10.1021/acs.chemrev.0c01291
PMID: 33938738
PMCID: PMC8824434

Publisher: American Chemical Society (ACS); AMERICAN CHEMICAL SOCIETY [ETC.]; AMERICAN CHEMICAL SOCIETY
Language: English
Country: United States of America
URL: https://pubs.acs.org/doi/10.1021/acs.chemrev.0c01291

Details >

Request Reprints/ePrints | Request Single Copy | Request Permission | Open Access - Creative Commons CC BY-NC-ND 4.0

Figure 25A

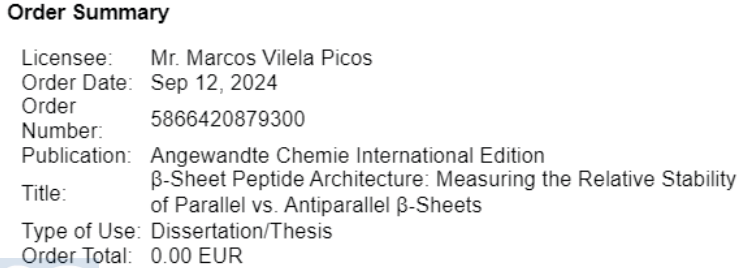

Order Summary

Licensee:	Mr. Marcos Vilela Picos
Order Date:	Sep 12, 2024
Order Number:	5866420879300
Publication:	Angewandte Chemie International Edition
Title:	β-Sheet Peptide Architecture: Measuring the Relative Stability of Parallel vs. Antiparallel β-Sheets
Type of Use:	Dissertation/Thesis
Order Total:	0.00 EUR

USC UNIVERSIDADE DE SANTIAGO DE COMPOSTELA

Figure 25B

CCC Marketplace

This is a License Agreement between Marcos Vilela Picos ("User") and Copyright Clearance Center, Inc. ("CCC") on behalf of the Rightsholder identified in the order details below. The license consists of the order details, the Marketplace Permissions General Terms and Conditions below, and any Rightsholder Terms and Conditions which are included below.

All payments must be made in full to CCC in accordance with the Marketplace Permissions General Terms and Conditions below.

Order Date	12-Sep-2024	Type of Use	Republish in a thesis/dissertation
Order License ID	1525581-1	Publisher	THE SOCIETY,
ISSN	1359-7345	Portion	Chart/graph/table/figure

LICENSED CONTENT

Publication Title	Chemical communications : Chem comm	Publication Type	Journal
Article Title	Versatile symport transporters based on cyclic peptide dimers.	Start Page	46
Author / Editor	ROYAL SOCIETY OF CHEMISTRY (GREAT BRITAIN)	End Page	49
Date	01/01/1996	Issue	1
Language	English	Volume	56
Country	United Kingdom of Great Britain and Northern Ireland	URL	http://www.rsc.org/Publishing/Journals/cc...
Rightsholder	Royal Society of Chemistry		

Figure 25C

CCC Marketplace

This is a License Agreement between Marcos Vilela Picos ("User") and Copyright Clearance Center, Inc. ("CCC") on behalf of the Rightsholder identified in the order details below. The license consists of the order details, the Marketplace Permissions General Terms and Conditions below, and any Rightsholder Terms and Conditions which are included below.

All payments must be made in full to CCC in accordance with the Marketplace Permissions General Terms and Conditions below.

Order Date	12-Sep-2024	Type of Use	Republish in a thesis/dissertation
Order License ID	1525582-1	Publisher	RSC Pub
ISSN	2040-3372	Portion	Chart/graph/table/figure

LICENSED CONTENT

Publication Title	Nanoscale	Publication Type	e-Journal
Article Title	Self-assembling Venturi-like peptide nanotubes.	Start Page	748
Author / Editor	Royal Society of Chemistry (Great Britain), National Center for Nanoscience and Technology.	End Page	753
Date	01/01/2009	Issue	2
Language	English	Volume	9
Country	United Kingdom of Great Britain and Northern Ireland	URL	http://www.rsc.org/Publishing/Journals/N...
Rightsholder	Royal Society of Chemistry		

Figure 25D

ACS Publications
Most Trusted. Most Cited. Most Read.

Self-Assembling Molecular Capsules Based on α,γ-Cyclic Peptides

Author: Haxel Lionel Ozores, Manuel Amorín, Juan R. Granja
Publication: Journal of the American Chemical Society
Publisher: American Chemical Society
Date: Jan 1, 2017

Copyright © 2017, American Chemical Society

PERMISSION/LICENSE IS GRANTED FOR YOUR ORDER AT NO CHARGE

This type of permission/license, instead of the standard Terms and Conditions, is sent to you because no fee is being charged for your order. Please note the following:

- Permission is granted for your request in both print and electronic formats, and translations.
- If figures and/or tables were requested, they may be adapted or used in part.
- Please print this page for your records and send a copy of it to your publisher/graduate school.
- Appropriate credit for the requested material should be given as follows: "Reprinted (adapted) with permission from {COMPLETE REFERENCE CITATION}. Copyright {YEAR} American Chemical Society." Insert appropriate information in place of the capitalized words.
- One-time permission is granted only for the use specified in your RightsLink request. No additional uses are granted (such as derivative works or other editions). For any uses, please submit a new request.

If credit is given to another source for the material you requested from RightsLink, permission must be obtained from that source.

BACK CLOSE WINDOW

USC UNIVERSIDADE DE SANTIAGO DE COMPOSTELA

Figure 26

Order Summary

Licensee:	Mr. Marcos Vilela Picos
Order Date:	Sep 12, 2024
Order Number:	5866540375575
Publication:	Angewandte Chemie International Edition
Title:	Photoswitchable Hydrogen-Bonding in Self-Organized Cylindrical Peptide Systems
Type of Use:	Dissertation/Thesis
Order Total:	0.00 EUR

Figure 27

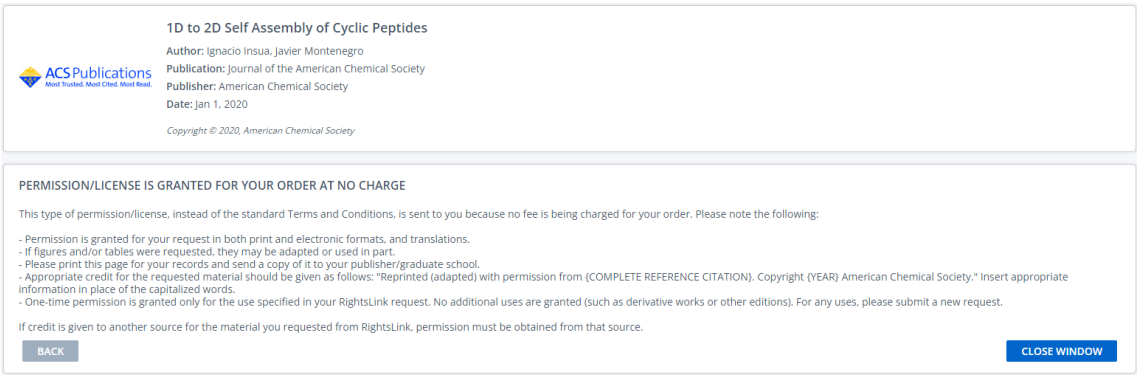

ACS Publications
Most Trusted. Most Cited. Most Read.

1D to 2D Self Assembly of Cyclic Peptides

Author: Ignacio Insua, Javier Montenegro
Publication: Journal of the American Chemical Society
Publisher: American Chemical Society
Date: Jan 1, 2020

Copyright © 2020, American Chemical Society

PERMISSION/LICENSE IS GRANTED FOR YOUR ORDER AT NO CHARGE

This type of permission/license, instead of the standard Terms and Conditions, is sent to you because no fee is being charged for your order. Please note the following:

- Permission is granted for your request in both print and electronic formats, and translations.
- If figures and/or tables were requested, they may be adapted or used in part.
- Please print this page for your records and send a copy of it to your publisher/graduate school.
- Appropriate credit for the requested material should be given as follows: "Reprinted (adapted) with permission from {COMPLETE REFERENCE CITATION}. Copyright {YEAR} American Chemical Society." Insert appropriate information in place of the capitalized words.
- One-time permission is granted only for the use specified in your RightsLink request. No additional uses are granted (such as derivative works or other editions). For any uses, please submit a new request.

If credit is given to another source for the material you requested from RightsLink, permission must be obtained from that source.

BACK CLOSE WINDOW

Figure 28A

CCC Marketplace

This is a License Agreement between Marcos Vilela Picos ("User") and Copyright Clearance Center, Inc. ("CCC") on behalf of the Rightsholder identified in the order details below. The license consists of the order details, the Marketplace Permissions General Terms and Conditions below, and any Rightsholder Terms and Conditions which are included below.

All payments must be made in full to CCC in accordance with the Marketplace Permissions General Terms and Conditions below.

Order Date	12-Sep-2024	Type of Use	Republish in a thesis/dissertation
Order License ID	1525721-1	Publisher	Royal Society of Chemistry
ISSN	1759-9962	Portion	Chart/graph/table/figure

LICENSED CONTENT

Publication Title	Polymer chemistry	Rightsholder	Royal Society of Chemistry
Article Title	Modular design for the controlled production of polymeric nanotubes from polymer/peptide conjugates	Publication Type	e-Journal
		Start Page	1956
Author / Editor	Royal Society of Chemistry (Great Britain)	Issue	9
Date	01/01/2010	Volume	2
Language	English	URL	http://www.rsc.org/Publishing/Journals/P...
Country	United Kingdom of Great Britain and Northern Ireland		

Figure 28B

Order Summary

Licensee:	Mr. Marcos Vilela Picos
Order Date:	Sep 12, 2024
Order Number:	5866560345786
Publication:	Angewandte Chemie International Edition
Title:	Secondary Self-Assembly of Supramolecular Nanotubes into Tubisomes and Their Activity on Cells
Type of Use:	Dissertation/Thesis
Order Total:	0.00 EUR

USC UNIVERSIDADE DE SANTIAGO DE

Figure 29 and 31C

Order Summary

Licensee:	Mr. Marcos Vilela Picos
Order Date:	Sep 12, 2024
Order Number:	5866570307141
Publication:	Chemistry - A European Journal
Title:	Double Orthogonal Click Reactions for the Development of Antimicrobial Peptide Nanotubes
Type of Use:	Dissertation/Thesis
Order Total:	0.00 EUR

Figure 30

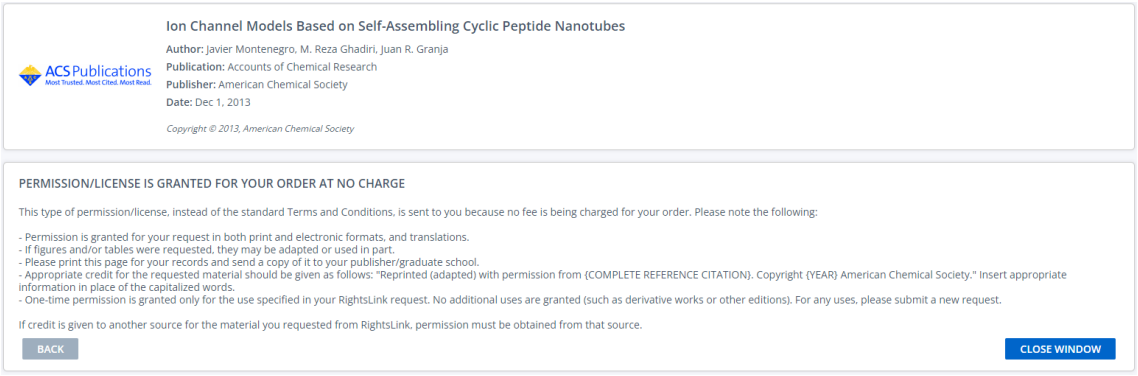

ACS Publications
Most Trusted. Most Cited. Most Read.

Ion Channel Models Based on Self-Assembling Cyclic Peptide Nanotubes

Author: Javier Montenegro, M. Reza Ghadiri, Juan R. Granja
Publication: Accounts of Chemical Research
Publisher: American Chemical Society
Date: Dec 1, 2013

Copyright © 2013, American Chemical Society

PERMISSION/LICENSE IS GRANTED FOR YOUR ORDER AT NO CHARGE

This type of permission/license, instead of the standard Terms and Conditions, is sent to you because no fee is being charged for your order. Please note the following:

- Permission is granted for your request in both print and electronic formats, and translations.
- If figures and/or tables were requested, they may be adapted or used in part.
- Please print this page for your records and send a copy of it to your publisher/graduate school.
- Appropriate credit for the requested material should be given as follows: "Reprinted (adapted) with permission from {COMPLETE REFERENCE CITATION}. Copyright {YEAR} American Chemical Society." Insert appropriate information in place of the capitalized words.
- One-time permission is granted only for the use specified in your RightsLink request. No additional uses are granted (such as derivative works or other editions). For any uses, please submit a new request.

If credit is given to another source for the material you requested from RightsLink, permission must be obtained from that source.

BACK CLOSE WINDOW

Figure 31A

Order Summary

Licensee:	Mr. Marcos Vilela Picos
Order Date:	Sep 13, 2024
Order Number:	5867001364248
Publication:	Colloids and Surfaces B: Biointerfaces
Title:	Membrane targeting antimicrobial cyclic peptide nanotubes – an experimental and computational study
Type of Use:	reuse in a thesis/dissertation
Order Total:	0.00 EUR

Figure 31B

CCC Marketplace

This is a License Agreement between Marcos Vilela Picos ("User") and Copyright Clearance Center, Inc. ("CCC") on behalf of the Rightsholder identified in the order details below. The license consists of the order details, the Marketplace Permissions General Terms and Conditions below, and any Rightsholder Terms and Conditions which are included below.

All payments must be made in full to CCC in accordance with the Marketplace Permissions General Terms and Conditions below.

Order Date	13-Sep-2024	Type of Use	Republish in a thesis/dissertation
Order License ID	1526028-1	Publisher	THE SOCIETY,
ISSN	1359-7345	Portion	Chart/graph/table/figure

LICENSED CONTENT

Publication Title	Chemical communications : Chem comm	Rightsholder	Royal Society of Chemistry
Article Title	Antibacterial cyclic D,L-alpha-glycopeptides.	Publication Type	Journal
Author / Editor	ROYAL SOCIETY OF CHEMISTRY (GREAT BRITAIN)	Start Page	3693
Date	01/01/1996	Issue	25
Language	English	Volume	0
Country	United Kingdom of Great Britain and Northern Ireland	URL	http://www.rsc.org/Publishing/Journals/cc...

USC UNIVERSIDADE DE SANTIAGO DE COMPOSTELA

Figure 32A

CCC Marketplace

This is a License Agreement between Marcos Vilela Picos ("User") and Copyright Clearance Center, Inc. ("CCC") on behalf of the Rightsholder identified in the order details below. The license consists of the order details, the Marketplace Permissions General Terms and Conditions below, and any Rightsholder Terms and Conditions which are included below.

All payments must be made in full to CCC in accordance with the Marketplace Permissions General Terms and Conditions below.

Order Date	13-Sep-2024	Type of Use	Republish in a thesis/dissertation
Order License ID	1526106-1	Publisher	ROYAL SOCIETY OF CHEMISTRY
ISSN	1463-9084	Portion	Chart/graph/table/figure

LICENSED CONTENT

Publication Title	Physical chemistry chemical physics	Publication Type	e-Journal
Article Title	Theoretical studies on the transport mechanism of 5-fluorouracil through cyclic peptide based nanotubes.	Start Page	1260
		End Page	1270
Author / Editor	Royal Society of Chemistry (Great Britain)	Issue	4
Date	01/01/1999	Volume	15
Language	English	URL	http://firstsearch.oclc.org/journal=1463-9...
Country	United Kingdom of Great Britain and Northern Ireland		
Rightsholder	Royal Society of Chemistry		

Figure 33A

Modular design of cyclic peptide – polymer conjugate nanotubes for delivery and tunable release of anti-cancer drug compounds

Author: Sophie K. Hill,Richard M. England,Sébastien Perrier
Publication: Journal of Controlled Release
Publisher: Elsevier
Date: March 2024

© 2024 The Authors. Published by Elsevier B.V.

Creative Commons

This is an open access article distributed under the terms of the Creative Commons CC-BY license, which permits unrestricted use, distribution, and reproduction in any medium, provided the original work is properly cited.

You are not required to obtain permission to reuse this article.

To request permission for a type of use not listed, please contact Elsevier Global Rights Department.

Are you the author of this Elsevier journal article?

Figure 33B

Order Summary

Licensee:	Mr. Marcos Vilela Picos
Order Date:	Sep 13, 2024
Order Number:	5867121015475
Publication:	Angewandte Chemie International Edition
Title:	Hierarchical Self-Assembled Photo-Responsive Tubisomes from a Cyclic Peptide-Bridged Amphiphilic Block Copolymer
Type of Use:	Dissertation/Thesis
Order Total:	0.00 EUR

Figure 34A

ACS Publications
Most Trusted. Most Cited. Most Read.

pH-Responsive, Amphiphilic Core–Shell Supramolecular Polymer Brushes from Cyclic Peptide–Polymer Conjugates

Author: Sophie C. Larnaudie, Johannes C. Brendel, Katrina A. Jolliffe, et al
Publication: ACS Macro Letters
Publisher: American Chemical Society
Date: Dec 1, 2017

Copyright © 2017, American Chemical Society

PERMISSION/LICENSE IS GRANTED FOR YOUR ORDER AT NO CHARGE

This type of permission/license, instead of the standard Terms and Conditions, is sent to you because no fee is being charged for your order. Please note the following:

- Permission is granted for your request in both print and electronic formats, and translations.
- If figures and/or tables were requested, they may be adapted or used in part.
- Please print this page for your records and send a copy of it to your publisher/graduate school.
- Appropriate credit for the requested material should be given as follows: "Reprinted (adapted) with permission from {COMPLETE REFERENCE CITATION}. Copyright {YEAR} American Chemical Society." Insert appropriate information in place of the capitalized words.
- One-time permission is granted only for the use specified in your RightsLink request. No additional uses are granted (such as derivative works or other editions). For any uses, please submit a new request.

If credit is given to another source for the material you requested from RightsLink, permission must be obtained from that source.

BACK CLOSE WINDOW

Figure 34B

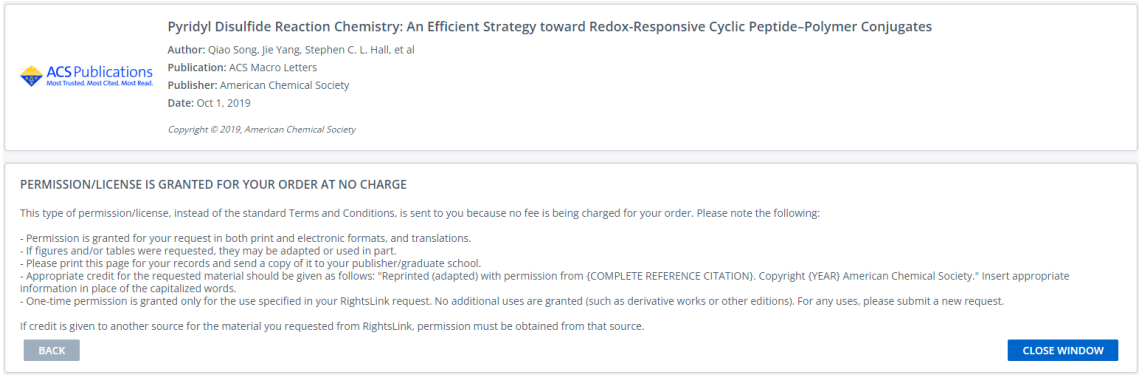

Pyridyl Disulfide Reaction Chemistry: An Efficient Strategy toward Redox-Responsive Cyclic Peptide–Polymer Conjugates

Author: Qiao Song, Jie Yang, Stephen C. L. Hall, et al
Publication: ACS Macro Letters
Publisher: American Chemical Society
Date: Oct 1, 2019

Copyright © 2019, American Chemical Society

PERMISSION/LICENSE IS GRANTED FOR YOUR ORDER AT NO CHARGE

This type of permission/license, instead of the standard Terms and Conditions, is sent to you because no fee is being charged for your order. Please note the following:

- Permission is granted for your request in both print and electronic formats, and translations.
- If figures and/or tables were requested, they may be adapted or used in part.
- Please print this page for your records and send a copy of it to your publisher/graduate school.
- Appropriate credit for the requested material should be given as follows: "Reprinted (adapted) with permission from {COMPLETE REFERENCE CITATION}. Copyright {YEAR} American Chemical Society." Insert appropriate information in place of the capitalized words.
- One-time permission is granted only for the use specified in your RightsLink request. No additional uses are granted (such as derivative works or other editions). For any uses, please submit a new request.

If credit is given to another source for the material you requested from RightsLink, permission must be obtained from that source.

BACK CLOSE WINDOW

Figure 34C

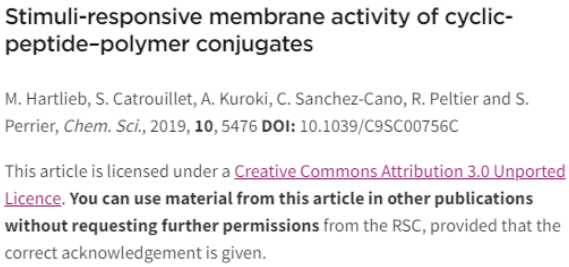

Stimuli-responsive membrane activity of cyclic-peptide–polymer conjugates

M. Hartlieb, S. Catrouillet, A. Kuroki, C. Sanchez-Cano, R. Peltier and S. Perrier, *Chem. Sci.*, 2019, **10**, 5476 **DOI:** 10.1039/C9SC00756C

This article is licensed under a Creative Commons Attribution 3.0 Unported Licence. **You can use material from this article in other publications without requesting further permissions** from the RSC, provided that the correct acknowledgement is given.

Figure 34D

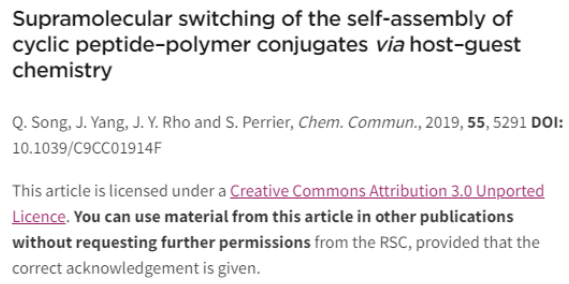

Supramolecular switching of the self-assembly of cyclic peptide–polymer conjugates *via* host–guest chemistry

Q. Song, J. Yang, J. Y. Rho and S. Perrier, *Chem. Commun.*, 2019, **55**, 5291 **DOI:** 10.1039/C9CC01914F

This article is licensed under a Creative Commons Attribution 3.0 Unported Licence. **You can use material from this article in other publications without requesting further permissions** from the RSC, provided that the correct acknowledgement is given.

Figure 35

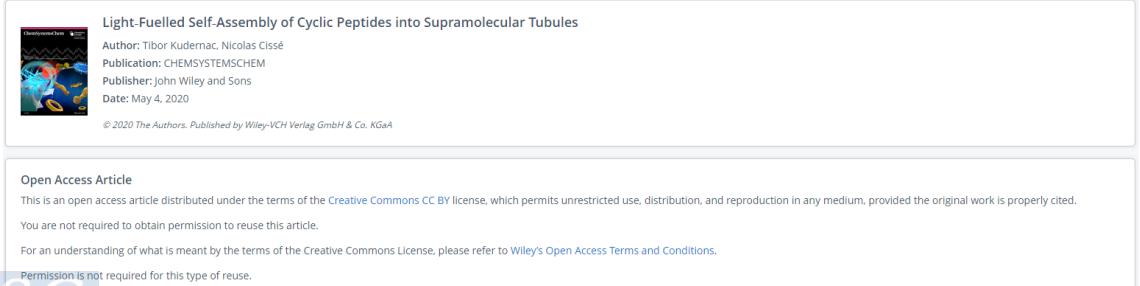

Light-Fuelled Self-Assembly of Cyclic Peptides into Supramolecular Tubules

Author: Tibor Kudernac, Nicolas Cissé
Publication: CHEMSYSTEMSCHEM
Publisher: John Wiley and Sons
Date: May 4, 2020

© 2020 The Authors. Published by Wiley-VCH Verlag GmbH & Co. KGaA

Open Access Article

This is an open access article distributed under the terms of the Creative Commons CC BY license, which permits unrestricted use, distribution, and reproduction in any medium, provided the original work is properly cited.

You are not required to obtain permission to reuse this article.

For an understanding of what is meant by the terms of the Creative Commons License, please refer to Wiley's Open Access Terms and Conditions.

Permission is not required for this type of reuse.

USC UNIVERSIDADE DE SANTIAGO DE COMPOSTELA

Figure 36A

CCC Marketplace

This is a License Agreement between Marcos Vilela Picos ("User") and Copyright Clearance Center, Inc. ("CCC") on behalf of the Rightsholder identified in the order details below. The license consists of the order details, the Marketplace Permissions General Terms and Conditions below, and any Rightsholder Terms and Conditions which are included below.

All payments must be made in full to CCC in accordance with the Marketplace Permissions General Terms and Conditions below.

Order Date	14-Sep-2024	Type of Use	Republish in a thesis/dissertation
Order License ID	1526364-1	Publisher	Royal Society of Chemistry
ISSN	2055-6764	Portion	Chart/graph/table/figure

LICENSED CONTENT

Publication Title	Nanoscale Horizons	Rightsholder	Royal Society of Chemistry
Article Title	pH-Triggered self-assembly and hydrogelation of cyclic peptide nanotubes confined in water micro-droplets.	Publication Type	e-Journal
		Start Page	391
Author / Editor	Royal Society of Chemistry (Great Britain),, Guo jia na mi ke xue zhong xin (China),	End Page	396
		Issue	4
Date	01/01/2016	Volume	3
Language	English		
Country	United Kingdom of Great Britain and Northern Ireland		

Figure 36B

Order Summary

Licensee:	Mr. Marcos Vilela Picos
Order Date:	Sep 14, 2024
Order Number:	5867691420927
Publication:	Angewandte Chemie International Edition
Title:	Spatially Controlled Supramolecular Polymerization of Peptide Nanotubes by Microfluidics
Type of Use:	Dissertation/Thesis
Order Total:	0.00 EUR

Figure 40A

CCC Marketplace

This is a License Agreement between Marcos Vilela Picos ("User") and Copyright Clearance Center, Inc. ("CCC") on behalf of the Rightsholder identified in the order details below. The license consists of the order details, the Marketplace Permissions General Terms and Conditions below, and any Rightsholder Terms and Conditions which are included below.

All payments must be made in full to CCC in accordance with the Marketplace Permissions General Terms and Conditions below.

Order Date	03-Oct-2024	Type of Use	Republish in a thesis/dissertation
Order License ID	1532381-1	Publisher	THE SOCIETY,
ISSN	1359-7345	Portion	Chart/graph/table/figure

LICENSED CONTENT

Publication Title	Chemical communications : Chem comm	Publication Type	Journal
Article Title	Photohealable ion gels based on the reversible dimerisation of anthracene.	Start Page	13371
		End Page	13374
Author / Editor	ROYAL SOCIETY OF CHEMISTRY (GREAT BRITAIN)	Issue	95
		Volume	54
Date	01/01/1996	URL	http://www.rsc.org/Publishing/Journals/cc...
Language	English		
Country	United Kingdom of Great Britain and Northern Ireland		
Rightsholder	Royal Society of Chemistry		

USC UNIVERSIDADE DE SANTIAGO DE COMPOSTELA

Figure 40B

Order Summary

Licensee:	Mr. Marcos Vilela Picos
Order Date:	Oct 3, 2024
Order Number:	5881381242394
Publication:	Angewandte Chemie International Edition
Title:	Strong, Self-Healable, and Recyclable Visible-Light-Responsive Hydrogel Actuators
Type of Use:	Dissertation/Thesis
Order Total:	0.00 EUR

Figure 41A

ACS Publications
Most Trusted. Most Cited. Most Read.

Dynamic Covalent Bond Based on Reversible Photo [4 4] Cycloaddition of Anthracene for Construction of Double-Dynamic Polymers

Author: Jiang-Fei Xu, Yu-Zhe Chen, Li-Zhu Wu, et al
Publication: Organic Letters
Publisher: American Chemical Society
Date: Dec 1, 2013

Copyright © 2013, American Chemical Society

PERMISSION/LICENSE IS GRANTED FOR YOUR ORDER AT NO CHARGE

This type of permission/license, instead of the standard Terms and Conditions, is sent to you because no fee is being charged for your order. Please note the following:

- Permission is granted for your request in both print and electronic formats, and translations.
- If figures and/or tables were requested, they may be adapted or used in part.
- Please print this page for your records and send a copy of it to your publisher/graduate school.
- Appropriate credit for the requested material should be given as follows: "Reprinted (adapted) with permission from {COMPLETE REFERENCE CITATION}. Copyright {YEAR} American Chemical Society." Insert appropriate information in place of the capitalized words.
- One-time permission is granted only for the use specified in your RightsLink request. No additional uses are granted (such as derivative works or other editions). For any uses, please submit a new request.

If credit is given to another source for the material you requested from RightsLink, permission must be obtained from that source.

BACK CLOSE WINDOW

Figure 41B

Photo-dissociation of self-assembled (anthracene-2-carbonyl)amino acid hydrogels

P. R. A. Chivers, R. S. Dookie, J. E. Gough and S. J. Webb, *Chem. Commun.*, 2020, **56**, 13792 **DOI:** 10.1039/D0CC05292B

This article is licensed under a Creative Commons Attribution 3.0 Unported Licence. **You can use material from this article in other publications without requesting further permissions** from the RSC, provided that the correct acknowledgement is given.

Figure 41C

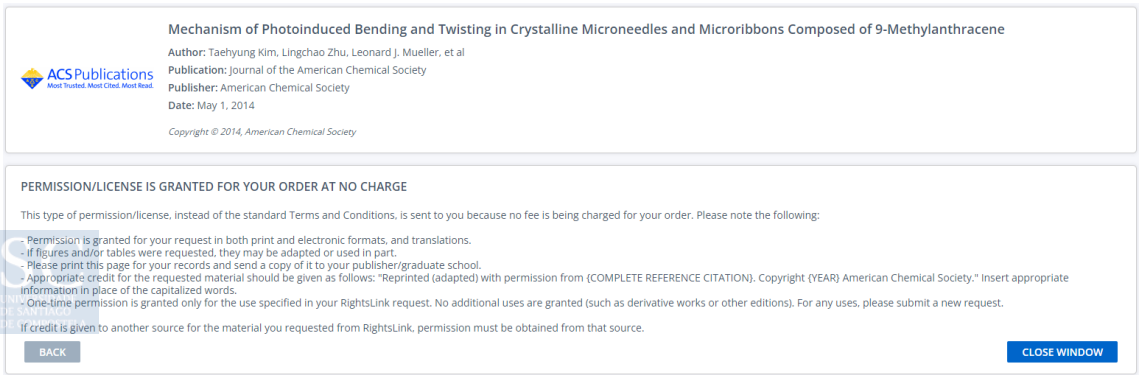

ACS Publications
Most Trusted. Most Cited. Most Read.

Mechanism of Photoinduced Bending and Twisting in Crystalline Microneedles and Microribbons Composed of 9-Methylanthracene

Author: Taehyung Kim, Lingchao Zhu, Leonard J. Mueller, et al
Publication: Journal of the American Chemical Society
Publisher: American Chemical Society
Date: May 1, 2014

Copyright © 2014, American Chemical Society

PERMISSION/LICENSE IS GRANTED FOR YOUR ORDER AT NO CHARGE

This type of permission/license, instead of the standard Terms and Conditions, is sent to you because no fee is being charged for your order. Please note the following:

- Permission is granted for your request in both print and electronic formats, and translations.
- If figures and/or tables were requested, they may be adapted or used in part.
- Please print this page for your records and send a copy of it to your publisher/graduate school.
- Appropriate credit for the requested material should be given as follows: "Reprinted (adapted) with permission from {COMPLETE REFERENCE CITATION}. Copyright {YEAR} American Chemical Society." Insert appropriate information in place of the capitalized words.
- One-time permission is granted only for the use specified in your RightsLink request. No additional uses are granted (such as derivative works or other editions). For any uses, please submit a new request.

If credit is given to another source for the material you requested from RightsLink, permission must be obtained from that source.

BACK CLOSE WINDOW

Figure 67A

Order Summary

Licensee:	Mr. Marcos Vilela Picos
Order Date:	Oct 5, 2024
Order Number:	5882421098969
Publication:	Angewandte Chemie International Edition
Title:	Intrinsically Photoswitchable α/β Peptides toward Two-State Foldamers
Type of Use:	Dissertation/Thesis
Order Total:	0.00 EUR

Figure 67B

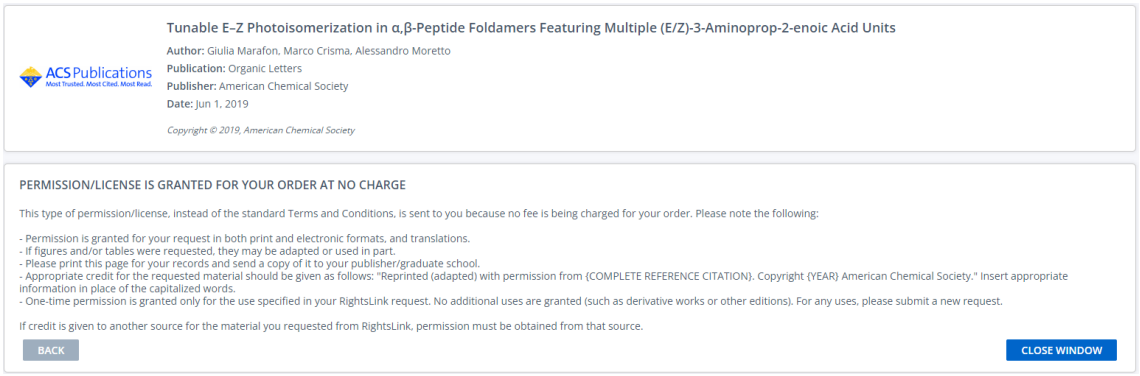

ACS Publications
Most Trusted. Most Cited. Most Read.

Tunable E–Z Photoisomerization in α,β-Peptide Foldamers Featuring Multiple (E/Z)-3-Aminoprop-2-enoic Acid Units

Author: Giulia Marafon, Marco Crisma, Alessandro Moretto
Publication: Organic Letters
Publisher: American Chemical Society
Date: Jun 1, 2019

Copyright © 2019, American Chemical Society

PERMISSION/LICENSE IS GRANTED FOR YOUR ORDER AT NO CHARGE

This type of permission/license, instead of the standard Terms and Conditions, is sent to you because no fee is being charged for your order. Please note the following:

- Permission is granted for your request in both print and electronic formats, and translations.
- If figures and/or tables were requested, they may be adapted or used in part.
- Please print this page for your records and send a copy of it to your publisher/graduate school.
- Appropriate credit for the requested material should be given as follows: "Reprinted (adapted) with permission from {COMPLETE REFERENCE CITATION}. Copyright {YEAR} American Chemical Society." Insert appropriate information in place of the capitalized words.
- One-time permission is granted only for the use specified in your RightsLink request. No additional uses are granted (such as derivative works or other editions). For any uses, please submit a new request.

If credit is given to another source for the material you requested from RightsLink, permission must be obtained from that source.

BACK CLOSE WINDOW

Figure 68A

Order Summary

Licensee:	Mr. Marcos Vilela Picos
Order Date:	Oct 5, 2024
Order Number:	5882431011479
Publication:	Angewandte Chemie International Edition
Title:	Photoresponsive Prion-Mimic Foldamer to Induce Controlled Protein Aggregation
Type of Use:	Dissertation/Thesis
Order Total:	0.00 EUR

Figure 68B

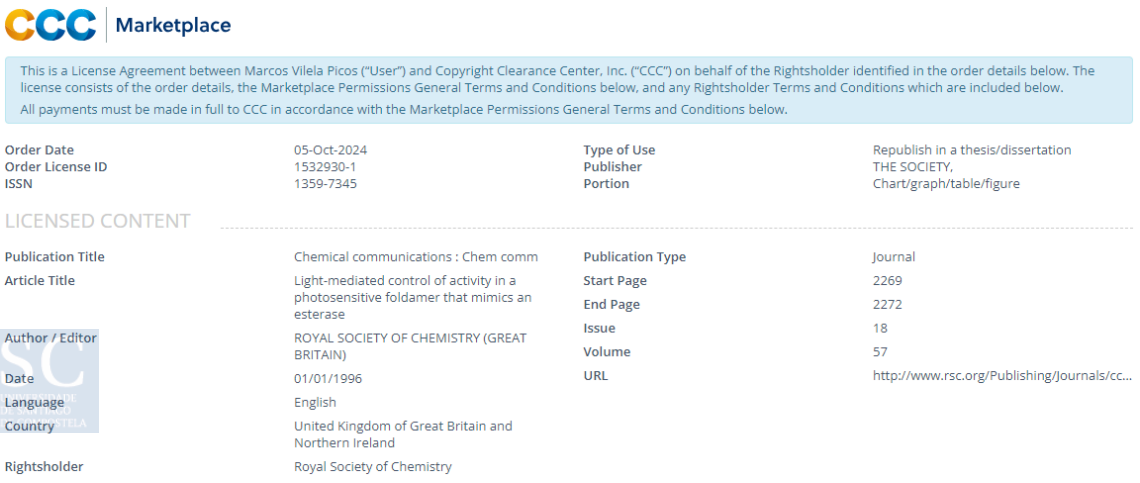

CCC Marketplace

This is a License Agreement between Marcos Vilela Picos ("User") and Copyright Clearance Center, Inc. ("CCC") on behalf of the Rightsholder identified in the order details below. The license consists of the order details, the Marketplace Permissions General Terms and Conditions below, and any Rightsholder Terms and Conditions which are included below.

All payments must be made in full to CCC in accordance with the Marketplace Permissions General Terms and Conditions below.

Order Date	05-Oct-2024	Type of Use	Republish in a thesis/dissertation
Order License ID	1532930-1	Publisher	THE SOCIETY,
ISSN	1359-7345	Portion	Chart/graph/table/figure

LICENSED CONTENT

Publication Title	Chemical communications : Chem comm	Publication Type	Journal
Article Title	Light-mediated control of activity in a photosensitive foldamer that mimics an esterase	Start Page	2269
		End Page	2272
Author / Editor	ROYAL SOCIETY OF CHEMISTRY (GREAT BRITAIN)	Issue	18
		Volume	57
Date	01/01/1996	URL	http://www.rsc.org/Publishing/Journals/cc...
Language	English		
Country	United Kingdom of Great Britain and Northern Ireland		
Rightsholder	Royal Society of Chemistry		

USC UNIVERSIDAD DE SANTIAGO DE COMPOSTELA

Figure 69A

CCC Marketplace

This is a License Agreement between Marcos Vilela Picos ("User") and Copyright Clearance Center, Inc. ("CCC") on behalf of the Rightsholder identified in the order details below. The license consists of the order details, the Marketplace Permissions General Terms and Conditions below, and any Rightsholder Terms and Conditions which are included below.
All payments must be made in full to CCC in accordance with the Marketplace Permissions General Terms and Conditions below.

Order Date	05-Oct-2024	Type of Use	Republish in a thesis/dissertation
Order License ID	1532968-1	Publisher	AMERICAN ASSOCIATION FOR THE ADVANCEMENT OF SCIENCE
ISSN	1095-9203	Portion	Chart/graph/table/figure

LICENSED CONTENT

Publication Title	Science	Publication Type	e-Journal
Article Title	One-step fabrication of supramolecular microcapsules from microfluidic droplets.	Start Page	690
Author / Editor	American Association for the Advancement of Science.	End Page	694
Date	01/01/1880	Issue	6069
Language	English	Volume	335
Country	United States of America	URL	http://www.sciencemag.org/archive
Rightsholder	American Association for the Advancement of Science		

Figure 69B

Cucurbit[n]uril-Based Microcapsules Self-Assembled within Microfluidic Droplets: A Versatile Approach for Supramolecular Architectures and Materials.

Liu, Ji; Lan, Yang; Yu, Ziyi; Tan, Cindy S.Y.; ...More *Accounts of chemical research*, 21 Feb 2017, Vol. 50, Issue 2, pages 208 - 217

ISSN: 00014842
DOI: 10.1021/acs.accounts.6b00429
PMID: 28075551
PMCID: PMC5474693

Publisher: AMERICAN CHEMICAL SOCIETY.; American Chemical Society; AMERICAN CHEMICAL SOCIEITY
Language: English
Country: United States of America
URL: https://pubs.acs.org/doi/10.1021/acs.accounts.6b00429

Details >

Request Reprints/ePrints | Request Single Copy | Request Permission | Open Access - Creative Commons CC BY-NC 4.0

Figure 70A

ACS Publications
Most Trusted. Most Cited. Most Read.

Microfluidic Assembly of Monodisperse Vesosomes as Artificial Cell Models

Author: Nan-Nan Deng, Maaruthy Yelleswarapu, Lifei Zheng, et al
Publication: Journal of the American Chemical Society
Publisher: American Chemical Society
Date: Jan 1, 2017

Copyright © 2017, American Chemical Society

PERMISSION/LICENSE IS GRANTED FOR YOUR ORDER AT NO CHARGE

This type of permission/license, instead of the standard Terms and Conditions, is sent to you because no fee is being charged for your order. Please note the following:

- Permission is granted for your request in both print and electronic formats, and translations.
- If figures and/or tables were requested, they may be adapted or used in part.
- Please print this page for your records and send a copy of it to your publisher/graduate school.
- Appropriate credit for the requested material should be given as follows: "Reprinted (adapted) with permission from {COMPLETE REFERENCE CITATION}. Copyright {YEAR} American Chemical Society." Insert appropriate information in place of the capitalized words.
- One-time permission is granted only for the use specified in your RightsLink request. No additional uses are granted (such as derivative works or other editions). For any uses, please submit a new request.

If credit is given to another source for the material you requested from RightsLink, permission must be obtained from that source.

BACK CLOSE WINDOW

USC UNIVERSIDADE DE SANTIAGO DE COMPOSTELA

Figure 70B

Order Summary

Licensee:	Mr. Marcos Vilela Picos
Order Date:	Oct 5, 2024
Order Number:	5882600947640
Publication:	Nature Materials
Title:	Sequential bottom-up assembly of mechanically stabilized synthetic cells by microfluidics
Type of Use:	Thesis/Dissertation
Order Total:	0.00 EUR

Figure 71

Order Summary

Licensee:	Mr. Marcos Vilela Picos
Order Date:	Oct 6, 2024
Order Number:	5882950835952
Publication:	Small
Title:	Microfluidic-Assisted Self-Assembly of Molecular Hydrogelator at Water–Water Interfaces for Continuous Fabrication of Supramolecular Microcapsules
Type of Use:	Dissertation/Thesis
Order Total:	0.00 EUR

Figures 100 and 101

Santiago de Compostela. October 8, 2024

Eva González Freire (DNI 53611721D) authorizes Marcos Vilela Picos (DNI 32725768B) to reprint or adapt figures of the doctoral thesis "*Application of two orthogonal click-type reactions for the preparation of cyclic peptides with antibacterial and anticancer activity*" in this doctoral thesis.

Firmado por Eva González, 08/10/2024, 16:38h

Eva González Freire

10.4. Annex IV: Declaration of all other images

The PhD candidate Marcos Vilela Picos declares that all those images that are not referenced to the corresponding reproduction or adaptation permission have been personally created.

Santiago de Compostela, December 2nd 2024.

USC UNIVERSIDADE DE SANTIAGO DE COMPOSTELA

The dynamic behaviour of supramolecular systems has facilitated the incorporation of stimuli-responsive capabilities into these materials, thereby broadening their range of applications. In this context, self-assembling cyclic peptide nanotubes emerge as a promising alternative for the construction of this type of systems. These tubular assemblies are formed by the controlled stacking of cyclic peptide units with a flat conformation through hydrogen bonding interactions.

This doctoral thesis proposes different strategies for obtaining stimuli-responsive cyclic peptide nanotubes in order to control their self-assembly process or to develop drug delivery applications. The results represent an initial step towards future new self-assembly properties and biological applications for cyclic peptide nanotubes.